[illegible]

Environmental Assessment of the Alaskan Continental Shelf

Final Reports of Principal Investigators

Volume 21

February 1984

U.S. DEPARTMENT OF COMMERCE
National Oceanic and Atmospheric Administration
National Ocean Service
Office of Oceanography and Marine Services
Ocean Assessments Division

U.S. DEPARTMENT OF THE INTERIOR
Minerals Management Service

Outer Continental Shelf Environmental Assessment Program

ENVIRONMENTAL ASSESSMENT
OF THE
ALASKAN CONTINENTAL SHELF

FINAL REPORTS OF PRINCIPAL INVESTIGATORS

VOLUME 21

FEBRUARY 1984

U.S. DEPARTMENT OF COMMERCE
NATIONAL OCEANIC AND ATMOSPHERIC ADMINISTRATION
NATIONAL OCEAN SERVICE
OFFICE OF OCEANOGRAPHY AND MARINE SERVICES
OCEAN ASSESSMENTS DIVISION

JUNEAU, ALASKA

The facts, conclusions, and issues appearing in this report are based on results of an Alaskan environmental studies program managed by the Outer Continental Shelf Environmental Assessment Program (OCSEAP) of the National Oceanic and Atmospheric Administration, U.S. Department of Commerce, and primarily funded by the Minerals Management Service, U.S. Department of the Interior, through interagency agreement.

Environmental Assessment of the Alaskan Continental Shelf

Final Reports of Principal Investigators

VOLUME 21 FEBRUARY 1984

CONTENTS

[The supplement to this report, "Multivariate Analysis of Petroleum Weathering in the Marine Environment - Sub Arctic. Volume II - Appendices," is contained in Volume 22 of OCSEAP Final Reports.]

Contract No. NA80RAC00018
Research Unit No. 597

Final Report

Multivariate Analysis of Petroleum Weathering in the Marine Environment - Sub Arctic

Volume I - Technical Results

Submitted by:

James R. Payne, Bruce E. Kirstein, G. Daniel McNabb, Jr.,
James L. Lambach, Robert Redding, Randolph E. Jordan,
Wilson Hom, Celso de Oliveira, Gary S. Smith, Daniel M. Baxter,
and Russel Gaegel (NOAA Kasitsna Bay laboratory manager)

James R. Payne, Principal Investigator
Division of Environmental Chemistry and Geochemistry
Science Applications, Inc.
La Jolla, CA 92038

January 18, 1984

VOLUME I

TABLE OF CONTENTS

TABLE OF CONTENTS

Section Page

TABLE OF CONTENTS

Section | Page

TABLE OF CONTENTS

Section Page

TABLE OF CONTENTS

LIST OF TABLES

LIST OF TABLES (continued)

LIST OF TABLES (continued)

LIST OF TABLES (continued)

LIST OF TABLES (continued)

LIST OF TABLES (continued)

LIST OF TABLES (continued)

LIST OF FIGURES

LIST OF FIGURES (continued)

LIST OF FIGURES (continued)

LIST OF FIGURES (continued)

LIST OF FIGURES (continued)

LIST OF FIGURES (continued)

LIST OF FIGURES (continued)

LIST OF FIGURES (continued)

LIST OF FIGURES (continued)

LIST OF FIGURES (continued)

LIST OF FIGURES (continued)

LIST OF FIGURES (continued)

LIST OF FIGURES (continued)

LIST OF FIGURES (continued)

LIST OF FIGURES (continued)

LIST OF FIGURES (continued)

LIST OF FIGURES (continued)

LIST OF FIGURES (continued)

LIST OF FIGURES (continued)

LIST OF FIGURES (continued)

LIST OF FIGURES (continued)

LIST OF FIGURES (continued)

LIST OF FIGURES (continued)

LIST OF FIGURES (continued)

LIST OF FIGURES (continued)

LIST OF FIGURES (continued)

LIST OF FIGURES (continued)

ACKNOWLEDGMENTS

This report represents the sustained efforts of many people in various capacities over a period of many months. Various consultants have contributed greatly to this project. N. L. Guinasso of Texas A&M provided initial guidance and review of existing oil-weathering models. Professor D. Mackay of the University of Toronto has contributed extensively through his decade of experience in oil-weathering, and we draw upon this vast experience for mass transfer, slick spreading and water-in-oil emulsification. Professor S. Middleman of the University of California at San Diego contributed extensively on the topics of diffusion coefficients and the state of mixedness of an oil slick. His contributions are presented in Sections 4.7 and 4.8. Dr. Fred Su at SAI provided some of the detailed mathematical derivations involving component-specific transport phenomena. Mr. Thomas Lovorn assisted in the mathematical derivations which will ultimately be required for modeling Oil/Suspended Particulate Material Interactions (Sections 4.10.5, 4.10.6, and 4.10.8). Mr. Mike Beckel and SAI's process laboratory staff completed the intertidal sediment extractions, and gas chromatography/mass spectrometry analyses were completed by John Nemmers and Norm Flynn. Drs. Osmond Holm-Hansen and Farooq Azam of Scripps Institute of Oceanography have been instrumental in the development and execution of experiments designed to examine the microbial degradation of spilled petroleum under simulated environmental conditions.

David J. Maiero is acknowledged for his contributions and expertise in selecting the intertidal sites for SPM collection and later intertidal corral experiments. Paul Mankiewicz, Beth Heffernan, Karen Meyers and Marinee Payne also provided laboratory assistance at Kasitsna Bay.

The photographic prints and reproductions presented in this report were prepared by Larry Haines of Design Photographics. Suzanne Goldman, Mabel O'Byrne and Angela Cohen produced the final copy of this report on the word-processor, and Charles R. Phillips aided in its final reproduction and

compilation. Rachel Hovde, Sylvie Barriault, Donna Michelson and Cheryl Fish are all in our debt for the countless hours required for typing the original draft manuscipts, preparing many of the figures and tables presented, and in overall management of the production of the report in its final form.

These people are all extended a special note of thanks; the efforts put forth by each were far above ordinary expectations.

1.0 INTRODUCTION

When fresh crude oil and/or refined petroleum products are released to the marine environment, they are immediately subject to a wide variety of chemical and physical alterations. The most predominant weathering processes include: evaporation; dispersion of whole oil droplets into the water column; dissolution of selected aromatic components; adsorption of dispersed and dissolved hydrocarbons onto suspended particulate material; water-in-oil emulsification (or mousse formation); microbial and photochemical oxidation; and, finally, advective removal of dispersed and dissolved components from the parent slick. Spreading and wind-driven drift of the surface oil from the point of origin also occur; however, these processes are not considered as weathering, per se. The magnitude and rates of these varying processes are dependent upon the specific chemical materials involved and on such "environmental" factors as turbulence, air and water temperature, suspended particulate material types and concentrations, oil composition, light intensity, nutrient availability, and microbial composition and abundance. The purpose of this program has been to investigate the rates and extent of the physical and chemical changes which occur to petroleum spills in the subarctic marine environment as a result of the combined actions of these abiotic and biotic factors. Among the processes examined and quantified are: evaporation, dispersion of whole oil droplets, dissolution of specific aromatics, microbial oxidation, emulsification (mousse formation), and adsorption onto suspended particulate material.

Our investigations have been designed to provide qualitative and quantitative information on the rates of loss and fates of specific compounds and "pseudo-compounds" during oceanic weathering. Ultimately, the final product or objective of this program has been to generate a combined component-specific and pseudo-component (boiling point or "distillation cut") model to simulate and predict spilled petroleum behavior as a result of physical/chemical weathering. These models were developed to encompass specific compound partitioning as well as overall oil mass balance considerations, and they have been tested with observed chemical changes from laboratory and field experiments. The algorithms which constitute the working computerized model can now be used in a predictive manner to determine the time-dependent chemical compositions and rheological properities of real or simulated oil spills. The oil weathering processes included in the mathematical model are evaporation, dispersion of oil into the water column, dissolution, water-in-oil emulsification (mousse formation), and oil slick spreading. When coupled to trajectory models, such a physical-chemical weathering model should allow environmental managers to better estimate the impacts from real and hypothetical oil spill situations. Furthermore, a thorough understanding of the time-dependent compositions and concentrations of spilled petroleum mixtures (including weathering products) will aid in extrapolating the findings from biological effects experiments to real environmental situations.

While this study was initially envisioned to be an experimental and modeling effort confined to SAI's La Jolla facilities, it was necessary and feasible to expand the program to include field studies in the Alaskan subarctic environment of NOAA's Kasitsna Bay laboratory facilities near Homer, Alaska. Therefore, additional flow-through seawater aquaria and wave tank experiments designed to simulate and quantify subarctic open ocean evaporation, dispersion, dissolution, and microbial and photochemical oxidation processes were completed at that facility. Also, in conjunction with other NOAA contractors (Drs. Griffiths and Morita; RU 190), experiments were completed to evaluate the long-term chemical fate of fresh and weathered oil in subtidal sediments. As an extension of the subtidal studies, additional field experiments were completed to examine the long-term (17 month) chemical fate of fresh oil in different subarctic intertidal regimes.

This final report is intended to be an independent document summarizing the overall program's activities to date; as such, it contains significant sections which have been discussed in detail in interim and progress reports. The main body of the report is divided into eight major chapters or sections. Each section is intended to be a complete "stand alone" presentation of various aspects of model development and verification of model predicted output as determined by laboratory and field experiments. To expedite a more thorough understanding of oil weathering processes, however, the separate sections are extensively cross referenced. Section 2.0 contains the Executive Summary of Program Activities for the overall study. Section 3.0 contains detailed oil characterizations for Murban, Cook Inlet, Prudhoe Bay, and Wilmington crude oils. Compound-specific analyses by GC, GC/MS and UV-Fluorescence are included along with true boiling point (TPB) distallation "pseudo-component" characterizations and the results of rheological properties determinations. Section 4.0 contains details of the Oil Weathering Model development, including derivations of all algorithms currently coded into the Oil Weathering Model. Two distinctly different approaches to modeling oil weathering behavior are considered, and these include a "pseudo-component" distillation cut approach which accounts for overall oil mass balance, and a component-specific evaporation/dissolution partitioning approach which is useful for biological considerations.

Section 4.0 is further divided into subsections which consider the algorithms required for: modeling a well-stirred versus diffusion controlled oil body (Sections 4.1 and 4.2); descriptions of component-specific evaporation and dissolution (Subsections 4.3 and 4.5); the measurement of Henry's Law coefficients for predicting evaporative behavior (Section 4.6); the mathematical derivations required and experimental measurements necessary for measurement of diffusion coefficients of volatile components through an oil slick (Section 4.7); the role of internal circulation within an oil slick for weathering of a thin oil film (Section 4.8); and the dispersion of whole oil droplets into the water column. (Complete listings of the computer code used in the Oil Weathering Model are presented in Appendices A through E.) Section 4.10 includes the algorithm development and mathematical derivations which ultimately will be required for modeling oil/suspended particulate material (SPM) interactions. This section further considers: SPM concentrations, size distributions and flocculation behavior as generated from cohesive and noncohesive sediments; the process of spontaneous dispersion of whole oil droplets; the interaction of "oil particles" and "dissolved components" with suspended particulate material; a description of the modeling requirements for studying the interaction of oil with suspended particulate material; and, finally, the boundary conditions which will be required for modeling dispersed oil/SPM interactions.

Section 5.0 considers the experimental program results generated from studies completed in La Jolla, California and Kasitsna Bay, Alaska. Results of experimental chamber evaporation/dissolution rate determinations at temperatures ranging from 3 to 20°C are discussed, and compound-specific concentrations in the oil, air, and water phases are presented as a function of time and weathering conditions. Determinations of oil/water partition coefficients required for dissolution modeling are considered, and then details of the expansion of the La Jolla-based studies to outdoor evaporation/dissolution studies in flow-through aquaria at Kasitsna Bay, Alaska, are presented. Extensive details are presented on the results of subarctic flow-through wave tank experiments where changes in oil physical properties and spill behavior are correlated with oil phase chemistry. Time-series dissolution of specific aromatics in the wave tank systems are also measured and discussed. Finally, the data from the La Jolla based evaporation/dissolution chamber experiments and Kasitsna Bay wave tank studies are used to validate computer model predictions. Comparisons of model predicted versus observed measurements of dispersion, oil phase viscosity, percent water incorporation, and evaporation (as determined by percent mass distilled considerations) for winter and summer spills are presented.

Section 6.0 presents the experimental results on measured oil/SPM interactions in beaker and wave tank studies, and then considers the long-term fate of fresh oil stranded in different intertidal regimes characteristic of southwestern Alaskan environments.

Section 7.0 presents the detailed results of flow-through microbial degradation studies completed in conjunction with Drs. Farooq Azam and Osmond

Holm-Hansen at Scripps Institution of Oceaography, and similar experiments completed at Kasitsna Bay, Alaska.

Section 8.0 presents the results of recent intercalibration programs completed through cooperative efforts with the NOAA/National Marine Fisheries Service Laboratory in Seattle, Washington.

As noted above, Appendices A through E present detailed code listings for various components of the overall weathering model. Appendix A lists the entire computer code as it existed in December, 1983. Appendix B includes the Oil Weathering Model User's Manual which was published as a separate document in July, 1983. Appendix C includes a code description for component-specific dissolution. Appendix D includes a code listing for dispersed oil-concentration profiles with a <u>time varying</u> oil flux, and Appendix E includes a code listing for dispersed oil concentration profiles with a <u>constant</u> oil flux. Appendix F presents analytical methods utilized throughout the oil weathering program, and Appendix G includes the results of X-ray diffraction analyses completed by Technology of Materials Company on suspended particulate material used for oil/SPM adsorption studies. Finally, because the information on long-term fate of sedimented oil is pertinent to the overall goals of this program, the results of our collaborative efforts with Drs. Griffiths and Morita of Oregon State University are included as Appendix H.

2.0 EXECUTIVE SUMMARY OF PROGRAM ACTIVITIES

2.1 INTRODUCTION

The ultimate purpose or objective of this program was to develop a computer model which would have predictive capabilities for oil-spill behavior under real world conditions. During model development, experiments were designed and conducted in evaporation/dissolution test chambers, in flow-through aquaria and in flow-through wave tanks under ambient subarctic environmental conditions at NOAA's Kasitsna Bay field laboratory to provide the necessary kinetic and thermodynamic data on the rates of transfer of molecular and "pseudo" (distillate cut) components in the oil. This report documents the development of the computer model and presents the measured kinetic and thermodynamic data for the following processes: evaporation, dissolution, dispersion of whole oil drops into the water column, adsorption of dispersed and dissolved oil onto suspended particulate material, and percent water uptake as a function of weathering conditions during the formation of water-in-oil emulsions (mousse). Specific rheological properties determinations were also made for oil/air and oil/water interfacial surface tension, density, and viscosity. Viscosity measurements were completed at a constant temperature of 38°C (to allow more accurate time-series comparisons) and at ambient temperatures during the oil weathering process (to provide data on the physical properties of spilled oil as it may be encountered during clean-up operations). Extensive whole oil rheological properties data sets and component-specific concentration data obtained from time-series oil, air and water column measurements during oil weathering experiments are presented in tabular and graphical form. These data are then compared with computer-model predicted oil behavior under carefully monitored subarctic environmental conditions for verification of the Oil Weathering Model.

The derivations presented here, and supporting data, are intended to serve as a data base and reference point for additional model development. With this report as a reference document and the Oil Weathering User's Manual, which was published as a separate document in July, 1983 (KIRSTEIN et al.), additional investigators, environmental managers and other interested parties can then better design and undertake future programs to predict the ultimate fate and impact of open-ocean oil spills under a wide variety of environmental conditions.

2.2 CRUDE OIL CHARACTERIZATION

The four oils studied in this program were analyzed by a variety of techniques including flame ionization detector (FID) gas chromatography, gas chromatography/mass spectrometry, and true boiling point (TBP) distillation separations for component-specific and overall oil mass-balance considerations, respectively. Separate distillate cuts were then subjected to characterization by the above methods, and time-series measurements of weathered oil interfacial surface tension, viscosity, density and percent water were completed under a variety of field conditions. Four crude oils were initially selected for preliminary evaluation, and these included Murban, Cook Inlet, Prudhoe Bay, and Wilmington crudes. Component-specific composition data presented in Section 3.0 (Oil Characterization) and rheological properties data (on ambient viscosity and density) along with preliminary distillate cut (% residuum) characterizations led to the selection of Prudhoe Bay crude oil for additional subarctic weathering studies. Of the four crudes, this crude was intermediate in API gravity (27.0) and it contained a wide variety of alkyl-substituted and relatively toxic aromatic hydrocarbons (e.g., see Figure 3-3, page 3-6 and Table 3-11, page 3-19) including the heteroaromatic sulfur compound dibenzothiophene, and its alkyl-substituted homologues (e.g., Figure 3-7, page 3-22). Also, the presence of an evenly repeating series of normal alkanes ranging from nC-3 to greater than nC-37 allowed "true boiling point" determinations of fractions lost due to environmental processes from more readily accessible gas chromatographic characterization data, and their presence aided in recognition of microbial processes affecting one compound class type in preference to another. By virtue of its production and transport from the North Slope, Prudhoe Bay crude oil also represented a crude which could potentially be released to the subarctic marine environment.

2.3 OIL WEATHERING MODEL DEVELOPMENT

Section 4.0 contains the complete mathematical derivations for all the currently utilized code in the Oil Weathering Model. In addition, derivations are presented for areas which are not currently encoded, but for which additional work may be warranted. The problem of a well-stirred versus diffusion controlled slab and its role in mathematical derivations for predicting evaporation and dissolution behavior is considered in depth. At this time the current Oil Weathering Model Code uses the well-stirred derivations. There are times, however, as a slick continues to age, where diffusion control processes will take over. Additional encoding of the derivations presented herein may provide a more accurate model for longer-term weathering processes and help in defining additional parameters which need to be measured. These considerations are also important for modeling and predicting the behavior of thick and thin oil lenses (patches) as observed in real world oil spill events (PAYNE, 1981).

Derivations are also presented for dispersion of whole oil droplets into the water column, component-specific dissolution of aromatics into the water column, component-specific evaporation from a finite slick, and component-specific dissolution. The problem with these component-specific approaches, however, is that none of them accounts for the overall mass balance of the slick. Therefore, it is necessary to characterize oil by a method which does account for the entire mass. The True Boiling Point distillation approach is a standard petroleum industry method which has been used for years in designing refining processes where it is important to control the physical-chemical behavior of different molecular weight and compound class (paraffin, naphtha, aromatic) groups in a manner to obtain the maximum yield of usable products from the parent crude oil resource. The utilization of a True Boiling Point characterization was, therefore, a natural development in the evolution of the oil weathering model. Extensive distillate cut data exist for over 800 of the world's currently produced crudes (COLEMAN et al., 1978). Therefore, once the oil weathering model is developed and tested with one crude, other crude oils (and refined products) from that data base can be modeled, with each distillate cut present in the subject crude of interest treated according to its thermodynamic, kinetic and physical properties. With this pseudo-component or distillate cut characterization approach it is then possible to get a more accurate estimate of the overall mass balance of the slick. One inherent problem with gas chromatographic methods is that they do not usually account for much of the non-distillable residuum (i.e., the fraction not distilled at 790°F). As the data in Tables 3-12 through 3-15 of Section 3.1 illustrate, weight percent nondistilled residuum increases in the series: Murban (19%), Cook Inlet (26%); Prudhoe Bay (36%) and Wilmington (53%). As such, Prudhoe Bay crude oil contains a 36% residual which would not otherwise be accounted for unless such a True Boiling Point distillation characterization approach were used. When the Oil Weathering Model is applied to other refined products--such as kerosene, gasoline or arctic diesel fuel--evaporation, dissolution and dispersion predictions can be made based on the published boiling point, viscosity and density data for these different distillate cuts. Solubility or oil/water partition coefficient data are also required, and these have been measured in this program and are utilized by the current Oil Weathering Model code.

Sections 4.2 through 4.9 present: derivations for measurement of Henry's Law coefficients; diffusion coefficients for volatile compounds moving through a slick; the role of internal circulation in weathering of a thin vs thick oil slab; and computer code for dispersion of oil drops into the water column from a time varying flux and a constant flux. Computer codes are published in Appendices A through E. Finally, mathematical formulations are derived for ultimate prediction of oil/suspended particulate material (SPM) interactions (Section 4.10). Subsections include predictions of SPM concentrations, size distributions and flocculation behavior for cohesive and noncohesive sediments. The process of spontaneous dispersion of oil micelles from an oil slick, "oil particle"/SPM interactions, "dissolved oil"/SPM interactions and modeling descriptions and definitions of boundary conditions for modeling dispersed oil/SPM interactions are also presented. Not all of the formulations derived in Section 4.0 are currently in the Oil Weathering Model, but as noted above, they serve as starting points for additional code development and provide indications of the required physical, chemical, and thermodynamic data required for modeling and verification.

2.4 EXPERIMENTAL RESULTS AND MODEL PREDICTED OIL WEATHERING BEHAVIOR

2.4.1 Temperature Controlled Evaporation/Dissolution Chamber Experiments in La Jolla, California

Section 5.0 presents the time-series chemical and physical properties data obtained during the controlled evaporation/dissolution chamber experiments in La Jolla and outdoor aquarium and wave tank systems operated under constant seawater flow-through conditions at Kasitsna Bay. Results are presented for air, oil, and water phase concentrations of individual aliphatic and aromatic hydrocarbons at 19 and 3°C under different wind speed conditions. As would be predicted from vapor pressure data, evaporation rates were depressed at lower temperatures and wind speeds, and a significantly longer accumulation time for the buildup of aromatic hydrocarbons in the water column was noted (e.g., see Figure 5-25, page 5-40 and Figure 5-31, page 5-47). However, equilibrium aromatic concentrations in the water column were higher under the colder conditions, and this presumably reflects the lessened evaporative losses under the colder temperature regime and thus, the longer lifetime of aromatic components in the parent oil source.

For predicting dissolution behavior of specific aromatic compounds, pure component water solubility data alone are not enough. Liquid/liquid (oil/water) partition coefficients (M-values) are required. These ratios are a function of the mole fraction of the dissolving component in the oil phase, its mutual solubility in the oil and seawater phases (activity coefficients), and (potentially) component-specific diffusivities. Such data are necessary for any predictive model validation, and Figure 5-32 (page 5-50) and Table 5-6 (page 5-53) present such data for Prudhoe Bay crude oil/seawater partitioning at 3 and 23°C.

2.4.2 Ambient Subarctic Aquaria and Wave-Tank Experiments at Kasitsna Bay, Alaska

To obtain additional oil weathering data for predicting the fate of oil in the subarctic marine environment, a significant amount of field experimentation was also necessary. In particular, such field experiments were required to evaluate the effects of specific parameters, such as microbial population densities, variable air/water temperature gradients, ambient nutrient and SPM levels, solar radiation input, rainfall, snowfall, and other similar factors which could not be properly simulated in laboratory environments. Recognizing this, after the laboratory and modeling activities had begun in La Jolla, NOAA and SAI investigators designed a major project expansion which would utilize NOAA's Kasitsna Bay, Alaska facility. Using indoor and outdoor aquariums, evaporation/dissolution and microbial degradation studies were continued. Flow-through seawater systems were utilized to maximize oil exposure to fresh seawater with nutrient levels and suspended particulate loads which would be more representative of those encountered in a real subarctic oil spill situation. Time-series data are discussed wherein chemical changes in the oil slick due to evaporation, dissolution and dispersion were monitored as a function of mixing energy and the presence or absence of dispersants (e.g., see Figures 5-34, page 5-56; 5-36, page 60; and 5-37, page 5-62; and Table 5-7, page 5-67). Rates of evaporation as a function of the viscosity (mixedness) of the slick were also examined in other experiments where fresh oil and artificially generated mousse were applied to seawater under different turbulent regimes.

In these flow-through aquaria where turbulence was propeller-induced, adequate turbulence regimes could not be generated to simulate open ocean conditions. Therefore, a series of four outdoor flow-through 2800 liter wave tanks were constructed for the purpose of evaluating oil weathering behavior under more natural conditions (Figure 5-49, page 5-77). The tanks were designed to simulate oil floating on the open-ocean water surface, with the slick constantly being exposed to previously uncontaminated seawater by wind drift and advection. In this manner, oil was constantly exposed to fresh seawater during the weathering process, and thus, dissolution behavior would more closely simulate that which would be encountered in the open ocean. In these experiments, however, the wave tanks served to "corral" the oil while the water was moved beneath it. By utilizing the wave tank turnover time and kinetic measurements of dissolved and dispersed hydrocarbon concentrations in the water column, dispersion flux calculations as a function of time were completed for the first 4 months of the spill. These wave tank data were then used for partial verification of Oil Weathering Model predictions, using data from model runs where input parameters were set to the approximate conditions of temperature, wind speed, wave height, slick size, etc. to simulate the wave tank experiments. Rheological properties determinations (Figure 5-67, page 5-100), and photographic documentation of the oil slick behavior up to 12 months for spills initiated in triplicate during the summer (July) and up to 5 months for a spill initiated in winter (November) are also presented (see Section 5.4.6).

In general, correlations of predicted oil weathering behavior and observed chemical changes are quite good. Correlations of chemical and physical property measurements with oil slick behavior are also considered--showing significant changes during the early stages of weathering (from a freely flowing slick), through water-in-oil emulsion or mousse formation (after several days), to the ultimate formation of tarballs if sites of nucleation were provided. Further, the effects of delayed evaporation/dissolution/dispersion weathering on a spill released under winter conditions are provided. In particular, time-dependent concentration data are also presented for specific components in the surface oil (e.g., Figures 5-104 and 5-105 on pages 5-128 and 5-129, and Table 5-10 on page 5-135), the water column (e.g., Figures 5-112 and 5-113 on pages 5-142 and 5-143, and Table 5-13, page 5-145) and the dispersed/particle bound oil (e.g., Figures 6-23 and 6-24, on pages 6-54 and 6-55, and Table 6-10, page 6-56) for summer and winter spill conditions. Computer predicted versus observed oil weathering characterizations are presented for up to 220 hours after initiation of the spills in the wave tank experiments (e.g., see Figure 5-123, page 5-175). Model predictions of oil viscosity, percent water incorporated, fraction lost by evaporation, and dispersion flux show fairly good agreement with observed data, and temperature dependent trends are clearly evident. Time-series computer predicted distillation curves and curves derived from gas chromatographic data also agree reasonably well, given the method of converting gas chromatographically derived data into True Boiling Point distillation data (Figures 5-124 and 5-125 on pages 5-180 and 5-181). Slight modifications to the Oil Weathering User's Manual input parameters were required to obtain optimal fit of the observed and predicted data, and this approach is documented in Section 5.5.2. By examining this approach, and studying the User's Manual in Appendix B, an example of the user-oriented approach used in developing the Model and its supporting documentation is readily obtained.

2.5 OIL/SPM INTERACTIONS AND THE LONG TERM FATE OF STRANDED OIL IN SELECTED INTERTIDAL REGIMES

Section 6.0 presents the results of investigations on the interactions between suspended particular material and dissolved/dispersed oil. Experiments were initially conducted to measure the effects of oil/SPM interactions on settling rates, skewness, kurtosis, and mean ϕ size of settled particulates. Subtle perturbations on settling properties were observed, and there did appear to be a slight suspension of the oil affected particles; however, the effect was not considered to be environmentally significant (e.g., Table 6-4, page 6-7 and Figure 6-2, page 6-8). Therefore, the emphasis of the oil/SPM interaction studies was focused on measuring component-specific interactions of the water soluble components of Prudhoe Bay crude oil and four suspended particulate material types characteristic of those which would be found in the southwestern waters of Alaska. The four representative suspended particulate material samples were further characterized with regard to their size distribution and relative surface area as measured by nitrogen adsorption, mineralogical properties as determined by X-ray diffraction, physical and compositional makeup as determined by scanning electron microscopy and percent surface organic carbon coating (Section 6.2). Chromatographic profiles and tabular data are presented for the oil, water and particulate phases from controlled beaker study experiments (e.g., Figure 6-16, page 6-37 and Table 6-8, page 6-36) and then later from suspended particulate material added to the wave tank systems. In the oil/SPM experiments in the outdoor wave tanks, effects of other weathering properties were included in the oil/SPM particulate interaction process. Dispersed oil/particulate measurements were made on the water column in the wave tank systems at times 0 minutes, 5 minutes, 1 hour, 2 hours, 4 hours, 8 hours, 12 hours, 1 day, 2 days, 4 days, 8 days, 12 days, 4 months, 6 months and 12 months after the spill (e.g., see Figures 6-23 and 6-24 on pages 6-54 and 6-55). Several differences were noted between the dispersed oil/particulate phase concentrations for the Kasitsna Bay SPM fine fraction compared to the Seldovia Salt Marsh SPM fine fraction and the control tank (which had no added <u>artificially</u> introduced SPM). The summer spill data suggest that in the presence of added Kasitsna Bay SPM a slightly higher initial water column buildup of dispersed oil occurs, with the suspended particulate material from that source then serving to maintain the dispersed oil concentrations for a slightly longer period compared to the Seldovia Salt Marsh SPM or control (see Figure 6-34, page 6-80). Alternatively, these results may indicate the more efficient scavenging of dispersed oil by the Salt Marsh SPM with concomitant removal by sedimentation. During the winter spill, when the added suspended particulate material type was glacial till (sampled from the base of the Grewingk Glacier), the results showed a higher initial spike concentration of dispersed oil with a much more rapid decrease in dispersed oil concentrations compared to the summer spills. This, presumably, also reflects the lower temperature at the time of the winter spill, and concomitant changes in oil rheological properties. Nevertheless, it is significant that oil dispersion was almost totally inhibited after as little as 6 to 9 days in the summer spills and a period of 6 to 8 days during the winter spill. In this latter case, however, evaporative processes were significantly retarded, and the presence of higher levels of lower molecular weight (more water soluble) components may have added to the process of spontaneous oil into water emulsification (micelle formation -- see Section 4.10.4). In all four experiments, after the oil had reached a viscosity of greater than 2,000 to 3,000 centipoise, dispersion was observed to drop off by several orders of magnitude from what was initially obtained in the tanks.

Dissolution of intermediate and higher molecular weight aromatic hydrocarbons was, however, observed to continue for periods of upwards of 6 months. During the initial 6 to 12 days, lower molecular weight aromatics ranging from benzene through its C_3 and C_4-substituted congeners were observed to be removed from the water by a combination of evaporative and advective processes (e.g., see Figures 5-117 through 5-120, pages 5-152 through 5-156). After 6 months, nanogram per liter levels of the alkyl-substituted naphthalenes and other alkyl-substituted aromatics were still observed. Time-series concentrations of all the truly dissolved identifiable aromatic components in the water column are presented in Tables 5-13 and 5-14 (pages 5-145 and 5-149).

Hydrocarbon loads in the wave tank bottom sediments were measured 13 days, 5 months, and 9 months after initiation of the spill events, and significant molecular-weight and compound class group fractionation was observed. Specifically, only aliphatic hydrocarbons were detected at significant concentrations (167 μg/g) in the sediments, even after as short a period as 13 days. With additional time, continued loss of lower molecular weight components up through nC-15 was observed in the wave tank sediments, and significant evidence of microbial degradation and aromatic hydrocarbon dissolution was observed (e.g., see Figures 6-31 and 6-32, pages 6-73 and 6-75).

In a collaboratory effort with Drs. Griffiths and Morita of Oregon State University, chemical analyses were undertaken on subtidal sediments which had been spiked with 0.1, 10, and 50 part per thousand (ppt) levels of fresh and artificially weathered Cook Inlet crude oil. The complete report submitted to Drs. Griffiths and Morita (in December, 1980) is included in its entirety as Appendix H. With this characterization of rate processes for suspended particulate material and sedimented oil, the next logical extension of this program was to study the long-term fate of fresh Prudhoe Bay crude oil spilled in different representative subarctic intertidal regimes. To this end, a series of 1-meter-square corral experiments were undertaken at four selected intertidal sites exhibiting different substrate types, energy regimes, fresh water/seawater influence, and organic carbon loading. Site selection included the glacial delta spit adjacent to the Grewingk Glacier; the intertidal mud flats within Kasitsna Bay; the estuarine environment of the Seldovia Salt Marsh; and the head of Jakolof Bay (which is a fresh water fed bay subject to significant ice scour). One liter of Prudhoe Bay crude was spilled in the corrals at three tidal heights, and time-series observational, photographic and chemical measurements were made for up to a period to 17 months following initial oil addition. Significant differences were noted among the intertidal substrate types, with the coarser grain sediments showing penetration and persistence of oil to a depth of 12-14 inches up to 17 months. Lower intertidal mud flats showed the most rapid cleansing of oil, primarily due to its lack of penetration on initial oiling. Some amounts of oil were observed to penetrate excavations left by burrowing organisms, however, the extent of overall oiling was generally much less, and most of the oil was observed to lift off of the intertidal sediment with the incoming tide. Further details are available in Section 6.4.

2.6 MICROBIAL DEGRADATION EXPERIMENTS CONDUCTED AT KASTISNA BAY AND SCRIPPS INSTITUITON OF OCEANOGRAPHY

Section 7.0 describes the results of detailed flow-through microbiological degradation studies undertaken under temperate and subarctic marine conditions (Scripps Institute of Oceanography and Kasitsna Bay, Alaska, respectively). In addition to the various physical and chemical degradative processes which effect the removal of hydrocarbons and heterocyclic components from an oil slick, there are biologically-related processes which contribute to the overall weathering of the oil. Microbial metabolism, ingestion by zooplankton, uptake and possible retention by marine invertebrates and vertebrates, and bioturbative effects (on sedimented oil) all serve to partition petroleum hydrocarbon into the water column, biomass, and sediment regimes of the ecosystem.

In this research program, the degradation of oil components by marine bacterial plankton populations were investigated, by both qualitative and quantitative approaches, in an attempt to determine the relative importance of this biological degradative mechanism. Continuous-flow experimental aquaria were utilized to simulate the microbial degradative impact upon oil spilled in both temperate and sub-arctic marine environments. The response of marine microbes to spilled oil was characterized quantitatively with the aid of radiolabeled substrate techniques which provided information on specific compounds susceptibility (via ^{14}C-labeled hydrocarbon degradation rate determinations), as well as overall metabolic responses (via ^{3}H-labeled substrate uptake). Qualitative characterizations of microbial degradation were inspected through time-series analyses of oil and seawater sample extracts by gas chromatography/mass spectrometry. These efforts provided information on relative degradation patterns of compound class types (i.e., aliphatic versus aromatic hydrocarbons), as well as tentative characterization of oxidized metabolic products.

Caution must be taken when attempting to extrapolate such data from controlled marine ecosystems to actual open ocean oil spills due to: (1) differences in the nature of the two systems, such as nutrient and dissolved oxygen levels, water temperature, growth substrate availability, etc.; (2) the inherent limitations of the ^{14}C-labeled substrate techniques on determining the total metabolism to CO_2; (3) assumptions that the model compounds will be degraded at the same rates when present in such a complicated matrix as crude petroleum; and (4) that these model compounds are representative or typical in terms of biodegradability. Nevertheless, comparisons of these degradation rate data to dissolution rate data (as derived from the wave tank studies performed at Kasitsna Bay), in conjunction with the ^{3}H-labeled substrate uptake data, nutrient data, and chemical characterization of oil and seawater extracts by GC and GC/MS supported the following statements:

- marine microbial populations responded to the input of petroleum by increased ^{3}H-thymidine incorporation into cellular DNA, although no significant impacts were observed for the rates of uptake for ^{3}H-glucose, and ^{3}H-leucine.

- significant increases in the degradation rates of all three ^{14}C-hydrocarbon substrates occurred within 48 hours of oil introduction, although, ^{14}C-hexadecane was degraded at slower rates ralative to either ^{14}C-naphthalene or ^{14}C-methylnaphthalene.

- nutrient supplementation (with inorganic nitrogen and phosphorus) in the experimental systems had no apparent influence on ^{14}C-hydrocarbon degradation rates except for some slight evidence from the Kasitsna Bay studies.

- generally low rates of ^{14}C-hydrocarbon degradation and bacterial growth (inferred from ^{3}H-thymidine uptake and epifluorescence enumeration) were apparent for the Kasitsna Bay study, and this is presumably due to the lower seasonal water temperatures.

- comparisons of dissolved compound concentrations from the Kasitsna Bay wavetank studies to the controlled ecosystem ^{14}C-hydrocarbon degradation rate data suggest, that for at least the first two weeks post-spill, physical dissolution is the dominant mechanism for specific compound removal from the oil/seawater interface.

- time-series analyses of the polar silica gel fractions of seawater extracts by GC and GC/MS suggest that microbial degradation has more of a long-term impact on dispersion of oil components through the continued formation of polar, water-soluble metabolites which pass into the water column from the oil/seawater interface.

Although the results of the ^{14}C hydrocarbon degradation studies, when compared to physical dissolution rate data, suggest that microbial degradation is not of enough significance to incorporate into the oil weathering model, the overall results of our studies do suggest that this biological degradative mechanism can be important in long-term weathering. This could be particularly true, for example, in a situation where oil would become stranded in an estuarine-type environment after a spill. If nutrients and dissolved oxygen were not limiting factors, microbial metabolism of petroleum components to more polar water-soluble species could eventually become an important mechanism for continued dissolution, especially in environments were photochemical processes may be limited due to short diurnal light periods and low solar intensities.

2.7 NOAA-SPONSORED INTERCALIBRATION PROGRAM PARTICIPATION

Finally, Section 8.0 presents the results of three recent intercalibration programs in which we have participated during the duration of this program. The results of environmental measurements are only valuable insofar as they are accurate and precise. This is particularly true if our measurements of chemical levels or properties are to be used for predictive assessments in which the data would be useful to environmental managers in the decision-making process as to what the impact of a potential spill under certain environmental conditions might be. While precision is a relatively easy parameter to measure by replicate determinations, accuracy is somewhat more intractable. Spiked sample recovery is valuable as far as determining what the efficiency of an extraction procedure is for compounds added by the investigator. It does little, however, to determine extraction efficiency of the subject compounds of interest as they are present in the original sample matrix. At this time, there are no Standard Reference Materials (SRM's) to assist in such determinations. Therefore, NOAA has initiated a number of interlaboratory/intercalibration programs wherein the results obtained on real environmental samples by a variety of participating laboratories can be compared. Section 8.0 contains the results of this laboratory's participation in those efforts and compares our data to those of other participating laboratories and the NOAA/National Analytical Facility when such data are available (Figure 8-1, page 8-3).

2.8 CONCLUSIONS AND RECOMMENDATIONS FOR ADDITIONAL RESEARCH

Based on the results of the algorithm development and chemical measurements completed in this program, it is clear that additional work is still required in the area of measuring pseudo-component and specific-component mass transfer rates from a diffusion controlled oil phase. As demonstrated in the development of mathematical formulations for oil under these conditions, a different set of boundary conditions and assumptions are required. Incorporation of the derivations presented for diffusion controlled processes into the computer code will result in considerable improvement, particularly for longer term oil weathering processes. This will also be important for modeling thin and thick oil patches as observed during several field investigations of spills-of-opportunity. Further work is also required for for development and validation of the mathematical formuations presented for modeling oil SPM interactions. The results of the wave tank studies were confounded by difficulties in separating truly particle-bound oil from dispersed oil droplets, and as such, the wave tank experiments did not provide all of the data which may have been desirable. Higher levels of suspended particulate material may have improved the sensitivity of the test, however, limitations within the wave tanks and SPM reservoir delivery systems did not allow generation of higher spiked levels of SPM concentrations. Furthermore, higher SPM levels in the wave tank studies may not have been realistic given measured concentrations of SPM in southwestern Alaskan waters.

Validation of the oil weathering model under higher turbulence regimes would also be an item of high priority. At this time the model is capable of predicting oil weathering behavior in real spill situations, and comparison of predicted and observed results during an investigation of a spill of opportunity would provide such data. Ironically, in most open ocean spills studied to date, component-specific measurements have been made while no attempt has been undertaken to approach determining the overall oil mass balance using a pseudo-component or distillate cut approach.

At this time, we are actively engaged in an investigation of the chemical behavior of oil released in the presence of sea ice, and a logical extension of that study might include longer term intertidal studies in selected arctic regimes. With regard to both arctic and subarctic intertidal zones, additional modeling and investigations in the area of along-shore transport processes, nearshore sediment re-suspension, and offshore transport of oiled beach substrates into subtidal regimes may merit further investigation.

2.9 NOAA/OCSEAP UTILIZATION OF THE OIL WEATHERING MODEL

The current version of the Open-Ocean Oil-Weathering model (named CUTVP2) is a general purpose oil-weathering computer code that considers many aspects of oil weathering. The model is based on a pseudocomponent characterization of oil which allows a total material balance to be considered. The pseudocomponent characterization adapted and used in this model is based on considerable refining industrial experience which translates into a readily available data base for essentially every crude oil and refined product ever produced.

The major oil-weathering processes which determine the material balance of spilled oil are evaporation, dispersion of oil droplets into water, spreading and water-in-oil emulsification (mousse). The spreading and emulsification processes can be "turned off" to simulate oil weathering on ice or land. The dissolution of molecular species from an oil slick into water accounts for only a few percent of the total mass of the slick; thus, this process is not considered in material balance predictions.

During the course of model development numerous derivations were completed which were directed at specific experimental results. An iterative approach of interpreting predicted and observed results then allowed further model refinement and experimental design to attain an understading of important variables. These derivations included the component-specific evaporation and dissolution in laboratory stirred tanks and outdoor flow-through wave tanks in Alaska. Also included in this report are derivations which calculate the water column concentrations of dispersed oil for both time-varying and constant source spill situations. The open-ocean oil-weathering code results were used to construct dispersed-oil source terms in the form of decaying exponentials which were then used as boundary conditions.

The open-ocean oil-weathering code was written in a manner that allows its use as a research tool. Most of the variables, parameters, and physical properties can be easily changed by way of keyboard entry. Thus, experimental results can be used to derive or determine parameters specific to experimental conditions. The open-ocean oil-weathering code can also be used as a learning tool because all the keyboard input has examples presented immediately before the user must enter the requested response. This important feature of the code is expected to facilitate its use, and result in improvements by way of other researchers participating in the refinement of understanding and parameter determinations.

The open-ocean oil-weathering code provides a means to interpret data from an actual oil spill. Samples of weathered oil from an actual oil spill can be taken to the laboratory and fractionated in a true-boiling-point distillation column. The distillation curve can be compared directly to the CUTVP2 predicted results; thus, the oil-weathering code predicts field observable oil compositions.

Throughout the time frame of this oil weathering research program (RU 597) considerable effort was expended in support of various synthesis meetings and in providing weathered-oil source terms for the National Marine Fisheries' efforts in developing the Bering Sea Fish-Oil Spill Interaction Model (RU 3010). In providing weathered-oil source terms for the Interaction Model both continuous and instantaneous spills were considered. For each of these types of spills, results calculated by the Open-Ocean Oil-Weathering Model were put in the form of decaying exponentials to represent the source terms for both evaporation and dispersion. These results were then delivered by letter report to NOAA and the RAND Corporation for use in calculating dispersed-oil plume concentrations in the water column.

Participation in the synthesis meetings for the St. Georges Basin (4-28-81), North Aleution Shelf (3-9-82), Navarin Basin (10-25-82), and Chukchi Sea (10-31-83) included presentation of oil source terms for various environmental scenarios. Oral presentations detailing the in-progress oil weathering experimental efforts were also given. The results of these participations and Oil Weathering Modeled scenarios were then incorporated into environmental impact statements for oil-lease sales in these respective areas.

Research activities related to the oil weathering program also led to an invited contribution to the 1981 National Academy of Sciences Ocean Sciences Board workshop on the publication Inputs, Fates and Effects of Petroleum in the Marine Environment. The background paper "A Review of the Formation and Behavior of Water-in-Oil Emulsions (Mousse) from Spilled Petroleum, and Tar Ball Distributions, Chemistries and Fates in the World's Oceans" (PAYNE, 1981) was prepared, and after peer review, presented at the workshop held at Clearwater Beach, Florida in November, 1981. More recently, the results of the triplicate summer wave tank experiments at Kasitsna Bay (and modeling activities related to those studies) were presented at the 1983 Oil Spills Conference at San Antonio, Texas (PAYNE, et al. 1983).

3.0 OIL CHARACTERIZATION

3.1 CHARACTERIZATION OF FOUR CRUDE OILS

At the onset of the program, four crude oils (representative of a wide variety of oil types) including two crudes produced in Alaska, were selected for detailed chemical analyses. The ultimate purpose of this investigation was to select one of the four crudes for additional detailed weathering characterizations. Crude oils are a naturally occurring complex mixture of organic and inorganic compounds, and the properties of a given crude are dependent upon the original depositional environment, the hydrocarbon sources and the degree of post-depositional maturation and migration. In general, most crudes can be classified into three categories:

- paraffin-based, exemplified by the continental crudes of the mid-United States,
- asphalt-based such as crudes produced in California and the Gulf of Mexico coast of the United States,
- mixed-base crudes such as those from the Middle East and Alaska.

Because the objective of this program was to develop a computer model which is applicable to a wide variety of crude petroleums it might be have been anticipated that at least one crude from each of the three classes (i.e., paraffin, asphaltic and mixed base) be studied. However, the paraffin-based crudes of the first category are not as likely to be involved in contamination of the marine environment, and these crudes have relatively low levels of aromatic compounds, which include the most toxic constituents of crude oil. For these reasons paraffin-based crudes were not included.

Table 3-1 presents gross characterization parameters of the four selected crude oils examined. These include: 1) a relatively high API gravity (lower specific gravity) Murban crude which is designated as an intermediate type or mixed-base crude - this particular crude oil has less sulfur and asphaltic material than most other Middle-East crudes (Evaluation of the

TABLE 3-1. GROSS CHARACTERIZATIONS OF FOUR SELECTED WHOLE CRUDE OILS.

Crude Oil	API* Gravity	Specific Gravity g/ml	Viscosity(100°F)* Kinematic cST	Viscosity(100°F)* Saybolt SUS	Pour Pt** °F	% Asphalt***	Ni ppm	V ppm	S %	N % ****
Murban, Aba Dhabi	40.5	0.829	2.8	35.9	-20	7	3.0	9.9	0.96	0.10
Cook Inlet, Alaska	35.4	0.848	17	85	-15	12	1.3	0.47	0.09	0.11
Prudhoe Bay, Alaska	27.0	0.893	19	84	-10	23	13.5	28.3	0.98	0.27
Wilmington, Calif.	19.4	0.938	100	470	<5*	24	100	80.6	1.8	0.83

Sources:

* Coleman, et al. 1978

** Evaluation of Worlds Important Crudes, 1973

*** Calculated from Conradson carbon value, Coleman et al., 1978

**** Ni, V, S, and N: this study

World's Important Crudes, 1973); 2) a slightly lower API gravity crude from Cook Inlet, Alaska, which is representative of oils produced in the sub-arctic environment and which by nature of its production and transport might be expected to be released at sea; 3) a lower API gravity Prudhoe Bay crude oil which would have a high probability of release in arctic regimes during production and in sub-arctic environments during transport and storage; and 4) a low API gravity crude from Wilmington, CA. The data in Table 3-1 illustrate that as the API gravity decreases (density increases) the viscosities of the whole crudes generally increase; the pour points are also observed to rise. Percent asphalt content is also observed to increase in going from the higher to lower API gravity crudes selected. Nickel, vanadium, sulfur and nitrogen contents are more variable among the crudes (data generated as part of this study); however, general increases in trace element concentrations are also observed in the trend from higher to lower API gravities. These considerations are important in that asphalts and the presence of trace elements such as nickel, vanadium and sulfur have been implicated in stabilization of water-in-oil emulsions (PAYNE, 1981) and as such, their presence or absence might also be a factor in selecting one representative crude for additional oil weathering studies.

In addition to the whole-crude physical property characterizations and trace element data presented in Table 3-1, each of these four oils was further characterized by separation into aliphatic, aromatic and polar fractions by liquid-solid (silica gel) column chromatography (see Methods, Appendix H), and each fraction was then examined by fused silica capillary column gas chromatography (flame ionization detector) and capillary column gas chromatograph/mass spectrometry (GC/MS). Figures 3-1 through 3-4 present the capillary column gas chromatograms obtained on the fractionated Murban, Cook Inlet, Prudhoe Bay and Wilmington Crude Oils, respectively. As the figures illustrate, the first three crudes are characterized by a regularly repeating series of n-alkanes and branched and cyclic hydrocarbons in the aliphatic fraction, whereas the Wilmington crude is characterized only by a large Unresolved Complex Mixture (UCM). Likewise, the aromatic fractions from Murban, Cook Inlet, and Prudhoe Bay crudes are very similar (Figures 3-1B

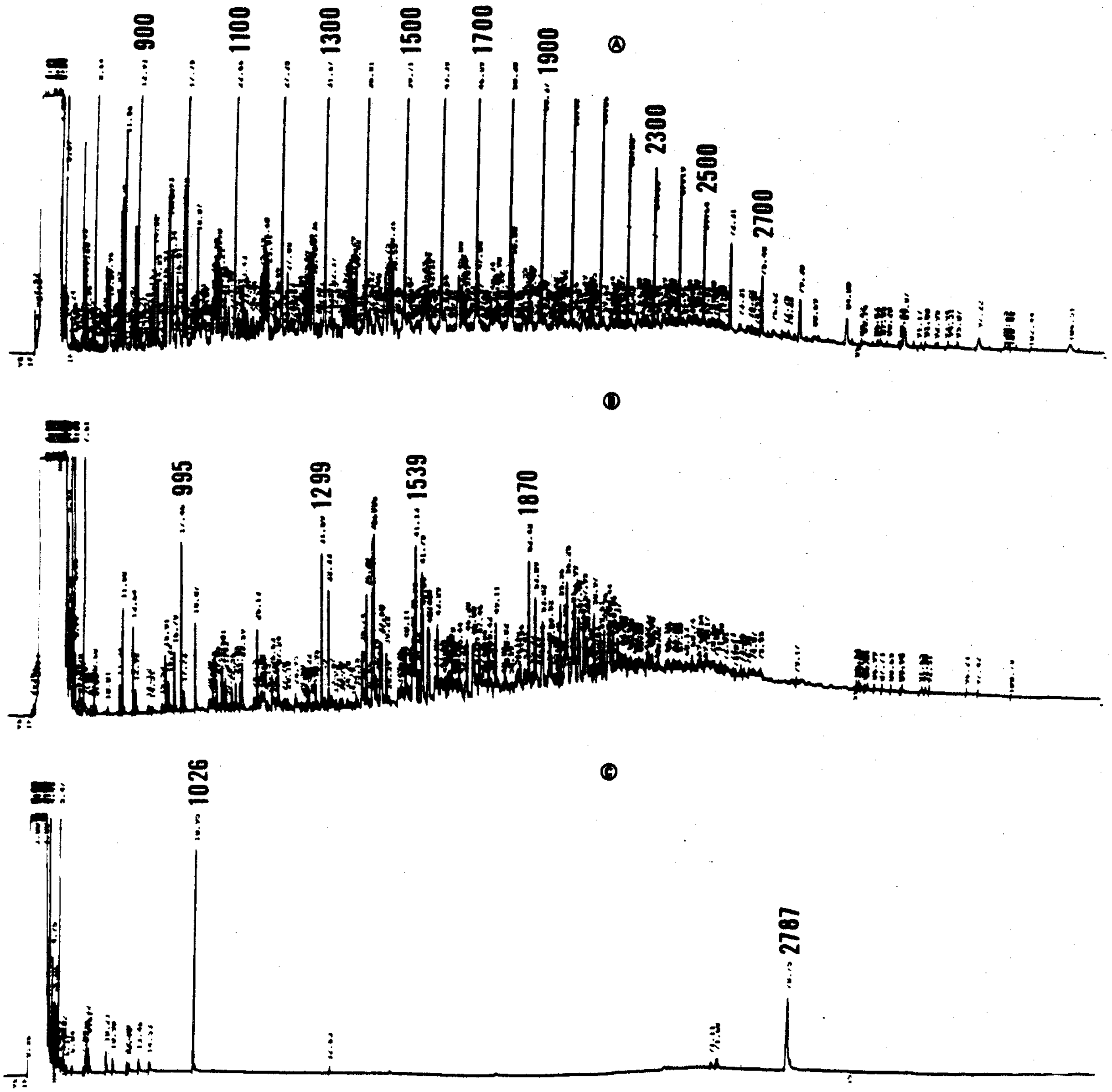

FIGURE 3-1. FLAME IONIZATION DETECTOR CAPILLARY GAS CHROMATOGRAMS OBTAINED ON L/C FRACTIONATED MURBAN CRUDE OIL: (A) ALIPHATIC FRACTION (F1); (B) AROMATIC FRACTION (F2); (C) POLAR FRACTION (F3). (KOVAT RETENTION INDICES ARE SHOWN ABOVE SELECTED PEAKS).

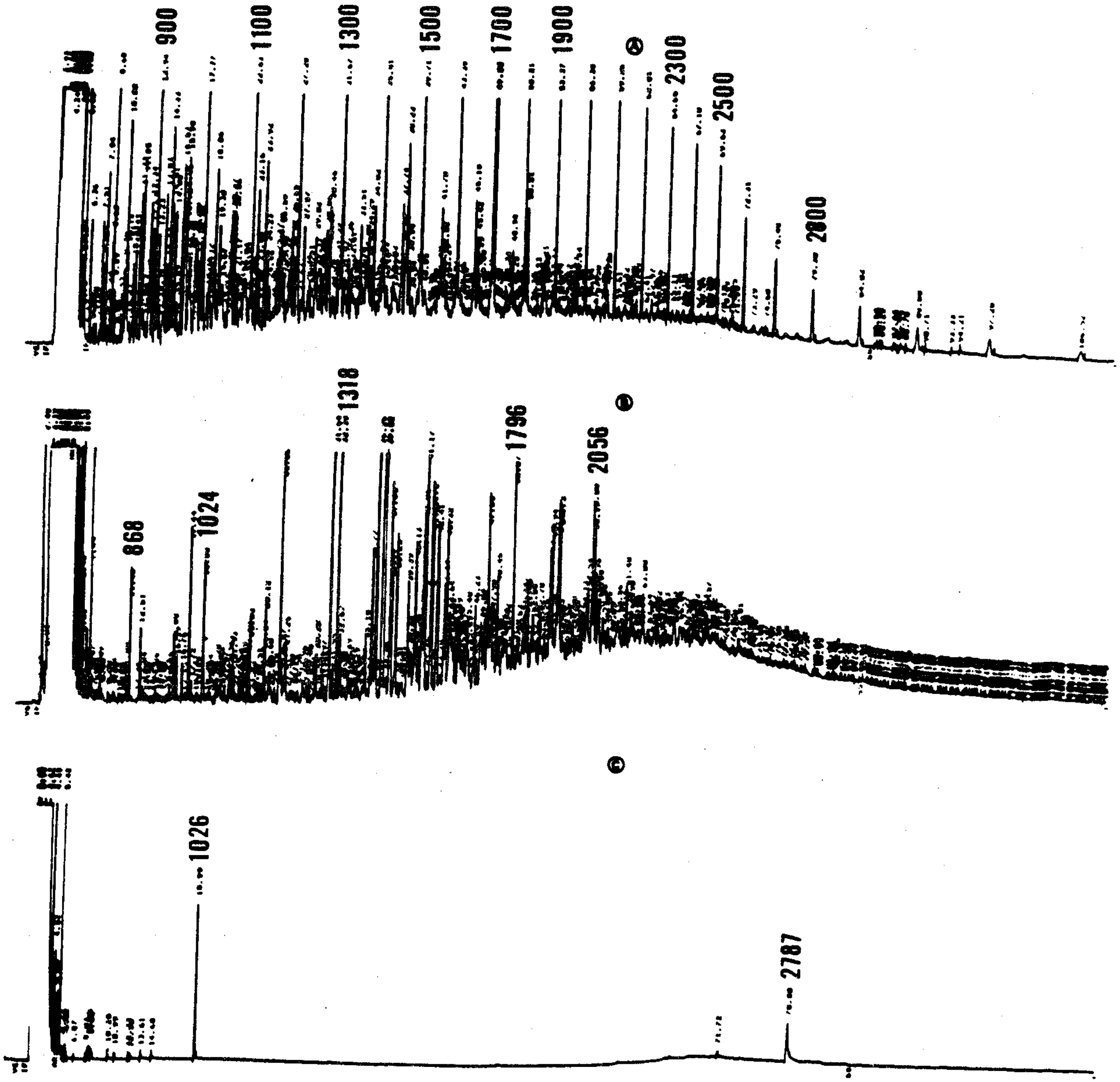

FIGURE 3-2. FLAME IONIZATION DETECTOR CAPILLARY GAS CHROMATOGRAMS OBTAINED ON L/C FRACTIONATED COOK INLET CRUDE OIL: (A) ALIPHATIC FRACTION (F1); (B) AROMATIC FRACTION (F2); (C) POLAR FRACTION (F3). (KOVAT RETENTION INDICES ARE SHOWN ABOVE SELECTED PEAKS).

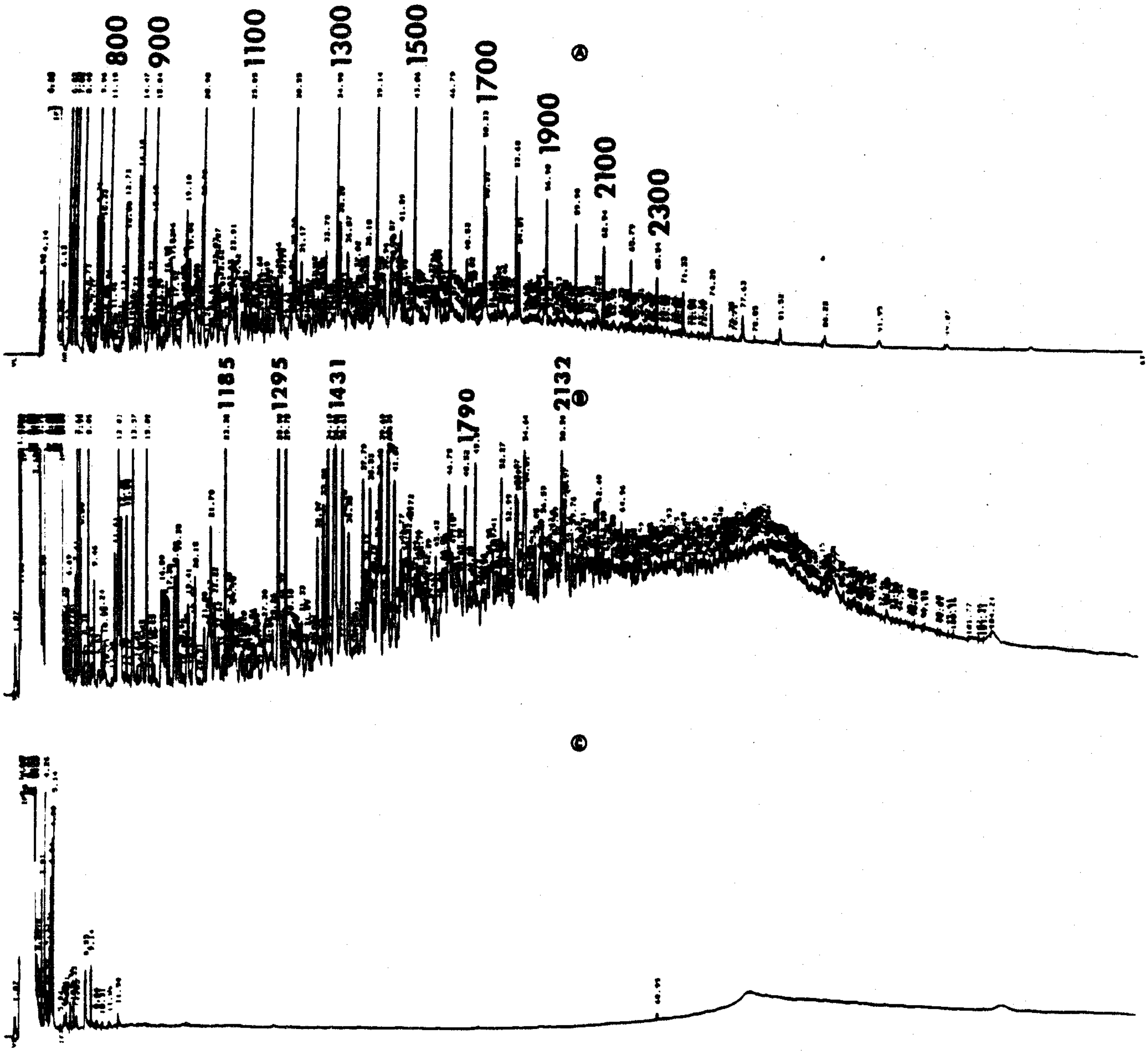

FIGURE 3-3. FLAME IONIZATION DETECTOR CAPILLARY GAS CHROMATOGRAMS OBTAINED ON L/C FRACTIONATED PRUDHOE BAY CRUDE OIL: (A) ALIPHATIC FRACTION (F1); (B) AROMATIC FRACTION (F2); (C) POLAR FRACTION (F3). (KOVAT RETENTION INDICES ARE SHOWN ABOVE SELECTED PEAKS).

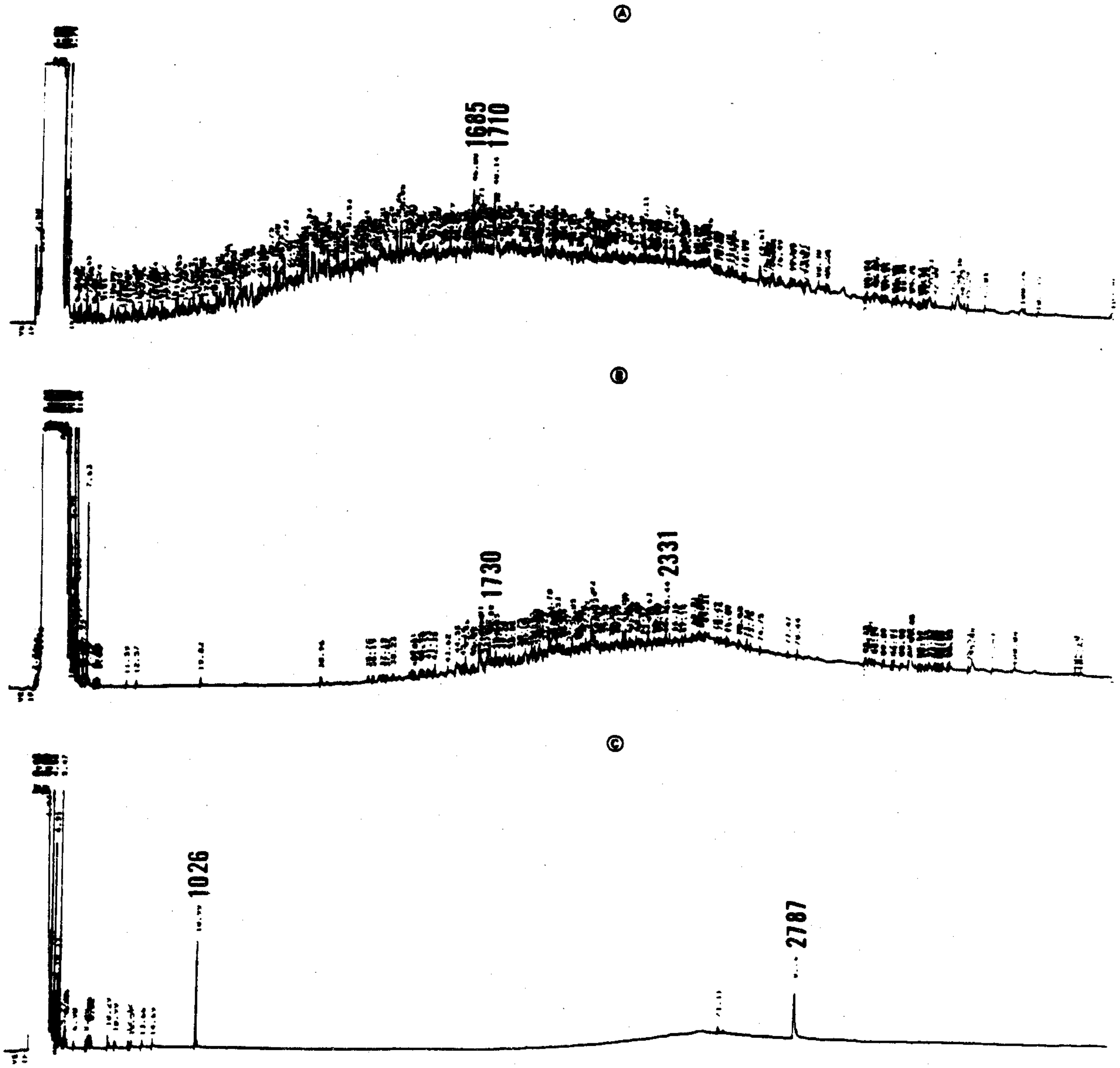

FIGURE 3-4. FLAME IONIZATION DETECTOR CAPILLARY GAS CHROMATOGRAMS OBTAINED ON L/C FRACTIONATED WILMINGTON CRUDE OIL: (A) ALIPHATIC FRACTION (F1); (B) AROMATIC FRACTION (F2); (C) POLAR FRACTION (F3). (KOVAT RETENTION INDICES ARE SHOWN ABOVE SELECTED PEAKS).

through 3-3B). The Wilmington crude oil aromatic distribution, however, is skewed to the higher molecular weight compounds. Polar components in the third fraction are observed to be limited in all four of these oils.

Gravimetric data obtained on the aliphatic and aromatic fractions and computer reduced compound-specific concentrations (organized by Kovat retention indices, Kovats 1958) are presented in Tables 3-2 and 3-3 for Murban crude; Tables 3-4 and 3-5 for Cook Inlet crude; Tables 3-6 and 3-7 for Prudhoe Bay crude and Tables 3-8 and 3-9 for Wilmington crude. Concentrations for the limited number of components present in the polar (F3) fractions from each oil are shown in Table 3-10. These data were generated on SAI's DEC-10 computer using an inhouse compound-specific data reduction program, and such data provide the basis for additional compound-specific weathering phenomena as will be discussed in detail in this report.

Figure 3-5 presents the reconstructed ion GC/MS chromatogram obtained on the aromatic fraction from Prudhoe Bay crude oil, and the individual aromatic components identified in this fraction are numbered on the chromatogram and listed in Table 3-11. Similar GC/MS data were obtained on the other crudes, however, comparative differences among the crudes can be better illustrated by graphic output such as that shown in Figures 3-6 through 3-8, rather than by tabulated compound identifications and concentrations.

Figure 3-6 presents the individual n-alkane concentrations for Murban crude, Cook Inlet crude and Prudhoe Bay crude, with the inset showing the relative concentrations of isoprenoid compounds in each of these oils. In that the Wilmington crude was not represented by an evenly repeating series of n-alkanes, aliphatic concentrations for that crude are not presented in Figure 3-6. The Cook Inlet crude and Prudhoe Bay crude show very similar trends. whereas the Murban crude is clearly characterized by relatively higher concentrations of the lower molecular weight hydrocarbons.

TABLE 3-2. MURBAN CRUDE OIL CONCENTRATIONS FOR ALIPHATIC FRACTION.

FRACTION#1 HP-RUN-DATE#10/22/1981 HP-RUN-NO# 37 HP-BOT-NO# 13

PEAK NUMBER	RETENTION TIME	KOVAT INDEX	KOVAT SUBGROUP	KOVAT GROUP	RESPONSE FACTOR	CONCENTRATION TOTAL
1.00	5.2100	0	0	0	1.440	1026.4
2.00	5.3900	0	0	0	1.440	195.91
3.00	7.4300	0	0	0	1.440	1079.7
4.00	7.6800	0	0	0	1.440	482.57
5.00	7.8600	0	0	0	1.440	279.37
6.00	8.6400	800	0	0	1.440	4477.0
7.00	9.7400	826	0	0	1.440	499.65
8.00	9.9600	831	0	0	1.440	504.46
9.00	10.920	853	0	0	1.440	488.62
10.0	11.560	868	0	0	1.440	3614.0
11.0	12.620	893	0	0	1.440	1145.9
12.0	12.930	900	0	0	1.440	6541.1
13.0	13.740	917	0	0	1.440	195.56
14.0	14.110	924	0	0	1.440	552.50
15.0	14.330	929	0	0	1.440	547.88
16.0	14.520	933	0	0	1.440	1266.2
17.0	14.850	940	0	0	1.440	898.38
18.0	15.530	953	0	0	1.440	971.73
19.0	16.340	970	0	0	1.440	1566.6
20.0	16.810	980	0	0	1.440	717.81
21.0	17.030	984	0	0	1.440	255.17
22.0	17.490	993	0	0	1.440	1678.0
23.0	17.790	1000	0	0	1.440	6646.0
24.0	18.670	1022	0	0	1.440	884.00
25.0	20.340	1052	0	0	1.440	780.98
26.0	20.580	1057	0	0	1.440	744.32
27.0	20.720	1060	0	0	1.440	353.39
28.0	20.900	1064	0	0	1.440	820.30
29.0	22.000	1086	0	0	1.440	760.69
30.0	22.660	1100	0	0	1.440	7770.6
31.0	23.430	1117	0	0	1.440	618.52
32.0	23.650	1121	0	0	1.440	314.79
33.0	23.870	1126	0	0	1.440	436.31
34.0	24.250	1134	0	0	1.440	296.63
35.0	24.440	1139	0	0	1.440	318.87
36.0	24.820	1147	0	0	1.440	483.82
37.0	25.190	1155	0	0	1.440	1258.0
38.0	25.400	1159	0	0	1.440	623.50
39.0	25.600	1164	0	0	1.440	1013.7
40.0	25.910	1170	0	0	1.440	719.59
41.0	26.200	1177	0	0	1.440	202.50
42.0	26.660	1187	0	0	1.440	530.62
43.0	26.870	1191	0	0	1.440	198.05
44.0	27.280	1200	0	0	1.430	7788.1
45.0	27.880	1213	0	0	1.440	508.39
46.0	28.510	1228	0	0	1.440	208.44
47.0	29.040	1240	0	0	1.440	222.20
48.0	29.870	1258	0	0	1.440	449.88
49.0	30.080	1263	0	0	1.440	877.04
50.0	30.360	1270	0	0	1.440	850.92
51.0	30.790	1279	0	0	1.450	286.46
52.0	31.230	1289	0	0	1.450	233.33
53.0	31.670	1300	0	0	1.450	8169.3
54.0	32.370	1316	0	0	1.440	535.79
55.0	32.650	1323	0	0	1.430	587.82
56.0	33.040	1333	0	0	1.420	276.92
57.0	33.520	1344	0	0	1.420	490.39
58.0	33.760	1350	0	0	1.410	232.95
59.0	34.080	1358	0	0	1.410	460.04
60.0	34.290	1363	0	0	1.400	725.68
61.0	34.580	1370	0	0	1.400	734.22
62.0	34.820	1376	0	0	1.390	695.01
63.0	35.810	1400	0	0	1.380	6548.0
64.0	36.220	1410	0	0	1.390	451.27
65.0	37.750	1449	0	0	1.440	665.58
66.0	38.080	1458	0	0	1.450	310.20
67.0	38.260	1462	0	0	1.460	807.97
68.0	38.550	1470	0	0	1.470	747.11
69.0	39.720	1500	0	0	1.510	6913.3
70.0	41.490	1548	0	0	1.500	637.40
71.0	41.690	1553	0	0	1.500	412.29
72.0	42.040	1563	0	0	1.500	787.86
73.0	42.310	1570	0	0	1.500	361.98
74.0	43.080	1591	0	0	1.500	194.35
75.0	43.390	1600	0	0	1.500	5925.5
76.0	45.080	1648	0	0	1.550	1821.5
77.0	45.420	1658	0	0	1.560	489.04
78.0	45.600	1663	0	0	1.560	291.18
79.0	45.870	1670	0	0	1.570	376.65
80.0	46.890	1700	0	0	1.600	5527.8
81.0	47.060	1710	0	0	1.500	497.15
82.0	48.340	1743	0	0	1.560	757.28
83.0	48.980	1763	0	0	1.540	315.89
84.0	49.250	1771	0	0	1.530	204.46
85.0	50.200	1800	0	0	1.510	4193.8
86.0	50.500	1815	0	0	1.440	632.91
87.0	51.550	1842	0	0	1.780	651.36
88.0	52.020	1857	0	0	1.880	294.55
89.0	52.200	1863	0	0	1.920	296.29
90.0	52.460	1871	0	0	1.970	418.88
91.0	53.370	1900	0	0	2.160	5078.5
92.0	56.380	2000	0	0	1.560	3791.2
93.0	57.490	2038	0	0	1.580	310.88
94.0	58.450	2071	0	0	1.590	219.71
95.0	59.260	2100	0	0	1.610	3161.2
96.0	60.340	2139	0	0	1.620	210.90
97.0	61.270	2172	0	0	1.640	321.56
98.0	62.020	2200	0	0	1.650	2950.3
99.0	63.000	2237	0	0	1.640	623.33
100.	64.650	2300	0	0	1.740	2698.1
101.	65.590	2337	0	0	1.700	211.89
102.	67.190	2400	0	0	1.630	2226.7
103.	68.040	2434	0	0	1.650	216.63
104.	69.440	2500	0	0	1.670	1925.0
105.	70.500	2532	0	0	1.680	213.54
106.	72.310	2600	0	0	1.720	1895.1
107.	75.480	2700	0	0	2.560	2243.8
108.	76.620	2729	0	0	2.320	294.82
109.	79.300	2800	0	0	1.770	1302.8
110.	84.000	2900	0	0	1.890	1066.3
111.	85.740	2929	0	0	1.870	258.29
112.	89.870	3000	0	0	1.920	866.60
113.	97.220	3100	0	0	2.630	1028.1
114.	106.51	3200	0	0	2.320	662.13
115.	106.51	3200	0	0	2.520	.00000

TOTAL RESOLVED HYDROCARBON = 154001.4
TOTAL UNRESOLVED HYDROCARBON = 155908.5
RESPONSE FACTOR AV. FOR C - 1000 TO 3000 FOR UCM = 1.714239
RATIO: RESOLVED/UNRESOLVED = 0.988402

SUM OF THE N-ALKANES = 75961.44
SUM OF THE EVEN N-ALKANES = 38150.2
SUM OF THE ODD N-ALKANES = 37811.24

RATIO: (PRISTANE+PHYTANE)/(N-ALKANES) = 1.487679E-2
RATIO: ODD/EVEN N-ALKANES = 0.991115
RATIO: PRISTANE/C-17 = 8.993653E-2
RATIO: PHYTANE/C-18 = 0.150916
RATIO: PRISTANE/PHYTANE = 0.785492
RATIO: (N-ALKANES)/(BRANCHED HYDROCARBONS) = 0.973365

Weight Distribution of Murban Crude by Fraction

Fraction	Weight (mg/g)
1	369
2	123
3	53.3

TABLE 3-3. MURBAN CRUDE OIL CONCENTRATIONS FOR AROMATIC FRACTION.

FRACTION:2. HP-RUN-DATE:10/22/1981 HP-RUN-NO: 38 HP-BOT-NO: 15

PEAK NUMBER	RETENTION TIME	KOVAT INDEX	KOVAT SUBGROUP	KOVAT GROUP	RESPONSE FACTOR	CONCENTRATION TOTAL
1.00	5.0700	0	0	0	1.440	22366.
2.00	5.1900	0	0	0	1.440	7550.2
3.00	5.2900	0	0	0	1.440	21853.
4.00	5.3400	0	0	0	1.440	11195.
5.00	5.4400	0	0	0	1.440	19563.
6.00	5.5500	0	0	0	1.440	18429.
6.50	5.6200	700	0	0	.0000	.00000
7.00	5.8600	708	0	0	1.440	1816.5
8.00	5.9300	711	0	0	1.440	186.15
9.00	6.3600	726	0	0	1.440	878.19
10.0	6.5600	733	0	0	1.440	41.969
11.0	6.6300	735	0	0	1.440	332.76
12.0	6.7700	740	0	0	1.440	43.073
12.5	8.4900	800	0	0	.0000	.00000
13.0	7.6100	780	0	0	1.440	282.57
14.0	11.240	863	0	0	1.440	59.163
15.0	11.580	871	0	0	1.440	199.52
16.0	12.640	895	0	0	1.440	163.78
16.5	12.840	900	0	0	.0000	.00000
17.0	12.920	902	0	0	1.440	43.927
18.0	15.910	963	0	0	1.440	198.62
19.0	16.220	969	0	0	1.440	64.858
20.0	16.790	981	0	0	1.440	126.05
21.0	17.460	995	0	0	1.440	352.77
21.5	17.710	1000	0	0	.0000	.00000
22.0	17.730	1000	0	0	1.440	44.710
23.0	18.870	1024	0	0	1.440	221.95
24.0	20.290	1053	0	0	1.440	41.222
25.0	21.050	1060	0	0	1.440	57.632
26.0	21.930	1086	0	0	1.440	94.191
27.0	22.560	1099	0	0	1.440	45.244
27.5	22.600	1100	0	0	.0000	.00000
28.0	22.950	1108	0	0	1.440	76.890
29.0	23.390	1117	0	0	1.440	67.528
30.0	23.590	1121	0	0	1.440	103.48
31.0	24.750	1146	0	0	1.440	55.852
32.0	25.130	1155	0	0	1.440	234.02
33.0	26.630	1187	0	0	1.440	67.137
34.0	27.240	1200	0	0	1.430	122.79
35.0	28.950	1239	0	0	1.440	47.257
36.0	30.950	1284	0	0	1.450	77.553
37.0	31.590	1299	0	0	1.450	430.37
38.0	31.620	1300	0	0	1.450	.00000
39.0	32.330	1317	0	0	1.440	290.31
40.0	32.670	1325	0	0	1.430	37.539
41.0	35.740	1399	0	0	1.380	158.27
42.0	35.760	1400	0	0	1.380	.00000
43.0	36.200	1411	0	0	1.390	338.86
44.0	36.820	1427	0	0	1.410	282.00
45.0	36.950	1430	0	0	1.420	206.19
46.0	37.150	1435	0	0	1.420	46.474
47.0	37.600	1447	0	0	1.440	120.51
48.0	37.750	1451	0	0	1.440	85.203
49.0	38.220	1463	0	0	1.460	117.97
50.0	39.660	1500	0	0	1.510	.00000
51.0	40.110	1512	0	0	1.510	143.78
52.0	40.790	1530	0	0	1.510	119.26
53.0	40.940	1534	0	0	1.510	126.10
54.0	41.130	1539	0	0	1.510	320.19
55.0	41.440	1548	0	0	1.500	83.104
56.0	41.750	1556	0	0	1.500	136.32
57.0	42.380	1573	0	0	1.500	60.466
58.0	43.020	1590	0	0	1.500	68.804
59.0	43.290	1598	0	0	1.500	161.38
60.0	43.360	1600	0	0	1.500	.00000
61.0	43.650	1608	0	0	1.510	71.931
62.0	44.270	1626	0	0	1.530	69.228
63.0	44.850	1631	0	0	1.530	41.585
64.0	45.440	1659	0	0	1.560	88.769
65.0	46.200	1681	0	0	1.580	132.38
66.0	46.800	1698	0	0	1.600	105.74
67.0	46.860	1700	0	0	1.600	.00000
68.0	47.080	1710	0	0	1.500	.00000
69.0	47.460	1718	0	0	1.580	196.08
70.0	48.420	1746	0	0	1.560	97.316
71.0	49.110	1767	0	0	1.540	186.79
72.0	50.020	1795	0	0	1.510	55.686
73.0	50.180	1800	0	0	1.510	.00000
74.0	50.510	1815	0	0	1.440	.00000
75.0	51.110	1829	0	0	1.700	45.577
76.0	51.290	1835	0	0	1.730	74.174
77.0	51.560	1843	0	0	1.790	52.425
78.0	52.010	1857	0	0	1.880	101.06
79.0	52.420	1870	0	0	1.970	470.68
80.0	53.090	1892	0	0	2.100	402.54
81.0	53.340	1900	0	0	2.160	.00000
82.0	53.820	1915	0	0	2.060	215.10
83.0	54.520	1939	0	0	1.920	106.13
84.0	54.670	1944	0	0	1.890	60.789
85.0	55.300	1964	0	0	1.770	75.466
86.0	55.560	1973	0	0	1.720	275.57
87.0	56.000	1988	0	0	1.630	73.068
88.0	56.250	1996	0	0	1.580	367.74
89.0	56.360	2000	0	0	1.560	.00000
90.0	56.810	2015	0	0	1.570	92.288
91.0	56.990	2021	0	0	1.570	231.47
92.0	57.400	2036	0	0	1.580	107.14
93.0	57.950	2055	0	0	1.590	237.79
94.0	58.970	2090	0	0	1.600	275.58
95.0	59.240	2100	0	0	1.610	.00000
96.0	59.610	2113	0	0	1.610	184.98
97.0	59.960	2126	0	0	1.620	239.34
98.0	60.440	2143	0	0	1.620	133.64
99.0	60.860	2158	0	0	1.630	137.60
100.	61.370	2177	0	0	1.640	140.03
101.	61.860	2195	0	0	1.640	58.671
102.	61.990	2200	0	0	1.650	.00000
103.	62.140	2205	0	0	1.650	63.213
104.	62.640	2217	0	0	1.660	56.003
105.	64.320	2288	0	0	1.730	59.906
106.	64.630	2300	0	0	1.760	.00000
107.	66.910	2389	0	0	1.640	52.644
108.	67.170	2406	0	0	1.630	.00000
109.	68.740	2464	0	0	1.660	48.519
110.	69.540	2497	0	0	1.670	62.154
111.	69.610	2500	0	0	1.670	.00000
112.	71.580	2573	0	0	1.700	46.185
113.	72.300	2600	0	0	1.720	.00000
114.	75.440	2700	0	0	2.560	.00000
115.	79.280	2800	0	0	1.770	.00000
116.	84.000	2900	0	0	1.850	.00000
117.	89.860	3000	0	0	1.920	.00000
118.	97.230	3100	0	0	2.630	.00000
119.	106.49	3200	0	0	2.320	.00000

```
TOTAL RESOLVED HYDROCARBON = 111906.1
TOTAL UNRESOLVED HYDROCARBON = 31166.35
RESPONSE FACTOR AV. FOR C - 1500 TO 3100 FOR UCM =  1.8[illegible]
RATIO: RESOLVED/UNRESOLVED = 3.590606

SUM OF THE N-ALKANES = 122.7935
SUM OF THE EVEN N-ALKANES = 122.7935
SUM OF THE ODD N-ALKANES = 0

RATIO: (PRISTANE+PHYTANE)/(N-ALKANES) = 0
RATIO: ODD/EVEN  N-ALKANES = 0
RATIO: PRISTANE/C-17 = 0
RATIO: PHYTANE/C-18 = 0
RATIO: PRISTANE/PHYTANE = 0
RATIO: (N-ALKANES)/(BRANCHED HYDROCARBONS) = 1.098496E-3
```

TABLE 3-4. COOK INLET CRUDE OIL CONCENTRATIONS FOR ALIPHATIC FRACTION.

FRACTION#1 HP-RUN-DATE#10/21/1981 HP-RUN-NO# 31 HP-BOT-NO# 1 FRACTION#1 HP-RUN-DATE#10/21/1981 HP-RUN-NO# 31 HP-BOT-NO# 1

PEAK NUMBER	RETENTION TIME	KOVAT INDEX	KOVAT SUBGROUP	KOVAT GROUP	RESPONSE FACTOR	CONCENTRATION TOTAL
2.00	5.0500	0	0	0	1.440	1236.4
3.00	5.1800	0	0	0	1.440	3096.1
4.00	5.2000	0	0	0	1.440	7834.8
5.00	5.3500	0	0	0	1.440	1968.5
6.00	5.5100	0	0	0	1.440	249.29
7.00	5.8000	700	0	0	1.440	2538.0
8.00	6.3600	719	0	0	1.440	509.92
9.00	7.5100	759	0	0	1.440	617.92
10.0	7.6300	764	0	0	1.440	147.39
11.0	7.7600	768	0	0	1.440	409.47
12.0	7.9400	774	0	0	1.440	1028.8
13.0	8.4000	790	0	0	1.440	186.35
14.0	8.6000	797	0	0	1.440	239.55
15.0	8.6800	800	0	0	1.440	1712.3
16.0	8.8900	805	0	0	1.440	306.56
17.0	9.5300	820	0	0	1.440	203.21
18.0	9.7900	826	0	0	1.440	457.30
19.0	10.000	831	0	0	1.440	1989.5
20.0	10.730	848	0	0	1.440	497.27
21.0	10.930	853	0	0	1.440	806.74
22.0	11.330	862	0	0	1.440	1751.6
23.0	11.550	867	0	0	1.440	2241.4
24.0	12.340	886	0	0	1.440	570.09
25.0	12.630	893	0	0	1.440	836.60
26.0	12.940	900	0	0	1.440	5395.7
27.0	13.230	906	0	0	1.440	611.01
28.0	13.360	909	0	0	1.440	242.75
29.0	13.830	918	0	0	1.440	790.75
30.0	14.110	924	0	0	1.440	607.16
31.0	14.330	929	0	0	1.440	1863.5
32.0	14.510	933	0	0	1.440	1241.1
33.0	14.860	940	0	0	1.440	1377.1
34.0	15.090	945	0	0	1.440	286.06
35.0	15.530	958	0	0	1.440	1712.3
36.0	15.860	960	0	0	1.440	188.38
37.0	15.980	963	0	0	1.440	369.79
38.0	16.890	982	0	0	1.440	273.42
39.0	17.020	986	0	0	1.440	356.85
40.0	17.260	987	0	0	1.440	335.92
41.0	17.440	993	0	0	1.440	1313.7
42.0	17.770	1000	0	0	1.440	6695.2
43.0	18.160	1008	0	0	1.440	588.12
44.0	18.320	1011	0	0	1.440	279.23
45.0	18.860	1022	0	0	1.440	2296.7
46.0	19.300	1031	0	0	1.440	1008.5
47.0	19.670	1039	0	0	1.440	162.95
48.0	19.990	1044	0	0	1.440	168.25
49.0	20.320	1052	0	0	1.440	254.38
50.0	20.470	1056	0	0	1.440	334.91
51.0	20.550	1057	0	0	1.440	162.66
52.0	20.680	1060	0	0	1.440	444.21
53.0	20.860	1064	0	0	1.440	1056.2
54.0	21.170	1070	0	0	1.440	360.05
55.0	21.620	1079	0	0	1.440	189.26
56.0	21.870	1086	0	0	1.440	287.08
57.0	22.040	1088	0	0	1.440	329.09
58.0	22.630	1100	0	0	1.440	7113.4
59.0	23.160	1111	0	0	1.440	1252.1
60.0	23.400	1117	0	0	1.440	587.10
61.0	23.600	1121	0	0	1.440	213.39
62.0	23.920	1128	0	0	1.440	1655.6
63.0	24.250	1134	0	0	1.440	840.32
64.0	24.460	1139	0	0	1.440	431.57
65.0	25.170	1155	0	0	1.440	911.25
66.0	25.390	1159	0	0	1.440	621.41
67.0	25.590	1164	0	0	1.440	784.67
68.0	25.900	1170	0	0	1.440	328.22
69.0	26.250	1178	0	0	1.440	146.67
70.0	26.650	1186	0	0	1.440	1012.6
71.0	26.860	1191	0	0	1.440	674.61
72.0	27.280	1200	0	0	1.430	7804.0
73.0	27.630	1207	0	0	1.440	245.19
74.0	27.870	1213	0	0	1.440	925.99
75.0	28.340	1224	0	0	1.440	279.52
76.0	28.510	1228	0	0	1.440	309.80
77.0	29.020	1239	0	0	1.440	659.24
78.0	29.870	1258	0	0	1.440	274.39
79.0	30.060	1263	0	0	1.440	882.64
80.0	30.460	1272	0	0	1.450	467.51
81.0	30.780	1279	0	0	1.450	316.81
82.0	30.970	1284	0	0	1.450	158.26
83.0	31.220	1289	0	0	1.450	565.67
84.0	31.670	1300	0	0	1.450	7596.8
85.0	31.970	1307	0	0	1.440	381.35
86.0	32.350	1316	0	0	1.440	670.89
87.0	32.670	1324	0	0	1.430	451.64
88.0	33.300	1339	0	0	1.420	185.11
89.0	33.510	1344	0	0	1.420	1142.6
90.0	34.080	1358	0	0	1.410	356.38
91.0	34.290	1363	0	0	1.400	521.84
92.0	34.580	1370	0	0	1.400	361.59
93.0	34.820	1376	0	0	1.390	1148.1
94.0	35.520	1392	0	0	1.380	357.53
95.0	35.810	1400	0	0	1.380	6143.5
96.0	36.820	1425	0	0	1.410	215.04
97.0	37.740	1449	0	0	1.440	1846.8
98.0	38.080	1458	0	0	1.450	276.84
99.0	38.220	1461	0	0	1.460	1847.4
100.	38.550	1470	0	0	1.470	619.79
101.	38.840	1477	0	0	1.480	252.12
102.	39.350	1490	0	0	1.500	224.17
103.	39.710	1500	0	0	1.510	6685.5
104.	40.050	1509	0	0	1.510	447.67
105.	41.480	1548	0	0	1.500	351.48
106.	41.700	1554	0	0	1.500	932.17
107.	42.020	1562	0	0	1.500	562.93
108.	42.290	1570	0	0	1.500	232.27
109.	43.390	1600	0	0	1.500	5339.2
110.	45.100	1648	0	0	1.550	1865.6
111.	45.420	1657	0	0	1.560	756.45
112.	45.590	1662	0	0	1.560	271.47
113.	45.860	1670	0	0	1.570	225.35
114.	46.900	1700	0	0	1.600	4852.8
115.	47.080	1710	0	0	1.500	3129.7
116.	48.340	1743	0	0	1.560	539.57
117.	48.980	1762	0	0	1.540	641.51
118.	49.250	1770	0	0	1.530	160.10
119.	50.210	1800	0	0	1.510	3485.1
120.	50.510	1815	0	0	1.640	1085.1
121.	51.530	1841	0	0	1.700	389.20
122.	52.010	1856	0	0	1.880	223.80
123.	52.810	1863	0	0	1.920	272.53
124.	53.110	1891	0	0	2.100	587.96
125.	53.370	1900	0	0	2.160	4624.1
126.	55.270	1963	0	0	1.780	183.31
127.	56.300	2000	0	0	1.560	3046.8
128.	57.500	2039	0	0	1.580	176.43
129.	59.250	2100	0	0	1.610	2912.6
130.	61.280	2173	0	0	1.640	198.28
131.	61.490	2181	0	0	1.640	210.20
132.	62.010	2200	0	0	1.650	2688.8
133.	64.650	2300	0	0	1.740	2613.3
134.	65.110	2318	0	0	1.720	240.29
135.	67.180	2400	0	0	1.630	2171.3
136.	69.630	2500	0	0	1.670	1794.5
137.	72.310	2600	0	0	1.720	1916.9
138.	75.480	2700	0	0	2.560	2245.0
139.	79.300	2800	0	0	1.770	1238.9
140.	84.020	2900	0	0	1.850	1136.3
141.	89.800	3000	0	0	1.920	984.75
142.	97.280	3100	0	0	2.630	989.39
143.	106.52	3200	0	0	2.320	530.60
144.	106.52	3200	0	0	2.520	.00000

TOTAL RESOLVED HYDROCARBON = 179155.5
TOTAL UNRESOLVED HYDROCARBON = 211498.7
RESPONSE FACTOR AV. FOR C - 700 TO 2900 FOR UCM = 1.701876
RATIO: RESOLVED/UNRESOLVED = 0.847076

SUM OF THE N-ALKANES = 70600.05
SUM OF THE EVEN N-ALKANES = 35349.81
SUM OF THE ODD N-ALKANES = 35250.23

RATIO: (PRISTANE+PHYTANE)/(N-ALKANES) = 0.0596988
RATIO: ODD/EVEN N-ALKANES = 0.997183
RATIO: PRISTANE/C-17 = 0.702859
RATIO: PHYTANE/C-18 = 0.311339
RATIO: PRISTANE/PHYTANE = 2.884348
RATIO: (N-ALKANES)/(BRANCHED HYDROCARBONS) = 0.650359

Weight Distribution of Cook Inlet Crude by Fraction

Fraction	Weight (mg/g)
1	803
2	64.6
3	127

TABLE 3-5. COOK INLET CRUDE OIL CONCENTRATIONS FOR AROMATIC FRACTION.

FRACTION:2 HP-RUN-DATE:10/21/1981 HP-RUN-NO: 32 HP-BOT-NO: 3

PEAK NUMBER	RETENTION TIME	KOVAT INDEX	KOVAT SUBGROUP	KOVAT GROUP	RESPONSE FACTOR	CONCENTRATION TOTAL
1.00	5.1500	0	0	0	1.440	2491.7
2.00	5.2100	0	0	0	1.440	792.16
2.50	5.6200	700	0	0	.0000	.00000
3.00	5.7500	705	0	0	1.440	2473.2
4.00	6.2300	721	0	0	1.440	1439.9
5.00	6.4200	728	0	0	1.440	150.45
6.00	7.0300	749	0	0	1.440	45.534
7.00	7.4400	763	0	0	1.440	422.83
7.50	8.4900	800	0	0	.0000	.00000
8.00	11.080	860	0	0	1.440	24.547
9.00	11.430	868	0	0	1.440	158.93
9.50	12.840	900	0	0	.0000	.00000
10.0	12.510	893	0	0	1.440	133.81
11.0	15.880	962	0	0	1.440	93.352
12.0	16.190	969	0	0	1.440	51.254
13.0	16.760	980	0	0	1.440	54.587
14.0	17.440	994	0	0	1.440	286.82
14.5	17.710	1000	0	0	.0000	.00000
15.0	18.880	1024	0	0	1.440	262.96
16.0	20.280	1053	0	0	1.440	33.044
17.0	21.930	1086	0	0	1.440	69.648
18.0	22.600	1100	0	0	1.440	27.983
18.0	22.600	1100	0	0	.0000	.00000
19.0	23.420	1118	0	0	1.440	65.698
20.0	23.630	1122	0	0	1.440	81.521
21.0	24.510	1141	0	0	1.440	33.662
22.0	24.750	1146	0	0	1.440	40.122
23.0	25.600	1165	0	0	1.440	40.225
24.0	26.180	1177	0	0	1.440	23.415
25.0	26.460	1188	0	0	1.440	410.90
26.0	26.870	1192	0	0	1.440	39.855
27.0	27.240	1200	0	0	1.430	.00000
28.0	27.260	1200	0	0	1.430	75.094
29.0	28.500	1228	0	0	1.440	28.949
30.0	28.960	1239	0	0	1.440	40.922
31.0	29.360	1248	0	0	1.440	28.678
32.0	29.600	1253	0	0	1.440	36.598
33.0	30.970	1285	0	0	1.450	49.908
34.0	31.620	1300	0	0	1.450	.00000
35.0	31.640	1300	0	0	1.450	1203.7
36.0	31.950	1307	0	0	1.440	54.034
37.0	32.390	1318	0	0	1.440	732.28
38.0	32.670	1325	0	0	1.430	87.609
39.0	33.490	1345	0	0	1.420	34.629
40.0	34.290	1364	0	0	1.400	20.120
41.0	34.990	1381	0	0	1.390	26.759
42.0	35.180	1385	0	0	1.390	85.658
43.0	35.760	1400	0	0	1.380	.00000
44.0	35.770	1400	0	0	1.380	241.85
45.0	36.250	1412	0	0	1.390	627.73
46.0	36.880	1428	0	0	1.410	571.89
47.0	37.020	1432	0	0	1.420	225.48
48.0	37.630	1447	0	0	1.440	257.14
49.0	37.770	1451	0	0	1.440	38.288
50.0	38.250	1463	0	0	1.460	281.57
51.0	38.510	1478	0	0	1.480	22.044
52.0	39.390	1493	0	0	1.500	142.38
53.0	39.660	1500	0	0	1.510	.00000
54.0	39.740	1502	0	0	1.510	72.082
55.0	40.130	1512	0	0	1.510	173.73
56.0	40.590	1525	0	0	1.510	62.959
57.0	40.820	1531	0	0	1.510	55.243
58.0	40.960	1535	0	0	1.510	148.61
59.0	41.170	1540	0	0	1.510	229.77
60.0	41.460	1548	0	0	1.500	26.979
61.0	41.780	1557	0	0	1.500	91.616
62.0	42.410	1574	0	0	1.500	498.40
63.0	43.140	1594	0	0	1.500	164.99
64.0	43.320	1598	0	0	1.500	169.26
65.0	43.360	1600	0	0	1.500	.00000
66.0	43.640	1608	0	0	1.510	70.557
67.0	44.310	1627	0	0	1.530	74.776
68.0	44.490	1632	0	0	1.530	47.388
69.0	45.000	1646	0	0	1.550	35.506
70.0	45.170	1651	0	0	1.550	38.891
71.0	45.480	1660	0	0	1.560	69.522
72.0	46.230	1682	0	0	1.580	97.685
73.0	46.490	1689	0	0	1.590	45.581
74.0	46.840	1699	0	0	1.600	180.54
75.0	46.860	1700	0	0	1.600	.00000
76.0	47.080	1710	0	0	1.500	.00000
77.0	47.160	1709	0	0	1.590	35.004
78.0	47.530	1720	0	0	1.580	293.69
79.0	47.900	1731	0	0	1.570	52.290
80.0	48.460	1748	0	0	1.550	154.86
81.0	49.030	1765	0	0	1.540	29.367
82.0	49.280	1771	0	0	1.530	21.953
83.0	49.740	1786	0	0	1.520	40.629
84.0	50.070	1796	0	0	1.510	323.08
85.0	50.180	1800	0	0	1.510	.00000
86.0	50.510	1815	0	0	1.440	.00000
87.0	50.630	1814	0	0	1.600	29.517
88.0	51.140	1830	0	0	1.700	93.923
89.0	51.320	1836	0	0	1.700	26.118
90.0	51.600	1844	0	0	1.800	68.087
91.0	52.080	1860	0	0	1.900	136.38
92.0	52.320	1867	0	0	1.950	64.794
93.0	52.590	1876	0	0	2.000	38.983
94.0	52.780	1882	0	0	2.040	93.215
95.0	53.260	1897	0	0	2.140	59.833
96.0	53.340	1900	0	0	2.160	.00000
97.0	53.750	1913	0	0	2.070	209.93
98.0	53.940	1919	0	0	2.040	221.00
99.0	54.200	1928	0	0	1.990	28.338
100.	54.570	1940	0	0	1.910	173.18
101.	54.730	1946	0	0	1.880	125.83
102.	55.850	1983	0	0	1.660	25.299
103.	56.080	1990	0	0	1.610	88.162
104.	56.360	2000	0	0	1.560	.00000
105.	57.130	2026	0	0	1.570	38.463
106.	58.000	2056	0	0	1.590	255.17
107.	58.170	2062	0	0	1.590	120.36
108.	58.360	2068	0	0	1.590	69.395
109.	58.680	2080	0	0	1.600	23.871
110.	59.080	2094	0	0	1.600	68.066
111.	59.240	2100	0	0	1.610	.00000
112.	59.300	2102	0	0	1.610	31.837
113.	59.550	2111	0	0	1.610	53.860
114.	60.560	2140	0	0	1.630	89.155
115.	61.150	2169	0	0	1.630	58.586
116.	61.400	2178	0	0	1.640	125.11
117.	61.900	2196	0	0	1.640	91.497
118.	61.990	2200	0	0	1.650	.00000
119.	63.080	2241	0	0	1.690	93.961
120.	64.620	2299	0	0	1.740	25.774
121.	64.630	2300	0	0	1.740	.00000
122.	66.840	2387	0	0	1.650	73.826
123.	67.170	2400	0	0	1.630	.00000
124.	67.270	2404	0	0	1.640	38.015
125.	69.570	2498	0	0	1.670	61.089
126.	69.610	2500	0	0	1.670	.00000
127.	72.380	2600	0	0	1.720	.00000
128.	72.810	2616	0	0	1.850	61.907
129.	75.370	2697	0	0	2.540	37.175
130.	75.440	2700	0	0	2.560	.00000
131.	76.980	2729	0	0	2.330	42.131
132.	79.280	2800	0	0	1.770	.00000
133.	84.000	2900	0	0	1.850	.00000
134.	89.860	3000	0	0	1.920	.00000
135.	97.230	3100	0	0	2.630	.00000
136.	106.09	3200	0	0	2.320	.00000

TOTAL RESOLVED HYDROCARBON = 20856.13
TOTAL UNRESOLVED HYDROCARBON = 32399.1
RESPONSE FACTOR AV. FOR C - 1500 TO 3100 FOR UCM = 1.803576
RATIO: RESOLVED/UNRESOLVED = 0.643726

SUM OF THE N-ALKANES = 0
SUM OF THE EVEN N-ALKANES = 0
SUM OF THE ODD N-ALKANES = 0

RATIO: (PRISTANE+PHYTANE)/(N-ALKANES) = 0
RATIO: ODD/EVEN N-ALKANES = 0
RATIO: PRISTANE/C-17 = 0
RATIO: PHYTANE/C-18 = 0
RATIO: PRISTANE/PHYTANE = 0
RATIO: (N-ALKANES)/(BRANCHED HYDROCARBONS) = 0

TABLE 3-6. PRUDHOE BAY CRUDE OIL CONCENTRATIONS FOR ALIPHATIC FRACTION.

PEAK NUMBER	RETENTION TIME	KOVAT INDEX	KOVAT SUBGROUP	KOVAT GROUP	RESPONSE FACTOR	CONCENTRATIO TOTAL
1.00	6.2700	0	0	0	1.900	222.26
2.00	6.6600	0	0	0	1.900	503.98
3.00	7.4000	700	0	0	1.900	772.90
4.00	8.7600	750	0	0	1.900	220.40
5.00	8.9900	759	0	0	1.900	1211.2
6.00	9.2900	770	0	0	1.900	151.87
7.00	9.8300	790	0	0	1.900	68.820
8.00	10.110	800	0	0	1.900	1672.0
9.00	11.080	821	0	0	1.900	30.366
10.0	11.350	827	0	0	1.900	93.765
11.0	11.650	833	0	0	1.900	194.96
12.0	11.790	836	0	0	1.900	107.53
13.0	12.470	851	0	0	1.900	31.594
14.0	12.640	855	0	0	1.900	48.322
15.0	13.030	863	0	0	1.900	593.76
16.0	13.410	871	0	0	1.900	1829.6
17.0	14.200	888	0	0	1.900	32.568
18.0	14.360	896	0	0	1.900	215.27
19.0	14.750	900	0	0	1.900	1000.3
20.0	15.150	908	0	0	1.900	41.808
21.0	15.610	917	0	0	1.900	29.476
22.0	15.800	921	0	0	1.900	253.00
23.0	16.130	927	0	0	1.900	24.606
24.0	16.310	931	0	0	1.900	29.959
25.0	16.430	933	0	0	1.900	147.04
26.0	16.820	941	0	0	1.900	173.72
27.0	17.620	957	0	0	1.900	193.63
28.0	17.840	961	0	0	1.900	98.313
29.0	17.990	964	0	0	1.900	385.73
30.0	18.320	971	0	0	1.900	464.17
31.0	18.980	984	0	0	1.900	525.15
32.0	19.620	997	0	0	1.900	233.69
33.0	19.780	1000	0	0	1.900	806.36
34.0	20.320	1011	0	0	1.900	32.441
35.0	20.470	1014	0	0	1.900	57.809
36.0	20.800	1023	0	0	1.900	143.15
37.0	21.110	1027	0	0	1.900	245.25
38.0	21.470	1034	0	0	1.900	176.60
39.0	21.690	1039	0	0	1.900	110.11
40.0	22.130	1048	0	0	1.900	99.164
41.0	22.400	1055	0	0	1.900	160.00
42.0	22.740	1060	0	0	1.900	325.59
43.0	23.270	1071	0	0	1.900	181.56
44.0	23.750	1081	0	0	1.900	32.780
45.0	23.870	1083	0	0	1.900	27.992
46.0	24.030	1086	0	0	1.900	44.553
47.0	24.190	1089	0	0	1.900	109.12
48.0	24.710	1100	0	0	1.800	1540.1
49.0	25.070	1108	0	0	1.900	31.424
50.0	25.240	1111	0	0	1.900	35.194
51.0	25.480	1117	0	0	1.900	169.07
52.0	25.680	1121	0	0	1.900	22.700
53.0	25.980	1127	0	0	1.900	140.61
54.0	26.270	1133	0	0	1.900	285.11
55.0	26.470	1138	0	0	1.900	82.415
56.0	26.630	1141	0	0	1.900	84.914
57.0	27.040	1150	0	0	1.900	101.47
58.0	27.360	1157	0	0	1.900	59.861
59.0	27.470	1159	0	0	1.900	57.131
60.0	27.690	1164	0	0	1.900	146.53
61.0	28.000	1171	0	0	1.900	306.20
62.0	28.430	1180	0	0	1.900	41.080
63.0	28.850	1189	0	0	1.900	288.49
64.0	29.060	1193	0	0	1.900	190.33
65.0	29.370	1200	0	0	1.880	1241.6
66.0	29.980	1213	0	0	1.890	272.23
67.0	30.630	1228	0	0	1.890	50.111
68.0	30.840	1233	0	0	1.890	56.531
69.0	31.240	1242	0	0	1.900	72.615
70.0	31.680	1252	0	0	1.900	284.49
71.0	31.960	1258	0	0	1.900	94.603
72.0	32.170	1263	0	0	1.900	165.73
73.0	32.570	1272	0	0	1.910	495.52
74.0	33.410	1292	0	0	1.910	25.825
75.0	33.760	1300	0	0	1.920	1247.9
76.0	34.010	1306	0	0	1.920	371.69
77.0	34.220	1311	0	0	1.920	46.336
78.0	34.500	1317	0	0	1.930	75.993
79.0	34.780	1324	0	0	1.930	270.40
80.0	35.730	1347	0	0	1.940	264.84
81.0	36.170	1358	0	0	1.940	109.84
82.0	36.380	1363	0	0	1.950	101.73
83.0	36.660	1370	0	0	1.950	90.982
84.0	36.920	1376	0	0	1.950	294.29
85.0	37.290	1385	0	0	1.960	24.823
86.0	37.630	1393	0	0	1.960	98.436
87.0	37.890	1400	0	0	1.960	1250.7
88.0	38.200	1407	0	0	1.970	51.772
89.0	38.630	1419	0	0	1.990	158.12
90.0	39.240	1434	0	0	2.010	169.75
91.0	39.790	1448	0	0	2.020	35.920
92.0	39.930	1452	0	0	2.030	102.34
93.0	40.160	1458	0	0	2.030	32.132
94.0	40.310	1462	0	0	2.040	210.76
95.0	40.630	1470	0	0	2.050	147.10
96.0	41.040	1480	0	0	2.060	31.088
97.0	41.780	1500	0	0	2.080	1485.5
98.0	42.080	1508	0	0	2.080	57.090
99.0	42.520	1520	0	0	2.090	47.566
100.	42.740	1526	0	0	2.090	25.778
101.	43.350	1542	0	0	2.090	34.977
102.	43.560	1548	0	0	2.090	115.13
103.	43.870	1557	0	0	2.090	166.07
104.	44.110	1563	0	0	2.090	50.379
105.	44.560	1575	0	0	2.090	28.248
106.	44.820	1583	0	0	2.100	99.971
107.	45.440	1600	0	0	2.100	1111.4
108.	45.640	1605	0	0	2.110	59.216
109.	46.030	1617	0	0	2.140	52.106
110.	46.350	1626	0	0	2.170	77.078
111.	46.660	1635	0	0	2.190	36.170
112.	47.150	1649	0	0	2.230	248.75
113.	47.610	1662	0	0	2.260	109.16
114.	47.900	1678	0	0	2.280	126.60
115.	48.910	1700	0	0	2.360	995.66
116.	49.110	1710	0	0	3.250	639.29
117.	49.980	1732	0	0	2.290	88.746
118.	50.360	1743	0	0	2.260	160.17
119.	50.640	1752	0	0	2.250	45.634
120.	50.830	1758	0	0	2.230	24.929
121.	51.000	1763	0	0	2.220	61.740
122.	51.690	1784	0	0	2.180	51.411
123.	52.210	1800	0	0	2.140	823.03
124.	52.530	1815	0	0	2.270	532.36
125.	53.340	1835	0	0	2.280	32.259
126.	53.580	1842	0	0	2.310	91.029
127.	54.470	1871	0	0	2.420	49.609
128.	55.140	1892	0	0	2.500	64.152
129.	55.370	1900	0	0	2.530	793.89
130.	55.640	1909	0	0	2.550	30.201
131.	57.100	1957	0	0	2.690	46.663
132.	58.370	2000	0	0	2.810	842.36
133.	59.520	2039	0	0	2.990	154.89
134.	60.530	2074	0	0	3.150	145.79
135.	61.260	2100	0	0	3.270	810.26
136.	63.020	2163	0	0	3.370	76.649
137.	63.600	2187	0	0	3.690	55.736
138.	64.000	2200	0	0	3.750	832.65
139.	65.030	2236	0	0	3.860	98.829
140.	65.730	2263	0	0	3.930	99.231
141.	66.720	2300	0	0	4.040	714.71
142.	69.310	2400	0	0	4.060	726.08
143.	70.990	2461	0	0	4.610	52.954
144.	72.830	2500	0	0	4.580	643.89
145.	73.010	2532	0	0	4.730	81.040
146.	73.800	2561	0	0	4.860	118.35
147.	75.010	2600	0	0	5.030	596.84
148.	76.100	2631	0	0	5.900	103.93
149.	77.840	2689	0	0	6.640	102.77
150.	78.880	2700	0	0	7.760	523.16
151.	82.520	2800	0	0	5.960	361.19
152.	87.880	2900	0	0	6.440	195.04
153.	89.230	2928	0	0	6.640	147.81
154.	93.500	3000	0	0	7.120	272.89
155.	102.11	3100	0	0	9.630	300.68
156.	110.50	3200	0	0	8.830	207.53
157.	110.59	3200	0	0	9.650	.00000

```
TOTAL RESOLVED HYDROCARBON = 42256.59
TOTAL UNRESOLVED HYDROCARBON = 152822.6
RESPONSE FACTOR AV FOR C = 1200 TO 3100 FOR UCM = 4.222611
RATIO RESOLVED/UNRESOLVED = 0.276507

SUM OF THE N-ALKANES = 15937.11
SUM OF THE EVEN N-ALKANES = 8266.371
SUM OF THE ODD N-ALKANES = 7670.736

RATIO: (PRISTANE+PHYTANE)/(N-ALKANES) = 7.351682E-2
RATIO: ODD/EVEN  N-ALKANES = 0.927945
RATIO: PRISTANE/C-17 = 0.642072
RATIO: PHYTANE/C-18 = 0.646825
RATIO: PRISTANE/PHYTANE = 1.200857
RATIO: (N-ALKANES)/(BRANCHED HYDROCARBONS) = [illegible]
```

Weight Distribution of Prudhoe Bay Crude by Fraction

Fraction	Weight (mg/g)
1	879
2	75
3	60

TABLE 3-7. PRUDHOE BAY CRUDE OIL CONCENTRATIONS FOR AROMATIC FRACTION.

FRACTION#2 HP-RUN-DATE: 9/22/1981 HP-RUN-NO: 72 HP-BOT-NO: 9

PEAK NUMBER	RETENTION TIME	KOVAT INDEX	KOVAT SUBGROUP	KOVAT GROUP	RESPONSE FACTOR	CONCENTRATION TOTAL
1.00	5.0700	[illegible]	0	0	1.720	190.88
1.50	5.1400	700	0	0	.0000	.00000
2.00	5.2400	704	0	0	1.720	30.523
3.00	5.3200	708	0	0	1.720	1050.7
4.00	5.3900	719	0	0	1.720	259.24
5.00	5.7200	725	0	0	1.720	40.506
6.00	6.3500	741	0	0	1.720	1362.0
7.00	6.6500	765	0	0	1.720	31.096
8.00	7.1300	786	0	0	1.720	29.295
9.00	7.2600	792	0	0	1.720	89.482
9.50	7.4500	800	0	0	.0000	.00000
10.0	7.4500	800	0	0	1.720	53.026
11.0	7.6400	805	0	0	1.720	26.509
12.0	10.040	861	0	0	1.720	474.62
13.0	10.390	870	0	0	1.720	1794.1
13.5	11.670	900	0	0	.0000	.00000
14.0	11.910	905	0	0	1.720	80.706
15.0	12.870	925	0	0	1.720	118.70
16.0	14.030	949	0	0	1.720	50.850
17.0	14.270	954	0	0	1.720	220.08
18.0	14.680	963	0	0	1.720	736.48
19.0	14.970	969	0	0	1.720	309.65
20.0	15.530	980	0	0	1.720	299.91
21.0	16.160	993	0	0	1.720	926.78
21.5	16.400	1000	0	0	.0000	.00000
22.0	17.040	1012	0	0	1.720	60.596
23.0	17.600	1023	0	0	1.720	452.93
24.0	18.240	1036	0	0	1.720	55.931
25.0	19.030	1053	0	0	1.720	304.00
26.0	19.250	1057	0	0	1.720	94.556
27.0	19.380	1060	0	0	1.720	75.839
28.0	19.770	1068	0	0	1.720	168.90
29.0	20.340	1080	0	0	1.720	326.51
30.0	20.660	1087	0	0	1.720	261.53
31.0	20.970	1093	0	0	1.720	31.137
31.5	21.320	1100	0	0	.0000	.00000
32.0	21.410	1102	0	0	1.720	25.859
33.0	21.630	1107	0	0	1.720	23.976
34.0	23.190	1140	0	0	1.720	164.11
35.0	23.480	1147	0	0	1.720	210.96
36.0	23.820	1154	0	0	1.720	152.70
37.0	24.090	1159	0	0	1.720	50.427
~~38.0~~	~~24.260~~	~~1164~~	~~0~~	~~0~~	~~1.720~~	~~134.86~~
39.0	24.500	1169	0	0	1.720	127.45
40.0	24.870	1177	0	0	1.720	85.472
~~41.0~~	~~25.290~~	~~1186~~	~~0~~	~~0~~	~~1.720~~	~~520.45~~
42.0	25.540	1191	0	0	1.720	27.458
43.0	25.710	1195	0	0	1.720	92.759
44.0	25.930	1200	0	0	1.720	135.14
45.0	25.940	1200	0	0	1.720	.00000
46.0	26.160	1205	0	0	1.720	27.698
47.0	26.450	1211	0	0	1.720	21.965
48.0	27.130	1227	0	0	1.720	171.69
49.0	27.670	1239	0	0	1.720	106.29
50.0	28.010	1247	0	0	1.720	109.41
51.0	28.240	1252	0	0	1.720	91.939
52.0	28.650	1262	0	0	1.720	76.356
53.0	28.950	1269	0	0	1.720	184.60
54.0	29.410	1279	0	0	1.720	57.255
55.0	29.600	1283	0	0	1.720	60.048
56.0	30.200	1297	0	0	1.720	1259.5
57.0	30.300	1300	0	0	1.720	.00000
58.0	30.560	1306	0	0	1.710	77.748
59.0	30.940	1315	0	0	1.700	737.95
60.0	31.270	1323	0	0	1.690	149.40
61.0	31.880	1338	0	0	1.670	46.984
62.0	32.140	1344	0	0	1.660	46.813
63.0	32.620	1356	0	0	1.650	25.069
64.0	32.870	1362	0	0	1.640	47.801
65.0	33.260	1372	0	0	1.630	30.491
66.0	33.760	1384	0	0	1.610	125.32
67.0	34.330	1398	0	0	1.600	176.99
68.0	34.410	1400	0	0	1.590	.00000
69.0	34.500	1402	0	0	1.600	33.488
70.0	34.780	1409	0	0	1.610	530.99
71.0	35.390	1425	0	0	1.630	359.91
72.0	35.510	1428	0	0	1.630	171.79
73.0	35.920	1438	0	0	1.640	25.701
74.0	36.160	1445	0	0	1.650	143.98
75.0	36.290	1448	0	0	1.650	40.603
76.0	36.770	1460	0	0	1.670	277.89
77.0	37.350	1475	0	0	1.690	84.677
78.0	37.980	1490	0	0	1.710	155.97
79.0	38.290	1500	0	0	1.720	.00000
80.0	38.320	1500	0	0	1.720	138.36
81.0	38.670	1510	0	0	1.710	209.85
82.0	39.110	1522	0	0	1.710	61.965
83.0	39.350	1528	0	0	1.710	76.088
84.0	39.480	1532	0	0	1.710	67.565
85.0	39.660	1537	0	0	1.700	163.18
86.0	39.980	1546	0	0	1.700	50.688
87.0	40.270	1554	0	0	1.700	360.57
88.0	40.910	1571	0	0	1.690	382.99
89.0	41.580	1589	0	0	1.680	83.018
90.0	41.790	1595	0	0	1.680	105.48
91.0	41.950	1600	0	0	1.680	.00000
92.0	42.180	1605	0	0	1.700	23.659
93.0	42.800	1624	0	0	1.770	65.828
94.0	42.990	1629	0	0	1.790	56.629
95.0	43.430	1642	0	0	1.830	51.286
96.0	43.970	1658	0	0	1.890	30.977
97.0	44.550	1674	0	0	1.950	23.556
~~98.0~~	~~44.720~~	~~1678~~	~~0~~	~~0~~	~~1.960~~	~~35.040~~
99.0	44.870	1683	0	0	1.980	24.234
100.	45.300	1696	0	0	2.020	26.795
~~101.~~	~~45.430~~	~~1700~~	~~0~~	~~0~~	~~2.040~~	~~.00000~~
102.	45.630	1710	0	0	2.200	106.89
103.	45.940	1715	0	0	1.990	179.71
104.	46.320	1727	0	0	1.960	80.158
105.	46.590	1735	0	0	1.930	24.762
106.	46.890	1744	0	0	1.900	102.48
107.	47.540	1764	0	0	1.850	202.37
108.	48.450	1791	0	0	1.760	194.08
109.	48.720	1800	0	0	1.740	.00000
110.	49.060	1815	0	0	1.700	.00000
111.	49.560	1826	0	0	1.990	46.389
112.	49.800	1834	0	0	2.070	83.400
113.	50.010	1841	0	0	2.130	43.118
114.	50.820	1866	0	0	2.380	227.34
115.	50.980	1871	0	0	2.430	36.169
116.	51.170	1878	0	0	2.480	33.360
117.	51.470	1887	0	0	2.570	131.40
118.	51.670	1893	0	0	2.630	61.880
119.	51.860	1900	0	0	2.690	.00000
120.	52.110	1908	0	0	2.630	98.167
121.	52.290	1914	0	0	2.580	102.86
122.	52.910	1935	0	0	2.410	180.41
123.	53.060	1940	0	0	2.370	75.793
124.	53.940	1969	0	0	2.130	72.737
125.	54.790	1997	0	0	1.900	25.529
126.	54.850	2008	0	0	1.890	.00000
127.	55.140	2010	0	0	1.890	22.683
128.	55.860	2035	0	0	1.890	80.907
129.	56.290	2050	0	0	1.900	218.64
130.	56.500	2057	0	0	1.900	67.069
131.	56.670	2063	0	0	1.900	28.102
132.	57.010	2075	0	0	1.900	52.511
133.	57.340	2087	0	0	1.900	119.85
134.	57.660	2098	0	0	1.910	45.806
135.	57.710	2100	0	0	1.910	.00000
136.	58.280	2120	0	0	1.900	65.863
137.	59.440	2163	0	0	1.880	67.791
138.	59.700	2172	0	0	1.880	112.33
139.	60.180	2189	0	0	1.870	26.102
140.	60.400	2200	0	0	1.870	.00000
141.	60.500	2202	0	0	1.870	45.016
142.	61.930	2256	0	0	1.870	67.085
143.	63.040	2298	0	0	1.870	23.278
144.	63.070	2300	0	0	1.870	.00000
145.	63.680	2324	0	0	1.830	23.304
146.	65.570	2400	0	0	1.700	.00000
147.	67.740	2489	0	0	1.660	29.996
148.	67.990	2500	0	0	1.650	.00000
149.	69.240	2552	0	0	1.650	41.619
150.	70.370	2600	0	0	1.650	.00000
151.	70.590	2607	0	0	1.700	25.283
152.	73.130	2700	0	0	2.300	.00000
153.	76.440	2800	0	0	1.640	.00000
154.	80.500	2900	0	0	1.660	.00000
155.	85.500	3000	0	0	1.830	.00000
156.	91.750	3100	0	0	3.440	.00000

FRACTION#2 HP-RUN-DATE: 9/22/1981 HP-RUN-NO: 72 HP-BOT-NO: 9

TOTAL RESOLVED HYDROCARBON = 22520.58
TOTAL UNRESOLVED HYDROCARBON = 36669.98
RESPONSE FACTOR AV. FOR C -1400 TO 3200 FOR UCM = 1.961737
RATIO RESOLVED/UNRESOLVED = 0.614142

SUM OF THE N-ALKANES = 0
SUM OF THE EVEN N-ALKANES = 0
SUM OF THE ODD N-ALKANES = 0

TABLE 3-8. WILMINGTON CRUDE OIL CONCENTRATIONS FOR ALIPHATIC FRACTI N.

```
FRACTION#1  HP-RUN-DATE:10/21/1981  HP-RUN-NO:  34  HP-BOT-NO:  7

 PEAK    RETENTION   KOVAT    KOVAT     KOVAT   RESPONSE   CONCENTRATION
NUMBER     TIME      INDEX   SUBGROUP   GROUP    FACTOR        TOTAL
------   ---------   -----   --------   -----   --------   -------------

 1.00     5.0100        0        0         0      1.440        540.74
 2.00     5.1600        0        0         0      1.440        17970.
 3.00     5.3200        0        0         0      1.440        1414.6
 4.00     5.7900        0        0         0      1.440        1043.3
 5.00     15.120        0        0         0      1.440        82.352
 6.00     16.460        0        0         0      1.440        76.485
 7.00     16.650        0        0         0      1.440        91.486
 8.00     17.790     1000        0         0      1.440        77.525
 9.00     18.210     1009        0         0      1.440        78.936
 10.0     19.060     1027        0         0      1.440        92.822
 11.0     19.670     1040        0         0      1.440        82.797
 12.0     20.900     1066        0         0      1.440        145.77
 13.0     21.400     1076        0         0      1.440        111.46
 14.0     21.710     1083        0         0      1.440        80.644
 15.0     23.200     1115        0         0      1.440        77.220
 16.0     23.460     1120        0         0      1.440        80.198
 17.0     23.960     1131        0         0      1.440        317.45
 18.0     24.640     1145        0         0      1.440        109.53
 19.0     24.900     1151        0         0      1.440        102.62
 20.0     25.750     1169        0         0      1.440        229.82
 21.0     26.400     1182        0         0      1.440        172.95
 22.0     26.720     1189        0         0      1.440        167.45
 23.0     27.230     1200        0         0      1.430        234.43
 24.0     28.520     1229        0         0      1.440        106.79
 25.0     29.530     1252        0         0      1.440        139.65
 26.0     30.010     1263        0         0      1.440        143.82
 27.0     31.580     1300        0         0      1.450        139.56
 28.0     33.270     1340        0         0      1.420        75.580
 29.0     33.530     1346        0         0      1.410        205.90
 30.0     34.210     1362        0         0      1.400        83.654
 31.0     35.760     1400        0         0      1.380        .00000
 32.0     36.910     1426        0         0      1.410        128.37
 33.0     37.780     1446        0         0      1.440        117.04
 34.0     38.090     1453        0         0      1.450        122.81
 35.0     38.460     1462        0         0      1.460        255.28
 36.0     38.850     1471        0         0      1.470        249.05
 37.0     40.100     1500        0         0      1.510        85.394
 38.0     42.500     1600        0         0      1.500        93.802
 39.0     44.520     1647        0         0      1.550        140.19
 40.0     46.080     1685        0         0      1.580        207.25
 41.0     46.300     1690        0         0      1.590        113.54
 42.0     46.710     1700        0         0      1.600        153.16
 43.0     48.140     1710        0         0      1.500        350.08
 44.0     50.200     1800        0         0      1.510        102.09
 45.0     51.710     1815        0         0      1.440        127.47
 46.0     53.340     1900        0         0      2.160        .00000
 47.0     56.030     2000        0         0      1.560        101.49
 48.0     57.160     2035        0         0      1.580        82.645
 49.0     59.240     2100        0         0      1.610        .00000
 50.0     63.110     2200        0         0      1.650        279.55
 51.0     65.270     2300        0         0      1.740        117.53
 52.0     66.050     2400        0         0      1.630        160.37
 53.0     69.610     2500        0         0      1.670        .00000
 54.0     72.300     2600        0         0      1.720        .00000
 55.0     74.610     2700        0         0      2.560        342.38
 56.0     79.280     2800        0         0      1.770        .00000
 57.0     84.000     2900        0         0      1.850        .00000
 58.0     91.530     3000        0         0      1.920        213.71
 59.0     94.360     3049        0         0      2.270        325.16
 60.0     97.230     3100        0         0      2.630        .00000
 61.0     100.76     3138        0         0      2.520        138.29
 62.0     106.49     3200        0         0      2.320        .00000
```

```
TOTAL RESOLVED HYDROCARBON = 29359.51
TOTAL UNRESOLVED HYDROCARBON = 179975
RESPONSE FACTOR AV. FOR C - 1000 TO 3100 FOR UCM =  1.762911
RATIO: RESOLVED/UNRESOLVED = 0.157569

SUM OF THE N-ALKANES = 2023.472
SUM OF THE EVEN N-ALKANES = 1185.446
SUM OF THE ODD N-ALKANES = 839.0259

RATIO: (PRISTANE+PHYTANE)/(N-ALKANES) = 0.236006
RATIO: ODD/EVEN  N-ALKANES = 0.706929
RATIO: PRISTANE/C-17 = 2.285709
RATIO: PHYTANE/C-18 = 1.249612
RATIO: PRISTANE/PHYTANE = 2.746258
RATIO: (N-ALKANES)/(BRANCHED HYDROCARBONS) = 7.683572E-2
```

Weight Distribution of Wilmington Crude by Fraction

Fraction	Weight (mg/g)
1	205
2	335
3	204

TABLE 3-9. WILMINGTON CRUDE OIL CONCENTRATIONS FOR AROMATIC FRACTION.

```
FRACTION:2  HP-RUN-DATE:10/21/1981  HP-RUN-NO:  35  HP-BOT-NO:  9

 PEAK    RETENTION  KOVAT    KOVAT    KOVAT  RESPONSE  CONCENTRATION
NUMBER     TIME     INDEX  SUBGROUP   GROUP   FACTOR       TOTAL

------  ---------  -----  --------   -----  --------  ------------

 1.00     5.3500       0        0        0     1.440       273.42
 2.00     5.6000       0        0        0     1.440       507.48
 2.50     5.6200     700        0        0     .0000       .00000
 3.00     5.8200     705        0        0     1.440       2570.7
 4.00     5.9000     706        0        0     1.440       170.29
 5.00     6.3600     717        0        0     1.440       1402.1
 6.00     6.6400     724        0        0     1.440       584.55
 7.00     7.6300     746        0        0     1.440       442.19
 8.00     27.240    1200        0        0     1.430       .00000
 9.00     31.620    1300        0        0     1.450       .00000
 10.0     35.760    1400        0        0     1.380       .00000
 11.0     39.660    1500        0        0     1.510       .00000
 12.0     43.360    1600        0        0     1.500       .00000
 13.0     44.550    1634        0        0     1.530       232.30
 14.0     46.810    1698        0        0     1.600       103.07
 15.0     46.660    1700        0        0     1.600       .00000
 16.0     47.080    1710        0        0     1.500       .00000
 17.0     47.360    1730        0        0     1.570       100.29
 18.0     50.160    1800        0        0     1.510       .00000
 19.0     50.510    1815        0        0     1.440       .00000
 20.0     53.340    1900        0        0     2.160       .00000
 21.0     53.700    1911        0        0     2.080       200.20
 22.0     56.050    1989        0        0     1.620       189.65
 23.0     56.360    2000        0        0     1.560       .00000
 24.0     57.390    2035        0        0     1.580       113.34
 25.0     57.920    2054        0        0     1.580       184.18
 26.0     59.240    2100        0        0     1.610       .00000
 27.0     61.090    2167        0        0     1.630       156.63
 28.0     61.370    2177        0        0     1.640       113.98
 29.0     61.990    2200        0        0     1.650       .00000
 30.0     64.630    2300        0        0     1.740       .00000
 31.0     65.440    2331        0        0     1.710       101.68
 32.0     67.170    2400        0        0     1.630       .00000
 33.0     69.610    2500        0        0     1.670       .00000
 34.0     72.300    2600        0        0     1.720       .00000
 35.0     75.440    2700        0        0     2.560       .00000
 36.0     79.280    2800        0        0     1.770       .00000
 37.0     84.000    2900        0        0     1.850       .00000
 38.0     89.860    3000        0        0     1.920       .00000
 39.0     97.230    3100        0        0     2.630       .00000
 40.0     106.49    3200        0        0     2.320       .00000


TOTAL RESOLVED HYDROCARBON = 7446.003
TOTAL UNRESOLVED HYDROCARBON = 67236.01
RESPONSE FACTOR AV. FOR C - 1600 TO 3100 FOR UCM =  1.321669
RATIO: RESOLVED/UNRESOLVED = 0.1107443

SUM OF THE N-ALKANES = 0
SUM OF THE EVEN N-ALKANES = 0
SUM OF THE ODD N-ALKANES = 0

RATIO: (PRISTANE+PHYTANE)/(N-ALKANES) = 0
RATIO: ODD/EVEN  N-ALKANES = 0
RATIO: PRISTANE/C-17 = 0
RATIO: PHYTANE/C-18 = 0
RATIO: PRISTANE/PHYTANE = 0
RATIO: (N-ALKANES)/(BRANCHED HYDROCARBONS) = 0
```

TABLE 3-10. POLAR (F3) FRACTION COMPONENTS FOR THE FOUR SELECTED CRUDES.

Murban Crude Oil Concentrations for Polar Fraction

Retention Time (min)	Kovat	Concentration (μg/g)
18.95	1026	121.
78.75	2787	116.

Cook Inlet Crude Oil Concentrations for Polar Fraction

Retention Time (min)	Kovat	Concentration (μg/g)
18.99	1026	151.
78.80	2787	111.

Prudhoe Bay Crude Oil Concentrations for Polar Fraction

Retention Time (min)	Kovat	Concentration (μg/g)
5.14	640	64.4
8.55	806	49.6
9.14	861	28.4

Wilmington Crude Oil Concentrations for Polar Fraction

Retention Time (min)	Kovat	Concentration (μg/g)
18.99	1026	211.
78.76	2787	224.

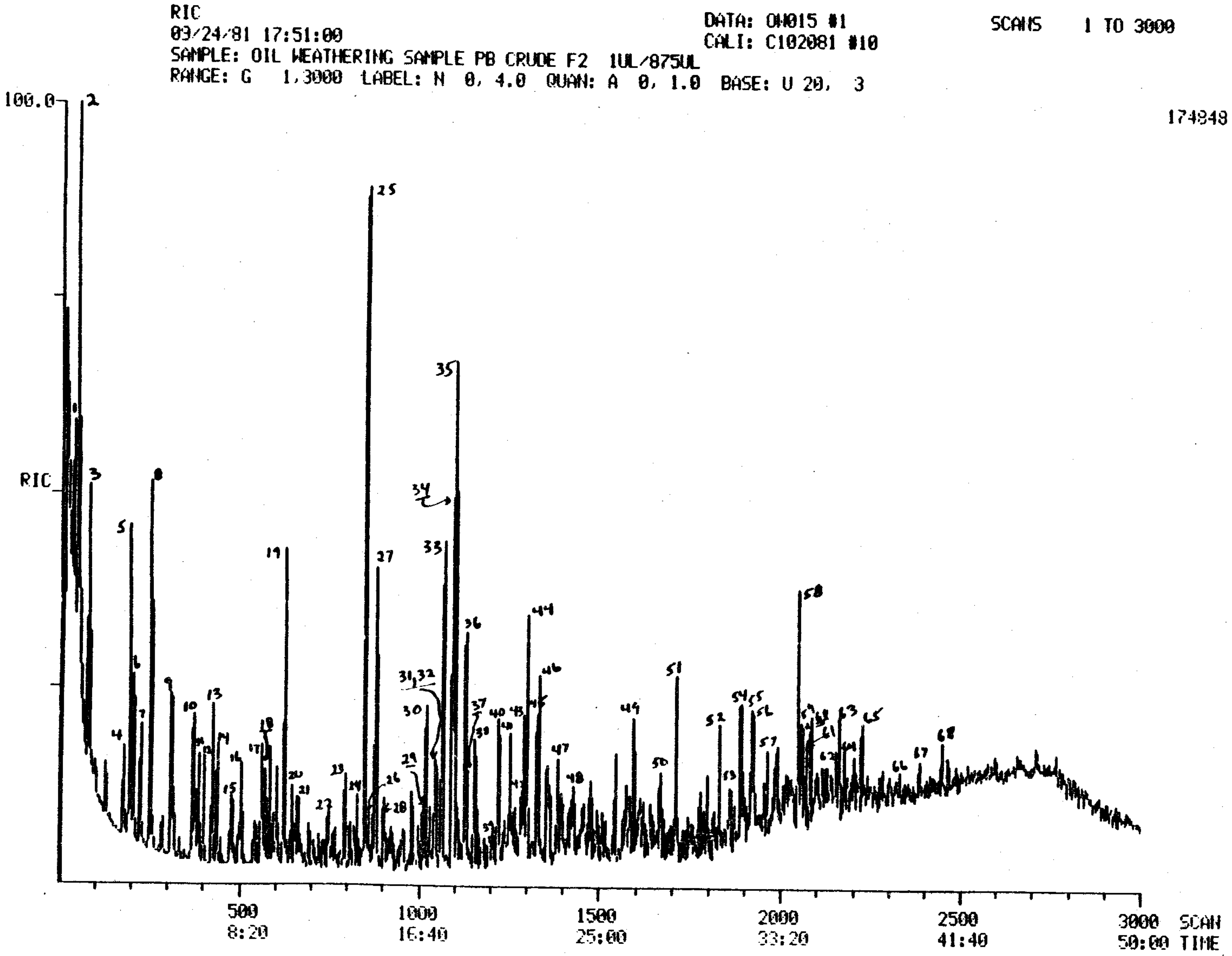

FIGURE 3-5. RECONSTRUCTED ION CHROMATOGRAM (RIC) GENERATED FROM GC/MS ANALYSES OF THE AROMATIC FRACTION (F2) OF PRUDHOE BAY CRUDE OIL. IDENTIFICATIONS OF THE NUMBERED PEAKS ARE PRESENTED IN TABLE 3-11.

TABLE 3-11. GC/MS IDENTIFICATIONS OF SELECTED COMPONENTS IN THE AROMATIC FRACTION OF PRUDHOE BAY CRUDE OIL (SEE FIGURE 3-5).

1	ethylbenzene
2	p-xylene
3	o-xylene
4	n-propylbenzene
5	ethylmethylbenzene
6	trimethylbenzene
7-9	C_3 benzenes
10	methylpropylbenzene
11-13	C_4 benzenes
14	ethyldimethylbenzene
15	C_4 benzene
16	tetramethylbenzene
17	unsaturated C_4 benzene (possibly a methylindane)
18	C_4 benzene
19	naphthalene
20,21	unsaturated C_5 benzenes (possibly C_2 indanes)
22	unsaturated C_6 benzene (possibly a C_2 tetralin)
23,24	C_6 benzenes
25	2-methylnaphthalene
26	unsaturated C_6 benzene (possibly a C_2 tetralin)
27	1-methylnaphthalene
28	unsaturated C_6 benzene (possibly a C_2 tetralin)
29	C_7 benzene
30	biphenyl
31	2-ethylnaphthalene
32	1-ethylnaphthalene
33-38	dimethylnaphthalenes
39	C_3 naphthalene
40	methylbiphenyl
41	2-isopropylnaphthalene
42	1-isopropylnaphthalene
43-46	trimethylnaphthalenes
47	fluorene
48	dimethylbiphenyl
49	methylfluorene
50	dibenzothiophene
51	phenanthrene
52,53	methyldibenzothiophenes
54-56	methylphenanthrenes
57	C_2 napthothiophenes
58-61	dimethylphenanthrenes
62-65	C_3 phenanthrenes
66	benzonaphthothiophene
67	chrysene or benz (a)anthracene
68	phthalate ester

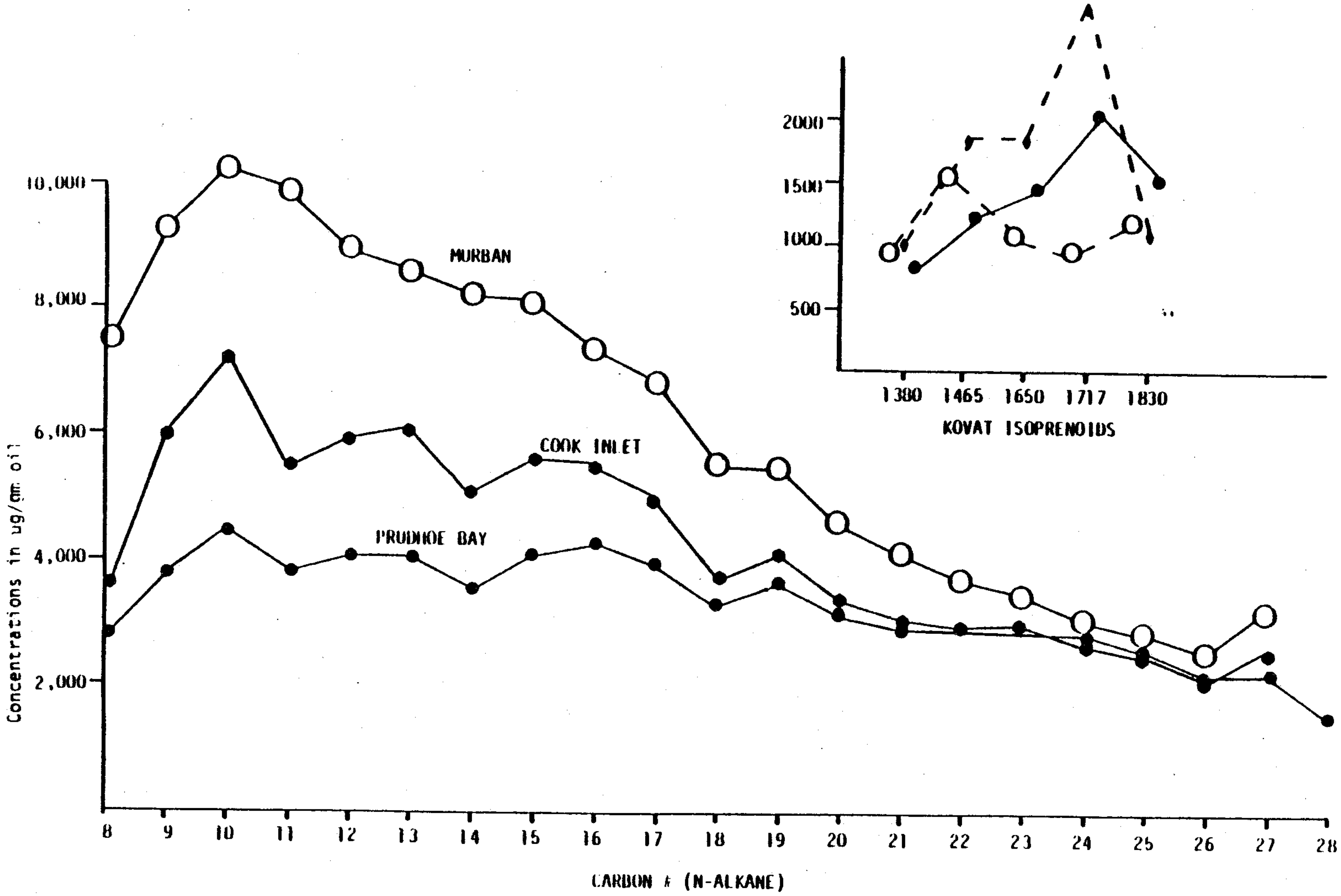

FIGURE 3-6. ALIPHATIC (n-alkane and isoprenoid) CARBON DISTRIBUTIONS FOR PRUDHOE BAY, COOK INLET AND MURBAN (middle east) CRUDE OILS.

Even more striking similarities of the two Alaskan crude oils are depicted in Figure 3-7, which shows the relative abundance of alkyl-substituted polynuclear aromatic (PNA) hydrocarbons as derived from selected ion monitoring GC/MS analyses. Figure 3-7A presents the relative abundance of the PNAs for Cook Inlet crude and Figure 3-7B presents the same data for Prudhoe Bay crude oil. It should be noted that in these oils, as in many other crudes, the alkyl-substituted polynuclear aromatic compounds are predominant over the non-substituted parent compounds. In Figure 3-7 the parent hydrocarbon is denoted by the first data point nearest the origin of the Absolute Carbon Number coordinate, and the degree of alkyl-substitution is then shown to increase with, for example, 11 representing methylnaphthalene, 12 representing dimethylnaphthalene, etc. In comparing Prudhoe Bay and Cook Inlet crudes it can be seen that the relative abundance of alkyl-substituted naphthalenes are nearly identical, and similar trends are observed for biphenyl, fluorene and phenanthrene. In this instance, Cook Inlet crude shows some evidence of slightly higher relative levels of alkyl-substituted phenanthrene. Of these two oils, only Prudhoe Bay crude oil contained significant concentrations of the alkyl-substituted sulfur-heteroaromatic dibenzothiophenes. This is also reflected in the difference in weight percent sulfur of the two crudes as shown by the data in Table 3-1. Figure 3-8 presents the relative abundance plots for the alkyl-substituted polynuclear aromatic hydrocarbons in Murban Crude and Wilmington crude. The alkyl-substituted naphthalene composition of Murban crude is similar to that observed for the two Alaskan crudes; however, this oil contains significantly higher levels of alkyl-substituted dibenzothiophenes, and again the weight percent sulfur in the crude is somewhat higher. The alkyl-substituted naphthalene distribution for Wilmington crude is significantly different from the other three oils considered, and of the four crudes it has the highest relative abundance of phenanthrene and fluorene.

Interestingly, there were no significant levels of dibenzothiophene detected. BALL and RALL (1962) have shown that the sulfur content of the low-boiling (up to 250°C) fractions of Wilmington crude is predominantly in

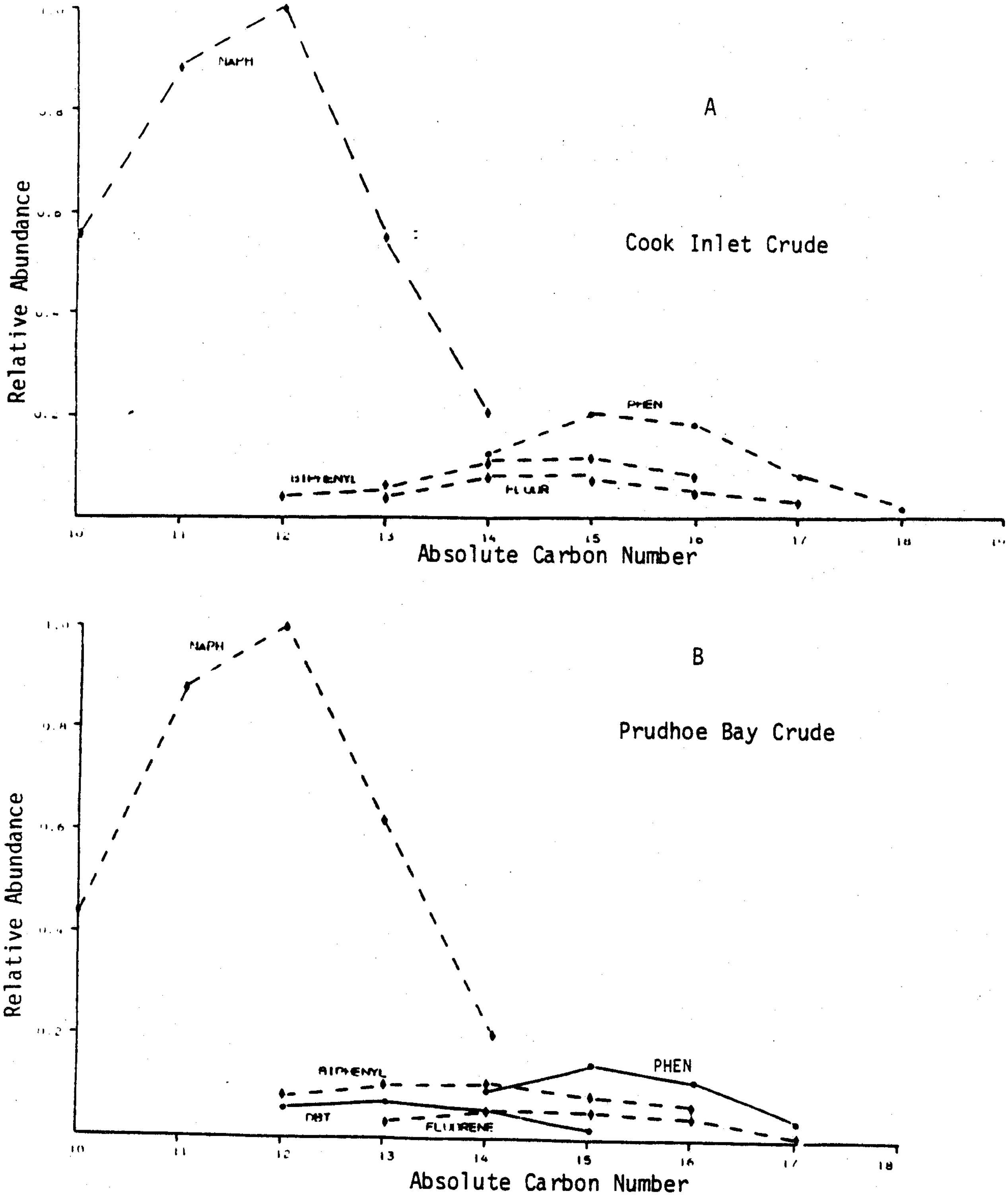

FIGURE 3-7. RELATIVE ABUNDANCE PLOTS FROM SELECTIVE ION MONITORING (GCMS) OF THE MAJOR ALKYL SUBSTITUTED AROMATIC SERIES DETECTED IN COOK INLET (TOP) AND PRUDHOE BAY (BOTTOM) OILS. (NAPH - naphthalene; PHEN- phenanthrenes; DBT - dibenzothiophenes; FLUOR - fluorenes)

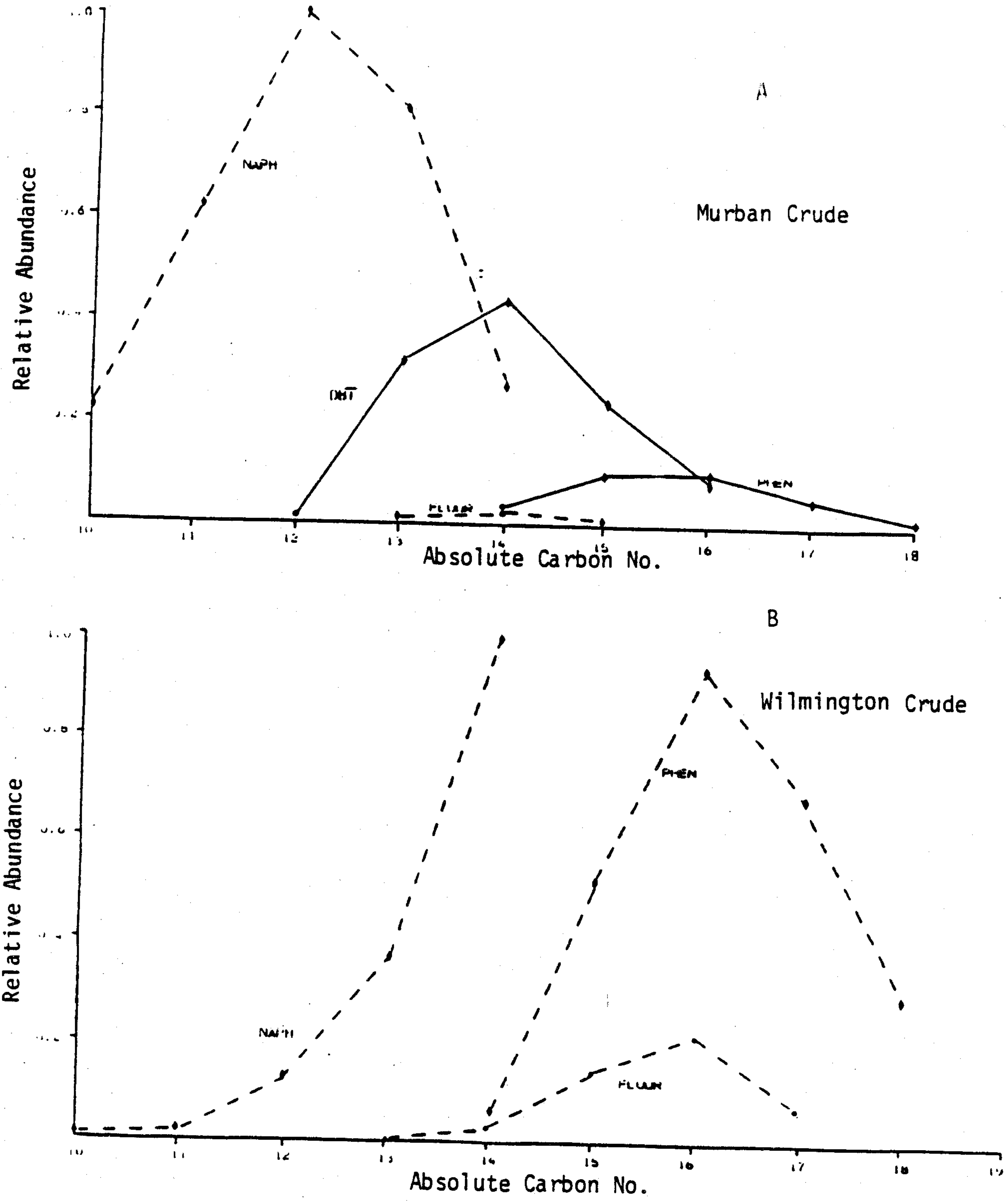

FIGURE 3-8. RELATIVE ABUNDANCE PLOTS FROM SELECTIVE ION MONITORING (GCMS) OF THE MOLECULAR ION FOR THE MAJOR ALKYL SUBSTITUTED AROMATIC SERIES DETECTED IN THE MURBAN (TOP) AND LONG BEACH (BOTTOM) CRUDE OILS. (Abbreviations as in Figure 3-7)

the form of alkyl thiophenes and saturated cyclic sulfides. The bulk of the sulfur-containing components, however, were in the residue and were not characterized in that study. It should be noted from the data in Table 3-1 that the Wilmington crude also had the highest levels of the trace elements nickel and vanadium.

Another significant feature of the relative abundance plots for aliphatic and aromatic hydrocarbons is that the crudes with higher API gravities (lower specific gravities) also tend to have higher relative concentrations of the lower molecular weight, and less dense, aliphatic and aromatic hydrocarbons. That is, the Wilmington crude with the lowest API gravity is not represented by lower molecular weight aliphatic materials and the aromatic fractions are skewed towards the more highly alkyl-substituted phenanthrenes and fluorenes. As the data in Table 3-1 illustrate, the lower API gravity crudes also tend to have higher weight percent asphalts.

Synchronous scanning spectrofluorometry has also been used to characterize the polynuclear aromatic hydrocarbons content of crude oil and sediments and waters exposed to crude oils (WAKEHAM, 1977; GORDON et al., 1976; VO-DINH et al., 1978; BOEHM and FIEST, 1980) and this technique was also used in our studies to characterize the four selected crude oils examined. Families of aromatic hydrocarbons can be revealed by this method (LLOYD, 1971) and synchronous scan UV fluorescence spectra of the four crudes are shown in Figures 3-9, 3-10 and 3-11. These spectra were obtained on a Perkin-Elmer model MPF-44A high performance fluorescence spectrofluorometer with the exitation and emission monochromoters offset by 30 nm. The combined excitation emission spectra were obtained over the range of 230 to 600 nm. In general, monocyclic aromatic hydrocarbons emit most strongly in the 280 to 290 nm region, dicyclic aromatics such as alkyl-substituted naphthalenes emit at about 310 to 320 nm; 3 and 4 ring aromatics emit in the range of 340 to 380 nm and compounds with greater than 5 rings emit in the range of 400 to 470 nm.

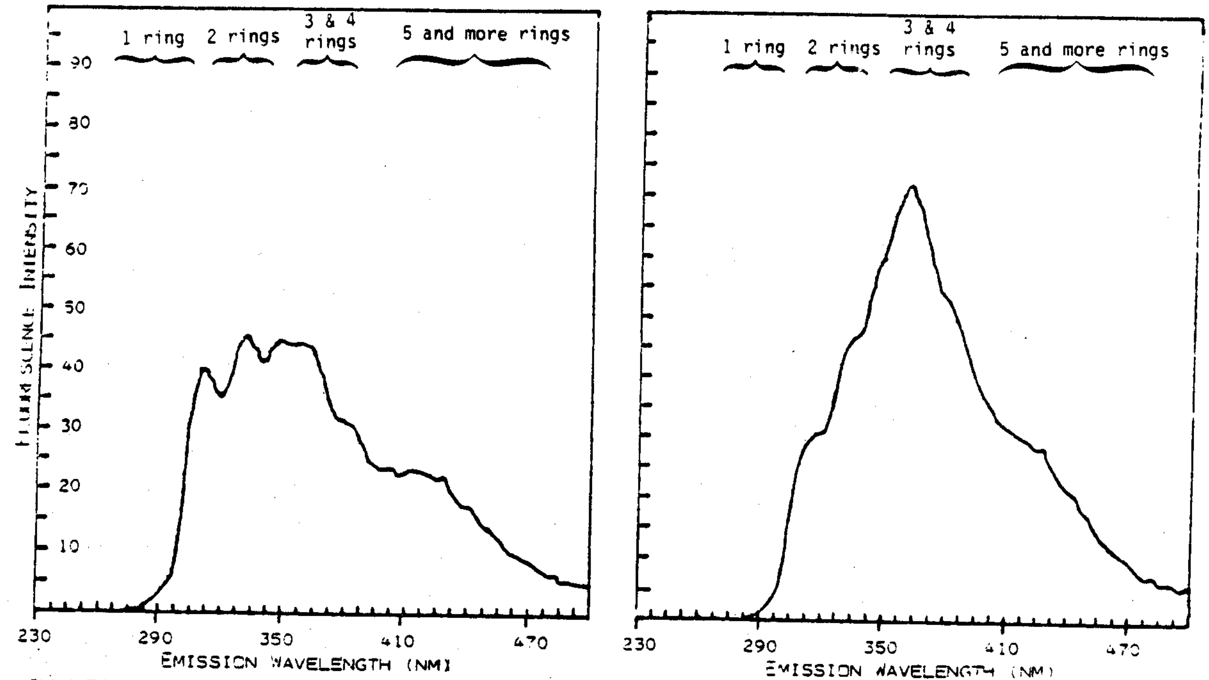

SYNCHRONOUS SCAN SPECTRA OF MURBAN CRUDE OIL (10 MG/ML)

SYNCHRONOUS SCAN SPECTRA OF WILMINGTON CRUDE OIL (10 MG/ML)

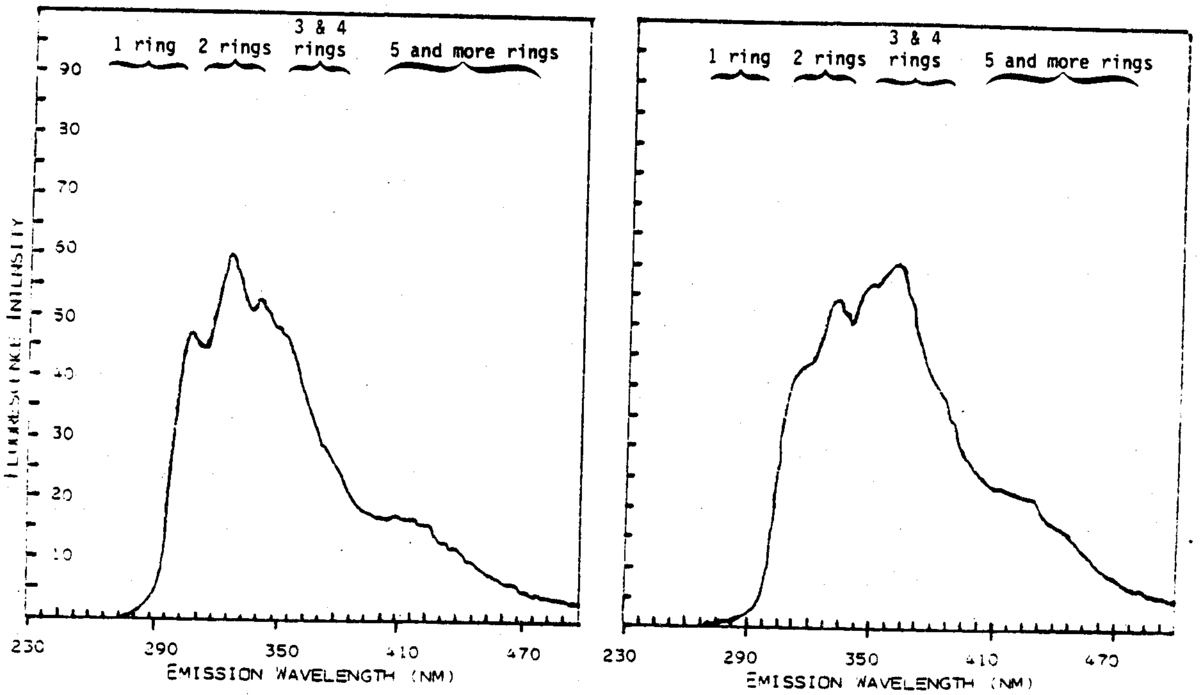

SYNCHRONOUS SCAN SPECTRA OF COOK INLET CRUDE OIL (10 MG/ML)

SYNCHRONOUS SCAN SPECTRA OF PRUDHOE BAY CRUDE (10 MG/ML)

FIGURE 3-9. SYNCHRONOUS SCAN UV FLUORESCENCE SPECTRUM OF 10 mg/ml CONCENTRATION OF THE FOUR SELECTED CRUDE OILS.

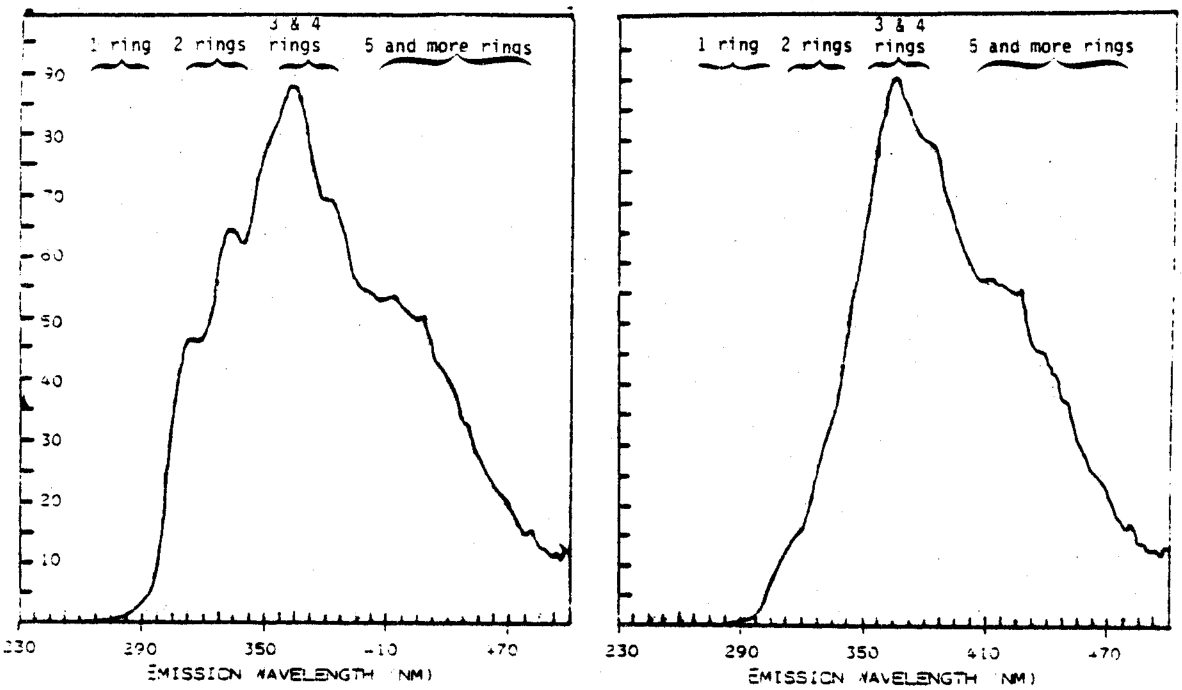

SYNCHRONOUS SCAN SPECTRA OF MURBAN CRUDE OIL (100 MG/ML)

SYNCHRONOUS SCAN SPECTRA OF WILMINGTON OIL (100 MG/ML)

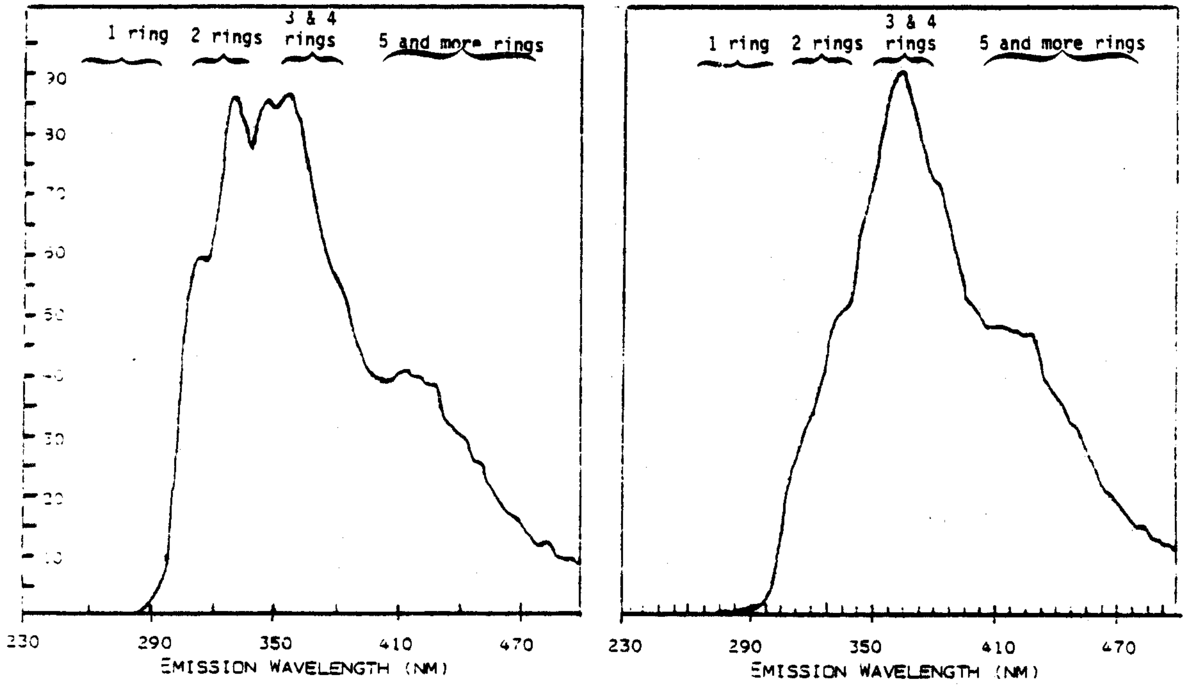

SYNCHRONOUS SCAN SPECTRA OF COOK INLET CRUDE OIL (100 MG/ML)

SYNCHRONOUS SCAN SPECTRA OF PRUDHOE BAY CRUDE OIL (100 MG/ML)

FIGURE 3-10. SYNCHRONOUS SCAN UV FLUORESCENCE SPECTRUM OF 100 mg/ml CONCENTRATIONS OF THE FOUR SELECTED CRUDE OILS.

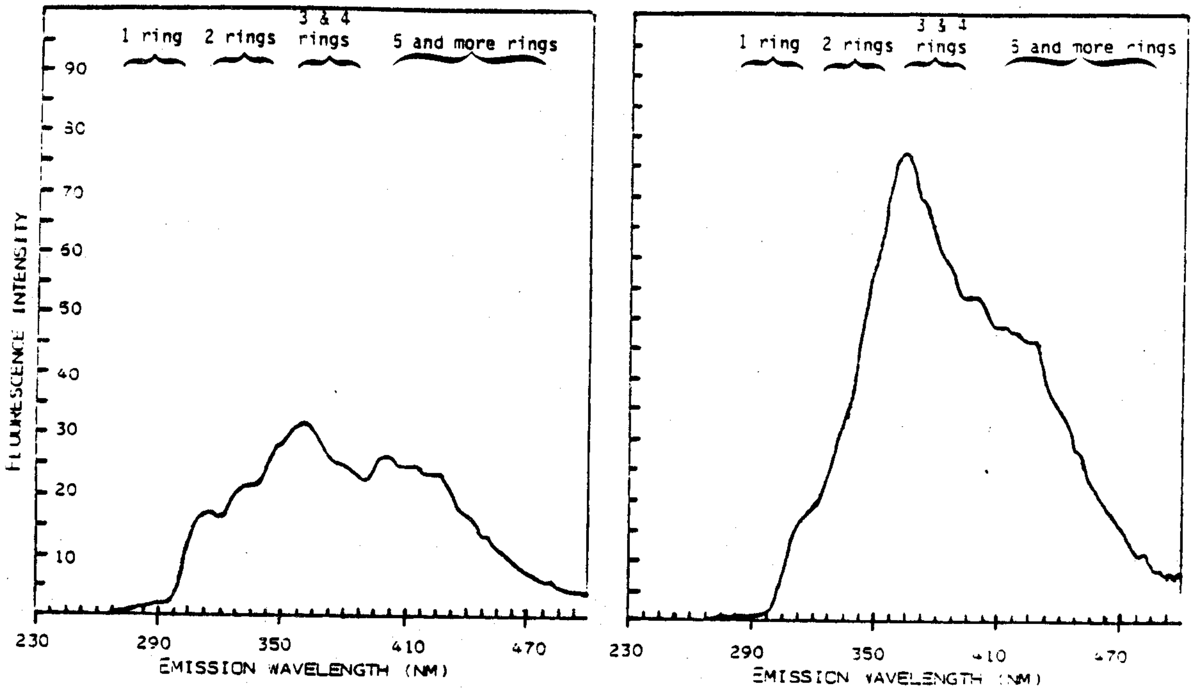

SYNCHRONOUS SCAN SPECTRA OF THE AROMATIC FRACTION OF MURBAN CRUDE OIL

SYNCHRONOUS SCAN SPECTRA OF THE AROMATIC FRACTION OF WILMINGTON CRUDE

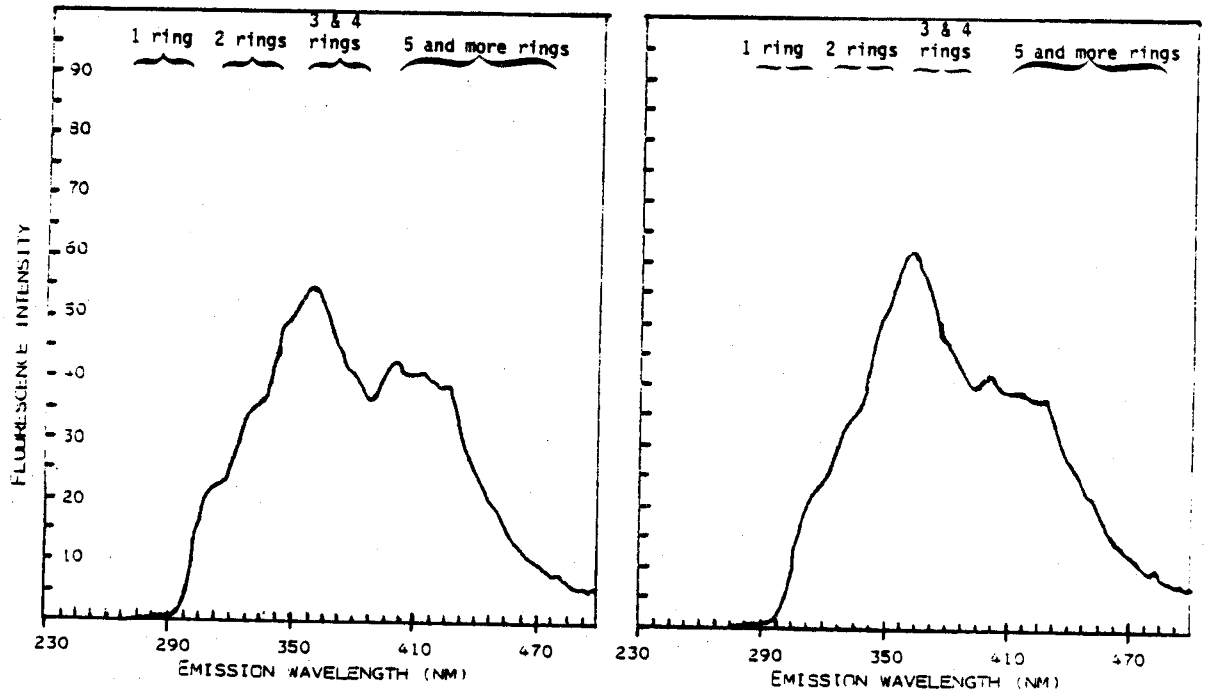

SYNCHRONOUS SCAN SPECTRA OF THE AROMATIC FRACTION OF COOK INLET CRUDE

SYNCHRONOUS SCAN SPECTRA OF THE AROMATIC FRACTION OF PRUDHOE BAY CRUDE

FIGURE 3-11. SYNCHRONOUS SCAN UV FLUORESCENCE SPECTRUM OF THE AROMATIC FRACTIONS OF THE FOUR SELECTED CRUDE OILS.

The four crudes shown in Figure 3-9 were scanned at concentrations of 10 mg/ml in spectral grade cyclohexane and the spectra shown in Figure 3-10 were obtained at concentrations of 100 mg/ml. It can be seen from the spectra presented in Figures 3-9 and 3-10 that at lower concentrations better fluorescence resolution for the small ringed compounds is obtained at the shorter wavelengths. At higher concentrations, greater fluorescence and resolution is observed for the 4 and 5 ring compounds, reflecting the effective energy transfer processes which occur at higher concentrations (JOHN and SOUTAR, 1976; VO-DINH et al. 1978)

From the spectra of the whole crude oil samples it appears that Cook Inlet and Murban crude oils contain a higher abundance of 2 and 3 ring aromatic compounds with Prudhoe Bay crude being intermediate and Wilmington having the lowest relative abundance of these compounds. As noted above, these compositional differences are also illustrated by the relative abundance PNA plots presented in Figures 3-7 and 3-8. The 4 and 5 ring aromatics appears to be more concentrated in the Wilmington and Murban crude oils. Figure 3-11 presents the synchronous scan UV-fluorescence spectra obtained on the aromatic fractions of each of the selected oils, and while the results are similar to those obtained for the unfractionated oils, a slight relative increase in fluorescence from the 3, 4, and 5 ring compounds can be observed.

While component-specific data are necessary for developing an oil weathering model, additional data are also required to enable a mass balance approach describing the state of an actively weathering oil slick. As will be discussed in the following sections on modeling, it is not possible to develop a mass balance model of oil weathering if only specific organic compounds, or even confined groups of compounds, are considered. Thus, to obtain information on the overall mass balance for various spilled crude oils, fractional distillation data are required of the type routinely used in the petroleum industry for overall oil characterizations. With such an approach, compounds can be grouped into pseudo-component classes based on their boiling points, and cumulative percent compositional data can be obtained on crudes as a function of the true boiling point distillation curve. Tables 3-12 through 3-15 present the fractional-distillation cut data (COLEMAN et al, 1978) for Murban, Cook Inlet, Prudhoe Bay and Wilmington crudes, respectively. The percent composition of each fractional cut is presented by boiling point, and the cumulative volume percent and API gravity of each distillation cut are also given. From these data, it can be seen that cumulative percent distilled can vary significantly from oil to oil, and it is also possible to see how different oil compositions are skewed to higher or lower molecular weight components. Note that the relative percent of nondistillable residue increases from Murban crude (19.1%) to Cook Inlet (25.6%) to Prudhoe Bay crude (36.3%) to Wilmington crude (53.3%) in line with the relative compositions of higher molecular weight materials, percent asphalt and (to a general extent) Kinematic and Saybolt viscosities. Not surprisingly, a relatively smooth decreasing trend in API gravity is also observed with each distillate cut. Figure 3-12 presents the true boiling point distillation curves showing the cumulative volume percent of each crude distilled vs. true boiling point in °F up to the limit of the nondistillable stillpot residual. Similar plots will be utilized extensively with the development of the pseudo component oil weathering model, and predicted vs. observed (as derived from capillary GC data) distillation curves will be used to compare oil weathering model output and observed field data.

In examining the detail from Tables 3-12 through 3-15, and the curves presented in Figure 3-12, it can be seen that significant portions of each of the crudes occur in the non-distillable residuum with boiling points above 790°F. Thus, while Murban and Cook Inlet crudes have 80% and 71% distillable components, Prudhoe Bay crude oil and Wilmington crude oil have distillable fractions consisting of only 62.6% and 46.3% of the starting oil, respectively. The steepness of the boiling point distillation temperature vs. percent distilled curves in Figure 3-12 also shows the relative differences in percent higher molecular weight non-boiling components. That is, the steeper the curve in Figure 3-12 the more components present boiling above 790°F. Figure 3-13 shows the cumulative boiling point distributions for the four crudes

TABLE 3-12. FRACTIONAL DISTILLATION DATA ON MURBAN BAB-BU HASA ABU DHABI CRUDE OIL.

Fraction No.	Cut Temp °F	Volume Percent	Cumulative Percent	°API 60°F	Cumulative % Based on Total Distillable Only
1	122	1.7	1.7	96.7	2.1
2	167	2.9	4.6	86.2	5.7
3	212	4.9	9.5	70.6	11.8
4	257	6.0	15.5	62.3	19.4
5	302	6.7	22.2	55.7	27.7
6	347	6.4	28.6	51.6	35.7
7	392	5.7	34.3	48.5	42.8
8	437	5.6	39.9	45.6	49.8
9	482	5.9	45.8	43.0	57.2
10	527	4.9	50.7	40.0	63.3
11	580	5.7	56.4	35.8	70.4
12	638	5.6	62.0	34.0	77.4
13	685	6.5	68.5	30.0	85.5
14	738	6.0	74.5	28.4	93.0
15	790	5.6	80.1	26.6	100

% Non-distillable residuum: 19.1; cumulative % 99.2; °API 16.7

% Asphalt in residuum: 30

TABLE 3-13. FRACTIONAL DISTILLATION DATA ON COOK INLET, ALASKA CRUDE OIL (McArthur River Field).

Fraction No.	Cut Temp °F	Volume Percent	Cumulative Percent	°API 60°F	Cumulative % Based on Total Distillable Only
1	122	2.4	2.4	89.2	3.4
2	167	2.5	4.9	77.2	6.9
3	212	5.9	10.8	65.0	15.1
4	257	6.1	16.9	59.5	23.7
5	302	5.1	22.0	55.4	30.8
6	347	5.2	27.2	50.8	38.1
7	392	4.9	32.1	46.5	45.0
8	437	5.1	37.2	43.0	52.2
9	482	5.2	42.4	39.6	59.5
10	527	5.0	47.4	37.0	66.5
11	580	3.3	50.7	32.8	71.1
12	638	5.2	55.9	31.3	78.4
13	685	7.0	62.9	28.7	88.2
14	738	4.2	67.1	26.6	94.1
15	790	4.2	71.3	25.0	100

% Non-distillable residuum: 25.6; cumulative % 96.9: °API 11.6

% Asphalt in residuum: 35

TABLE 3-14. FRACTIONAL DISTILLATION DATA ON PRUDHOE BAY, ALASKA CRUDE OIL.

Fraction No.	Cut Temp °F	Volume Percent	Cumulative Percent	°API 60°F	Cumulative % Based on Total Distillable Only
1	122	-	-	-	-
2	167	2.1	2.1	72.7	3.4
3	212	2.6	4.7	64.2	7.5
4	257	3.5	8.2	56.7	13.1
5	302	3.6	11.8	51.6	18.8
6	347	3.7	15.5	47.6	24.8
7	392	3.5	19.0	45.2	30.4
8	437	4.3	23.3	41.5	37.2
9	482	4.8	28.1	37.8	44.9
10	527	5.0	33.1	34.8	52.9
11	580	2.8	35.9	30.6	57.3
12	638	6.5	42.4	29.1	67.7
13	685	6.8	49.2	26.2	78.6
14	738	6.0	55.2	24.0	88.2
15	790	7.4	62.6	22.5	100

% Non-distillable residuum: 36.3; cumulative % 98.9; °API 11.4

% Asphalt in residuum: 57

TABLE 3-15. FRACTIONAL DISTILLATION DATA ON WILMINGTON, CALIFORNIA CRUDE OIL.

Fraction No.	Cut Temp °F	Volume Percent	Cumulative Percent	°API 60°F	Cumulative % Based on Total Distillable Only
1	122	-	-	-	-
2	167	-	-	-	-
3	212	2.3	2.3	68.6	5.0
4	257	2.4	4.7	58.7	10.2
5	302	2.4	7.1	53.0	15.3
6	347	2.5	9.6	48.1	20.7
7	392	2.8	12.4	43.2	26.8
8	437	3.6	16.0	38.8	34.6
9	482	4.4	20.4	35.4	44.1
10	527	5.3	25.7	32.3	55.5
11	580	4.7	30.4	26.8	65.7
12	638	6.3	36.7	24.5	79.3
13	685	4.1	40.8	22.3	88.1
14	738	5.5	46.3	20.3	100
15	790	*	-		

% Non-distillable residuum: 53.5; cumulative % 99.6; °API 8.9

% Asphalt in residuum: 42

* Distillation discontinued at 740°F

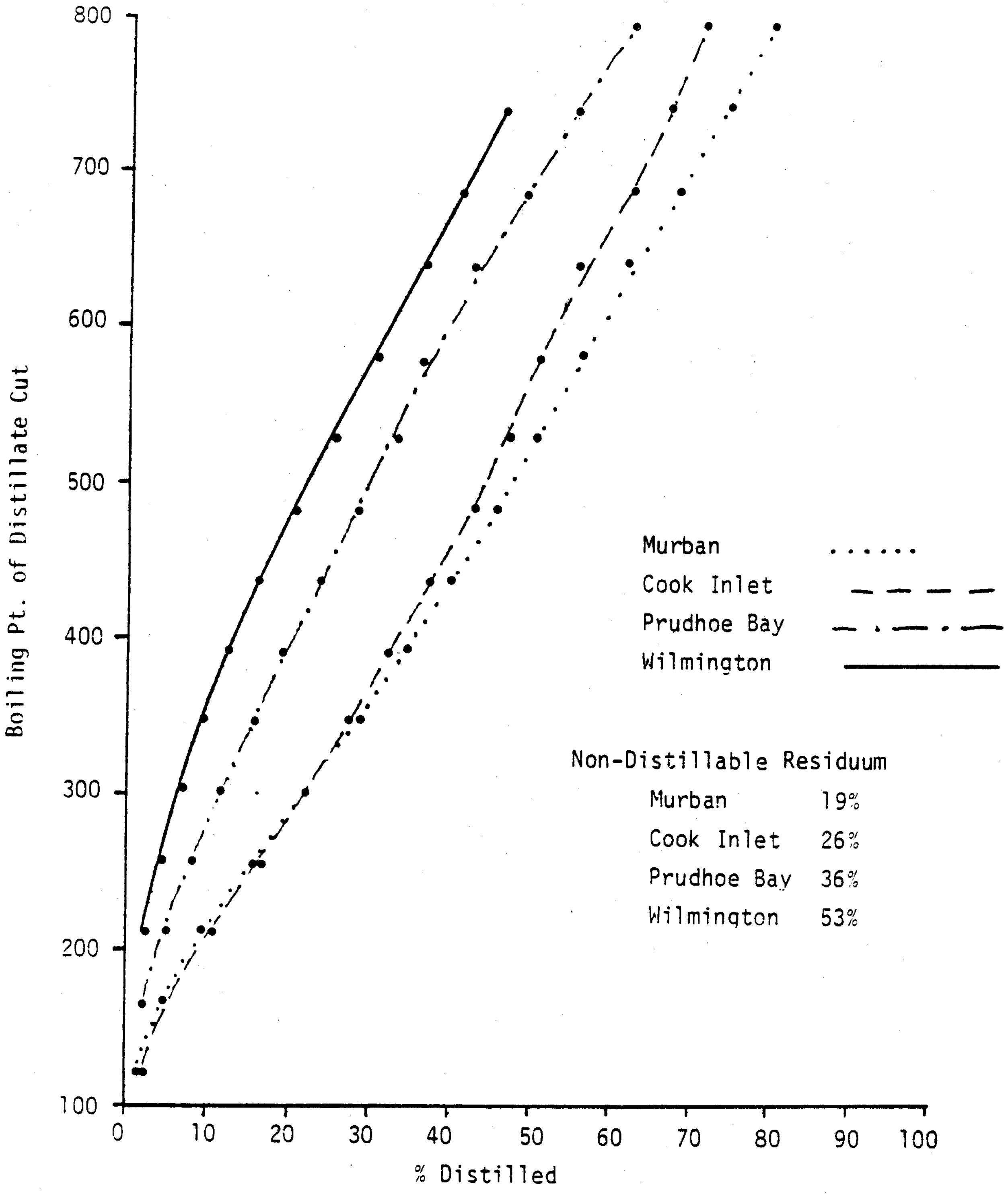

FIGURE 3-12. BOILING POINT DISTILLATION CURVES FOR THE FOUR SELECTED CRUDE OILS STUDIED.

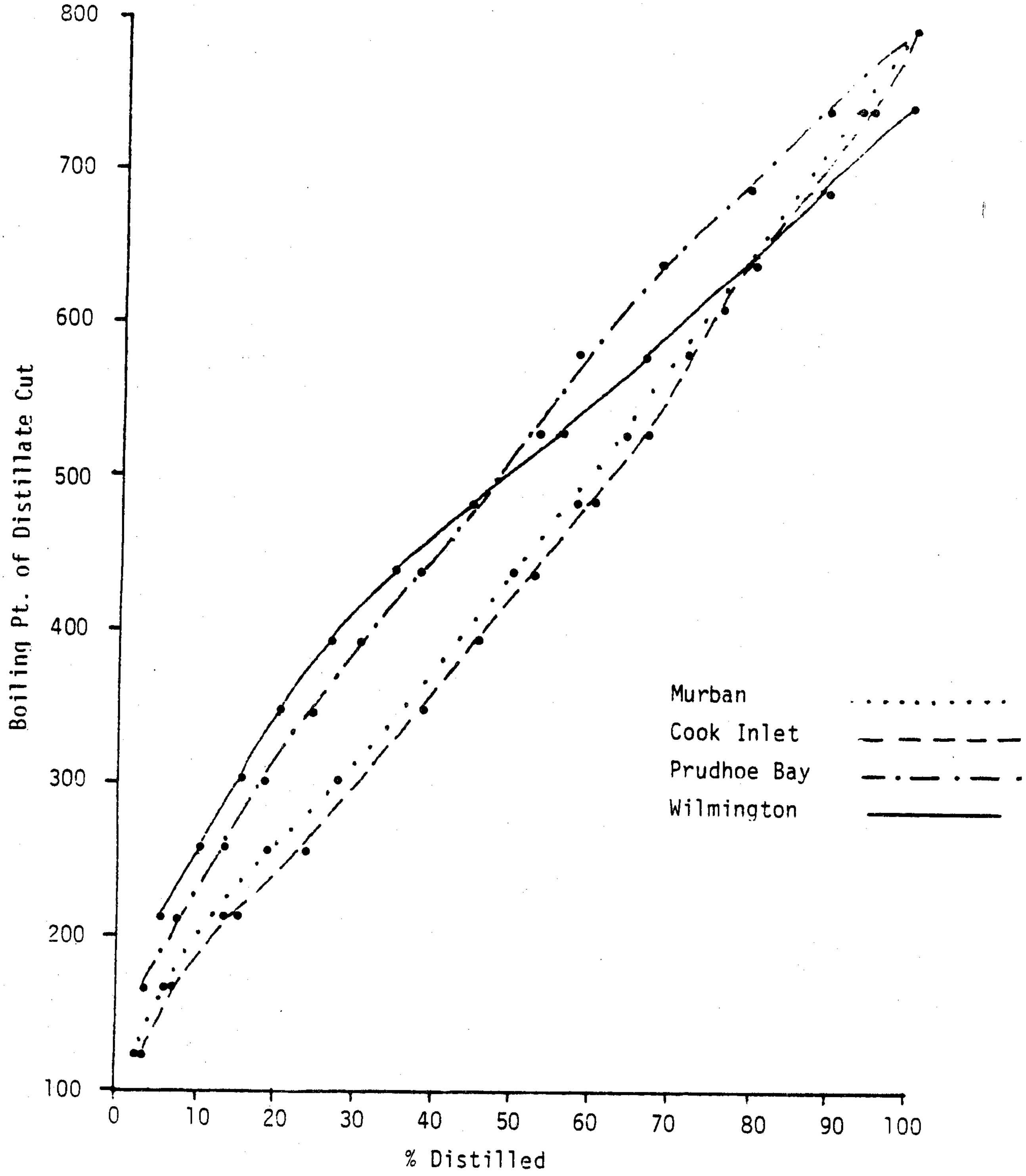

FIGURE 3-13. CUMULATIVE BOILING POINT DISTILLATION CURVES FOR THE TOTAL DISTILLABLE FRACTIONS OF THE FOUR CRUDE OILS STUDIED.

based on the total distillable fractions only. That is, it is a temperature vs. percent distilled curve for the fraction of the oil which can be distilled below 790°F, and thus, the weight of each distillate cut has been normalized to the overall weight of the total distillate obtained. These data illustrate that at a given temperature, less total material of the distillable fraction has been distilled for Prudhoe Bay and Wilmington crude vs Murban and Cook Inlet crude, and this again reflects the somewhat higher molecular weight component concentrations of the Prudhoe Bay and Wilmington crude oils.

In line with this characterization approach Prudhoe Bay crude oil was subjected to a true boiling point distillation at atmospheric pressure using the TBP apparatus shown in Figure 3-14. An aliquot of 1.5 l of fresh Prudhoe Bay crude oil was subjected to a 15 theoretical plate packed column distillation. This distillation was carried out at a reflux ratio of 6:1 and followed the procedure outlined in (TIEGE, 1980). A total of 13 distillate fractions and the pot bottom residues were collected and then subjected to characterization by FID-GC. Figures 3-15 and 3-16 present the FID-GC obtained on the whole crude oil and selected distillate cuts. Boiling points for each cut are presented in the figure legends. The chromatogram in Figure 3-15A is of whole unfractionated Prudhoe Bay crude oil. Resolved components from heptane (KOVAT index 700) through nC-32 (KOVAT index 3200) can be observed. The chromatogram in Figure 3-15B is of distillate cut 1 and most of the collected components were so volatile that they were masked by the solvent peak which for these characterizations was carbon disulfide. Chromatogram C shows the components present in distillate cut #3 and in this instance the measured peaks include compounds in the KOVAT 700 to 800 range. Distillate cut #5 shown in Chromatogram D contains components in the KOVAT index 700 to 850 range with a maximum at nC-8 (KOVAT index 800). Higher boiling distillate cuts are shown in Figure 3-16, and the Chromatogram A shows distillate cut #7 which is centered around nC-9 (KOVAT index 900) with a range extending from KOVAT index 750 to 1000. Distillate cut 11 is centered around nC-10 (KOVAT index 1000) and includes components boiling between nC-9 and nC-10. Distillate cut 12 (Chromatogram C) shows a clean fractionation with all the components in the

Figure 3-14. True Boiling Point (TBP) 15 Theoretical Plate Distillation Apparatus used for Characterization of Whole and Weathered Crude Oils for Experimental Verification of Mass Balance Predictions.

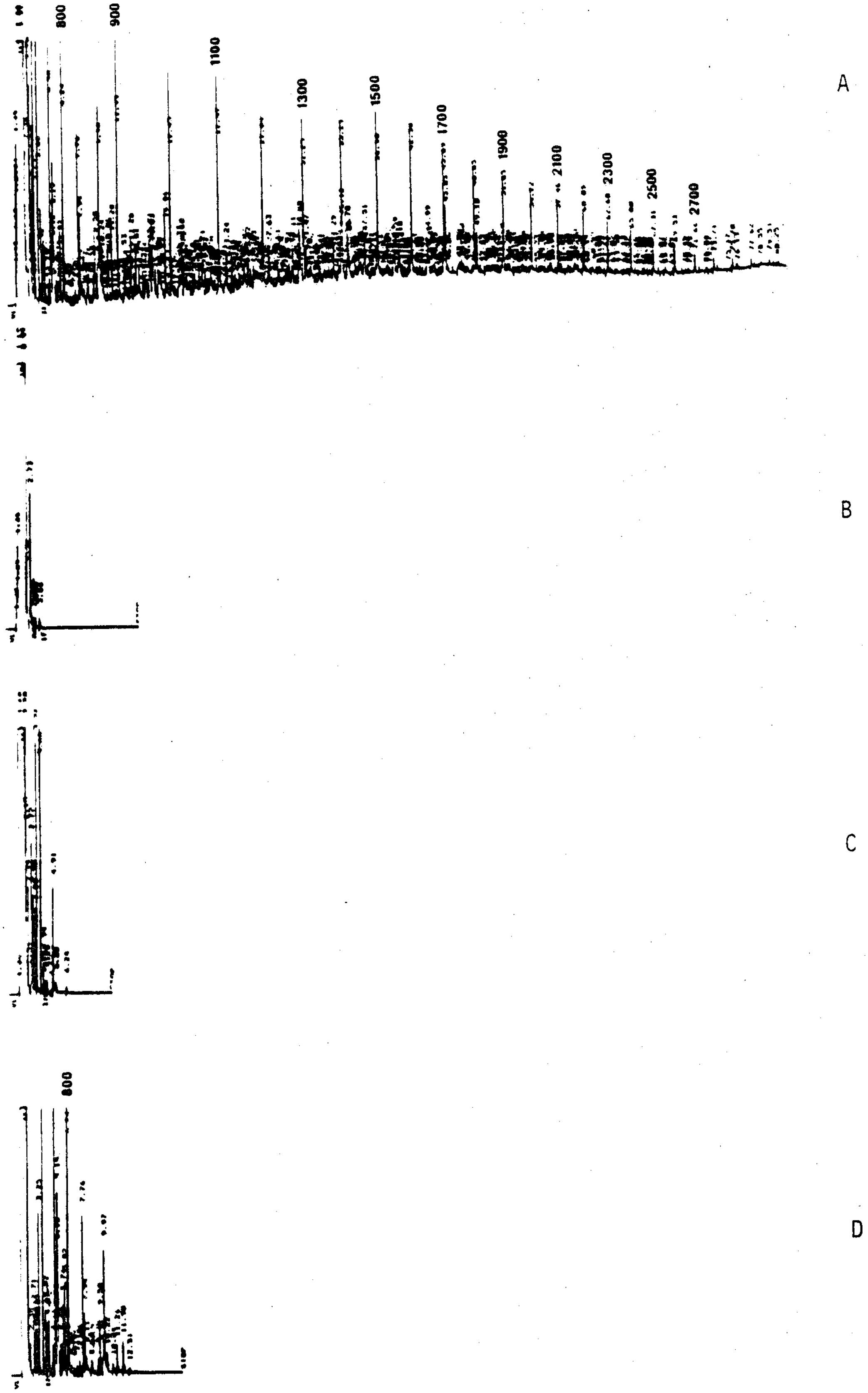

Figure 3-15. GC-FID Chromatograms of Distillate Cuts of Fresh Prudhoe Bay Crude Oil. (A) Fresh Oil Before Distillation, (B) Cut #1, (107°-151°F), (C) Cut #3 (186°-209°F), and (D) Cut #5 (233°-259°F).

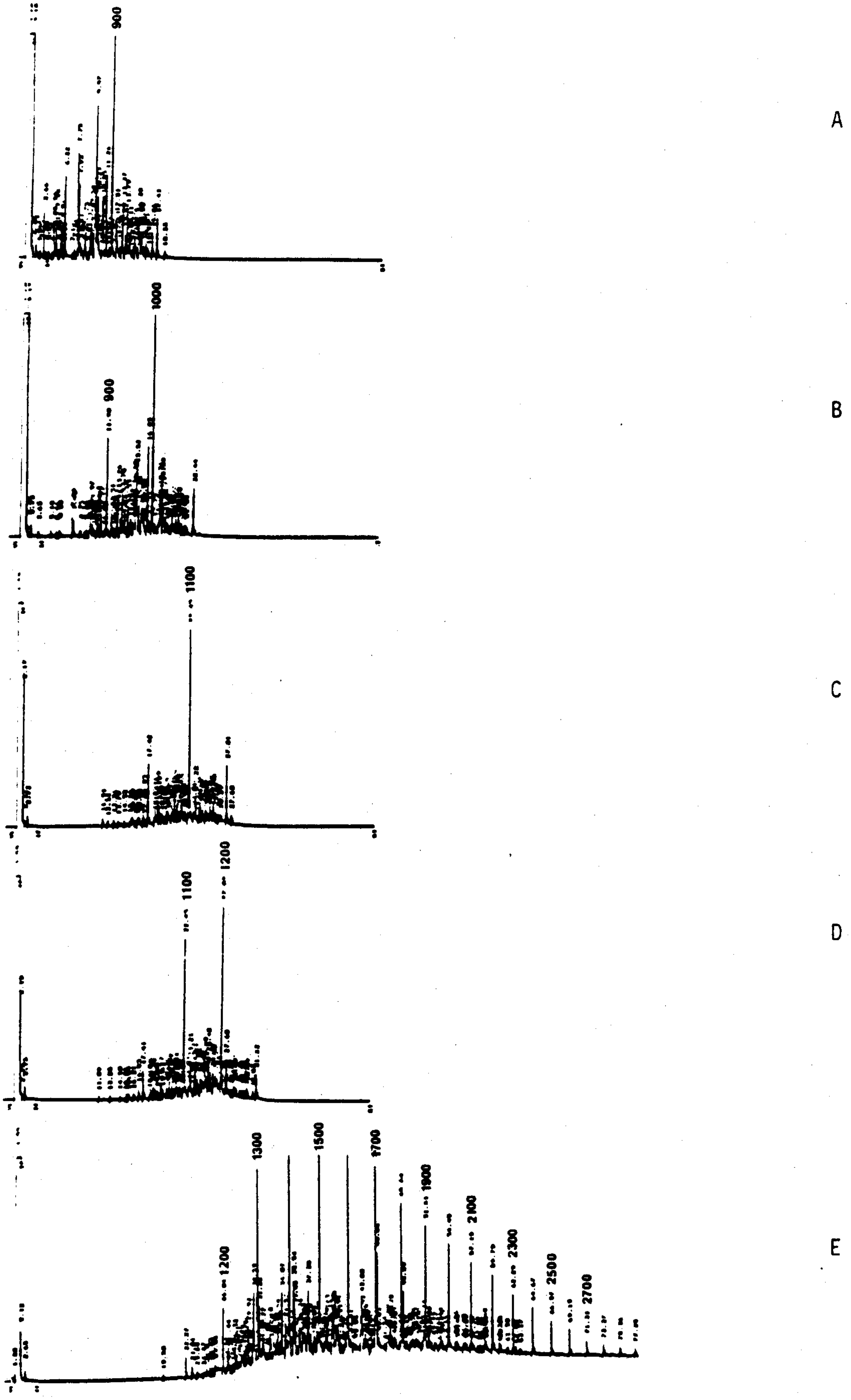

Figure 3-16. GC-FID Chromatograms of Distillate Cuts of Fresh Prudhoe Bay Crude Oil. (A) Cut #7 (282°-304°F), (B) Cut #9 (324°-348°F), (C) Cut #11 (369°-393°F), (D) Cut #12(393°-414°F), and (E) Pot Residue (Bottoms) After Distillation.

nC-10 to nC-12 range present with the majority of mass contributed by nC-11 (KOVAT index 1100). Cut #12 which was the last cut obtained under atmospheric distillation conditions contained a trace of nC-10 with the majority of components observed between nC-11 and nC-13 (Chromatogram D). The chromatogram generated from the still bottom residues for nondistilled residual under atmospheric conditions is shown in Figure 3-16E and in this case all components below nC-11 (KOVAT index 1100) are clearly removed with the majority of the mass of oil made up by the resolved n-alkanes from nC-12 (KOVAT index 1200) through nC-30 (KOVAT index 3000) and the unresolved complex mixture eluting between KOVAT index range 1200 and 2300.

Table 3-16 presents the experimental fractional distillation data obtained on the Prudhoe Bay crude oil sample distilled under atmospheric conditions. Comparison of the experimental data in Table 3-16 with those published by (Petroleum Publishing Co., 1973) shows very close agreement.

3.2 SELECTION OF PRUDHOE BAY CRUDE OIL FOR FURTHER OIL WEATHERING STUDIES

Based on these results, Prudhoe Bay crude oil was selected as being the best candidate for extensive sub-arctic weathering studies. Prudhoe Bay crude oil has an API gravity somewhat lower than the Murban or Cook Inlet crudes, yet its aliphatic fraction is represented by an evenly repeating series of alkanes (unlike the Wilmington crude) which facilitates examination of evaporation, dissolution and microbial degradation processes. Also, Prudhoe Bay crude oil has a relatively high percent asphaltic fraction and intermediate levels of nickel, vanadium, sulfur and nitrogen, making it an ideal oil for extended studies investigating the formation of water-in-oil emulsions or mousse (PAYNE, 1981). As demonstrated by the synchronous scan UV fluorescence data and the selected ion monitoring relative abundance plots for the polynuclear aromatic hydrocarbons, Prudhoe Bay crude oil is intermediate in overall aromatic hydrocarbon composition. On this basis, the Prudhoe Bay crude is a good representative selection for toxicity determinations on weathered crude oil. Finally, while both Cook Inlet crude oil and Prudhoe Bay

Table 3-16. Comparison of Atmospheric Distillation Data for Prudhoe Bay (North Shore) Oil

SAI Cut #	SAI TBP Cut Temp.	SAI Cumulative Volume % Distilled	Published* TBP Cut Temp	Published Cumulative Volume % Distilled
"Lights"	<107°F	1.3	<97°F	2.6
1	107-151	2.9	97-178	
2	151-186	4.7		4.1
3	186-209	6.3	178-214	6.2
4	209-233	8.0	214-242	8.2
5	233-259	9.8	242-270	10.2
6	259-282	11.5	270-296	12.2
7	282-304	13.2	296-313	13.2
8	304-324	14.8	313-342	
9	324-348	16.3		15.2
10	348-369	17.9	342-366	17.1
11	369-393	19.4	366-395	19.1
12	393-414	20.9	395-415	21.1

*Evaluation of World's Important Crudes Petroleum Publishing Co., Tulsa, OK (1973) crude oil have a higher potential of being released in sub-arctic environments, the selection of Prudhoe Bay crude over Cook Inlet crude was supported by the fact that it contains relatively higher levels of the alkyl-substituted dibenzothiophenes.

4.0 OIL WEATHERING MODEL DEVELOPMENT

The objectives for a mathematical model of oil weathering on the ocean surface are to temporally predict both the mass of oil remaining in the slick and the chemical composition and physical properties of the oil slick. These two objectives require that oil composition be described in terms of both specific components and component categories, or "pseudocompounds". Pseudocomponent classification has been widely used in the petroleum industry to describe crude oil because of the inherent interest in bulk oil characteristics and accounting for total mass. A specific-component description is of interest in describing spilled oil as a changing source of foreign chemicals to an aquatic ecosystem, but the complexity of oil composition makes it impractical to keep track of bulk oil mass in terms of individual components.

The open-ocean oil-weathering model presented in this report has been developed over the last three years. Additional stand-alone models have been derived and used to guide experimental and development work, and are presented also. The most developed models are mass transport models which describe evaporation and dissolution processes. These two processes described molecular transport in contrast to the dispersion oil-weathering process. The dispersion process describes the transport of discrete oil drops into the water column due to wind/wave action and other parameters. The models presented here implicitly describe how a pseudocomponent (bulk oil) model provides information that must be used to describe specific component transport. These models incorporate the concepts of interfacial mass transfer, the considerations of both mechanically well-stirred and stagnant oil phases, the effects of slick spreading, and the boundary conditions imposed on the oil by the environment. In addition, these models include descriptive predictions of specific compound concentrations in the air and water columns in contact with a slick or other spilled oil phase.

Both portions of the model require distinct and independent mathematical formulations. In order to predict the mass of oil remaining in a slick as a function of time, a method of characterizing the bulk oil with respect to the various transport processes that alter and dissipate oil must be utilized. The total oil mass cannot be characterized by its individual components because of their number and complexity, and the limitations of analysis. To compensate for these limitations, the pseudo-component approach "cuts" oil into a number of fractions, assigning appropriate physical properties to each.

In attempting to predict the mass of oil remaining in a slick, the two most important mass transport processes to consider are evaporation and dispersion. Of these two, evaporation appears to have the greater influence, certainly over short time scales, making vapor pressure an especially important oil characteristic. Adequate description of the dissolution process, on the other hand, requires water solubility information. The pseudo-component approach to describe these processes is to cut the oil into a number of fractions based on properties of distillation fractions.

The pseudo-component approach, which is that taken in virtually all previous efforts to model oil weathering, is singularly useful for providing a total material balance verses time for spilled oil (especially for slicks). However, this approach does not predict the time-dependent material balance for specific chemical components. In order to obtain component-specific information, component-specific physical properties (e.g., solubilities, vapor pressures and other phase partitioning parameters) must be used. There have been no other functional component-specific models developed previously. Ironically, most of the data generated when an actual oil spill has occurred have been component-specific concentrations across phase boundaries, and virtually no pseudo-component concentration data have been reported.

Although evaporation and dispersion are the oil-weathering processes of most importance during the initial stages of a spill, other longer-term weathering processes destroy and produce compounds to a degree that is important to any component-specific model. In the case of photo or autoxidation, a compound may chemically react to become an aldehyde, ketone, alcohol or acid, all of which are more soluble in the water column that are the precursor hydrocarbon compounds. Similarly, metabolites of microbial degradation have physical properties markedly different from their corresponding parent compounds. Such "fringe" processes, which are not unimportant, are typically more complex than are the evaporation and dispersion processes, increasing the complexity of their mathematical descriptions.

In discussing the segments of the model which follow, three basic aspects have been considered for each oil weathering process:

(1) physical properties (of bulk oil and specific components)

(2) mass balance equations (for specific components and pseudocomponents)

(3) environmental parameters (which the oil encounters upon being spilled)

Physical properties include the thermodynamic and transport characteristics required to describe a particular process. In the cases of evaporation and dissolution, <u>thermodynamic</u> properties are the vapor pressures, Henry's Law coefficients, solubilities, and mixing rules, while the <u>transport</u> properties include diffusivities, viscosities and, again, mixing rules.

4.1 Pseudo-Component Evaporation of Oil

Predicting the quantity of oil in the slick as a function of time requires that a total mass balance approach be used. It is not possible to write a total material balance for crude oil by using component-specific information. If one tries to use component specific information, it soon becomes apparent that all the components in crude oil will never be identified, thus precluding an accounting of the total mass of the oil. No predictive equations have ever been successfully developed based on specific components where the purpose of prediction was a total mass balance for oil.

The question then is raised as to how one uses bulk properties of the oil to make specific predictions? The petroleum industry refers to these bulk properties of oil as "characterization parameters". The characterization of an oil must be done with respect to a specific prediction as the objective. For example, when the prediction (process design or mathematical model) is a process that involves vapor-liquid transport, the characteristic parameters are then vapor pressures or partial pressures. When the prediction is the performance of a catalytic reformer where naphthas are converted to aromatics, the characteristics required on the catalytic reformer feedstock are combined contents of paraffins-olefins-naphthas-aromatics, referred to as PONA. Kinetic equations use PONA values as starting concentrations along with kinetic constants to predict the product from the catalytic reforming process. Both these examples illustrate a pseudo-component model, sometimes referred to as a "lumped" model.

In predicting the mass of oil remaining in an oil slick as a function of time as evaporation proceeds, characterization of the oil must be with respect to vapor pressure. An overall mass balance utilizes the vapor pressure and environmental parameters to predict loss of oil and, therefore, mass of oil remaining in the slick. The following discussion considers: 1) the procedure for characterizing crude oils with respect to pseudo-component vapor pressures and 2) the pertinent equations for the overall mass balance as they apply to the use of the overall oil weathering model.

4.1.1 Pseudo-Component Characterization of Crude Oil

The standard inspections on a crude oil include distillation, density of the distillate cuts, and viscosity of the distillate cuts. There are virtually no component-specific data that can be obtained which will allow adequate prediction of the bulk properties of the oil. The standard distillation data come from either a true boiling point (TBP) distillation or an ASTM (American Society for Test and Materials) D-86 distillation; both are usually carried out at one atmosphere total pressure. Each of these distillations can be carried out at 40 mm Hg total pressure to obtain information on the less volatile fractions of the oil.

Either distillation is conducted in a manner such that the distillate fractions are collected separately (i.e., the fraction distilling at 50 to 75°C is physically separated from the fraction distilling at 75 to 100°C). The total number of fractions collected is usually five to seven, but can be as many as 20. Characteristic data for the distillate fractions include the temperatures at the beginning and end of each fraction (or "cut"), sometimes in the form of a continuous curve of temperature vs percent distillate. The API (American Petroleum Institute) gravity for each cut is then measured, as is occasionally the viscosity of each cut.

Given the boiling point (1 atm) and API gravity of each cut (or pseudo-component), the vapor pressure of the cut as a function of temperature can be calculated. First, the molecular weight and critical temperature of the cut are calculated according to the following correlation (FALLON and WATSON, 1944):

$$y = C_1 + C_2X_1 + C_3X_2 + C_4X_1X_2 + C_5X_1^2 + C_6X_2^2 \tag{4.1}$$

where X_1 is the boiling point (°F) at one atmosphere, X_2 is the API gravity, and the constants C_1 to C_5 have the values indicated in Table 4-1. Similarly, the critical temperature can be calculated from the same equation form using the indicated constant values in Table 4-1.

Next the equivalent paraffin carbon number is calculated according to (GAMSON and WATSON, 1944):

$$N_c = (MW - 2)/14 \tag{4.2}$$

TABLE 4-1. CORRELATION EQUATION CONSTANTS FOR THE CHARACTERIZATION OF NARROW BOILING PETROLEUM FRACTIONS (see text for equation form).

PROPERTY	C_1	C_2	C_3	C_4	C_5	C_6
Molecular weight $t_b \leq 500°F$	6.241E+01	-4.595E-02	-2.836E-01	3.256E-03	4.578E-04	5.279E-04
Molecular weight $t_b > 500$	4.268E+02	-1.007	-7.491	1.380E-02	1.047E-03	2.621E-02
Critical temperature $t_b \leq 500$	4.055E+02	1.337	-2.662	-2.169E-03	-4.943E-04	1.454E-02
Critical temperature $t_b > 500$	4.122E+02	1.276	-2.865	-2.888E-03	-3.707E-04	2.288E-02
b'	1.237E-02	2.516E-01	4.039E-02	-4.024E-02	-----	-----
Kinematic vis, cs @ 122°F API $\leq$ 35	-4.488E-01	-9.344E-04	1.583E-02	-5.219E-05	5.2688-06	1.536E-04
Kinematic vis, cs @ 122°F API > 35	-6.019E-01	1.793E-03	-3.159E-03	-5.1E-06	9.067E-07	3.522E-05

The critical volume is then calculated according to:

$$V_c = (1.88 + 2.44N_c)/0.044 \tag{4.3}$$

and the critical pressure is calculated from:

$$P_c = \frac{20.8T_c}{(V_c - 8)} + P_c' \tag{4.4}$$

where $P_c' = 10$ to correct the critical pressure correlation from a strictly paraffinic mixture to a naphtha-aromatic-paraffin mixture. Next a parameter (b) is calculated according to

$$b = b' - 0.02 \tag{4.5}$$

where

$$b' = C_1 + C_2N_c + C_3N_c^2 + C_4N_c^3 \tag{4.6}$$

and the values of the constants C_1 to C_4 are indicated in Table 4.1.

A final parameter designated as A is then calculated according to:

$$A = \frac{T_{r_b}}{T_{r_b} - 1} \left\{ \log_{10} (P_{r_b}) + \exp\left[-20(T_{r_b} - b)^2\right] \right\} \tag{4.7}$$

where T_{r_b} and P_{r_b} are the reduced temperature and pressure at the normal boiling point. The vapor pressure equation which can be used down to 10 mm Hg is:

$$\log_{10} P_r = \frac{-A(1 - T_r)}{T_r} - \exp\left[-20(T_r - b)^2\right] \tag{4.8}$$

where A, b, T_c and P_c were determined from the normal boiling point and API gravity of the cut. The temperature at which the vapor pressure is 10 mm Hg can be obtained by the root-finding algorithm of Newton-Raphson.

Below 10 mm Hg, the vapor pressure is calculated according to the Clausius-Clapeyron equation as follows (GAMSON and WATSON, 1944):

$$\ln \frac{P_2}{P_1} = \frac{\lambda_0}{RT_c} \int_{T_{r_1}}^{T_{r_2}} \frac{(1 - Tr)^{0.38}}{T_r^{\,2}} \, dT_r \tag{4.9}$$

and is based on the law which states the ratio of the heat of vaporization, λ, to $(1 - T_r)^{0.38}$ is a constant at any temperature. The latent heat of vaporization is calculated from the slope of the natural log of the vapor pressure equation with respect to the temperature at the temperature where the vapor pressure is 10 mm Hg. Thus, in the above equation, P_2 is the 10 mm Hg vapor pressure at the temperature, T_r, previously determined.

A sample calculation for the characterization of Prudhoe Bay crude oil is presented in Tables 4-2 and 4-3A. Table 4-2 presents the standard inspections (COLEMAN, 1978; PPC, 1973) for the crude and is the starting point for the characterization calculations. Note that the distillation in Table 4-2 was conducted at 40 mm Hg for cuts 11 to 15. Thus, these cut temperatures must be corrected to one atmosphere (API, 1976). Table 4-3A presents the computer generated output along with the corrected cut temperatures. The characterizations of Cook Inlet, Murban, and Wilmington crudes are presented in Tables 4-3B through 4-3D, and the vapor pressures at 55°F calculated from these characterizations are presented in Table 4-4 for all four crudes.

Table 4-2 STANDARD INSPECTIONS FOR PRUDHOE BAY CRUDE OIL (COLEMAN, 1978)

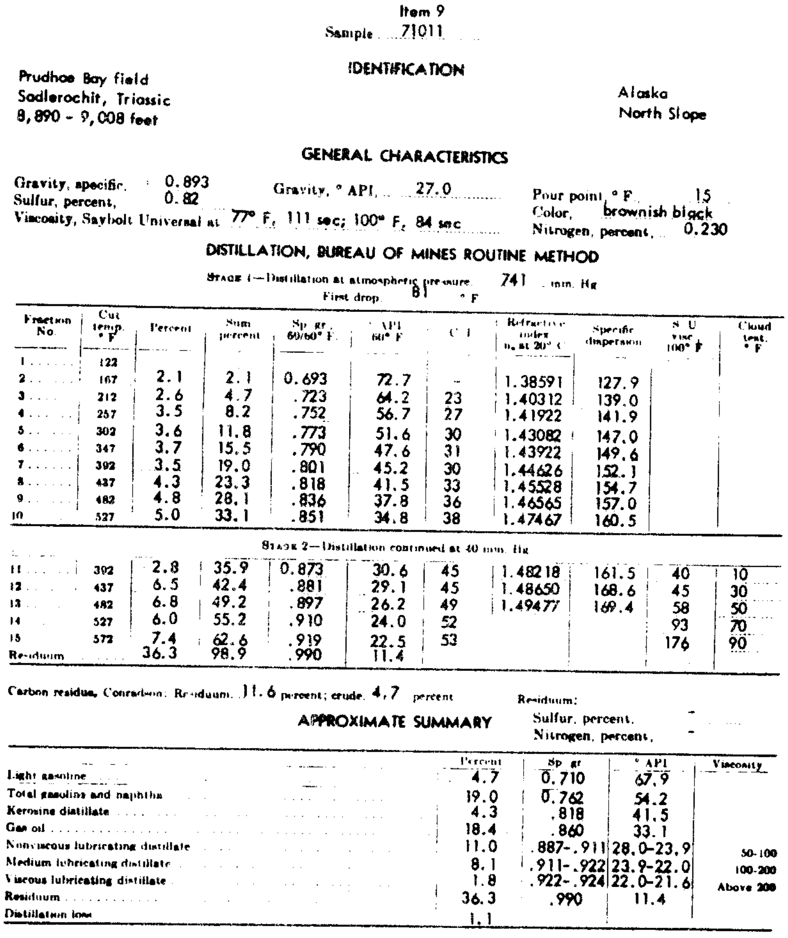

Item 9
Sample 71011

IDENTIFICATION

Prudhoe Bay field
Sodlerochit, Triassic
8,890 - 9,008 feet

Alaska
North Slope

GENERAL CHARACTERISTICS

Gravity, specific, 0.893
Gravity, ° API, 27.0
Pour point, ° F, 15
Sulfur, percent, 0.82
Color, brownish black
Viscosity, Saybolt Universal at 77° F, 111 sec; 100° F, 84 sec
Nitrogen, percent, 0.230

DISTILLATION, BUREAU OF MINES ROUTINE METHOD

Stage 1—Distillation at atmospheric pressure, 741 mm. Hg
First drop, 81 ° F

Fraction No.	Cut temp. ° F	Percent	Sum percent	Sp. gr., 60/60° F.	° API 60° F	C. I.	Refractive index n_D at 20° C	Specific dispersion	S. U. visc. 100° F	Cloud test, ° F
1	122									
2	167	2.1	2.1	0.693	72.7	--	1.38591	127.9		
3	212	2.6	4.7	.723	64.2	23	1.40312	139.0		
4	257	3.5	8.2	.752	56.7	27	1.41922	141.9		
5	302	3.6	11.8	.773	51.6	30	1.43082	147.0		
6	347	3.7	15.5	.790	47.6	31	1.43922	149.6		
7	392	3.5	19.0	.801	45.2	30	1.44626	152.1		
8	437	4.3	23.3	.818	41.5	33	1.45528	154.7		
9	482	4.8	28.1	.836	37.8	36	1.46565	157.0		
10	527	5.0	33.1	.851	34.8	38	1.47467	160.5		

Stage 2—Distillation continued at 40 mm. Hg

Fraction No.	Cut temp. ° F	Percent	Sum percent	Sp. gr., 60/60° F.	° API 60° F	C. I.	Refractive index n_D at 20° C	Specific dispersion	S. U. visc. 100° F	Cloud test, ° F
11	392	2.8	35.9	0.873	30.6	45	1.48218	161.5	40	10
12	437	6.5	42.4	.881	29.1	45	1.48650	168.6	45	30
13	482	6.8	49.2	.897	26.2	49	1.49477	169.4	58	50
14	527	6.0	55.2	.910	24.0	52			93	70
15	572	7.4	62.6	.919	22.5	53			176	90
Residuum		36.3	98.9	.990	11.4					

Carbon residue, Conradson: Residuum, 11.6 percent; crude, 4.7 percent

Residuum:
Sulfur, percent, -
Nitrogen, percent, -

APPROXIMATE SUMMARY

	Percent	Sp. gr.	° API	Viscosity
Light gasoline	4.7	0.710	67.9	
Total gasoline and naphtha	19.0	0.762	54.2	
Kerosine distillate	4.3	.818	41.5	
Gas oil	18.4	.860	33.1	
Nonviscous lubricating distillate	11.0	.887-.911	28.0-23.9	50-100
Medium lubricating distillate	8.1	.911-.922	23.9-22.0	100-200
Viscous lubricating distillate	1.8	.922-.924	22.0-21.6	Above 200
Residuum	36.3	.990	11.4	
Distillation loss	1.1			

Table 4-3A CHARACTERIZATION OF TBP DISTILLATE CUTS FROM PRUDHOE BAY CRUDE OIL

```
CODE VERSION IS CUTVP2 OF FEBRUARY 83
ITEM      9, SAMPLE 71011

       TB        API       SPGR        VOL        MW         TC         PC         VC          A          B         T10        VIS     NC NS
 1  1.67E+02  7.27E+01  6.81E-01  2.12E+00  8.92E+01  9.31E+02  3.83E+01  3.88E+02  3.23E+00  1.98E-01  4.60E+02  4.14E-01   3  1
 2  2.12E+02  6.42E+01  7.11E-01  2.63E+00  1.02E+02  9.85E+02  3.65E+01  4.37E+02  3.31E+00  2.11E-01  4.96E+02  4.92E-01   3  1
 3  2.57E+02  5.67E+01  7.39E-01  3.54E+00  1.14E+02  1.04E+03  3.51E+01  4.86E+02  3.39E+00  2.23E-01  5.31E+02  6.01E-01   3  1
 4  3.02E+02  5.16E+01  7.60E-01  3.64E+00  1.28E+02  1.09E+03  3.36E+01  5.41E+02  3.49E+00  2.34E-01  5.68E+02  7.47E-01   3  1
 5  3.47E+02  4.76E+01  7.77E-01  3.74E+00  1.43E+02  1.14E+03  3.22E+01  6.01E+02  3.61E+00  2.45E-01  6.04E+02  9.43E-01   3  1
 6  3.92E+02  4.52E+01  7.87E-01  3.54E+00  1.61E+02  1.18E+03  3.06E+01  6.71E+02  3.77E+00  2.55E-01  6.42E+02  1.20E+00   3  1
 7  4.37E+02  4.15E+01  8.04E-01  4.35E+00  1.78E+02  1.23E+03  2.94E+01  7.40E+02  3.91E+00  2.64E-01  6.80E+02  1.56E+00   3  1
 8  4.82E+02  3.78E+01  8.22E-01  4.85E+00  1.96E+02  1.27E+03  2.83E+01  8.11E+02  4.06E+00  2.72E-01  7.18E+02  2.05E+00   3  1
 9  5.27E+02  3.48E+01  8.36E-01  5.06E+00  2.12E+02  1.32E+03  2.76E+01  8.77E+02  4.18E+00  2.79E-01  7.55E+02  2.00E+00   3  1
10  5.80E+02  3.06E+01  8.58E-01  2.83E+00  2.36E+02  1.37E+03  2.65E+01  9.71E+02  4.37E+00  2.87E-01  8.01E+02  3.04E+00   3  1
11  6.38E+02  2.91E+01  8.66E-01  6.57E+00  2.72E+02  1.42E+03  2.49E+01  1.11E+03  4.68E+00  2.97E-01  8.53E+02  5.26E+00   3  1
12  6.85E+02  2.62E+01  8.82E-01  6.88E+00  2.99E+02  1.46E+03  2.40E+01  1.22E+03  4.89E+00  3.03E-01  8.95E+02  9.26E+00   3  1
13  7.38E+02  2.40E+01  8.94E-01  6.07E+00  3.35E+02  1.51E+03  2.29E+01  1.36E+03  5.20E+00  3.10E-01  9.44E+02  1.88E+01   3  1
14  7.90E+02  2.25E+01  9.03E-01  7.48E+00  3.76E+02  1.55E+03  2.18E+01  1.52E+03  5.58E+00  3.17E-01  9.94E+02  4.05E+01   3  1
15  8.50E+02  1.14E+01  9.73E-01  3.67E+01  6.00E+02  0.00E+00  0.00E+00  0.00E+00  0.00E+00  0.00E+00  0.00E+00  1.81E+02   0  0

BULK API GRAVITY =  27.0

TB = NORMAL BOILING TEMPERATURE, DEG F
API = API GRAVITY
VOL = VOLUME PER CENT OF TOTAL CRUDE
MW = MOLECULAR WEIGHT
TC = CRITICAL TEMPERATURE, DEG RANKINE
PC = CRITICAL PRESSURE, ATMOSPHERES
VC = CRITICAL VOLUME, CC/MOLE
A AND B ARE PARAMETERS IN THE VAPOR PRESSURE EQUATION
T10 IS THE TEMPERATURE IN DEG R WHERE THE VAPOR PRESSURE IS 10 MM HG
VIS IS THE KINEMATIC VISCOSITY IN CENTISTOKES AT 122 DEG F
NC = ERROR CODE, SHOULD BE LESS THAN 20
NS = ERROR CODE, SHOULD BE EQUAL TO 1
IGNORE THE ERROR CODES FOR COMPONENT NUMBER 15 IF IT IS A RESIDUUM
```

Table 4-3B CHARACTERIZATION OF TBP DISTILLATE CUTS FROM COOK INLET CRUDE OIL

```
CODE VERSION IS CUTVP2 OF FEBRUARY 83
ITEM     7, SAMPLE 72025

        TB        API       SPGR       VOL        MW         TC         PC         VC         A          B          T10        VIS     NC NS
 1   1.22E+02  8.92E+01  6.30E-01  2.48E+00  7.80E+01  8.75E+02  4.01E+01  3.44E+02  3.15E+00  1.83E-01  4.25E+02  3.74E-01  3  1
 2   1.67E+02  7.72E+01  6.66E-01  2.58E+00  9.07E+01  9.27E+02  3.77E+01  3.94E+02  3.25E+00  1.99E-01  4.61E+02  4.20E-01  3  1
 3   2.12E+02  6.50E+01  7.08E-01  6.09E+00  1.02E+02  9.84E+02  3.64E+01  4.38E+02  3.32E+00  2.12E-01  4.96E+02  4.92E-01  3  1
 4   2.57E+02  5.95E+01  7.28E-01  6.30E+00  1.16E+02  1.04E+03  3.47E+01  4.93E+02  3.42E+00  2.24E-01  5.32E+02  5.99E-01  3  1
 5   3.02E+02  5.54E+01  7.44E-01  5.26E+00  1.31E+02  1.08E+03  3.30E+01  5.52E+02  3.55E+00  2.36E-01  5.69E+02  7.41E-01  3  1
 6   3.47E+02  5.08E+01  7.63E-01  5.37E+00  1.46E+02  1.13E+03  3.16E+01  6.13E+02  3.67E+00  2.47E-01  6.05E+02  9.33E-01  3  1
 7   3.92E+02  4.65E+01  7.81E-01  5.06E+00  1.62E+02  1.18E+03  3.04E+01  6.77E+02  3.79E+00  2.56E-01  6.43E+02  1.19E+00  3  1
 8   4.37E+02  4.30E+01  7.97E-01  5.26E+00  1.80E+02  1.23E+03  2.92E+01  7.47E+02  3.94E+00  2.65E-01  6.80E+02  1.54E+00  3  1
 9   4.82E+02  3.96E+01  8.13E-01  5.37E+00  1.98E+02  1.27E+03  2.81E+01  8.21E+02  4.10E+00  2.73E-01  7.19E+02  2.02E+00  3  1
10   5.27E+02  3.70E+01  8.25E-01  5.16E+00  2.16E+02  1.32E+03  2.72E+01  8.91E+02  4.23E+00  2.80E-01  7.56E+02  2.67E+00  3  1
11   5.80E+02  3.28E+01  8.47E-01  3.41E+00  2.41E+02  1.37E+03  2.61E+01  9.91E+02  4.43E+00  2.89E-01  8.02E+02  2.97E+00  3  1
12   6.38E+02  3.13E+01  8.54E-01  5.37E+00  2.79E+02  1.42E+03  2.45E+01  1.14E+03  4.75E+00  2.99E-01  8.55E+02  5.05E+00  3  1
13   6.85E+02  2.87E+01  8.68E-01  7.22E+00  3.07E+02  1.46E+03  2.35E+01  1.25E+03  4.99E+00  3.05E-01  8.97E+02  8.67E+00  3  1
14   7.38E+02  2.66E+01  8.80E-01  4.33E+00  3.45E+02  1.50E+03  2.24E+01  1.40E+03  5.33E+00  3.12E-01  9.47E+02  1.72E+01  3  1
15   7.90E+02  2.50E+01  8.89E-01  4.33E+00  3.87E+02  1.54E+03  2.14E+01  1.57E+03  5.73E+00  3.18E-01  9.98E+02  3.65E+01  3  1
16   8.50E+02  1.16E+01  9.72E-01  2.64E+01  6.00E+02  0.00E+00  0.00E+00  0.00E+00  0.00E+00  0.00E+00  0.00E+00  1.79E+02  0  0

BULK API GRAVITY =  35.4

TB = NORMAL BOILING TEMPERATURE, DEG F
API = API GRAVITY
VOL = VOLUME PER CENT OF TOTAL CRUDE
MW = MOLECULAR WEIGHT
TC = CRITICAL TEMPERATURE, DEG RANKINE
PC = CRITICAL PRESSURE, ATMOSPHERES
VC = CRITICAL VOLUME, CC/MOLE
A AND B ARE PARAMETERS IN THE VAPOR PRESSURE EQUATION
T10 IS THE TEMPERATURE IN DEG R WHERE THE VAPOR PRESSURE IS 10 MM HG
VIS IS THE KINEMATIC VISCOSITY IN CENTISTOKES AT 122 DEG F
NC = ERROR CODE, SHOULD BE LESS THAN 20
NS = ERROR CODE, SHOULD BE EQUAL TO 1
IGNORE THE ERROR CODES FOR COMPONENT NUMBER 16 IF IT IS A RESIDUUM
```

Table 4-3C CHARACTERIZATION OF TBP DISTILLATE CUTS FROM MURBAN CRUDE OIL

```
CODE VERSION IS CUTVP2 OF FEBRUARY 83
ITEM 99999, SAMPLE 99999
        TB        API       SPGR      VOL       MW        TC        PC        VC        A         B         T10       VIS     NC NS
 1  1.22E+02  9.67E+01  6.10E-01  1.71E+00  7.95E+01  8.73E+02  3.95E+01  3.58E+02  3.16E+00  1.85E-01  4.25E+02  3.93E-01  3  1
 2  1.67E+02  8.62E+01  6.39E-01  2.91E+00  9.39E+01  9.21E+02  3.67E+01  4.07E+02  3.29E+00  2.03E-01  4.62E+02  4.35E-01  3  1
 3  2.12E+02  7.06E+01  6.80E-01  4.91E+00  1.05E+02  9.78E+02  3.56E+01  4.49E+02  3.37E+00  2.14E-01  4.97E+02  4.96E-01  3  1
 4  2.57E+02  6.23E+01  7.18E-01  6.02E+00  1.17E+02  1.03E+03  3.42E+01  5.00E+02  3.46E+00  2.26E-01  5.33E+02  5.98E-01  3  1
 5  3.02E+02  5.57E+01  7.43E-01  6.82E+00  1.31E+02  1.08E+03  3.30E+01  5.53E+02  3.55E+00  2.36E-01  5.69E+02  7.41E-01  3  1
 6  3.47E+02  5.16E+01  7.60E-01  6.52E+00  1.47E+02  1.13E+03  3.15E+01  6.16E+02  3.68E+00  2.47E-01  6.06E+02  9.31E-01  3  1
 7  3.92E+02  4.85E+01  7.73E-01  5.72E+00  1.64E+02  1.18E+03  3.01E+01  6.85E+02  3.83E+00  2.57E-01  6.43E+02  1.18E+00  3  1
 8  4.37E+02  4.56E+01  7.85E-01  5.62E+00  1.83E+02  1.22E+03  2.88E+01  7.59E+02  4.00E+00  2.67E-01  6.81E+02  1.52E+00  3  1
 9  4.82E+02  4.30E+01  7.97E-01  6.02E+00  2.03E+02  1.26E+03  2.76E+01  8.30E+02  4.19E+00  2.75E-01  7.20E+02  1.98E+00  3  1
10  5.27E+02  4.00E+01  8.11E-01  4.91E+00  2.22E+02  1.31E+03  2.67E+01  9.13E+02  4.29E+00  2.82E-01  7.57E+02  2.61E+00  3  1
11  5.80E+02  3.58E+01  8.31E-01  5.72E+00  2.48E+02  1.36E+03  2.56E+01  1.02E+03  4.50E+00  2.91E-01  8.04E+02  3.71E+00  3  1
12  6.38E+02  3.40E+01  8.40E-01  5.62E+00  2.87E+02  1.41E+03  2.40E+01  1.17E+03  4.84E+00  3.01E-01  8.57E+02  4.82E+00  3  1
13  6.85E+02  3.00E+01  8.61E-01  6.52E+00  3.12E+02  1.45E+03  2.33E+01  1.27E+03  5.04E+00  3.06E-01  8.98E+02  8.39E+00  3  1
14  7.38E+02  2.84E+01  8.70E-01  6.02E+00  3.53E+02  1.49E+03  2.21E+01  1.43E+03  5.41E+00  3.13E-01  9.49E+02  1.62E+01  3  1
15  7.90E+02  2.66E+01  8.80E-01  5.62E+00  3.95E+02  1.53E+03  2.11E+01  1.60E+03  5.83E+00  3.19E-01  1.00E+03  3.42E+01  3  1
16  8.50E+02  1.67E+01  9.39E-01  1.94E+01  6.00E+02  0.00E+00  0.00E+00  0.00E+00  0.00E+00  0.00E+00  0.00E+00  1.35E+02  0  0

BULK API GRAVITY =  40.5

TB = NORMAL BOILING TEMPERATURE, DEG F
API = API GRAVITY
VOL = VOLUME PER CENT OF TOTAL CRUDE
MW = MOLECULAR WEIGHT
TC = CRITICAL TEMPERATURE, DEG RANKINE
PC = CRITICAL PRESSURE, ATMOSPHERES
VC = CRITICAL VOLUME, CC/MOLE
A AND B ARE PARAMETERS IN THE VAPOR PRESSURE EQUATION
T10 IS THE TEMPERATURE IN DEG R WHERE THE VAPOR PRESSURE IS 10 MM HG
VIS IS THE KINEMATIC VISCOSITY IN CENTISTOKES AT 122 DEG F
NC = ERROR CODE, SHOULD BE LESS THAN 20
NS = ERROR CODE, SHOULD BE EQUAL TO 1
IGNORE THE ERROR CODES FOR COMPONENT NUMBER 16 IF IT IS A RESIDUUM
```

Table 4-3D CHARACTERIZATION OF TBP DISTILLATE CUTS FROM WILMINGTON CRUDE OIL

```
CODE VERSION IS CUTVP2 OF FEBRUARY 83
ITEM     94, SAMPLE 71052
                                                                                                         VC          A           B          T10         VIS      NC NS
        TB         API        SPGR        VOL         MW         TC          PC
  1  2.12E+02  6.86E+01  6.95E-01  2.31E+00  1.04E+02  9.80E+02  3.59E+01  4.45E+02  3.35E+00  2.13E-01  4.97E+02  4.94E-01  3  1
  2  2.57E+02  5.87E+01  7.31E-01  2.41E+00  1.15E+02  1.04E+03  3.40E+01  4.91E+02  3.41E+00  2.24E-01  5.32E+02  5.99E-01  3  1
  3  3.02E+02  5.30E+01  7.54E-01  2.41E+00  1.29E+02  1.09E+03  3.34E+01  5.45E+02  3.51E+00  2.35E-01  5.68E+02  7.45E-01  3  1
  4  3.47E+02  4.81E+01  7.74E-01  2.51E+00  1.44E+02  1.14E+03  3.21E+01  6.03E+02  3.62E+00  2.45E-01  6.05E+02  9.42E-01  3  1
  5  3.92E+02  4.32E+01  7.96E-01  2.81E+00  1.59E+02  1.19E+03  3.10E+01  6.63E+02  3.73E+00  2.54E-01  6.41E+02  1.21E+00  3  1
  6  4.37E+02  3.80E+01  8.17E-01  3.61E+00  1.75E+02  1.24E+03  2.99E+01  7.27E+02  3.85E+00  2.63E-01  6.78E+02  1.58E+00  3  1
  7  4.82E+02  3.54E+01  8.33E-01  4.42E+00  1.93E+02  1.28E+03  2.87E+01  7.98E+02  4.00E+00  2.71E-01  7.16E+02  2.00E+00  3  1
  8  5.27E+02  3.23E+01  8.49E-01  5.32E+00  2.09E+02  1.33E+03  2.80E+01  8.61E+02  4.12E+00  2.77E-01  7.54E+02  2.02E+00  3  1
  9  5.80E+02  2.68E+01  8.79E-01  4.72E+00  2.29E+02  1.39E+03  2.72E+01  9.40E+02  4.26E+00  2.85E-01  7.98E+02  3.20E+00  3  1
 10  6.30E+02  2.45E+01  8.92E-01  6.33E+00  2.59E+02  1.44E+03  2.57E+01  1.06E+03  4.52E+00  2.94E-01  8.49E+02  5.80E+00  3  1
 11  6.85E+02  2.23E+01  9.04E-01  4.12E+00  2.86E+02  1.48E+03  2.47E+01  1.17E+03  4.74E+00  3.00E-01  8.91E+02  1.04E+01  3  1
 12  7.30E+02  2.03E+01  9.16E-01  5.52E+00  3.20E+02  1.52E+03  2.36E+01  1.30E+03  5.03E+00  3.08E-01  9.40E+02  2.16E+01  3  1
 13  8.50E+02  8.90E+00  9.91E-01  5.35E+01  6.00E+02  0.00E+00  0.00E+00  0.00E+00  0.00E+00  0.00E+00  0.00E+00  2.10E+02  0  0

BULK API GRAVITY =  19.4

TB = NORMAL BOILING TEMPERATURE, DEG F
API = API GRAVITY
VOL = VOLUME PER CENT OF TOTAL CRUDE
MW = MOLECULAR WEIGHT
TC = CRITICAL TEMPERATURE, DEG RANKINE
PC = CRITICAL PRESSURE, ATMOSPHERES
VC = CRITICAL VOLUME, CC/MOLE
A AND B ARE PARAMETERS IN THE VAPOR PRESSURE EQUATION
T10 IS THE TEMPERATURE IN DEG R WHERE THE VAPOR PRESSURE IS 10 MM HG
VIS IS THE KINEMATIC VISCOSITY IN CENTISTOKES AT 122 DEG F
NC = ERROR CODE, SHOULD BE LESS THAN 20
NS = ERROR CODE, SHOULD BE EQUAL TO 1
IGNORE THE ERROR CODES FOR COMPONENT NUMBER 13 IF IT IS A RESIDUUM
```

Table 4-4 VAPOR PRESSURE OF TBP DISTILLATE CUTS FOR FOUR CRUDE OILS

```
CRUDE OIL CHARACTERIZATION AND PSEUDOCOMPONENT EVAPORATION MODEL
IDENTIFICATION: WILMINGTON, CALIFORNIA

ITEM     94, SAMPLE 71052
VAPOR PRESSURE IN ATMOSPHERES AT  5.540E+01 DEG F

          VP

 1      2.389E-02
 2      6.720E-03
 3      1.613E-03
 4      3.583E-04
 5      7.427E-05
 6      1.411E-05
 7      2.361E-06
 8      3.822E-07
 9      4.110E-08
10      2.372E-09
11      1.997E-10
12      9.010E-12

MEAN MOLECULAR WEIGHT OF THE CRUDE =  3.206E+02
```

```
CRUDE OIL CHARACTERIZATION AND PSEUDOCOMPONENT EVAPORATION MODEL
IDENTIFICATION: NURBAN, ABU DHABI

ITEM 99999, SAMPLE 99999
VAPOR PRESSURE IN ATMOSPHERES AT  5.540E+01 DEC F

          VP

 1      2.279E-01
 2      7.565E-02
 3      2.368E-02
 4      6.517E-03
 5      1.555E-03
 6      3.350E-04
 7      6.459E-05
 8      1.110E-05
 9      1.657E-06
10      2.699E-07
11      2.295E-08
12      1.901E-09
13      7.944E-11
14      2.403E-12
15      4.950E-14

MEAN MOLECULAR WEIGHT OF THE CRUDE =  2.158E+02
```

```
CRUDE OIL CHARACTERIZATION AND PSEUDOCOMPONENT EVAPORATION MODEL.
IDENTIFICATION: COOK INLET, ALASKA

ITEM      7, SAMPLE 72025
VAPOR PRESSURE IN ATMOSPHERES AT  5.540E+01 DEG F

          VP

 1      2.280E-01
 2      7.673E-02
 3      2.430E-02
 4      6.680E-03
 5      1.561E-03
 6      3.402E-04
 7      6.809E-05
 8      1.217E-05
 9      1.945E-06
10      3.071E-07
11      2.770E-08
12      1.275E-09
13      9.292E-11
14      3.248E-12
15      7.181E-14

MEAN MOLECULAR WEIGHT OF THE CRUDE =  2.206E+02
```

```
CRUDE OIL CHARACTERIZATION AND PSEUDOCOMPONENT EVAPORATION MODEL
IDENTIFICATION: PRUDHOE BAY, ALASKA

ITEM      9, SAMPLE 71011
VAPOR PRESSURE IN ATMOSPHERES AT  5.540E+01 DEC F

          VP

 1      7.751E-02
 2      2.440E-02
 3      6.852E-03
 4      1.644E-03
 5      3.617E-04
 6      7.046E-05
 7      1.283E-05
 8      2.115E-06
 9      3.394E-07
10      3.193E-08
11      1.556E-09
12      1.255E-10
13      4.983E-12
14      1.264E-13

MEAN MOLECULAR WEIGHT OF THE CRUDE =  2.739E+02
```

4.1.2 Pseudo-Component Evaporation Model on the Ocean Surface

The evaporation model which predicts the oil remaining in a slick is derived from the physical properties of the oil cuts and a total material balance. From the previous discussion a number of pseudo-components are defined. For each pseudo-component the vapor pressure, molecular weight and initial quantity are known, and a material balance can be written to include each:

$$\frac{dM_i}{dt} = -K_i A X_i P_i^* \quad \text{for } i = 1, 2, \ldots\ldots\ldots \begin{array}{l}\text{total number}\\ \text{of components}\end{array} \tag{4.10}$$

where it is assumed that the oil slick is well stirred and a pseudo-Raoult's law applies as the mixing rule. In this rate equation, M_i is the number of moles of component i in the oil slick, P_i^* is the vapor pressure at the prevailing environmental temperature, A is the area of the slick, K_i is an over-all mass-transfer coefficient based on partial pressure driving forces, and x_i is the mole fraction of component i in the slick. The differential equations are all coupled through the mole fraction term where the total number of moles appears in the denominator.

The over-all mass-transfer coefficient can be calculated two different ways. One way is the approach of MACKAY and MATSUGU, 1976.

$$K = 0.0292\ U^{0.78}\ X^{-0.11}\ Sc^{-0.67} \tag{4.11}$$

where U is the wind velocity in m/hr, X is the slick diameter (assumes circular slick), and Sc is the Schmidt number (2.7). This expression is a correlation and is the proper mass transfer coefficient to multiply by the partial pressure to obtain the rate. Here K is specific to a particular cut i through the Schmidt number.

Implicit in the rate equation for the i-th component is the assumption that the partial pressure in the bulk atmosphere is zero. It can then be seen that the mass transfer coefficient above takes into account (through the X term) an averaging effect whereby the evaporation rate on the downwind portion of the slick is lower than the upwind portion due to the fact that P_i becomes finite in the air immediately over the oil slick in the down-wind direction.

Another approach to calculating overall mass transfer coefficients is that of TREYBAL, 1955, and LISS, 1974:

$$\frac{1}{K_g} = \frac{1}{k_g} + \frac{H^*}{k_\ell} \tag{4.12}$$

where k_g is the individual gas-phase mass-transfer coefficient, k_ℓ is the individual liquid-phase mass-transfer coefficient and H* is the Henry's law coefficient which is defined by:

$$P_i \equiv H^* x_i \tag{4.13}$$

The units on k_g for a <u>partial pressure</u> driving force are typically moles/(m^2 · hr · atm), the units on k_g for a <u>mole fraction</u> driving force are moles/(m^2 · hr), and the units on H* are atm. The individual mass transfer coefficients, k_ℓ and k_g, must then be obtained from actual data in a manner similar to that used to deduce K in equation (4.11).

The other bulk property of interest for the oil slick is its viscosity. When oil is spilled on the ocean surface, the viscosity is low enough so that mixing occurs and the well-mixed oil-phase assumption is valid. However, as evaporation occurs the viscosity increases because the low-viscosity fractions are removed. The viscosity "blending" relationship used to predict the bulk viscosity as a function of composition is:

$$\frac{\mu}{\mu_o} = \exp(K_4F) \tag{4.14a}$$

where μ_o is the viscosity of the unweathered oil at 25°C, F is the fraction weathered (i.e., how much has evaporated and dissolved), and K_4 is an oil-dependent constant (TEBEAU, et al., 1982). Previously, a viscosity blending rule was used as (REID, et al., 1977).

$$\ln\mu_{mix} = \sum_{i=1} x_i \ln\mu_i \quad \text{for } i = 1, 2, \ldots\ldots\ldots \tag{4.14b}$$

where μ_i is the viscosity of each (unweathered) cut and x_i is the mole fraction. In order to use equation (4.14b) it is necessary to have as input the μ_i at some reference temperature. If the μ_i are not available then μ_i can be estimated from the correlation form indicated in equation (4.1) where the predicted quantity is $\log_{10}$ of the kinematic viscosity at 122°F in centistokes and the constants C_1 to C_5 are presented in Table 4-1 (HOUGEN, 1965). This viscosity mixing rule has been found to be inadequate in that it always predicted a bulk oil viscosity that was too low; thus, the reason for its replacement.

The bulk viscosity predicted from equation (4.14a) is scaled with respect to temperature according to the Andrade equation (GOLD, 1969) which is

$$\ln\frac{\mu_1}{\mu_0} = B\left[\frac{1}{T_1} - 0.00335\right] \tag{4.15}$$

where μ_o is the viscosity of the bulk oil at 25°C, and B is an oil-dependent constant. None of the above viscosity equations take into account water-in-oil emulsion (mousse) formation (MACKAY, 1980).

The area for mass transfer in equation (4.10) is calculated from the rate at which the oil spreads on the water surface. Considerable research has been devoted to the spreading of oil on the water surface; however, many of the resulting models are still relatively elementary. The spreading model used is due to MACKAY, 1980 since this model is based on observations.

Using arguments based on observations the area of the slick is calculated according to the differential equation

$$\frac{dA}{dt} = K_3 Z^{1.33} A^{0.33} \tag{4.16}$$

where A is the slick area, Z is the thickness and K_3 is a constant. This equation is sometimes referred to as the thick-slick area (MACKAY, et al, 1980). Other spreading equations such as those based on gravity-surface tension theories have been found to be inadequate on the open sea surface.

The prediction of water-in-oil emulsification (mousse) is important in oil-weathering material balances because of the viscosity change due to the incorporation of water into oil. The water-in-oil emulsification formation is based on three parameters (MACKAY, et al., 1980) which appear in the following equation:

$$(1 - K_2W) \exp\left[\frac{-2.5W}{1-K_1W}\right] = \exp\left[-K_3t\right] \tag{4.17a}$$

where W is the weight fraction water in the oil-water mixture, K_1 is a constant in a viscosity equation due to Mooney (MOONEY, 1951), K_2 is a coalescing-tendency constant, and K_3 is a lumped water-incorporation rate constant. The viscosity equation due to Mooney is

$$\mu = \mu o \exp\left[\frac{-2.5W}{1-K_1W}\right] \tag{4.17b}$$

where μ_0 is the parent oil viscosity and K_1 is usually around 0.62 to 0.65 and apparently does not change much with respect to different types of oils. The constant K_2 above must satisfy the relation $K_2W < 1$ in order for the water incorporation rate term (right-hand side of equation 4.17a) to be >0. Thus, K_2 is the inverse of the maximum weight fraction water in the mixture. K_3 is the water incorporation rate constant and is a function of the wind speed.

The dispersion (oil into water) weathering process is described by two equations (MACKAY, 1980). These equations are:

$$F = K_a \ (V + 1)^2 \tag{4.17c}$$

$$F_B = (1 + K_b \mu^{\frac{1}{2}} \delta \chi)^{-1} \tag{4.17d}$$

where F is the fraction of sea surface subject to dispensions per second, V is the wind speed in m/sec and K_a is a constant. F_B is the fraction of droplets of oil below a critical size which do not return to the slick, K_b is a constant, μ is the oil viscosity in centipoise, χ is the slick thickness in meters, and δ is the oil/water interfacial surface tension in dynes/cm. The mass fraction that leaves the slick as dispersed droplets is F_b F and this fraction applies to each cut of oil.

Figure 4-1 presents an abbreviated flow chart of the calculation performed in the open-ocean oil-weathering code. The majority of the coding is In settling up the required physical properties and kinetic constants. The actual integration routine is relatively small.

Figures 4-2(a) through 4-2c present plotted results for calculated oil weathering results in Table 4-5. The plot routine that produces Figures 4-2(a) through 4-2(c) is not part of the oil-weathering code. The plot routine reads a plot file which is generated by the oil-weathering code. The plot file is essentially numerical results only (no formatting) and contains

FIGURE 4-1. ABBREVIATED BLOCK FLOW DIAGRAM FOR OPEN-OCEAN OIL-WEATHERING CODE.

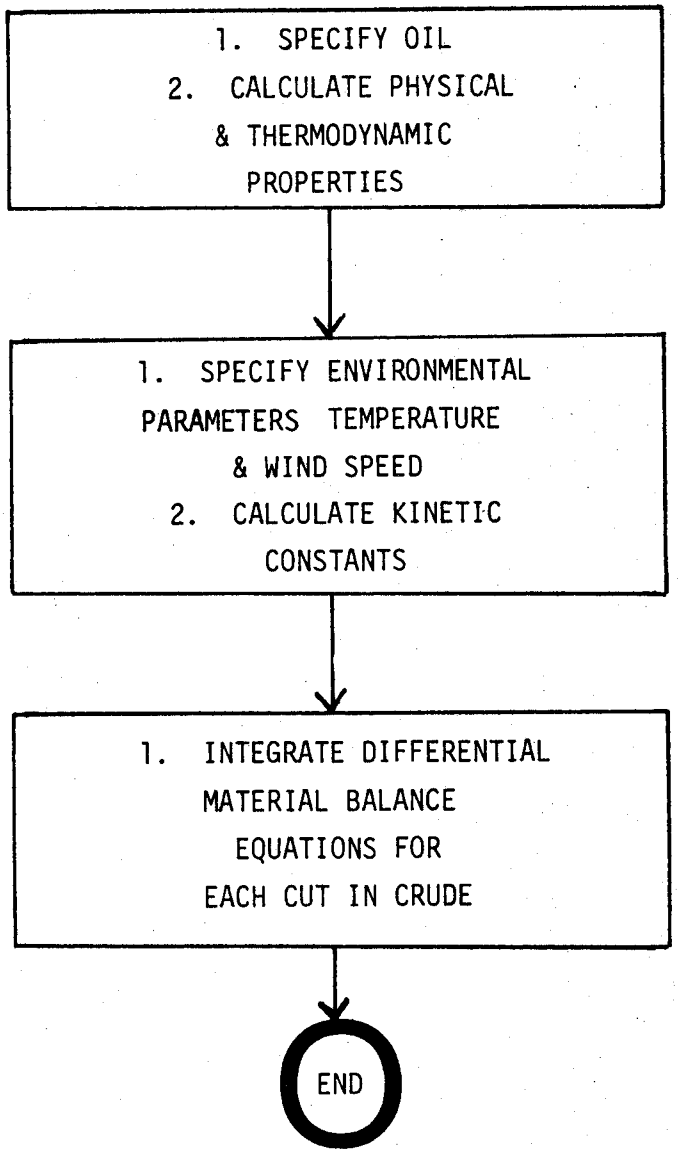

Figure 4-2(a)

PREDICTED TBP DISTILLATION CURVES

FOR WEATHERED OIL AT 55 F & 10 KNOTS
STEN= 30,KB= 50, VOL= 5000 BBLS
PRUDHOE BAY, ALASKA

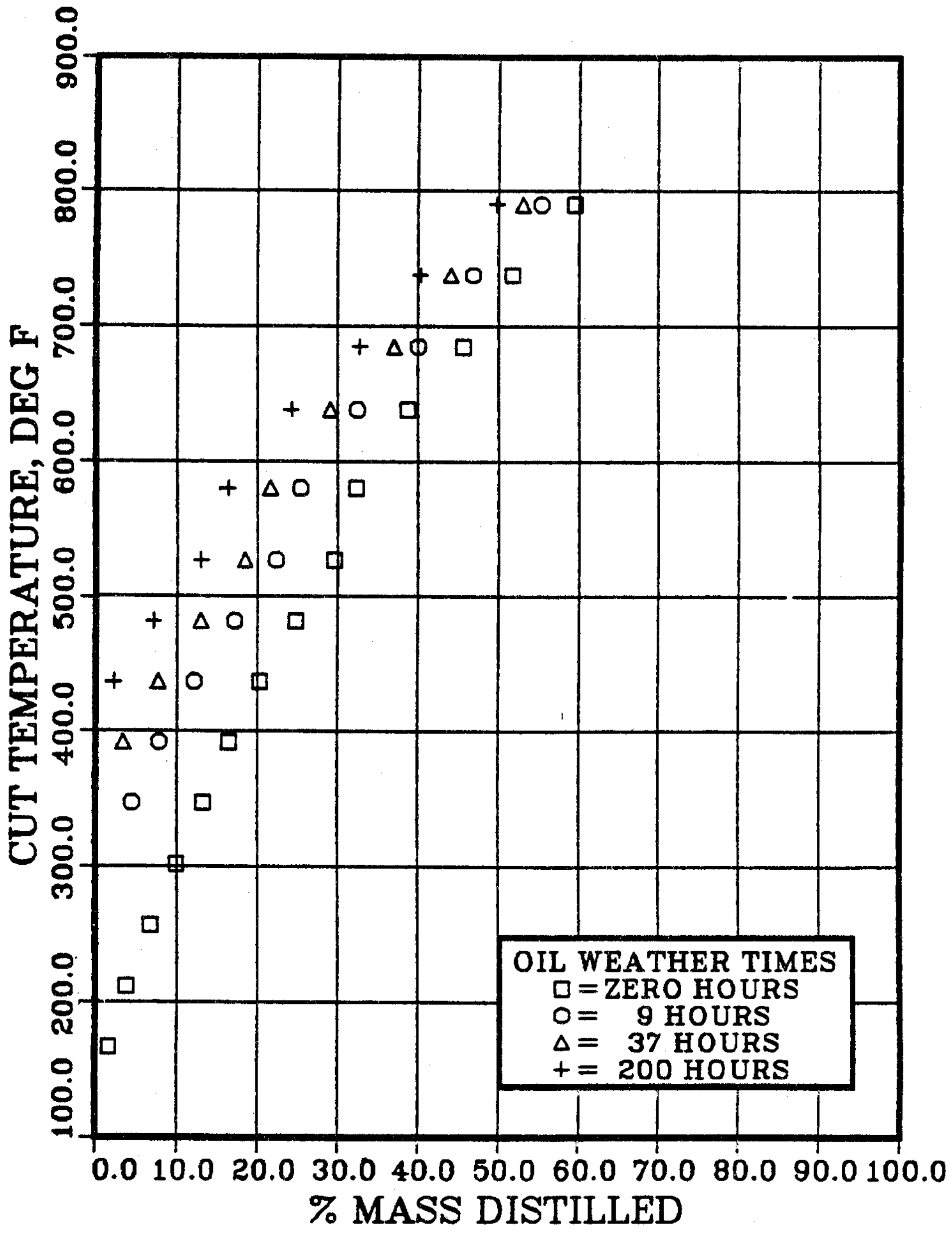

Figure 4-2(b)

PREDICTED GC DISTILLATION CURVES

FOR WEATHERED OIL AT 55 F & 10 KNOTS
STEN= 30, KB= 50, VOL= 5000 BBLS
PRUDHOE BAY, ALASKA

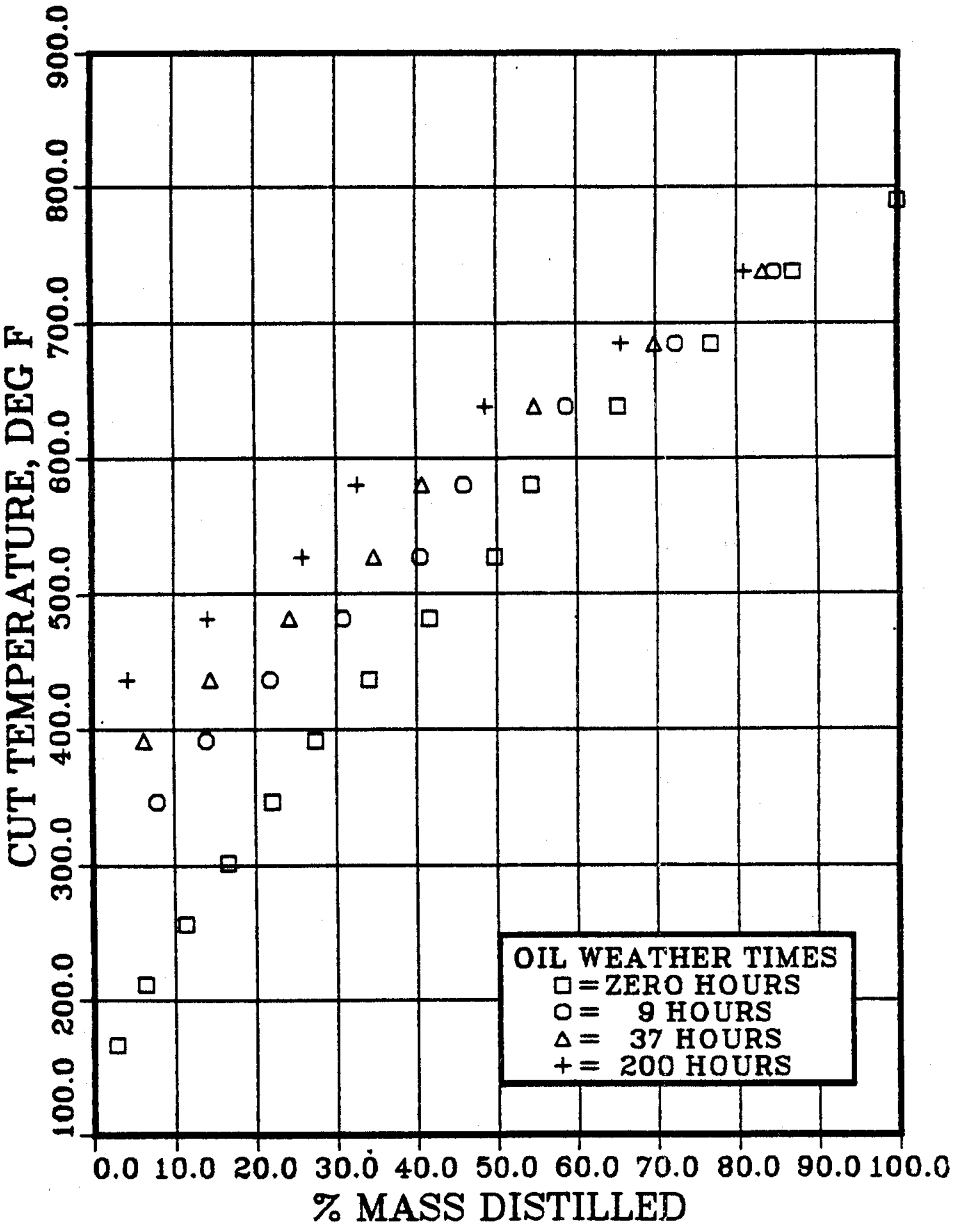

Figure 4-2(c)

PREDICTED MASS FRACTION REMAINING
FOR WEATHERED OIL AT 55 F & 10 KNOTS
STEN= 30, KB= 50, VOL= 5000 BBLS
PRUDHOE BAY, ALASKA

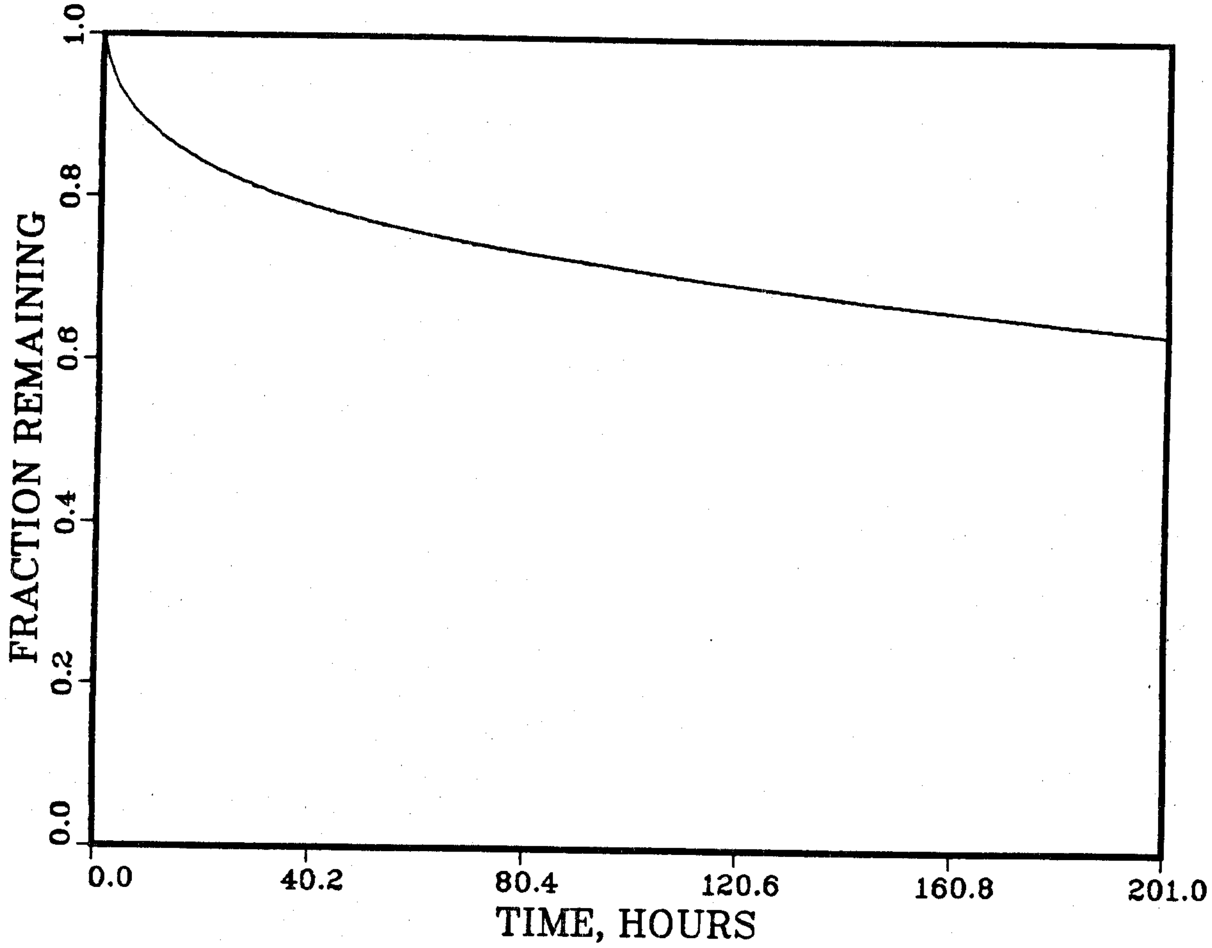

all the calculated numbers for the purpose of further manipulation which can be print, tape or plot.

Figure 4-2(a) is a predicted true boil point (TBP) distillation curve for the weathered crude. Thus, this is a prediction of the oil-composition versus time that can be field tested. Figure 4-2(b) presents a predicted gas-chromatograph distillation curve which is essentially the same as Figure 4-2(a) except for the normalization. It has been arbitrarily assumed that the gas chromatograph will not transport the 850°F+ material.

Figure 4-2(c) presents the predicted mass fraction of the slick remaining. This figure shows the combined effects of evaporation and dispersion, which are the two primary oil-weathering processes that remove oil from an oil slick. Dissolution does not account for more than a few percent of the mass loss of a slick; hence, dissolution is not included in the material balance differential equation list.

Figure 4-5 is an example of abbreviated output (80-column) which presents numerical results for the weathering of Prudhoe Bay crude at 55°F in a 10-knot wind. The cut information which numbers 1-15 presents the physical properties of the cuts: molecular weight, vapor pressures, density and boiling point. The kinetic parameters are contained in the mass-transfer coefficient code (2 in this case), wind speed and temperature. The integrated material balance presents the volume remaining in the slick, the density, area, thickness, weight % water-in-oil, evaporation rate, mass per unit area and compositional information. More detailed output is also generated but it quite lengthy, and an example of such is presented in Appendix B: User's Manual.

Table 4-5   ABBREVIATED OUTPUT FROM OPEN-OCEAN OIL-WEATHERING CODE

```
OIL WEATHERING FOR PRUDHOE BAY, ALASKA

CODE VERSION IS CUTVP2 OF FEBRUARY 83
TEMPERATURE=  55.0 DEG F, WIND SPEED=  10.0 KNOTS
SPILL SIZE=  5.000E+03 BARRELS
MASS-TRANSFER COEFFICIENT CODE=  2

FOR THE OUTPUT THAT FOLLOWS, MOLES=GRAM MOLES
GMS=GRAMS, VP=VAPOR PRESSURE IN ATMOSPHERES
BP=BOILING POINT IN DEG F, API=GRAVITY
MW=MOLECULAR WEIGHT

 CUT   MOLES       GMS        VP         BP         API      MW
   1  1.28E+05  1.14E+07  7.66E-02  1.67E+02  7.27E+01   89
   2  1.46E+05  1.48E+07  2.41E-02  2.12E+02  6.42E+01  101
   3  1.82E+05  2.07E+07  6.74E-03  2.57E+02  5.67E+01  113
   4  1.71E+05  2.19E+07  1.62E-03  3.02E+02  5.16E+01  127
   5  1.61E+05  2.30E+07  3.55E-04  3.47E+02  4.76E+01  143
   6  1.37E+05  2.20E+07  6.90E-05  3.92E+02  4.52E+01  160
   7  1.55E+05  2.77E+07  1.25E-05  4.37E+02  4.15E+01  177
   8  1.61E+05  3.15E+07  2.06E-06  4.82E+02  3.78E+01  195
   9  1.57E+05  3.34E+07  3.30E-07  5.27E+02  3.48E+01  212
  10  8.13E+04  1.92E+07  3.10E-08  5.80E+02  3.06E+01  236
  11  1.65E+05  4.50E+07  1.51E-09  6.38E+02  2.91E+01  272
  12  1.61E+05  4.80E+07  1.21E-10  6.85E+02  2.62E+01  298
  13  1.28E+05  4.29E+07  4.79E-12  7.38E+02  2.40E+01  334
  14  1.42E+05  5.35E+07  1.21E-13  7.90E+02  2.25E+01  375
  15  4.71E+05  2.83E+08  0.00E+00  8.50E+02  1.14E+01  600

MOUSSE CONSTANTS: MOONEY= 6.20E-01, MAX H20= 0.70, WIND**2= 1.00E-03
DISPERSION CONSTANTS: KA= 1.08E-01, KB= 5.00E+01, S-TENSION= 3.00E+01
VIS CONSTANTS: VIS25C= 3.50E+01, ANDRADE = 9.00E+03, FRACT = 1.05E+01

FOR THE OUTPUT THAT FOLLOWS, TIME=HOURS
BBL=BARRELS, SPGR=SPECIFIC GRAVITY, AREA=M*M
THICKNESS=CM, W=PERCENT WATER IN OIL (MOUSSE)
DISP=DISPERSION RATE IN GMS/M*M/HR
ERATE=EVAPORTION RATE IN GMS/M*M/HR
M/A=MASS PER M*M OF OIL IN THE SLICK
I=FIRST CUT WITH GREATER THAN  1% (MASS) REMAINING
J=FIRST CUT WITH GREATER THAN 50% (MASS) REMAINING

TIME  BBL     SPGR  AREA   THICKNESS   W  DISP     ERATE      M/A    I  J
  0 5.0E+03 0.88 4.0E+04 2.0E+00     0 1.6E+01 0.0E+00 1.8E+04 1  1
  1 4.8E+03 0.88 9.7E+04 7.9E-01     2 1.3E+01 1.7E+02 7.0E+03 1  2
  2 4.7E+03 0.89 1.3E+05 5.7E-01     5 1.2E+01 7.4E+01 5.1E+03 2  3
  3 4.6E+03 0.89 1.6E+05 4.7E-01     7 1.1E+01 4.4E+01 4.2E+03 2  4
  4 4.6E+03 0.89 1.8E+05 4.1E-01     9 9.7E+00 3.0E+01 3.7E+03 2  4
  5 4.5E+03 0.89 2.0E+05 3.7E-01    12 8.9E+00 2.2E+01 3.3E+03 3  4
  6 4.5E+03 0.89 2.1E+05 3.3E-01    14 8.3E+00 1.7E+01 3.0E+03 3  4
  7 4.4E+03 0.90 2.3E+05 3.1E-01    16 7.7E+00 1.4E+01 2.8E+03 3  4
  8 4.4E+03 0.90 2.4E+05 2.9E-01    18 7.2E+00 1.1E+01 2.6E+03 3  5
  9 4.3E+03 0.90 2.6E+05 2.7E-01    20 6.7E+00 9.1E+00 2.4E+03 3  5
 10 4.3E+03 0.90 2.7E+05 2.5E-01    22 6.3E+00 7.8E+00 2.3E+03 4  5
 11 4.3E+03 0.90 2.8E+05 2.4E-01    24 5.9E+00 6.8E+00 2.2E+03 4  5
 12 4.3E+03 0.90 2.9E+05 2.3E-01    26 5.5E+00 6.0E+00 2.1E+03 4  5
 13 4.2E+03 0.90 3.0E+05 2.2E-01    27 5.2E+00 5.4E+00 2.0E+03 4  5
 14 4.2E+03 0.90 3.1E+05 2.1E-01    29 4.9E+00 4.8E+00 1.9E+03 4  5
 15 4.2E+03 0.90 3.2E+05 2.1E-01    31 4.7E+00 4.3E+00 1.8E+03 4  5
 16 4.2E+03 0.90 3.3E+05 2.0E-01    32 4.4E+00 3.9E+00 1.8E+03 4  5
 17 4.1E+03 0.90 3.4E+05 1.9E-01    34 4.1E+00 3.5E+00 1.7E+03 4  5
 18 4.1E+03 0.90 3.5E+05 1.8E-01    36 3.9E+00 3.2E+00 1.7E+03 4  5
 20 4.1E+03 0.90 3.6E+05 1.8E-01    37 3.7E+00 2.9E+00 1.6E+03 4  6
 21 4.1E+03 0.90 3.7E+05 1.7E-01    39 3.5E+00 2.7E+00 1.6E+03 4  6
```

Table 4-5 continued

```
FOR THE OUTPUT THAT FOLLOWS, TIME=HOURS
BBL=BARRELS, SPGR=SPECIFIC GRAVITY, AREA=M*M
THICKNESS=CM, W=PERCENT WATER IN OIL (MOUSSE)
DISP=DISPERSION RATE IN GMS/M*M/HR
ERATE=EVAPORTION RATE IN GMS/M*M/HR
M/A=MASS PER M*M OF OIL IN THE SLICK
I=FIRST CUT WITH GREATER THAN  1% (MASS) REMAINING
J=FIRST CUT WITH GREATER THAN 50% (MASS) REMAINING

TIME  BBL    SPGR   AREA  THICKNESS  W  DISP     ERATE     M/A    I  J
  23 4.0E+03 0.90 3.9E+05 1.7E-01   41 3.2E+00 2.3E+00 1.5E+03 4  6
  24 4.0E+03 0.90 4.0E+05 1.6E-01   43 3.0E+00 2.1E+00 1.5E+03 4  6
  25 4.0E+03 0.90 4.0E+05 1.6E-01   44 2.8E+00 2.0E+00 1.4E+03 4  6
  26 4.0E+03 0.90 4.1E+05 1.5E-01   45 2.7E+00 1.9E+00 1.4E+03 5  6
  27 4.0E+03 0.90 4.2E+05 1.5E-01   47 2.6E+00 1.8E+00 1.4E+03 5  6
  28 4.0E+03 0.90 4.3E+05 1.5E-01   48 2.4E+00 1.7E+00 1.3E+03 5  6
  30 3.9E+03 0.90 4.4E+05 1.4E-01   49 2.3E+00 1.6E+00 1.3E+03 5  6
  31 3.9E+03 0.90 4.4E+05 1.4E-01   50 2.2E+00 1.5E+00 1.3E+03 5  6
  32 3.9E+03 0.90 4.5E+05 1.4E-01   51 2.1E+00 1.4E+00 1.2E+03 5  6
  33 3.9E+03 0.90 4.6E+05 1.4E-01   52 2.0E+00 1.3E+00 1.2E+03 5  6
  34 3.9E+03 0.90 4.6E+05 1.3E-01   53 1.9E+00 1.3E+00 1.2E+03 5  6
  35 3.9E+03 0.90 4.7E+05 1.3E-01   54 1.9E+00 1.2E+00 1.2E+03 5  6
  37 3.9E+03 0.90 4.8E+05 1.3E-01   55 1.8E+00 1.2E+00 1.2E+03 5  6
  38 3.8E+03 0.90 4.8E+05 1.3E-01   56 1.7E+00 1.1E+00 1.1E+03 5  6
  39 3.8E+03 0.90 4.9E+05 1.2E-01   57 1.6E+00 1.1E+00 1.1E+03 5  6
  40 3.8E+03 0.90 5.0E+05 1.2E-01   58 1.6E+00 1.0E+00 1.1E+03 5  6
  41 3.8E+03 0.91 5.0E+05 1.2E-01   58 1.5E+00 9.9E-01 1.1E+03 5  6
  42 3.8E+03 0.91 5.1E+05 1.2E-01   59 1.5E+00 9.5E-01 1.1E+03 5  6
  43 3.8E+03 0.91 5.1E+05 1.2E-01   60 1.4E+00 9.1E-01 1.1E+03 5  6
  44 3.8E+03 0.91 5.2E+05 1.2E-01   60 1.4E+00 8.8E-01 1.1E+03 5  6
  45 3.8E+03 0.91 5.2E+05 1.1E-01   61 1.4E+00 8.5E-01 1.0E+03 5  6
  46 3.8E+03 0.91 5.3E+05 1.1E-01   61 1.3E+00 8.2E-01 1.0E+03 5  6
  47 3.8E+03 0.91 5.3E+05 1.1E-01   62 1.3E+00 7.9E-01 1.0E+03 5  6
  48 3.8E+03 0.91 5.4E+05 1.1E-01   63 1.2E+00 7.7E-01 1.0E+03 5  6
  49 3.7E+03 0.91 5.4E+05 1.1E-01   63 1.2E+00 7.4E-01 9.9E+02 5  6
  50 3.7E+03 0.91 5.5E+05 1.1E-01   63 1.2E+00 7.2E-01 9.8E+02 5  6
  51 3.7E+03 0.91 5.5E+05 1.1E-01   64 1.1E+00 6.9E-01 9.7E+02 5  6
  61 3.7E+03 0.91 6.0E+05 9.7E-02   67 9.3E-01 5.2E-01 8.8E+02 5  7
  71 3.6E+03 0.91 6.4E+05 8.9E-02   69 8.0E-01 4.2E-01 8.1E+02 6  7
  81 3.5E+03 0.91 6.8E+05 8.3E-02   69 7.2E-01 3.5E-01 7.6E+02 6  7
  91 3.5E+03 0.91 7.1E+05 7.8E-02   70 6.6E-01 3.0E-01 7.1E+02 6  7
 101 3.4E+03 0.91 7.5E+05 7.3E-02   70 6.1E-01 2.6E-01 6.7E+02 6  7
 111 3.4E+03 0.91 7.8E+05 7.0E-02   70 5.7E-01 2.3E-01 6.3E+02 6  7
 121 3.4E+03 0.91 8.1E+05 6.6E-02   70 5.3E-01 2.0E-01 6.0E+02 6  7
 131 3.3E+03 0.91 8.3E+05 6.3E-02   70 4.9E-01 1.8E-01 5.8E+02 6  7
 141 3.3E+03 0.91 8.6E+05 6.1E-02   70 4.6E-01 1.6E-01 5.5E+02 6  7
 151 3.2E+03 0.91 8.8E+05 5.8E-02   70 4.3E-01 1.5E-01 5.3E+02 6  8
 161 3.2E+03 0.91 9.1E+05 5.6E-02   70 4.1E-01 1.3E-01 5.1E+02 6  8
 171 3.2E+03 0.91 9.3E+05 5.4E-02   70 3.8E-01 1.2E-01 4.9E+02 6  8
 181 3.1E+03 0.91 9.5E+05 5.2E-02   70 3.6E-01 1.1E-01 4.8E+02 6  8
 191 3.1E+03 0.91 9.8E+05 5.1E-02   70 3.4E-01 1.0E-01 4.6E+02 6  8
```

In summary the open-ocean oil-weathering code considers the following processes:

- evaporation
- dispersion
- spreading
- physical property changes
- mousse formation

The oil-weathering code User's Manual presented in the Appendix presents detailed input-output information along with a code listing. It is imperative that any user be knowledgable with respect to the common terms used to describe oil in the environment. Thus, the User's Manual and the code itself was written to aid the user in gaining the knowledge necessary. All that is required to use the code is the User's Manual and to LOGIN on the computer (as described).

4.2 The Influence of Mechanical State on an Oil Slick

In essentially all of the previously published modeling work on oil weathering by the processes of evaporation and dissolution, the oil phase has been modeled as a well-stirred phase, resulting in a decaying exponential prediction for concentrations. Another modeling assumption which might be applied to an oil phase is that diffusion controls the mass transfer of components, at least under certain conditions. The well-stirred oil assumption is not universally appropriate since there can be conditions under which an oil phase is stagnant and not mechanically stirred. However, if the rate of evaporation (or dissolution) is the rate limiting step, then the concentration gradients in the oil phase can "keep up" with the evaporation rate at the surface and the oil phase appears well-stirred (i.e., no concentration gradients exist). The rate of evaporation or dissolution can be expected to be rate limiting when the partial pressure or solubility of the component of interest is quite small, or when a crust or skin has formed on the oil surface.

The following discussion examines a criterion for invoking the well-stirred oil phase assumption by examining results from corresponding heat transfer problems. This criterion is then examined for the physical properties of the components of interest for evaporation from an oil slick. Finally, the results of a numerical experiment are presented which demonstrate that a decaying exponential model can fit the data from an evaporation experiment where the evaporation is diffusion controlled within the bulk oil phase.

4.2.1 Modeling Assumptions

In heat transfer problems involving flat plates and a surface heat transfer coefficient, there are two problem solutions termed the "thin" and "thick" plate solutions. A thin plate does not have sufficient internal thermal resistance relative to the surface resistance to support temperature gradients. In other words, the surface resistance to heat transfer is much greater than the internal resistance. As a result the temperature of a thin plate is essentially uniform and the thin plate problem solution is the same as that obtained for a well-stirred phase comprising the plate. A particular plate can be classified as thermally thick or thin according to the Biot number (ROHSENOW and HARTNETT, 1973) which is:

$$Bi \equiv \frac{h\delta}{K} \quad \text{(dimensionless)} \tag{4.18}$$

where h is the surface conductance, δ is the plate thickness and K is the thermal conductivity. Roughly, for a flat plate with the convective boundary condition:

$$\text{thin, } Bi<0.1 \text{ ; thick, } Bi>0.1 \tag{4.19}$$

The Biot number as defined above is the same as H in the solutions for the temperatures of a well-stirred fluid in contact with a slab with "radiation" boundary conditions (JAEGER, 1945).

The corresponding Biot number for mass transfer problems involving flat plates is obtained by examining the following equations for heat and mass transfer:

$$-K \left.\frac{dT}{dx}\right|_{x=0} = h(T_m - T) \tag{4.20}$$

where T is the temperature of the solid at the interface and T_m is the temperature of the convective medium. The corresponding equation for mass transfer is:

$$-\mathcal{D} \left.\frac{dc}{dx}\right|_{x=0} = h(C_m - C_m^*) \tag{4.21}$$

where $\mathcal{D}$ is the diffusion coefficient in the slab, C is the concentration in the slab at the interface, C_m is the concentration of the convective medium, C_m^* is the hypothetical concentration of the convective medium in equilibrium with C, and h is now the convective mass-transfer coefficient. The equilibrium relationship required is assumed to be a Henry's law type expressed as:

$$C_m^* = \xi C \tag{4.22}$$

Equations (4.21) and (4.22) are not in the same form because of the equilibrium relationship that exists in the mass transfer case. However, making the change of variable $C_m^* = \xi C$ in the later equation yields:

$$-\mathcal{D}\frac{dc}{dx}\bigg|_{x=0} = \xi h(\bar{C}_m - C) \tag{4.23}$$

Now, compared to the heat transfer Biot number, the Biot mass-transfer number becomes:

$$\mathrm{Bi(mass)} = \frac{h\xi\delta}{\mathcal{D}} \tag{4.24}$$

In order to use the Biot number criterion to determine if an oil slick is diffusion-controlled, the quantity ξ in the Henry's law expression is required. The following calculation illustrates the assumptions and data required to calculate ξ. The starting point for the calculation is:

$$C_a = \xi C_\ell \tag{4.25}$$

where C_a is the concentration in the air, gm/cc; C^ℓ is the concentration in the liquid, gm/cc; and ξ is dimensionless.

In the absence of experimental measurements of ξ, a conventional Raoult's law is assumed:

$$P_i = x_i P_{vP} \tag{4.26}$$

where P_i is the partial pressure of component i, x_i is the mole fraction, and P_{vp} is the pure component vapor pressure. In order to use this expression, it must be assumed that:

$$C_a = \left[\frac{M_i}{RT}\right] P_{vp} \left[\frac{M_o}{\rho_o} \; \frac{1}{M_i}\right] C_\ell \tag{4.27}$$

where M_i is the molecular weight of i the component of interest, M_o is the mean molecular weight of the oil, and ρ_o is the bulk oil density. The quantity RT/M_i converts C_a to partial pressure and the quantity $M_o/(\rho_o \; M_i)$ converts C^ℓ to mole fraction; thus recovering Raoult's law as used here. The dimensionless Henry's law constant sought becomes:

$$\xi \equiv \frac{P_{vp} M_o}{\rho_o RT} \tag{4.28}$$

which has units of (gm-mole i)/(gm-mole oil) and is unitless according to the use of mole fraction in Raoult's law.

In order to illustrate the calculation of the Biot mass-transfer number, the vapor pressures for hydrocarbons containing 6 to 18 carbon atoms can be predicted from (BUTLER, 1975):

$$P_i = \exp\left[10.94 - 1.06N_i\right] \tag{4.29}$$

where P_i is the vapor pressure in mm Hg at 20°C and N_i is the number of carbon atoms. The quantity ξ becomes:

$$\xi = \frac{\exp\,[10.94 - 1.06N_i]\,M_o}{760\rho_o RT} \tag{4.30}$$

Assuming a mean molecular weight for the oil of 300 gms/gm-mole and a bulk oil density of 0.8 gm/cm^3, Equation (4.30) becomes:

$$\xi = 2 \times 10^{-5} \exp\,[10.94 - 1.06N_i] \tag{4.31}$$

at 20°C, and the above can be used to calculate the Biot mass-transfer number.

In order to calculate the Biot mass-transfer number, the diffisivity of the component of interest, the convective mass-transfer coefficient and oil thickness must be estimated. For the diffusivity a value of 10^{-6} cm^2/sec is used (REID, 1977); a slick thickness of 0.5 cm, and for the convective mass-transfer coefficient a value of 1000 cm/hr (0.28 cm/sec; LISS, 1974). The Biot mass-transfer number becomes:

$$Bi \equiv 1.4 \times 10^{-5}\xi \tag{4.32}$$

or, using the expression for:

$$Bi = 2.8 \exp\,[10.94 - 1.06N_i] \tag{4.33}$$

Table 4-6 presents the Biot mass transfer number for hydrocarbons containing 6 to 20 carbon atoms. This table indicates that the "thin" plate solution (i.e., the well-stirred phase assumption) is satisfactory, and that it can be used for hydrocarbons n-C_{14} and higher in carbon number. Thus, for these compounds the evaporation rate is so small that the diffusion transport rate can "keep up", and the concentration profiles within the oil are "flat". However, for hydrocarbons containing 13 carbon atoms or less, the evaporation rate is much greater than the diffusion rate. As a result concentration profiles can be present in the oil phase and the well-stirred oil-phase assumption should not be used.

Table 4-6. BIOT MASS TRANSFER NUMBER($\mathcal{D}=10^{-6}$ cm^2/sec, $\delta=0.5$ cm, h=1000 cm/hr, T=20°C).

N_i (carbon atoms)	Bi (dimensionless)	
6	273	
7	94	
8	33	
9	11	
10	4	
11	1.4	
12	0.5	
13	0.16	diffusion controlled (convection>diffusive rate)
14	0.05	(diffusive rate>convective)
15	0.02	well-stirred
16	0.006	
17	0.002	
18	0.0008	
19	0.0003	
20	0.0001	

It is important to recognize the assumptions used to calculate the Biot mass-transfer number. The diffusivity assumed is 10^{-6} cm^2/sec, and it is conceibale that a value of 10^{-7} to 10^{-9} cm^2/sec is real. Since the diffusivity appears in the denominator of the Biot mass transfer number, all the values presented in Table 4-6 could increase accordingly. Also there are no data available to determine the real value of the equilibrium constant, ξ, and it is not readily known how close to reality the calculated values are.

4.2.2 Material Transport Under Diffusion-Controlled Evaporation

The previous discussion presents information on the criterion for the assumption of a well-stirred oil phase for modeling the evaporation oil-weathering process. It was pointed out that many assumptions were required to perform the calculation of the Biot mass transfer number and these assumptions definitely require refinement. However, whether or not the evaporation process is diffusion-controlled it must be recognized that experimentally the well-stirred oil phase model, which is a decaying exponential, appears to fit the observed data quite well. Therefore, it is worthwhile to examine the mathematics of a diffusion controlled slab from which components are evaporating and compare the observable variable with a first order decay law. The observable variable is the concentration of the component of interest in the air stream, or the bulk average concentration in the fluid, as a function of time.

The numerical experiment performed here was that of calculating the theoretical air phase concentration of a component evaporating from a diffusion-controlled slab, and then fitting by least squares a decaying exponential to the "data".

The concentration profiles in a diffusion controlled slab from which a component of interest is evaporating are (CARSLAW and JAEGER, 1959):

$$\frac{C}{C_0} = \frac{4}{\pi} \sum_{n=1}^{\infty} \frac{(-1)^{n+1}}{(2n-1)} \cos\left\{\frac{(2n-1)\pi x}{2\ell}\right\} \exp\left[-\frac{(2n-1)^2\pi^2\theta}{4}\right] \qquad (4.34)$$

where C_0 is the initial concentration throughout and θ is the dimensionless time: $\mathcal{D}t/\ell^2$. The evaporation rate, and hence the concentration of the component of interest in an air stream above the surface,is the derivative of the above expression evaluated at the evaporating surface. The derivative need not be multiplied by the area and diffusivity since these quantities only "scale" the calculated concentration, and thus the calculated concentration in the air stream is in arbitrary units.

The results of this numerical experiment are presented in Figures 4-3 through 4-5. In each of the figures the fitting curve, which is A*exp[-kθ], has four symbols marking it, and the theoretical curve is the one with no symbols running from a dimensionless time of 0.1 to 1.5. In Figure 4-4 the fitted curve covers one **e-folding** time; i.e., the time required for the theoretical curve to decrease by 1/e = 0.367, beginning at θ = 0.1. In Figures 4-4 and 4-5 the fitted curves cover two and three e-folding times, respectively.

FIGURE 4-3. THEORETICAL AIR CONCENTRATION OF AN EVAPORATING COMPONENT ABOVE A DIFFUSION CONTROLLED SLAB AND A LEAST SQUARES EXP (-kΘ) FOR A e-FOLDING TIME

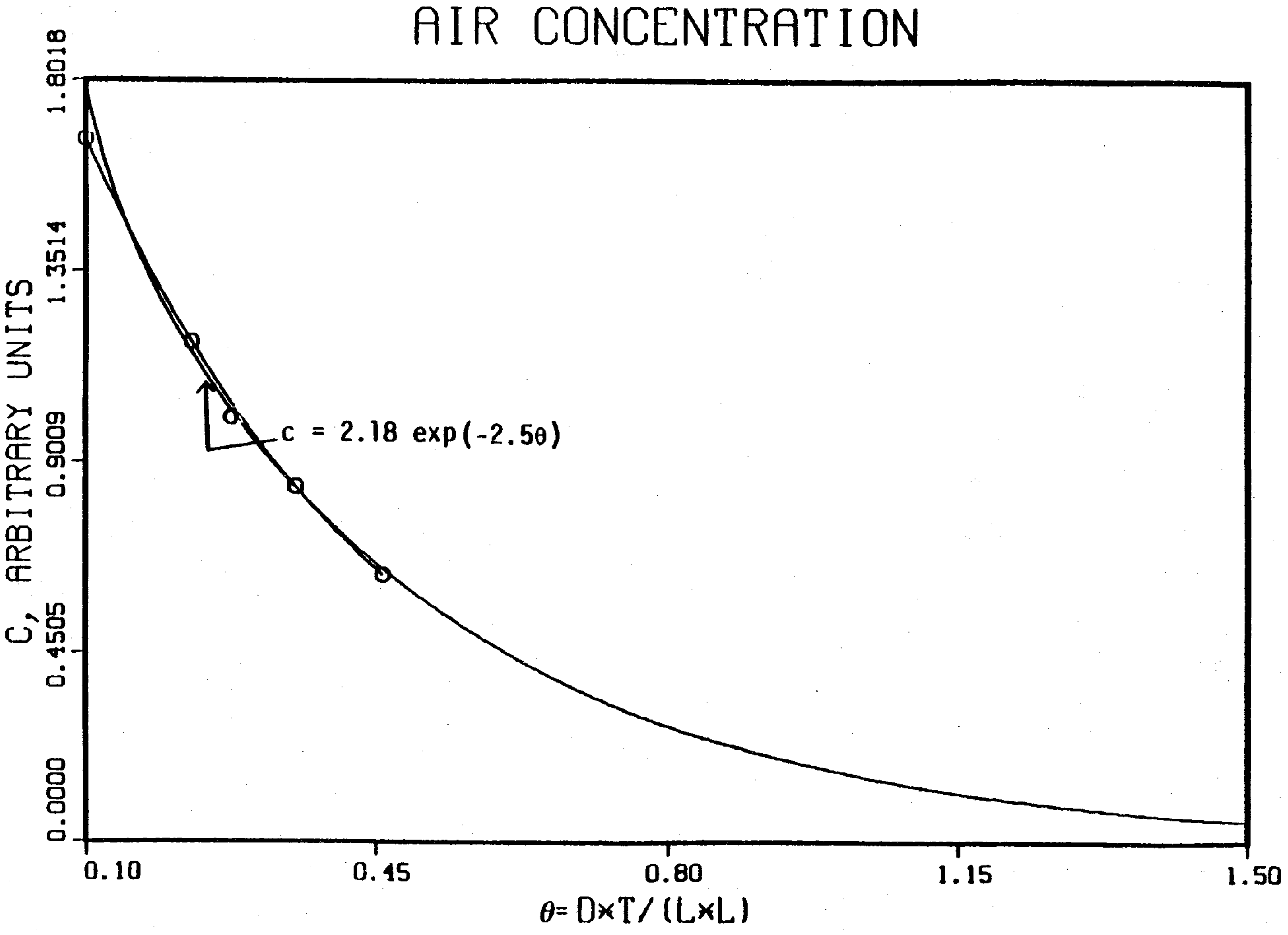

Figure 4-4. THEORETICAL AIR CONCENTRATION OF AN EVAPORATING COMPONENTS ABOVE A DIFFUS
CONTROLLED SLAB AND A LEAST SQUARES EXP (-kθ) FOR 2 e-FOLDING TIMES

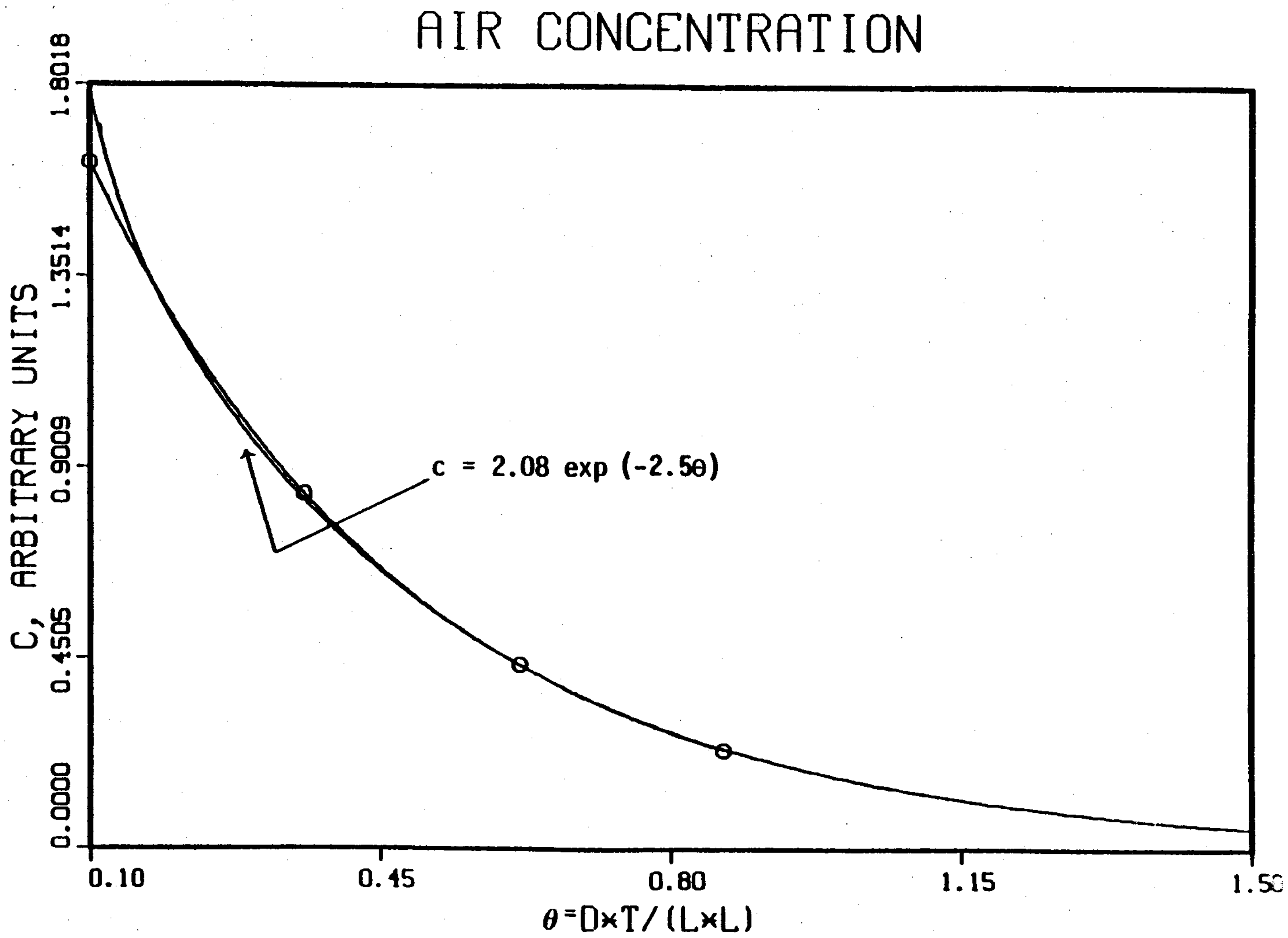

FIGURE 4-5. THEORETICAL AIR CONCENTRATION OF AN EVAPORATING COMPONENT ABOVE A DIFFUSION CONTROLLED SLAB AND A LEAST SQUARE EXP (-kθ) FOR 3 e-FOLDING TIMES

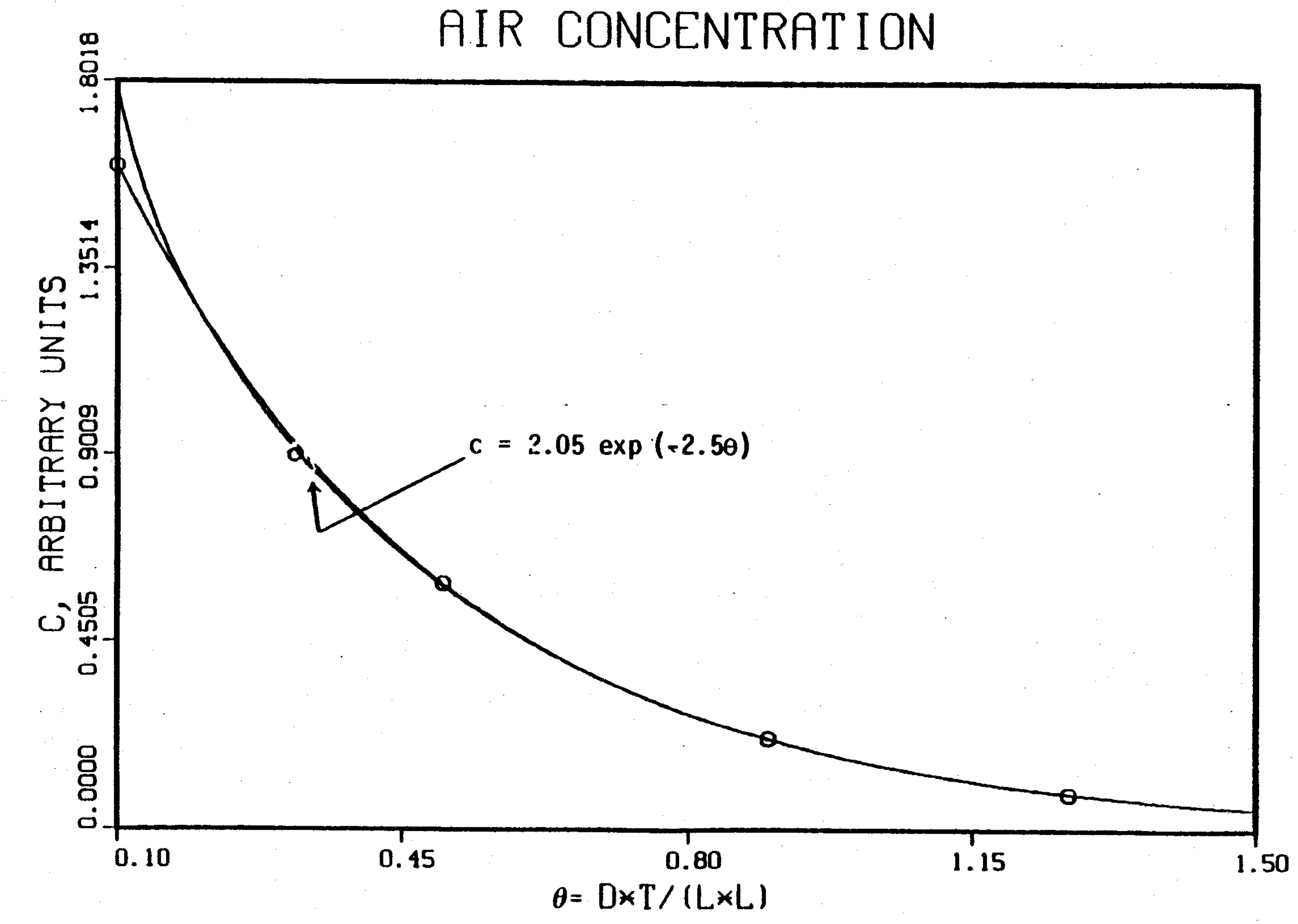

The result of this numerical experiment is that the fitted $A*\exp[-k\theta]$ curves cannot be distinguished in a laboratory experiment from the theoretical curve. In other words, performing a laboratory experiment on evaporation, fitting the data to $A*\exp[-k\theta]$, and obtaining an apparently good fit of the data is not sufficient to draw a conclusion about which mechanism is controlling.

The results of this numerical experiment can be used to obtain a single exponential expression to predict the decay of the air-phase concentration above a diffusion-controlled slab in the following way. Note that over the range of dimensionless time from 0.1 to 1.5 the "k" in the exponential fit is about -2.5. Thus, exp[-kt] where $k = 2.5\mathcal{D}t/\ell^2$, and t is time in seconds, provides a good fit to the data over the range of the independent variable examined.

These discussions have presented criteria to determine if an evaporating oil slick should be modeled as a well-stirred or stagnant phase. The method for that determination has been based on the Biot mass-transfer number in much the same way the presence of laminar flow is based on the Reynolds number. However, the data required to calculate the Biot mass-transfer number are not readily available, and estimates of these data must be made.

The primary reason for wanting to know if the oil phase is well-stirred or stagnant is that each of these states require different data and equations for model development. If an oil slick is diffusion-controlled, wind speed will not affect the average, time-dependent composition of the diffusing component in the oil mass. On the other hand, if the oil phase is well-stirred the wind speed will have an affect on the average composition of the oil.

Even though an oil phase can be diffusion controlled, it has been demonstrated that a decaying exponential will fit the air phase concentration data quite well. Thus, if an experiment is conducted to determine if evaporation from an oil slick is occurring from a well-stirred phase, it is necessary to obtain a good fit to the data but not sufficient to distinguish a well-stirred from a diffusion-controlled phase.

4.3 Component-Specific Evaporation from a Finite Oil Slick

The component-specific approach to model the evaporation process cannot predict the total mass of oil remaining in a slick. This approach can yield component-specific concentrations in the oil as a function of time when coupled to a pseudo-component overall material balance. For each specific component the rate of loss of component i from the slick takes the same form as a pre-defined pseudo-component:

$$\frac{dC_i}{dt} = -KAH_iC_i \qquad \text{for } i = 1, 2, \ldots\ldots\ldots \tag{4.35}$$

where C_i is the concentration of component i in the oil, H_i is the Henry's law coefficient for the i-th component, and K and A are the same as those used in the pseudo-component equations. There is no "closure" on the total mass of oil remaining in the slick when the above equation is used because the index i does not include all species. Therefore, the closure of the material balance can be handled in any of three ways:

1) ignore the decreasing slick mass and integrate equation (4.35) directly;
2) decrease the slick mass for those compounds for which a differential equation is written;
3) use the pseudo-component material balance to calculate a total slick mass and use this information in the differential equation.

Using the last approach, the rate of loss of component i from the slick is written the same as before but now with the concentration C_i as:

$$C_i = g_i/M_T \tag{4.36}$$

where g_i is the mass of i and M_T is the total mass of oil. M_T is calculated from the pseudo-component differential equations.

This approach to component-specific evaporation modeling will predict an increase in concentration with respect to time for those compounds with very low or essentially zero vapor pressures. While approach 2) above would also do the same, the error in predicting the total mass of oil remaining in the slick is not known, and it is believed the pseudo-component prediction will yield the best results when coupled to the component-specific model.

4.4 Component-Specific Evaporation from a Semi-Infinite Oil Slick

The foregoing discussion on evaporation of components, from an oil slick does not take into account the fact that the partial pressure in the air of all the components being transported from the oil through evaporation will not necessarily be zero. For example, when the Henry's law coefficient of a compound is very low, it takes only a very small amount of it to saturate the air, which is the case with a very volatile compound such as naphthalene. Also, since the air above an oil slick is not of infinite "volume" due to finite turbulent diffusivities which form transport boundaries, it is necessary to consider the effects of these conditions on component-specific transport.

Consider an oil slick being continuously emitted from a point source onto the ocean surface as shown in Figure 4-6. This slick is referred to as the semi-infinite slick. By writing differential material balances for both the oil and air phases the following set of equations describes the evaporation of component i:

Figure 4-6. CONTINUOUS OIL SLICK WITH ORIGIN AT x = 0; SURFACE IS IN y-x PLANE

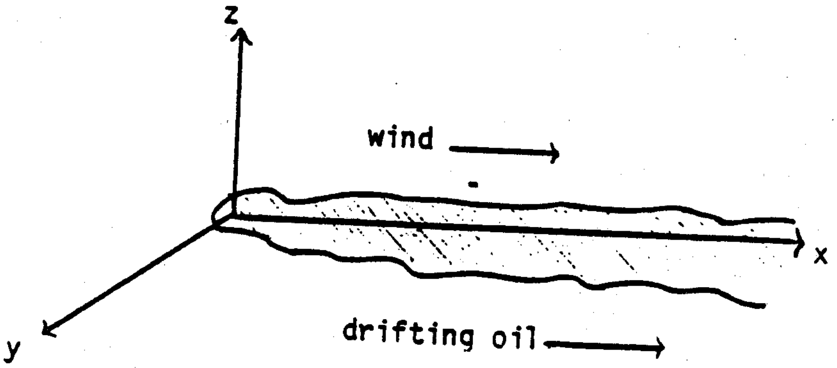

$$U_a \frac{\partial C_a}{\partial x} = \bar{\mathscr{D}}_z \frac{\partial^2 C_a}{\partial z^2} \tag{4.37}$$

$$C_a(x) = 0 \quad \text{at} \quad Z = \infty \tag{4.38}$$

$$C_a(Z) = 0 \quad \text{at} \quad x = 0 \tag{4.39}$$

$$\frac{dC_H}{dx} = \frac{H\bar{\mathscr{D}}_z}{\bar{U}_o \delta} \left. \frac{dC_a}{dz} \right|_{z=0} \tag{4.40}$$

$$\frac{dC_H}{dx} = - \frac{K_o}{\bar{U}_o \delta} \left[C_H - \left. C_a \right|_{z=0} \right] \tag{4.41}$$

$$C_H = HC_i \quad \text{at} \quad x = 0 \tag{4.42}$$

where C is the concentration of the species of interest with the subscript "a" denoting the air, H denoting the oil, i denotes the X = 0 concentration, U_a is the mean wind speed, $\bar{\mathscr{D}}_z$ is the turbulent diffusivity in the air, H is the Henry's law coefficient, U_0 is the oil velocity, δ is the slick thickness, and K_0 is the over-all mass-transfer coefficient. This derivation essentially follows that of SUTTON (1943) in which the evaporation of water from lakes was studied. A modification of Sutton's derivation was made here where the over-all mass-transfer coefficient was introduced so that the results of other researchers can be utilized. The width of the slick does not appear in the above equations as a result of the assumption that the slick width is constant. This assumption will generally be valid only in the case where the oil is emitted to the surface slowly.

Equations (4.37) through (4.42) can be solved by Laplace transforms. The quantity of interest is the concentration of a specific component in the oil, and the solution is:

$$\frac{C}{C_o} = \frac{1}{\alpha} \exp\left[kx\alpha^2\right] \operatorname{erfc}\left[\alpha\sqrt{kx}\right] + \frac{1}{\beta} \exp\left[kx\beta^2\right] \operatorname{erfc}\left[\beta\sqrt{kx}\right] \qquad (4.43)$$

where α and β are the roots of:

$$q^2 + \frac{\tilde{H}}{K} q + \frac{\tilde{H}}{k} = 0 \qquad (4.44)$$

which may be complex. The other terms are defined as:

$$\tilde{H} = \frac{K_o}{\bar{U}_o \delta} \qquad (4.45)$$

and

$$K \equiv \frac{H\bar{\mathcal{D}}_z}{\bar{U}_o \delta} \qquad (4.46)$$

and

$$k \equiv \frac{\bar{U}_a}{\bar{\mathcal{D}}_z} \qquad (4.47)$$

This model for a semi-infinite oil slick will not predict an increase in concentration with respect to time for the less volatile compounds in the oil phase due to the fact that an over-all material balance is not considered here as it is in the pseudo-component model. However, the above model will predict what combinations of parameters are important in invoking the zero air phase concentration assumption. Equations 4.43 through 4.47 show that the oil-phase concentration can be adequately predicted by assuming a zero air-phase partial pressure for small distances from the oil release point. However, for large distances from the oil release point, the zero air-phase partial-pressure assumption is not always adequate to predict the oil-phase concentrations and the above equations must be used.

Figures 4-7 and 4-8 present the calculations of the relative concentration of a specific compound in a semi-infinite oil slick for the parameters indicated in the figure legends. Also presented in these figures is the oil concentration when a zero partial pressure for this species is assumed to exist in the air phase. For the case of a 10 knot wind, the error introduced in assuming a zero partial pressure is approximately a factor of 10 at a down-wind distance of one kilometer. This error rapidly increases with distance and thus shows that the zero-partial-pressure assumption should <u>not</u> be used, but that equations 4.43 thrugh 4.47 must be used to predict the oil-phase concentration as a function of downwind distance for the parameters specified. The case of a 40 knot wind is presented in Figure 4-8 and shows that the error at one kilometer is essentially zero and does not become significant until 5 kilometers. This result is expected because a strong wind lowers the partial pressure above the slick. For less than a 10 knot wind the error in assuming a zero partial pressure will be quite large. These results are being used to determine when the zero partial-pressure assumption can (or can not) be involved.

FIGURE 4-7. PREDICTED OIL-PHASE CONCENTRATION IN A SEMI-INFINITE OIL SLICK FOR A 10 KNOT WIND.

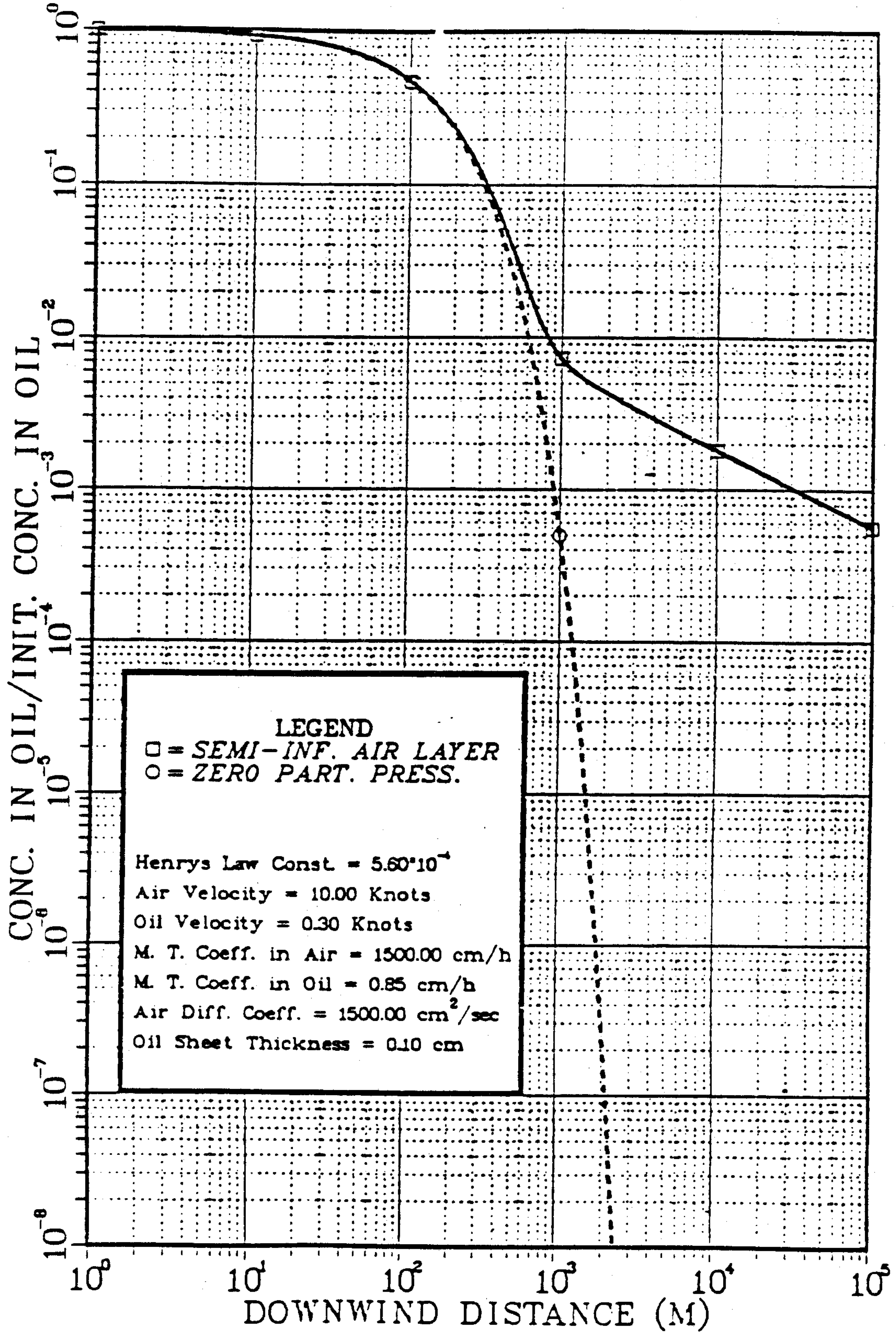

FIGURE 4-8. PREDICTED OIL-PHASE CONCENTRATION IN A SEMI-INFINITE OIL SLICK FOR A 40 KNOT WIND.

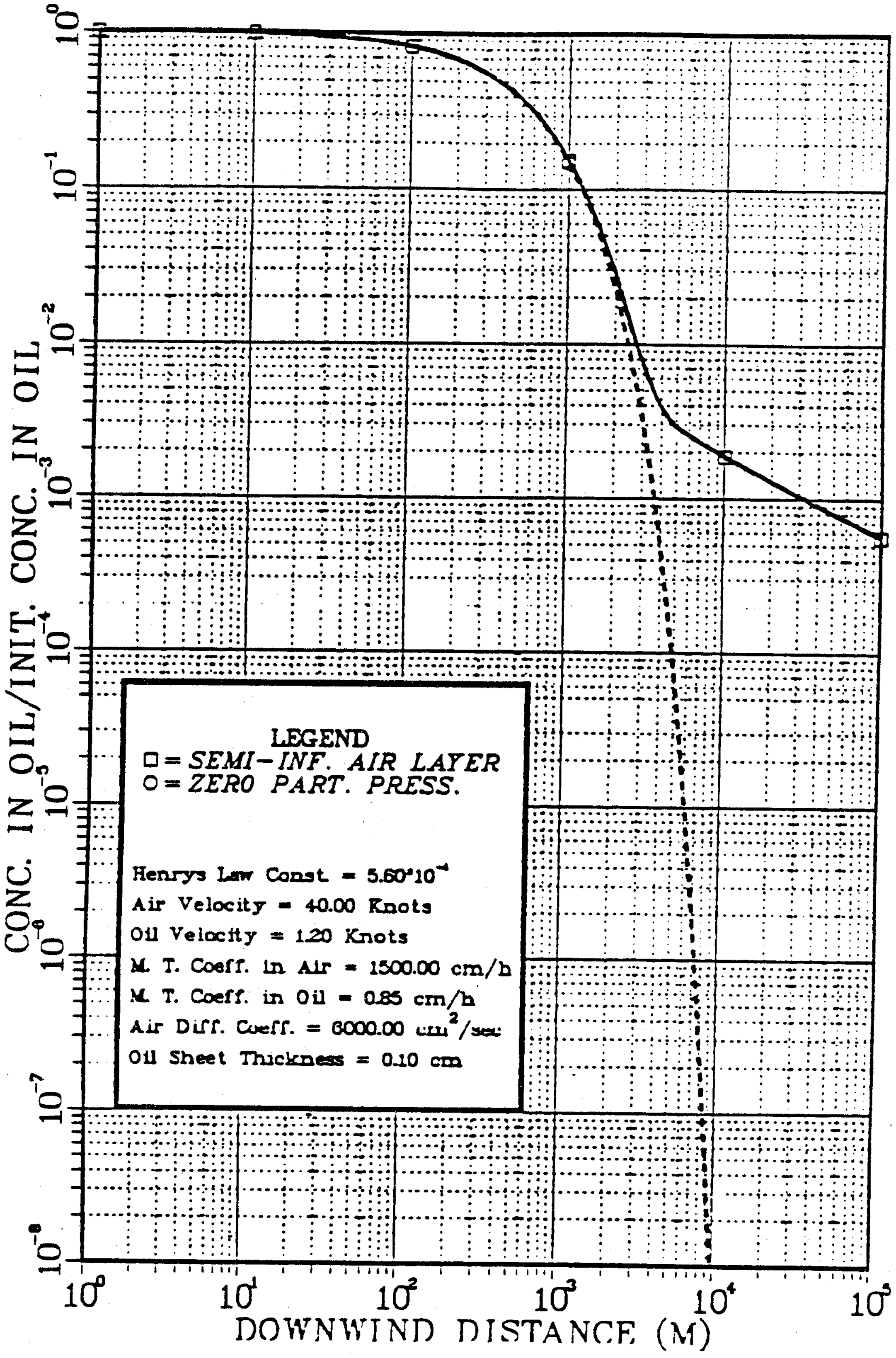

4.5 COMPONENT-SPECIFIC DISSOLUTION FROM A SEMI-INFINITE OIL SLICK

The dissolution of specific components from an oil slick into the water column is described mathematically in much the same way as evaporation. However, dissolution accounts for only a small reduction of the slick mass compared to evaporation. The pertinent physical property required to describe dissolution is the liquid-liquid partition coefficient which is the analogy of Henry's Law for evaporation.

Unfortunately there is no characterization process for dissolution that can be applied to the bulk oil in the same manner that distillation is used to characterize the oil with respect to evaporation. There have been two attempts to classify the oil into pseudo-components with respect to solubility, one by YANG and WANG (1977), but was not carried through to the quantitative stage, and another due to MACKAY (1980) where only two major "cuts" were recognized. Since dissolution apparently accounts for a relatively small mass loss from the slick, an independent component-specific approach to dissolution is presented here.

The physical property data required are liquid-liquid partition coefficients, referred to in the content of this work as m-values. It must be emphasized that pure component solubility data alone are not useful in obtaining m-values, because these types of data only yield information about the chemical potential of the species in the aqueous phase. What is required along with pure component solubility data is the chemical potential of the species in the oil phase. Henry's Law data coupled with solubility and vapor pressure data will provide m-value through calculation, while liquid-liquid equilibrium experiments measure the m-value directly.

For the case of a species dissolving from an oil slick into the water column, consider a water column which is uniform with respect to a vertical turbulent diffusivity. Then transport in the water column is described by

$$\frac{\partial C_w}{\partial t} = \bar{\mathcal{D}}_w \frac{\partial^2 C_w}{\partial x^2} \qquad (4.48)$$

where C_w is the water column concentration of the species of interest, t is time, X is distance (depth) and $\bar{\mathcal{D}}_w$ the turbulent diffusivity. The water column is clean at t = 0 so that

$$C_w\,(X) = 0 \qquad \text{at } t = 0 \qquad (4.49)$$

Since mass cannot transfer across the bottom at $X = \ell$ (this defines the coordinate frame)

$$\frac{dC_w}{dX} = 0 \qquad \text{at } x = \ell\,,\ t > 0 \qquad (4.50)$$

At the oil-water interface the mass fluxes from the oil and into the water must be equal which yields

$$A\delta \frac{dC_o}{dt} = A\bar{\mathcal{D}}_w \frac{dC_w}{dX} \qquad \text{at } x = 0,\ t > 0 \qquad (4.51)$$

where A is the interfacial area, C_o is the oil-phase concentration of the species of interest, and δ is the oil-phase thickness. Thus $A\delta$ is the volume of oil and the left-hand term above is a species balance in a well-stirred oil phase. This equation is rewritten as

$$\frac{dC_o}{dt} = \frac{\bar{\mathcal{D}}_w}{\delta} \frac{dC_w}{dX} \qquad \text{at } x = 0,\ t > 0 \qquad (4.52)$$

The component flux from the oil is written as

$$-A\bar{\mathscr{D}}_w \frac{dC_w}{dX} = AK_o\ (C_m - C_w) \qquad \text{at } X = 0,\ t > 0 \tag{4.53}$$

where C_m is a hypothetical water-phase concentration that is in equilibrium with the oil-phase concentration, and K_o is an over-all mass-transfer coefficient based on water-phase concentrations. The above equation is analogous to a heat transfer equation for the flux of energy across a film resistance. However, mass transfer requires that some form of a potential be used to write the driving force rather than observable concentrations. It is not correct to write the driving force for mass transfer as the concentration difference between the two phases. The reason for this is apparent when a simple system such as pure benzene and water is considered. At equilibrium the concentration of benzene in the water is on the order of 1700 ppm. Thus, the benzene concentration difference between the two phases is not zero, yet mass transfer does not occur. Therefore, in order to write a driving force for mass transfer the concentration in one of the phases must be related to the other phase on a thermodynamic basis. Once this relationship is defined, the mass transfer problem looks like a heat transfer problem where the temperature is the potential for heat transfer. Thus, in the preceding expression, C_m is a water-phase concentration (hypothetical) in equilibrium with the bulk oil-phase concentration C_o. As a result of this problem definition an oil-water partition coefficient is required. The oil-water partition coefficient is defined as follows:

$$m \equiv \left.\frac{C_o}{C_w}\right| \quad \text{at equilibrium} \tag{4.54}$$

At this point do not relate C_o and C_w above to those same symbols appearing in the previous equations. Because of the way the previous equations are written, it is convenient to keep C_w in them as it appears now.

This means C_o must change. The recipe for doing this is embodied in the mass transfer resistance equation $(C_m - C_w)$ term. Here C_m is that hypothetical concentration in water in equilibrium with the concentration in the oil. Therefore the oil-phase concentration must be changed according to

$$C_o = mC_m \tag{4.55}$$

And C_o must be replaced with mC_m in equation (4.52) to yield

$$\frac{dC_m}{dt} = \frac{\bar{\mathscr{D}}_w}{m\delta}\frac{dC_w}{dX} \qquad \text{at } X = 0,\ t > 0 \tag{4.56}$$

Rewriting equation (4.53) to cancel the area yields

$$\frac{dC_w}{dX} + \frac{K_o}{\bar{\mathscr{D}}_w}(C_m - C_w) = 0 \tag{4.57}$$

Finally, the initial concentration in the oil is $C_o^{\,o}$ which must be divided by m to yield $C_m^{\,o}$ to yield

$$C_m^o = \frac{C_o^o}{m} \tag{4.58}$$

The equation set is contained in equations (4.48); (4.49); (4.50); (4.56); (4.57) and (4.58). The analytical solutions to this equation set can be obtained using the technique of Laplace transforms which is described by Jaeger (Jaeger, 1945). This reference solves the analogous heat transfer problem from which the solution to the mass transfer problem can be written immediately.

The analytical solution for the water-phase concentration is

$$\frac{C_w}{C_o^o/m} = \frac{1}{1+k'} - 2\tilde{H} \sum_{n=1}^{\infty} \frac{(\alpha_n^2 - k'\tilde{H})\cos\alpha_n(1-X/\ell)\exp(-\alpha_n^2 T)}{P_n \cos\alpha_n} \tag{4.59}$$

and for the oil-phase concentration

$$\frac{C_m}{C_o^o/m} = \frac{1}{1+k'} + 2k'\tilde{H}^2 \sum_{n=1}^{\infty} \frac{1}{\tilde{P}_n} \exp(-\alpha^2 T) \tag{4.60}$$

where α_n is the n-th positive root of

$$\tan\alpha_n = \frac{\tilde{H}\alpha_n}{\alpha_n^2 - k'\tilde{H}} \tag{4.61}$$

$$\tilde{H} = \ell h \tag{4.62}$$

$$h = \frac{K_o}{\bar{\mathcal{D}}_w} \tag{4.63}$$

$$k' = \frac{\ell}{m\delta} \tag{4.64}$$

$$T = \bar{\mathcal{D}}_w t/\ell^2 \text{ (dimensionless time)} \tag{4.65}$$

$t \equiv$ time

and

$$P_n \equiv \alpha_n^4 + \alpha_n^2(\tilde{H}^2 + \tilde{H} - 2k'\tilde{H}) + k'\tilde{H}^2(1+k') \qquad (4.66)$$

These equations provide useful information in that the effect of the parameters of the problem can readily be determined. For example, note that the parameter k' is a ratio of the capacitance of each phase for the component of interest, and that the partition coefficient m multiples the oil phase thickness δ to yield an equivalent oil-phase thickness. Also, the time required to attain steady state can be determined by examining the n = 1 exponential term, i.e., when $\exp(\alpha_1 T) \approx 0.01$ the $n \geq 2$ terms have essentially decayed to zero.

In order to make the analytical solutions for component-specific dissolution usable they have been programmed in FORTRAN to allow easy investigations of the results. The details of this particular code, input-output information, and a code listing are presented in Appendix C: Code Description for Component-Specific Dissolution.

The types of compounds to which the above problem solution can be applied are presented in Table 4-7 (MACKAY and SHIU, 1977). These compounds represent the polynuclear aromatic hydrocarbons which are likely to have the significant environmental toxic effects. The solutions represented by the above equations apply only strictly for the case where there is no evaporation. This condition is approximated when there is a crust on the oil or the solution to the corresponding evaporation problem applies only strictly for the case where there is no dissolution, which is approximated when the evaporation rate is much greater than the dissolution rate. When evaporation and dissolution are both important, a "three-slab" problem results; however, this particular condition would be unlikely in a mathematical sense.

4.6 Measurement of Henry's Law Coefficient

The need for specific thermodynamic information to describe interphase mass transport was presented in the discussions of component-specific evaporation and dissolution. The vapor-liquid equilibrium data required are called Henry's law coefficients (H). The Henry's law coefficient pertains to that portion of the phase equilibrium diagram where the ratio of phase concentrations is constant, which is the case when the concentration of the species of interest in one phase is small (e.g., oxygen in water).

Henry's law coefficients appear in the flux expressions and the overall mass-transfer coefficients which describe interphase mass transfer. The reason for the appearance of H in the flux expression is that a concentration difference between two phases is not sufficient information to identify in which direction mass will transfer. If the system is not at equilibrium, mass

Table 4-7. COMPOUNDS OF IMPORTANCE IN AQUATIC ENVIRONMENT (MACKAY & SHIU, 1977).

	Solubilities	
	Exptl	
Compd	mg/L	x_w, mole fraction $\times 10^9$
Indan, C_9H_{10}	109.1 ± 1.02	16650
Naphthalene, $C_{10}H_8$	31.7 ± 0.26	4460
1-Methylnaphthalene, $C_{11}H_{10}$	28.5 ± 0.3	3550
2-Methylnaphthalene, $C_{11}H_{10}$	25.4 ± 0.2	3220
1,3-Dimethylnaphthalene, $C_{12}H_{12}$	8.0 ± 0.5	920
1,4-Dimethylnaphthalene, $C_{12}H_{12}$	11.4 ± 0.1	1310
1,5-Dimethylnaphthalene, $C_{12}H_{12}$	3.38 ± 0.04	377
2,3-Dimethylnaphthalene, $C_{12}H_{12}$	3.0 ± 0.01	347
2,6-Dimethylnaphthalene, $C_{12}H_{12}$	2.0 ± 0.02	233
1-Ethylnaphthalene, $C_{12}H_{12}$	10.7 ± 0.3	1240
1,4,5-Trimethylnaphthalene, $C_{13}H_{14}$	2.1 ± 0.1	215
Biphenyl, $C_{12}H_{10}$	7.0 ± 0.06	815
Acenaphthlene, $C_{12}H_{10}$	3.93 ± 0.014	459
Fluorene, $C_{13}H_{10}$	1.98 ± 0.04	214
Phenanthrene, $C_{14}H_{10}$	1.29 ± 0.07	130
Anthracene, $C_{14}H_{10}$	0.073 ± 0.005	7.57
2-Methylanthracene, $C_{15}H_{12}$	0.039 ± 0.004	3.67
9-Methylanthracene, $C_{15}H_{12}$	0.261 ± 0.002	24.4
9,10-Dimethylanthracene, $C_{16}H_{14}$	0.056 ± 0.0005	4.90
Pyrene, $C_{16}H_{14}$	0.135 ± 0.005	12.0
Fluoranthene, $C_{16}H_{10}$	0.26 ± 0.002	22.8
1,2-Benzofluorene, $C_{17}H_{10}$	0.045 ± 0.0012	3.75
2,3-Benzofluorene, $C_{17}H_{10}$	0.0020 ± 0.00003	0.956
Chrysene, $C_{18}H_{12}$	0.0020 ± 0.00017	0.158
Triphenylene, $C_{18}H_{12}$	0.043 ± 0.00013	3.39
Naphthacene, $C_{18}H_{12}$	0.00057 ± 0.00003	0.037
1,2-Benzanthracene, $C_{18}H_{12}$	0.014 ± 0.0002	1.10
7,12-Dimethyl-1,2-benzanthracene, $C_{20}H_{16}$	0.061 ± 0.0006	4.26
Perylene, $C_{20}H_{12}$	0.0004 ± 0.00002	0.0283
3,4-Benzopyrene, $C_{20}H_{12}$	0.0038 ± 0.00031	0.273
3-Methylcholanthrene, $C_{21}H_{16}$	0.0029 ± 0.000021	0.192
Benzo[g,h,i]perylene, $C_{22}H_{12}$	0.00026 ± 0.00001	0.0173
Coronene, $C_{24}H_{12}$	0.00014 ± 0.00002	0.00856

will transfer in the direction toward equilibrium. The information required to determine which way mass will transfer is the chemical potential of the species in each phase because the chemical potential is the potential for mass transfer. The Henry's law coefficient provides the method to map the concentration in one phase to the same chemical potential basis as the other phase. By using H, the correct driving force can be written for mass transfer.

The over-all mass-transfer coefficient also utilizes H in a manner that takes into account the relative solubility of the species of interest in each phase. There is virtually no way to determine the relative mass transfer resistances without H (TREYBAL, 1955; LISS, 1974).

The technique originally described by MCAULIFFE (1966) to measure henry's law coefficients using gas chromatography involves multiple equilibrations of equal volumes of aqueous and gaseous phases. A large glass syringe with a Luer-Lok fitting is filled 1:1 with liquid and clean nitrogen or air. The syringe is then capped off and agitated vigorously to create an equilibrium between phases. Most of the gas is then flowed through a gas sample loop which is an integral part of the analytical system (a gas chromatograph). At some point in this flow, a valve is turned and the gas in the loop (typically 0.1 to 10 ml) is introduced into the gas chromatograph. The rest of the gas is discharged from the syringe and fresh gas is introduced. The process is repeated a number of times.

The mathematical description of this procedure using equal volumes was given by McAuliffe and yields:

$$\log G_n = an + b \tag{4.66}$$

$$a = -\log (H + 1) \tag{4.67}$$

$$b = \log HX_o \tag{4.68}$$

where G_n is the amount of the compound of interest in the gas during the n-th equilibration, H is Henry's law coefficient, and X_0 is the original amount of the compound in the system. Equation (4.66) shows that a plot of the log of compound concentration (or GC peak height) vs equibration number n gives a straight line. The negative slope of this line gives the log of (H + 1).

In measurements of Henry's law coefficients for petroleum components, it is not necessarily convenient to use equal volumes of liquid and gaseous phases. Some compounds have large distribution coefficients and some have relatively small values. Also, when the fresh oil/air system is measured, it has been found to not be desirable to deal with 25 ml of oil in the partitioning syringe. Therefore, a re-derivation of equations (4.66) through (4.67) for unequal volumes of gas/liquid is presented. Considering a measurement system with unequal liquid and gas volumes, V_L and V_g, respectively, G_i can be defined as the amount of a distributing component in the gas phase during the i-th equilibration. Similarly, L_i is the amount in the liquid phase during the i-th equilibration. The total amount of the substance is:

$$X_i = G_i + L_i \tag{4.69}$$

and the Henry's law coefficient becomes:

$$H = \frac{\text{concentration in gas}}{\text{concentration in liquid}} = \frac{G_i V_L}{V_g L_i} \tag{4.70}$$

r can be defined as:

$$r = \frac{V_L}{V_g} \tag{4.80}$$

and as a result the gas phase amount, G_i, can be re-expressed:

$$G_i = X_i - L_i = X_i - \frac{rG_i}{H} = \frac{Hx_i - rG_i}{H} \tag{4.81}$$

$$HG_i = Hx_i - rG_i \tag{4.82}$$

$$G_i = \frac{HX_i}{r + H} \tag{4.83}$$

$$G_i = \frac{(H/r)x_i}{1 + H/r} \tag{4.84}$$

Similarly, the liquid phase amount, L_i, can be written:

$$L_i = \frac{x_i}{1 + H/r} \tag{4.85}$$

The fractional amounts the component in the gas and liquid phases, f_g and f_L, respectively, can be expressed as:

$$f_g = \frac{G_i}{x_i} = \frac{(H/r)x_i}{x_i(1 + H/r)} = \frac{H/r}{(1 + H/r)} \tag{4.86}$$

$$f_L = \frac{L_i}{x_i} = \frac{x_i}{x_i(1 + H/r)} = \frac{}{(1 + H/r)} \tag{4.87}$$

For subsequent equilibrations (i.e., i+1, i+2 .... i+n), equation (4.84) can be generalized to:

$$G_{i+1} = \frac{(H/r)}{1 + H/r}\left[x_i - \frac{H/r}{1 + H/r}x_i\right] \tag{4.88}$$

or simplifying the above

$$G_{i\,+\,1} = \frac{(H/r)X_i}{(1 + H/r)^2} \tag{4.89}$$

going through steps (4.84) through (4.89) again for $X_{i\,+\,1}$ in place of X_i in (4.84) yields

$$G_{i\,+\,2} = \frac{(H/r)X_i}{(1 + H/r)^3} \tag{4.90}$$

Now redefine the i index where i = 1 to yield

$$G_3 = \frac{(H/r)X_i}{(1 + H/r)^3} \tag{4.91}$$

Note that X_i is the amount initially in the liquid phase loaded into the syringe and that to get to equation (4.91) above it required <u>3</u> equilibrations.

Generalizing for m equilibrations yields

$$G_m = \frac{(H/r)x_1}{(H/r + 1)^m} \tag{4.92}$$

G_m can be experimentally obtained as component-specific gas chromatographic data, and if equation (4.92) is rearranged to logrithmic form it takes on a linear form (y = mx + b), and a plot of log G_m vs (m) has a slope equal to -log(H/r +1). Only one phase of the system needs to be sampled, any ratio of volumes can be used, many compounds can be measured at one time, and standards do not have to be run since only relative amounts are used in the calculations.

Henry's Law coefficients have been measured in this study using equation (4.92). A 50 ml glass Hamilton gas-tight syringe with a Luer fitting is used along with a sample loop (of varying sizes) installed into a six-port Valco valve which allows the loop gas to be initially purged to the atmosphere prior to introduction into the carrier gas of the gas chromatograph. The valve is enclosed in an insulated enclosure, heated, and temperature controlled. The gas is delivered to the valve by 1/16-inch tubing. In order to avoid inconsistencies and pressure differences which could effect equilibrium, the syringe is discharged with a Sage Instruments Syringe infusion pump set at a very slow rate. A Hewlett-Packard 5731A gas chromatograph with a flame ionization detector and 3385A Automatic Integration System has been employed. A 6-ft glass column packed with 1% SP-1000 on Carbopak B 60/80 is currently being used, and plans for future studies incorporate the use of a 30-m glass capillary column using SE-54 or SE-30 as the liquid phase.

In order to verify the ability of this experimental technique, a number of measurements have been made on hydrocarbons dissolved in distilled water. The extent of "known" Henry's law data is very limited, however a few literature values (MACKAY, 1975) have been found for comparison. Typically, the compound of interest is equilibrated with distilled water in a separatory funnel for a number of hours. Then the water can be taken from the funnel stopcock directly into the syringe. Figure 4-9 presents a plot of resultant data for benzene and Table 4-8 presents some of the data obtained so far in this program which can be compared to previously measured values.

The technique is reproducible, with a scatter in the data of about 10 to 20 percent. All of the Henry's Law values are in approximate agreement with the literature values except for iso-octane. This has not been explained, but it is suspected that the previously cited value is incorrect.

FIGURE 4-9. EXPERIMENTAL DATA FOR BENZENE

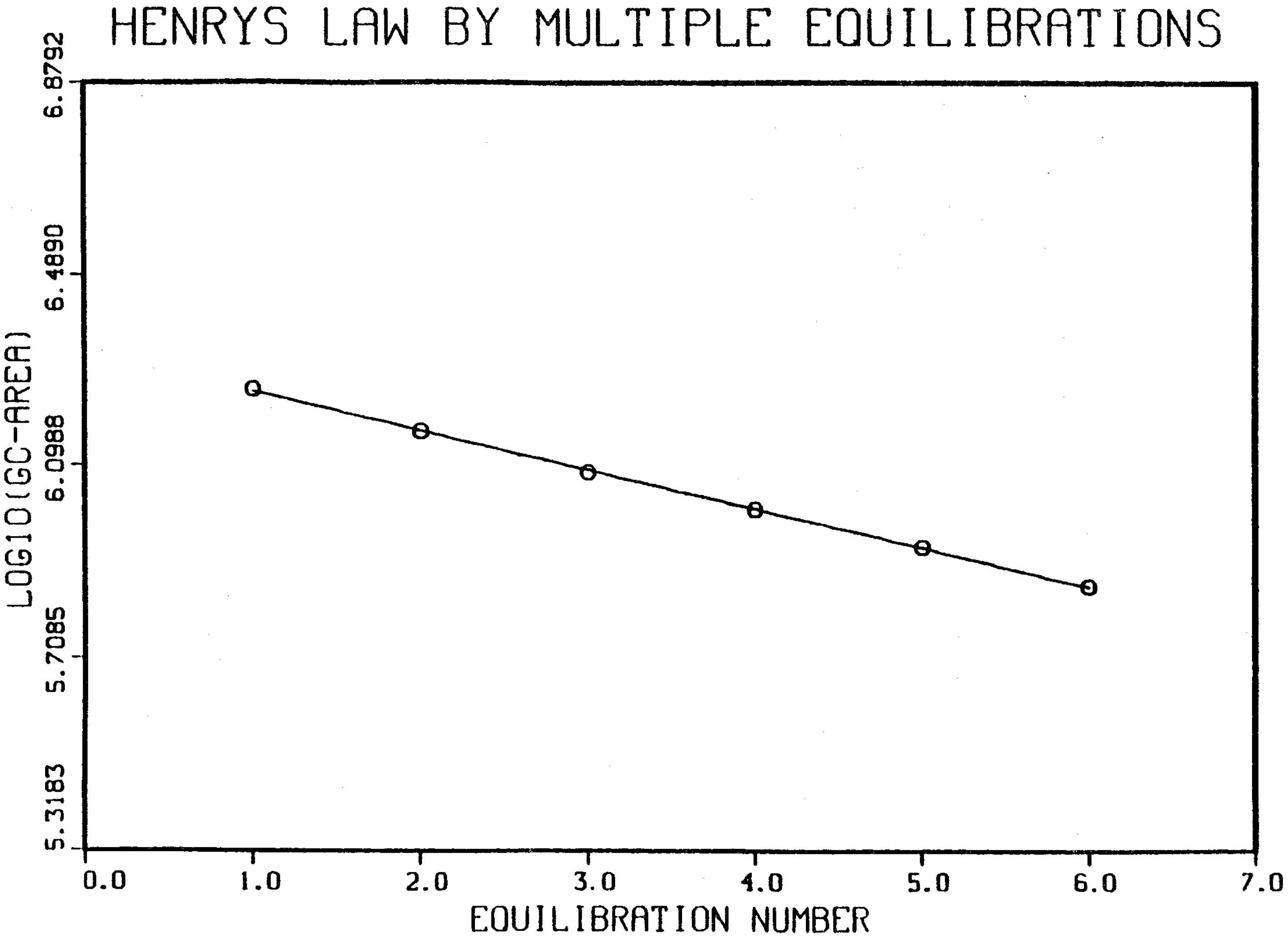

TABLE 4-8. HENRY'S LAW RESULTS.

Compound	Ratio $\frac{V_\ell}{V_s}^{**}$	r^*	H(atm m^3/mole)	H(literature)	$\frac{H}{H(\text{lit.})} \times 100$
Benzene	25/25	-.9980	5.5×10^{-3}	5.5×10^{-3}	100
Benzene	14/36	-.9997	4.3×10^{-3}		78
Benzene	25/25	-.9998	5.0×10^{-3}		98
Benzene	25/25	-.9998	5.0×10^{-3}		91
Benzene	14/36	-.9998	4.9×10^{-3}		90
Benzene	14/36	-.9999	4.8×10^{-3}		87
Toluene	25/25	-.9999	5.3×10^{-3}	6.68×10^{-3}	79
Toluene	21/19	-.9890	5.6×10^{-3}		84
Iso-octane	31/19	-.990	~0.18	3.04	5.9
Iso-octane	31/19	-.997	0.098		3.2
n-Hexane	31/19	---	0.87	1.20	72.5
n-Hexane	36/14	---	1.04	1.20	87.1
Benzene/Toluene***	26/24	-.9985/-.9948	$5.04 \times 10^{-3}/5.07 \times 10^{-3}$	$5.5 \times 10^{-3}/6.68 \times 10^{-3}$	91/76

* correlation coefficient

** V_ℓ = volume of liquid, V_g = volume of gas

*** combined Benzene/Toluene

In order to get H values for compounds that have very low partial pressures in oil, a slightly different approach is being taken. Instead of sampling the gas, the liquid (oil) is sampled after every 5 or 10 equilibrations. The partitioning theory presented for water is applicable, however the measurement technique is the same except that the liquid sample involves the oil being dissolved in an appropriate amount of solvent (CS_2) and analyzed directly.

4.7 DIFFUSION COEFFICIENTS FOR VOLATILE COMPONENTS THROUGH OIL

To fully develop a model for oil weathering it is necessary to have diffusion coefficients for a variety of components in oil. Two problems pose obstacles to straight-forward application of the diffusion equations to describe the migration of components within an oil mass. First, the oil is usually in the form of a continually spreading slick and the continually altering thickness of the slick is a complicating factor. In addition, as lighter components are lost from the surface of the slick and skins begin to form, the impact on transfer of components across that interface is major. It is important, therefore, to be able to account for changing slick thickness and for slick skin permeability.

This section treats these points, beginning with multicomponent diffusion and commenting on the problems of developing a model that accounts for slick thinning. As an outgrowth of this, an approach is explained for treating laboratory experimental data in a way that can yield diffusion coefficients free from the effect of thinning. Problems associated with modeling skin formation are discussed, and an approach is presented.

Diffusion through a thinning slick can be thought of in terms of one-dimensional diffusion through a plane slab of thickness b. Assuming an impenetrable barrier at the plane boundary ($y = 0$). Also, at $y = b$, it is assumed that the ambient medium is sufficiently stirred that all volatiles are at zero concentration in that plane.

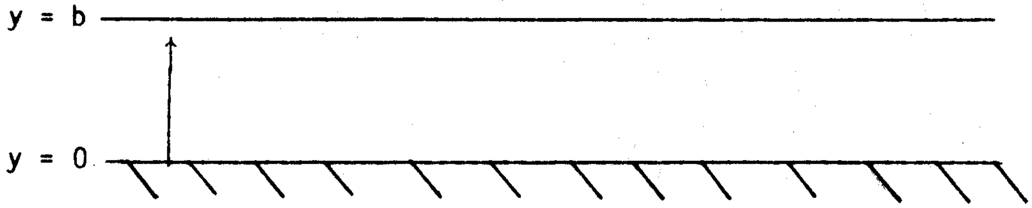

If $b = b_0$ = constant, and if diffusivity is also constant, the (molar) concentration of any species is given by:

$$\frac{C}{C_0} = \frac{4}{\pi} \sum_{n=0}^{\infty} \frac{(-1)^n}{(2n+1)} \exp\left[\frac{-(2n+1)^2 \pi^2 \mathcal{D} t}{4 b_0^2}\right] \cos\left[\frac{(2n+1)\pi y}{2 b_0}\right] \qquad (4.93)$$

where C_0 is the (assumed uniform) concentration at t = 0. After some interval of time, t, the amount of the volatile species remaining in the slab is:

$$\int_0^b c\,dy = \frac{8 C_0 b}{\pi^2} \sum_{n=0}^{\infty} \frac{1}{(2n+1)^2} \exp\left[\frac{-(2n+1)^2 \pi^2 \mathcal{D} t}{4 b^2}\right] \qquad (4.94)$$

and the mass loss up to time t is:

$$M C_0 b_0 \left[1 - \int_0^{\phi} (C/C_0)\, dy/b_0\right] \qquad (4.95)$$

where M = molecular weight and $\phi \equiv b/b_0$.

If an assumption is made that the volumes of all components are addictive, then the mass loss may be related to slab thickness as follows:

$$\rho_L(b_o - b) = \sum_i M_i C_{o_i} b_o \left[1 - \int_o^{\phi} (C/C_o)_i \; dy/b_o \right] \tag{4.96}$$

where ρL is the mass density of the slab, and the summation is over all volatile species.

If one makes a "quasi-steady state" assumption, stipulating that equation (4.94) is valid even for b varying with time, then an algebraic equation for b(t) is obtained:

$$1 - \phi = \sum_i m_i \left[1 - \frac{8\phi}{\pi^2} \sum_{n=0} \frac{1}{(2n+1)^2} \exp\left[\frac{-(2n+1)^2 \pi^2 \mathscr{D}_i t}{4b^2} \right] \right] \tag{4.97}$$

or

$$1 - \phi = \sum_i m_i \left[1 - \frac{8\phi}{\pi^2} \sum_{n=0} \frac{1}{(2n+1)^2} \exp\left[\frac{-(2n+1)^2 \pi^2 \tau_i}{4\phi^2} \right] \right] \tag{4.98}$$

where

$$\phi = b/b_o, \quad \tau_i = \mathscr{D}_i t/b_o{}^2, \quad m_i = \frac{M_i C_{o_i}}{\rho_L} \tag{4.99}$$

One would expect this quasi-steady state assumption to be reasonably accurate for short time ($\phi \approx 1$).

In principle one could use equation (4.98) to calculate diffusion coefficients $\mathscr{D}_i$ from observations of $\phi(\tau)$. For a multicomponent system this would be impractical, since a multivariable fit of data on $\phi(\tau)$ would be required. Since the accuracy of equation (4.98) for large time periods is questionable, and since one would have to go to large time in order to have reasonable precision in data for $\phi(\tau)$, the use of equation (4.98) for determination of $\mathscr{D}_i$ is not suggested for multicomponent systems.

Having completed this analysis, it was concluded that the proper alternative approach should be to determine diffusion coefficients by monitoring the role of release of each species from the slab, at short time intervals ($\phi = 1$). This is done by measuring the appearance of each species in an inert stream that sweeps across the slab. If a sweep stream, initially free of every diffusing species, is provided at a flowrate q_0 (volume/time), then the concentration of each species in that stream may be found, assuming constant pressure isothermal conditions in the sweep stream. If ρ_G is the density of the sweep gas, then the rate of flow of gas into the system is $\rho_G q_0$.

The mass rate of flow of diffusants into the System is $\sum AM_iN_i$, where A is the exposed area of the slab and N_i is the molar flux of species i from the slab. The mass fraction of species i in the exit stream is:

$$x_i = \frac{AM_iN_i}{\rho_G q_0 + \sum AM_iN_i} \tag{4.100}$$

It is anticipated that $\sum AM_iN_i << \rho_G q_0$, therefore:

$$x_i = \frac{AM_iN_i}{\rho_G q_0} \tag{4.101}$$

Hence, from a measurement of each X_i, each N_i is found, to then be correlated to individual component diffusivities $\mathscr{D}$.

To avoid problems with the reduction in slab thickness, an expression for N_i that is accurate over small time interval is derived from the Leveque solution:

$$N_i = C_{oi}\sqrt{\mathcal{D}_i/\pi t} \tag{4.102}$$

Thus, $x_i(t)$ should be measured to determine $N_i(t)$, and from the slope of a plot of N_i vs $t^{-1/2}$, $\mathcal{D}$ can be found.

Although the previous discussion avoids treating the reduction in slab thickness as a variable in measuring diffusion coefficients, it is important to get some idea of the rate of thinning. From equation (4.98) for a single diffusing species, we must solve for ϕ:

$$\phi = \frac{1 - m}{1 - \frac{8m}{\pi^2} \sum\limits_{n=0} \frac{1}{(2n + 1)^2} \exp\left[\frac{-(2n + 1)^2 \pi^2 \tau}{4\phi^2}\right]} \tag{4.103}$$

Again for short time intervals, it is convenient to use the Leveque solution for N, and find ϕ from:

$$\phi = 1 - \frac{2m}{\sqrt{\pi}} \tau^{1/2} \tag{4.104}$$

Another approach to this problem is to apply the perturbation solution as described by DUDA and VRENTAS (1969). Since only the first few terms are used, the available solution is restricted to small values of M. A comparison of solutions is:

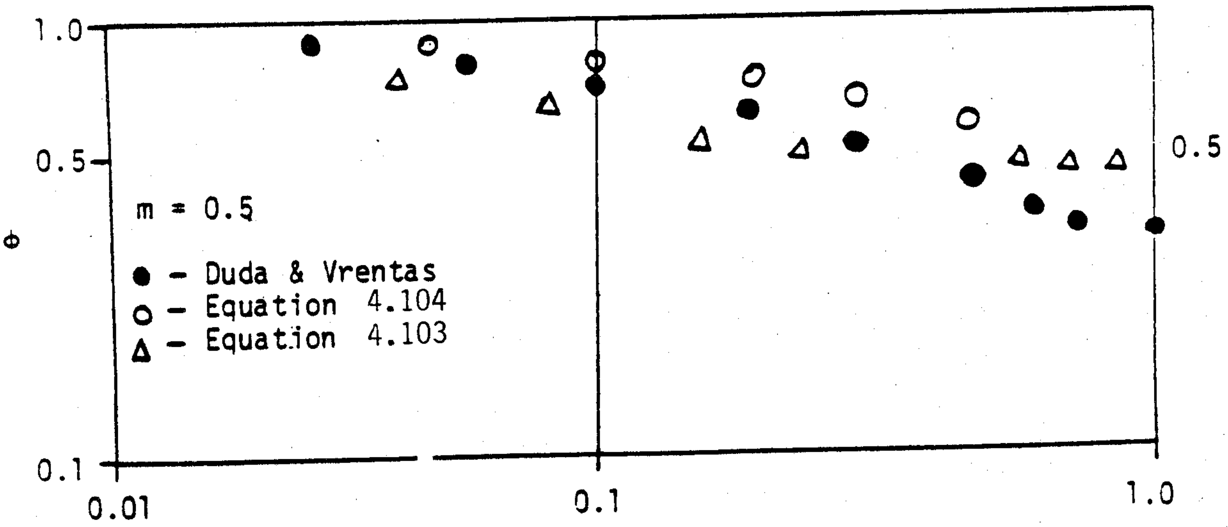

Equation (4.104) is expected to be valid only for small τ. Equation (4.103) shows (correctly) that ϕ approaches a value of 1-m at long τ. Also, the Duda and Vrentas solution in inaccurate over its mid-range, where it predicts that ϕ falls below $\phi = 0.5$. It does correctly give $\phi = 0.5$ as τ exceeds 3. The Duda and Vrentas solution is probably accurate at small τ. The value of m = 0.5 examined here ($m = N_b$ in their notation) is a little large for their perturbation solution.

It is interesting to examine the fractional loss of a species from the slab, as a function of time. We expect that slab thinning will increase the rate of loss, but we do not know the degree of this increase. If the thickness remained uniform, the fraction of each species remaining would be found from:

$$f = 1 - \frac{8}{\pi^2} \sum_{n=0} \frac{1}{(2n+1)^2} \exp\left[\frac{-(2n+1)^2\pi^2\tau}{4}\right] \qquad (4.105)$$

or, for short times:

$$f \approx \frac{2}{\sqrt{\pi}} \tau^{1/2} \qquad (4.106)$$

The following figure shows f calculated using the above equations as well as f using the Duda and Vrentas solution. As expected, taking account of slab thinning leads to more rapid loss of diffusible species.

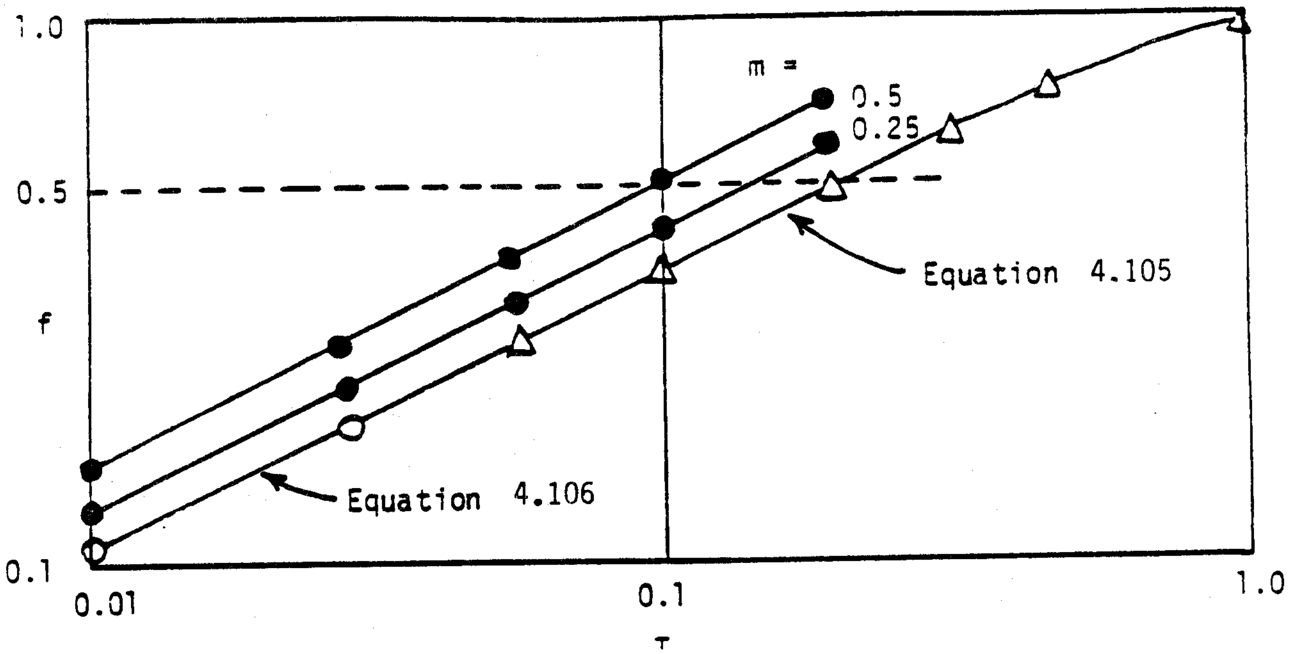

Even though the Duda and Vrentas solution is suspect in its mid-range for such large values of m, it is still useful to observe the effect of slab thinning on the half-time for release of a volatile component. For a slab of uniform thickness, the half-time is found to be $\tau_{1/2} = 0.2$. For m = 0.25 we find $\tau_{1/2} = 0.15$, and for m = 0.5, the value is reduced to $\tau_{1/2} = 0.1$.

4.8 THE ROLE OF INTERNAL CIRCULATION IN THE WEATHERING OF A THIN OIL SLICK

When a slick of oil floats upon a rough sea, its motion is determined by the local wind and wave action. These external forces could be strong enough to produce motion within the slick. Previous analyses of weathering have focused on mass transfer by diffusion within the slick, and on convection across the slick/water and slick/air interfaces. Our efforts have attempted to produce a model that allows an estimate of the extent of internal motion, and the degree to which that motion enhances mass transfer of components to the environment.

The simplest model is derived from Figure 4-10 which shows an idealized oil slick. The slick is taken to be a slab of uniform thickness, H, and length, L, in the wind direction and we assume L>>H. Further, the width normal to the wind direction, W, also is assumed to satisfy W>>H. The wind generates a shear stress τ on the upper surface, which produces a velocity, V, in the wind direction, along the plane of the slick/air interface. We assume that the slick is stationary with respect to the water, or equivalently that V is measured relative to the mean velocity of the slick with respect to the water. Thus the physical model is as shown in Figure 4-11.

We are interested in the velocity profile v(y), and in then examining the effect of velocity on mass transfer at the slick/air interface. The velocity profile, under the approximations, satisfies:

$$0 = - \frac{\partial p}{\partial x} + \mu \frac{\partial^2 v}{\partial y^2} \qquad (4.107)$$

$v = V \quad \text{at} \quad y = H$

$v = 0 \quad \text{at} \quad y = 0$

and is found to be:

$$v = V \frac{y}{H} - \frac{1}{2\mu} y(H - y) \frac{\partial p}{\partial x} \qquad (4.108)$$

We have assumed that $\alpha p/\alpha x$ is independent of y, equivalent to the assumption that the velocity is everywhere parallel to the planes (i.e., at both y = 0 and y = H). Of course this would not be true near the edges of the slick, where the flow reverses and returns across the lower region of the slick. We envision the flow induced in the slick by the wind to be like the motion of a tractor tread. The gradient $\alpha p/\alpha x$ is not known, but may be found by invoking the assumption that there is no net flow of oil in the x-direction:

$$\int_0^H v \, dy = 0 \qquad (4.109)$$

FIGURE 4-10. OIL SLICK ON THE SEA.

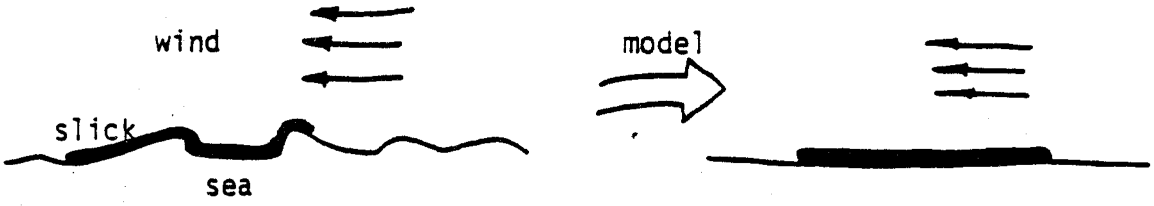

FIGURE 4-11. CIRCULATION WITHIN THE SLICK

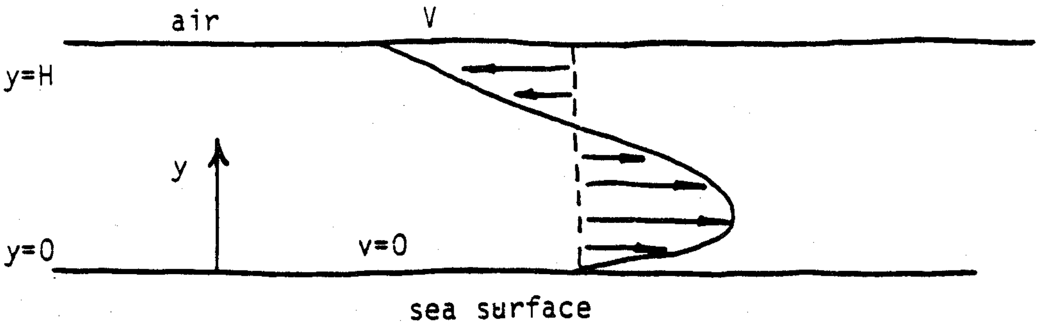

Upon imposing this constraint we find:

$$\frac{\partial p}{\partial x} = \frac{6\mu V}{H^2} \qquad (4.110)$$

and the velocity field is given as:

$$v = V\frac{y}{H}\left(2 - \frac{3y}{H}\right) \qquad (4.111)$$

Next we examine the effect of this velocity field on mass transfer across the plane y = H. The basic case for comparison is the pure diffusion control situation, where there is no motion within the slab. From the classical solution to the pure diffusion problem we find:

$$\frac{C}{C_o} \approx \frac{8}{\pi^2}\exp\left(-\frac{\pi^2}{4}\frac{\mathcal{D}}{H^2}t\right) \quad \text{for} \quad \frac{\mathcal{D}t}{H^2} > 0.2 \qquad (4.112)$$

where $\mathcal{D}$ is the diffusion coefficient of some species through the oil, and C/C_0 is the fraction of the diffusible species remaining after time t. We may regard the term:

$$t_D \equiv \frac{4H^2}{\pi^2\mathcal{D}} \qquad (4.113)$$

to be a diffusion "time scale".

We can now impose a shear stress exerted by the wind which can set the slick liquid into circulation. Circulation aids diffusion by bringing regions of high concentration in the diffusible species into closer contact with the interface. In a sense this reduces the diffusion distance and should speed up the rate of removal by diffusion. We have investigated the magnitude of this enhanced removal, and how it might be correlated with slick and wind parameters.

A model can be formed along the physical bounds shown in Figure 4-12. Near the region $y = H$, we assume a classic Leveque-type diffusion problem. The circulating flow is mixed in the lower part of the slick and becomes the feed for the Leveque flow. Schematically, we separate the upper and lower regions into a diffusion region and a mixing region, connected by the circulating flow q. The magnitude of the circulating flow can be obtained from:

$$q/W = \int_{\frac{2}{3}H}^{H} v\,dy = \frac{4HV}{27} = \frac{H^2\tau}{27\mu} \tag{4.114}$$

where W is the unit width in the z-direction. Along the slick/air interface the velocity is related to the shear stress τ by:

$$\tau = \mu \left.\frac{\partial v}{\partial y}\right|_H = 4\,\mu\,\frac{V}{H} \tag{4.115}$$

An average velocity of circulation as may be defined as:

$$\overline{V} = \frac{q/W}{H/3} = \frac{H\tau}{9\mu} \tag{4.116}$$

The Leveque solution gives:

$$\frac{C_2}{C_1} = 1 - 0.186(3)^{1/3}\left(\frac{9\,\mathcal{D}\,L}{\overline{V}B^2}\right)^{2/3} \tag{4.117}$$

where C_1 and C_2 are defined as in Figure 4-12, $B = \frac{1}{3}H$ and $V = H\tau/9\mu$; more simply:

$$\frac{C_2}{C_1} = 1 - 21.7\left(\frac{\mathcal{D}\,L\,\mu}{\tau H^3}\right)^{2/3} \tag{4.118}$$

For a simple stirred tank of volume ν, a material balance can be stated as:

$$\nu\,\frac{d\,C_2}{dt} = q\left(C_2 - C_1\right) = -\,21.7\left(\frac{\mathcal{D}\,L\,\mu}{\tau H^3}\right)^{2/3} q\,C_2 \tag{4.119}$$

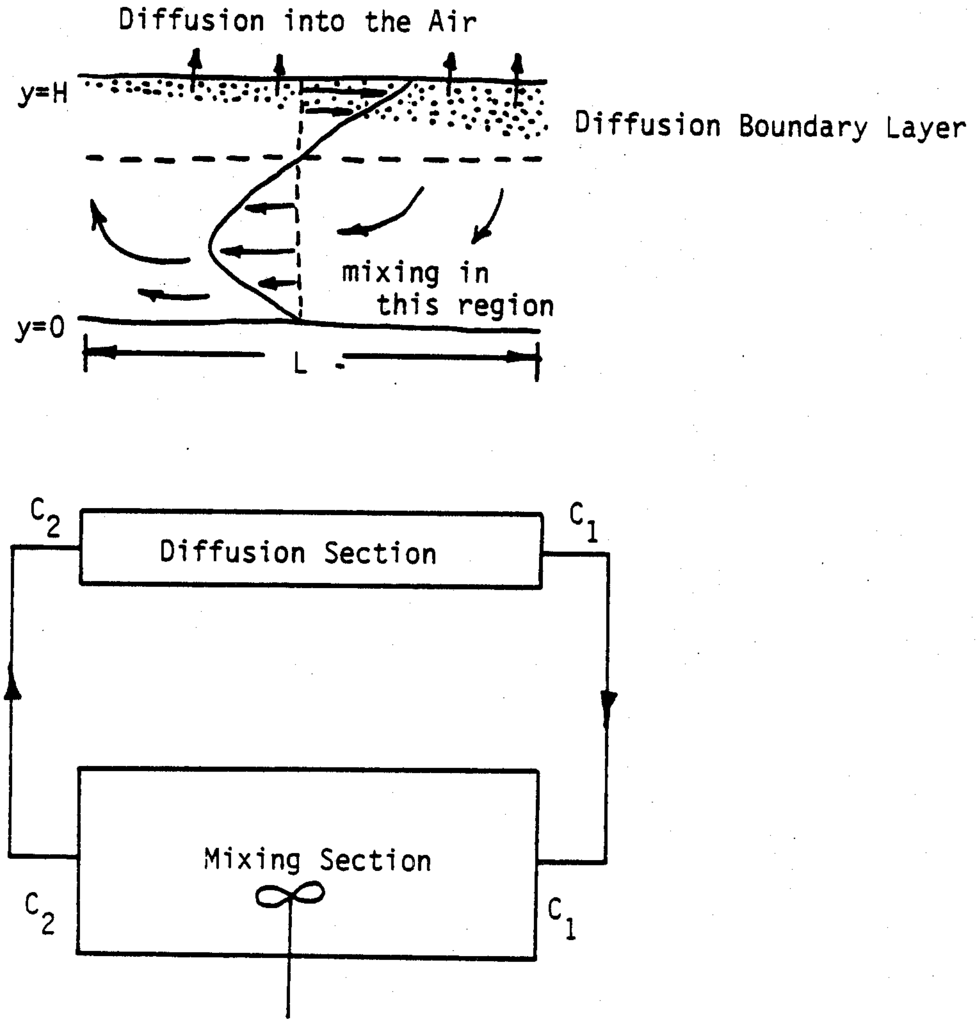

FIGURE 4-12. A MODEL FOR DIFFUSION WITH CIRCULATION

and the solution for C_2 is expressed:

$$\frac{C_2}{C_{2_0}} = \exp\left(- t/t_c\right) \qquad (4.120)$$

Thus we find, using Equations (4.114) and (4.119), that an appropriate time scale for circulation-enhanced loss is:

$$t_c = 0.8\left(\frac{L\mu H^3}{\mathcal{D}^2 \tau}\right)^{1/3} \qquad (4.121)$$

Of particular interest is the ratio t_D/t_c, which provides a measure of enhanced removal associated with circulation. We find:

$$E = \frac{t_D}{t_c} = \frac{1}{2}\left(\frac{\tau H^3}{L\mu\mathcal{D}}\right)^{1/3} \qquad (4.122)$$

If we go back to Equation (4.115), we may write E as:

$$E = \frac{1}{2}\left(\frac{4\,VH^2}{L\mathcal{D}}\right)^{1/3} = 0.79\left(\frac{VH}{\mathcal{D}}\ \frac{H}{L}\right)^{1/3} \qquad (4.123)$$

Even though we do not know V (it is related to the unknown τ) equation (4.123) is a useful form because it has the appearance of a Peclet number:

$$Pe = VH/\mathcal{D} = \frac{\tau H^2}{4\mu\mathcal{D}} \qquad (4.124)$$

and:

$$E = 0.79(Pe/A)^{1/3} \qquad (4.125)$$

where the aspect ratio $A = L/H$ appears.

While this model has several assumptions and uncertainties, it provides the opportunity to assess the role of certain physical events that occur during the weathering process:

Slick Spreading

As H decreases and L increases, we see that E decreases. Thus, as spreading occurs, diffusion control dominates any effects of internal circulation.

Viscosity increase through loss of volatiles

Since a rough approximation for diffusion coefficients of volatiles in a viscous liquid suggests that $\mathcal{D} \propto 1/\mu$, we expect that the Peclet number will remain constant at fixed H. Thus the aging of the slick per se does not change the balance between diffusion and convection as the dominant mode of volatiles loss.

In order to assess the importance of internal circulation, in the context of this model, we must estimate the magnitude of E. This requires data from which the shear stress at the sea surface may be estimated. However, typical values of V, H, and D (e.g., $V = 10$ cm/s, $H = 2$ cm, $\mathcal{D} = 10^{-7}$ cm^2/s) and aspect ratio ($L/H = 200$) give an estimate for E of about 10^2, representing a significant enhancement in the rate of loss of volatiles. This circulation model assumes that the slick may spread across the sea surface, but that its motion is laminar. Another type of internal circulation is possible, driven by wave action which is shown in Figure 4-13.

A localized area within a large slick may alternately be thinned and thickened as the surface of the sea undergoes wave motion. We might regard this as a complete mixing process at that local level, and a model which accounts for this phenomenon might be taken along the following lines:

- diffusion occurs from a uniform slab;
- the slab is instantaneously mixed periodically;
- diffusion occurs during intervals between mixing

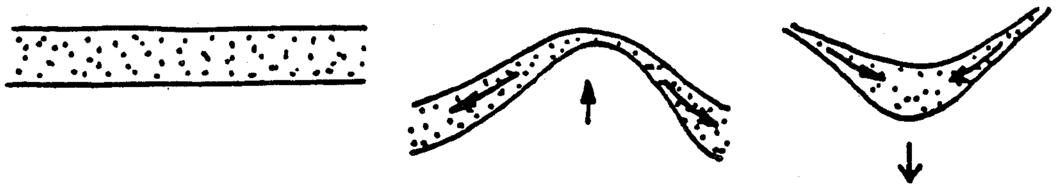

FIGURE 4-13. WAVE ACTION AS A MEANS OF PERIODIC MIXING ON A LOCAL SCALE.

This is a relatively simple model to assess. Define t_M as the time interval between mixes (We expect that t_M is related to the temporal periodicity of the waves). If the slick has a mean concentration, C_0, of some species at time t = 0, then after an interval, t_M, the slick will be mixed and its mean concentration will be:

$$C_1 = C_o \left[1 - \left(4 \mathcal{D} t_M / \pi H^2 \right)^{1/2} \right] \tag{4.126}$$

$$= C_o (1 - F) \tag{4.127}$$

The slick will then continue to lose volatiles by diffusion, as before, except that the initial mean concentration is now C_1. In general, we would find, after n "mixes":

$$C_n = C_{n-1} (1 - F) \tag{4.128}$$

and the solution of this difference equation, assuming F is constant, is:

$$C_n = C_o (1 - F)^n \tag{4.129}$$

We may compare this solution to that for quiescent diffusion in the absence of mixing:

$$C/C_o = \frac{8}{\pi^2} \exp\left(- \frac{\pi^2}{4} \frac{\mathcal{D}}{H^2} t \right) + \frac{8}{9\pi^2} \exp\left(- \frac{9\pi^2}{4} \frac{\mathcal{D} t}{H^2} \right) + \ldots \tag{4.130}$$

and if we plot C/C_0 vs t/H^2 (Figure 4-14) we see that:

$$t = n t_M \tag{4.131}$$

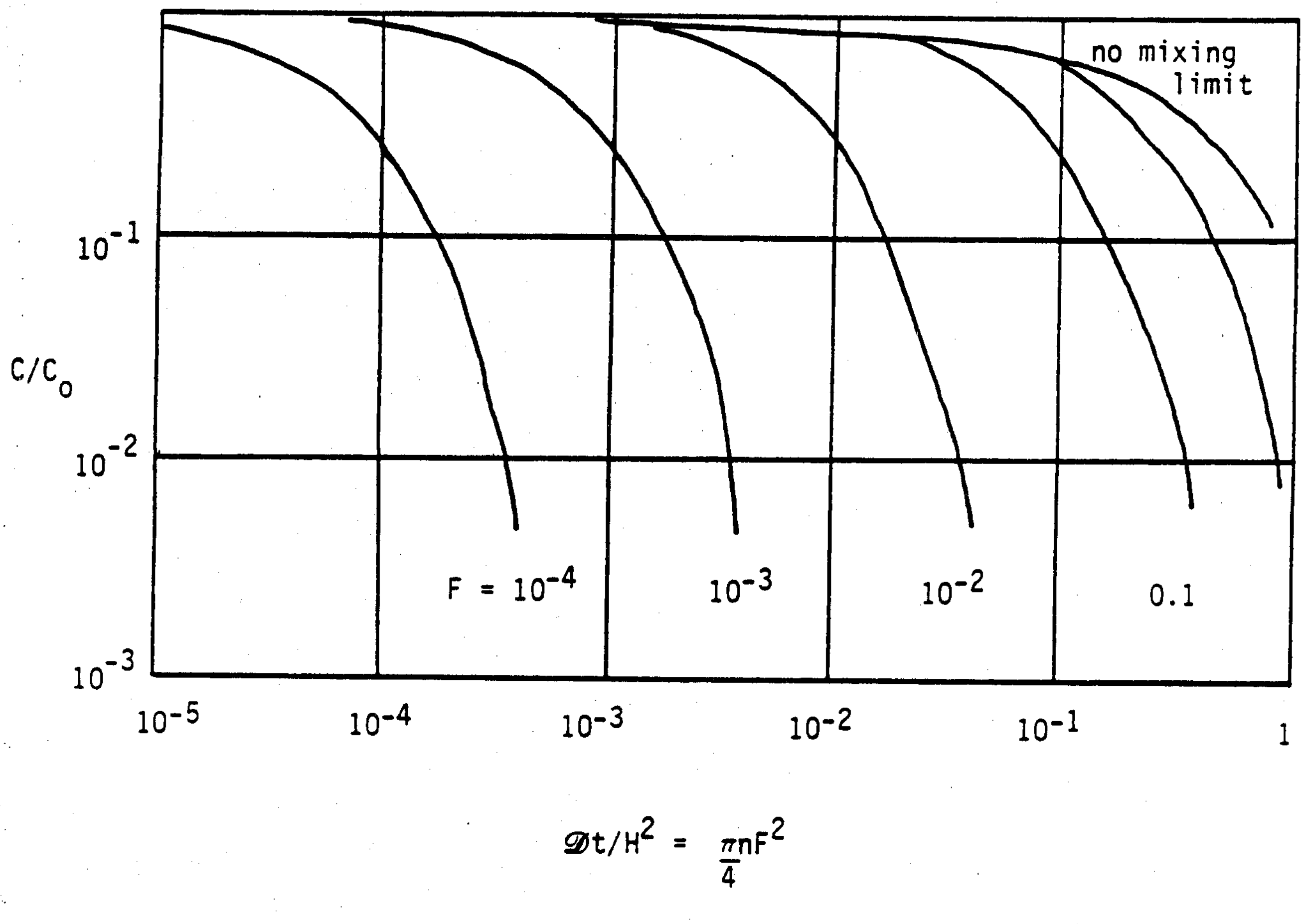

FIGURE 4-14. EFFECT OF MIXING ON CONCENTRATION

As expected, periodic mixing enhances the rate of loss of volatiles, the extent of enhancement depending upon the parameter F. From the half-times of these curves we may define a measure of the extent of enhancement by mixing, E_M, as:

$$E_M = \frac{\tau_{1/2}\,\text{(pure diffusion)}}{\tau_{1/2}\,\text{(periodic mixing)}} \tag{4.132}$$

Figure 4-15 shows E_m plotted as a function of F. Reasonable values of F can be estimated from:

$$F = \left(4\mathscr{D} t_M/\pi H^2\right)^{1/2} \tag{4.133}$$

We expect that H is of order 1 cm, with a range of perhaps 0.5 to 2 cm. The magnitude of $\mathscr{D}$ will depend strongly upon which volatile species is considered and might range from 10^{-8} to 10^{-6} cm^2/s. The wave interval, t_M, might take on values in the range 1 to 10 sec. F, then, would be in the range $10^{-4} \leq F \leq 10^{-2}$. If these estimates are reasonable, then it appears that this periodic mixing mechanism exerts a tremendous degree of enhancement of loss of volatiles on the slick in comparison to the pure, static diffusion model.

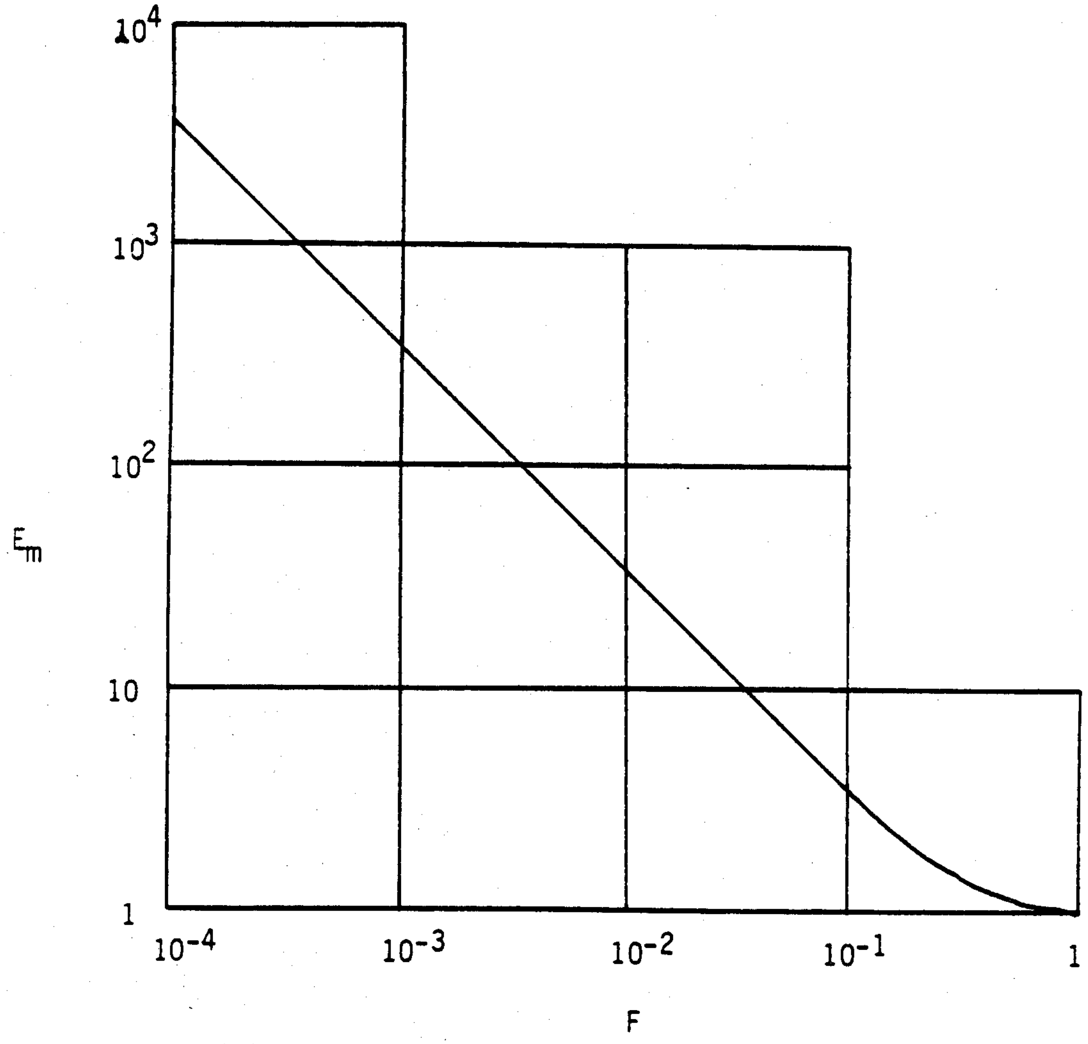

FIGURE 4-15. DEPENDENCE OF ENHANCEMENT FACTOR ON F

4.9 DISPERSION OF OIL DROPS INTO WATER

Oil enters the water column not only on the molecular level as dissolved species, but also as discrete drops. The oil drops enter the water column as a result of turbulence at the surface. This turbulence which is due to wind and waves creates small oil drops which do not return to the parent slick. These drops are then swept away by the local currents and eddy diffusivity. Examination of the knowledge of the dispersing of oil into the water column (MACKAY, et al., 1980) indicates that this process puts more oil into the water column than dissolution. The calculation of water-column oil-drop concentration versus time and depth can be based on the results of the dispersion model in the current open-ocean oil-weathering computer code. The results from the oil-weathering code are in the form of a flux versus time. In order to use these results the water-column concentration calculation must be written in terms of a flux boundary condition.

Consider the concentration of oil drops in the water column to be described in the vertical direction by

$$\frac{\partial C}{\partial t} = k \frac{\partial^2 C}{\partial x^2} \qquad 0 \leq x \leq \ell \tag{4.134}$$

At the bottom of the ocean

$$\frac{dC}{dx} = 0 \qquad \text{at } x = 0 \tag{4.135}$$

since mass cannot transport across this boundary. Also

$$C(x) = 0 \qquad \text{at } t = 0 \tag{4.136}$$

which describes a clean water column at time zero. The first equation above implies that the oil drops are neutrally buoyant.

The flux of oil drops into the water at $x = \ell$ is assumed to be represented by a sum of decaying exponentials. For one of these exponentials

$$k \frac{dC}{dx} = ae^{-bt} \qquad \text{at } x = \ell \tag{4.137}$$

where a and b are determined from a fit of the available dispersion rate data. This then requires that a solution be generated for each (a,b) set and the results added to obtain the sum.

The solution to the equation set described above is

$$C(\chi,t) = \frac{a}{b\ell} - \frac{a \cos\left(\sqrt{\frac{b}{k}}\, x\right) e^{-bt}}{(kb)^{\frac{1}{2}} \sin\left(\sqrt{\frac{b}{k}}\ell\right)} +$$

$$\frac{2a}{\ell} \sum_{n=1}^{\infty} \frac{(-1)^n \cos\,(n\Pi\, x/\ell) e^{-kn^2 \Pi^2 t/h^2}}{(b - kn^2\Pi^2/\ell^2)} \tag{4.138}$$

Typical units for the various constants above are $a \equiv \text{gm/cm}^2\text{sec}$, $b \equiv 1/\text{sec}$, $\ell \equiv \text{cm}$, and $k \equiv \text{cm}^2/\text{sec}$. The total mass put into the water column is

$$m = \int_0^{\infty} ae^{-bt}\, dt \tag{4.139}$$

or

$$M = \frac{a}{b} \tag{4.140}$$

which agrees with the concentration predicted from $C(x,t)$ when $t \to \infty$, i.e., $C(x,t \to \infty) = a/b\ell$.

The equation which describes $C(X,t)$ above has been programmed in FORTRAN so that numerical investigations can be easily performed. The code listing and user instructions are in Appendix D: Code Listing for Dispersed-Oil Concentration Profile with a **Time-Varying Flux.** In order to illustrate the use of this code three examples are presented here. The dispersion rate data were obtained directly from the open-ocean oil-weathering model and are listed in Table 4-9 for three wind speeds. These data are plotted in Figures 4-16(a) through 4-16(c). The coordinates are $\log_{10}$ of the rate versus time, and these plots show that a two-line fit will represent the data. The entire range of 200 hours for each wind speed can be represented as

$$k \frac{dc}{dx} = a_1 e^{-b_1 t} + a_2 e^{-b_2 t} \quad \text{at } x = \ell \tag{4.141}$$

The values of a_1, b_1, etc., for each wind speed are listed in Table 4-10.

Table 4-9

Dispersion Rate Data Obtained from Open-Ocean Oil-Weathering Model

Time (Hours)	Dispersion Rate ($gm/m^2/hr$) (and wind speed)		
	10 knots	20 knots	40 knots
5	5.0	9.5	12
10	3.7	4.5	10
20	2.4	2.8	7.5
50	0.87	1.5	3.5
100	0.52	1.1	1.4
150	0.41	---	0.73
200	0.33	0.5	0.45

Figure 4-16A.

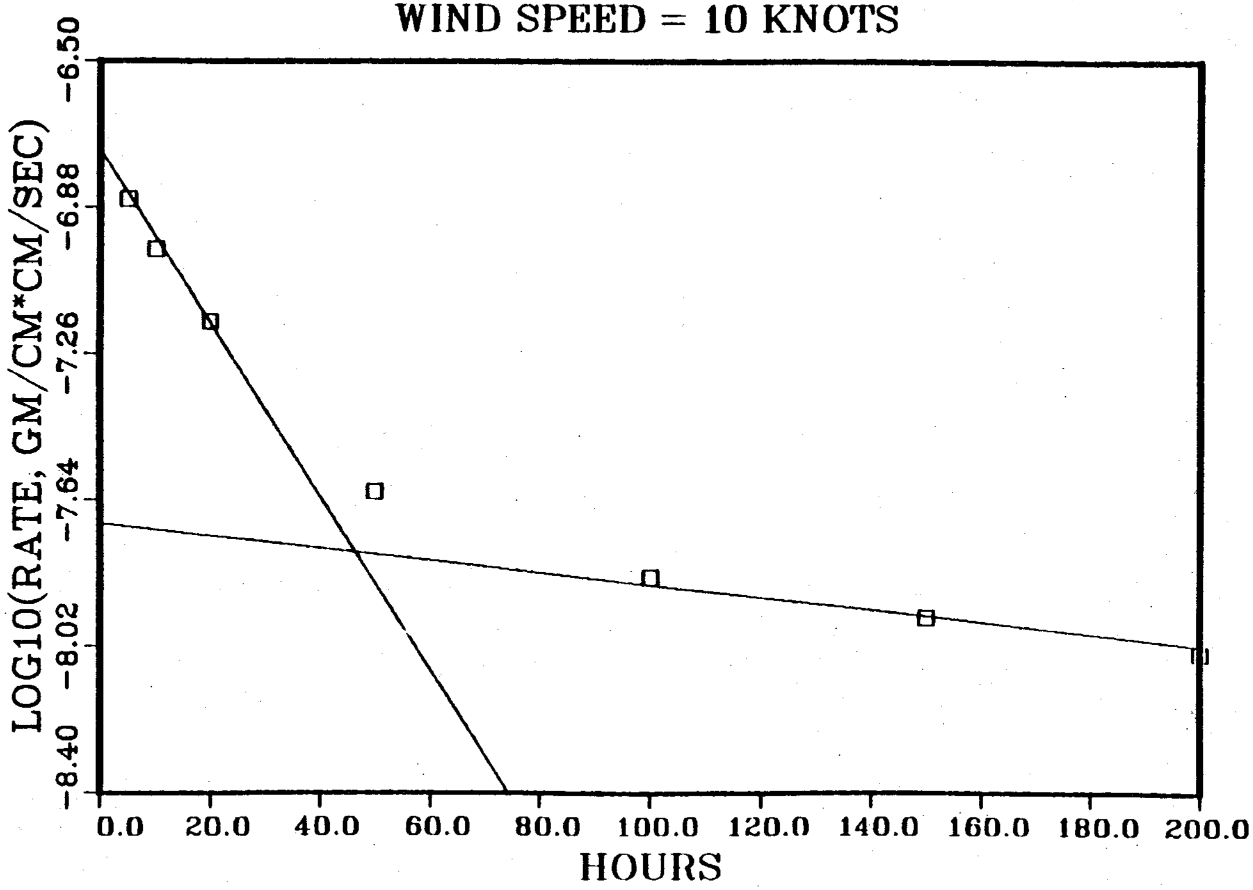

DISPERSION RATE VERSUS TIME
FROM OPEN–OCEAN OIL–WEATHERING MODEL
WIND SPEED = 10 KNOTS

Figure 4-16B.

DISPERSION RATE VERSUS TIME
FROM OPEN–OCEAN OIL–WEATHERING MODEL
WIND SPEED = 20 KNOTS

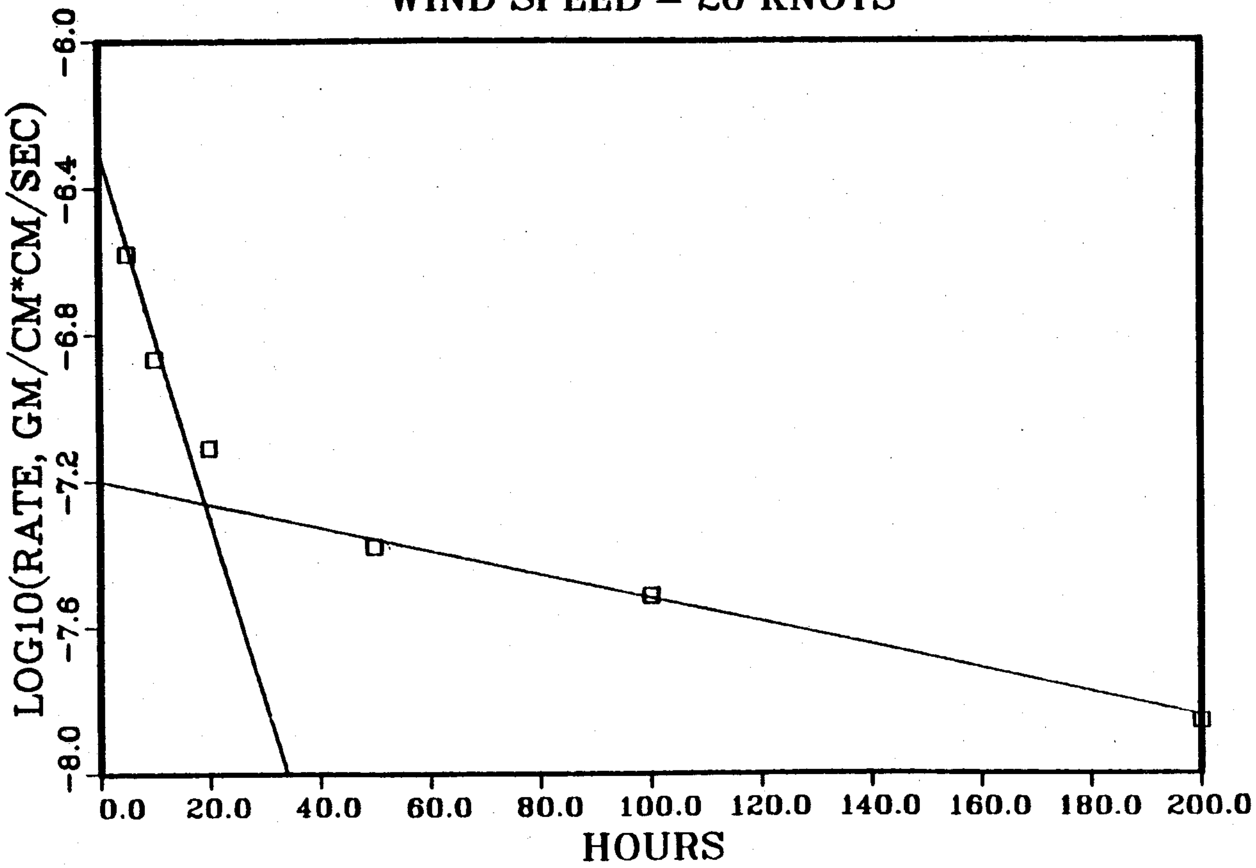

Figure 4-16C.

DISPERSION RATE VERSUS TIME
FROM OPEN–OCEAN OIL–WEATHERING MODEL
WIND SPEED = 40 KNOTS

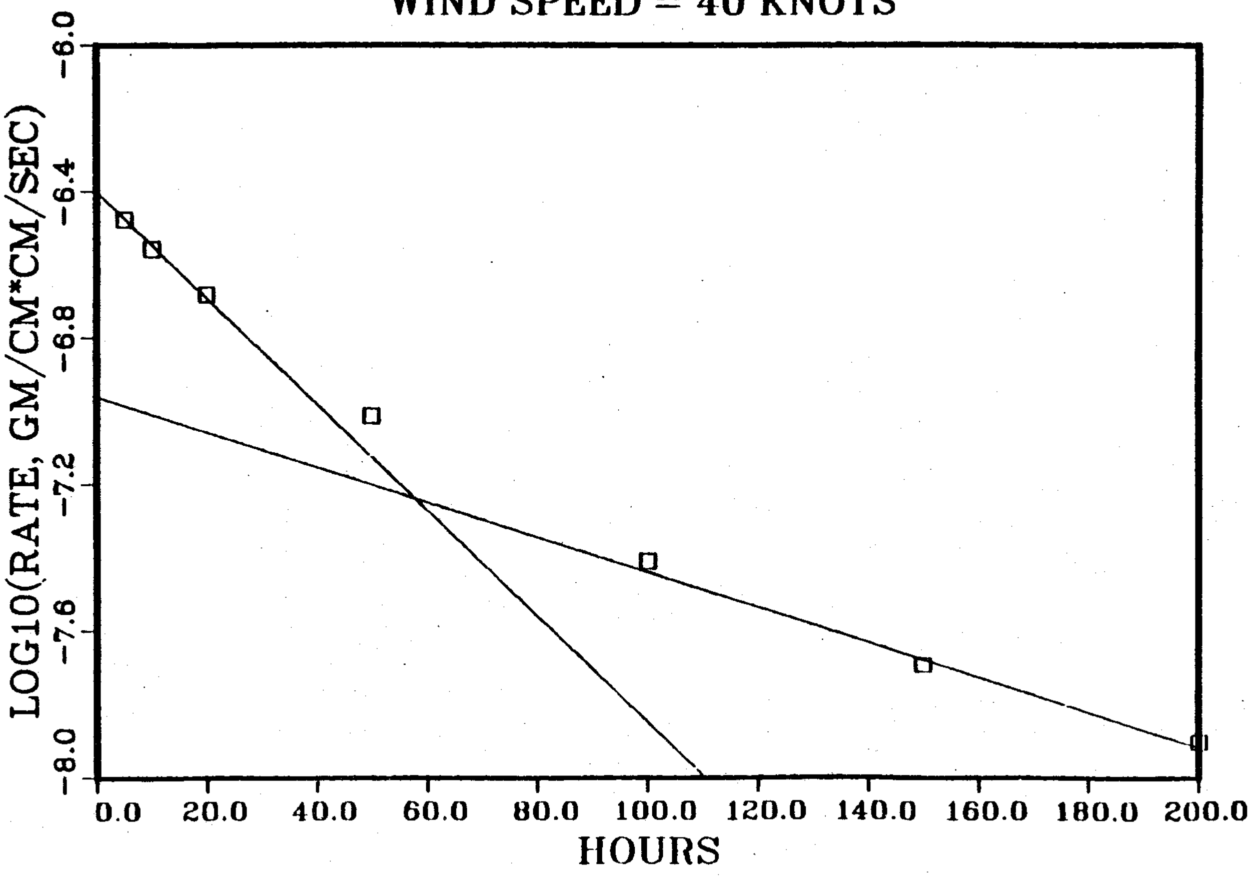

Table 4-10

Equation Constants for Two-Line Fit for Dispersion Rate Data

Wind Speed (knots)	a_1 gm/cm^{2}sec	b_1 1/sec	a_2	b_2
10	1.89×10^{-7}	1.4×10^{-5}	2.03×10^{-8}	1.02×10^{-6}
20	6.4×10^{-8}	2.03×10^{-6}	5.1×10^{-7}	3.19×10^{-5}
40	1.12×10^{-7}	3.05×10^{-6}	4.04×10^{-7}	9.3×10^{-6}

$$\text{flux} = a_1 e^{-b_1 t} + a_2 e^{-b_2 t}$$

An example of detailed results are presented in Table 4-11 for 20-knot wind speed. The input data are always printed in the output file along with the total dispersion rate from the (a,b) data sets entered. In this example there are two (a,b) data sets, i.e., the two straight lines in Figure 4-16B for a 20-knot wind speed. The output that follows the time = infinity water-column concentration value through the line stating "end of calculation for A(2), B(2)" is intermediate output. The final concentration profiles are listed in the box on page three of Table 4-11. Since columns and rows of numbers are sometimes tedious to examine, the results for the example case and the two other wind speeds in Table 4-10 have been plotted in Figures 4-17A through 4-17F. In each figure the pertinent parameters are listed to provide a complete record of the calculated results. For these examples a vertical diffusivity of 185 cm^2/sec was used (PELTO, 1983). For each of the three wind speeds the 50-meter depth cases always exhibit very curved concentration profiles up through 24 hours. In contrast the 10-meter depth cases exhibit very flat concentration profiles indicating that the dispersed-oil input rate at the ocean surface is the rate controlling step.

Table 4-11. Detailed Results for the Calculation of Dispersed-Oil Concentration Profiles in the Water Column.

```
CONCENTRATION OF DISPERSED OIL IN THE WATER COLUMN, CALCULATED BY EXPONENTIAL FITS TO A GIVEN DISPERSION RATE

VERTICAL DIFFUSIVITY =  1.850D+02 CM*CM/SEC, DEPTH =     50. METERS, MAXIMUM TIME =     24. HOURS

K*PIE*PIE/L/L =  7.304D-05 1/SEC

NUMBER OF TERMS IN THE SERIES =  100, NUMBER OF EXPONENTIAL FITS =  2

THE EXPONENTIAL FIT COEFFICIENTS FOR THE DISPERSION RATE (RATE=A*EXP(-B*TIME)) ARE:
UNITS ARE A==GM/CM*CM/SEC, B==1/SEC

               AI(J)            BI(J)
  1          6.400D-08        2.030D-06
  2          5.100D-07        3.190D-05

THE DISPERSION RATE FROM THE ABOVE A,B DATA SET FOR A WIND SPEED OF  20. KNOTS IS:

         TIME         RATE
         HOUR       CM/M*M/HR
       2.400D+00    1.620D+01
       4.800D+00    1.280D+01
       7.200D+00    1.022D+01
       9.600D+00    8.244D+00
       1.200D+01    6.738D+00
       1.440D+01    5.587D+00
       1.680D+01    4.705D+00
       1.920D+01    4.027D+00
       2.160D+01    3.504D+00
       2.400D+01    3.100D+00

THE TIME = INFINITY WATER-COLUMN CONCENTRATION OF DISPERSED OIL =  6.305D-06 GM/CC

A CHECK OF THE INITIAL CONDITIONS FOR THE J = 1   A,B INPUT SET

        DEPTH          EBL           SUM       CONC AT T=0
        METER        COS TERM       SERIES

      0.000D+00     5.718D-06    -5.839D-07     3.488D-09
      5.000D+00     5.883D-06    -4.224D-07    -1.045D-11
      1.000D+01     6.032D-06    -2.734D-07    -1.570D-11
      1.500D+01     6.164D-06    -1.411D-07    -1.668D-11
      2.000D+01     6.280D-06    -2.561D-08    -1.702D-11
      2.500D+01     6.378D-06     7.264D-08    -1.718D-11
      3.000D+01     6.459D-06     1.534D-07    -1.726D-11
      3.500D+01     6.522D-06     2.164D-07    -1.731D-11
      4.000D+01     6.567D-06     2.616D-07    -1.733D-11
      4.500D+01     6.594D-06     2.887D-07    -1.735D-11
      5.000D+01     6.603D-06     2.978D-07    -1.735D-11

DISPERSED-OIL CONCENTRATIONS, GM/CC, IN THE WATER COLUMN FOR VARIOUS TIMES AND DEPTHS FOLLOW

                                                 H O U R S
 DEPTH  2.40D+00  4.80D+00  7.20D+00  9.60D+00  1.20D+01  1.44D+01  1.68D+01  1.92D+01  2.16D+01  2.40D+01
 METER
   0.0  4.88D-07  6.82D-07  8.26D-07  9.46D-07  1.05D-06  1.15D-06  1.24D-06  1.33D-06  1.42D-06  1.51D-06
   5.0  3.36D-07  5.28D-07  6.72D-07  7.93D-07  9.02D-07  1.00D-06  1.10D-06  1.19D-06  1.28D-06  1.37D-06
  10.0  2.21D-07  3.99D-07  5.39D-07  6.59D-07  7.67D-07  8.69D-07  9.67D-07  1.06D-06  1.15D-06  1.24D-06
  15.0  1.38D-07  2.94D-07  4.25D-07  5.42D-07  6.50D-07  7.52D-07  8.51D-07  9.47D-07  1.04D-06  1.13D-06
  20.0  8.13D-08  2.11D-07  3.31D-07  4.42D-07  5.48D-07  6.50D-07  7.50D-07  8.47D-07  9.42D-07  1.04D-06
  25.0  4.53D-08  1.48D-07  2.54D-07  3.59D-07  4.63D-07  5.64D-07  6.64D-07  7.62D-07  8.59D-07  9.53D-07
  30.0  2.38D-08  1.01D-07  1.94D-07  2.93D-07  3.94D-07  4.94D-07  5.94D-07  6.93D-07  7.90D-07  8.86D-07
  35.0  1.18D-08  6.85D-08  1.50D-07  2.42D-07  3.40D-07  4.40D-07  5.40D-07  6.39D-07  7.37D-07  8.33D-07
  40.0  5.54D-09  4.72D-08  1.19D-07  2.07D-07  3.02D-07  4.01D-07  5.01D-07  6.00D-07  6.98D-07  7.95D-07
  45.0  2.71D-09  3.52D-08  1.01D-07  1.86D-07  2.80D-07  3.78D-07  4.77D-07  5.77D-07  6.75D-07  7.73D-07
  50.0  1.90D-09  3.13D-08  9.49D-08  1.78D-07  2.72D-07  3.70D-07  4.69D-07  5.69D-07  6.68D-07  7.65D-07
```

Table 4-11, pg 2 Detailed Results for the Calculation of Dispersed-Oil Concentration Profiles in the Water Column. (Continued)

```
THE DERIVATIVE WITH RESPECT TO X OF THE WATER COLUMN CONCENTRATION FOLLOWS, IN GM/(CM**4)

                                                    H O U R S
  DEPTH    2.40D+00  4.80D+00  7.20D+00  9.60D+00  1.20D+01  1.44D+01  1.68D+01  1.92D+01  2.16D+01  2.40D+01
  METER
    0.0    3.40D-10  3.34D-10  3.28D-10  3.23D-10  3.17D-10  3.11D-10  3.06D-10  3.01D-10  2.95D-10  2.90D-10
    5.0    2.66D-10  2.83D-10  2.87D-10  2.87D-10  2.85D-10  2.81D-10  2.77D-10  2.73D-10  2.68D-10  2.63D-10
   10.0    1.97D-10  2.33D-10  2.47D-10  2.52D-10  2.52D-10  2.50D-10  2.47D-10  2.44D-10  2.40D-10  2.36D-10
   15.0    1.38D-10  1.87D-10  2.08D-10  2.16D-10  2.19D-10  2.19D-10  2.17D-10  2.14D-10  2.11D-10  2.08D-10
   20.0    9.04D-11  1.45D-10  1.70D-10  1.82D-10  1.87D-10  1.88D-10  1.87D-10  1.84D-10  1.82D-10  1.79D-10
   25.0    5.57D-11  1.09D-10  1.36D-10  1.49D-10  1.54D-10  1.56D-10  1.56D-10  1.54D-10  1.52D-10  1.50D-10
   30.0    3.21D-11  7.83D-11  1.04D-10  1.17D-10  1.23D-10  1.25D-10  1.25D-10  1.24D-10  1.22D-10  1.20D-10
   35.0    1.72D-11  5.33D-11  7.51D-11  8.62D-11  9.13D-11  9.33D-11  9.35D-11  9.29D-11  9.18D-11  9.05D-11
   40.0    8.44D-12  3.28D-11  4.86D-11  5.68D-11  6.06D-11  6.21D-11  6.24D-11  6.20D-11  6.13D-11  6.04D-11
   45.0    3.36D-12  1.56D-11  2.38D-11  2.82D-11  3.02D-11  3.10D-11  3.12D-11  3.10D-11  3.07D-11  3.03D-11
   50.0    0.00D+00  0.00D+00  0.00D+00  0.00D+00  0.00D+00  0.00D+00  0.00D+00  0.00D+00  0.00D+00  0.00D+00

GRAMS OIL
 IN WATER  5.48D-04  1.09D-03  1.62D-03  2.14D-03  2.65D-03  3.15D-03  3.64D-03  4.13D-03  4.60D-03  5.07D-03
PER CM*CM

  AVERAGE
   GM/CC   1.10D-07  2.17D-07  3.23D-07  4.27D-07  5.29D-07  6.30D-07  7.29D-07  8.25D-07  9.21D-07  1.01D-06

********************************  END OF CALCULATION FOR A(1), B(1)

THE TIME = INFINITY WATER-COLUMN CONCENTRATION OF DISPERSED OIL =  3.197D-06 GM/CC

A CHECK OF THE INITIAL CONDITIONS FOR THE J = 2   A,B INPUT SET

         DEPTH          EBL            SUM         CONC AT T=0
         METER        COS TERM        SERIES

       0.000D+00     -3.674D-06     -6.844D-06      2.779D-08
       5.000D+00     -2.227D-06     -5.424D-06     -8.326D-11
       1.000D+01     -6.835D-07     -3.881D-06     -1.251D-10
       1.500D+01      8.889D-07     -2.309D-06     -1.329D-10
       2.000D+01      2.423D-06     -7.745D-07     -1.356D-10
       2.500D+01      3.853D-06      6.556D-07     -1.369D-10
       3.000D+01      5.118D-06      1.920D-06     -1.375D-10
       3.500D+01      6.163D-06      2.965D-06     -1.379D-10
       4.000D+01      6.943D-06      3.745D-06     -1.381D-10
       4.500D+01      7.425D-06      4.227D-06     -1.382D-10
       5.000D+01      7.588D-06      4.390D-06     -1.383D-10

DISPERSED-OIL CONCENTRATIONS, GM/CC, IN THE WATER COLUMN FOR VARIOUS TIMES AND DEPTHS FOLLOW

                                                    H O U R S
  DEPTH    2.40D+00  4.80D+00  7.20D+00  9.60D+00  1.20D+01  1.44D+01  1.68D+01  1.92D+01  2.16D+01  2.40D+01
  METER
    0.0    3.28D-06  3.91D-06  4.06D-06  4.02D-06  3.91D-06  3.79D-06  3.67D-06  3.57D-06  3.49D-06  3.42D-06
    5.0    2.33D-06  3.14D-06  3.46D-06  3.56D-06  3.56D-06  3.52D-06  3.46D-06  3.41D-06  3.37D-06  3.33D-06
   10.0    1.56D-06  2.45D-06  2.89D-06  3.10D-06  3.20D-06  3.24D-06  3.25D-06  3.25D-06  3.24D-06  3.23D-06
   15.0    9.92D-07  1.86D-06  2.37D-06  2.67D-06  2.85D-06  2.96D-06  3.03D-06  3.08D-06  3.11D-06  3.14D-06
   20.0    5.94D-07  1.37D-06  1.91D-06  2.27D-06  2.52D-06  2.70D-06  2.83D-06  2.92D-06  2.99D-06  3.04D-06
   25.0    3.35D-07  9.82D-07  1.51D-06  1.92D-06  2.23D-06  2.46D-06  2.64D-06  2.77D-06  2.87D-06  2.95D-06
   30.0    1.78D-07  6.86D-07  1.19D-06  1.62D-06  1.97D-06  2.25D-06  2.47D-06  2.64D-06  2.77D-06  2.88D-06
   35.0    8.87D-08  4.73D-07  9.41D-07  1.38D-06  1.77D-06  2.08D-06  2.34D-06  2.54D-06  2.69D-06  2.81D-06
   40.0    4.21D-08  3.31D-07  7.65D-07  1.21D-06  1.62D-06  1.96D-06  2.24D-06  2.46D-06  2.63D-06  2.76D-06
   45.0    2.07D-08  2.50D-07  6.60D-07  1.11D-06  1.53D-06  1.88D-06  2.18D-06  2.41D-06  2.59D-06  2.73D-06
   50.0    1.46D-08  2.24D-07  6.25D-07  1.08D-06  1.50D-06  1.86D-06  2.16D-06  2.39D-06  2.58D-06  2.72D-06
```

Table 4-11, pg 3 Detailed Results for the Calculation of Dispersed-Oil Concentration Profiles in the Water Column. (Continued)

```
THE DERIVATIVE WITH RESPECT TO X OF THE WATER COLUMN CONCENTRATION FOLLOWS, IN CM/(CM**4)

                                                H O U R S
  DEPTH    2.40D+00   4.80D+00   7.20D+00   9.60D+00   1.20D+01   1.44D+01   1.68D+01   1.92D+01   2.16D+01   2.40D+01
  METER
    0.0    2.09D-09   1.59D-09   1.21D-09   9.15D-10   6.95D-10   5.27D-10   4.00D-10   3.04D-10   2.31D-10   1.75D-10
    5.0    1.73D-09   1.46D-09   1.17D-09   9.23D-10   7.18D-10   5.54D-10   4.26D-10   3.26D-10   2.49D-10   1.90D-10
   10.0    1.33D-09   1.28D-09   1.10D-09   8.95D-10   7.13D-10   5.59D-10   4.34D-10   3.34D-10   2.56D-10   1.96D-10
   15.0    9.58D-10   1.08D-09   9.89D-10   8.37D-10   6.81D-10   5.42D-10   4.24D-10   3.29D-10   2.53D-10   1.94D-10
   20.0    6.45D-10   8.78D-10   8.59D-10   7.54D-10   6.26D-10   5.04D-10   3.98D-10   3.10D-10   2.40D-10   1.84D-10
   25.0    4.05D-10   6.82D-10   7.18D-10   6.52D-10   5.51D-10   4.49D-10   3.57D-10   2.79D-10   2.17D-10   1.67D-10
   30.0    2.37D-10   5.05D-10   5.71D-10   5.35D-10   4.60D-10   3.78D-10   3.02D-10   2.37D-10   1.85D-10   1.42D-10
   35.0    1.28D-10   3.52D-10   4.25D-10   4.08D-10   3.56D-10   2.95D-10   2.37D-10   1.86D-10   1.45D-10   1.12D-10
   40.0    6.35D-11   2.20D-10   2.81D-10   2.75D-10   2.42D-10   2.02D-10   1.63D-10   1.28D-10   1.00D-10   7.74D-11
   45.0    2.54D-11   1.05D-10   1.39D-10   1.39D-10   1.23D-10   1.02D-10   8.27D-11   6.54D-11   5.11D-11   3.95D-11
   50.0    0.00D+00   0.00D+00   0.00D+00   0.00D+00   0.00D+00   0.00D+00   0.00D+00   0.00D+00   0.00D+00   0.00D+00

GRAMS OIL
 IN WATER  3.85D-03   6.77D-03   8.99D-03   1.07D-02   1.20D-02   1.29D-02   1.37D-02   1.42D-02   1.46D-02   1.50D-02
PER CM*CM

  AVERAGE
    GM/CC  7.70D-07   1.35D-06   1.80D-06   2.14D-06   2.39D-06   2.59D-06   2.73D-06   2.84D-06   2.93D-06   2.99D-06

 *********************************  END OF CALCULATION FOR A(2), B(2)
```

```
 CONCENTRATIONS VERSES TIME AND DEPTH FOR 2 A,B DATA SETS (ADD UP THE PREVIOUS RESULTS)

                                                H O U R S
  DEPTH    2.40D+00   4.80D+00   7.20D+00   9.60D+00   1.20D+01   1.44D+01   1.68D+01   1.92D+01   2.16D+01   2.40D+01
  METER
    0.0    3.77D-06   4.59D-06   4.88D-06   4.97D-06   4.96D-06   4.94D-06   4.91D-06   4.90D-06   4.91D-06   4.93D-06
    5.0    2.66D-06   3.67D-06   4.13D-06   4.35D-06   4.46D-06   4.52D-06   4.56D-06   4.60D-06   4.65D-06   4.70D-06
   10.0    1.78D-06   2.85D-06   3.43D-06   3.76D-06   3.97D-06   4.11D-06   4.22D-06   4.31D-06   4.39D-06   4.48D-06
   15.0    1.13D-06   2.16D-06   2.79D-06   3.21D-06   3.50D-06   3.71D-06   3.88D-06   4.03D-06   4.15D-06   4.27D-06
   20.0    6.76D-07   1.58D-06   2.24D-06   2.71D-06   3.07D-06   3.35D-06   3.58D-06   3.77D-06   3.93D-06   4.08D-06
   25.0    3.81D-07   1.13D-06   1.77D-06   2.28D-06   2.69D-06   3.02D-06   3.30D-06   3.53D-06   3.73D-06   3.91D-06
   30.0    2.02D-07   7.87D-07   1.38D-06   1.91D-06   2.37D-06   2.75D-06   3.07D-06   3.34D-06   3.56D-06   3.76D-06
   35.0    1.00D-07   5.42D-07   1.09D-06   1.63D-06   2.11D-06   2.52D-06   2.88D-06   3.18D-06   3.43D-06   3.64D-06
   40.0    4.77D-08   3.78D-07   8.84D-07   1.42D-06   1.92D-06   2.36D-06   2.74D-06   3.06D-06   3.33D-06   3.56D-06
   45.0    2.34D-08   2.85D-07   7.61D-07   1.30D-06   1.81D-06   2.26D-06   2.65D-06   2.99D-06   3.27D-06   3.51D-06
   50.0    1.65D-08   2.55D-07   7.20D-07   1.25D-06   1.77D-06   2.23D-06   2.62D-06   2.96D-06   3.25D-06   3.49D-06

 THE DERIVATIVE OF THE CONCENTRATION WITH RESPECT TO X FOR 2 A,B DATA SETS

                                                H O U R S
  DEPTH    2.40D+00   4.80D+00   7.20D+00   9.60D+00   1.20D+01   1.44D+01   1.68D+01   1.92D+01   2.16D+01   2.40D+01
  METER
    0.0    2.43D-09   1.92D-09   1.53D-09   1.24D-09   1.01D-09   8.39D-10   7.06D-10   6.05D-10   5.26D-10   4.65D-10
    5.0    1.99D-09   1.74D-09   1.46D-09   1.21D-09   1.00D-09   8.36D-10   7.03D-10   5.98D-10   5.17D-10   4.53D-10
   10.0    1.53D-09   1.52D-09   1.34D-09   1.15D-09   9.65D-10   8.09D-10   6.81D-10   5.78D-10   4.96D-10   4.32D-10
   15.0    1.10D-09   1.27D-09   1.20D-09   1.05D-09   9.01D-10   7.61D-10   6.41D-10   5.43D-10   4.64D-10   4.02D-10
   20.0    7.35D-10   1.02D-09   1.03D-09   9.36D-10   8.13D-10   6.92D-10   5.84D-10   4.95D-10   4.22D-10   3.63D-10
   25.0    4.60D-10   7.91D-10   8.54D-10   8.00D-10   7.06D-10   6.05D-10   5.12D-10   4.33D-10   3.69D-10   3.17D-10
   30.0    2.69D-10   5.84D-10   6.76D-10   6.52D-10   5.83D-10   5.02D-10   4.27D-10   3.61D-10   3.07D-10   2.63D-10
   35.0    1.46D-10   4.05D-10   5.00D-10   4.95D-10   4.47D-10   3.88D-10   3.30D-10   2.79D-10   2.37D-10   2.03D-10
   40.0    7.19D-11   2.53D-10   3.29D-10   3.32D-10   3.03D-10   2.64D-10   2.25D-10   1.90D-10   1.61D-10   1.38D-10
   45.0    2.88D-11   1.21D-10   1.63D-10   1.67D-10   1.53D-10   1.33D-10   1.14D-10   9.64D-11   8.18D-11   6.98D-11
   50.0    0.00D+00   0.00D+00   0.00D+00   0.00D+00   0.00D+00   0.00D+00   0.00D+00   0.00D+00   0.00D+00   0.00D+00

GRAMS OIL
 IN WATER  4.40D-03   7.86D-03   1.06D-02   1.28D-02   1.46D-02   1.61D-02   1.73D-02   1.84D-02   1.93D-02   2.00D-02
PER CM*CM


  AVERAGE
    GM/CC  8.80D-07   1.57D-06   2.12D-06   2.56D-06   2.92D-06   3.22D-06   3.46D-06   3.67D-06   3.85D-06   4.01D-06

 *********************************  END OF CALCULATION FOR ALL 2 OF THE A,B SETS
```

Figure 4-17A.

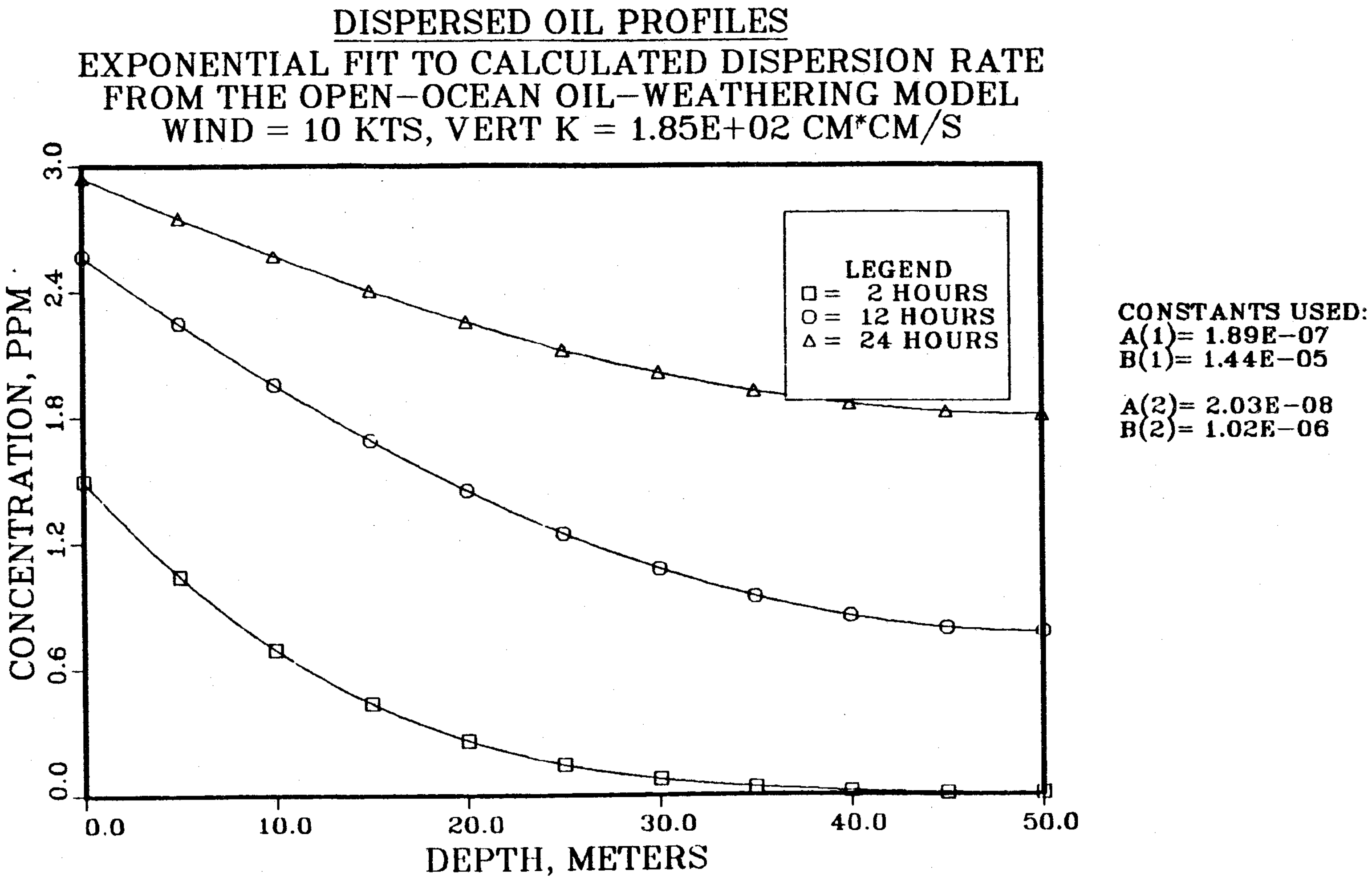
DISPERSED OIL PROFILES
EXPONENTIAL FIT TO CALCULATED DISPERSION RATE
FROM THE OPEN-OCEAN OIL-WEATHERING MODEL
WIND = 10 KTS, VERT K = 1.85E+02 CM*CM/S
CONCENTRATION, PPM
0.0
0.6
1.2
1.8
2.4
3.0
DEPTH, METERS
0.0
10.0
20.0
30.0
40.0
50.0
LEGEND
□ = 2 HOURS
○ = 12 HOURS
△ = 24 HOURS
CONSTANTS USED:
A(1)= 1.89E-07
B(1)= 1.44E-05
A(2)= 2.03E-08
B(2)= 1.02E-06

Figure 4-17B.

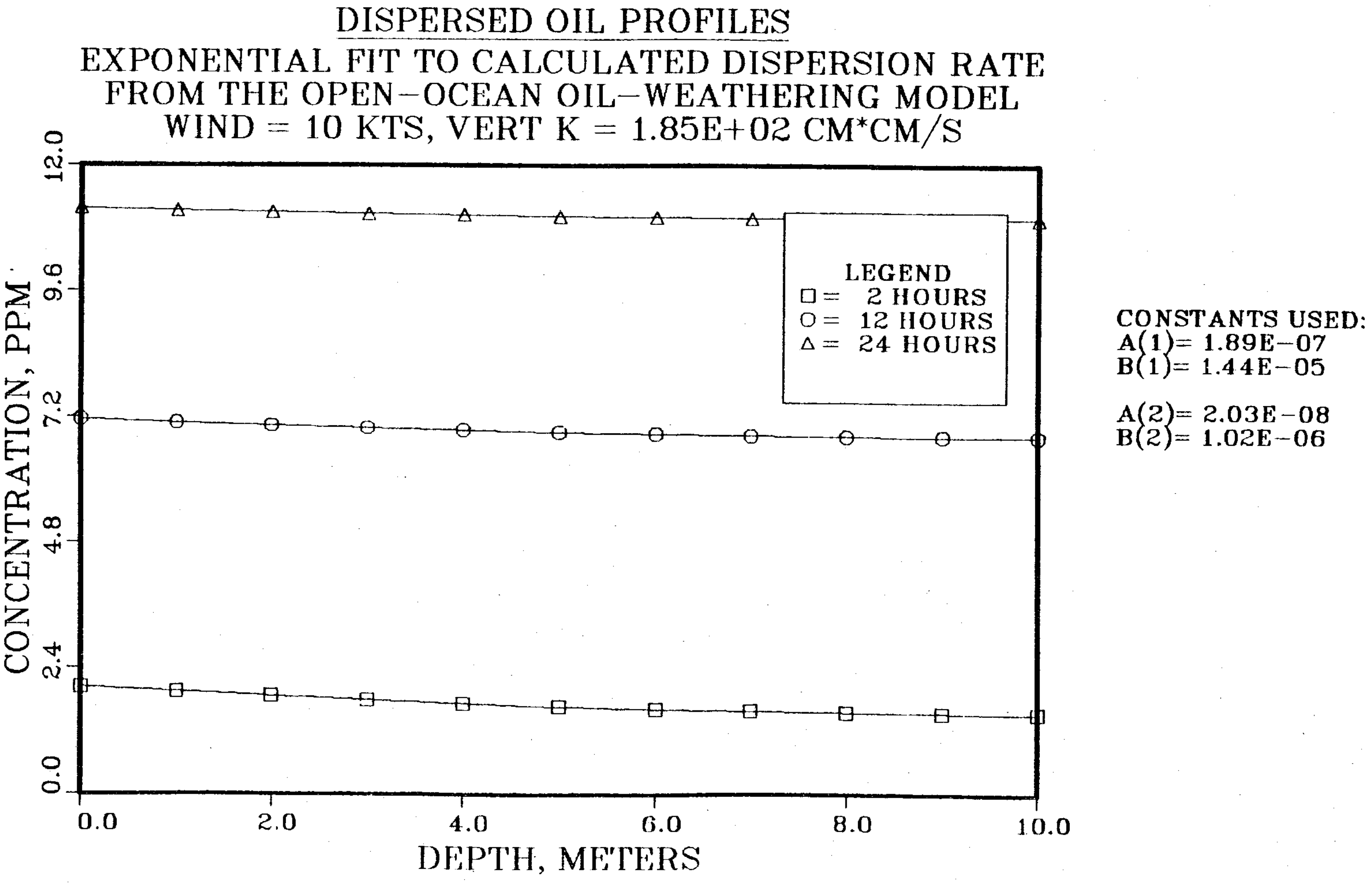
DISPERSED OIL PROFILES
EXPONENTIAL FIT TO CALCULATED DISPERSION RATE
FROM THE OPEN-OCEAN OIL-WEATHERING MODEL
WIND = 10 KTS, VERT K = 1.85E+02 CM*CM/S
CONCENTRATION, PPM
0.0
2.4
4.8
7.2
9.6
12.0
DEPTH, METERS
0.0
2.0
4.0
6.0
8.0
10.0
LEGEND
□ = 2 HOURS
○ = 12 HOURS
△ = 24 HOURS
CONSTANTS USED:
A(1)= 1.89E-07
B(1)= 1.44E-05
A(2)= 2.03E-08
B(2)= 1.02E-06

Figure 4-17C.

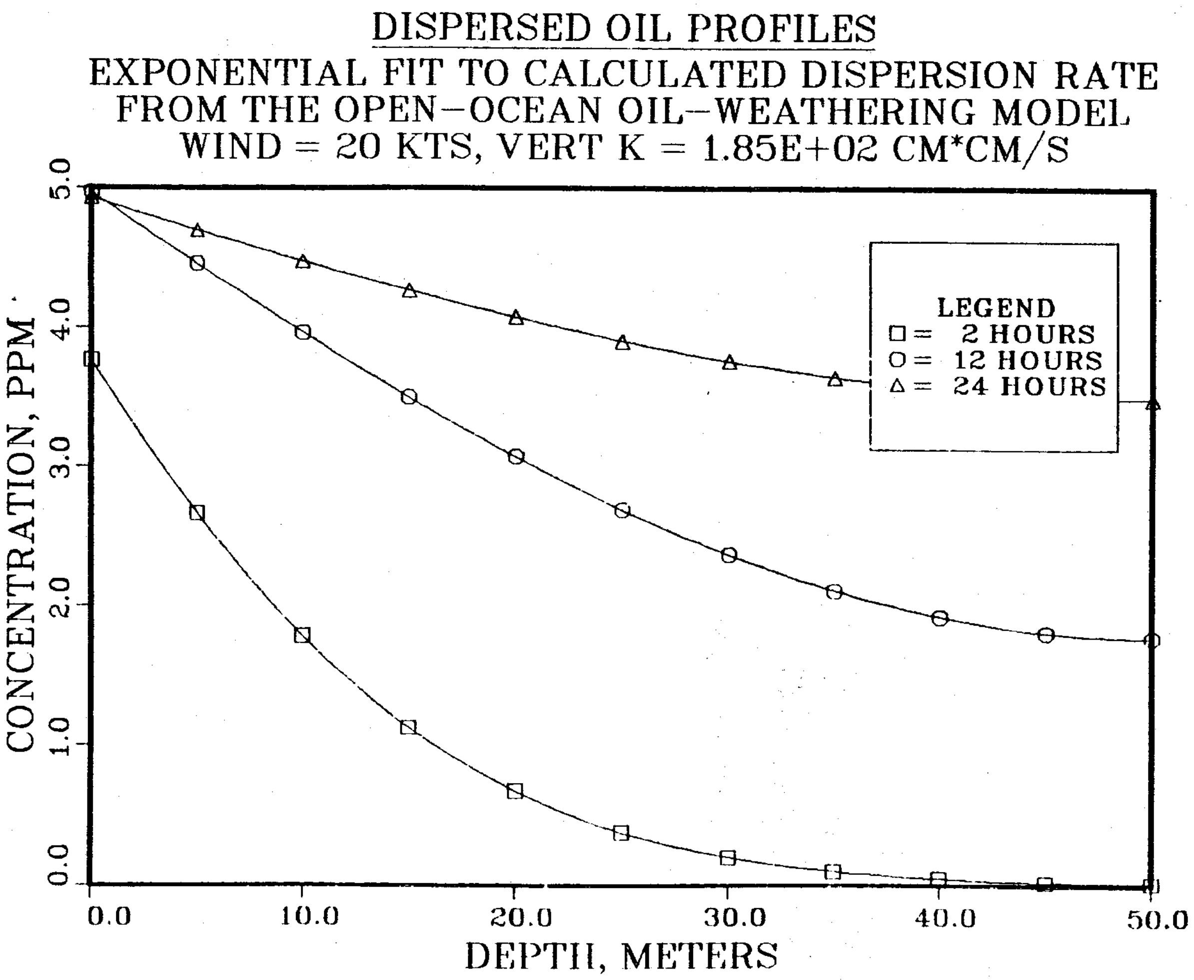

CONSTANTS USED:
A(1)= 6.40E-08
B(1)= 2.03E-06

A(2)= 5.10E-07
B(2)= 3.19E-05

Figure 4-17D.

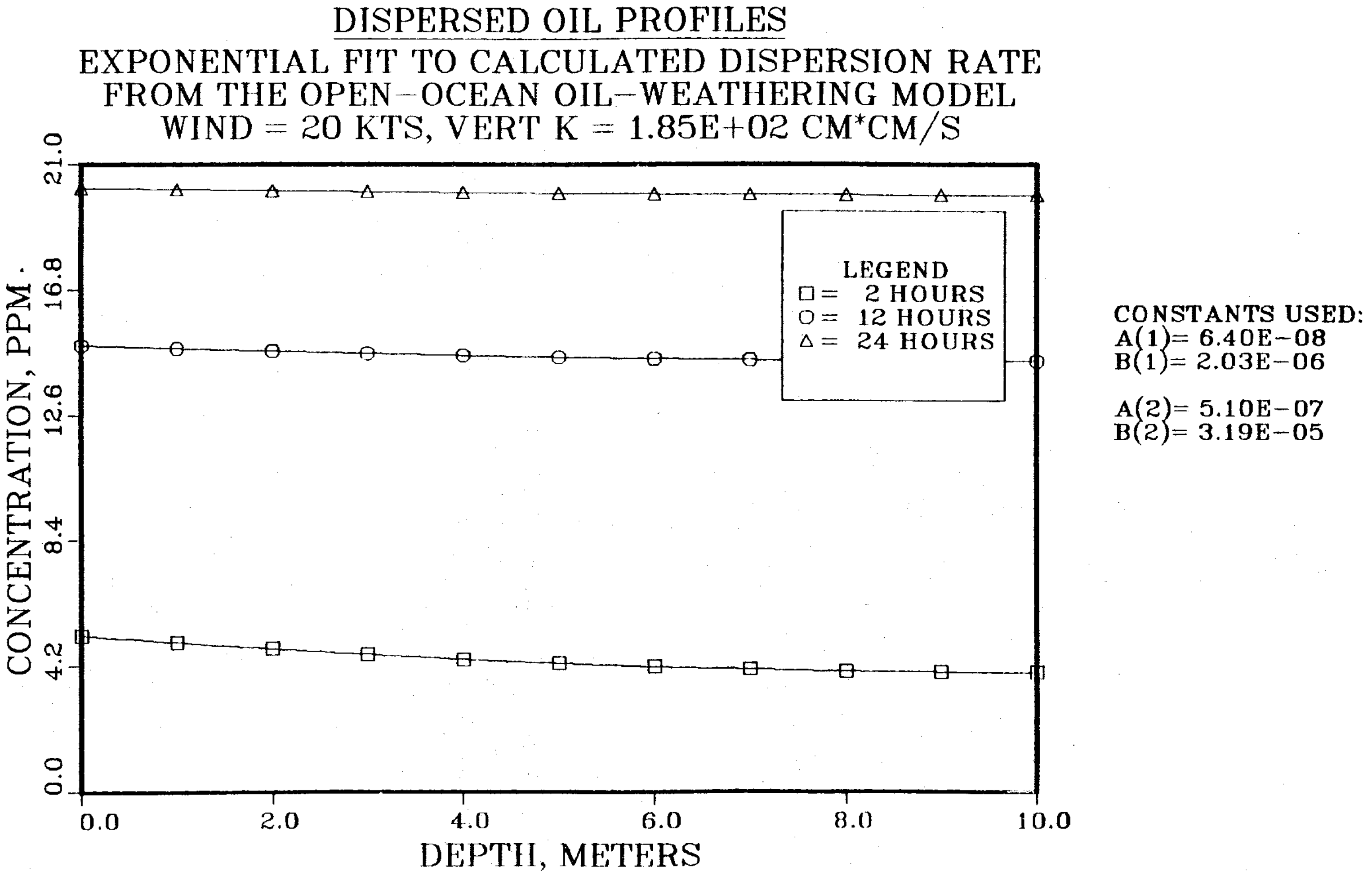
DISPERSED OIL PROFILES
EXPONENTIAL FIT TO CALCULATED DISPERSION RATE
FROM THE OPEN-OCEAN OIL-WEATHERING MODEL
WIND = 20 KTS, VERT K = 1.85E+02 CM*CM/S
CONCENTRATION, PPM
21.0
16.8
12.6
8.4
4.2
0.0
DEPTH, METERS
0.0
2.0
4.0
6.0
8.0
10.0
LEGEND
□ = 2 HOURS
○ = 12 HOURS
△ = 24 HOURS
CONSTANTS USED:
A(1)= 6.40E-08
B(1)= 2.03E-06
A(2)= 5.10E-07
B(2)= 3.19E-05

Figure 4-17E.

DISPERSED OIL PROFILES

EXPONENTIAL FIT TO CALCULATED DISPERSION RATE
FROM THE OPEN–OCEAN OIL–WEATHERING MODEL
WIND = 40 KTS, VERT K = 1.85E+02 CM*CM/S

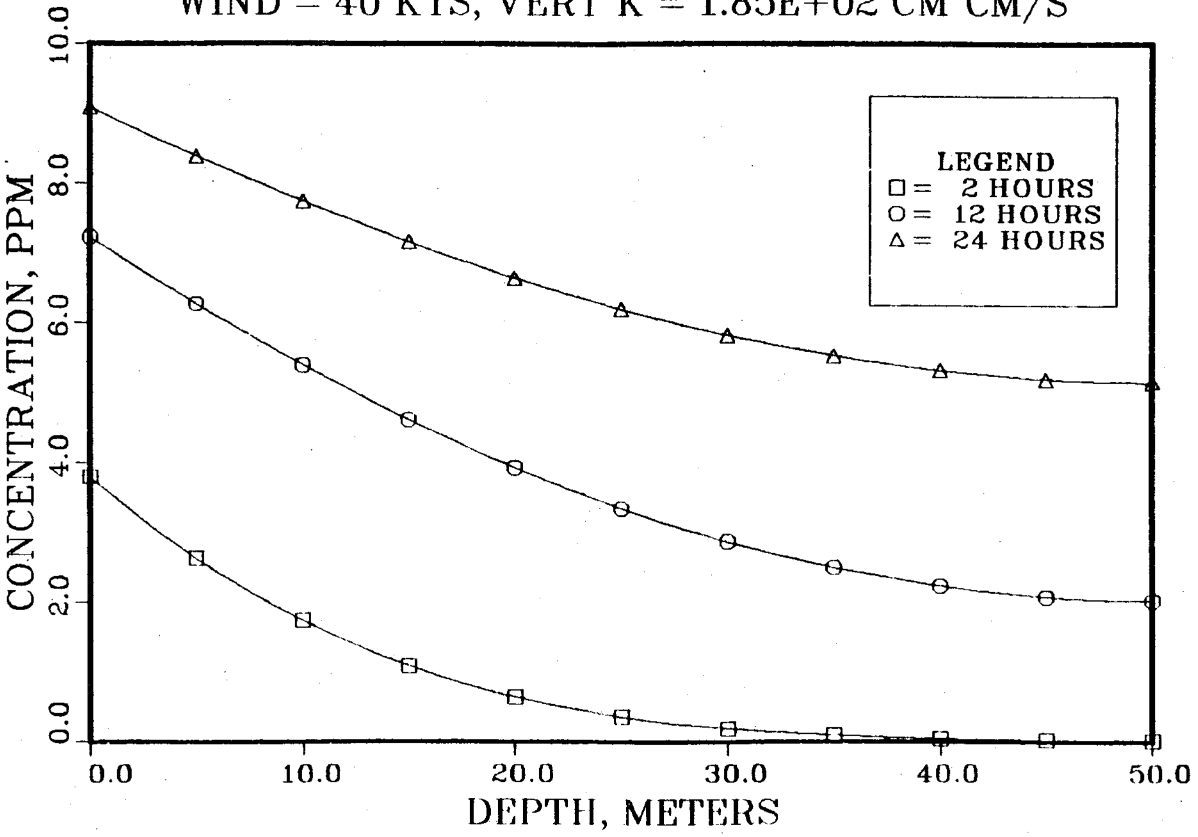

CONSTANTS USED:
A(1)= 1.12E–07
B(1)= 3.06E–06

A(2)= 4.04E–07
B(2)= 9.26E–06

Figure 4-17F.

DISPERSED OIL PROFILES
EXPONENTIAL FIT TO CALCULATED DISPERSION RATE
FROM THE OPEN-OCEAN OIL-WEATHERING MODEL
WIND = 40 KTS, VERT K = 1.85E+02 CM*CM/S

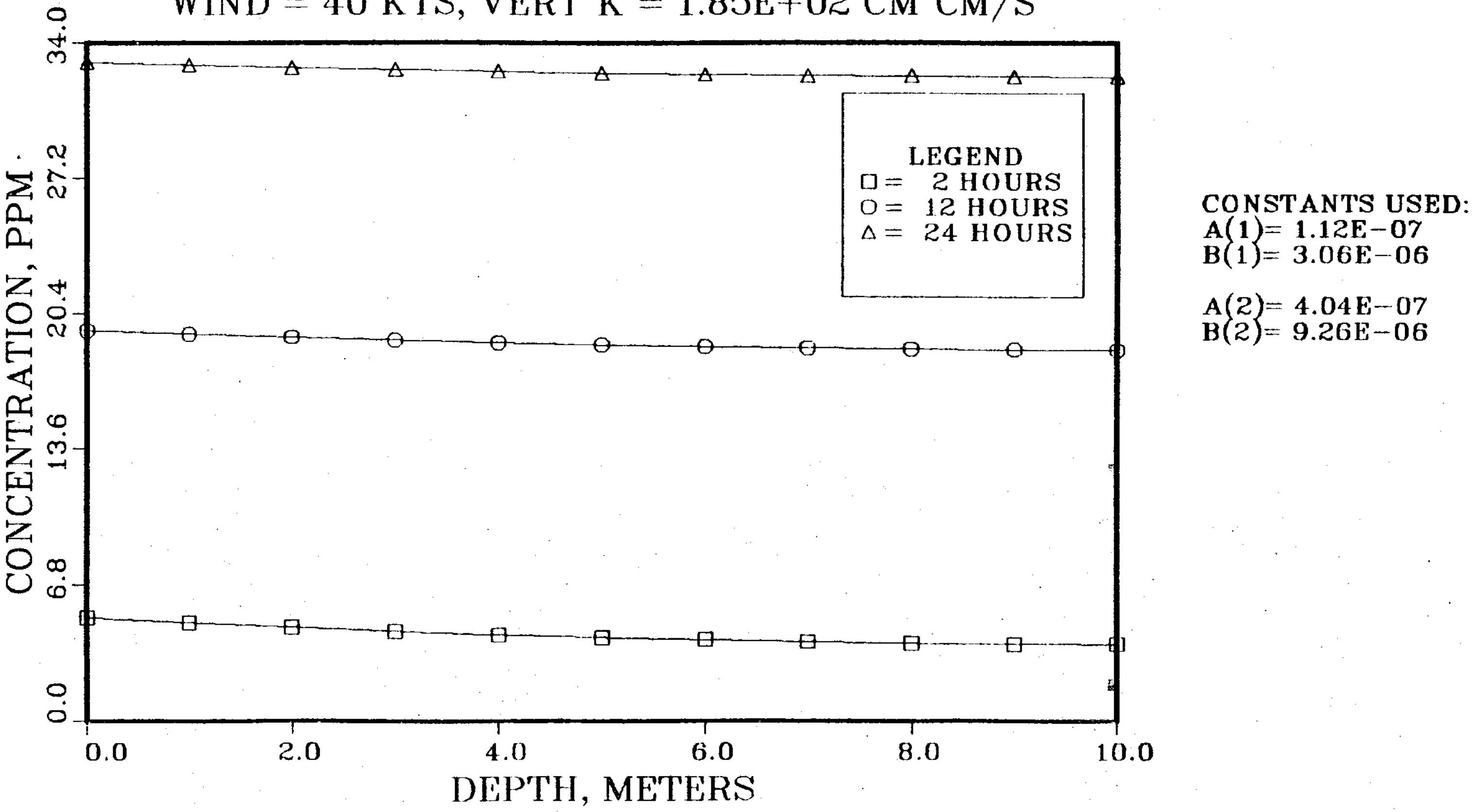

The actual concentrations predicted in these examples must be regarded as upper-bound values because horizontal diffusion and currents in reality will decrease these predicted concentrations. However, in comparison to predicted dissolved concentrations from the previous section, it is clear that dispersed-oil concentrations are greater than dissolved-oil concentrations, and that the dispersed-oil profiles have a much faster response time, i.e., line out fast. The reason for the rapid dispersed-oil concentration-profile response is due to direct coupling to a source in contrast to a mass-transfer resistance for the dissolved-oil concentration profile response.

The previous derivation presented here considered a time-varying dispersion flux is modeled as the sum of decaying exponentials. Another derivation of potential use is to consider the dispersion flux to be constant. Therefore, the problem and resulting solution considered here are for a constant flux of oil at the ocean surface and a zero concentration gradient at the ocean floor. The solutions to the problems defined by the other boundary conditions can be derived following the technique used here. Consider the dispersed oil to be transported in the water column according to

$$\frac{\partial C}{\partial t} = K\frac{\partial^2 C}{\partial X^2} \quad \text{for } 0 < X < \ell \tag{4.142}$$

With an initially clean water column

$$c(x,0) = 0 \tag{4.143}$$

At the ocean bottom

$$\frac{dc}{dx} = 0 \qquad \text{at } x = 0 \tag{4.144}$$

and at the ocean surface a constant flux of oil exists as

$$-k \frac{dc}{dx} = -W \qquad \text{at } x = \ell \tag{4.145}$$

The coordinate frame is defined by the above problem definition where the ocean surface is at $x = \ell$ and the ocean floor at $x = 0$. A positive flux is defined as mass transferring in the +x direction; thus dc/dx is multiplied by -1. The vertical eddy diffusivity is k, and the source flux is W.

The solution to the above set of equations can be obtained by using the technique known as the Laplace Transform (Carslaw and Jaeger, 1967). The Laplace Transform of the concentration is

$$\bar{c} \equiv \int_0^\infty e^{-pt} c(x,t)dt \tag{4.146}$$

Applying the above to the partial differential equation yields the ordinary differential equation

$$\frac{d^2\bar{c}}{dx^2} - q^2\bar{c} = 0 \tag{4.147}$$

where

$$q \equiv \sqrt{\frac{p}{k}} \tag{4.148}$$

The solution for c is

$$\bar{c} = c_1 e^{qx} + C_2 e^{-qx} \tag{4.149}$$

where C_1 and C_2 are two constants. The Laplace Transform of the boundary condition at $x = 0$ yields $dc/dx = 0$ which yields $C_1 = C_2$. The Laplace Transform of the boundary condition at $x = \ell$ yields $dc/dx = Q/p$ where $Q = w/k$. Using this result yields

$$\bar{c} = \frac{Q \cosh qx}{qp \sinh q\ell} \qquad (4.150)$$

The inverse of the above equation yields $c(x,t)$; and this equation is the same as equation (8), section 12.5 of Carslaw and Jaeger. Thus, the final result is

$$c(x,t) = W\left(\frac{4t}{k}\right)^{\frac{1}{2}}\left[\sum_{n=0}^{\infty} \operatorname{ierfc}\left\{\frac{(2n+1)\ell - x}{2\sqrt{kt}}\right\} + \sum_{n=0}^{\infty} \operatorname{ierfc}\left\{\frac{(2n+1)\ell + x}{2\sqrt{kt}}\right\}\right] \qquad (4.151)$$

where $\operatorname{ierfc}(\xi)$ is the first repeated integral of the error function. The function $\operatorname{ierfc}(\xi)$ can be calculated from

$$\operatorname{ierfc}(\xi) = \frac{1}{\sqrt{\pi}}\, e^{-\xi^2} - \xi \operatorname{erfc}(\xi) \qquad (4.152)$$

and $\operatorname{ierfc}(\xi)$ is the complementary error function.

The computer code and user instruction for equation (4.151) is presented in Appendix E: Code Listing for Dispersed-Oil Concentration Profiles with a Constant Flux, and calculates $c(x,t)$ for given input parameters of the eddy diffusivity, constant oil flux, ocean depth, maximum time, number of terms in the $\operatorname{ierfc}(\xi)$ series, and number of terms in the $\operatorname{erfc}(\xi)$ series. A sample calculation result is presented in Table 4-12.

TABLE 4-12. EXAMPLE OF RESULTS FROM CALCULATING DISPERSED-OIL CONCENTRATION PROFILES IN WATER COLUMN FOR A CONSTANT FLUX SOURCE.

```
CONCENTRATION PROFILES IN THE WATER COLUMN FOR DISPERSED OIL (NEUTRAL DENSITY)
CALCULATED FOR A CONSTANT FLUX (IERC SOLUTION) AT THE OCEAN SURFACE

VERTICAL EDDY DIFFUSIVITY =  1.85D+02 CM*CM/SEC, DISPERSED OIL FLUX =  2.22D-08 CM/CM*CM/SEC
OCEAN DEPTH =  50.0 METERS, MAXIMUM TIME =  12.5 HOURS, NUMBER OF TERMS IN IERFC SERIES =  99
NUMBER OF TERMS IN ERF SERIES =  99

DISPERSED-OIL CONCENTRATIONS, CM/CC, IN THE WATER COLUMN FOR VARIOUS TIMES AND DEPTHS FOLLOW

                                                     H O U R S
 DEPTH
 METER    1.25D+00   2.50D+00   3.75D+00   5.00D+00   6.25D+00   7.50D+00   8.75D+00   1.00D+01   1.13D+01   1.25D+01

   0.0    1.24D-07   1.75D-07   2.14D-07   2.47D-07   2.76D-07   3.03D-07   3.28D-07   3.51D-07   3.74D-07   3.95D-07
   5.0    7.27D-08   1.21D-07   1.59D-07   1.92D-07   2.21D-07   2.47D-07   2.71D-07   2.94D-07   3.17D-07   3.38D-07
  10.0    3.89D-08   8.03D-08   1.15D-07   1.45D-07   1.73D-07   1.98D-07   2.22D-07   2.45D-07   2.67D-07   2.88D-07
  15.0    1.88D-08   5.06D-08   8.05D-08   1.08D-07   1.33D-07   1.57D-07   1.80D-07   2.02D-07   2.23D-07   2.44D-07
  20.0    8.09D-09   3.03D-08   5.44D-08   7.80D-08   1.01D-07   1.23D-07   1.44D-07   1.65D-07   1.86D-07   2.06D-07
  25.0    3.10D-09   1.72D-08   3.55D-08   5.51D-08   7.50D-08   9.49D-08   1.15D-07   1.35D-07   1.55D-07   1.75D-07
  30.0    1.05D-09   9.18D-09   2.24D-08   3.81D-08   5.52D-08   7.31D-08   9.16D-08   1.11D-07   1.30D-07   1.49D-07
  35.0    3.16D-10   4.64D-09   1.38D-08   2.62D-08   4.07D-08   5.69D-08   7.40D-08   9.20D-08   1.11D-07   1.29D-07
  40.0    8.53D-11   2.25D-09   8.45D-09   1.83D-08   3.09D-08   4.56D-08   6.17D-08   7.90D-08   9.69D-08   1.15D-07
  45.0    3.31D-11   1.13D-09   5.61D-09   1.38D-08   2.52D-08   3.90D-08   5.45D-08   7.12D-08   8.88D-08   1.07D-07
  50.0    7.65D-12   8.14D-10   4.71D-09   1.24D-08   2.34D-08   3.68D-08   5.21D-08   6.86D-08   8.61D-08   1.04D-07
```

4.10 INTERACTIONS OF PRUDHOE BAY CRUDE OIL WITH SUSPENDED PARTICULATE MATERIAL

4.10.1 Introduction

The interaction of oil in the water column with suspended particulate matter can occur by way of two different mechanisms. The first mechanism is on a molecular scale with dissolved oil species sorbing from the water phase onto the suspended solids. The second mechanism is on a macroscopic scale with dispersed drops of oil colliding with the suspended solids. The resulting loaded particulate are ultimately deposited on the sea floor. The objective of predicting the interaction of oil with suspended particulates is to assess the biological implications of the oil that finally resides on the sediments.

The interaction of oil with suspended particulates involves a number of mass transport processes which are illustrated in Figure 4-18. All these transport processes are dependent on the source terms for oil and sediment. The oil source term can be dissolution of molecular species or dispersion of drops of oil from the parent slick. The dispersion process can be wind-induced turbulence or spontaneous emulsification. These three oil source terms are labeled 1-3 in Figure 4-18. The sediment source term (in the figure) occurs as the result of turbulence at the ocean floor and is labeled as path 6. (Other sediment source terms are discussed in the following section.) The interaction of oil and suspended particles in the water column occurs by sorption of molecularly dissolved species, labeled as 8, spontaneously dispersed drops colliding with suspended particles, labeled as 11, and finally as turbulence dispersed drops also colliding with particles, labeled as 7. The sediment returns to the sea floor, path 9, with sorbed oil, or associated with oil drops, or with no oil. Oil can also transport to the sea floor as unassociated drops, path 4, or as dissolved species, path 5. Once oil is on the sea floor, it can be further mixed into the deposited sediments by turnover mechanisms, which are labeled path 10.

Figure 4-18. Transport and Interaction Path Diagram for Oil and Suspended Particulate Matter

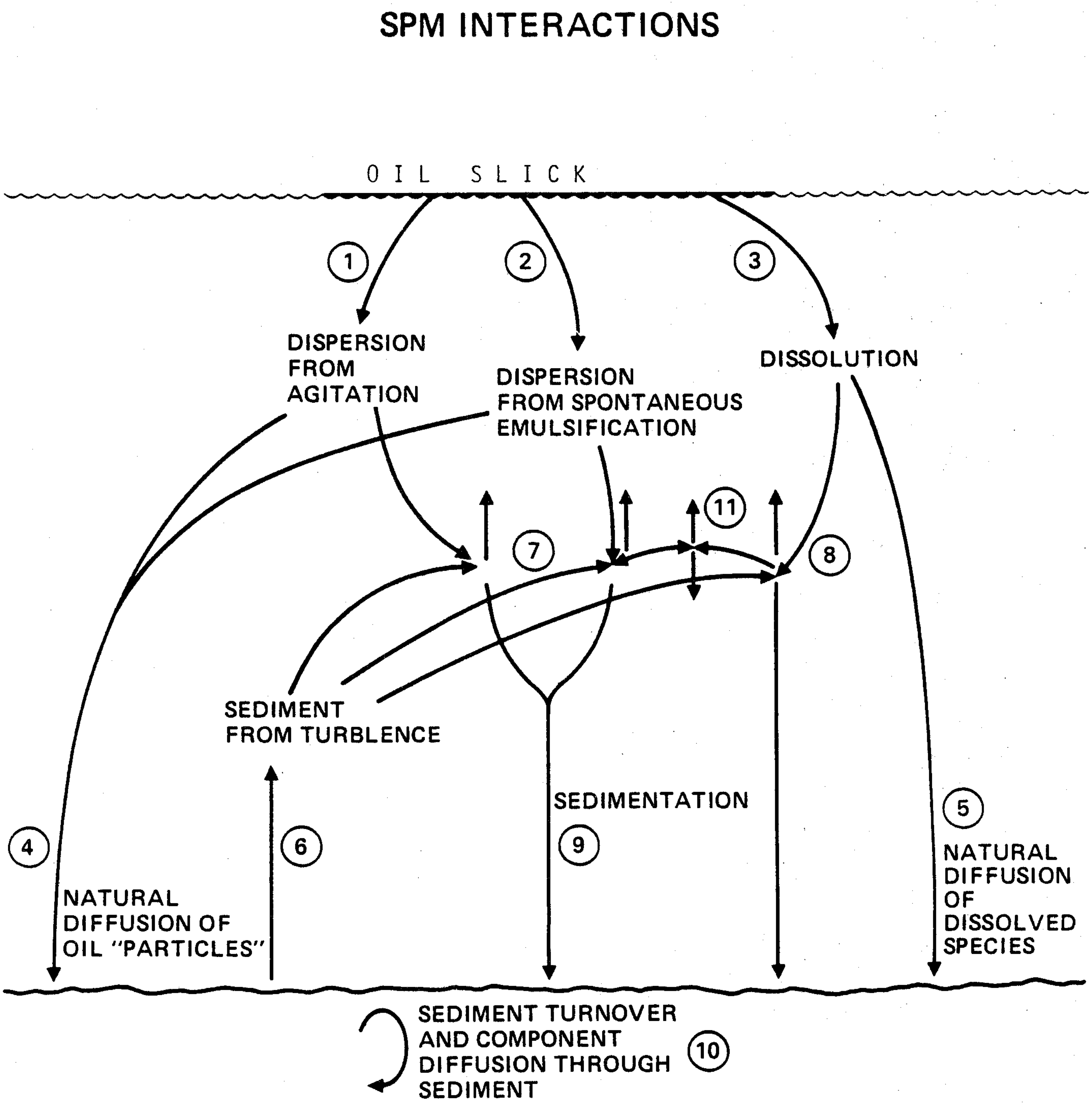

The mathematical description of the interaction of oil in the water column with suspended particulate matter requires both thermodynamic and kinetic information. The kinetic information must describe the strength of the oil source terms (rates), the transport (movement) of oil and sediment in the water column due to the local turbulent diffusivity, and the suspension-deposition rates of sediment on the sea floor. The thermodynamic information must describe the phase equilibrium of the molecular species for the water-solid sorption. The sorption phenomena can conceptually be described the same way that vapor-liquid distributions are described by Henry's Law. Usually, for the case of dissolved hydrocarbons in the water column, the sorption ratio which relates the dissolved species concentration to the sorbed concentration is a constant for very low concentrations. Also to be considered is the oil-water equilibrium of dissolving species, and this equilibrium has been described extensively in the open literature as a partition coefficient, or M value.

In the sections that follow, discussions on suspended particle loading, dissolved oil interactions, spontaneous emulsification, dispersed oil/particulate interactions and the applied mathematics applicable to specific oil-particle interactions in postulated environmental conditions are presented. It must be emphasized that the current state of knowledge with respect to a complete description is not possible because of the complex nature of the processes involved, both in a physical chemistry and kinetic sense. Very little is known about the oil-particle kinetics which may be the most important because they presumably account for transporting most of the oil to the sea floor.

4.10.2 Suspended Particle Loading

Suspended particulate matter (SPM) can originate from many sources and is brought to natural waters by a number of mechanisms. Natural sources of SPM include terrestrial surface weathering and river run off, hydrothermal activities, biosynthesis, and volcanic emanation. Man-made sources are sewage discharge, dredging, continental drilling, and agricultural excavation. SPMs vary greatly in their composition, from inorganic oxides to carbonates, to clays, to organic detritus, to mixtures of all of the above. SPM concentrations range from a few hundred milligrams per liter in sewage effluent, to a few tens of milligrams per liter in rivers and estuaries, to a few tenths and hundredths of a milligram per liter in the open ocean (Huang, 1976).

Because SPM materials display the diversity shown above and because the nature of SPM is critical in its oil sorption properties, quite a bit of detailed information is required to make predictions of the fate of oil in the presence of SPM. Primarily, the size distribution, surface area, concentration, and chemical composition (including Total Organic Carbon Loading) of SPM are pertinent to understanding the physical and chemical interactions between petroleum and SPM. For modeling purposes, information about the size distribution and concentration constitute a source term, or a total amount of SPM available to interact with and possibly sink the oil. The surface area and chemical composition of the SPM, along with the concentration and size distribution will determine the actual kinetics and thermodynamics of the oil/SPM interactions.

In a study of SPM distribution and transport in the Bering sea, Baker (1983) found that near shore particle concentrations were uniform vertically, and that they dropped off rapidly with increasing distance from shore. Further from shore the water column was characterized by a three layer structure. The surface layer displayed a high turbidity resulting from in situ phytoplankton growth and offshore advection and diffusion of shore and river derived particles. The broad middle layer had horizontally and vertically uniform particle concentrations. The bottom layer had increased turbidity resulting from resuspension of bottom sediments. Seasonal particle concentrations varied less than 25%, although winter storms did temporarily homogenize the three layer system described above. Particle size distributions measured followed a power law curve:

$$N = -kD^{-c} \tag{4.152}$$

where N = number of particles larger than a given size
D = particle diameter
k,c are constants

The derivative with respect to size of this cumulative distribution is:

$$dN/dD = aD^{-b} \tag{4.153}$$

where a = ck
b = c+1

In the above expressions, a represents the dN/dD value at D = 1 micron and b represents the slope of the distribution when plotted on full logarithmic paper. The slope is a measure of the number of large particles relative to the number of small particles. When $b>3$, small particles dominate the distribution. When $b<3$, large particles dominate. Typical values for b and a in the Bering sea were 4.1 and 3.9×10^5 away from shore and 3.4 and 3.1×10^5 near shore, respectively.

Further investigations are required in order to determine if the above SPM parameters vary widely from location to location. If they do not, then an "average" SPM loading and size distribution for each environment (near-shore and open sea) can be used in an oil/SPM model. If they do, then much more site specific information will be required for input. Also, more must be known about the effects of high winds (storms) on the three layer system described above. If such winds resuspend large amounts of sediment and/or re-

redistribute SPM between layers, they may play an important role in determining the amount of SPM available for sorption of oil.

Ultimately, the final input to an SPM model must include a total SPM concentration and size distribution (possibly dependent on sea state), from which a number density (particles per liter) can be calculated. Also, some information about the chemical makeup of the sediment should be known, especially the total organic carbon content (discussed below). These data, along with information concerning location (i.e., distance from shore, etc.), may then be used to predict the SPM's interactions with both dissolved and dispersed oil.

4.10.3 SPM Concentration, Size Distribution and Flocculation

The purpose of constructing and oil/SPM model is to provide both a conceptual and a quantitative framework within which to predict the fate of dissolved and dispersed oil in a sediment laden water column. The range in possible SPM source terms is illustrated with the following examples.

Predictive models of oil/SPM interaction must include (inherently, if not explicitly) the SPM concentration and size distribution. Therefore it is necessary to develop the capability to predict the likely SPM concentration and size distribution under various sediment and environmental conditions. This information will also aid in properly selecting sediment samples with which to perform oil/SPM experiments in the laboratory. These experiments will, in turn, provide the bulk parameterizations necessary for a practical model.

Cohesive Sediments

Sediments can be lumped into two broad classes - cohesive and non-cohesive. Cohesive sediments are formed of clay minerals with median particle diameter less than 40μm to 100μm and a significant fraction less than 2μm. The processes of movement of cohesive sediment are considerably different and more complicated than the processes of movement of non-cohesive sediment. The erosion velocity increases with increasing grain size from 200μm upward. For diameters smaller than 200μm and especially below about 50μm, the cohesiveness and duration of consolidation are important (Postma, 1967).

Owen (1977) identifies four physical parameters that need to be evaluated for a particular cohesive sediment:

1. the critical shear stress, τ_e, above which erosion occurs;
2. a rate-of-erosion constant, M;
3. the limiting shear stress, τ_d, below which deposition occurs;
4. the settling velocity, V_s.

The relationships among these parameters are (OWEN, 1977):

$$\text{Erosion:} \quad \left(\frac{dm}{dt_e}\right) = M \left(\frac{\tau}{\tau_e} - 1\right) \qquad (4.154)$$

$$\text{Deposition:} \quad \left(\frac{dm}{dt_d}\right) = CV_s \left(1 - \frac{\tau}{\tau_d}\right) \qquad (4.155)$$

where dm/dt is the rate of mass transfer and C is the near bottom sediment concentration.

The critical shear stress and the erosion rate constant are functions of the cohesive strength of the sediment. The cohesive strength is a function of the type of clay mineral, the particle size, the quantity and type of cations present in solution, and the water content and organic content of the sediment (Drake, 1976; Owen, 1977). Because of the complexity of cohesion, Drake (1976) states that "there is currently no reliable means of predicting [cohesive] sediment entrainment as a function of boundary shear stress". This indicates that presently each geographical area of concern may need to be characterized by laboratory or in-situ measurements.

Once in suspension the fine clay particles tend to form flocs. The flocs settle out but will not be deposited unless the bottom shear stress is less than the initial bonding strength of the settling flocs (Owen, 1977). Therefore, t_d depends upon the bottom sediment characteristics and the dispersion of the settled flocs depends critically upon the bottom boundary conditions.

Finally, the settling velocity spectrum of the flocs will be a function of the sediment concentration and the turbulent characteristics of the water column. The turbulent shear causes interparticle collisions and conversely limits the maximum size of the flocs. Furthermore, as flocs form, they entrap water (and/or oil) thereby reducing their effective density (Tambo and Watanabe, 1979). Therefore, laboratory measurements of clay settling velocity in quiesent water are of questionable value in relation to the natural environment.

It is conceivable that flocs will have higher settling velocities as a result of adsorbing oil. Chase (1979) examined the settling behavior of natural aquatic particulates and concluded that for particles less than 100μm diameter, Stoke's settling law underestimated the aggregated settling rates by up to an order of magnitude. He suggested that viscous drag reduction by surface coating on the flocs was responsible for the enhanced settling rates. After careful examination of Chase's data, Hawley (1982) developed equations which predict aggregate settling rates as a funtion of aggregate size up to 40μm. Furthermore, Hawley concluded that except in regions of high shear aggregation depends primarily upon collisions due to differential settling because each size class has a spectrum of settling velocities.

It is not presently feasible to incorporate all of these processes into a comprehensive model; however, Hunt (1982a, 1982b) developed an empirical expression which can be used to quantitavely predict removal of particles in the region of particle sizes where the shear mechanism dominates. This is generally in the 1 to 10μm range - the same size range as oil micelles. Following Hunt, the rate of change of total suspended-particle volume, V(t), is

$$dV(t)/dt = -bV^2(t) \tag{4.156}$$

or

$$V(t)/V_o = \frac{1}{1 + V_o bt} \tag{4.157}$$

where b has units $ppm^{-1}s^{-1}$ for V(t) in ppm by volume and V_o is the intial volume concentration. The time at which V is 1/2 V_o is $t =(V_o b)^{-1}$. Furthermore, $V_o bt$ is nearly proportional to $V_o Gt$ where G is the turbulent shear rate. The following empirical expression is based on Hunt's kaolinite data

$$b = 1.9 \times 10^{-5} G^{1/2} \text{ (collisions } ppm^{-1}s^{-1}) \tag{4.158}$$

for G in s^{-1}. The turbulent shear rate G is calculated from

$$G=(\varepsilon/\nu)^{1/2} \tag{4.159}$$

where ε is the energy dissipation rate and ν the kinematic viscosity. The dissipation rate measured by Grant et al (1968) in the ocean ranged from 2.5 x $10^{-2}\mathrm{cm}^2\mathrm{s}^{-3}$ at 15 m to 4.8 x $10^{-4}\mathrm{cm}^2\mathrm{s}^{-3}$ at 90 m. The corresponding range of G is 0.2 s^{-1} to 1.6 s^{-1}.

The initial clay particle volume concentration has a wide range of values. At 20 mg/l concentration and a typical specific gravity of 2.5, the volume concentration is 8 ppm. For oil concentrations of 0.2 mg/ℓ and specific gravity of 0.8, the volume concentration is 0.25 ppm. Since the concentration of the clay is much greater than the oil, the rate of removal of the oil will be governed by the rate of removal of the clay due to the flocculation and settling. This assumes that the oil micelle and clay particle stick when they collide. Thus, for G=1 s^{-1} and neglecting dispersion, the volume concentration of the clay size class and oil micelles are reduced by 50% in

$$t_{1/2} = \frac{1}{V_o b} = 1.8 \text{ hours}$$

For oil only, $t_{1/2}$ = 48 hours.

Less time is required to reduce the volume concentration of clay/oil suspension because the large number of clay particles increases the probability of collision and settling. Assuming that the oil micelles collide only with clay particles, the predicted oil/SPM particle volume concentration is 0.125 ppm after approximately 2 hours.

It should be noted that $t_{1/2}$ is not the time required for complete removal from the water column because the flocs and oil/SPM particles must still settle to the bottom. The time required to settle out will, of course, depend on the depth, density and floc size.

Non-Cohesive Sediment

The suspension of non-cohesive sediment - sand size and larger - is somewhat simpler than suspension of cohesive sediment. The shear stress required to initiate movement of sand is mainly a function sand size and specific gravity. Deposition occurs when the shear stress falls below that required for movement.

Smith and McLean (1977b) derived the following expression for concentration of sediment size class n, C_n, and the total sediment concentration, C_s, for a steady state, horizontally uniform, multi-component flow:

$$\frac{C_n}{1-C_s} = \frac{C_{no}}{1-C_{so}} \exp \left(-W_n \int_o^z \frac{dZ}{K_n}\right) \tag{4.160}$$

where subscript 'o' indicates value at a reference level $z=z_o$, W_n is the settling velocity of component n, $K_n=kU_*f(z)$ is the vertical eddy diffusivity of component n, k = 0.4 and U_* is the friction velocity. U_* is defined as $\sqrt{S_b/\rho}$ where S_b is the bottom shear stress and ρ is the fluid density. Prior to transport of bed material in a fully rough turbulent flow, Z_o is the depth within the sediment at which the mean current is zero. It is related to the bed roughness by $Z_o=k/30$ where k is a measure of the bed roughness obtained from the bottom sediment grain sizes (Komar, 1976). Once the tranport of bed material has begun, Z_o increases and is taken to be the top of the bed load layer (Smith and McClean, 1977a).

Smith and McLean (1977b) proposed that the sediment concentration at the reference level Z_o is obtained by the empirical expression

$$C_{no} = \frac{f_n}{\left(1 + \frac{1}{\gamma_o C_b S_n}\right)} \tag{4.161}$$

where f_n is the fraction of the bed sample in size class n; C_b is the concentration of sediment in the bed (=1-porosity); $\gamma_0 = 2.4 \times 10^{-3}$ a constant based on Columbia River data; and

$$S_n = \frac{\tau_b}{\tau_n} - 1 \qquad (4.162)$$

where τ_n is the shear stress required to intiate movement of component n. Smith (1977) identifies this reference level concentration as the weakest link in the computations.

The sediment concentration profile is determined simultaneously with the current profile using a numerical iterative technique. Adams and Weatherly (1981) and Cacchione and Drake (1982) have used this approach to investigate the effects of the suspended sediment stratification on bottom boundary layers in the Florida current and shallow Norton Sound, respectively. Smith and McLean (1977b) solved for the concentration profiles for a sediment characterized by 10 size classes between 125µm and 595µm with a median size of 297µm and a friction velocity $U_* = 4.52$ cm s^{-1}. This value is comparable to the mean value of $U_* = 4$ cm s^{-1} measured by Cacchione and Drake (1982) at 18 m depth in Norton Sound in storm-generated currents.

Relating the profiles calculated by Smith and McLean to the shallow water conditions in Norton Sound, the predicted surface concentration is $C = C_b x 10^{-6}$ where C_b is the bed concentration. For $C_b = 0.65$, $C = 0.65x10^{-6}$ composed primarily of 125µm particles. For a spedific gravity of 2.65, C = 1.7 mg/ℓ and the number concentration is 0.65 particles cm^{-3}. This compares to a number concentration of 3800 micelles cm^{-3} for 0.25 ppm oil composed of 5µm micelles.

Since the sand grains are much larger than the oil micelles, the interaction between between oil and SPM will likely be governed by differential settling. However, the interaction among oil micelles will likely be governed by turbulent shear. For a turbulent shear of $G=10\ s^{-1}$, Hunt's (1982a) expression gives 6×10^{-5} collisions $ppm^{-1}s^{-1}$ and 18 hours for the process of oil-coalescing-with-oil to reduce the volume concentration of oil by 50%. In this process, oil micelles collide, coalesce and rise to the surface. The time for removal will increase if coalescence is hindered by surface tension of the oil micelle. For SPM scavenging oil micelles the theoretical collision rate for differential settling is expressed as

$$\beta = \frac{\Pi}{4} (d_n + d_o)^2 \left| U_n - U_o \right| N_n N_o \tag{4.163}$$

where subscript 'n' indicates sediment and 'o' indictes oil. For $d_n = 125\mu m$, $d_o = 5\mu m$, $U_n = 1cm\ s^{-1}$, $U_o = 3 \times 10^{-4}\ cm\ s^{-1}$, $N_n = 0.65\ cm^{-3}$, $N_o = 3800\ cm^{-3}$, the collision rate and $t_{1/2}$ are $\beta = 0.33$ collisions $cm^{-3}s^{-1}$ and $t_{1/2} = 1.6$ hours. Since β does not include corrections for inefficient collisions $t_{1/2}$ is a minimum value. If the collisions are only 1% efficient the $t_{1/2}$ increaes to 160 hrs.

Suspension and concentration/size distribution profiles of cohesive sediments cannot be reliably predicted at this time. However, once the concentration is known (empirically or otherwise), empirical expressions have been developed which can quantitatively predict volume removal rate of the clay or clay and oil suspension. On the other hand, the suspension and concentration/size distribution profiles of non-cohesive sediment can be predicted if bottom boundary concentrations can be specified. However, the predictions remain to be verified along with the collision rates predicted by the theoretical expression for differential settling. In both cases, SPM can potentially accelerate the removal of oil from the water column but experimental verification of the rates is required.

4.10.4 SPONTANEOUS EMULSIFICATION (DISPERSION)

Spontaneous emulsification is a phenomenon first observed in 1878 by Johannes Gad (Gad, 1878). Gad found that a solution of lauric acid in oil, when placed on top of aqueous alkali, would spontaneoously form emulsions (i.e., without mechanical agitation). In industry, suitable surfactants are usually added to mixtures to aid in emulsification, very often with slight shaking or mixing. However, there are many examples in the literature where two immiscible phases are brought together gently and still form emulsions. Some systems that have been investigated are: solutions of ethyl alcohol in toluene in contact with water (Gurwitsch, 1913 and Raschevsky, 1928), solutions of oleic acid in oil on alkaline solutions (V. Stackelburg, et al., 1949), benzene, toluene, or xylene placed on strong solutions of dodecylamine hydrochloride (Kaminski and Mcbain, 1949), and solutions of long chain salts in contact with solutions of cetyl alcohol or cholesterol in oil (Davies, 1972). Many such 3-component, 2-phase systems have been studied in order to determine the mechanisms that produce spontaneous emulsification. These small systems are relatively straightforward to examine, and some progress has been made in identifying the mechanisms involved (Groves, 1978). However, with large complex systems such as petroleum/water, very little if any work has been done to determine whether spontaneous emulsification occurs and to what extent.

During the measurement of M values (oil/water partition coefficients) for oil-weathering physical properties, oil was added gently to a separatory funnel of water. Small "micelles" or oil droplets were observed in the aqueous phase. This observation indicates that some sort of spontaneous or self emulsification takes place at the petroleum/water interface. These droplets were examined under a microscope and estimated to be one to ten microns in diameter. Further work must be performed to determine the importance, mechanism, and extent of spontaneous emulsification in aqueous systems.

The three mechanisms that have been found to be important in spontaneous emulsification all involve rapid diffusion of a solute across a boundary between two immiscible solvents. This rapid diffusion of a solute either changes the properties of the boundary (i.e., interfacial tension, pressure, local solute concentration), causing droplets of one solvent to break away into the other, or simply carry solvent molecules with it, which accumulate into droplets (Davies, 1957). It would be reasonable to expect, therefore, that oil droplets created by one of these mechanisms could be enriched in the component(s) that are rapidly diffusing.

In order to develop a model to describe suspended particulate/oil interactions in which spontaneous emulsification is occurring, the following information must be obtained:

1) mass in water of spontaneously emulsified oil.
2) droplet density of spontaneously emulsified oil.
3) size distribution of spontaneously emulsified oil.
4) chemical composition of spontaneously emulsified oil.

In order to determine the above, experiments must be performed in which crude oil is very gently spread onto a surface of water, and allowed to equilibrate. Care must be taken throughout the experiments to avoid stirring or agitating the oil/water system so that mechanically caused dispersion does not occur. The water must then be filtered (0.45 μm) in order to separate dissolved and particulate oil and then analyzed by gas chromatography to determine the concentration and composition of the droplets. Unfiltered water samples must also be examined under a microscope in order to measure the number density and size distribution of the droplets. These analyses must be performed on oil at varying stages of weathering in order to determine how long spontaneous emulsification is active and to attempt to correlate bulk oil properties (i.e., density, surface tension, viscosity) to the rate of spontaneous emulsification. If such correlations can be determined, they can be incorporated into the lumped-parameter oil-weathering model.

4.10.5 Oil "Particle"/SPM Interactions

From a mechanistic or kinetic point of view, the interaction between dispersed oil or oil "particles" with suspended particulate matter, SPM, has not been extensively studied. Poirier and Theil in 1941 measured the volume of oil that could be adsorbed and sedimented by one gram of ten different sediments in static water columns. They found that the volume sedimented was roughly proportional to the inverse of the grain size of the sediment. Gearing and Gearing in 1982 studied the fate of petroleum hydrocarbons under simulated storm conditions in marine microcosms. They found that increasing the SPM load to 160 milligrams per liter from the normal level of three to five milligrams per liter did not change the overall fate of No. 2 fuel oil added to the microcosms in an oil/water dispersion. Mackay, et al. (1982) used varying amounts of chemical dispersants in sea water to measure the rise and fall of oil in association with sedimenting matter. The results were subjected to a simple correlation procedure to determine the magnitude and effect of the following variables: dispersant type, sediment type, particle size and concentration, dispersant dose and oil type. Wade and Quinn (1979) studied the effect of chronic low level input of No. 2 fuel oil into marine microcosms. They discovered that the majority of the hydrocarbon associated with small size sediment particles (3 to 455 micron) and that substantial accumulation in the bottom sediments did not occur until approximately 135 days from the first addition of oil.

A time-dependent kinetic model to describe these observed phenomena (dispersed oil/SPM interactions), however, has never been fully developed. Since it is becoming apparent that this process is the first stage of the most prolific oil sedimentation mechanism, it is important that such a model be developed. The parameters and/or conditions that might influence the rate of "reaction" between dispersed oil and SPM are numerous. The concentration of dispersed oil and SPM, size distribution of the droplets and SPM, composition of the oil and SPM, and the density of the oil and SPM will all have some effect on the rate of association.

The starting point for developing a model for these systems will be a simple second order rate equation:

$$d[C]/dt = k[A][B] \tag{4.164}$$

where [C] = concentration of associated oil/SPM "particles" in particles per volume (number density)

[A] = concentration of oil "particles" in particles per volume (number density)

[B] = concentration of SPM in particles per volume (number density)

The number densities for [A] and [B] can either be measured (by microscope) or calculated if the total dispersed oil concentration and droplet size distribution are known. However determination of [C] is more difficult since it is hard to distinguish between "oiled" particles and "unoiled" particles optically, and separation of "oiled" particles from droplets and "unoiled" particle by physical means (i.e., filtration) is difficult. Before the experiments described below can be accomplished, methods for determining these three concentrations independently must be developed.

In order to determine the rate constant, k, its dependence on particle size, oil and SPM composition, and other factors, must be found. With regard to particle size, for example, it may be that very small oil droplets will not "react" with SPM as readily as larger ones due to their high surface tension. Oil and SPM composition might also have effects on the rate. Many authors have noted a difference in sedimentation abilities of minerals (Mackay, et al., 1982; Poirier and Theil, 1941; Meyers and Quinn, 1973). Also, total SPM organic carbon content has been found to influence dissolved hydrocarbon/SPM sorption (Karickhoff, et al., 1978) and may also affect droplet association. Other factors such as release point (surface/subsurface) and electrical properties should also be considered. In order to determine which variables are important in determining the rate constant, k, a controlled system will be required in which conditions (concentrations, distributions, sediment types, etc.) can be varied and the resultant SPM/oil interactions studied. After such experiments, the resultant rate equation can be solved and incorporated into a lumped-parameter oil-weathering model. The parameters found important can be measured on true-boiling-point cuts of crude oil and used as input to the model, which will then predict the time dependent concentrations of oil droplets, SPM, and oil/SPM droplets in the water column.

To illustrate how the rate "constant" k is a function of SPM, oil and environmental parameters, consider the general form:

$$k_{ij} = N_j V_j E_{ij} \, 4\pi R_j^2 \qquad (4.165)$$

where i indicates micelle size class, j indicates SPM size class, N_j=number concentration of size class j; V_{ij}= velocity of class j relative to micelle size i; R_j=radius of class j; and E_{ij} is the "collection efficiency" of i by j. E_{ij} will depend upon hydrodynamic, gravitational, inertial, surface and electrical forces. N_j will be a function of depth z.

The following case is an example of how hydrodynamic forces affect the collection efficiency between sand SPM and oil micelles. A "spherical" sand SPM would be 100% efficient if it collected all micelles within its cross-sectional area.

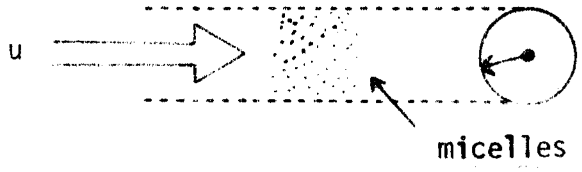

100% efficient

However, due to fluid flow around the SPM, some/oil micelles will be deflected around the SPM and will not impact it.

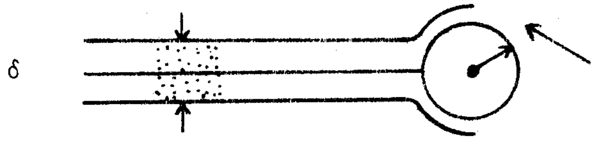

flow streamline separating
impact and non-impact regions.

Oil micelles within the distance δ will impact; micelles outside the distance δ will not impact. The length δ is the "stopping distance" of the micelle. The stopping distance is the distance required for the micelle to be brought to rest by viscosity when it has a velocity u relative to the fluid. Micelles outside δ will stop before they impact the SPM and then be carried with the fluid around the SPM. Due to inertia, micelles within δ will not have room to stop and they will impact the SPM. The distance δ is

$$\delta = \frac{2\rho a^2}{9\eta} U \tag{4.166}$$

where ρ = oil micelle density
a = micelle radius
η = kinematic viscosity of water
U = relative velocity of micelle and fluid

The ratio of δ to R, is the radius of the SPM.

$$\delta/R = \frac{2\rho a^2}{9\eta} \frac{U}{R} = \text{Stokes Number } (S_{tk}) \tag{4.167}$$

Actual measurements show that to a good approximation (Twomey, 1977)

$$\begin{aligned} \text{Collection Efficiency} &= S_{tk} \text{ if } S_{tk} < 1 \\ &= 1 \text{ if } S_{tk} \geq 1 \end{aligned}$$

in the case of potential flow around the collecting SPM particle.

These results indicate that large, sand size, SPM may not be very effective in scavenging small micelles. For example, the efficiency of 500 μm SPM collecting 10 μm micelles is only 0.4% (essentially zero percent) but increases to 10% for 50 μm micelles. This implies that the smallest micelles may have to coalesce into larger micelles before they can be effectively scavenged by sand size SPM.

4.10.6 Dissolved Oil/SPM Interactions

The sorption of organic compounds onto SPM has been studied extensively. The partitioning of polynuclear aromatic hydrocarbons (Means, et al., 1980, phthalic acid esters (Sullivan, et al., 1982), polychlorinated biphenyls (Steen, et al., 1978; Pavlou and Dexter, 1979), fatty acids (Meyers and Quinn, 1973), and hydrophobic pollutants in general (Karickhoff, et al., 1979) between water and SPM phases have all been measured.

For most systems the water/sediment partition coefficient (K_p) is a constant over a broad range of water-phase concentrations, thus:

$$K_p = X/C \qquad (4.168)$$

where X = equilibrium concentration of compound sorbed onto sediment, relative to dry weight of sediment (ppb)

C = equilibrium concentration of compound in water phase (ppb)

Once K_p is known (measured) for one or a few concentrations, predictions can be made concerning adsorption at other concentrations. Such predictions have been very successful with most simple systems (Pavlou and Dexter, 1979; Karickhoff, et al., 1979). However, complex systems, such as petroleum/water are not as straightforward. It is impossible to measure K_p for every component of oil. In addition, experiments are difficult to conduct on oil because dispersion of droplets will, in general, also be present. These droplets will interfere with the equilibrium, and it will be difficult to distinguish between oil due to dispersion and oil due to dissolution in subsequent sample handling and preparation for analyses.

For these reasons it is desirable to find a method for measuuring K_p for a lumped model in which direct partitioning between water and sediment is avoided. One such method has been developed (Karickhoff, et al., 1979) and should be attempted using the oil/water system. Basically the method involves relating K_p to the organic carbon content of the sediment, the size distribution of the sediment, and the octanol/water partition coefficient.

Karickhoff (Karickhoff, et al., 1979) found that individual sediment particle sizes adsorbed in amounts proportional to their organic carbon content, thus:

$$K_p = K_{oc} \cdot (oc) \qquad (4.169)$$

where K_{oc} = organic carbon partition coefficient
oc = organic carbon content

Further, if the sediment size distribution and organic carbon content of each fraction are known, then K_p can be expressed as a sum over all of the particle sizes:

$$K_p = \sum_i K_{oci} \cdot (f)_i \cdot (oc)_i \qquad (4.170)$$

where $(f)_i$ = fraction of each particle size of the total sediment mass

Finally, in order to relate K_p to an easily measured and/or tabulated parameter, K_{oc} was correlated with K_{ow}, the octanol/water partition coefficient. A least squares fit using data from a series of polycyclic aromatics and chlorinated hydrocarbons in equilibrium with a coarse silt sediment gave:

$$K_{oc} = 0.63\, K_{ow} \qquad (r^2 = 0.96) \qquad (4.171)$$

Means, et al. (1980) used the same method to study adsorption of polycyclic aromatics on a variety of soils and sediments and obtained the same result except with a constant of 0.48 rather than 0.63. Using this result, K_p for coarse silt can then be expressed as:

$$K_p(\text{coarse silt fraction}) = 0.63 \cdot K_{ow}(\text{silt}) \cdot f(\text{silt}) \cdot (oc(\text{silt})) \qquad (4.172)$$

and the total K_p would be a sum of such terms over all of the particle sizes:

$$K_p = \sum_i C_i \cdot K_{owi} \cdot f_i \cdot (oc)_i \qquad (4.173)$$

where C_i = the ratio of K_{oc} to K_{ow} for the i-th fraction

Karickhoff suggested a number of ways to simplify the above sum. For most sediments, the organic carbon content of the sand fraction (>50 micron) is much smaller than it is in the smaller particles. Thus K_{oc} for the sand fraction is estimated to be some fraction of the K_{oc} for the finer material (usually 20%). Also, the K_{oc}'s for the various fine fractions (<50 microns) do not vary significantly in most sediments. Therefore, these fractions need not be distinguished, they can be considered as one fraction. With these simplifications the sum for K_p reduces to:

$$K_p = C.f \cdot (0.2) \cdot K_{ow} \cdot (oc(sand)) + C \cdot (1-f) \cdot K_{ow} \cdot (oc(fines)) \qquad (4.174)$$

where f = fraction of sand particles (usually small or SPM)
C = average C_i (approximately 0.5)

In order to utilize this formulation in an oil-weathering model, octanol/water partition coefficients would be measured on each cut of the true boiling point distillation of crude oil. These values can then be used along with organic carbon contents of the SPM of interest to calculate K_p for each cut. K_p would then be utilized to predict adsorption of dissolved oil onto SPM in the water column.

4.10.7 Modeling Description of the Interaction of Oil with Suspended Particulate Matter

Transport of oil through the water column occurs by turbulent diffusion of dissolved molecules or by turbulent diffusion of oil droplets. Dissolved molecules enter the water column from the oil slick by virtue of the (slight) solubility of the hydrocarbons. Oil droplets on the order of microns in diameter enter the water column by virtue of wind-driven action or by spontaneous emulsification. When suspended particulate matter is present in the water, each of these forms of oil will interact with the particulate. The interaction can be of a thermodynamic nature, or particle-droplet collision.

The material balance derivations that follow consider each of these two interactions separately in order to gain insight about these processes. These derivations illustrate what transport processes are occurring and the physical properties, both thermodynamic and kinetic, required to generate predictions about the concentration of "oil" in the water column. The derivations are one-dimensional and do not consider a convection term. However, extending the concepts to a general situation is straightforward. These one-dimensional derivations are the type that can be used in controlled experiments conducted to deduce the parameters of interest. However, note that thermodynamic quantities can be measured in static experiments and need not be deduced from dynamic situations.

In order to derive a time-dependent material balance for dissolved species interacting and transporting with suspended particulate matter, consider a water column with a uniform loading of suspended particulate matter. (Additional boundary conditions imposed by water column density gradients and bottom effects are considered in the following section). Oil at the water surface is "dissolving" into the water. A material balance for the dissolving species which have the potential for adsorbing onto the suspended particulate is derived from:

$$\text{IN} - \text{OUT} = \text{ACCUMULATION} \qquad (4.175)$$

In order to derive the material balance a one-dimensional system is considered. The material balance must consider the adsorption capacity of the suspended solids and the fact that the suspended solids are mobile as determined by the eddy diffusivity.

The capacitance of the suspended solids for adsorbing dissolved species is (usually) expressed as a Henry's-Law type relationship as

$$Z = K_p C \tag{4.176}$$

where Z is the concentration on the solid phase (suspended particulate) in units of (usually) gm per gm of solid, and C is the aqueous phase concentration in gm/ml. The units K_p are then ml/gm. K_p is termed the distribution coefficient, adsorption coefficient or partition coefficient, depending on the field of science and engineering being studied.

The accumulation term is written for a differential volume element as

$$\text{ACCUMULATION} = A\Delta X\left[\varepsilon + K_p \rho_s\right] \frac{\partial C}{\partial t}\bigg|_{\overline{X}} \tag{4.177}$$

where A is the area of the volume element with the mass flux normal to this area, Δx is the width of the element, ε is the volume fraction of water, and ρ_s is the mass of sorbing solid per unit volume. Therefore $\varepsilon \partial C/\partial t$ represents the accumulation in the water in the volume element due to a change in concentration, and $K_p \rho_s$ represents the accumulation on the solid phase in the volume element due to the sorptive capacity.

The "in" flux term is written as

$$\text{IN} = -A\mathscr{D}_e \frac{dC}{dx}\bigg|_X \; -A\mathscr{D}_e^* \frac{dC^*}{dx}\bigg|_X \tag{4.178}$$

Here two gradients are considered. The first gradient term is that gradient in the aqueous phase and represents the turbulent transport of the dissolved species by eddy diffusion. The second term with the * superscript represents the turbulent transport of the species (of interest) that is sorbed on the suspended particulate. It must be recognized that the suspended particulate transport sorbed mass by virtue of turbulence. Thus, the suspended particles are diffusing (moving) and the particles become identified by the concentration of species sorbed onto them. The OUT term is the same as the IN term except it is evaluated at X+ΔX. Writing the complete differential material balance yields

$$-A\mathcal{D}_e \frac{dC}{dx}\bigg|_X - A\mathcal{D}_e^* \frac{dC^*}{dx}\bigg|_X + A\mathcal{D}_e^* \frac{dC^*}{dx}\bigg|_{X+\Delta X}$$

$$+A\mathcal{D}_e^* \frac{dC^*}{dx}\bigg|_{X+\Delta X} = A\Delta X\left[\varepsilon + K_p\,\rho_s\right]\frac{\partial C}{\partial t}\bigg|_{\overline{X}} \qquad (4.179)$$

Since ε is usually very close to unity, ε can be set to 1. Note that C* and C are related according to $C^* = K_p\rho_s C$ and that $\mathcal{D}e = \mathcal{D}e^*$. This last equality states that the turbulent diffusivity for dissolved components and particulate are the same. Putting in these (simplyfing) expressions yields

$$-\mathcal{D}_e\,(1 + K_p\rho_s)\,\frac{dC}{dx}\bigg|_X + \mathcal{D}_e(1+K_p\rho_s)\,\frac{dC}{dx}\bigg|_{X+\Delta X}$$

$$=\Delta X(1+K_p\rho_s)\,\frac{\partial C}{\partial t}\bigg|_{\overline{X}} \qquad (4.180)$$

Simplyfing and taking the limit as $\Delta X \to 0$ yields

$$\frac{\partial C}{\partial t} = \mathscr{D}_e \frac{\partial^2 C}{\partial X^2} \qquad (4.181)$$

Thus, it appears that the capacitance of the mobile sorbing suspended particulate matter does not affect the rate of transport of the species of interest. However, the capacitance term does appear in the boundary condition at the source because the boundary flux must equate to both gradients, i.e., at the oil-water interface

$$\text{flux} = - \mathscr{D}_e \left(1 + K_p \rho_s\right) \frac{dC}{dx} \qquad (4.182)$$

The "flux" above is determined in part by the parameters of the oil phase. Since solving two-slab problems are sometimes tedious, the flux can be specified as a sum of decaying exponents of the form ae^{-bt}. By obtaining a solution, C, for each (a,b) set and then summing over all sets, virtually any source boundary condition can be approximated.

From this material balance derivation it is apparent that the suspended particulate matter will suppress the dissolved concentration because mass is required to satisfy the sorption (thermodynamic) expression. However, a concentration profile in the water column will move with the same speed as if suspended particulate matter were not present.

The transport of dispersed oil droplets occurs by turbulent diffusion and these oil droplets interact with suspended particulate by collisions. The result of a collision can be a rebounding of the same two particles or a coalescing of the two particles into one. The objective of a material balance for dispersed oil is then to predict as a function of time and depth the concentration of dispersed oil that exists as droplets only, and as oil associated with particulate. In order to derive a material balance for dispersed oil, a specification with respect to the state of the suspended particulate must be made. For the case being considered here, a uniform concentration of suspended particulate is assumed.

A material balance for the dispersed oil droplets which are assumed to transport through the water column according to the eddy diffusivity is

$$\frac{\partial C_o}{\partial t} = \mathcal{D}_e \frac{\partial^2 C_o}{\partial x^2} - KC_sC_o \qquad (4.183)$$

where C_o is the concentration of oil droplets per unit volume, C_s is the concentration of suspended particulate per unit volume, and k is a reaction rate constant for the collision <u>and</u> sticking of an oil droplet and a suspended particulate. Likewise, for the suspended particulate matter

$$\frac{\partial C_s}{\partial t} = \mathcal{D}_e \frac{\partial^2 C_s}{\partial X^2} - KC_sC_o \qquad (4.184)$$

and for an oil-particle species

$$\frac{\partial C_1}{\partial t} = \mathcal{D}_e \frac{\partial^2 C_1}{\partial X^2} + KC_sC_o \qquad (4.185)$$

where C_1 is the concentration of oil-particulate due to a single sticking collision.

Each of the reaction terms above should actually be a summation over all possible collisions of the specific species and all other species. However, experimental evidence apparently indicates a rate considering only C_s and C_o might be sufficient (Mackay and Hossain, 1982).

In the case where C_s is in large excess, the reaction rate expression will be of the form k_sC_s. However, in the Bering and Beaufort Seas the suspended particulate loadings can be quite small (Baker, 1983); thus, the two-component problem with both C_o and C_s will have to be considered.

The boundary conditions for the dispersed oil droplets depends on the oil slick and local parameters. These oil droplets may enter the water column due to wind-driven turbulence and/or spontaneous emulsification. The boundary conditions for the suspended particulate will depend on the resuspension/deposition phenomena that occurs at the ocean floor and other SPM source terms.

The material balance equations presented here consider the particles, both oil and sediment, to be neutrally buoyant or that they move according to the local eddy diffusivity. Thus, there is no gravity term. Future analyses of this assumption are required to determine what particle sizes will be transported by the local turbulence so that the particles appear neutrally buoyant.

4.10.8 Boundary Conditions for Modeling Dispersed Oil/SPM Interactions

Boundary Conditions are required for solutions to the mass balance equations. When an oil "particle" rises to the surface, it may stick or be reentrained based on sea state conditions. At the bottom, the oil may stick and adsorb onto the sediment or may be reentrained.

The boundary conditions at the surface and at the bottom are similar. That is,

$$-A_z \frac{\partial C}{\partial z} + (1-A)WC = 0 \qquad (4.186)$$

where A is the probability that the micelle will "stick" at the surface or bottom and remain there. If all micelles stick and stay then A = 1; if none do, then A = 0. The value of A will be different for the surface and bottom and will depend on environmental conditions and boundary characteristics.

At the thermocline, there is a change in the turbulent parameters between the upper and lower layer.

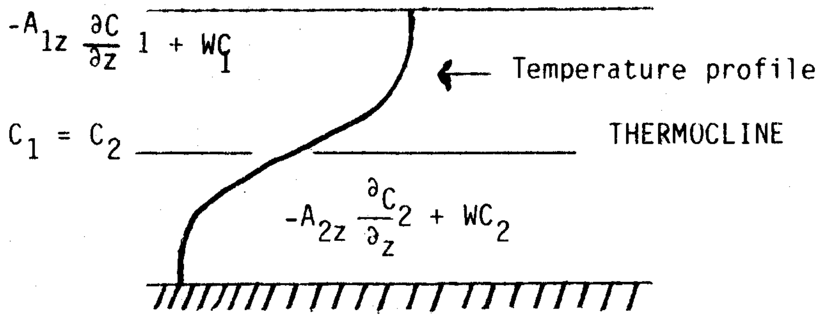

At the thermocline:

$$-A_1 \frac{\partial C}{\partial z} 1 + W_1 C_1 = -A_2 \frac{\partial C}{\partial z} 2 + W_2 C_2 \qquad (4.187)$$

$$C_1 = C_2 \qquad (4.188)$$

These boundary conditions alone do not indicate a build up of particles at the thermocline. In fact, the continuity of flux across the thermocline ensures that there will be no accumulation. However, there may be a maximum in the concentration profile at the thermocline under certain conditions.

To illustrate, consider the steady state case of vertical gradients only for oil/SPM particles that sink. Furthermore, let the particle sinking velocity be constant but the vertical eddy diffusivity vary with depth. Then the mass balance equation can be written as

$$A_2 \frac{\partial^2 C}{\partial z^2} - \left(W - \frac{\partial A_z}{\partial_z}\right) \frac{\partial C}{\partial z} + R = 0 \qquad (4.189)$$

where R is the source of oil/SPM particles.

The oil/SPM profile may look like:

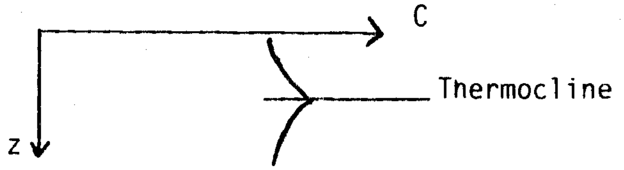

The conditions for the maximum are:

$\frac{\partial^2 C}{\partial z^2} > 0 \qquad \frac{\partial C}{\partial z} > 0$ above thermocline

$\frac{\partial^2 C}{\partial z^2} < 0 \qquad \frac{\partial C}{\partial z} = 0$ in thermocline

$\frac{\partial^2 C}{\partial z^2} > 0 \qquad \frac{\partial C}{\partial z} < 0$ below thermocline

For the maximum to exist under these conditions, we must have

$$\frac{\partial A_z}{\partial z} < W \tag{4.190}$$

above the thermocline and

$$\frac{\partial A_z}{\partial z} > W > 0 \tag{4.191}$$

below the thermocline. This is consistent with the general distribution of A_z which shows a minimum in the thermocline.

4.10.9 Current Status of Modeling Oil/SPM Interactions

At this time none of the previously desdribed formulations for modeling oil/SPM interactions have been incorporated into the Open-Ocean Oil-Weathering Model Code. These derivations were presented to illustrate the approach which is required to include these interactions and to define the physical and chemical parameters of importance which would need to be characterized before modeling such interactions can be successfully pursued. However, it is important to note that the oil/SPM interactions is an "add-on" calculation to the oil-weathering code. The oil-weathering calculations only provide a source term for dispersed oil. Thus, the Open-Ocean Oil-Weathering Code is a stand-alone calculation with respect to oil/SPM interactions and the oil/SPM interaction calculation is carried out afterwards because there is not oil/SPM feedback to the weathering oil slick.

5.0 EXPERIMENTAL PROGRAM RESULTS -- LA JOLLA, CALIFORNIA AND KASITSNA BAY, ALASKA

5.1 EXPERIMENTAL CHAMBER EVAPORATION/DISSOLUTION RATE DETERMINATIONS

Evaporation and dispersion are the two major weathering processes affecting oil after it is released into seawater; in some instances most of the volatile compounds may be lost by evaporative processes within 24 to 48 hours (JORDAN and PAYNE, 1980). The composition of an oil slick, its surface area and physical properties, the wind velocity, air and sea temperatures, sea state, and the intensity of solar radiation can all affect hydrocarbon evaporation rates (WHEELER, 1978).

Given sufficient time, evaporative processes can remove most of the volatile hydrocarbons with molecular weights less than nC-15, and in general pentadecane is the lightest normal alkane commonly found in weathered oils and tar balls (PAYNE, 1981). Further, it is rare to find hydrocarbons lighter than nC-12 in seawater extracts not associated with oil spill events. The volatile compounds encompassed below nC-15 make up anywhere from 20-50% of most crude oils, and the distillation curve data shown in Figure 3-12 illustrate that these components make up 50% of the overall mass of Murban crude, 46% of Cook Inlet crude, 31% of Prudhoe Bay crude and 25% of Wilmington crude oils. Hydrocarbon components with molecular weights less than nC-15 can make up as much as 75% or more in refined petroleum products and they constitute 10% or less of residual fuel oils such as Bunker C (CLARK and BROWN, 1977).

While other studies have been completed to determine the relative importance of evaporation vs dissolution for such compounds as benzene and cyclohexane (HARRISON et al., 1975; MCAULIFFE, 1977; SMITH and MCINTYRE, 1971), carefully controlled experiments were clearly required to examine the simultaneous affects of evaporation and dissolution on oil weathering. Acquisition of such data is critical for modification of algorithms and input components for the oil-weathering computer model and verification of predicted output where environmental parameters such as wind speed and air and water temperature could be controlled. To support this requirement, an evaporation/dissolution chamber was constructed to allow simultaneous, compound-specific concentration determinations in air, oil and water phases such that evaporative and dissolution process rates could be determined as a function of time. Figure 5-1 presents three schematic diagrams of the evaporation/dissolution chamber showing its component parts and functional design, and Figure 5-2 shows the assembled evaporation/dissolution chamber. The circular design of the tank allows air to pass over the slick on a one time basis where an estimated 90% of the air flow is diverted up the exhaust vent shown in Figure 5-1A and out of the exhaust port into a vented duct. The velocity of the air stream is controlled by baffled systems on the blower shown in the foreground of Figure 5-2, and air velocities over the slick are measured using a Kurz air velocity meter installed 5 cm above the oil/seawater interface. To minimize sample contamination during experimental studies, the tank has been fabricated entirely of glass, stainless steel, anodized aluminum and teflon. The circular design was chosen over other shapes (e.g., rectangular) such that wind driven oil would not accumulate or pile up at one end of the chamber. In this manner a continuous oil slick can be maintained to simulate the conditions of airflow over a large surface oil mass.

For ambient temperature (19 to 23°C) studies, the chamber was assembled in a dedicated laboratory facility controlled by standard air conditioning. Lower temperature studies at 13 and 3°C have been conducted within a specially designed cold room where air and water temperatures could be carefully controlled and maintained. (In this enclosed chamber, lower molecular weight hydrocarbons lost due to evaporation processes are vented outside the laboratory.) Seawater for the system was obtained from the flow-through seawater aquarium supply source at Scripps Institution of Oceanography and filtered (0.45 μm glass fiber filters) before use. During an experimental run, time series air samples were obtained by adsorbing volatile components onto Tenax© columns (using a technique described in greater detail in Appendix F), water column samples were obtained through the stopcocks in the sides of the chamber and "grab" oil samples were obtained through a specially designed

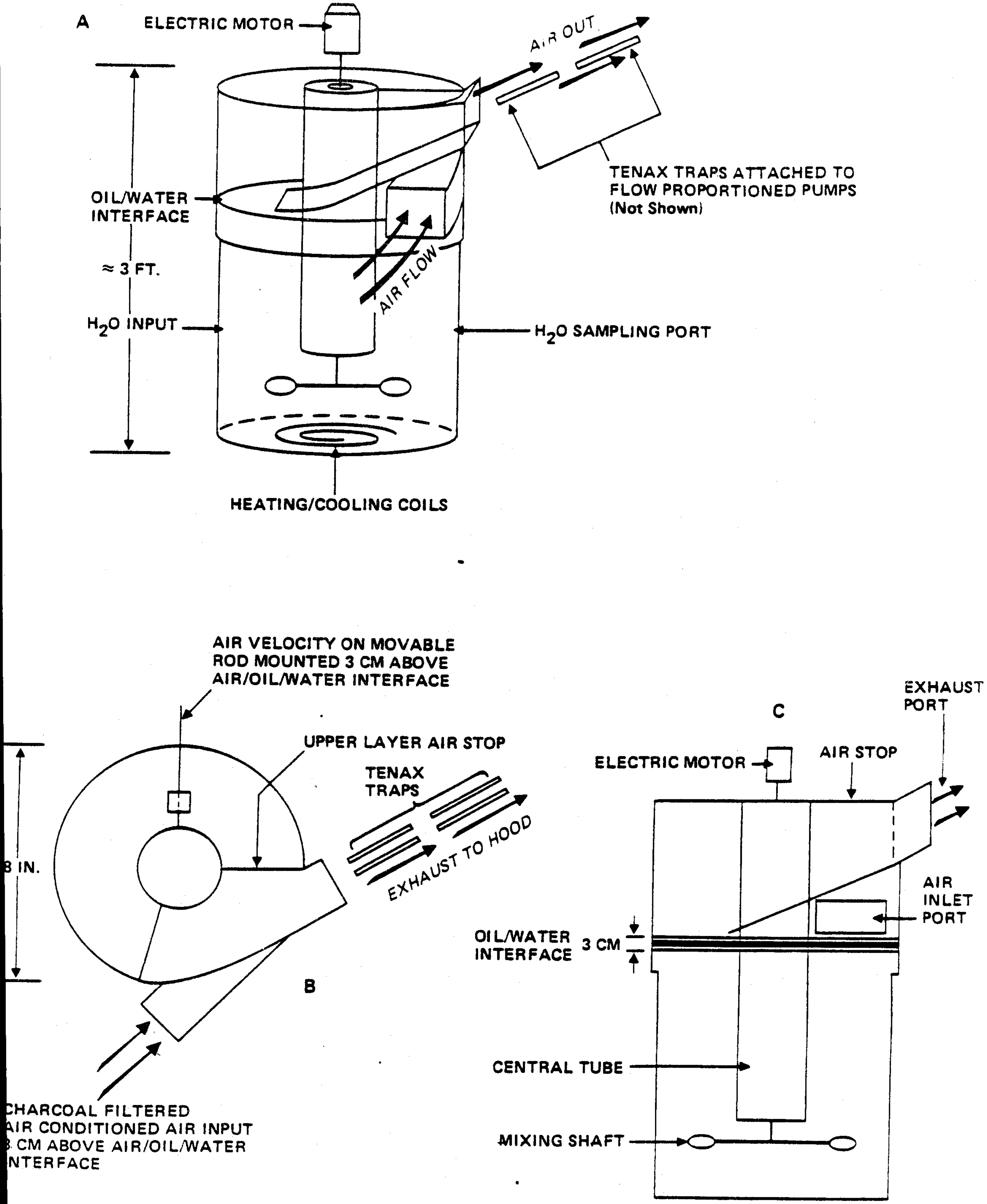

FIGURE 5-1. PROTOTYPE TANK DESIGN FOR EVAPORATION/DISSOLUTION EXPERIMENTS.

Figure 5-2. Assembled Evaporation/Dissolution Chamber Utilized For Component Specific Evaporation/Dissolution Rate Determinations As a Function Of Temperature and Wind Speed -- La Jolla, CA.

sampling port in the top of the air-flow manifold. To ensure homogenity in the water column, the water was agitated from below by means of a variable-speed rotating paddle capable of generating eddy diffusion coefficients ranging from 10 to 100 cm^2/sec.

5.1.1 Results of Evaporation/Dissolution Chamber Experiments at 19°C - La Jolla

Before experimental studies on such a complex mixture as Prudhoe Bay crude oil were initiated, evaporation/dissolution experiments were completed using a simple, three component mixture consisting of benzene, toluene, and cyclohexane at less than full saturation concentrations. The application of the results from these experiments toward the oil weathering model development was presented in detail in Sections 2.4.4 and 2.4.6, respectively, of our November 1980 Interim Quarterly Report (PAYNE et al., 1980).

After completing preliminary evaluation of the evaporation/dissolution chamber with the three component mixture mentioned above, a series of oil weathering experiments were undertaken with Prudhoe Bay crude oil at ambient (19 to 23°C) temperatures and at 3°C in the presence and absence of Corexit 9527. Time-series oil and water samples collected in conjunction with these experiments were fractionated into aliphatic, aromatic and polar components and analyzed by capillary Flame Ionization Detector (FID) gas chromatography. All original and reduced chromatographic data were stored in the experiment (EXP) data base of the oil weathering model. Individual compound concentrations could then be retrieved from the computer data base for any desired fraction as a function of time and environmental conditions. Data for atmospheric volatile compound concentrations were obtained and reduced manually (Tenax trap experiments); however, the reduced data output were then entered into the computer for generation of time series decay curves for volatile compound losses.

Figure 5-3 presents time series packed column FID gas chromatograms obtained on the volatile components in the air above the spilled oil slick at

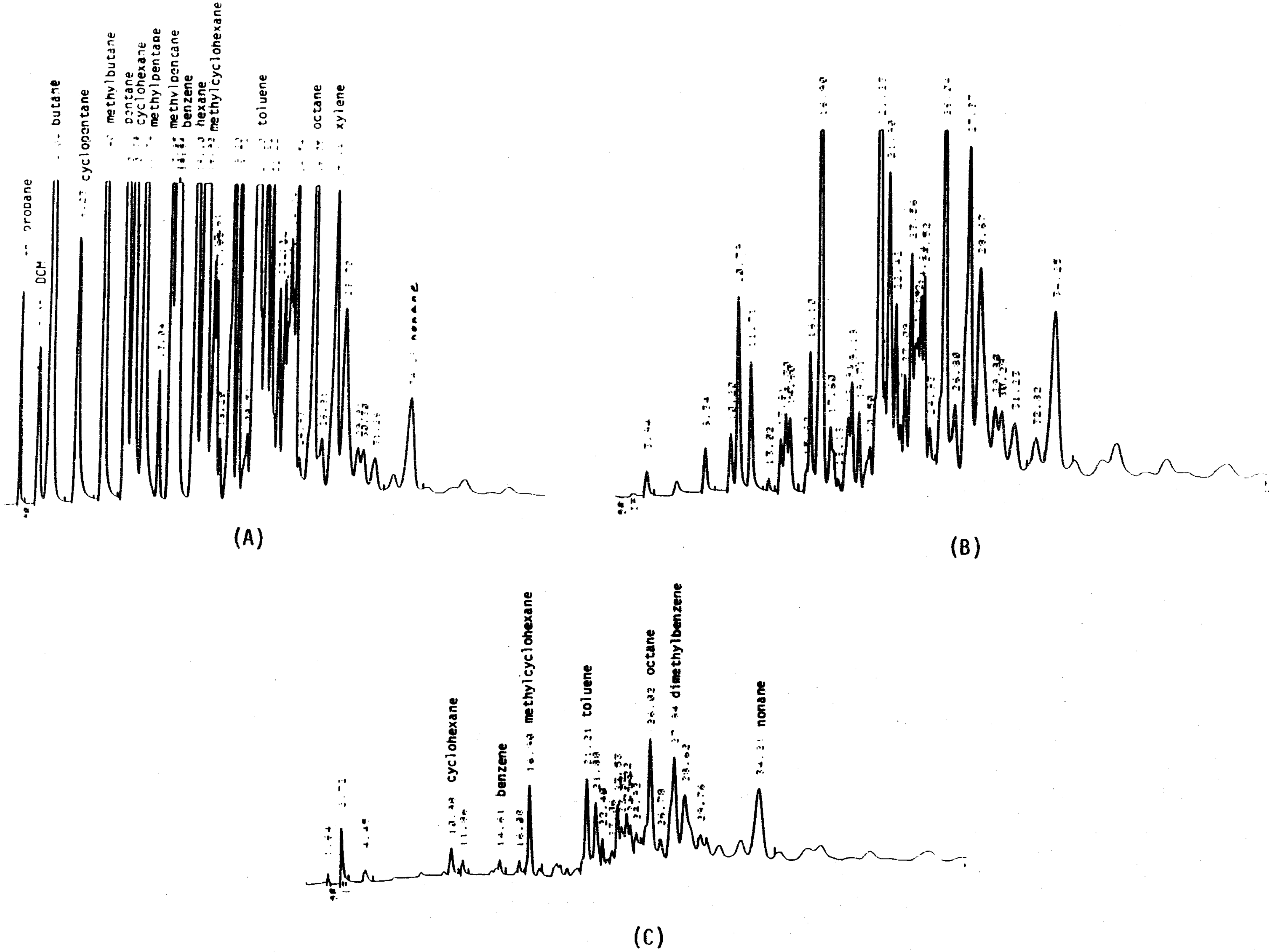

FIGURE 5-3. PACKED COLUMN FLAME IONIZATION DETECTOR GAS CHROMATOGRAMS OBTAINED ON HEAT-DESORBED VOLATILE COMPONENTS TRAPPED ON TENAX® FROM EVAPORATION/DISSOLUTION EXPERIMENT COMPLETED AT 19°C UNDER INFLUENCE OF A 7 KNOT WIND (E/D-4). (A) AIR SAMPLE 15 MINUTES AFTER THE SPILL (FRONT TRAP); (B) AIR SAMPLE 6 HOURS AFTER THE SPILL (FRONT TRAP); (C) AIR SAMPLE 12 HOURS AFTER THE SPILL (FRONT TRAP). ALL SAMPLES OBTAINED BY VACUUM TRAPPING EXHAUST AIR STREAM FROM EVAPORATION/

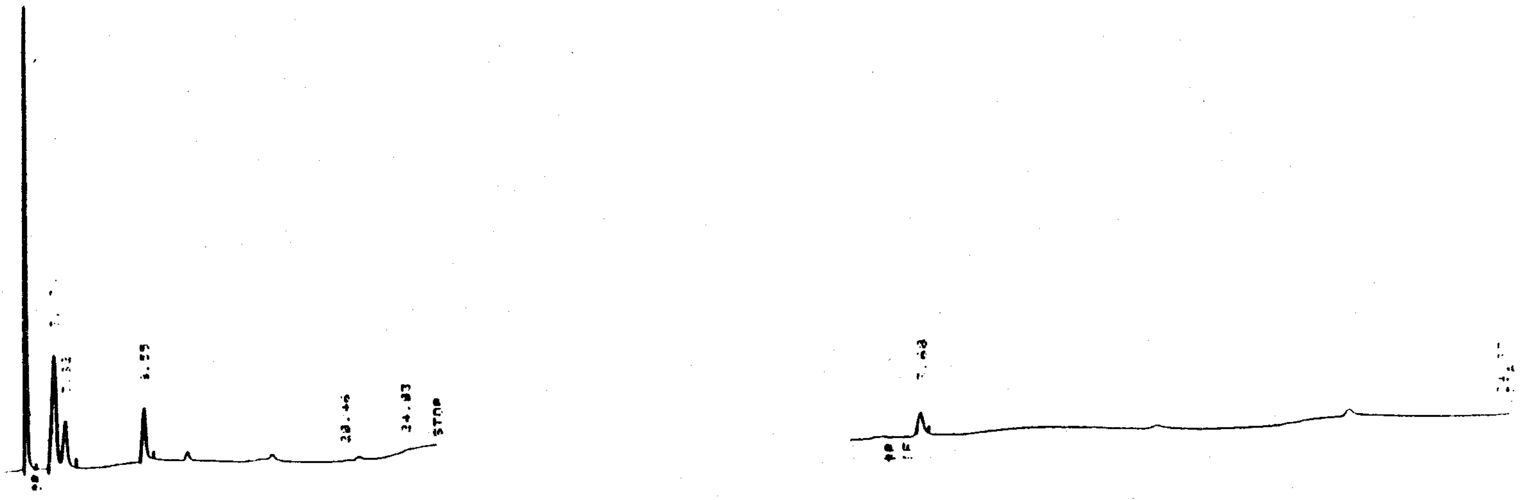

(D)

(E)

FIGURE 5-3 (continued). PACKED COLUMN FLAME IONIZATION DETECTOR GAS CHROMATOGRAMS OBTAINED ON HEAT-DESORBED VOLATILE COMPONENTS TRAPPED ON TENAX® FROM EVAPORATION/DISSOLUTION EXPERIMENT COMPLETED AT 19°C UNDER INFLUENCE OF A 7 KNOT WIND (E/D-4). (D) BACKUP IN-SERIES TRAP 15 MINUTES AFTER THE SPILL SHOWING LIMITED BREAKTHROUGH OF ONLY 4 INDIVIDUAL ALIPHATIC COMPONENTS; (E) BACKGROUND AIR SAMPLE (CONTROL) COLLECTED BEFORE SPILL INITIATED. ALL SAMPLES OBTAINED BY VACUUM TRAPPING EXHAUST AIR STREAM FROM EVAPORATION/DISSOLUTION CHAMBER AT A FLOW RATE OF 25 ML/MIN FOR 60 SECONDS.

19°C (Evaporation/Dissolution Run 4; denoted E/D-4). This technique allows quantitation of lower molecular weight compounds ranging from propane through nonane as a function of time. As the chromatograms in Figure 5-3, B and C illustrate, very rapid losses of lower molecular weight components below octane are observed. The chromatogram in Figure 5-3D shows the in-series back-up Tenax trap from the 15 minute sample, and only limited breakthrough of lower molecular weight compounds such as butane and methylbutane are noted. Figure 5-3E presents a time-zero Tenax background air control sample showing no component contamination before the spill occurred. Additional details on the sampling procedure and methodology for analyses of volatiles using this Tenax trap procedure are presented in Appendix F - Analytical Methods.

From the type of data obtained and shown in Figure 5-3, it is possible to generate time series airborne concentrations of these volatile compounds as shown by the data in Table 5-1 and the graphs in Figure 5-4. Clearly, airborne concentrations of monocyclic aromatics such as benzene and toluene are observed to fall off rapidly to non-detectable levels within 7 to 8 hours under these conditions. Similar exponential decay curves are observed for volatile aliphatic compounds such as pentane, methylpentane and octane (Figure 5-5).

Simultaneously collected water samples analyzed by a purge and trap technique similar to that developed by BELLAR and LICHTENBERG, (1974) allow determination of water column concentrations of these same volatile components as a function of time; Table 5-2 and Figure 5-6 present such time series data (from E/D-4) for benzene, toluene, cyclohexane and xylene. In the water column data, an initial increase in aromatic hydrocarbon concentrations is noted with the concentration maximum occurring after 4-5 hours. Under these conditions, the absolute maxima of individual compounds are determined by the oil phase and seawater solubilities of the compound of interest and its mole fraction in the parent oil. After the maximum concentration buildup at 4-5 hours (controlled by compound specific mass transfer coefficients) exponential decreases in the water-borne concentrations are then noted due to gradual seawater/air partitioning and evaporative loss of these compounds.

TABLE 5-1. TIME-SERIES AIR-BORN CONCENTRATIONS (μg/l) OF VOLATILE COMPONENTS ABOVE PRUDHOE BAY CRUDE OIL WEATHERING AT 19°C UNDER A 7 KNOT WIND (Tenax Samples from E/D-4).

Compound	time 0	30 min	45 min	1 hour	1 hour 15 min	1 hour 30 min	1 hour 45 min	2 hrs	2.5 hrs	3 hrs	4 hrs	5 hrs	6 hrs	8 hrs
Butane	11.9	3.54	3.05	2.65	1.17	ND	ND	ND	ND	ND	ND	ND	ND	ND
Cyclopentane	2.46	0.761	0.689	0.382	ND	ND	ND	ND	ND	ND	ND	ND	ND	ND
Methylbutane	7.30	2.22	2.59	1.08	1.19	0.675	1727	0.439	0.592	0.241	ND	ND	ND	ND
Pentane	16.1	3.88	3.50	1.79	1.64	0.816	0.682	0.496	0.426	0.222	ND	ND	ND	ND
Cyclohexane	7.52	2.70	2.80	1.39	1.36	0.816	0.682	0.488	0.454	0.323	0.320	0.253	0.85	ND
Methylpentane	7.32	2.34	2.21	1.14	1.19	0.537	0.565	0.400	0.557	0.180	ND	ND	ND	ND
Benzene	3.8	1.17	1.18	0.670	0.670	0.653	1.08	0.748	0.636	0.355	0.160	0.443	0.003	ND
Hexane	12.0 μg/l	4.78	6.29	3.30	3.89	2.12	2.39	2.62	4.95	0.806	1.68	1.77	0.550	ND
Methylcyclohexane	15.6	5.64	5.63	3.11	3.14	1.48	1.47	1.25	1.23	0.717	0.247	0.222	ND	ND
Toluene	14.3 μg/l	4.98	5.17	2.97	2.79	1.55	1.42	0.975	0.864	0.484	0.20	0.253	ND	ND
Ethyl Benzene	1.47	0.576	0.555	0.318	0.306	ND	ND	ND	ND	ND	ND	ND	ND	ND
Cumene & n-octane	6.08μg/l	2.63	2.60	1.75	1.63	1.35	1.27	1.20	1.09	0.806	0.520	0.348	ND	ND

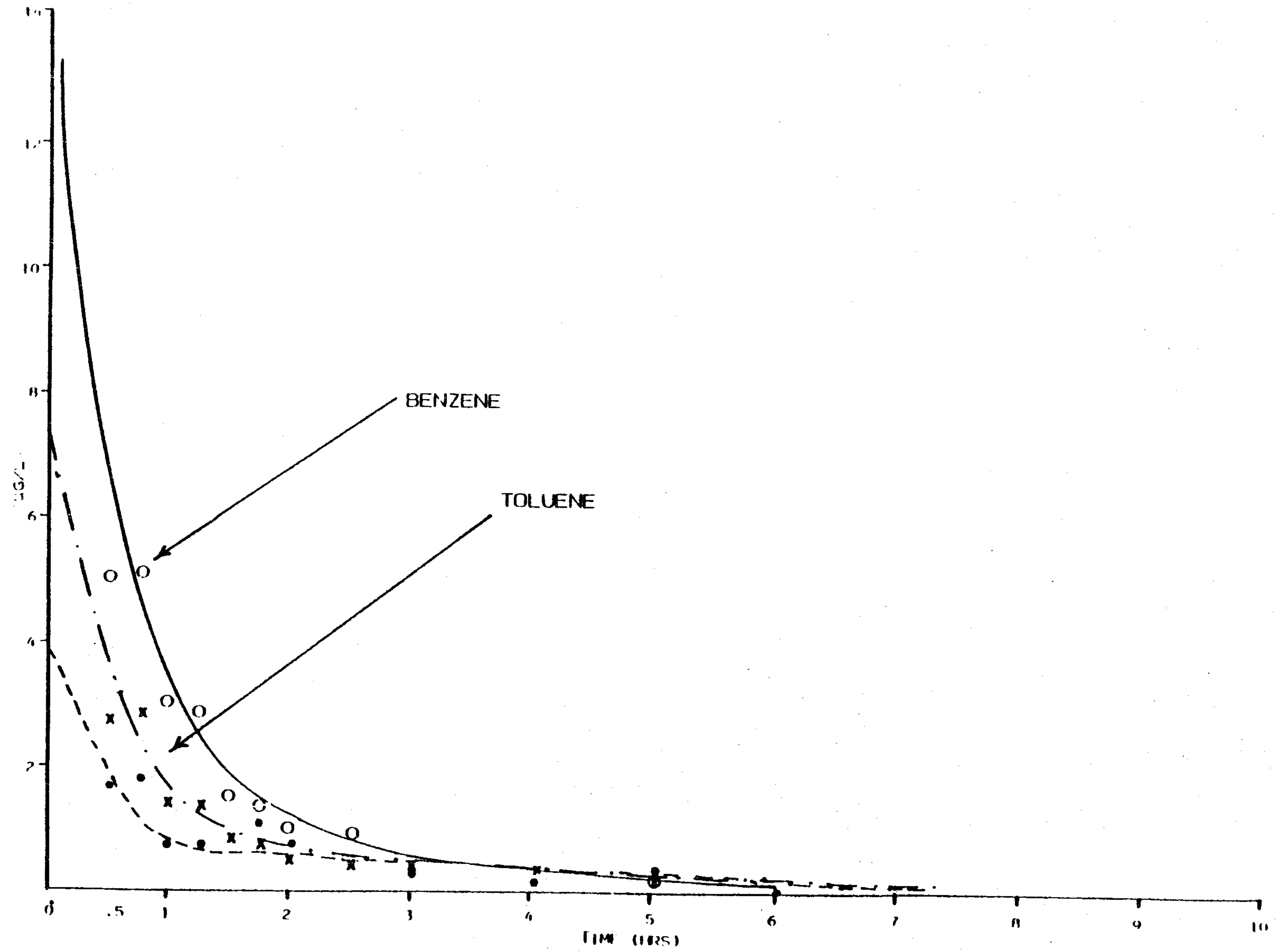

FIGURE 5-4. VOLATILE AROMATIC COMPONENT CONCENTRATIONS IN THE AIR STREAM ABOVE A 200 ml "SLICK" OF PRUDHOE BAY CRUDE OIL WEATHERING AT 19°C UNDER INFLUENCE OF A 7 KNOT WIND. (Evaporation/dissolution chamber run 4).

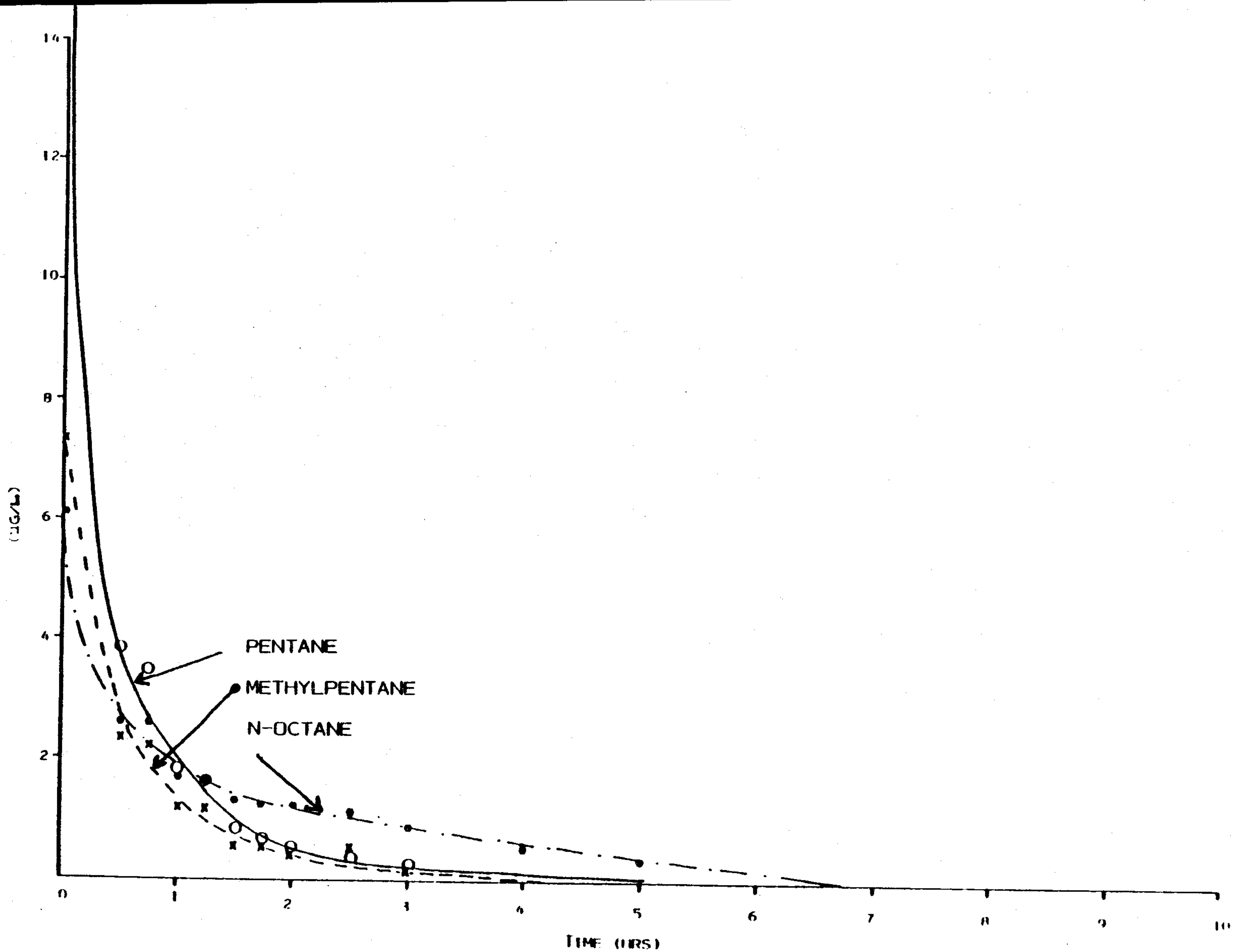

FIGURE 5-5. VOLATILE ALIPHATIC COMPONENT CONCENTRATIONS IN THE AIR STREAM ABOVE A 200 ml "SLICK" OF PRUDHOE BAY CRUDE OIL WEATHERING AT 19°C UNDER INFLUENCE OF A 7 KNOT WIND. (Evaporation/dissolution chamber run 4).

TABLE 5-2. TIME-SERIES WATER COLUMN CONCENTRATIONS (μg/l) OF LOWER MOLECULAR WEIGHT ALIPHATIC AND AROMATIC COMPONENTS FROM PRUDHOE BAY CRUDE OIL WEATHERING AT 19°C UNDER INFLUENCE OF A 7 KNOT WIND (Evaporation/dissolution Exp-4; purge and trap analyses after Bellar and Lichtenberg, 1974).

Compound	15 min	30 min	45 min	1 hour	1.5 hours	2 hours	2.5 hours	6 hours	11 hours	20 hours	26 hours	32 hours	38 hours	44 hours	50 hours	56 hours	62 hours
Cyclopentane	43.7	48.7	54.6	54.6	48.7	63.9	61.7	64.0	48.0	31.0	25.2	19.4	13.0	8.21	3.59	ND	ND
Methylbutane	21.4	23.2	24.2	24.2	24.4	27.0	26.0	27.3	21.1	15.1	13.3	10.8	7.51	5.01	2.75	ND	ND
Pentane	96.2	90.1	98.4	98.0	58.6	108.0	105.0	67.4	58.6	42.0	30.4	40.6	25.6	17.8	6.2	2.6	ND
Cyclohexane	50.2	50.0	52.4	53.0	61.4	62.4	62.6	59.8	44.0	30.4	26.8	21.2	15.0	10.2	6.2	1.8	ND
Methylpentane	57.6	54.7	57.2	57.4	59.8	64.6	66.3	57.6	42.8	29.7	25.1	21.9	15.1	10.2	4.60	ND	ND
Benzene	424.0	494.0	588.0	647.0	661.0	669.0	688.0	482.0	309.0	136.0	1.21	69.0	21.6	0.800	ND	ND	ND
Methylcyclohexane	36.6	28.0	28.1	27.0	27.7	30.1	31.5	26.4	18.7	13.9	12.7	11.0	8.01	5.61	3.32	ND	ND
Toluene	377.0	354.0	492.0	650.0	604.0	608.0	680.0	406.0	231.0	77.0	ND	49.6	3.80	ND	ND	ND	ND
Ethyl Benzene	19.5	11.4	19.3	375.0	26.8	25.8	34.3										
n-Octane	6.40	4.20	4.6	6.6	5.2	4.2	5.41	3.40	3.20	2.80	1.60	1.80	1.60	1.20	1.20	1.20	ND

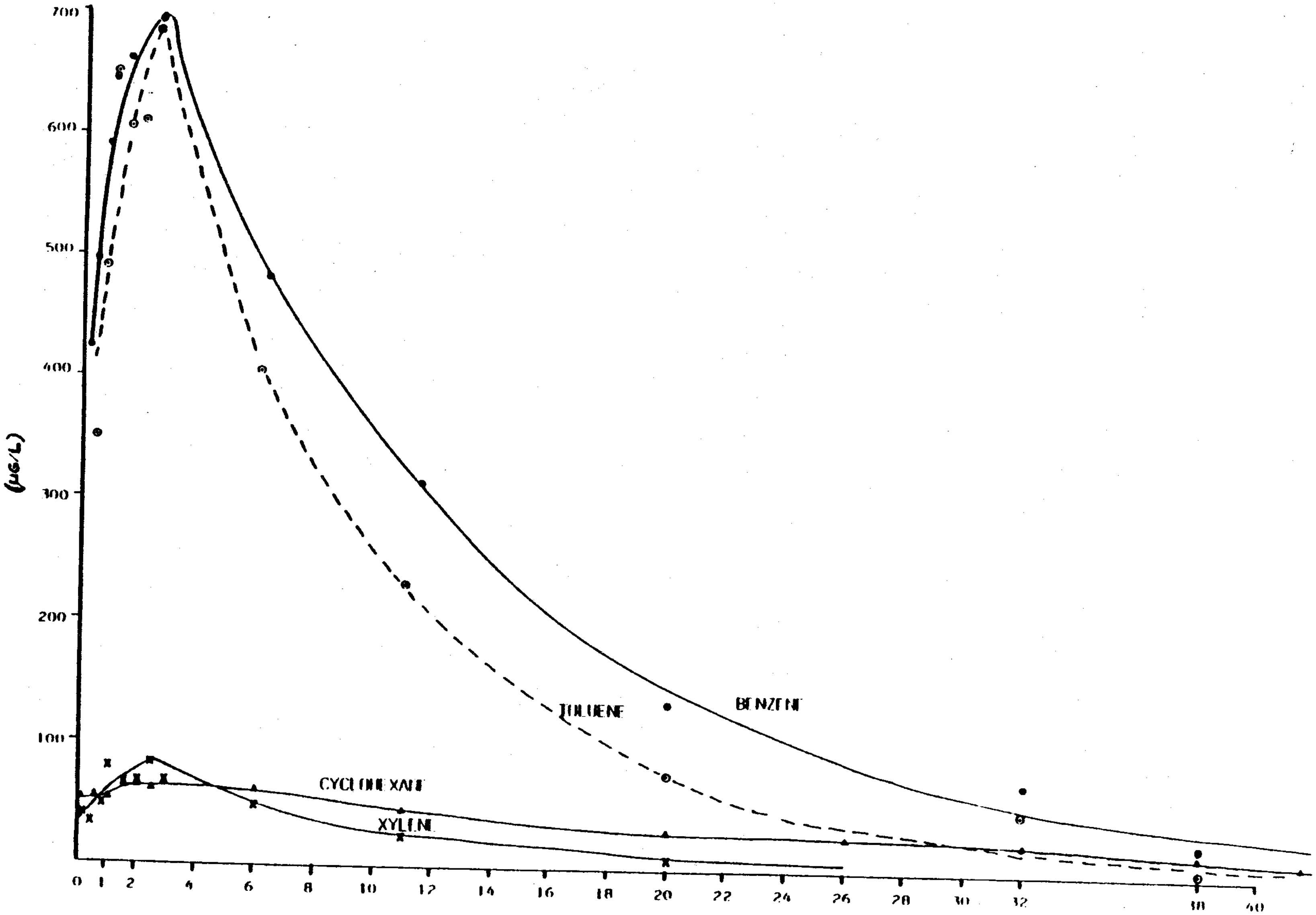

FIGURE 5-6. WATER COLUMN CONCENTRATIONS OF LOWER MOLECULAR WEIGHT AROMATIC COMPONENTS FROM PRUDHOE BAY CRUDE OIL WEATHERING AT 19°C UNDER INFLUENCE OF A 7 KNOT WIND. (Evaporation/dissolution Exp-4; purge and trap analyses after Bellar & Lichtenberg, 1974).

Intermediate and higher molecular weight component-specific data can only be generated by more detailed time-series sampling, methylene chloride extraction and fractionation of oil and water phases followed by capillary gas chromatographic analyses. Figure 5-7 presents the time-series FID capillary column gas chromatograms obtained on the aliphatic fractions of the oil samples from one such evaporation run (E/D-4) undertaken at 19°C under the influence of 7 knot winds. Sampling times for the chromatograms shown in Figure 5-7 are as follows: A, 0 hours; B, 2 hours; C, 1 day; D, 3 days; E, 7 days; F, 12 days; G, 24 days; and H, 41 days. Quite clearly, general evaporative trends can be observed from the chromatograms in Figure 5-7, and rapid loss of compounds below Kovat index 1000 are observed after as little as 2 hours. The time series concentration profiles for the intermediate and higher molecular weight compounds are somewhat more subtle with only limited additional losses occurring, and Tables 5-3 and 5-4 present time series concentrations of selected aromatic hydrocarbons in the oil and sub-surface water column, respectively.

Examination of the myriad of peaks in the time series chromatograms and the data in Tables 5-3 and 5-4 clearly shows the efficacy of developing a sound data management system for handling the extensive array of compound-specific data in the oil and water phases during the weathering process. Specifically, for each sample phase (oil, water and air) at each sampling time, literally hundreds of component-specific concentrations are generated. While such data can be worked up manually and plotted as shown in Figures 5-8 through 5-13, comparisons of oil weathering behavior as a function of temperature (or the presence or absence of dispersants, etc.) can best be accomplished through computer manipulation of data. Further, comparison of predicted vs. observed compound-specific (or even pseudo-component or distillation cut) data for oil weathering behavior can only be handled with an advanced data system such as the one utilized in this program. During development of this GC data base system, however, it was necessary to manually reduce and plot some of the initial individual-compound time-dependent concentrations

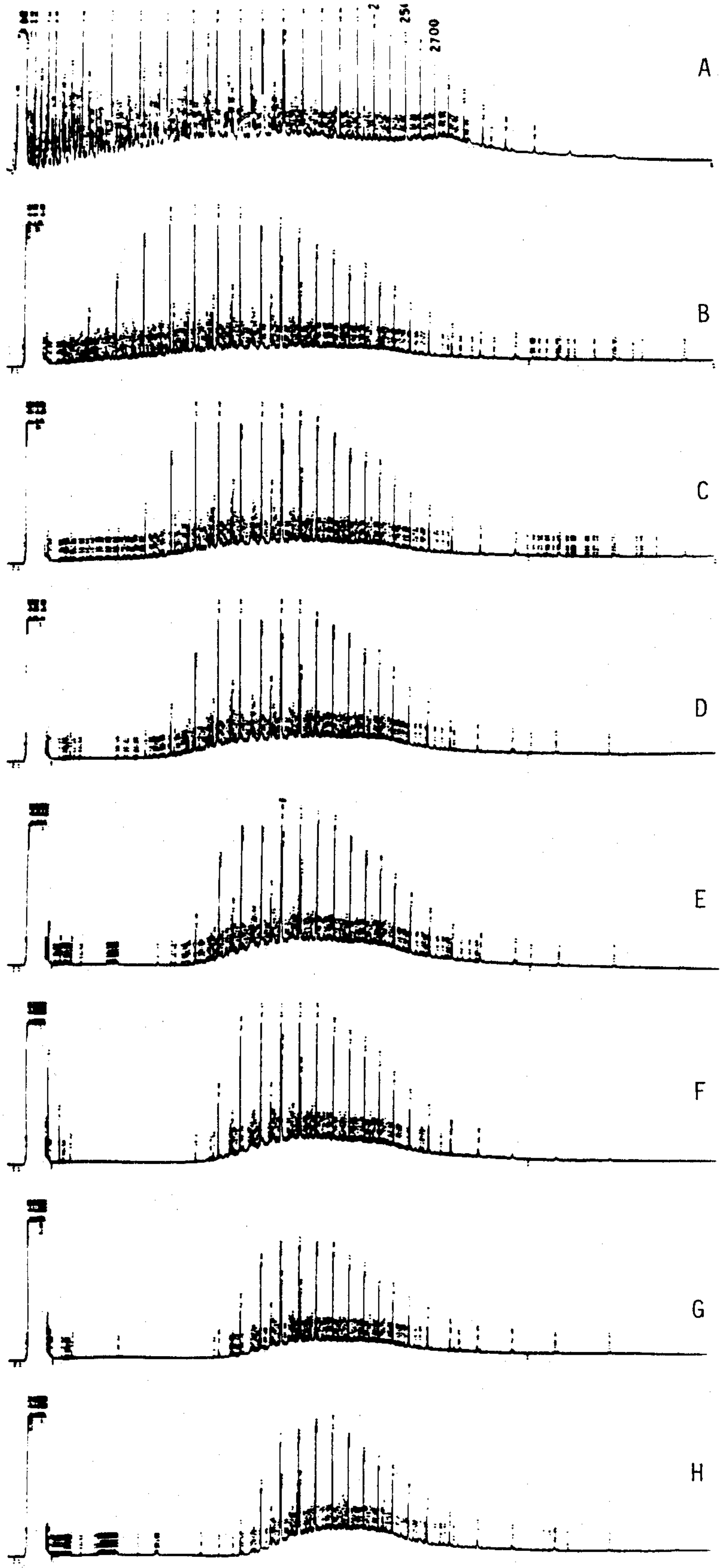

FIGURE 5-7. FLAME IONIZATION DETECTOR CAPILLARY GAS CHROMATOGRAMS OBTAINED ON PRUDHOE BAY CRUDE OIL WEATHERING AT 19°C UNDER INFLUENCE OF A 7 KNOT WIND (E/D-4). SAMPLING TIMES: (A) ZERO HOURS; (B) 2 HOURS; (C) 1 DAY; (D) 3 DAYS; (E) 7 DAYS; (F) 12 DAYS; (G) 24 DAYS; AND (H) 41 DAYS.

TABLE 5-3. TIME DEPENDENT AROMATIC COMPOUND CONCENTRATIONS IN OIL EXTRACTS BENEATH A SLICK UNDERGOING EVAPORATION/DISSOLUTION WEATHERING AT 19° UNDER A 7 KNOT WIND. (Concentration in ug/l).

			SAMPLING TIME																	
COMPOUND	RT (min.)	KOVAT	0-HRS.	1.5	3.0	6.0	8.75	12.0	24.0	35.75	48.0	72.5	149	169	195	220	288	337	384	460
ethylbenzene	7.27	857	26.9		16.3	14.7														
1,4 & 1,1-dimethylbenezene	7.64	867	184.	124.	131.	119.1	78.5	26.6	26.1											
1,2-dimethylbenezene	8.59	893	114.	94.1	102.	69.6	61.3	21.4	17.2											
propylbenzene	11.38	951	12.6	15.9	14.8	15.9														
1-ethyl-2-methylbenzene	11.81	959	138.	105.	103.	71.6	50.8	13.8												
1-methylethylbenzene	12.68	977	74.7	78.3	72.1	49.9	31.7													
1,2,4,-trimethylbenzene	13.40	991	263.	320.	303.	280.	126.	60.3	18.1											
1,2,X--trimethylbenzene	14.86	1019	230.	284.	274.	186.	120.	56.5												
2,3-dihydro-1H-indane	15.49	1031		21.6	19.7	12.7														
2,1-dihydro-1-methyl-1H-indane	18.21	1082	120	122	114	95.3	66.7	79.2												
1,2,3,5-tetramethylbenzene	21.65	1148	83.8	127	126	97.8	69.1	56.6	23.7											
1,2,3,4-tetramethylbenzene	22.09	1156	83.2	148	139	128	102	55.8												
naphthalene	23.26	1179	294	521	513	424	304	227	79.1		38.3	18.1								
1-methylnaphthalene	29.57	1304	560	948	990	905	738	697	441	120	366	310	84.1	[illegible]	31.3	21.2				
2-methylnaphthalene	28.77	1288	890	1500	1530	1430	1150	1050	661	161	517	419	88.8	35.4	24.8	16.8				
1,1-biphenyl	32.85	1375	162	144	160	144	122	125	161	131	80.9	75.8	32.0	22.1	15.8	16.6	8.87			
2-ethylnaphthalene	33.45	1387	124	223	234	220	196	182	130	24	148	144	80.1	57.9	50.7	38.1	25.3	27.8		
1,5-dimethylnaphthalene	33.94	1398	580	828	859	812	716	708	613	244	557	576	244	204	247	185	124	124	79.7	59.4
2,3-dimethylnaphthalene	34.62	1413	208	221	227	205	167	195	160	140	147	127	77.1		127	31.3	65.5	77.7	56.7	45.9
1,1-methylene-bisbenzene	37.64	1481	281	459	469	475	394	391	339	208	300	411	328	272	251	272	190	194	156	137
dibenzothiophene	48.32	1744	246	316	334	310	276	285	318	267	299	156	321	297	112	114	152	427	356	449
phenanthrene	49.34	1771	207	267	270	264	230	238	260	246	244	200	274	248	271	259	175	111	281	351
4-methyldibenzothiophene	52.05	1845	176	240	249	250	223	221	253	222	244	273	264	211	252	241	114	136	259	360
2-methylphenanthrene	53.58	1887	120	161	158	149	151	150	160	157	147	162	150	159	158	148	163	199	179	198
x-methylphenanthrene	54.42	1911	188	212	215	213	178	192	216	193	200	207	180	201	177	141	143	253	224	272
2,3-dimethylphenanthrene	58.36	2027	242	264	275	264	225	243	275	254	243	271	255	241	252	181	214	347	302	382

TABLE 5-4. TIME DEPENDENT AROMATIC COMPOUND CONCENTRATIONS IN WATER EXTRACTS BENEATH A SLICK UNDERGOING EVAPORATION/DISSOLUTION WEATHERING AT 19°C UNDER A 7 KNOT WIND. (Concentration in μg/l).

Compound	RT (min)	Kovat	0 hr	1.5	3.0	6.0	8.75	12.0	24.0	35.75	48.0	72.5	140.75	163.25	194.
Ethylbenzene	7.27	857		10.6	21.0	22.7	17.6	17.5	3.54	5.32	4.51		1.71		2.
1,4 & 1,3-dimethylbenzene	7.64	867		55.2	73.7	98.7	44.5	64.4	18.6	29.7	16.1		9.15		6.
1,2 dimethylbenzene	8.59	893		30.2	41.5	55.9	42.3	40.7	120.	17.4	8.42		2.61		1.
Propylbenzene	11.38	951		3.19	128	88.6	170	61.0		59.4	2.92				
1-ethyl-2 methylbenzene	11.81	959		6.97	13.2	18.2	8.64	13.8		4.92	1.92				
1-methylethylbenzene	12.68	977		3.89	7.81	11.2	8.85	9.01	2.32	4.09	1.08				
1,2,4-trimethylbenzene	13.40	991		12.6	10.9	21.9	3.01	14.1	6.26	3.75	3.11				
1,2,x-trimethylbenzene	14.86	1019		8.16	10.6	18.6	7.40	13.9	8.30	9.48					
2,3 dihydro 1H-Indane	15.49	1031			1.51	2.17	2.81	1.38		1.14	4.25				
2,3-dihydro 1methyl-1H-Indane	18.21	1082			1.61	2.92	3.81	2.05	1.17	2.17					
1,2,3,5 tetramethylbenzene	21.65	1148								1.77					
1,2,3,4 tetrahydronapthalene	22.09	1156				2.51	1.87	2.00	1.00	2.95	1.47				
Napthalene	23.26	1179		14.4	17.2	35.5	6.77	32.0	32.4	18.3	21.6				
1 Methylnapthalene	29.57	1304		4.43	1.48	7.52		2.32	24.6	24.4	22.4	9.32	4.09	1.67	
2 Methylnapthalene	28.77	1288		5.98	1.81	9.36		1.76	10.6	32.2	26.6	8.27	4.09	2.17	1.4
1,1 bi-phenyl	32.85	1375						1.98	4.06	5.59	3.90	2.05	1.31		
2 ethylnapthalene	33.45	1387								2.17					
1,5-dimethylnapthalene	33.94	1398							3.86	1.67		2.54	2.76	1.51	
2,3-dimethylnapthalene	34.62	1413							1.40		1.19		1.49		1.
1,1-methylene bisbenzene	37.64	1481									1.50				
1,6,7-trimethylnapthalene	39.52	1525													
Dibenzothiophene	48.32	1744													
Phenanthrene	49.34	1771													
4 methyldibenzothiophene	52.05	1845													
2-methylphenanthrene	53.58	1887													
x-methylphenanthrene	54.42	1911													
2,3-dimethylphenanthrene	58.36	2027													

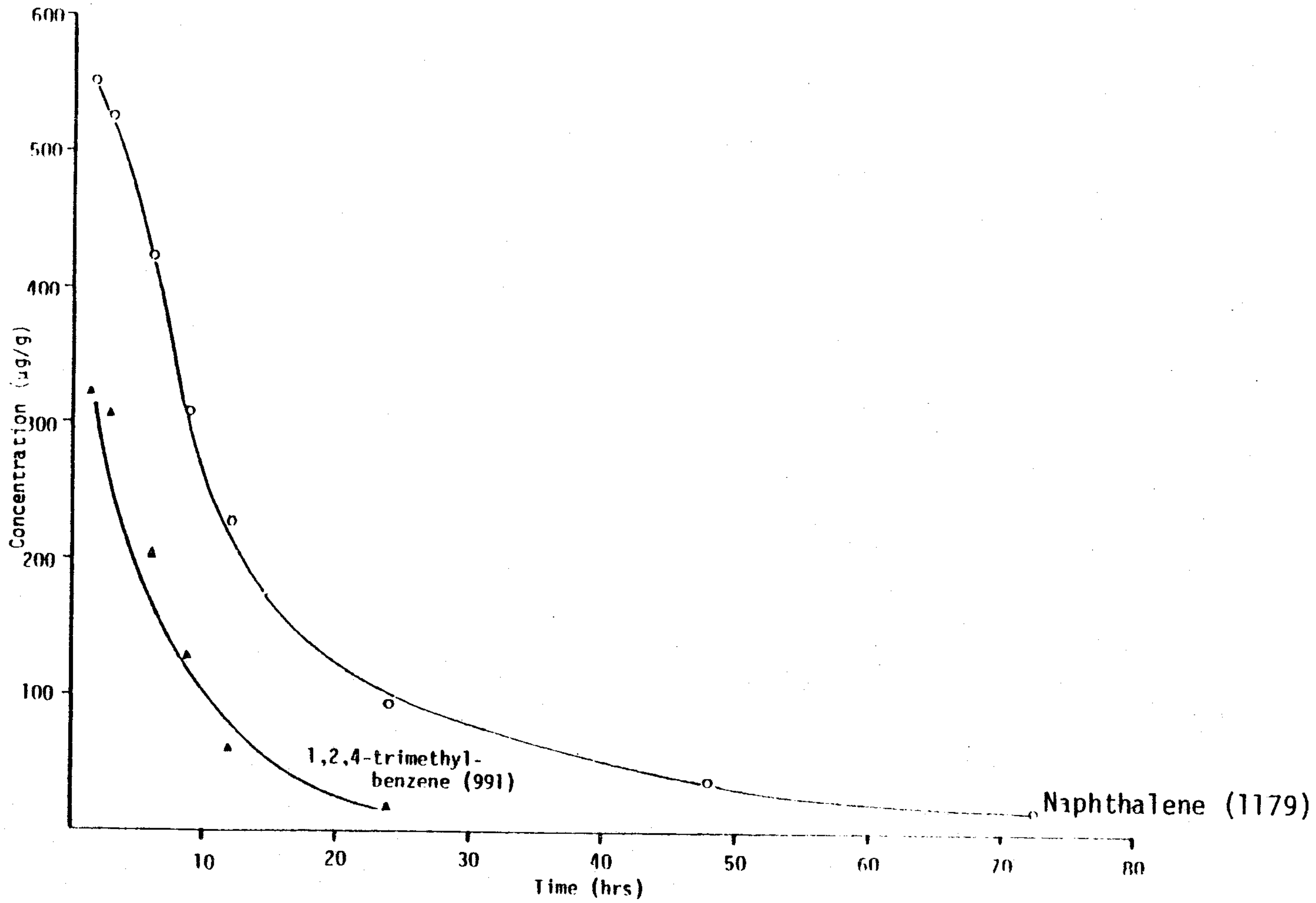

FIGURE 5-8. TIME-DEPENDENT CONCENTRATION IN OIL WEATHERING AT 19°C UNDER INFLUENCE OF A 7 KNOT WIND.

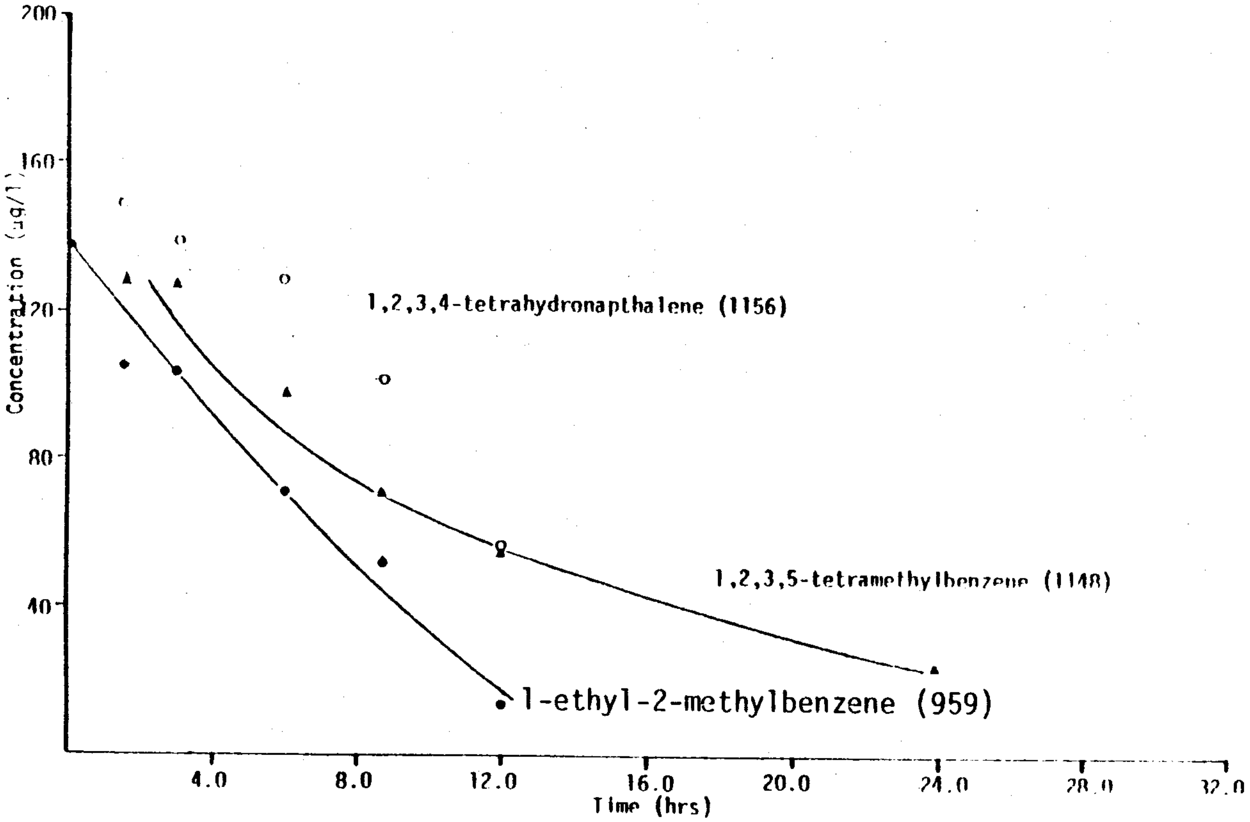

FIGURE 5-9. TIME-DEPENDENT CONCENTRATION IN OIL WEATHERING AT 19°C UNDER INFLUENCE OF A 7 KNOT WIND.

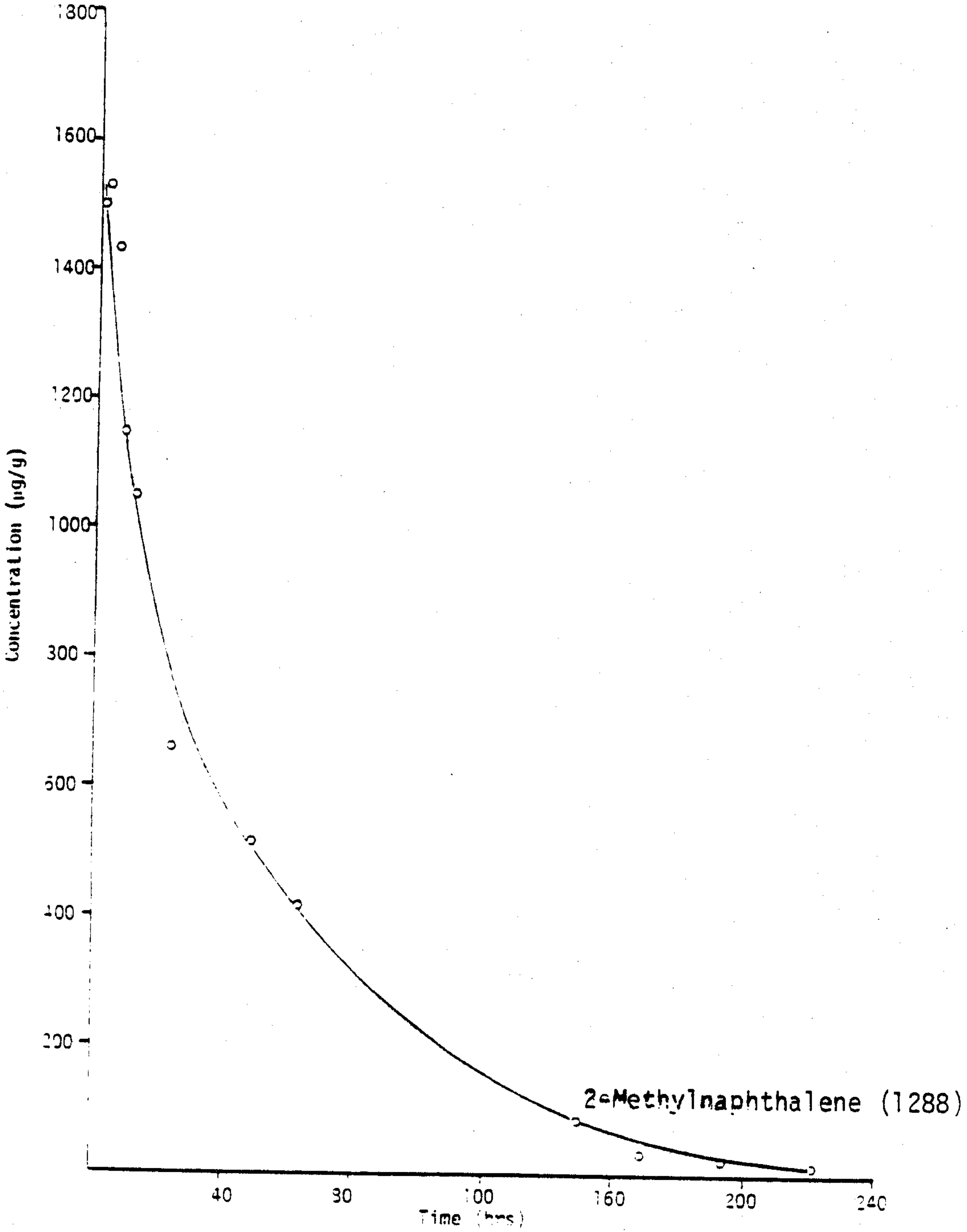

FIGURE 5-10. TIME-DEPENDENT CONCENTRATION IN OIL WEATHERING AT 19°C UNDER INFLUENCE OF A 7 KNOT WIND.

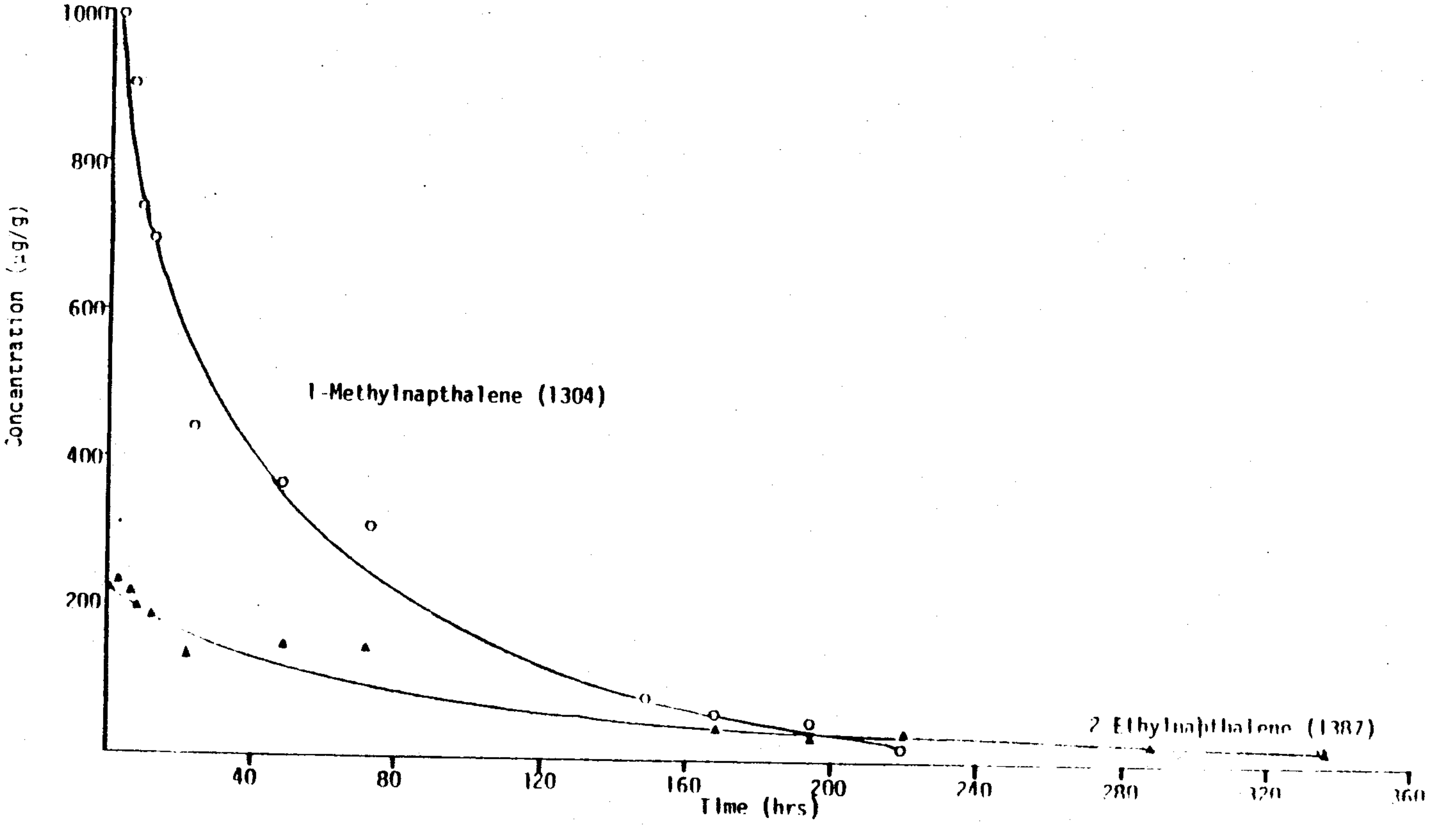

FIGURE 5-11. TIME-DEPENDENT CONCENTRATION IN OIL WEATHERING AT 19°C UNDER INFLUENCE OF A 7 KNOT WIND.

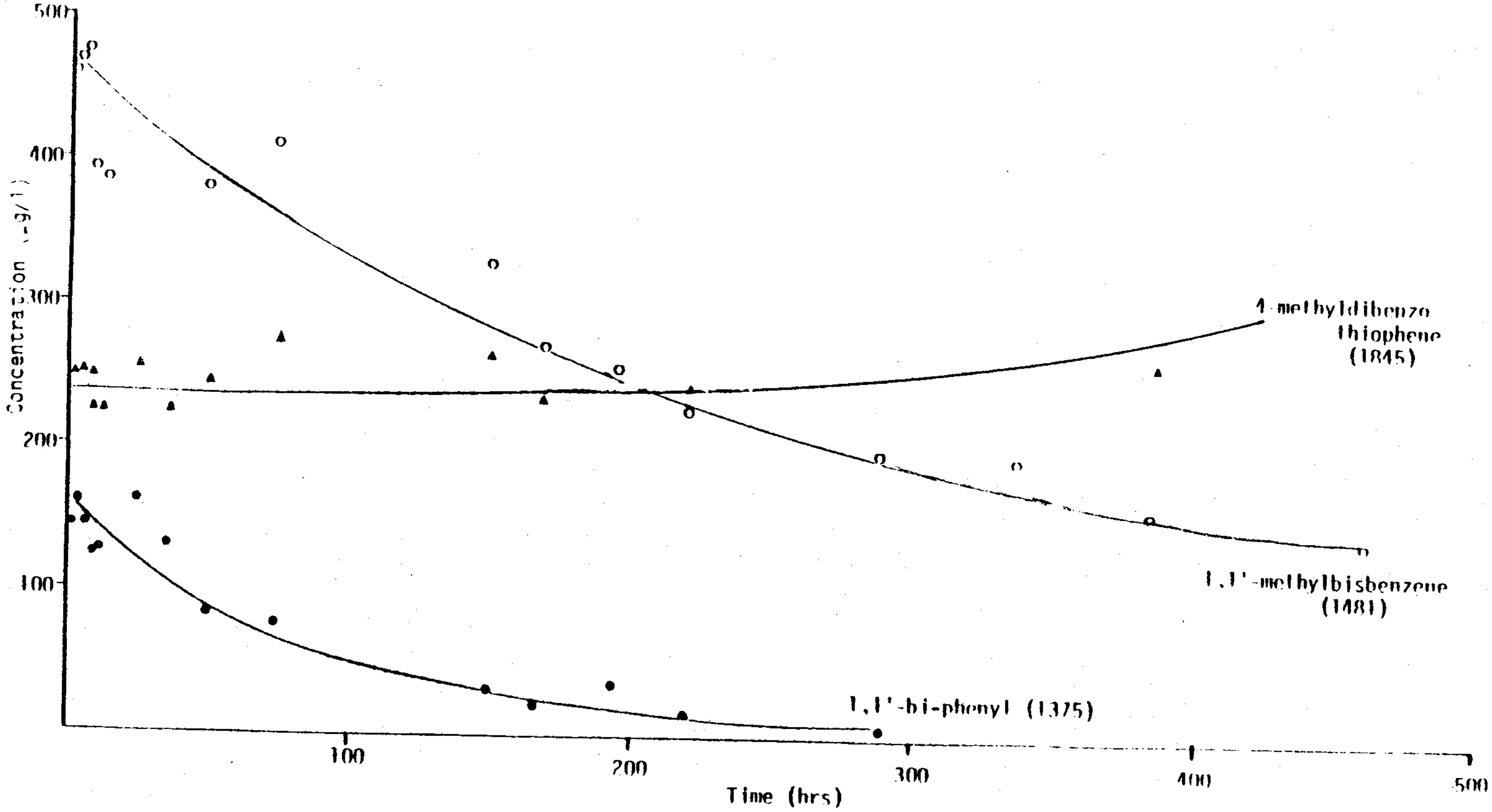

FIGURE 5-12. TIME-DEPENDENT CONCENTRATION IN OIL WEATHERING AT 19°C UNDER INFLUENCE OF A 7 KNOT WIND.

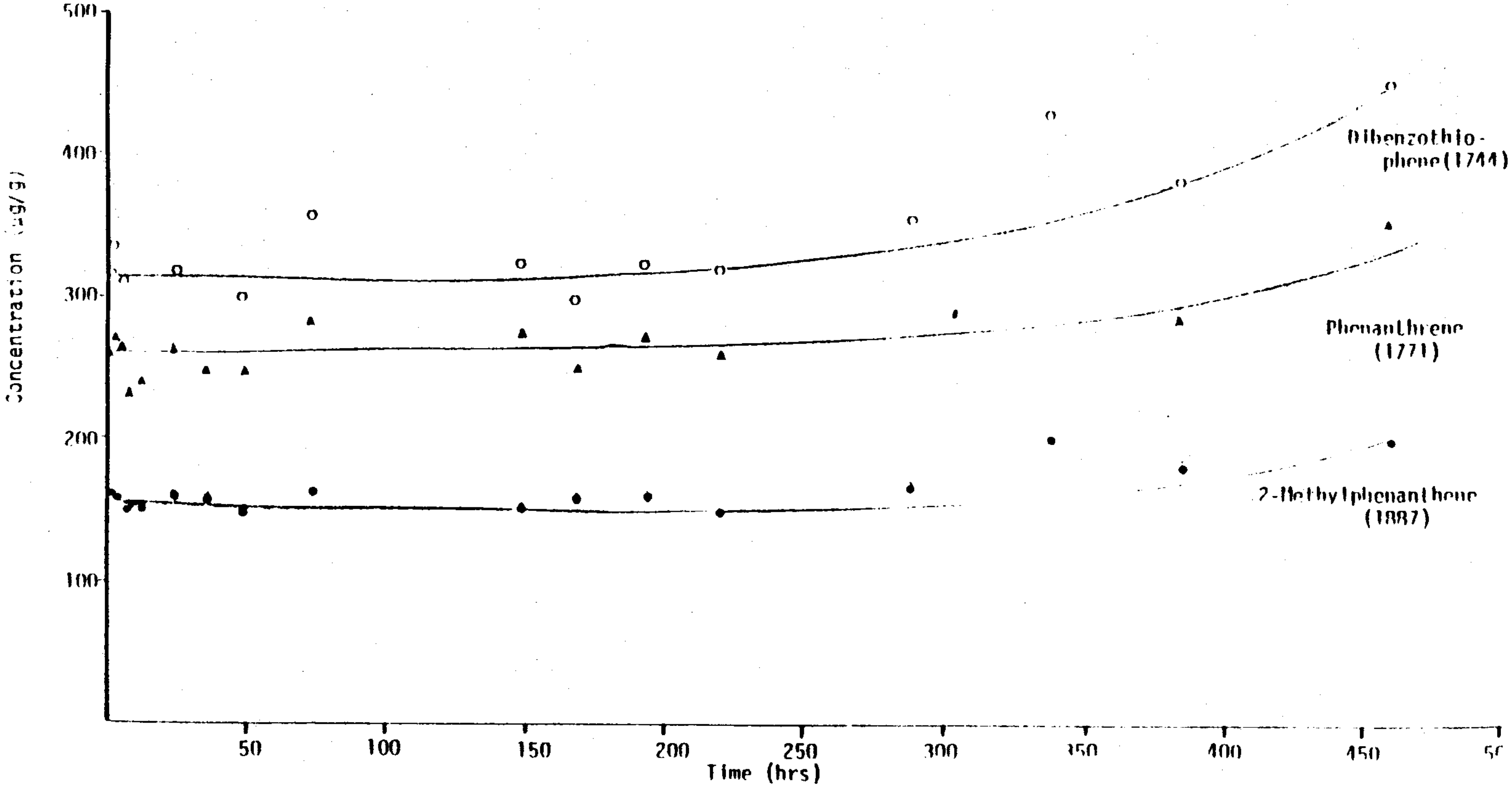

FIGURE 5-13. TIME-DEPENDENT CONCENTRATION IN OIL WEATHERING AT 19°C UNDER INFLUENCE OF A 7 KNOT WIND.

as shown in Figures 5-8 through 5-13. Figures 5-14 and 5-15 present the more recently computer generated plots of the oil phase component concentrations from E/D-4.

The oil slick component concentration graphs (Figures 5-8 through 5-15) show the exponential decrease of the lower molecular weight components from the slick and the longer-term stability and residence of the higher molecular weight polynuclear aromatics, heterocyclic PNA's and their respective alkyl-substituted homologs.

The concentrations of lower molecular weight compounds such as ethylbenzene and 1,2-diethylbenzene were observed to decrease very rapidly in the first several hours, and after a period of 6 hours ethylbenzene (KOVAT 857) was no longer observed in the surface oil. Likewise, 1-ethyl-2-methylbenzene (KOVAT 959) showed a very rapid decrease in concentration with no detectable material present after 12 hours (Figure 5-9). Evaporation and dissolution of 1,2,4-trimethylbenzene (KOVAT 991) were somewhat slower (Figure 5-8), but its exponential decay resulted in no detectable material after approximately 24 hours, and the concentration of its isomer, 1,2,3-trimethylbenzene (KOVAT 1019) is seen to decrease rapidly in a 12-hour period. Tetramethylbenzene (KOVAT 1148) was observed to decrease exponentially over the first 24 hours to the point where it was no longer observed (Figure 5-9). Tetrahydronaphthalene (KOVAT 1156) was also lost before 12 hours occurred, and naphthalene decreased in an exponential fashion over a 74 hour period to where it was no longer detectable (Figures 5-8 and 5-9). The alkyl-substituted polynuclear aromatics showed longer residence times in the oil, with 2-methylnaphthalene (KOVAT 1288) and 1-methylnaphthalene (KOVAT 1304) present for 220 hours (Figures 5-10 and 5-11). They too showed an exponential decrease in concentration in the oil, and 1,1-biphenyl (KOVAT 1375) and 2-ethylnaphthalene (KOVAT 1387) showed similar effects as their concentrations dropped off exponentially to the point where they were no longer observed after 250 hours (Figures 5-11 and 5-12). The compounds with molecular weights above alkyl-substituted naphthalenes showed longer residence times in the oil, and this is illustrated in Figure

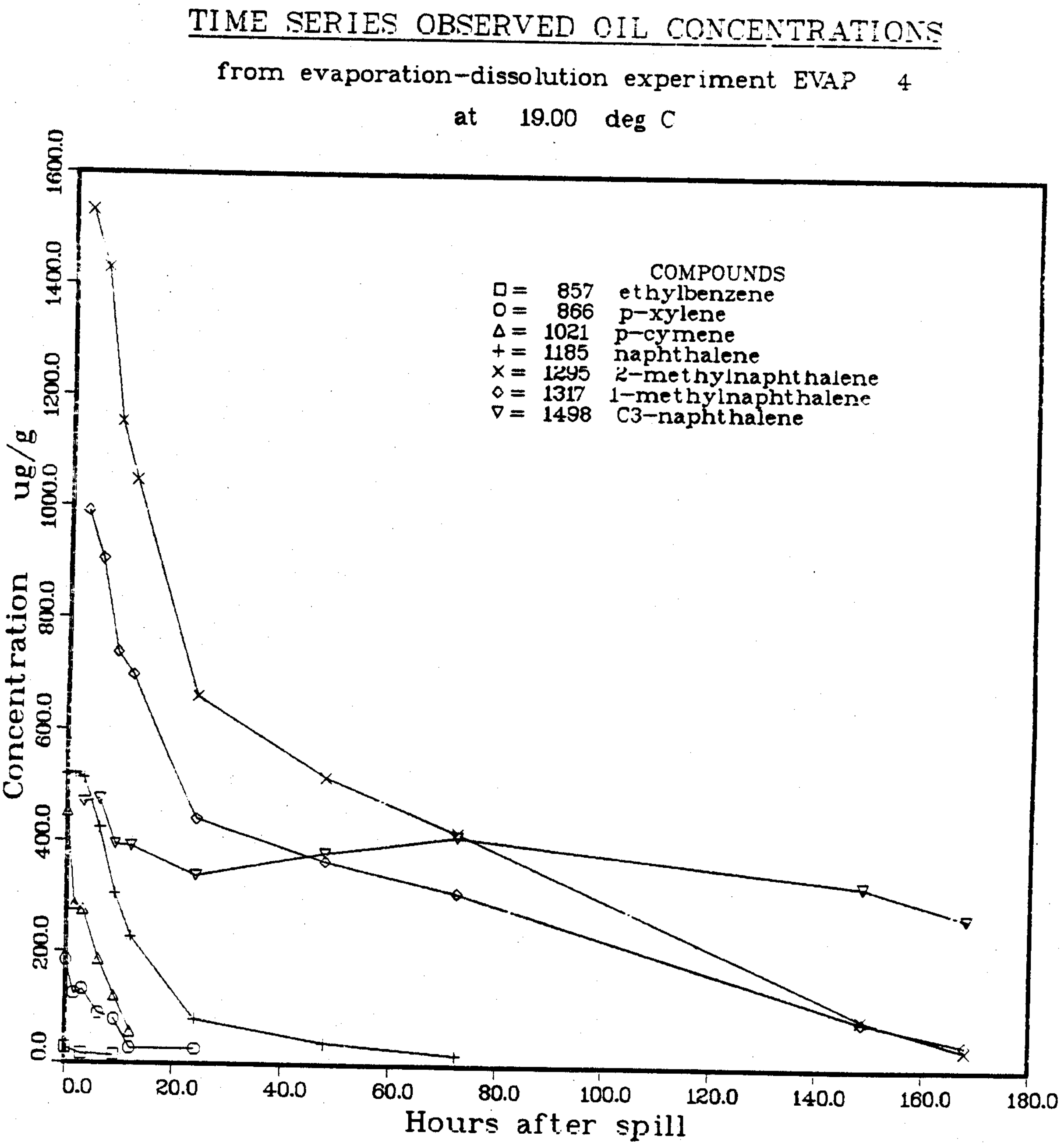

FIGURE 5-14. COMPUTER GENERATED TIME-SERIES PLOTS OF SPECIFIC COMPONENT CONCENTRATIONS REMAINING IN PRUDHOE BAY CRUDE OIL WEATHERING AT 19°C UNDER INFLUENCE OF A 7 KNOT WIND. (E/D-4 DATA FROM EXP DATA BASE OF OIL WEATHERING MODEL).

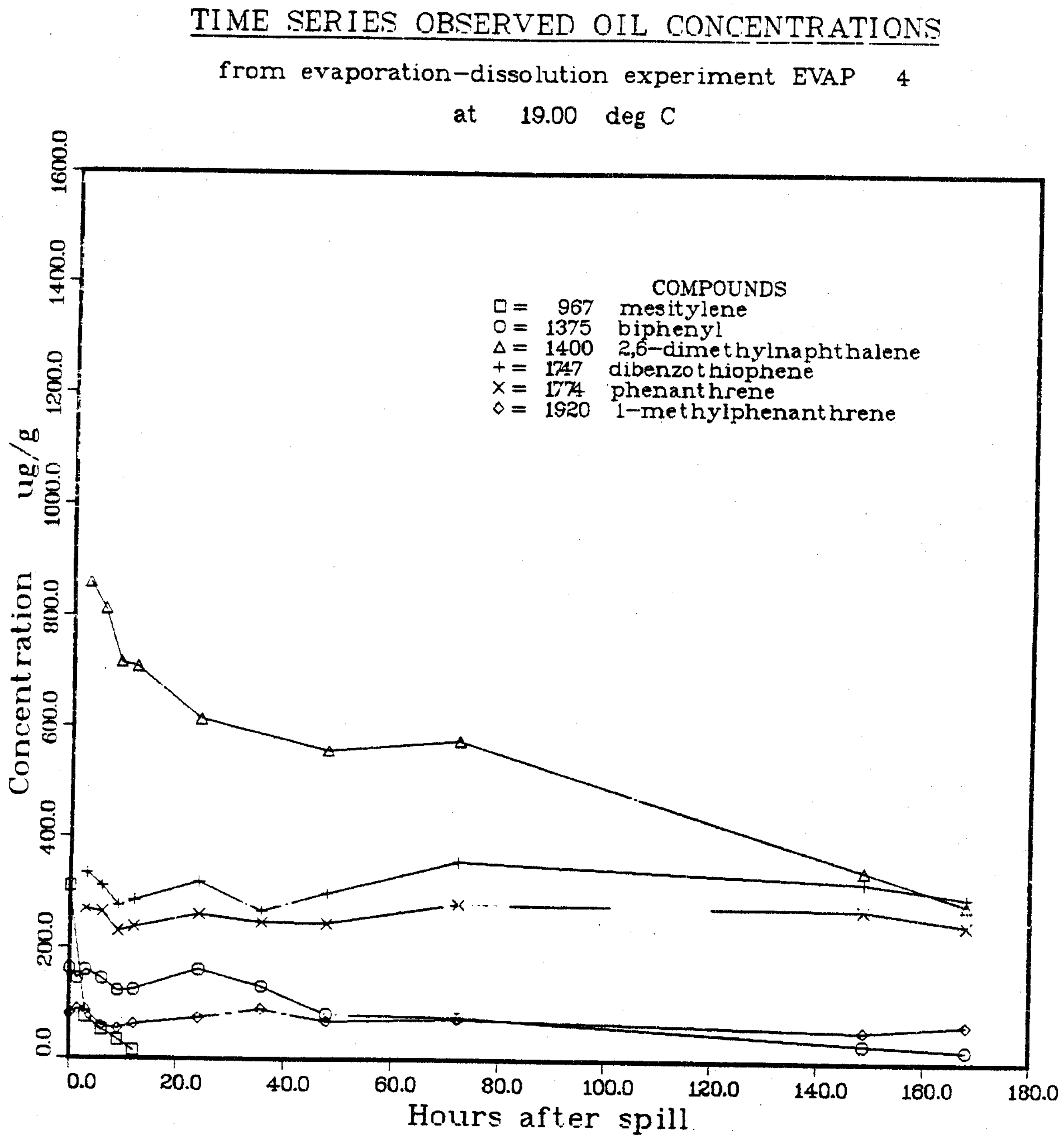

FIGURE 5-15. COMPUTER GENERATED TIME-SERIES PLOTS OF SPECIFIC HIGHER MOLECULAR WEIGHT COMPONENT CONCENTRATIONS REMAINING IN PRUDHOE BAY CRUDE OIL WEATHERING AT 19°C UNDER INFLUENCE OF A 7 KNOT WIND. (E/D-4 DATA FROM EXP DATA BASE OF OIL WEATHERING MODEL).

5-12 for 1,1-methylene bis-benzene (KOVAT 1487) which was still present after 475 hours although its concentration had dropped by a factor of 4 in an exponential fashion during that period.

Dibenzothiophene, the major sulfur heterocyclic aromatic compound in Prudhoe Bay crude oil, did not show a significant decrease over a 500-hour period due to either evaporation or dissolution (Figure 5-13). In fact, the relative concentration of dibenzothiophene increased slightly in the weathered-oil-residue due to the loss of the lower molecular weight components. Phenanthrene (KOVAT 1771) also showed a slight increase in relative concentration as did the alkyl-substituted 4-methyldibenzothiophene (KOVAT 1845) and 2-methylphenanthrene (KOVAT 1887; Figure 5-13). Although these compounds do have limited water solubilities, as reported by CLARK and MACLEOD (1977), they are not readily dissolved from the oil into the water column, and they are apparently not removed to any appreciable degree by evaporation after the slick becomes diffusion controlled.

Water column concentrations of these same aromatic compounds are presented in Table 5-4 and Figures 5-16 through 5-21 show the manually plotted time-dependent concentration changes for several selected compounds. Figure 5-22 presents the computer generated plots of many of the same compounds for comparison. Initial increases of concentrations of the lower molecular weight aromatics in the water column occur within the first 5 to 10 hours while higher molecular weight component concentrations peak at after a slightly longer period. Interestingly, after approximately 10 hours, exponential decreases in the water column concentrations occurred due to evaporative loss through air/sea exchange. While the methylene chloride extraction technique does not allow evaluation of benzene and toluene (due to hexane and benzene solvent interference during capillary chromatography), these concentrations can be determined by the purge and trap results as shown in Table 5-2 and Figure 5-6. It is possible with the methylene chloride extraction and subsequent fraction ation procedure to quantify the water column and oil slick concentrations for other aromatics, ranging from ortho-, meta- and para-xylenes(1-2, 1-3, and

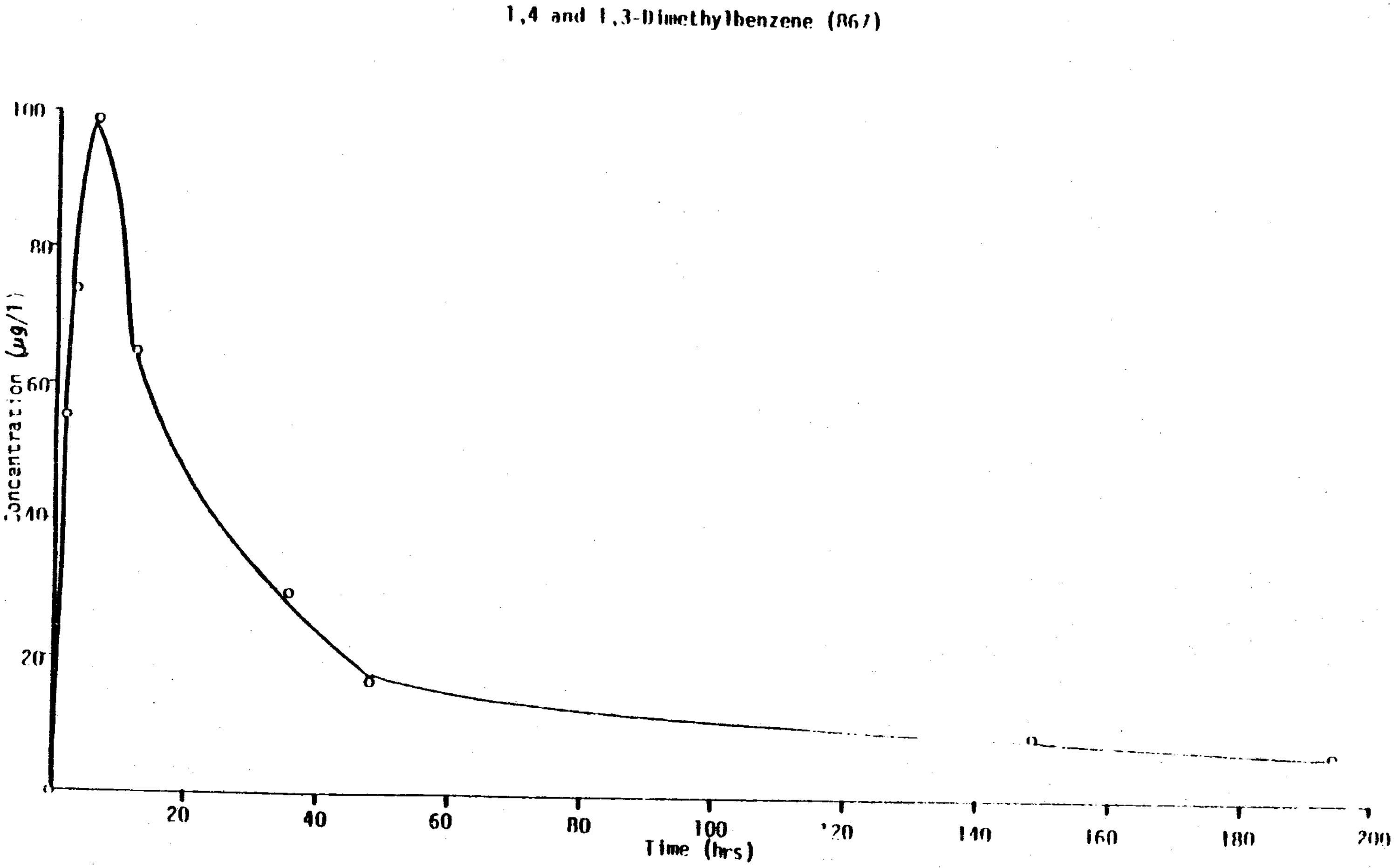

FIGURE 5-16. TIME-DEPENDENT CONCENTRATION IN THE WATER COLUMN WEATHERING AT 19°C UNDER INFLUENCE OF A 7 KNOT WIND.

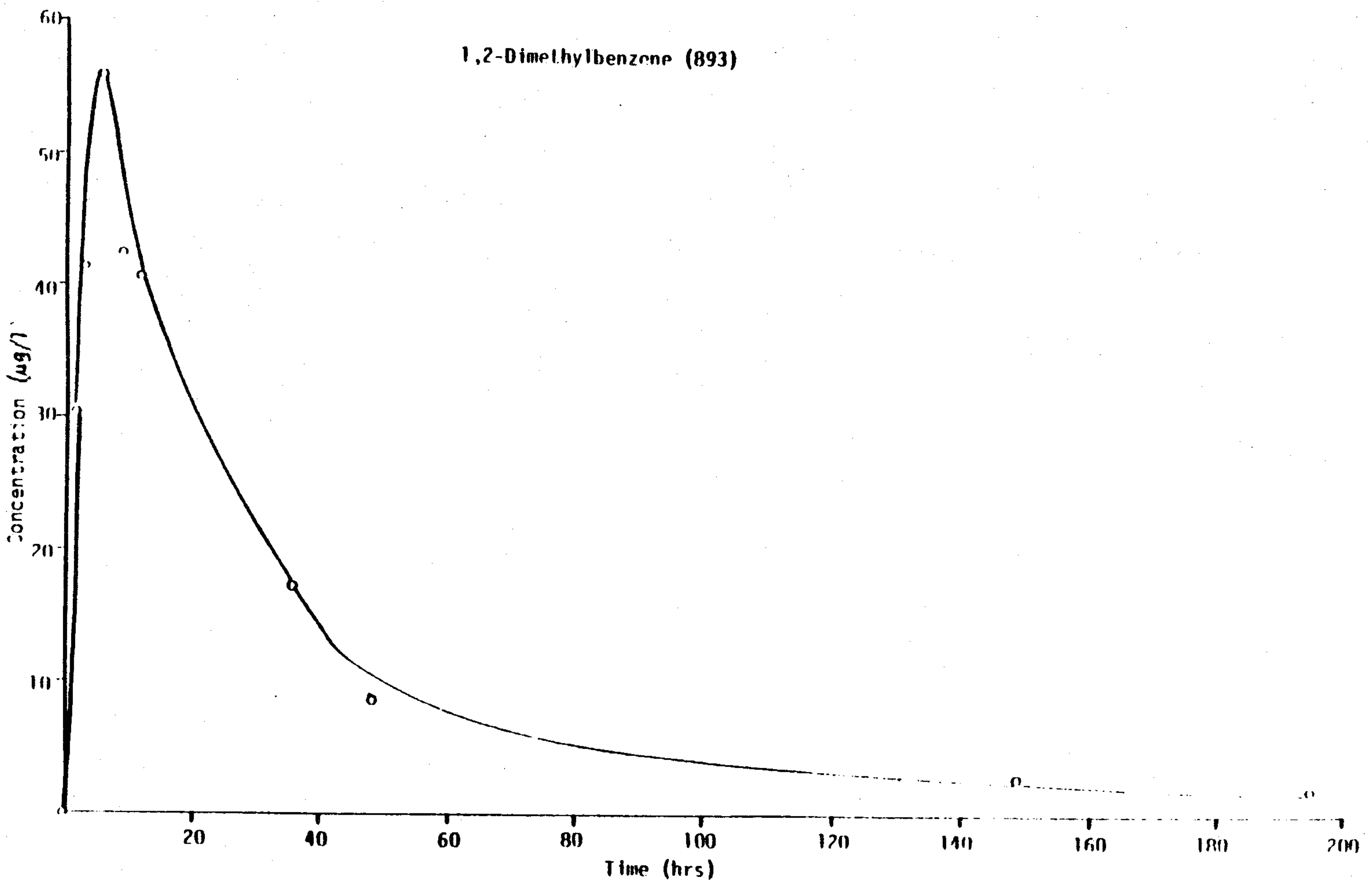

FIGURE 5-17. TIME-DEPENDENT CONCENTRATION IN THE WATER COLUMN WEATHERING AT 19°C UNDER INFLUENCE OF A 7 KNOT WIND.

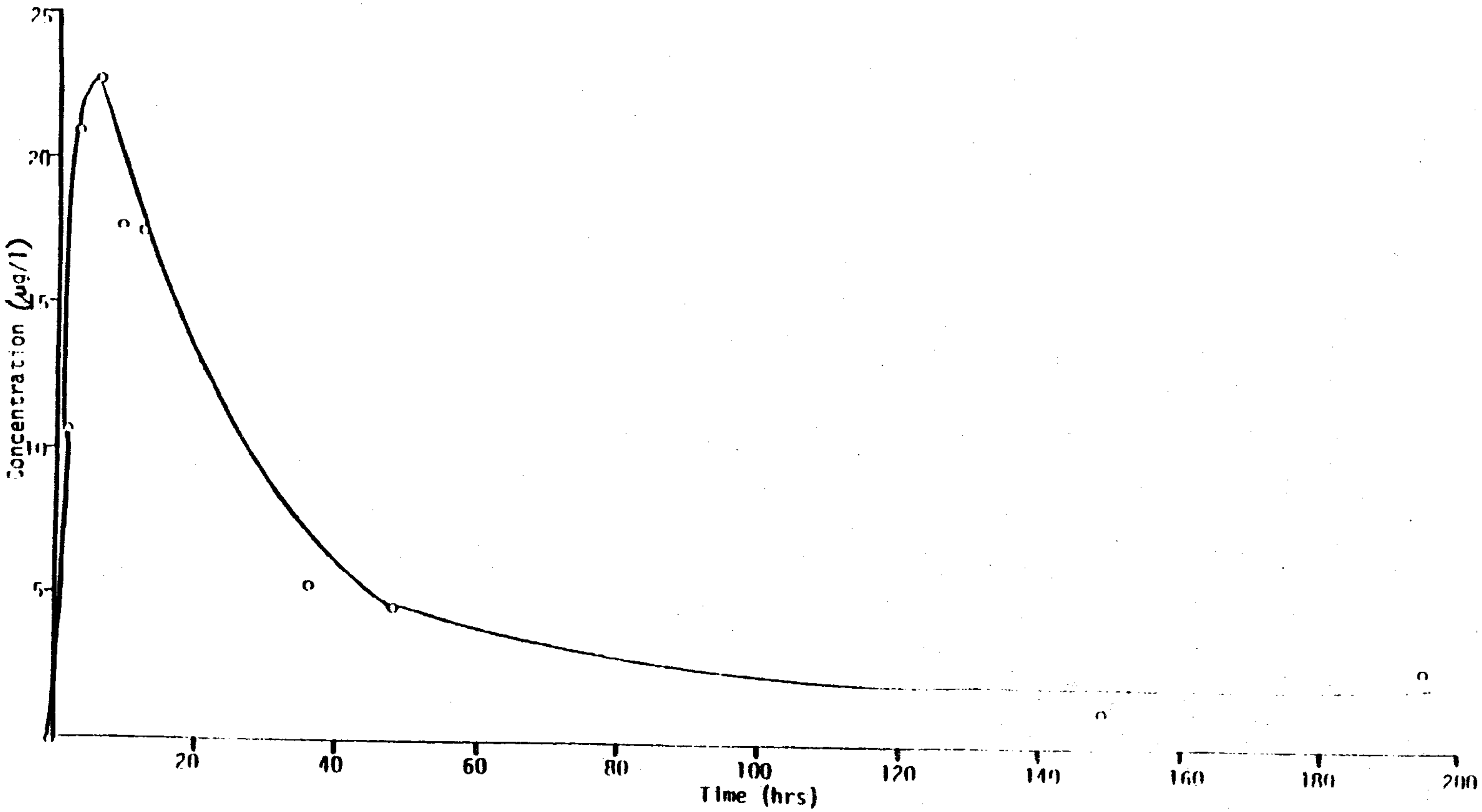
Ethylbenzene (857)

FIGURE 5-18. TIME-DEPENDENT CONCENTRATION IN THE WATER COLUMN WEATHERING AT 19^{o}C UNDER INFLUENCE OF A 7 KNOT WIND.

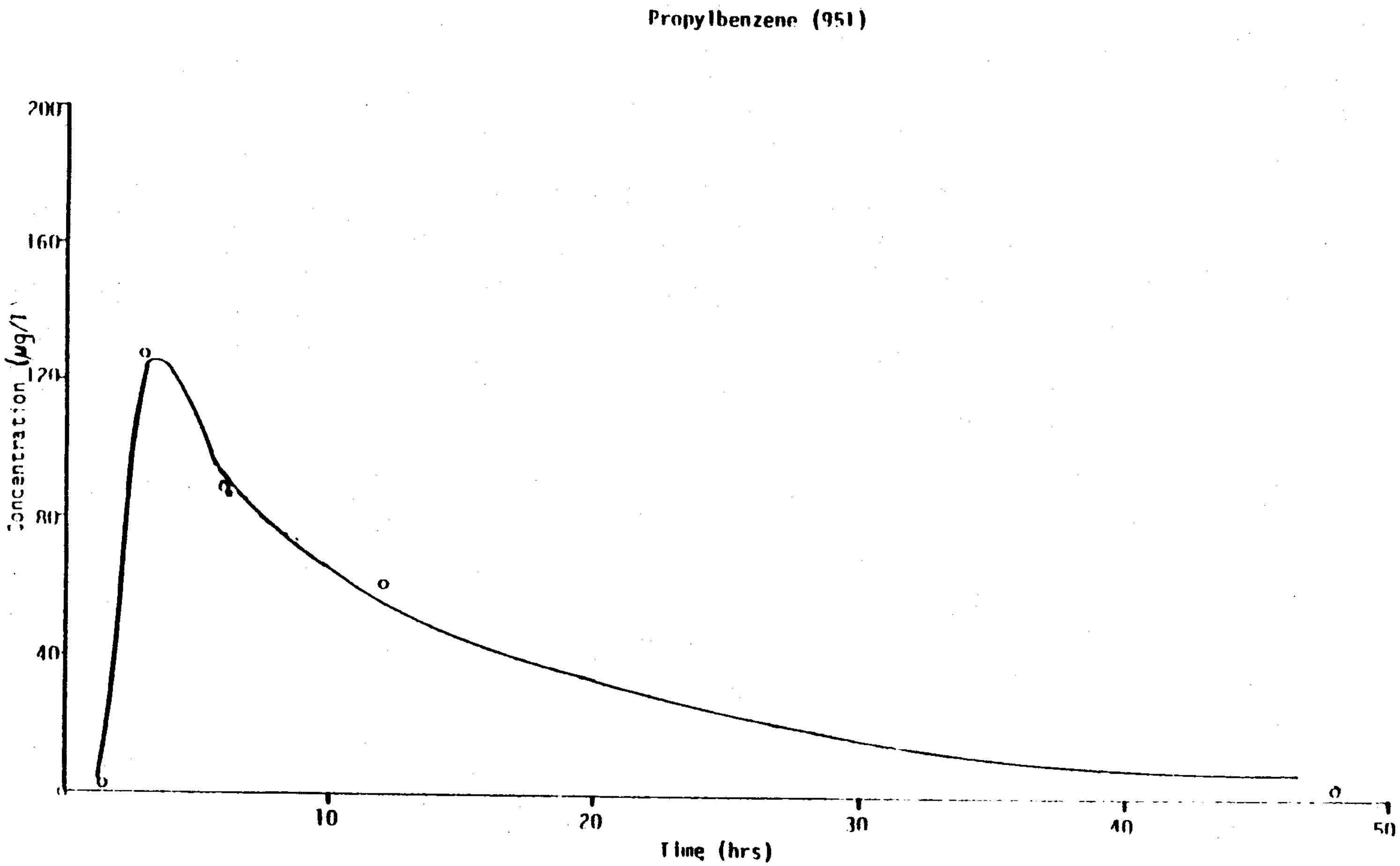

FIGURE 5-19. TIME-DEPENDENT CONCENTRATION IN THE WATER COLUMN WEATHERING AT 19°C UNDER INFLUENCE OF A 7 KNOT WIND.

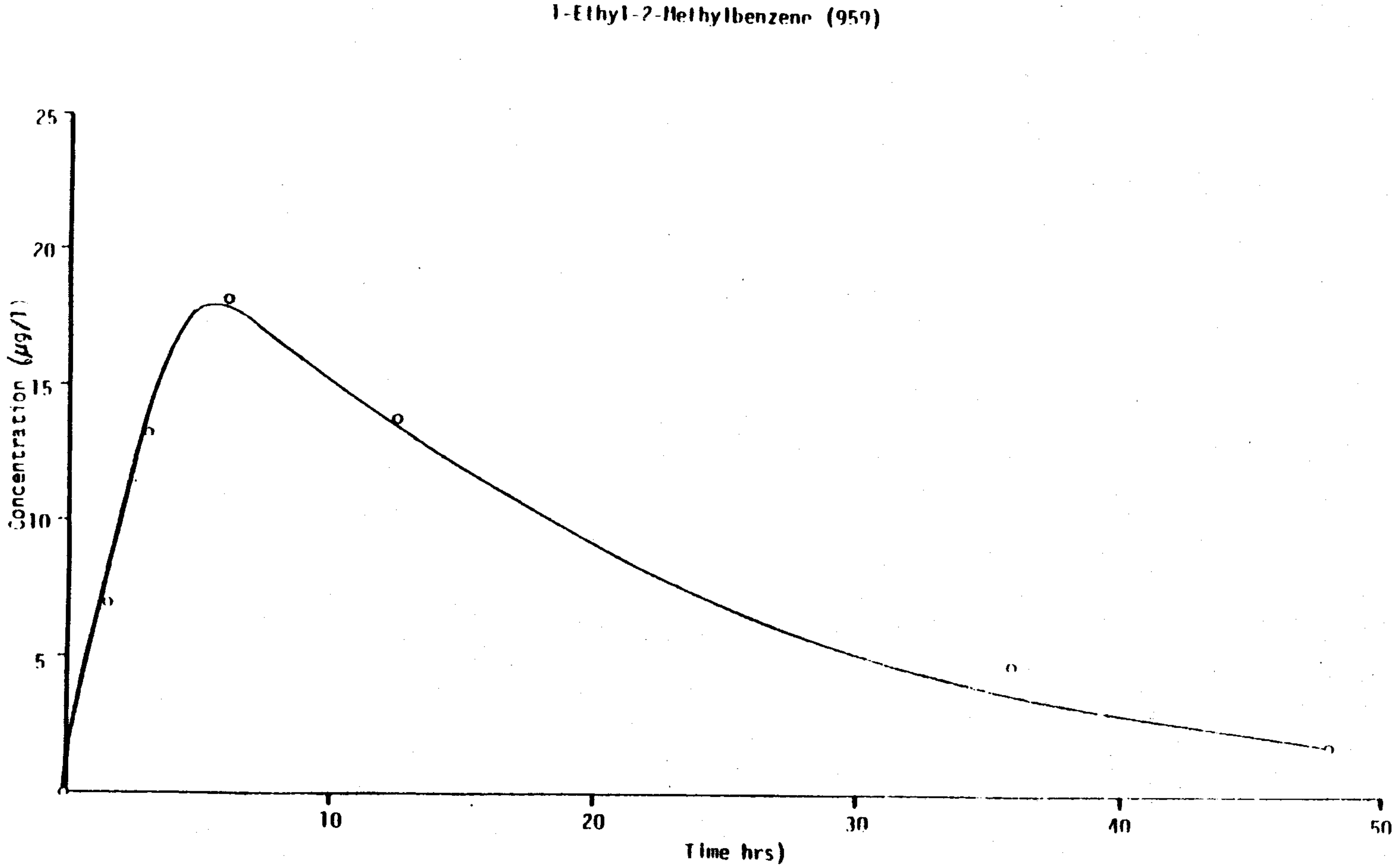

FIGURE 5-20: TIME-DEPENDENT CONCENTRATION IN THE WATER COLUMN WEATHERING AT 19°C UNDER INFLUENCE OF A 7 KNOT WIND.

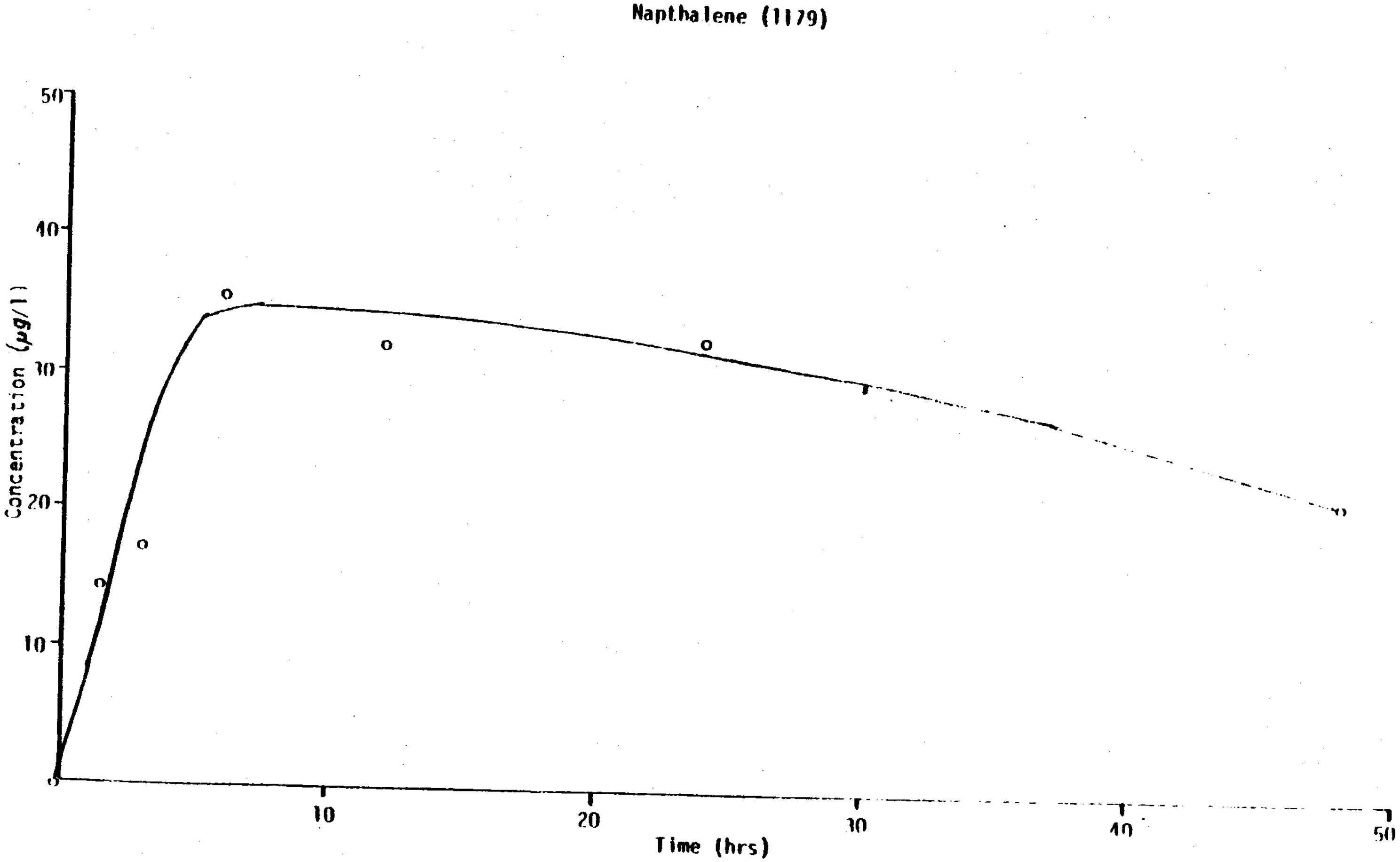

FIGURE 5-21. TIME-DEPENDENT CONCENTRATION IN THE WATER COLUMN WEATHERING AT 19°C UNDER INFLUENCE OF A 7 KNOT WIND.

1-4-dimethylbenzenes) through alkyl-substituted phenanthrenes. Figure 5-16 shows the time-dependent changes and concentrations of meta- and para-xylene with time. The initial buildup to 100 μg/l in the first 5 hours was very similar to that observed when the purge and trap technique was used for similar measurements as reported in Figure 5-6. Validation of the compatability of the measurement techniques is provided by the similar values and trends obtained by these two significantly different methods (purge and trap FID GC vs methylene chloride extraction, SiO_2 fractionation and FID chromatography). Likewise, concentration buildup and declines for ortho-xylene and ethylbenzene were similar when measured by both techniques. Figure 5-17 shows the time-dependent concentration changes in the water column for ortho-xylene, and these data also clearly parallel those observed for the other two isomers. Similar profiles are obtained for ethylbenzene, propylbenzene and 1-ethyl-2-methylbenzene in the subsequent Figures (5-18 through 5-20). Polynuclear aromatics starting with naphthalene show somewhat later concentration maxima and longer retention in the water column as shown by the data in Figures 5-21 and 5-22.

Each of the maximum concentrations reached during the initial stages of dissolution reflect the mole fraction of the component in the oil and the relative activity coefficients of the compound in the oil and the water. In almost all instances, however, the concentrations in the water column in the evaporation/dissolution chamber do not reach the higher values obtained during the closed system (separatory funnel) oil/seawater partition coefficient determinations described in the next section (5.2). This presumably reflects the rapid loss from the oil of the specific components due to evaporative processes and the concomitant decrease in overall mole fraction of these lower molecular weight materials in the oil. Finally, as these materials are ultimately removed from the oil slick reservoir itself, the water column concentrations undergo a decrease beneath the slick. In the case of the higher molecular weight naphthalenes and alkyl-substituted naphthalenes, this decrease does not occur until 10 to 20 hours after the spill incident (20 hours for 1-methylnaphthalene, 35 hours for 2-methylnaphthalene, 35 hours for

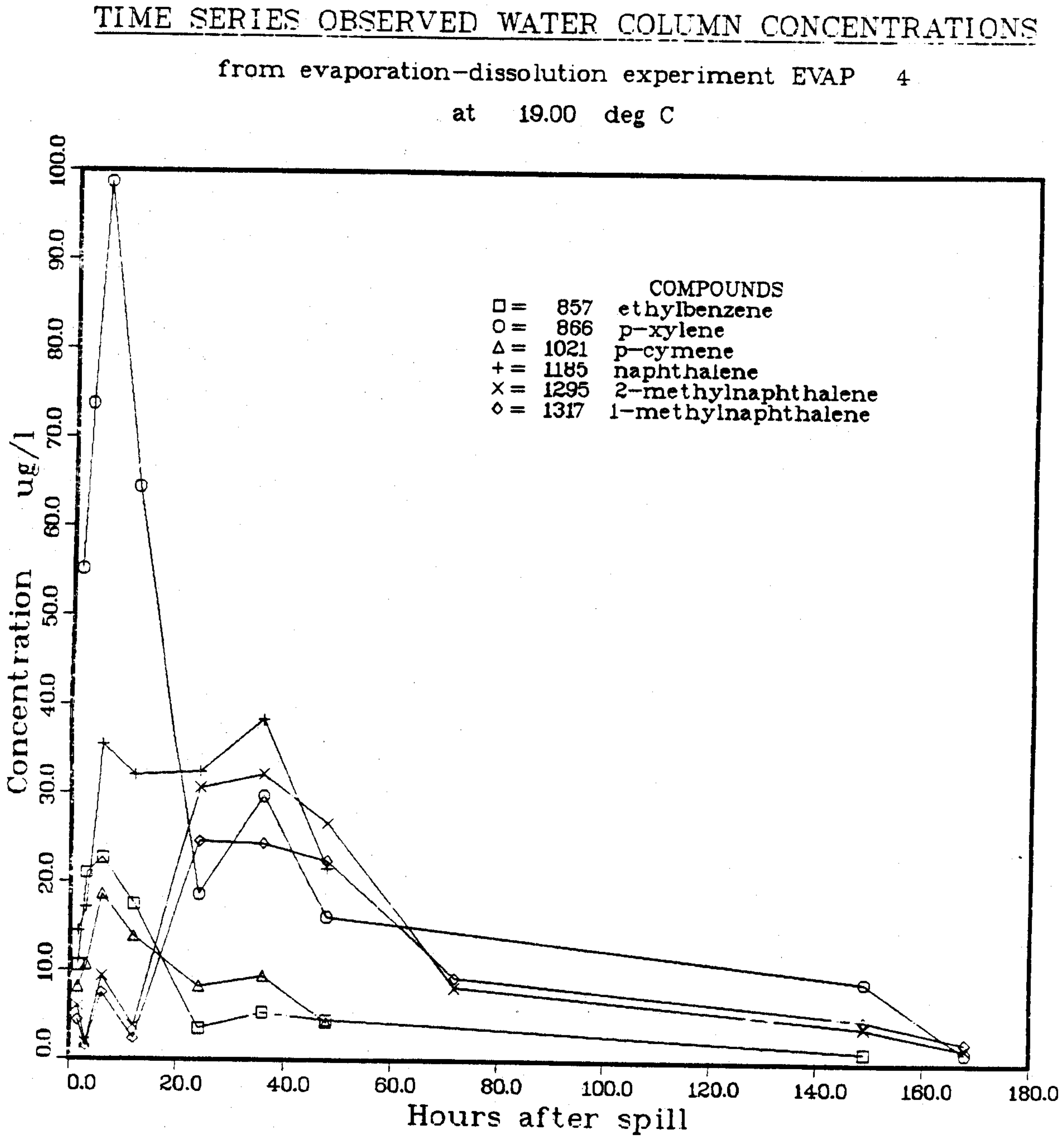

FIGURE 5-22. COMPUTER GENERATED TIME-SERIES PLOTS OF SPECIFIC COMPONENT CONCENTRATIONS REMAINING IN THE WATER BENEATH A PRUDHOE BAY CRUDE OIL SLICK WEATHERING AT 19°C UNDER INFLUENCE OF A 7 KNOT WIND. (E/D-4 DATA FROM EXP DATA BASE OF OIL WEATHERING MODEL).

biphenyl). This is presumably due to the longer residence time of these higher molecular weight materials in the oil causing their longer residence time in the water column beneath the slick.

During the initial evaporation/dissolution experiment using Prudhoe Bay crude oil, the oil was added from a height of 6-8" above the water and significant plunging of oil droplets into the water column was noted. While such droplet formation no doubt occurs in a real-spill event, such behavior significantly complicates development of algorithms for evaporation and dissolution because of the greatly enhanced surface area of the oil droplets exposed to the water column. Development of dissolution algorithms to account for this droplet formation is much more complicated. Therefore, in subsequent evaporation/dissolution experiments, the oil was added via a horizontally placed transfer tube located 0.5 cm above the water surface. In this manner, the oil was observed to spread as a smooth slick over the water and significant 1 to 10-mm oil droplet dispersion was prevented. In that the algorithms for dissolution require input parameters such as the surface area of the oil slick exposed to the water, it was believed that this approach would provide much better experimental data to compare against computer predicted output for evaporation and dissolution weathering in the stirred tank experiments. Further, during the initial evaporation/dissolution experiments using a 7 knot wind, 5 to 10-cm holes were "blown" in the surface slick. While such breakup of surface slicks in ocean systems is also known to occur, this behavior in the evaporation/dissolution chamber complicates modeling of the observed results and generation of agorithms. For this reason, in subsequent evaporation/dissolution experiments, the wind speed was dropped to 1 knot such that buildup of volatile components would not occur in the air above the slick but that holes were not blown into the slick at the same time.

To evaluate these changes in the experimental procedure, a second 19°C evaporation/dissolution experiment was undertaken and Figures 5-23 and 5-24 present the computer plotted time-series observed oil concentrations from that experiment. Quite clearly, the reduction in wind speed affects the rate

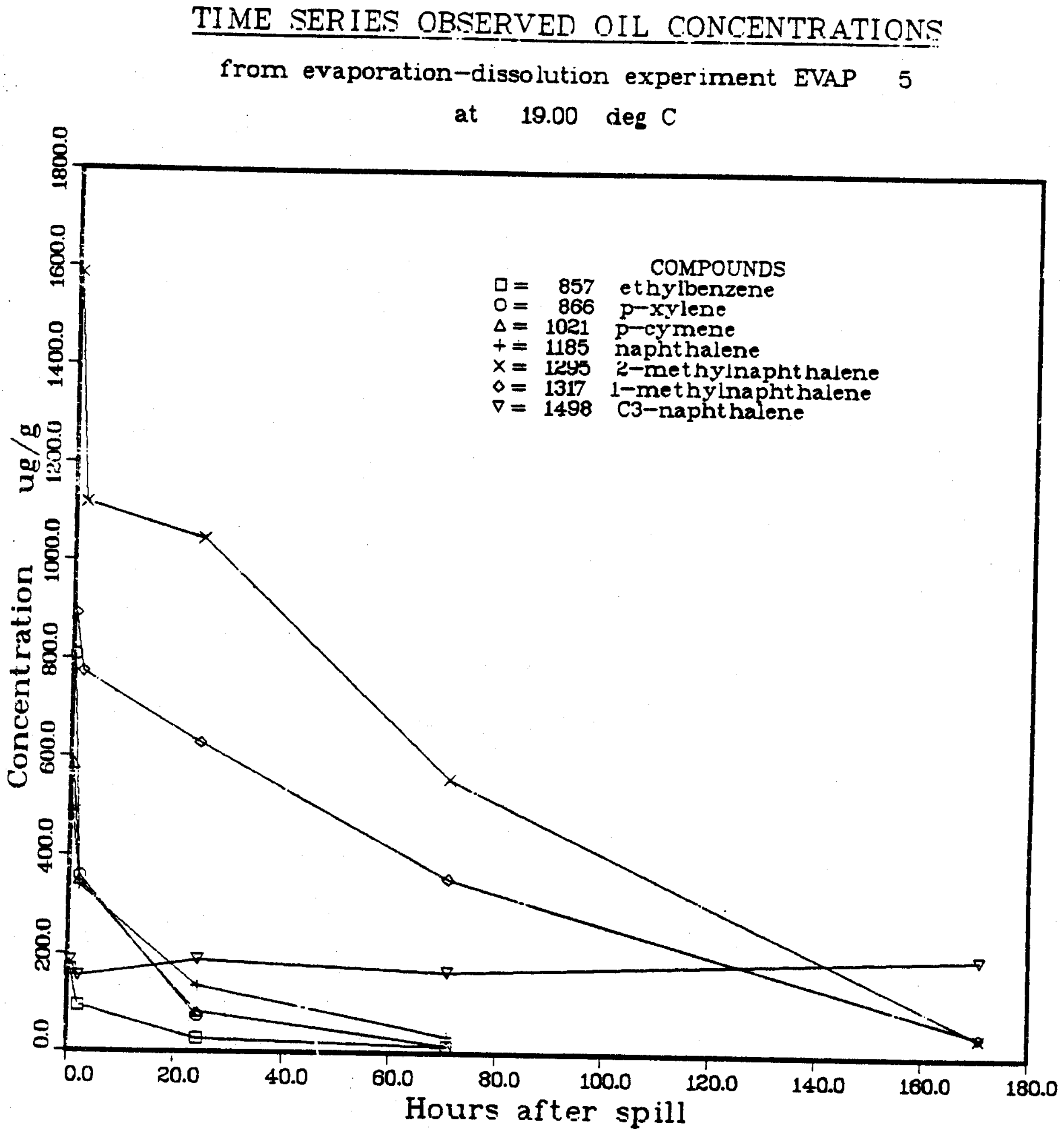

FIGURE 5-23. COMPUTER GENERATED TIME-SERIES PLOTS OF SPECIFIC COMPONENT CONCENTRATIONS REMAINING IN PRUDHOE BAY CRUDE OIL WEATHERING AT 19°C UNDER INFLUENCE OF A 1 KNOT WIND. (E/D-5 DATA FROM EXP DATA BASE OF OIL WEATHERING MODEL).

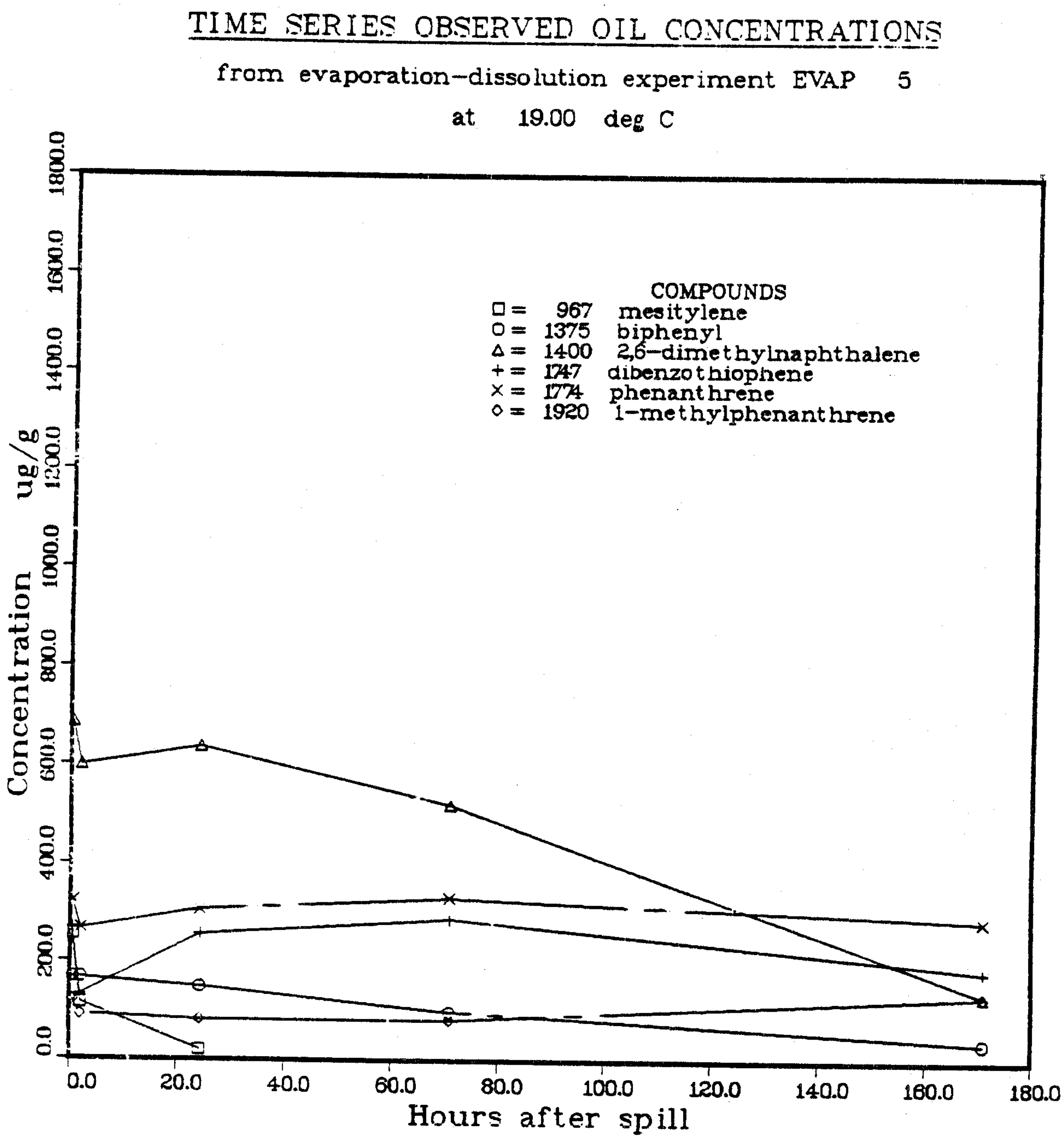

FIGURE 5-24. COMPUTER GENERATED TIME-SERIES PLOTS OF SPECIFIC COMPONENT CONCENTRATIONS REMAINING IN THE WATER BENEATH A PRUDHOE BAY OIL SLICK WEATHERING AT 19°C UNDER INFLUENCE OF A 1 KNOT WIND. (E/D-5 DATA FROM EXP DATA BASE OF OIL WEATHERING MODEL).

of loss of the lower molecular weight components as can be seen by comparing Figures 5-23 and 5-14. Longer residence times of compounds from ethylbenzene through naphthalene are observed in the slick under these conditions. The residence time of higher molecular weight components such as mesitylene (Kovat 967) through 1-methylphenanthrene are not drastically affected. That is, their residence time in the slick is significant over the 180 hours of experiment as would be anticipated. Reduction of the formation of oil in water dispersed droplets also significantly affects the amounts of hydrocarbons dissolved in the water column, as would be expected from the significantly decreased oil/water interfacial surface area. Figure 5-25 presents the computer generated plot of the water column concentrations from evaporation/dissolution experiment 5 where the oil was added to the evaporation/dissolution chamber with the horizontally positioned addition tube. Comparison of the data in Figure 5-22 with 5-25 shows that a factor of 2 to 3 decrease is observed in the water column concentrations as a result of this more gentle oil-addition procedure. As noted above, these modifications to the experimental procedure were necessitated by the requirement to maintain as carefully a controlled oil/water surface area as possible for verification of algorithms derived to predict dissolution phenomena. Results of observed vs predicted water column concentrations from these experiments are presented in Section 5.5.1.

5.1.2 Results of Evaporation/Dissolution Chamber Experiments at 3°C - La Jolla

Figures 5-26 and 5-27 present the gas chromatograms on the aliphatic and aromatic fractions of time series oil samples collected from an evaporation/dissolution experiment conducted under a 1-2 knot wind at 3°C (E/D-6). In this instance, time series samples were collected 30 minutes after the spill and at times 2 hours, 1 day, 3 days, 6 days, 12 days and 21 days following the initial spill event. On comparing these chromatograms to the chromatograms shown earlier in Figure 5-7, it can be seen that loss of lower molecular weight components due to volatilization is slightly inhibited at this lower temperature. This is perhaps best observed in examining the

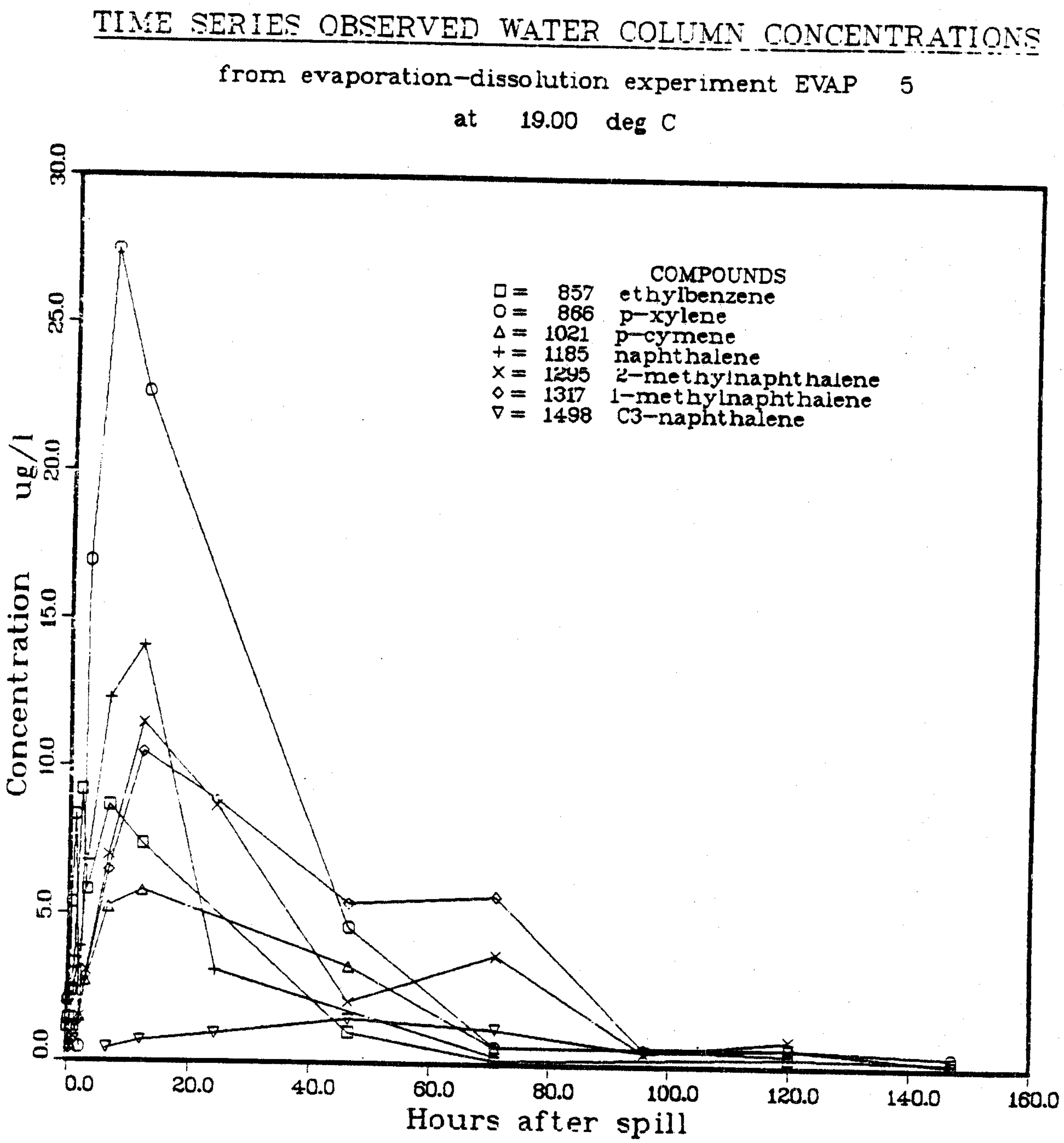

FIGURE 5-25. COMPUTER GENERATED TIME-SERIES PLOTS OF SPECIFIC COMPONENT CONCENTRATIONS REMAINING IN THE WATER BENEATH A PRUDHOE BAY CRUDE OIL SLICK WEATHERING AT 19°C UNDER INFLUENCE OF A 1 KNOT WIND. (E/D-5 DATA FROM EXP DATA BASE OF OIL WEATHERING MODEL).

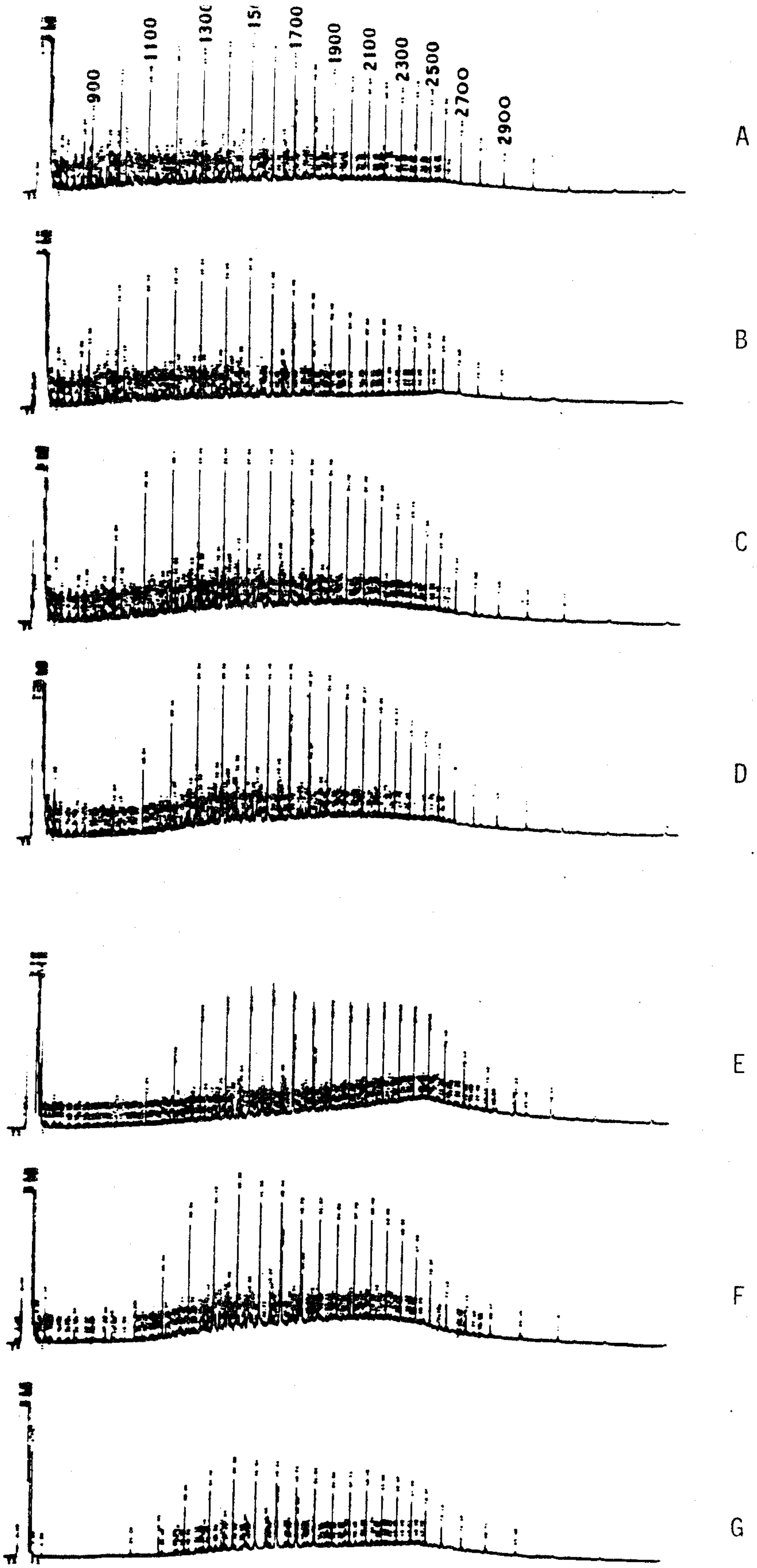

FIGURE 5-26. FLAME IONIZATION DETECTOR CAPILLARY GAS CHROMATOGRAMS OF ALIPHATIC COMPONENTS REMAINING IN PRUDHOE BAY CRUDE OIL WEATHERING AT 3°C UNDER INFLUENCE OF A 1 KNOT WIND (E/D-6). TIME-SERIES SAMPLING POINTS AFTER THE "SPILL": (A) 30 MINUTES; (B) 2 DAYS; (C) 1 DAY; (D) 3 DAYS; (E) 6 DAYS; (F) 12 DAYS; AND (G) 21 DAYS.

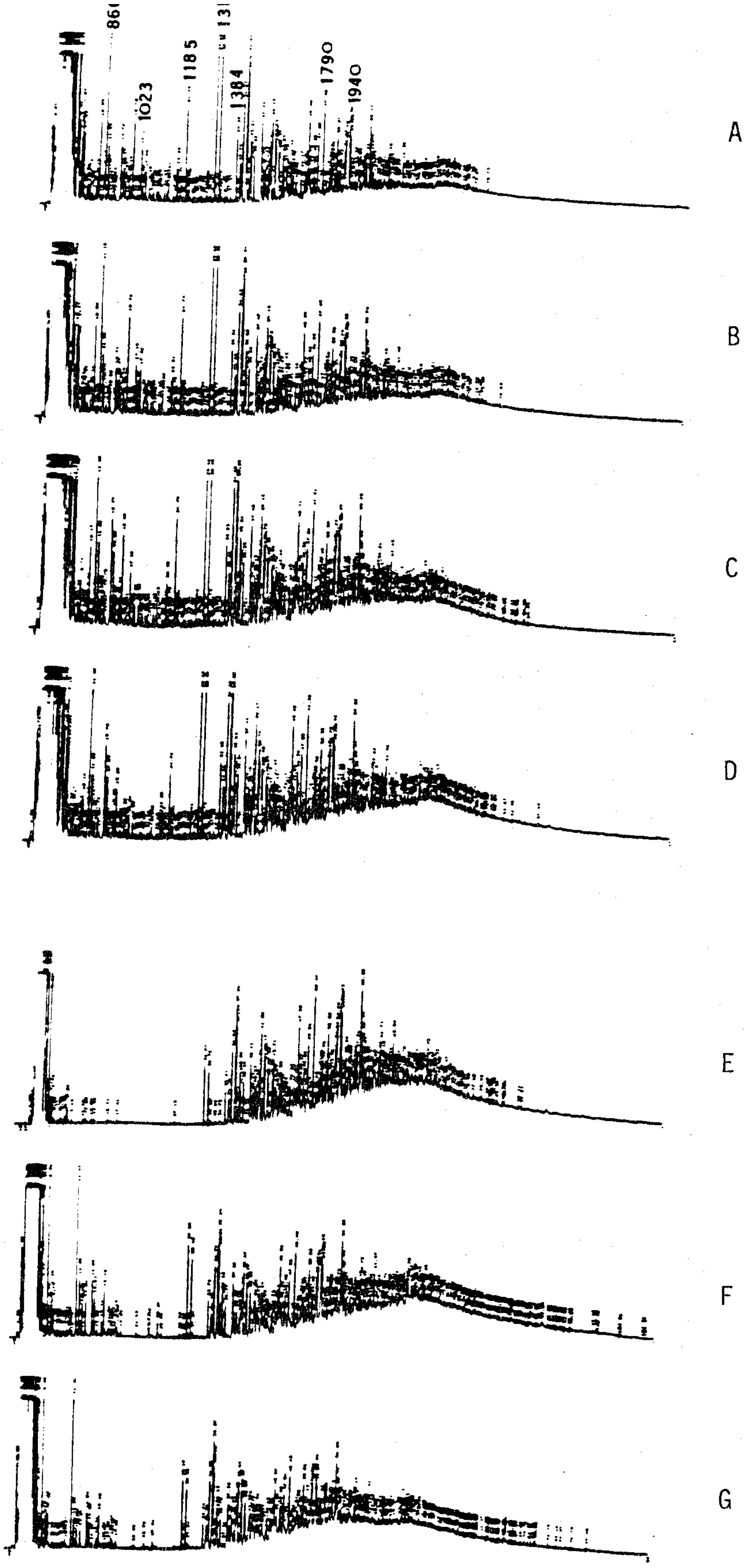

FIGURE 5-27. FLAME IONIZATION DETECTOR CAPILLARY GAS CHROMATOGRAMS OF AROMATIC COMPONENTS REMAINING IN PRUDHOE BAY CRUDE OIL WEATHERING AT 3°C UNDER INFLUENCE OF A 1 KNOT WIND (E/D-6). TIME-SERIES SAMPLING POINTS AFTER THE "SPILL": (A) 30 MINUTES; (B) 2 HOURS; (C) 1 DAY; (D) 3 DAYS; (E) 6 DAYS; (F) 12 DAYS; AND (G) 21 DAYS.

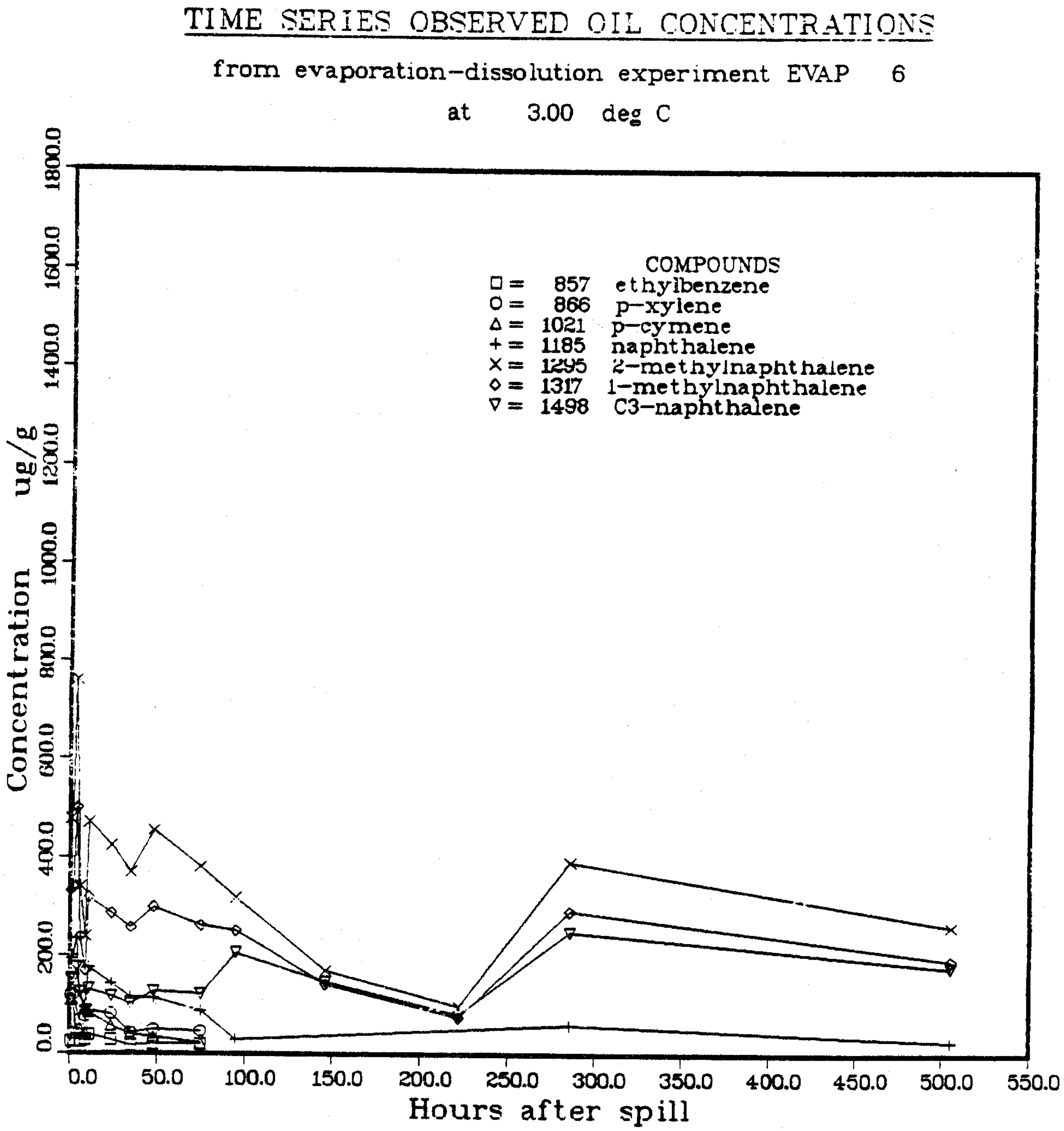

FIGURE 5-28. COMPUTER GENERATED TIME-SERIES PLOTS OF SPECIFIC COMPONENT CONCENTRATINS REMAINING IN PRUDHOE BAY CRUDE OIL WEATHERING AT 3°C UNDER INFLUENCE OF A 1 KNOT WIND. (E/D-6 DATA FROM EXP DATA BASE OF OIL WEATHERING MODEL).

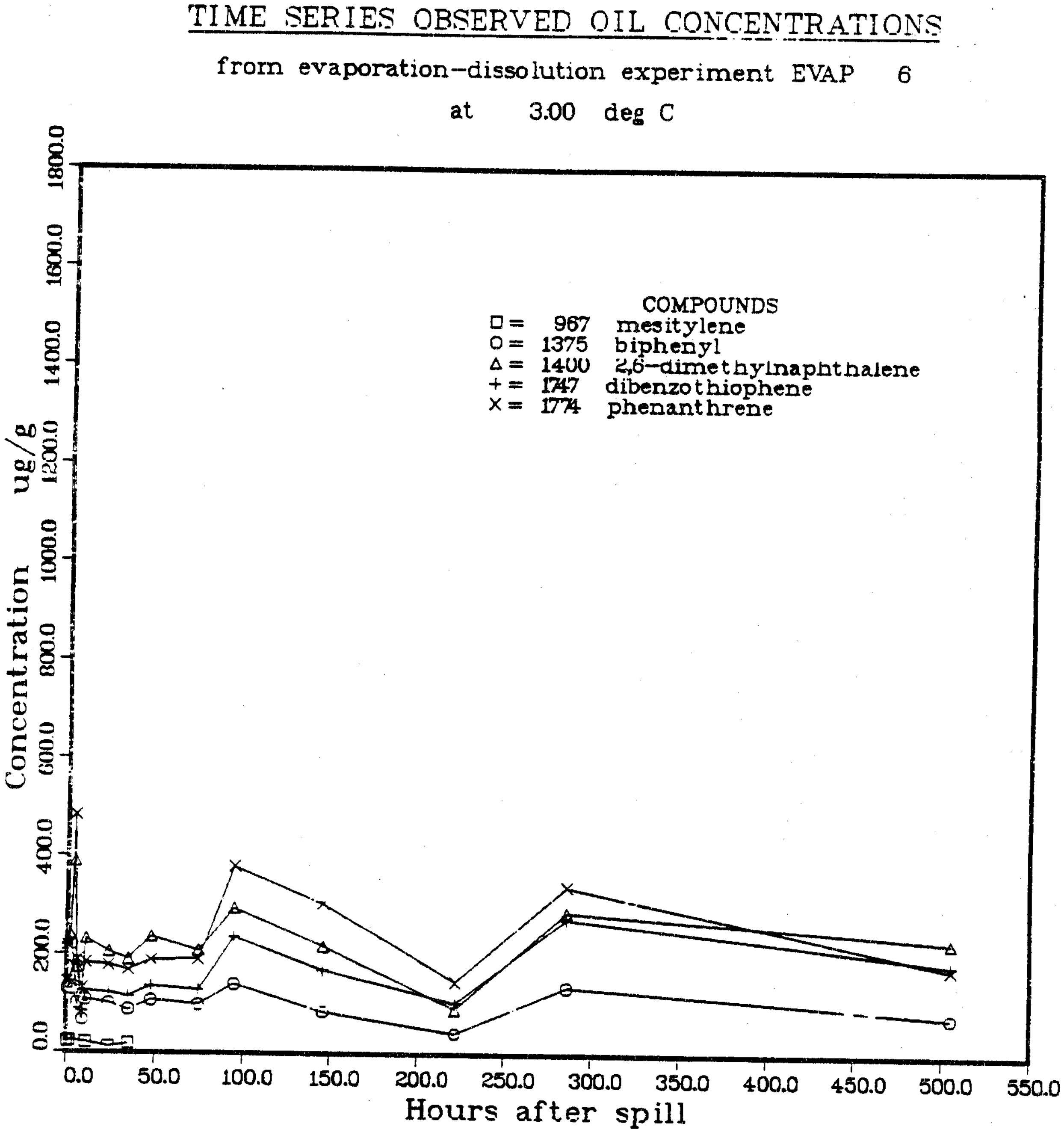

FIGURE 5-29. COMPUTER OPERATED TIME-SERIES PLOTS OF SPECIFIC HIGHER MOLECULAR WEIGHT COMPONENT CONCENTRATIONS REMAINING IN PRUDHOE BAY CRUDE OIL WEATHERING AT 3°C UNDER A INFLUENCE OF A 1 KNOT WIND. (E/D-6 DATA FROM EXP DATA BASE OF OIL WEATHERING MODEL).

computer generated plots of specific compound concentrations in the oil vs time as shown in Figure 5-28 and 5-29.

Comparison of these latter figures to the computer plotted figures (5-23 and 5-24) for the 19°C experiment show significantly longer residence times of the intermediate molecular weight components compared to those lost at the higher temperature (note difference in time scales for Figures 5-28 and 5-29 vs 5-23 and 5-24). The lower molecular weight components (up to p-cymene) appear to be lost at approximately the same rates (after 60 hrs) in both experiments. The same relative increases in concentrations of higher molecular weight compounds such as dibenzothiophene, phenanthrene and methylphenanthrene can be observed in both experiments. Gas chromatograms for the time series water column samples obtained in the 3°C evaporation/dissolution experiment are presented in Figure 5-30. These chromatograms show the slow build-up of the relatively more water soluble lower and intermediate molecular weight alkyl-substituted aromatics in the water column. In this instance, however, the maximum water column concentrations are reached after approximately 50 hours and longer as shown by the computer plot of water column concentrations for this experiment (Figure 5-31). The selected chromatograms and time-series concentration plots show the early water column buildup of the lower molecular weight compounds of interest such as toluene, ortho- and para-xylenes and alkyl-substituted benzenes. The higher molecular weight compounds such as naphthalene and alkyl-substituted naphthalenes then reach maximum concentrations in the water column at 40-60 hours and then remain in the water column, not being lost through air/sea exchange and evaporation, for longer periods of time. It is quite interesting to compare the chromatographic profiles of the water column extracts (Figure 5-30) with the aromatic fractions of the oil sample extracts (Figure 5-27). Clearly, the aromatics present in the water column are skewed towards the lower molecular weight range. The lower molecular weight compounds in the oil are rapidly lost due to the combined effects of evaporation/dissolution such that, with time, only the higher molecular weight aromatic compounds remained in the slick up to the 21 days that this experiment was run.

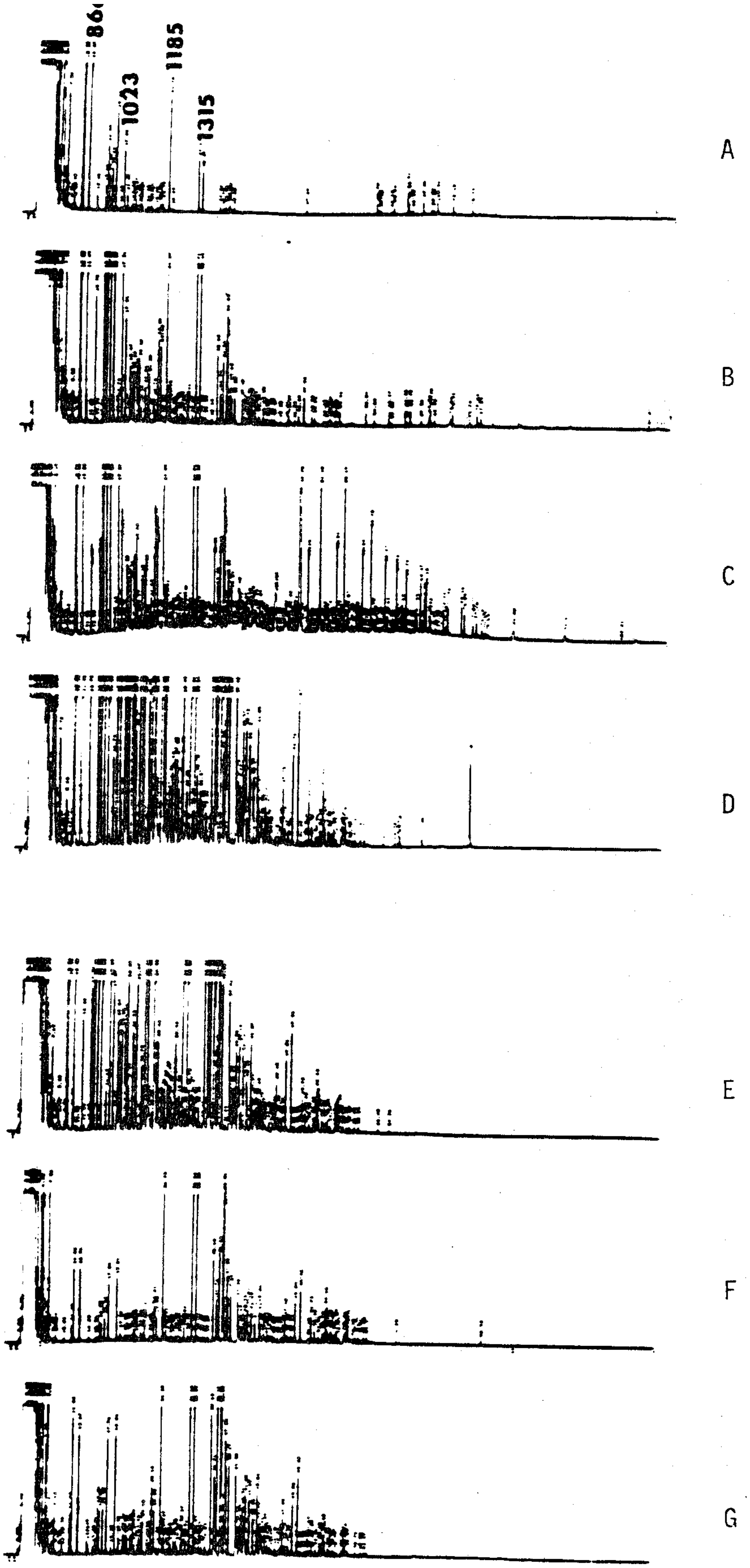

FIGURE 5-30. FLAME IONIZATION DETECTOR CAPILLARY GAS CHROMATOGRAMS OF THE AROMATIC COMPONENTS REMAINING IN THE WATER COLUMN BENEATH A PRUDHOE BAY CRUDE OIL SLICK WEATHERING AT 3°C UNDER INFLUENCE OF A 1 KNOT WIND (E/D-6). TIME-SERIES SAMPLING POINTS AFTER THE "SPILL": (A) 30 MINUTES; (B) 2 HOURS; (C) 1 DAY; (D) 3 DAYS (E) 6 DAYS; (F) 12 DAYS; and (G) 21 DAYS.

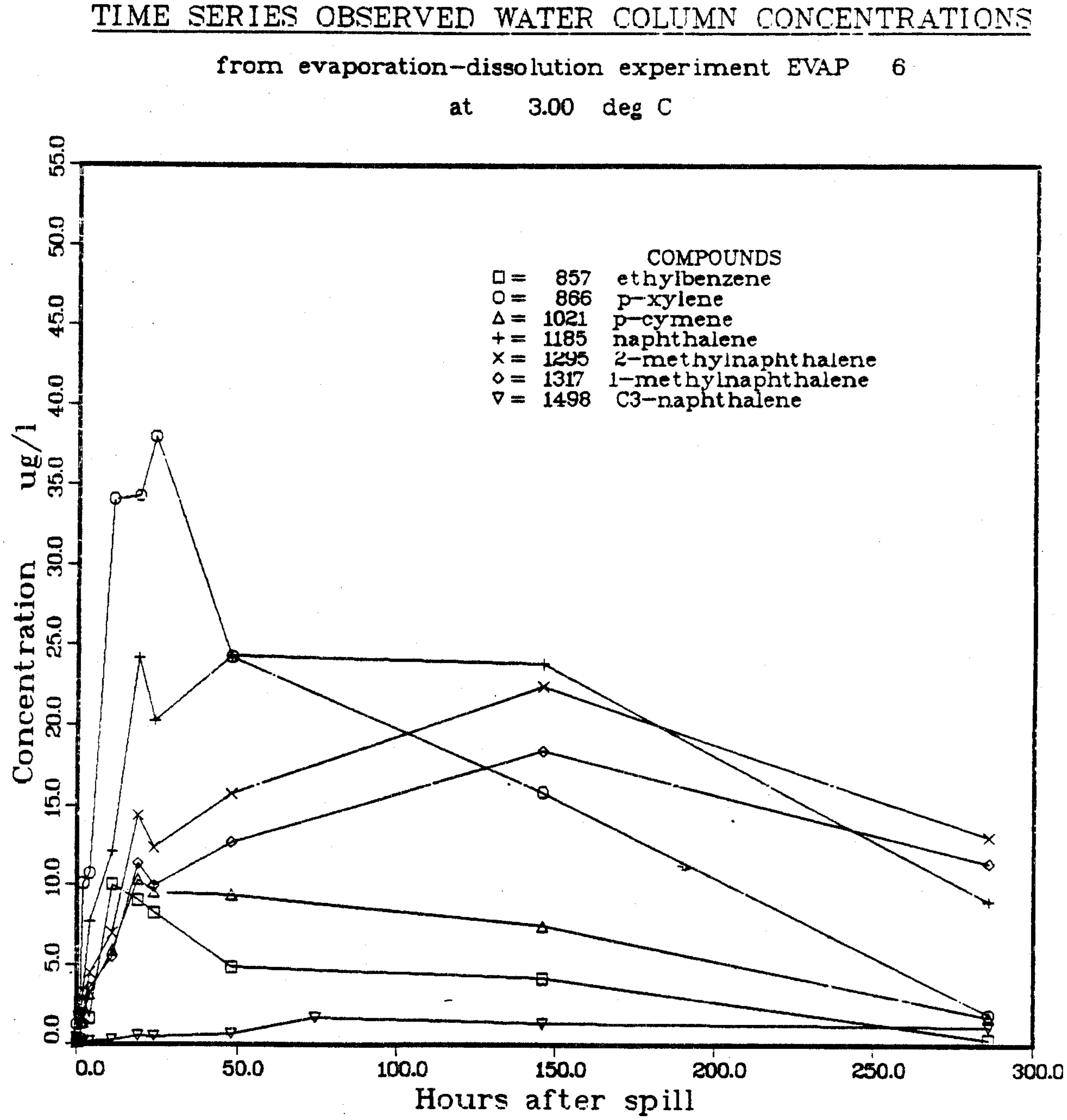

FIGURE 5-31. COMPUTER GENERATED TIME-SERIES PLOTS OF SPECIFIC AROMATIC COMPONENT CONCENTRATIONS REMAINING IN THE WATER COLUMN BENEATH A PRUDHOE BAY CRUDE OIL SLICK WEATHERING AT 3°C UNDER INFLUENCE OF A 1 KNOT WIND. (E/D-6 DATA FROM EXP DATA BASE OF OIL WEATHERING MODEL).

5.2 DETERMINATION OF LIQUID/LIQUID PARTITION COEFFICIENTS AND WATER SOLUBILITIES OF COMPONENT PETROLEUM HYDROCARBONS AS A FUNCTION OF TEMPERATURE

In order to adequately predict evaporation/dissolution phenomena with the oil weathering model, thermodynamic data in the form of equilibrium distribution coefficients are required to describe interphase mass transfer. These data are typically referred to as Henry's Law coefficients for evaporation or liquid-liquid partition coefficients (M-values) for dissolution. These data are used to describe how far from equilibrium the three phases are in terms of concentrations, and the departure from equilibrium measured on an arbitrary scale multiplied by the appropriate mass transfer coefficients yield the mass flux across the phase boundary from oil into the water and atmosphere.

To determine the liquid-liquid partition coefficients (M-values) for all of the components of interest in Prudhoe Bay crude oil, a series of equilibrium experiments were undertaken at 3, 13 and 23°C. In these experiments known volumes of oil and water were equilibrated in separatory funnels for 48 hours, with their phases being vigorously shaken at time zero and then allowed to settle with occasional swirling over the first 24-hour period. Additional mixing (swirling) was done 13 hours before sampling, and the phases were allowed to separate without further agitation. Water and oil phase samples were then removed and the samples were extracted with equal volumes of methylene chloride (800 ml).

During initial attempts at M-value determinations, a number of problems were encountered due to the formation of 1 to 5 μm micelles of dispersed oil in the water column phase. Incorporation of micelles into the aqueous phase led to anomalously high levels of "dissolved" petroleum hydrocarbons (exceeding solubility limits in some cases) in the aqueous phase. This micelle phenomenon yielded M-value partition coefficients (oil phase concentration ÷ water phase concentration) which were anomalously low, and with these M-values initially predicted rates of dissolution of higher molecular weight components were too high. In addition to the microscopic examinations of the aqueous phases from these M-value experiments which confirmed the presence of micelles, indirect evidence of micelle formation was obtained by the presence of higher molecular weight n-alkanes in the aqueous phase. These compounds have extremely limited water solubilities (less than 0.8 µg/L for compounds with molecular weight greater than nC-18; SUTTON AND CALDER, 1974) and their presence in water column extracts was taken as evidence of micelle formation.

Because of these initial difficulties due to the oil-in-water dispersions, a number of additional M-value experiments were then undertaken where the oil and water phases were not as vigorously agitated. Figure 5-32 presents FID capillary gas chromatograms of (A) the whole unfractionated oil, (B) the aliphatic fraction of the surface oil, (C) the aromatic fraction of the surface oil, and (D) the unfractionated water column extract from under the slick. Initially, M-value determinations were attempted using L/C fractionated water column samples; however, only trace levels of aliphatic components were detected in the fractionated samples, and some breakthrough of the lower molecular weight aromatics (benzene, toluene, xylenes, and ethylbenzene) during the liquid column chromatography was noted. This phenomenon complicated ratio determinations for oil phase and water phase concentrations, so later M-value determinations were completed using unfractionated water column samples. Because the majority of the components which are subject to dissolution are aromatic hydrocarbons, this procedure does not limit the data obtained. Figure 5-33 presents the reconstructed ion gas chromatogram of the water column extract, and Table 5-5 lists the identifications of the aromatic compounds of interest.

From this latter series of partition coefficient experiments, M-values for individual compounds at various temperatures were obtained, and Table 5-6 presents the calculated values for oil/seawater partitioning at 3 and 23°C. These values were obtained using a sub-program in the overall oil weathering model called M-VAL, which matches the oil phase and water phase specific compound concentrations by Kovat retention indices. Also shown in Table 5-6 are the identifications of selected compounds as determined by the GC/MS analysis of the water column and fractionated (F2) oil sample extracts.

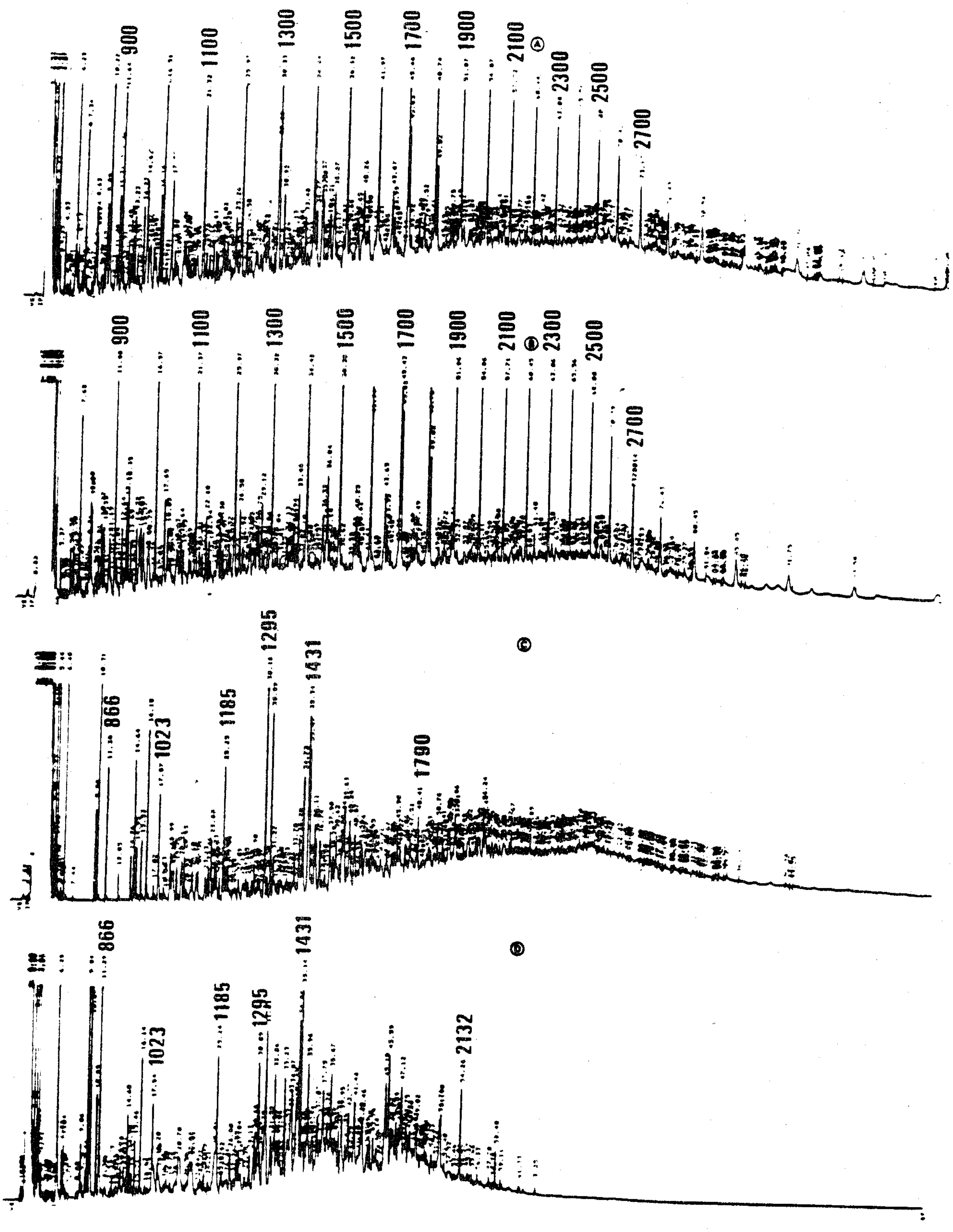

FIGURE 5-32. FLAME IONIZATION DETECTOR CAPILLARY GAS CHROMATOGRAMS OBTAINED ON SPECIFIC SAMPLES USED FOR COMPOUND SPECIFIC OIL/SEAWATER PARTITION COEFFICIENT (M-VALUE) DETERMINATIONS. (A) UNFRACTIONED OIL; (B) ALIPHATIC FRACTION OF THE SURFACE OIL; (C) AROMATIC FRACTION OF THE SURFACE OIL AND (D) THE UNFRACTIONATED WATER COLUMN EXTRACT BENEATH THE SLICK. (KOVAT INDICES ARE SHOWN ABOVE MAJOR PEAKS).

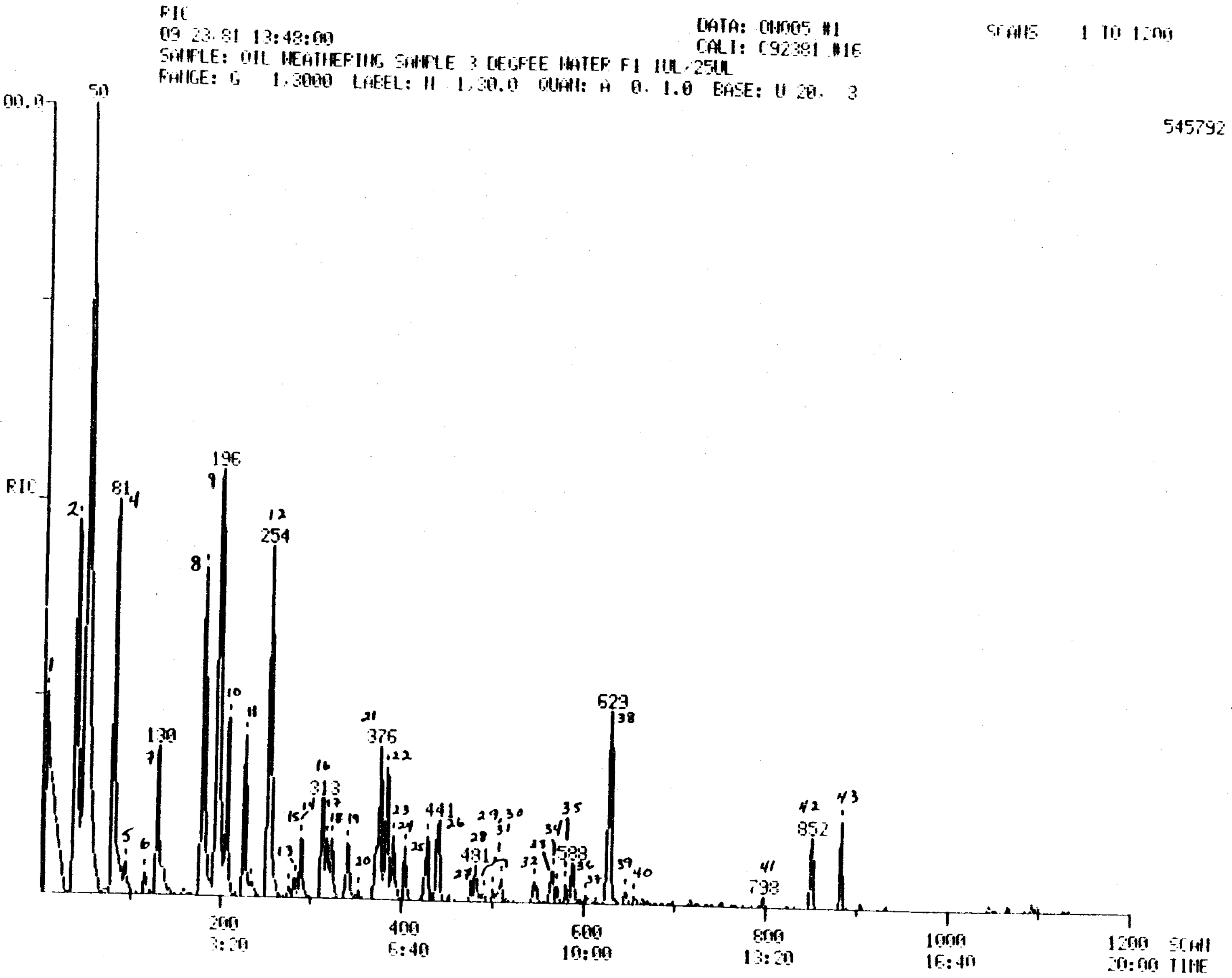

FIGURE 5-33. RECONSTRUCTED ION CHROMATOGRAM (RIC) FROM CAPILLARY GC/MS ANALYSES OF WATER COLUMN EXTRACTS FROM OIL/SEAWATER PARTITION COEFFICIENT EXPERIMENTS. IDENTIFICATIONS OF THE NUMBERED PEAKS IN THE CHROMATOGRAM ARE PRESENTED IN TABLE 5-5.

TABLE 5-5. COMPOUNDS IDENTIFIED BY GC/MS ANALYSES OF WATER COLUMN EXTRACTS FROM OIL/SEAWATER PARTITION COEFFICIENT (M-VALUE) EXPERIMENTS.

1	methyl chloride (solvent)
2	ethylbenzene
3	p-xylene
4-	o-xylene
5	nonane
6	C_9H_{16}
7	cumene
8	n-propylbenzene
9	ethylmethylbenzene
10	trimethylbenzene
11,12	C_3 benzenes
13	decane
14,15	C_4 benzenes
16-18	C_3 benzenes
19	unsaturated C_3 benzene
20	methylisopropylbenzene
21	methylpropylbenzene
22	C_4 benzene
23	ethyldimethylbenzene
24-28	C_4 benzenes
29	t-amylbenzene
30	C_4 benzene
31	tetramethylbenzene
32,33	unsaturated C_4 benzenes
34	C_4 benzene
35	C_5 benzene
36	tetralin
37	C_5 benzene
38	naphthalene
39	C_2 indane
40	unsaturated C_5 benzene (possibly a methyltetralin or a C_2 indane)
41	methyltetralin
42	2-methylnaphthalene
43	3-methylnaphthalene

TABLE 5-6. OIL/SEAWATER LIQUID-LIQUID PARTITION COEFFICIENTS (M-VALUES) DETERMINED AT 3 AND 23°C.

M - Values Determined at 3^o and 23^o

Kovats	M - Values			Compounds
	3^ooil/3^o-wat	23^o -oil/23^o -wat	23^o -oil/23^o -wat	
765	652	688	583	toluene
859	2,660	2,690	2,250	ethylbenzene
867	3,030	3,060	2,550	p-xylene
892	2,730	2,260	1,900	o-xylene
923	8,840	8,520	7,310	cumene
953	13,400	14,645	14,800	n-propylbenzene
961	12,100	10,800	9,370	ethylmethylbenzene
967	14,900	13,600	11,800	mesitylene
979	10,800	9,350	7,840	C_3 benzene
992	------	11,200	9,080	C_3 benzene
1021	14,800	5,830	9,660	p-cymene
1035	3,530	1,990	2,450	naphthalene
1066	68,800	------	38,800	C_4 benzene
1086	10,740	4,290	2,530	ethyldimethylbenzene
1121	57,300	6,530	12,600	tetramethylbenzene
1163	------	26,300	22,000	naphthalene
1185	5,570	6,720	6,900	naphthalene
1199	------	19,900	15,500	C_5 benzene unsaturated
1237	------	5,180	5,240	2-methylnaphthalene
1284	3,900	1,110	1,070	C_6 benzene
1296	35,800	14,900	11,000	2-methylnaphthalene
1316	30,400	5,320	4,830	1-methylnaphthalene
1338	------	4,690	4,060	
1343	10,100	951	951	
1371	3,210	466	424	C_7 benzene
1425	128,000	------	93,400	dimethylnaphthalene
1428	67,000	------	23,200	dimethylnaphthalene
1461	------	44,500	53,900	
1469	5,670	889	1,000	n-octylbenzene
1476	58,300	9,030	6,920	C_3 naphthalene
1499	------	6,910	6,590	
1510	23,300	7,130	6,460	2-isopropylnaphthalene
1523	47,300	6,120	6,610	
1528	------	10,000	10,600	1-isopropyl naphthalene
1537	47,400	7,930	6,660	trimethyl naphthalene
1546	4,600	925	714	

TABLE 5-6. OIL/SEAWATER LIQUID-LIQUID PARTITION COEFFICIENTS (M-VALUES) DETERMINED AT 3 AND 23°C. (Continued).

M - Values Determined at 3° and 23° (continued)

Kovats	M - Values			Compounds
	3°oil/3°-wat	23° -oil/23° -wat	23^{C} -oil/23° -wat	
1589	7,880	1,730	1,440	
1642	13,400	2,150	2,160	
1715	71,800	------	9,460	methyl fluorene
1743	------	8,030	6,950	
1841	9,760	5,270	4,080	
1867	30,100	11,900	10,800	methyldibenzothiophene
2154	------	5,280	3,920	

These values are then used in the evaporation/dissolution oil weathering model as described in Section 4.0 of this report. Section 5.5 presents the results of predicted vs observed evaporation and dissolution behavior for specific compounds as measured in the evaporation/dissolution chamber at 23 and 3°C and in the wave tank experiments completed at Kasitsna Bay.

5.3 OUTDOOR EVAPORATION/DISSOLUTION STUDIES IN FLOW-THROUGH AQUARIA AT KASITSNA BAY, ALASKA

Part of the Summer 1980, Kasitsna Bay program involved construction of outdoor flow-through aquaria for long-term sub-arctic evaporation/dissolution and microbial degradation studies. Figure 5-34 presents a schematic diagram of the outdoor flow-through tank arrangement, and Figure 5-35A shows the arrangement of the tanks during water column sampling. Figure 5-35B shows the mechanical stirrers used to provide turbulence during the Spring 1981 program. In September and October of 1980 four long-term microbial degradation experiments were begun: flow was maintained in two tanks where oil was allowed to weather in the presence and absence of Corexit 9527 (Tanks 3 and 7, respectively), and two tanks were maintained in a static condition where similarly treated oils were allowed to weather in the absence of continuous seawater flow (Tanks 5 and 2, respectively).

At the onset of the Spring, 1981 program, the four outdoor tanks were again examined and sampled, and two of the systems (Tanks 3 and 7) were left undisturbed to allow continued longer term microbial degradation of the partially weathered oil over the summer months. Additional details on the results obtained from these and other long-term microbial degradation experiments are described in Section 7.0.

A more ambitious series of evaporation/dissolution experiments were then undertaken during the Spring 1981 program in these outdoor tanks using the matrix design as presented in Figure 5-34. That is, evaporation/dissolution phenomena were examined with fresh Prudhoe Bay crude oil and

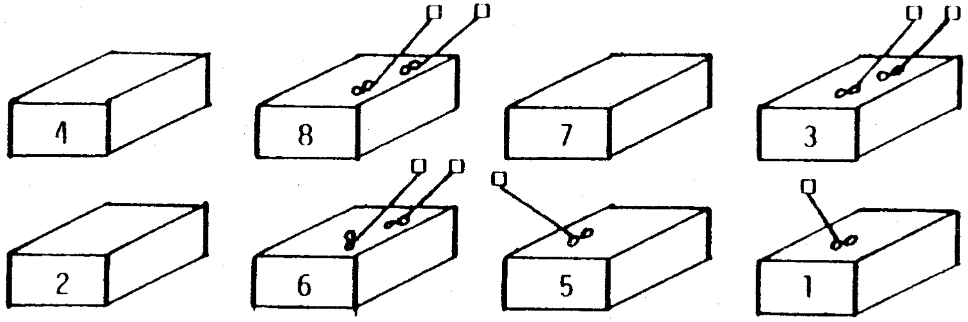

Kasitsna Bay Revised New Experimental Plan 5-1-81

Tank No.	Mousse	Oil	Turbulance	Corexit	Flow
6	+	-	+	+	+
4	+	-	-	-	+
8	+	-	+	-	+
2	+	-	-	+	+
5	-	+	+	+	+
3	-	7 month old weathered oil	+	+	–
1	-	+	+	-	+
7	-	7 month old weathered oil	-	-	+

FIGURE 5-34. SCHEMATIC DIAGRAM OF OUTDOOR FLOW-THROUGH TANK CONFIGURATION AT KASITSNA BAY, ALASKA. THE MATRIX PRESENTS THE EXPERIMENTAL DESIGN AND TANK CONFIGURATION AS USED DURING THE SPRING/SUMMER 1981 FIELD PROGRAM.

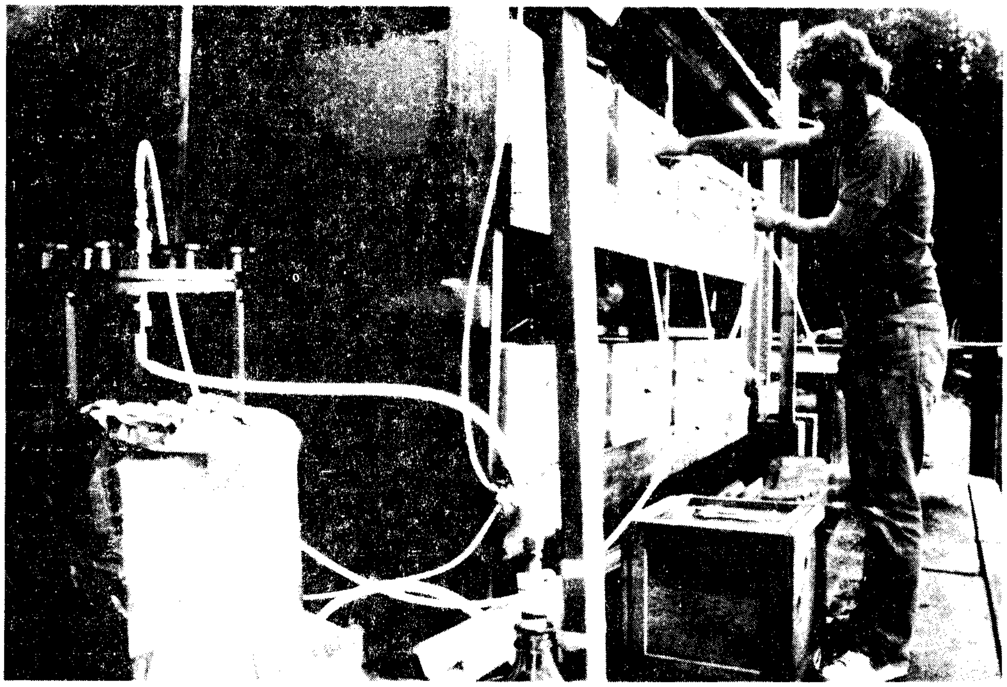

FIGURE 5-35A. ARRANGEMENT OF OUTDOOR FLOW-THROUGH TANKS DURING WATER COLUMN SAMPLING.

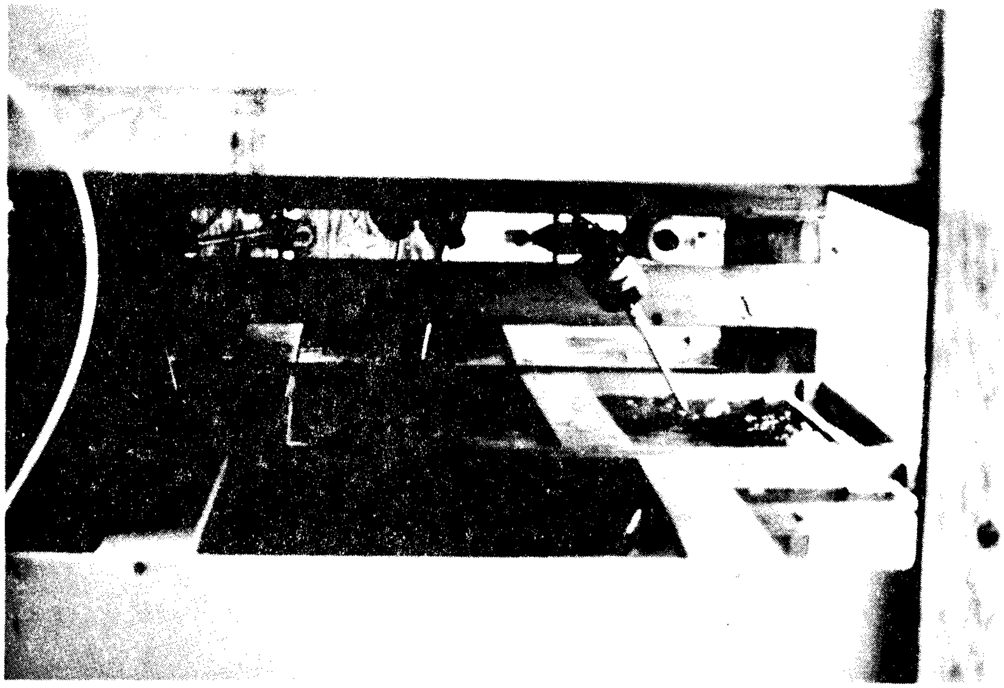

FIGURE 5-35B. MECHANICAL STIRRERS USED TO INTRODUCE TURBULENCE TO SELECTED TANKS AS ILLUSTRATED BY THE MATRIX IN FIGURE 5-34.

artificially generated mousse in the presence and absence of turbulence and in the presence and absence of the dispersant Corexit 9527 as shown in Figure 5-34.

Time-series capillary column chromatographic profiles were obtained at Kasitsna Bay on the oil fractions during the experimental runs, and digitized data were recorded on magnetic tape and returned to La Jolla for incorporation into the data base for the oil weathering model. As in the evaporation/dissolution experiments in La Jolla, two types of water samples were obtained, with the first being 25-ml whole water samples in Pierce septum-capped vials for analysis of volatile organics by the purge and trap technique. In addition, 20 to 40-L samples of the discharged water from each tank were obtained and extracted with methylene chloride for later laboratory fractionation and GC and GC/MS analyses.

Numerous samples were collected to provide quantitative data on evaporation/dissolution rates of oil under a wide variety of conditions; however, only three selected experiments are addressed in this report. Specifically, these include evaporation/dissolution results from: fresh oil in the presence of turbulence (Tank 1); artificially generated mousse in the presence of turbulence (Tank 8); and fresh crude oil plus Corexit in the presence of turbulence (Tank 5).

The importance of examining the evaporation/dissolution behavior of an artificially generated water-in-oil emulsion stemmed from the fact that significant increases in viscosity and specific gravity have been observed for many water-in-oil emulsions, and these increases have been shown to affect spreading, dispersion, interaction with suspended particulate material and presumably evaporation/dissolution (PAYNE, 1981). TWARDUS (1980) indicated that no quantitative data existed on how mousse affects evaporation, but it was suspected that once mousse formation occurred, evaporation would occur at reduced rates. Similar predictions have been made by NOGATA and KONDO (1977), and, in our Spring 1981 experiments, attempts were made to quantify any differences in lower molecular weight volatile compound losses from fresh Prudhoe Bay crude oil and artificially (shaker table) generated mousse where evaporation was prevented during mousse formation in a sealed teflon container. Specifically, in this experiment, a water-in-oil emulsion (or artificial mousse) was generated with fresh Prudhoe Bay crude oil by mixing 80 parts filtered seawater with 20 parts fresh oil in sealed teflon containers on a shaker table for 48 hours.

This fresh mousse was then poured onto the water surface in Outdoor Tank #8 and propeller driven turbulence was introduced to determine if differential rates of lower molecular weight hydrocarbon losses occurred in the more viscious water-in-oil emulsion compared to fresh Prudhoe Bay crude (Tank No. 1). As in the corresponding evaporation/dissolution chamber experiments in La Jolla, volatile compound concentrations were measured in the air 1 to 2 inches above the slick by pumping measured volumes of air through stainless steel columns packed with Tenax® at different time intervals following the spills. In both Tanks 1 and 8, turbulence was induced by propeller mixing. The water and air temperatures at the time of sampling were 6° and 6 to 12°C, respectively. After sampling, the Tenax® traps were capped with stainless Swagelok© fittings and stored at room temperature until FID GC analyses, using the procedures described in Appendix F. Backup columns in series with the front columns showed no breakthrough of lower molecular weight material and 95+% recovery on the front traps. Interestingly, the qualitative appearance of the temperature programmed chromatograms of the volatiles from both systems were remarkedly similar (PAYNE, 1981), and the time-series data presented graphically in Figures 5-36A and 5-36B illustrate that essentially identical losses of lower molecular weight compounds ranging from butane to xylene were obtained for both the fresh oil and fresh mousse. The data in Figure 5-36C, however, show slightly longer retention of these compounds in mousse spread on seawater in the absence of turbulence. One of the static (non-propeller mixed) mousse systems (Tank 2) was also treated with Corexit 9527 immediately

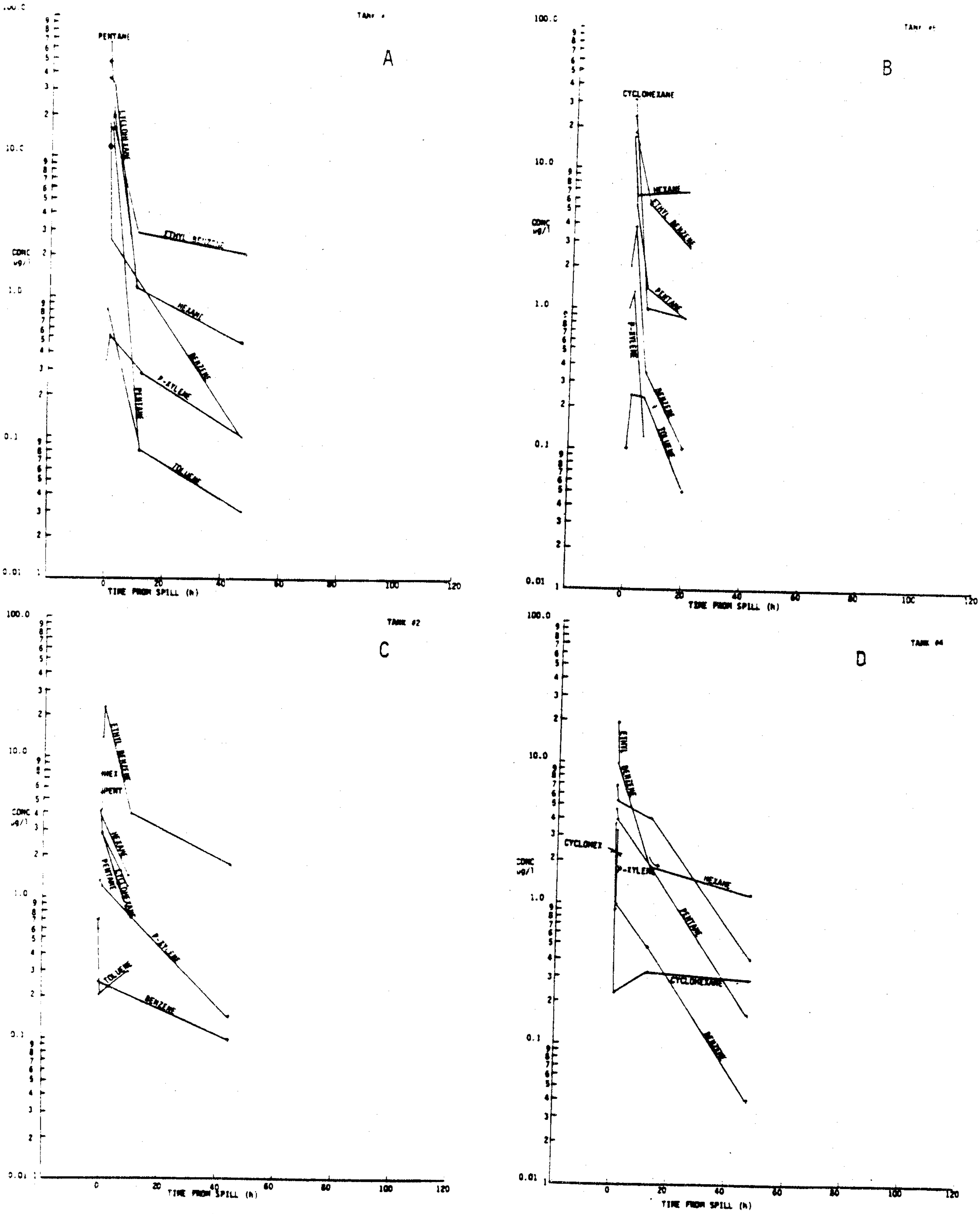

FIGURE 5-36. TENAX TRAP/FID GC DATA ON SUB-ARCTIC VOLATILE COMPONENT LOSS FROM PRUDHOE BAY CRUDE OIL AND MOUSSE ON FLOW-THROUGH SEAWATER ENCLOSURES IN KASITSNA BAY, ALASKA. A) FRESH OIL AND TURBULANCE; B) FRESH MOUSSE AND TURBULENCE; C) FRESH MOUSSE (NO TURBULANCE); D) FRESH MOUSSE AND COREXIT 9527 (NO TURBULANCE). WATER TEMP 6°C, AIR TEMP 6-13°C.

after the spill (Figure 5-36D), but this apparently did not affect evaporation loss compared to the non-dispersant treated control (Figure 5-36C).

Figure 5-37 presents selected time-series glass capillary gas chromatographic profiles obtained on the fresh oil samples in the flow-through tank in the presence of turbulence (Tank 1). The sampling points in Figure 5-37 are for times of: 1 hour, 26 hours, 4 months and 6 months. Figure 5-38 presents the time-series gas chromatographic profiles obtained on the artificially generated mousse in the presence of turbulence at sampling times 0, 30 hours and 4 months (Tank 8). Very similar losses of the lower molecular weight components below nC-9 appeared to have occurred in both the fresh oil and artificial mousse experiments however, slightly longer retention of lower molecular weight components is suggested in the artificial mousse case when examining the four month data (Figure 5-38C). Also, while only limited or no microbial degradation is suggested during the first 24 to 30-hour period, more significant microbial utilization of the aliphatics as opposed to the branched chain isoprenoids can be observed in the four month old samples from both the fresh crude and artificially generated mousse. In the fresh oil plus turbulence experiment, the nC-17/pristane and nC-18/phytane ratios dropped to 0.38 and 0.51, respectively after four months, and in the chromatogram of the four month old weathered mousse (Figure 5-38C) the nC-17/pristane and nC-18/phytane ratios dropped to 0.75 and 0.92, respectively. The values for these ratios in fresh Prudhoe Bay crude oil are 1.7 and 1.6, respectively. It should also be noted that after four months of weathering in both systems, the unresolved complex mixture had increased significantly. The effects of microbial degradation are even more striking in Figure 5-37D which presents the weathered sample from the fresh oil plus turbulence tank after 6 months of weathering during the sub-arctic summer months from June through October, 1981. In the 6 months old sample (Figure 5-37D) the isoprenoid compounds, pristane (Kovat 1710) and phytane (Kovat 1815) dominate all of the other resolved components. Additional discussions of microbial degradation of surface oil are presented in Sections 7.1 through 7.3.

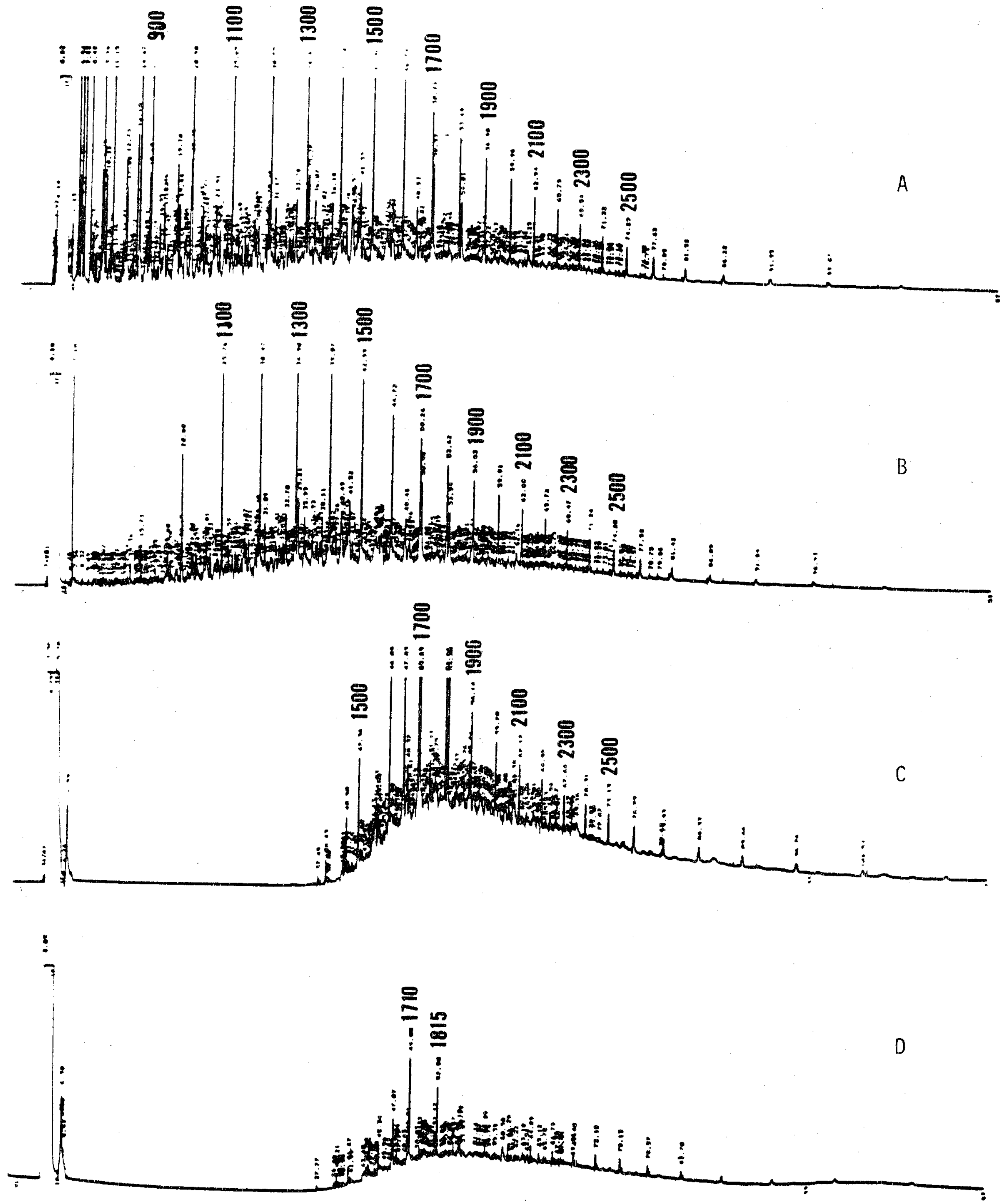

FIGURE 5-37. FLAME IONIZATION DETECTOR CAPILLARY GAS CHROMATOGRAMS OBTAINED ON PRUDHOE BAY CRUDE OIL WEATHERING IN THE PRESENCE OF PROPELLER DRIVEN TURBULENCE IN THE OUTDOOR FLOW-THROUGH AQUARIA (TANK #1) AT KASITSNA BAY, ALASKA. TIME-SERIES SAMPLING POINTS AFTER THE "SPILL": (A) 1 HOUR; (B) 26 HOURS, (C) 4 MONTHS; AND (D) 6 MONTHS.

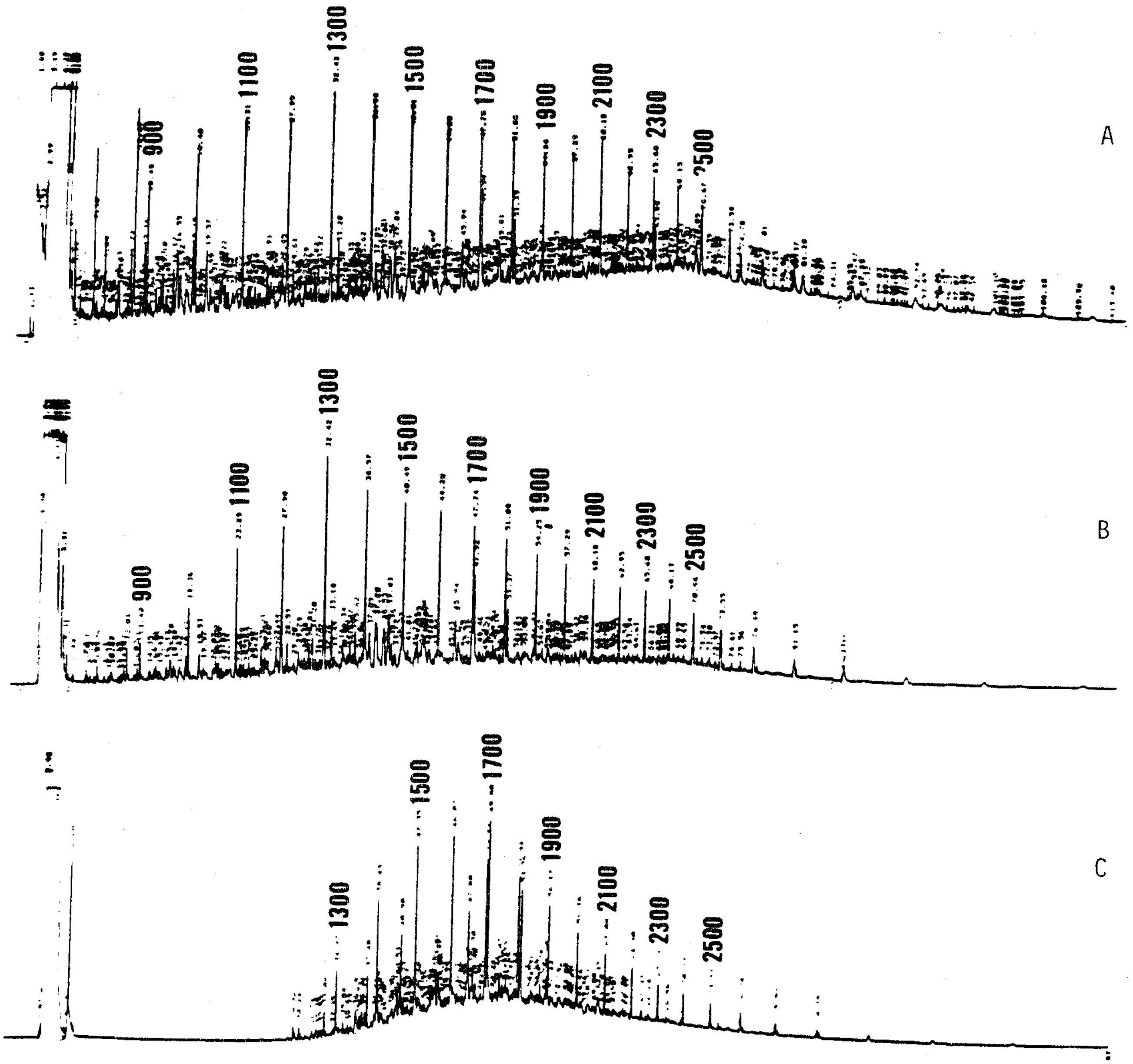

FIGURE 5-38. FLAME IONIZATION DETECTOR CAPILLARY GAS CHROMATOGRAMS OBTAINED ON ARTIFICALLY GENERATED MOUSSE (USING PRUDHOE BAY CRUDE OIL) WEATHERING IN THE PRESENCE OF PROPELLER DRIVEN TURBULENCE IN THE OUTDOOR FLOW-THROUGH AQUARIA (TANK #8) AT KASITSNA BAY, ALASKA. TIME-SERIES SAMPLING POINTS AFTER THE "SPILL" (A) 5 MIN; (B) 30 HOURS; AND (C) 4 MONTHS.

Easier comparisons of the relative retention of the higher molecular weight components can be made by examination of the computer generated time-series concentration profiles obtained from capillary FID gas chromatographic analyses of the oil and mousse from the well-stirred tanks as shown in Figure 5-39. Kovat indices for the compounds in each plot are identified in the figures, and these data confirm that compounds in the range of nC-9 through nC-11 are preferentially retained in the mousse sample for longer periods of time (Figures 5-39A and C). Figures 5-40A and 5-40B show the time-series concentrations of components with Kovat indices ranging from 1300 to 2000 for the oil and artificially generated mousse samples, respectively. A similar relative increase in these higher molecular weight compound concentrations (in μg/g oil) is noted for both the oil and mousse after approximately 25 hours, and this is due to the removal of significant mass of the oil by evaporation of the lower molecular weight components (compounds with molecular weights above nC-15 are not lost during this time frame). Absolute concentrations of the individual components in each of the mousse sample plots (on a μg/g of mousse basis) are lower than those of the fresh oil because of the additional mass of seawater (80% by weight) in the water-in-oil emulsions.

Thus, in the presence of turbulence in these studies, the higher viscosity of the 80% water-in-oil mousse did not significantly affect evaporative loss of the lower molecular weight components boiling below xylene, but some reduction in evaporation was noted for intermediate molecular weight compounds (Kovat indices 800 to 1100) in the mousse. More significant differences were noted in the amounts of oil and fresh mousse that were dissolved and dispersed into the water column due to the turbulent regimes, and Table 5-7 presents selected time series water column concentrations for the two systems. The three orders of magnitude difference between the fresh oil and fresh mousse systems clearly reflects the latter's resistance towards dissolution and dispersion to droplets.

Figure 5-41 presents the glass capillary gas chromatograms on the time series oil samples from outdoor tank #5 from the Spring 1981 experiments

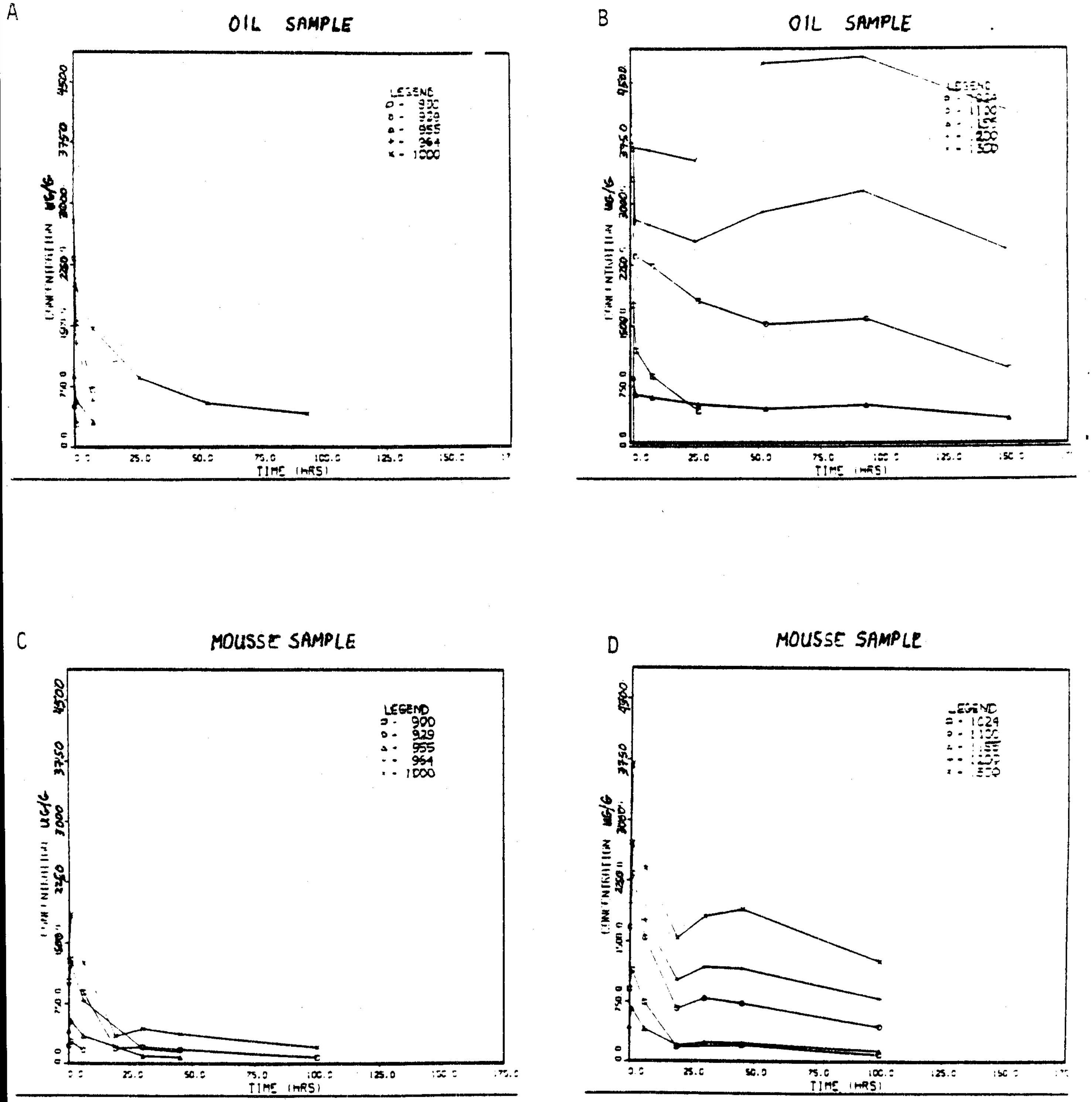

FIGURE 5-39. COMPUTER GENERATED PLOTS OF CAPILLARY FID-GC INTERMEDIATE MOLECULAR WEIGHT COMPONENTS REMAINING IN PRUDHOE BAY CRUDE OIL AND MOUSSE WEATHERING UNDER SUB-ARCTIC CONDITIONS ON FLOW-THROUGH SEAWATER ENCLOSURES AT KASITSNA BAY, ALASKA. KOVAT INDICES ARE IDENTIFIED ON EACH PLOT. A AND B-FRESH PRUDHOE BAY CRUDE AND TURBULANCE; C AND D-FRESH PRUDHOE BAY MOUSSE AND TURBULANCE. TEMPERATURE AS IN FIGURE 5-34.

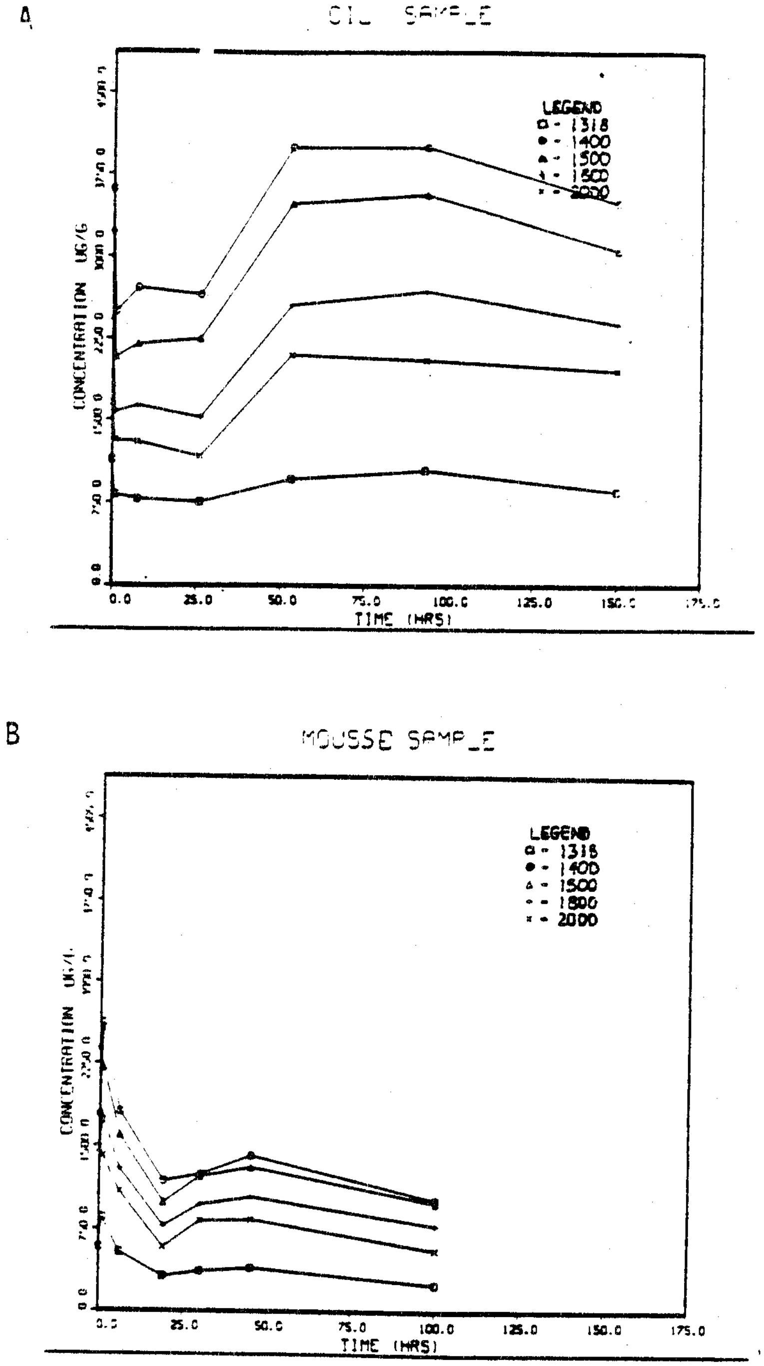

FIGURE 5-40. COMPUTER GENERATED PLOTS OF CAPILLARY FID-GC DATA ON HIGHER MOLECULAR WEIGHT COMPONENTS REMAINING IN PRUDHOE BAY CRUDE OIL AND MOUSSE WEATHERING UNDER SUB-ARCTIC CONDITIONS ON FLOW-THROUGH SEAWATER ENCLOSURES AT KASITSNA BAY, ALASKA. KOVAT INDICES ARE IDENTIFIED ON EACH PLOT AND ENVIRONMENTAL CONDITIONS ARE AS IN FIGURE 5-34.

TABLE 5-7. TIME-SERIES WATER COLUMN CONCENTRATIONS (μg/l) OF DISSOLVED AND DISPERSED HYDROCARBONS FROM FRESH PRUDHOE BAY CRUDE OIL AND MOUSSE WEATHERING ON FLOW-THROUGH SEAWATER ENCLOSURES (TURBULENT REGIME) AT KASITSNA BAY, ALASKA. (WATER TEMPERATURE 6°C, AIR TEMPERATURE 6-13°C). CONCENTRATIONS DETERMINED BY CAPILLARY TEMPERATURE-PROGRAMMED FID GAS CHROMATOGRAPHY.

Fresh Oil	0 hrs	1 hrs	7.5 hrs	26 hrs	53 hrs
Resolved Components	7200	4740	1400	10110⁺	659
Unresolved Complex Mixture	3140	1460	420	447	114

Fresh Mousse*	0 hrs	1 hrs	6 hrs	19 hrs	30 hrs	45 hrs	100 hrs
Resolved Components	23	7	29	18	10	24	34
Unresolved Complex Mixture	ND	ND	12	45	37	69	59

*Water column concentrations corrected for total oil volume added as "mousse."

ND = none detected

+Possibly due to excessive oil droplet entrainment

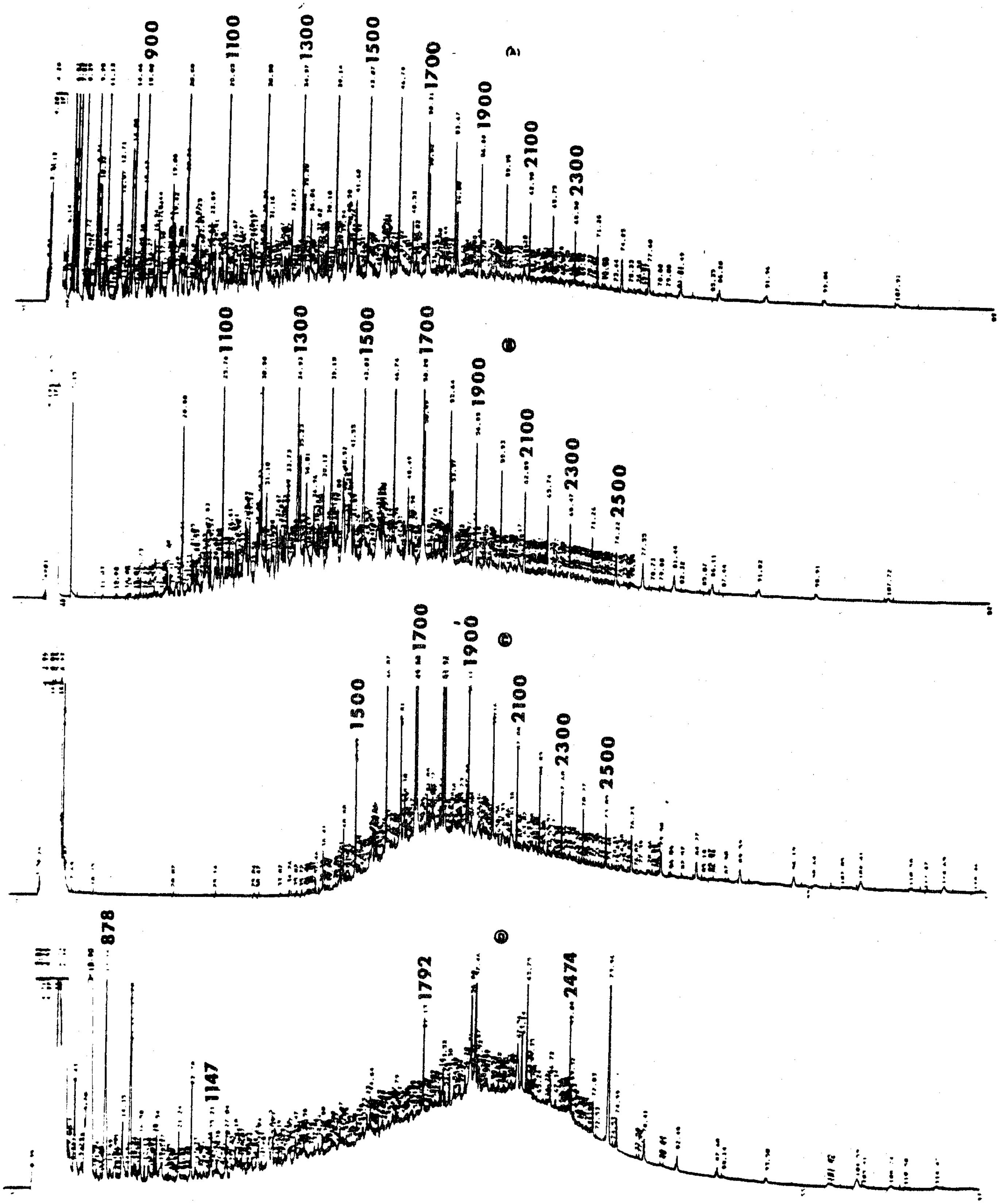

FIGURE 5-41. FLAME IONIZATION DETECTOR CAPILLARY GAS CHROMATOGRAMS OBTAINED ON PRUDHOE BAY CRUDE OIL PLUS COREXIT (OIL:COREXIT = 20:1) WEATHERING IN THE PRESENCE OF PROPELLER DRIVEN TURBULANCE IN THE OUTDOOR FLOW-THROUGH AQUARIA (TANK #5) AT KASITSNA BAY, ALASKA. TIME-SERIES SAMPLING POINTS AFTER THE "SPILL": (A) 1 HOURS; (B) 23 HOURS; (C) 4 MONTHS. CHROMATOGRAM D WAS OBTAINED ON THE POLAR (F3) FRACTION OBTAINED FROM AN ACIDIFIED WATER COLUMN SAMPLE AFTER 4 MONTHS OF IN SITU WEATHERING.

(fresh oil plus Corexit, 20:1, in the presence of turbulence). These data are included to allow direct comparison to the fresh oil plus turbulence experiment in tank #1 over the same time frame as shown in Figure 5-37. As in the non Corexit fresh oil experiment, the most effective initial weathering mechanism was due to evaporation as compounds below Kovat indices 1000 were clearly lost during the first 24 hours. Visual observation of the water column extracts from this tank, however, also indicated that enhanced removal of oil into the water column occurred as a result of the dispersant.

As noted above, the tanks were maintained in a flow-through condition during the period of April to October 1981 to allow indigenous microbial populations to be fully operative, and Figure 5-41C shows the chromatographic profiles obtained on the Corexit treated oil after 4 months of weathering. Interestingly, the chromatogram is nearly identical to the chromatogram in Figure 5-38C, the patchy mousse from stirred Tank 1 which was not treated with Corexit in April. As in the other case, most of the components below nC-14 have been removed by evaporation and dissolution processes during the warmer summer months, and the change in the nC-17/pristane and nC-18/phytane ratios to values of 1.1 and 1.0, respectively, illustrates the effects of microbial degradation. Surprisingly, the decrease in these ratios is not as great as that observed for Tank 1, although this is quite possibly due to the fact that the oil sample from Tank 5 was scraped from the side of the tank and not taken from the water surface. Unfortunately, some time during the four month weathering period between April and July, the water level in Tank 5 increased and overflowed and much of the oil was lost. After the water level was returned to the appropriate height in the outdoor tank, the stranded oil was then not subject to additional degradation from water-borne micro-organisms.

This observation is in line with similar findings by BLUMER et al. (1973) where they studied stranded oil on intertidal rocks from the beaches of Bermuda. In their studies, oil which was stranded in the upper intertidal zones away from the water showed only limited degradation due to bacterial processes, and weathering was limited to evaporation and photo-oxidation.

The chromatogram in Figure 5-41D shows the water column extract of the aromatic fraction under the oil after 4 months of weathering during the spring and summer months. Because the tank overflowed sometime during that period, it might a priori be expected that more of the water soluble components would be lost due to air-sea exchange. Furthermore, since the tanks were maintained in a flow-through condition during this period, removal of water soluble components by advection might be anticipated. There are still significant levels of aromatic components remaining in the water column over this time period, although the lower molecular weight aromatics from benzene through naphthalene have been removed.

As noted in above, additional time series (up to 150 hours) samples and chromatograms were obtained on the other outside tank experiments shown schematically in Figure 5-34. Some of these tank experiments are considered in Section 7.0 which deals with longer term microbial degradation results.

5.4 AMBIENT SUB-ARCTIC WAVE TANK EXPERIMENTS AT KASITSNA BAY

5.4.1 Introduction

As noted in the previous section (5.3), the outdoor microbial degradation tanks were utilized for initial evaporation/dissolution experiments during the Spring 1981 Kasitsna Bay program where turbulence was induced via propeller mixing. Even with this approach, however, the turbulence regime was not entirely satisfactory, and it did not closely approximate that which would be observed in open ocean oil spill situations. Therefore, to quantify more natural changes to oil in a subarctic marine environment, four continuous-flowing outdoor wave tanks were constructed at Kasitsna Bay during the Summer 1981 and 1982 Field Programs. These wave tanks were used to study the physical and chemical changes caused by evaporation, dissolution, water-in-oil emulsification, photo-oxidation, and microbial degradation under more realistic environmental conditions during all subarctic weather seasons.

The wave tanks and the flow-through seawater system were designed to simulate oil moving over a constantly regenerating water column, as would be encountered during wind-driven drift of a slick. In this instance, however, the tanks served to "corral" the oil, and the seawater was "moved" beneath it by a flowing seawater system which ensured each 2,800 liter tank had a turnover time of one tank volume every three hours. Turbulence was introduced into the tanks by paddle wheels at the water input end of the tanks, and water was removed from the center of the tanks by a discharge pipe whose orifice was 2 to 3 centimeters (cm) from the bottom.

These sections (5.4.2 to 5.4.6) describe the wave tank construction and utilization and present the results of triplicate determinations of changes in oil behavior due to alterations in its rheological properties with weathering. Time-series data are presented for changes in: oil density, percent water incorporated during water-in-oil emulsification, oil/air interfacial surface tension, oil/water interfacial surface tension, and oil viscosity. Sections 5.4.7 and 5.4.8 present the results of triplicate component-specific concentration measurements in the oil and water column as a function of time. These data are then compared with computer-based oil-weathering model predictions in Section 5.5).

5.4.2 Wave Tank Construction

Four flow-through wave tanks were constructed at the Kasitsna Bay facility to allow replicate evaluations of the fate of an open ocean oil spill under ambient Sub-Arctic conditions. The wave tanks were fabricated using 3/4" AC exterior plywood, glued at every joint, painted with 2-part epoxy resin, and sealed with silicone sealant (Figure 5-42). Figure 5-43 shows the dimensions of one 2800 liter wave tank. To prevent buckling of the sides due to water pressure from the filled tank, five sets of braces (constructed of 2 x 4 lumber and secured with bolts) were installed on each tank.

Seawater for the wave tank system was provided by a submersible pump located approximately 10 ft below low, low tide in Kasitsna Bay. The sea-

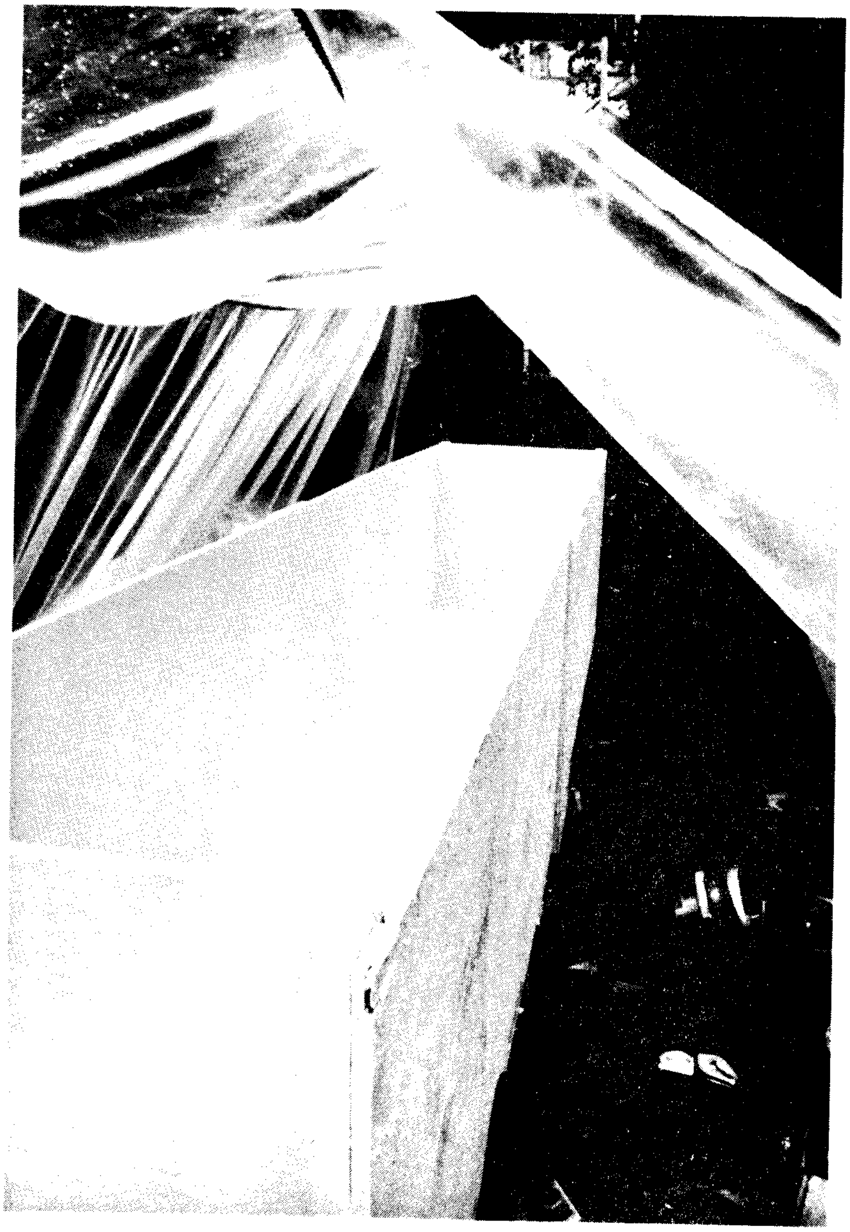

Figure 5-42. Curing of two-part epoxy used to seal 2800 liter wave tanks. Note the plastic tarp used to protect the tank system from rainfall.

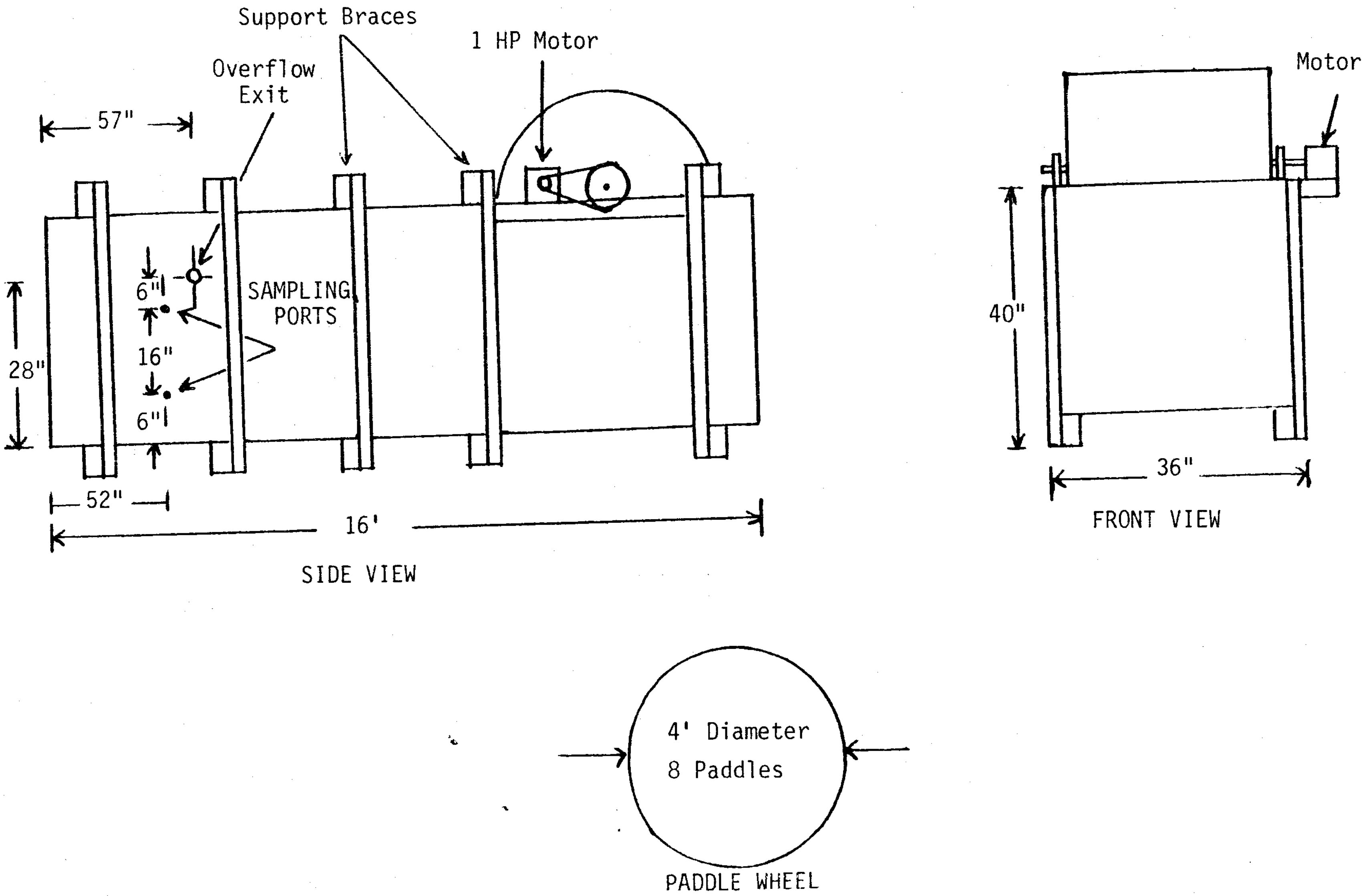

Figure 5-43. Dimensions of the Wave Tank (not to scale)

water lines were insulated to prevent freezing and buried in the intertidal zone to avoid damage from storms (Figure 5-44). During insulation of the seawater system, the wave tank construction was completed and paddle wheels were fabricated of three-quarter inch exterior plywood for wave turbulence generation in the tanks (Figure 5-45). Paddle wheels were not painted or sealed. Each paddle wheel was four feet in diameter and contained eight equally spaced paddles. The paddle wheels were placed at one end of the tanks (Figure 5-46 and 5-47), and a 60 inch platform was built on each side of the tank to support the bearings. The drive shaft was attached to the wheel with a six bolt plate.

To drive the paddle wheel, a double wide chain drive mechanism was used. A 39-tooth gear was attached to the 1 1/4" diameter drive shaft, and the drive motor had a 14-tooth gear (Figure 5-48). The characteristics of the electric motor are listed below:

Balor Industrial Motor
Single Phase
Spec 35C 13-157
Serial F186
1 H.P.
1725 RPM
Hz 60
pH 1
DES L
P.F. 68%

Rated @ 40°C ambient continuous use
V.L. 3510 Catalog Number
Frame 56C
280 V-230V/115V
14.6/6.2 amps
Ser F 1.15
Class BC
Code K
Full Load Efficiency 67%

The motor was mounted transverse to the shaft and a gear box was attached to the motor to achieve the desired paddle wheel rotational speed of 11 RPM.

Electrical power was supplied by 220V power lines (Romex underground cable) through four inch ABS pipe. Each wave tank motor was individually powered and had its own circuit breaker.

Figure 5-44. Burial of insulated seawater lines and electrical cable for the submersible pump supplying seawater to the wave tank system.

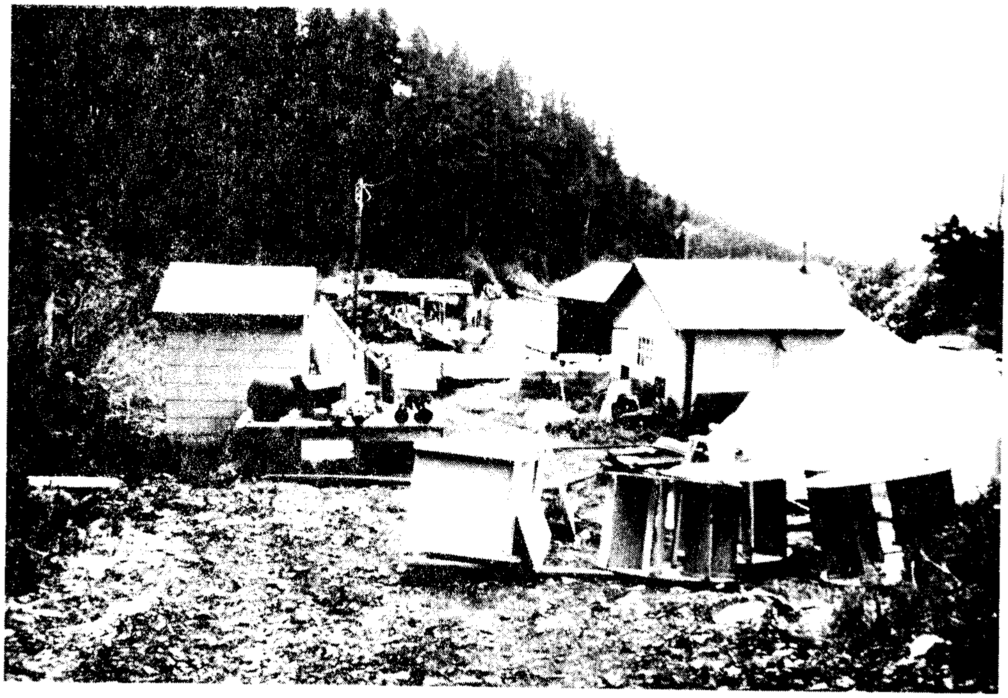

Figure 5-45. Construction of plywood paddle wheels during wave tank installation.

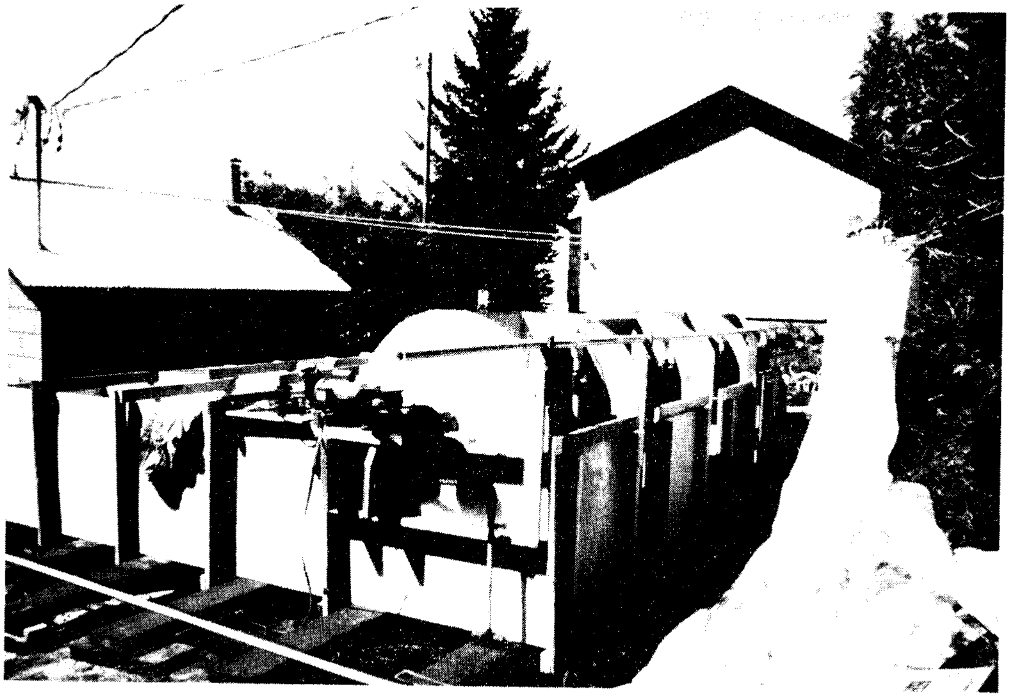

Figure 5-46. Installation of paddle wheels and vertical seawater delivery lines. The seawater source line can be observed in the foreground on the 4 x 8 timbers supporting the wave tank systems.

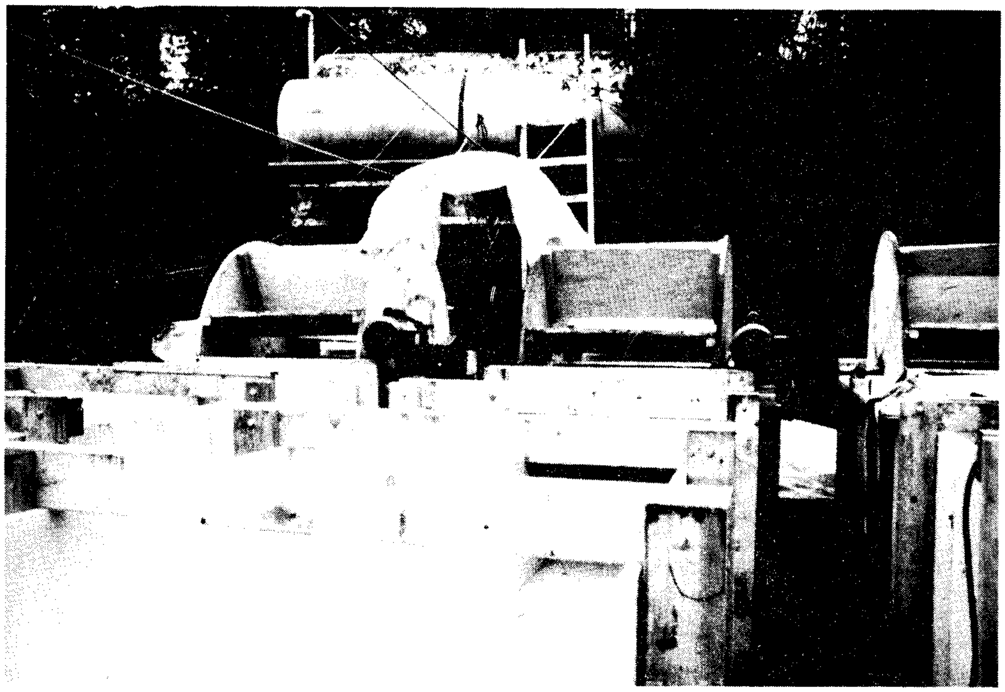

Figure 5-47. Support braces used to secure the wave tanks.

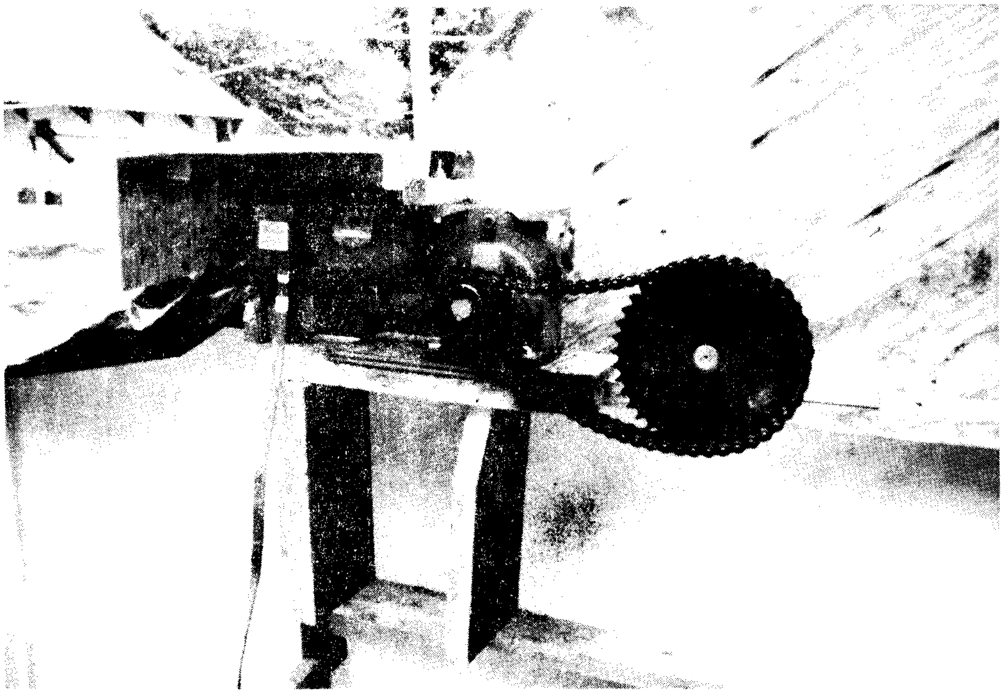

Figure 5-48. One horsepower electrical motor and gear drive mechanism used to propel the paddle wheels.

Figure 5-49. Overview of the wave tank systems after completion (photographed during oil weathering experiments).

Figure 5-49 shows an overview of the completed system, and Figure 5-50 presents a flow diagram for seawater delivery and discharge. Water was pumped into the wave tank area and entered the distribution system via 1 1/2" flexible black pipe. The remainder of the delivery system was made of 1 1/2" white PVC tubing. All incoming lines were either glued or secured tight with worm clamps. Seawater was distributed along a horizontal feed line with vertical delivery lines controlled by ball valves behind each paddle wheel (Figure 5-51). Each ball valve was a full bore type valve seated in Teflon with a full range adjustable control, from complete stop to a full-open position. There were five vertical exit points that were valve controlled. The first went to a wash stand for cleaning glass carboys and the remaining four supplied the wave tanks. With a tank volume of ~2800 liters and a flow rate of 15-16 l/min, there was a complete tank-volume turnover every three hours. To prevent back siphoning, in the event of pump failure, the vertical delivery lines did not extend below the surface of the water in the tanks (see Figure 5-50).

The level of the water inside the wave tanks was maintained at 28" through a self-regulating siphoning exit tube placed 28 inches from the bottom of the tank. Figure 5-52 presents a flow diagram for the siphoning pipe and Figure 5-53 shows the arrangement of the discharge siphon on the outside of one tank. Basically, there is a tee on the inside of the tank with a stand pipe that extends to within two inches of the tank bottom. This allows only water from the deepest part of the tank to overflow, and thereby, prevents removal of any oil diectly from the surface, which would affect the overall mass balance. Another standpipe extents from the tee to a point well above the upper edge of the tank (Figure 5-52) and serves as a vent to prevent any unwanted siphoning which would otherwise drain the tank if input seawater flow was interrupted. The exit pipes on the exterior of the tanks have a built in diversion so that flow measurements can be made with relative ease (Figure 5-53). The exiting water collects in a 2" PVC pipe (that runs the width of all four wave tanks) which is also vented to prevent the creation of another siphon (Figures 5-50 and 5-54). The outflowing water is then discharged onto Kasitsna Bay.

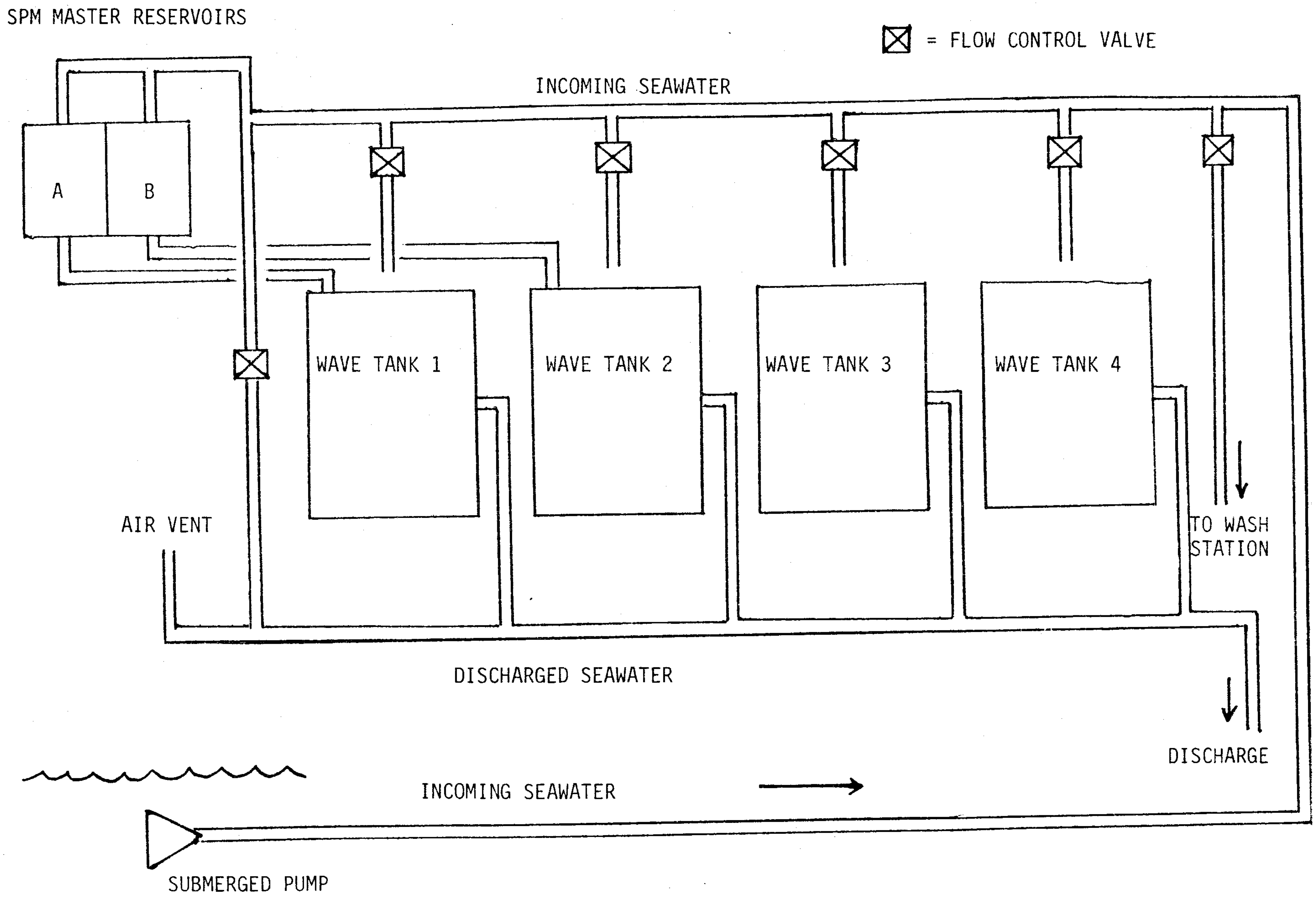

Figure 5-50. General layout of the Wave Tank Flow System

Figure 5-51. Close-up of the seawater delivery line for the four 2800 liter wave tanks.

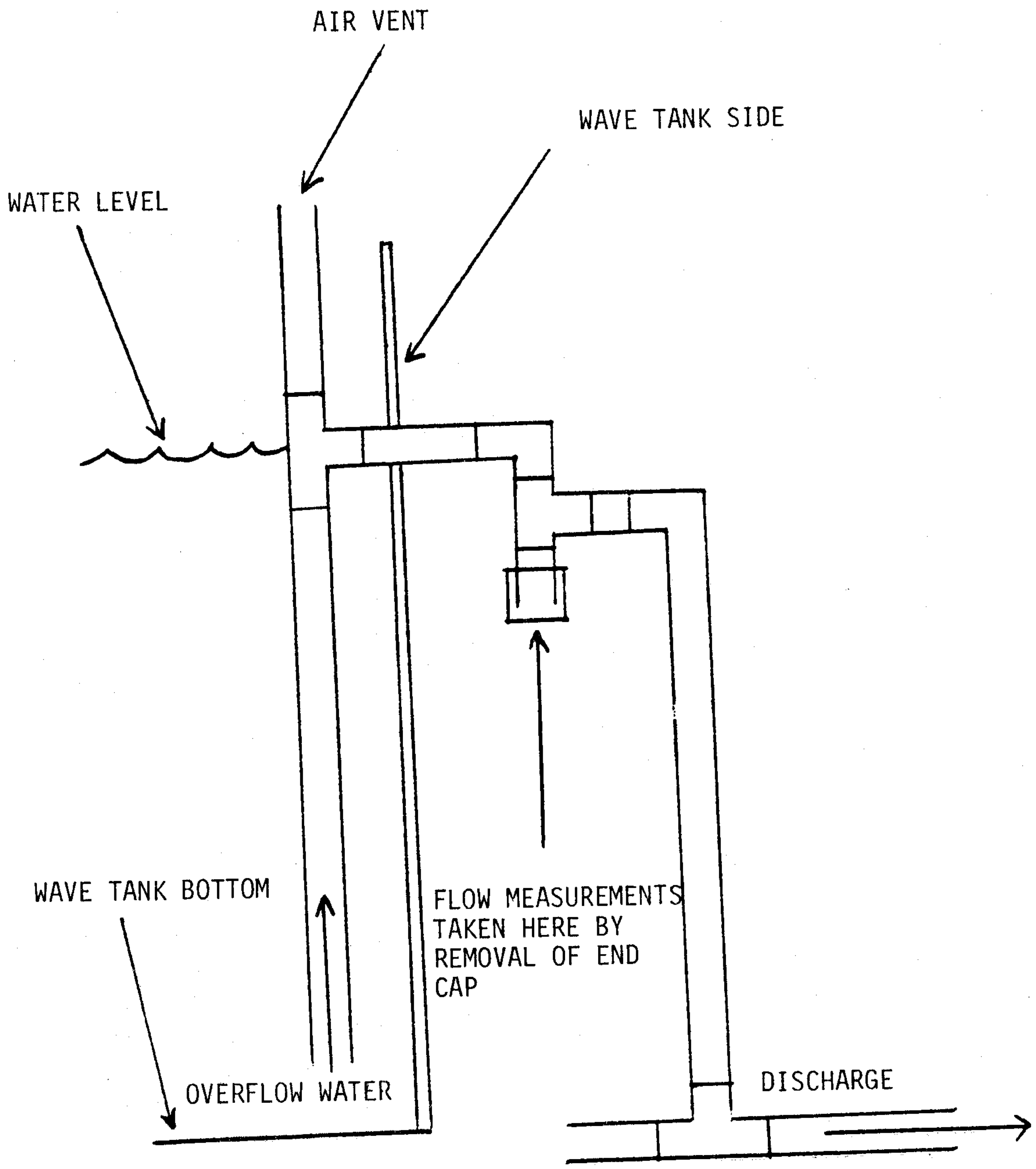

Figure 5-52. Arrangement of the self-regulating overflow siphon

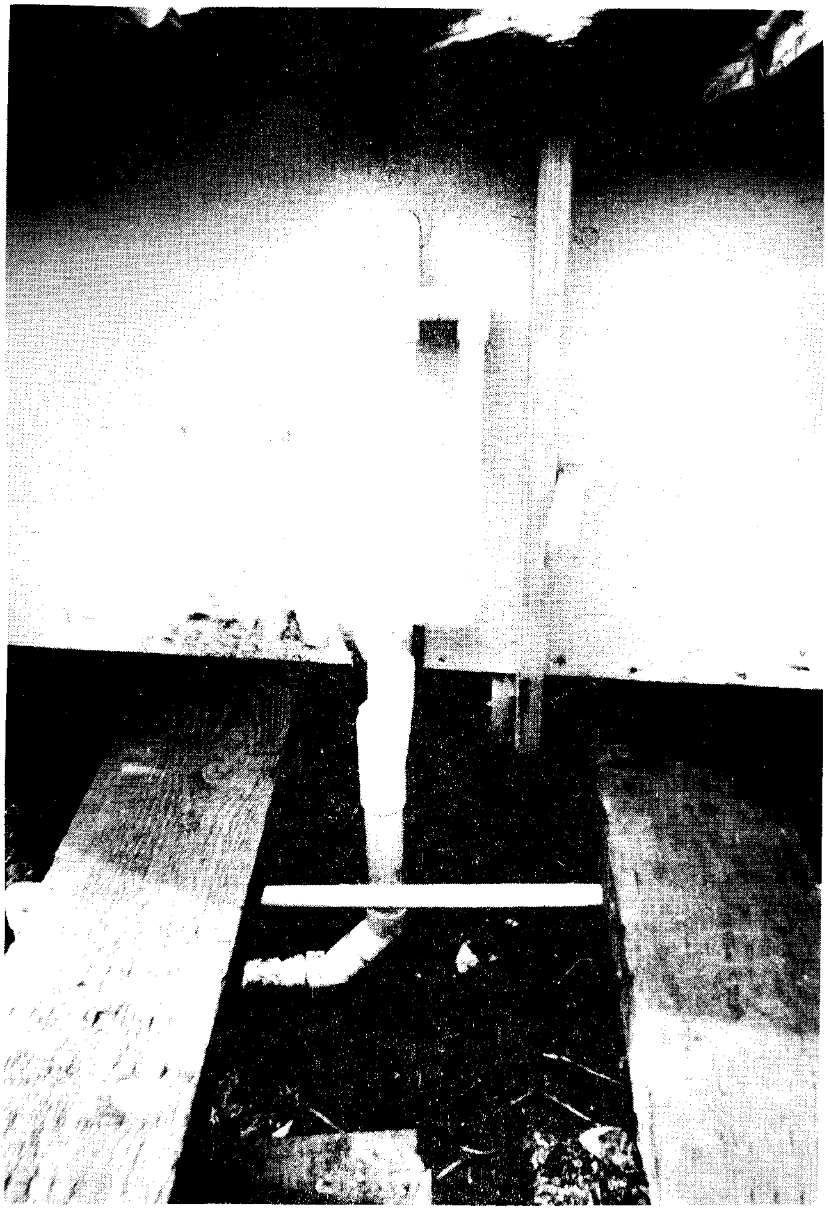

Figure 5-53. Wave tank overflow syphon system on the outside of wave tank 4. The PVC plug on bottom of the uppermost "T" can be removed for tank-discharge flow-rate determinations.

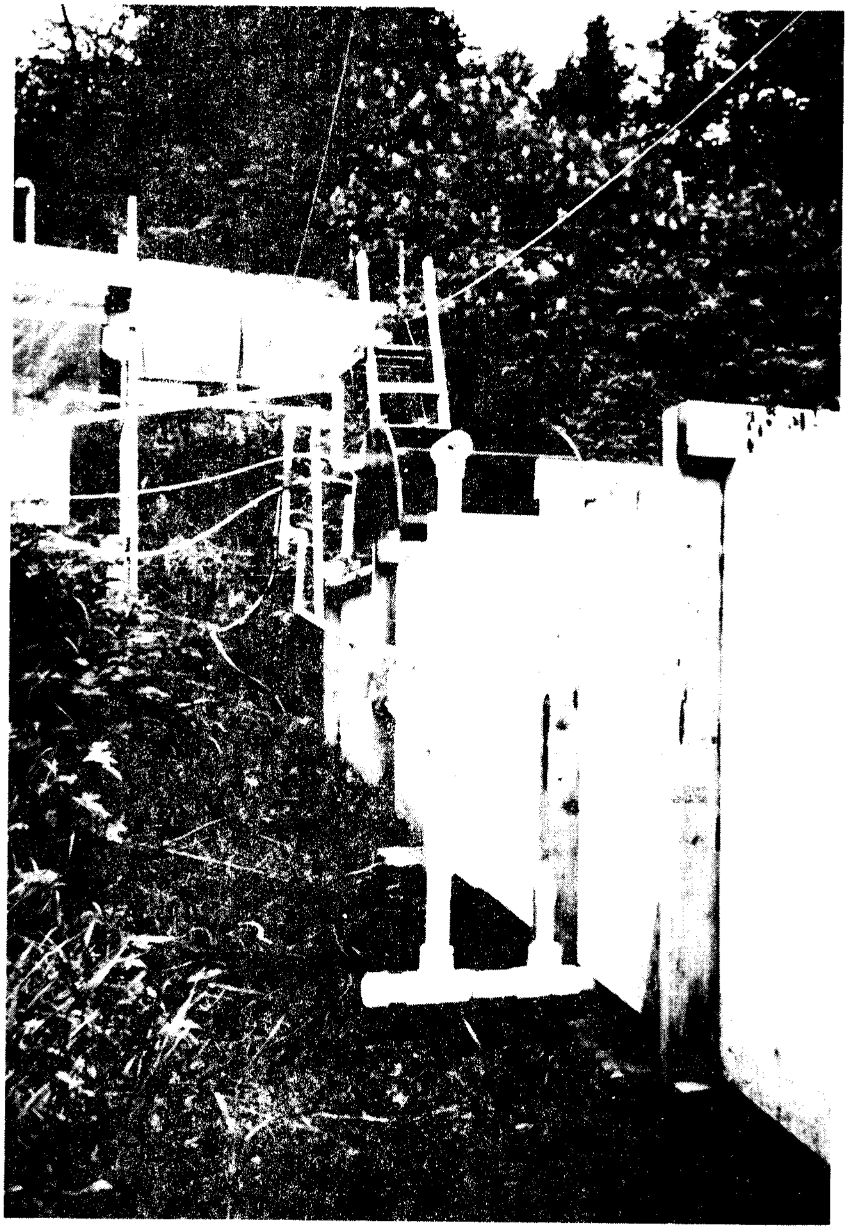

Figure 5-54. Stand pipe on seawater drainage plumbing installed to prevent unwanted syphoning of the wave tank system. The auxiliary feed line for the SPM reservoir tanks can be observed in the background of the figure.

Half inch stainless steel Swagelock bulkhead fittings were installed, as sampling ports, 6 inches below the surface of the water and 6 inches above the bottom of the wave tank (see Figure 5-43). These sampling ports were located 52 inches from the end of the tank, opposite the paddle wheel.

5.4.3 SPM Master Reservoir Construction

A bifurcated tank was built for the purpose of continously feeding the primary wave tanks with water containing elevated levels of suspended particulate matter. Figure 5-55 presents the dimensions of the Master SPM resevoir tank. The tank was constructed, primarily, of 3/4" AC exterior plywood, which was sealed with 2- part epoxy resin.

Seawater was supplied to the 175 liter reservoirs from the submerged pump via a divert valve in the overall wave tank delivery system (Figure 5-56). Appropriate weighed amounts of sediment were added to the reservoirs and suspended by propeller action mixing from mounted stir motors (Figure 5-57 and 5-58). The stir motors used were TAMCO chemical mixers with specifications shown below:

Model 2M034	AC/DC Motor
115V, 1/15 H.P.	0-5000 RPM

Seawater, containing elevated levels of SPM, was delivered from the resevoirs to the wave tanks via Teflon tubing which terminated at the paddle wheel end of tanks 1 and 2. Inside the resevoir, a short piece of Teflon tube was connected to a bulkhead fitting, and the intake end was fastened to a float (Figure 5-58). Attaching the intake to a float insured that the feed would maintain a fixed position (constant head) below the surface of the water at all times. Also, a screen was placed around the intake to prevent clogging of the lines by large particles.

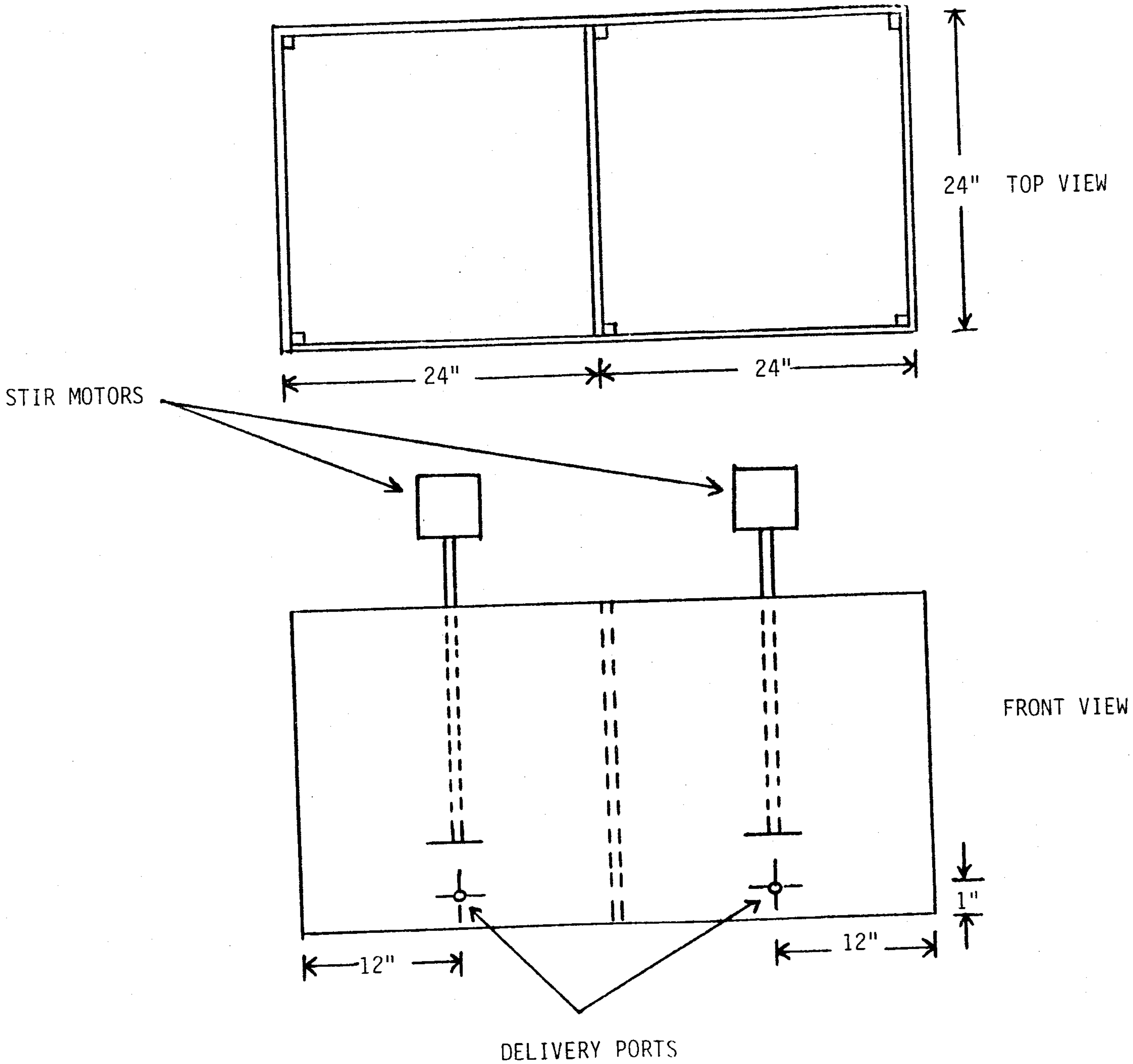

Figure 5-55. Dimensions of the SPM Master Reservoirs (not to scale)

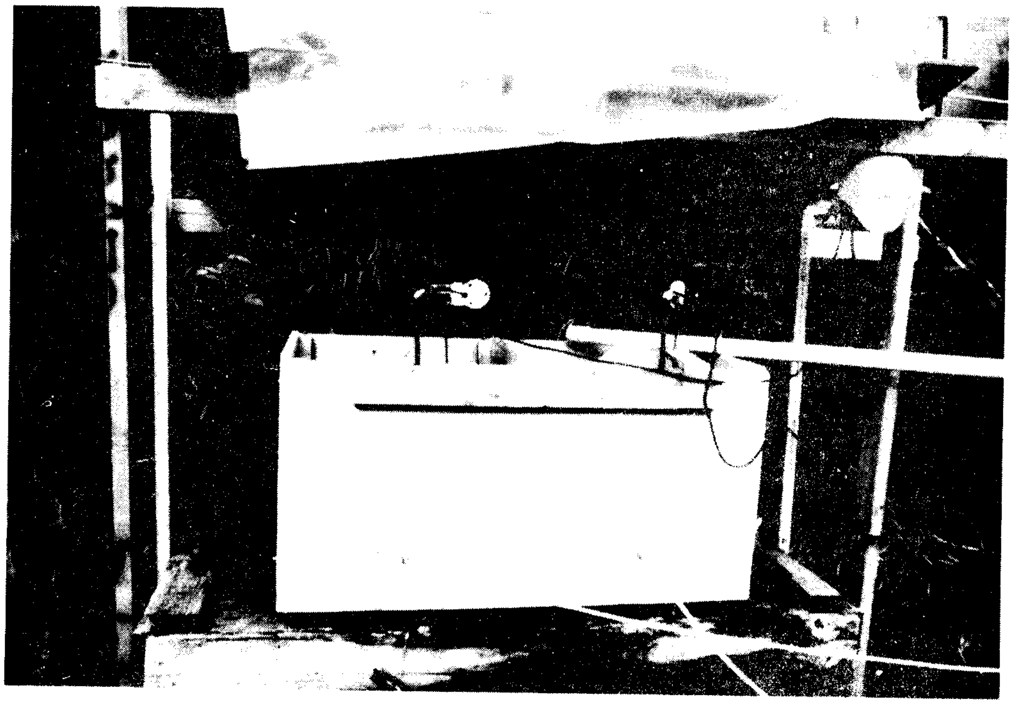

Figure 5-56. Bifurcated SPM reservoir showing stirring motors used to suspend particulate material and the seawater feed line for periodic refill of the SPM reservoir system. The Teflon lines attached to the bottom of the tank flow directly into wave tanks 1 and 2.

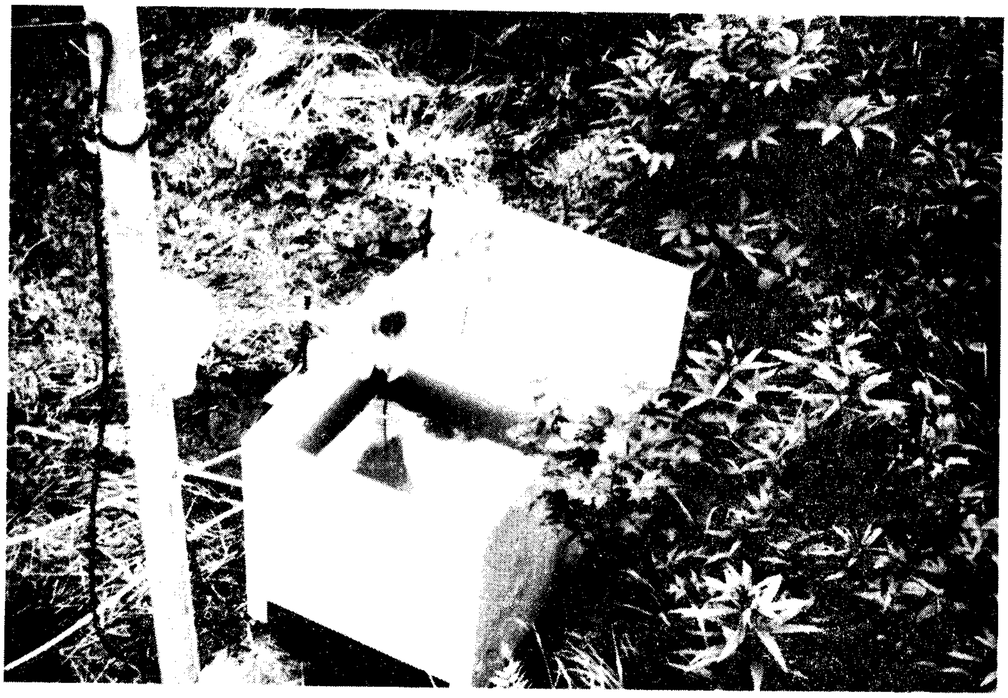

Figure 5-57. SPM reservoir system after addition of sedimentary material for SPM loading of wave tank 1.

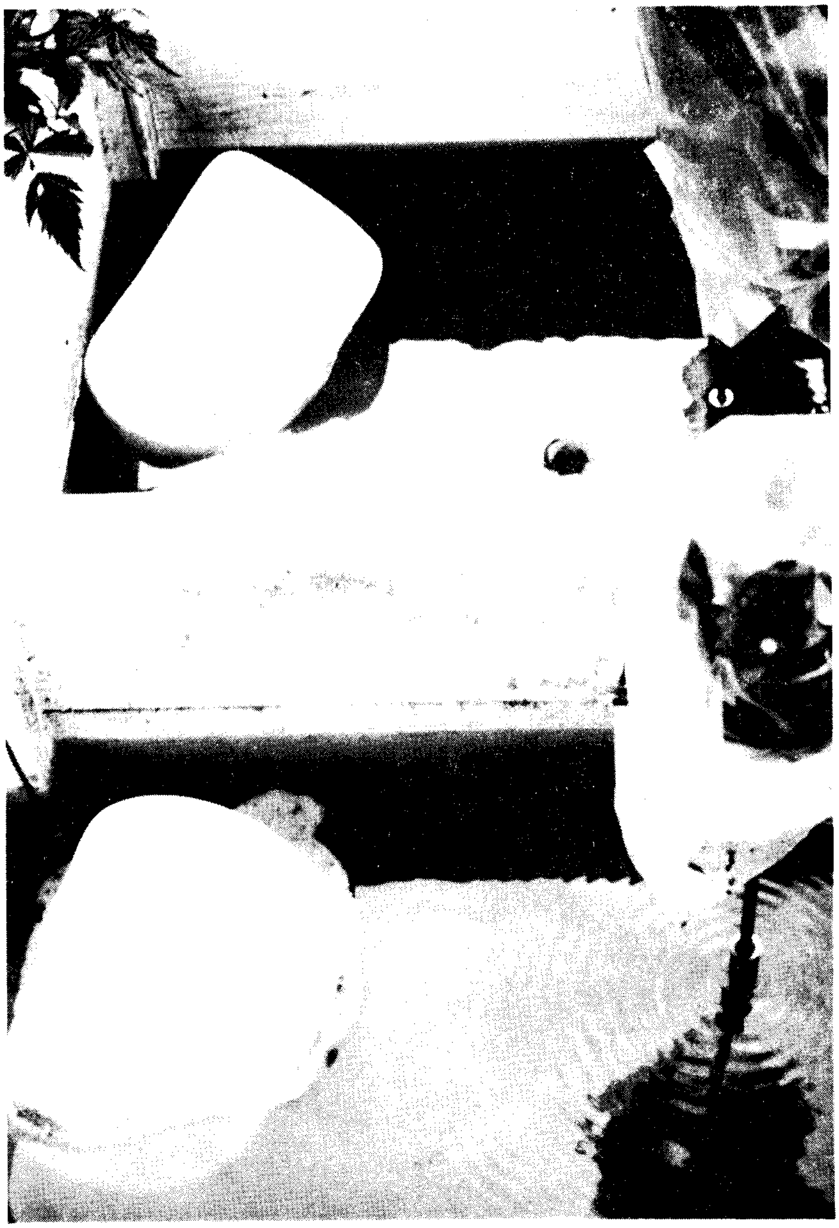

Figure 5-58. Closeup of the bifurcated SPM reservoir tank showing the float system to which the discharge lines were attached. Discharged lines were suspended approximately 3" below each float, such that a constant feed of SPM-laden water would be introduced to the wave tanks regardless of the water level in the SPM reservoir system.

Initially, water from the SPM reservoirs was gravity fed to the wave tanks, and the desired flow was achieved by constricting the tubing with a chem-clamp. In later experiments, flow was controlled with peristaltic pumps.

5.4.4 Wave Tank Water Column Sampling and Extraction

In order to monitor the concentration of dissolved and dispersed hydrocarbons in the water column beneath the spilled oil in the wave tanks, 20 liter bulk water samples were collected according to the following schedule: At 0 minutes, 5 minutes, 1 hour, 2 hours, 4 hours, 8 hours, 12 hours, 24 hours, 48 hours, 3 days, 6 days, 9 days, 12 days, 4 months, 9 months, and 12 months after a spill of 16 liters of Prudhoe Bay crude oil.

Figure 5-59 presents a diagram of the sampling procedure. Seawater samples were obtained through a sampling port located six inches below the water surface and 52 inches from the quiescent end of the tank (Figure 5-60). A vacuum pump was used to pull the water through Teflon tubing to a filter apparatus and then into a 20 liter glass carboy (Figure 5-61). To avoid possible contamination, all sampling equipment was constructed of only Teflon, glass, or stainless steel. To ensure that only truly dissolved compunds were sampled, and to obtain values for dispersed/particle bound oil, the water was filtered through pre-kilned 0.45µm glass fiber filters. The filter apparatus used was a 293 mm diameter Millipore manifold.

Once sampled, the water was extracted according to the following scheme. The pH was adjust to 2 using Hydrochloric acid, and 500 mls of CH_2Cl_2 were added and stirred vigorously for two minutes. The CH_2Cl_2 was then forced, through stainless steel tubing using pressurized N_2, into a separatory funnel. This extraction was repeated two more times using 250 mls of CH_2Cl_2, and the separatory funnel containing the combined CH_2Cl_2 extracts was then used for physical removal of water, with the organic phase being delivered into a round bottom flask.

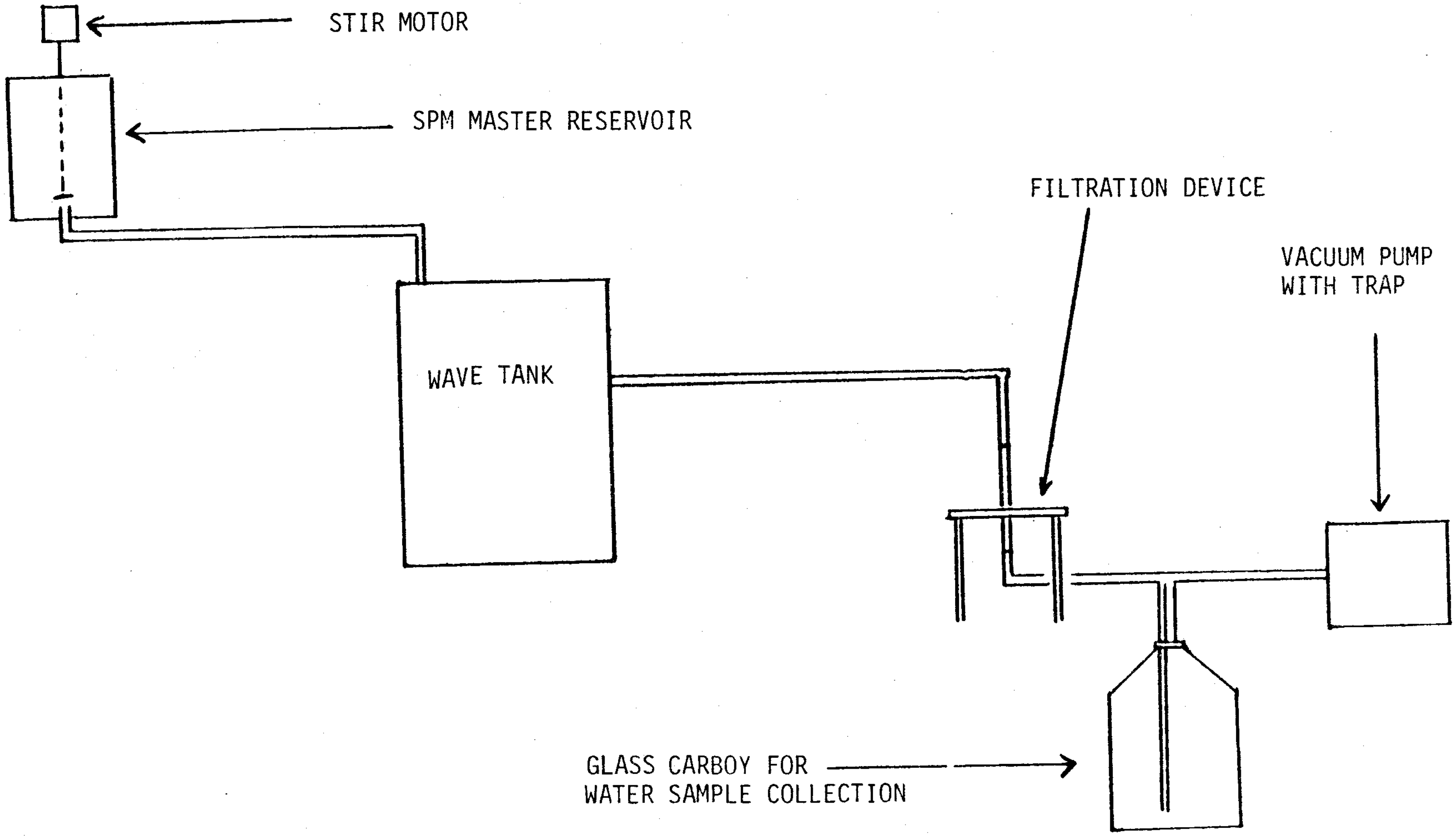

Figure 5-59. Water Column and Dispersed/Particle Bound Oil Sampling Diagram

Figure 5-60. Subsurface sampling of seawater via Teflon transfer line attached to stainless steel bulkhead fitting approximately 6" below the air/sea interface.

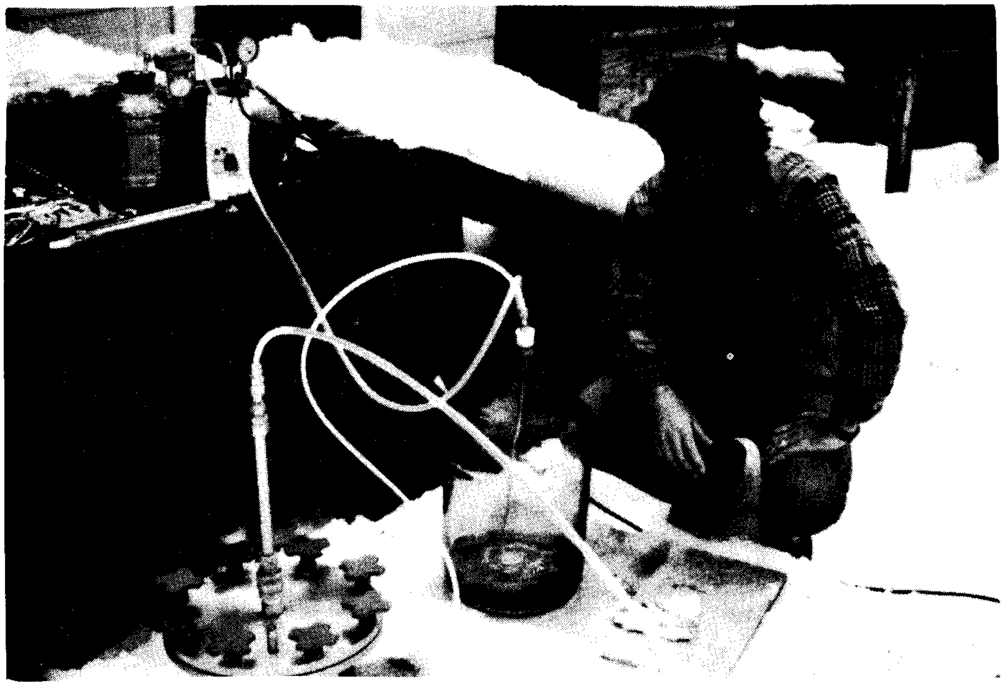

Figure 5-61. Filter/carboy collection system used for sampling suspended particulate material/dispersed oil and dissolved hydrocarbon components in the water system.

Figure 5-62. Removal of the 293 mm diameter 0.45 micrometer glass fiber filter for SPM/particulate material determinations.

Extract concentration was completed by Kurderna-Danish evaporation and final Pre-Injection Volume (PIV) adjustments were completed by passing a stream of N_2 over the sample. The extracts were then transferred into crimp top vials for immediate analysis by FID-GC at Kasitsna Bay. Spike/recovery experiments completed at Kasitsna Bay using a variety of aliphatic and aromatic standards demonstrated an extraction efficiency of better than 70% for most of the components of interest.

5.4.5 Particulate Sampling and Extraction

The level of adsorption of oil by various types of suspended particulate matter and the amount of dispersion of discreet oil droplets was measured by extraction and analysis of the 0.45µm glass fiber filters used in line with the water sampling method. Thus, for each "dissolved" water sample collected, an accompanying particulate phase sample was obtained (Figures 5-62 and 5-63). Filters were either extracted and analyzed immediately at Kasitsna Bay or folded into pre-cleaned aluminum foil and frozen until extraction in La Jolla.

Extraction of the filter pads was accomplished using the following procedure. The filters were cut into small pieces and placed into a 1000 ml round bottom flask. To remove water, 100 mls of CH_3OH were added and refluxed with the sample for 15 minutes. The CH_3OH was then decanted into a sepratory funnel. Next, 200 mls of CH_2Cl_2 were added to the round bottom flask and refluxed for 30 minutes. The reflux with 200 mls of fresh CH_2Cl_2 was repeated, and all extracts were decanted and combined into the separatory funnel. In order to remove the CH_3OH from the extract, 200 mls of 3% NaCl water were added to the sepratory funnel. The CH_2Cl_2 layer was then delivered into a round bottom flask, and the remaining aqueous phase was back extracted with 25 mls of CH_2Cl_2 three times. This back extract was also delivered into the round bottom flask. Spike-recovery experiments with aliphatic and aromatic standards showed extraction efficiency to be approximately 70%.

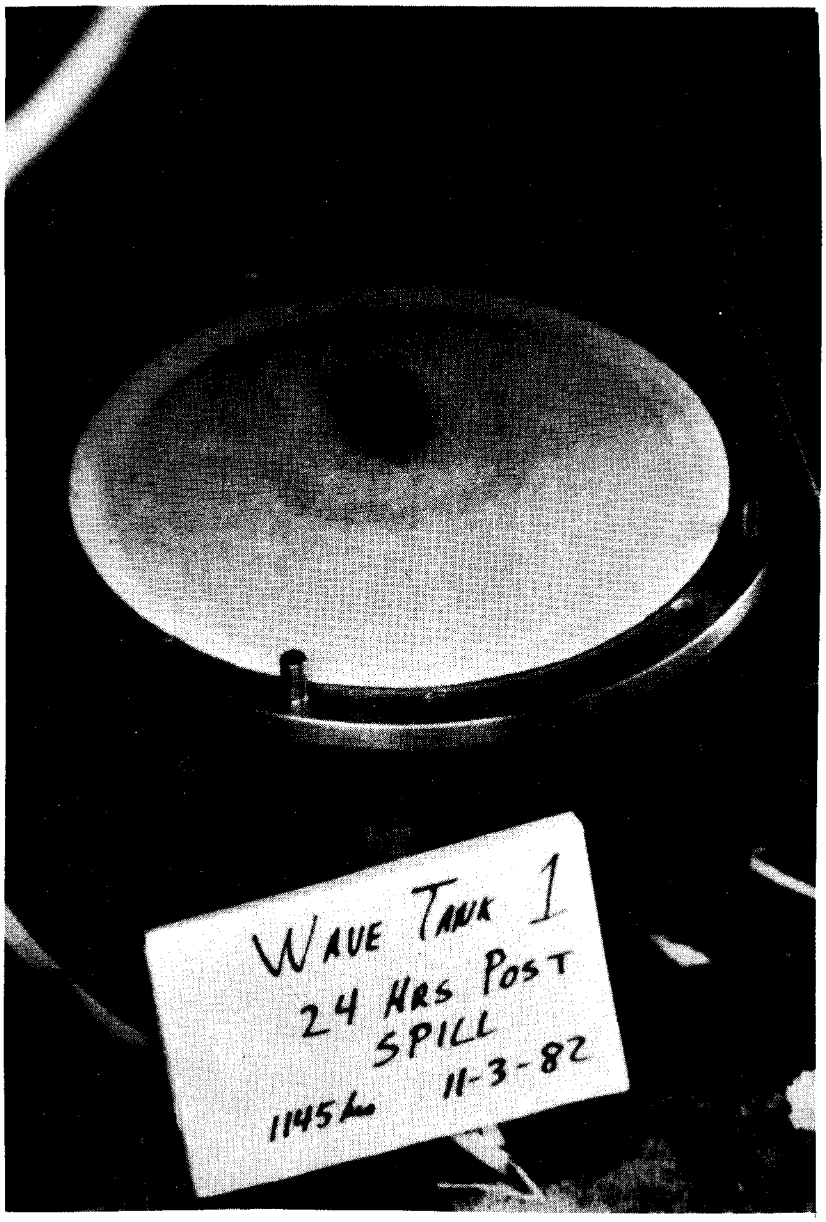

Figure 5-63. Closeup of suspended particulate material isolated for hydrocarbon analyses from wave tank 1, 24 hours after initiation of the spill.

The filter extracts were then reduced in volume by KD evaporation followed by passing a stream of N_2 over the sample until the desired PIV was obtained. The extracts were then transferred to crimp top vials for analysis by FID-GC.

5.4.6 Observations from Kasitsna Bay Wave Tank Oil Weathering Experiments and Oil Physical Properties Determinations

The first wave-tank oil weathering experiments were initiated in triplicate in July 1982. In monitoring oil weathering behavior during the summer of 1982, essentially identical changes were observed in all three tanks. After four months of ambient weathering, some differences were noted in the tanks, and these will be considered later in this section. In the following discussion, however, the appearance of the slick in wave tank 1 only will be considered as it was representative of what was observed in each of the tanks during the initial 4 month weathering period. At the initiation of the spill the air temperature was 55°F (13°C) and the water temperature was 11°C. During the first 12 days of the experiment the air temperature remained fairly constant during the day, and daylight extended from approximately 0400 hours to 2200 hours. Oil subsamples were obtained immediately before each spill, and then chemical and rheological properties determinations were completed as a function of time as described earlier.

Figure 5-64 shows the wave turbulence at time zero before initiation of the spill. With the paddle wheel and wave tank configuration as described in the previous section, four to six inch standing waves and breaking wave turbulence due to backwash at the end of the tank were established. Prior to initiation of any oil/wave tank experiments, the seawater system and tanks were allowed to flush for two weeks with paddle wheel turbulence, and seawater blanks analyzed before initiation of oil weathering experiments showed no evidence of significant levels of phthalates, plasticizers or other petroleum like components.

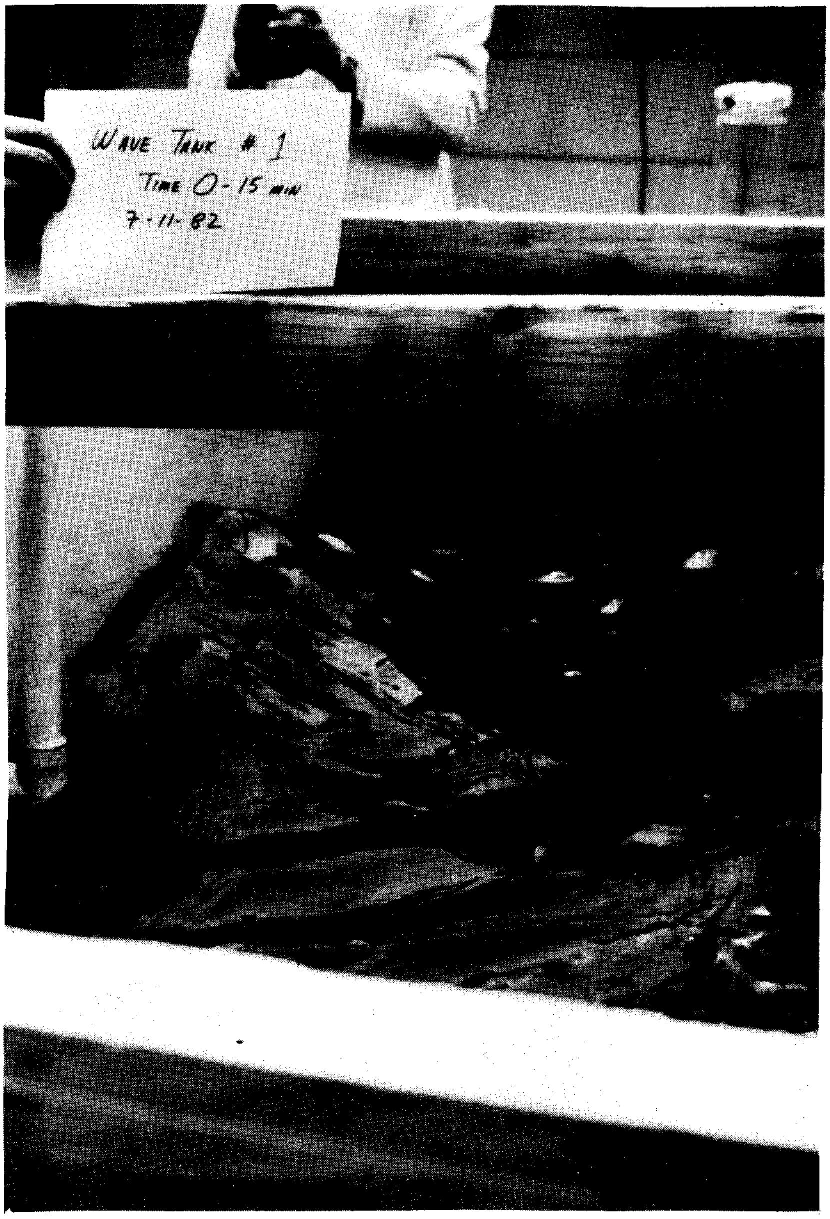

Figure 5-64. Time zero wave turbulence in wave tank 1 before initiation of a 16 liter spill of fresh Prudhoe Bay crude oil in July 1982.

The spill in Wave Tank 1 was initiated by addition of 16 l of fresh Prudhoe Bay crude oil on July 11, 1982 (Figure 5-65). Figure 5-66 shows the appearance of the oil slick five minutes after the initiation of the spill. Sheen can be seen eminating from the edge of the surface oil/open water interface, and the oil was noted to immediately stain the sides of the wave tank. After approximately 15 minutes the oil was effectively corraled toward the end of the tank, and an irregular discontinuity between the surface oil and open water was observed to migrate from as far as two meters to as close as one meter to the paddle wheel generating the wave turbulence. Sea state estimates indicated the wave turbulence was similar to that which might be expected from a 2 knot wind. Tables 5-8 and 5-9 and Figure 5-67 present oil/water and oil/air interfacial surface tensions and other physical properties data from the oil measured during the wave tank experiments.

Approximately eight hours into the spill, the oil viscosity had increased from approximately 30 to 100 centipoise as measured in a 38°C constant temperature bath housed within the main laboratory. With this increasing viscosity and approximately 0.1 percent water content, the oil took on a stiffer appearance and dispersion of oil droplets into the water was noted to be slightly reduced (Figure 5-68). Figure 5-69 presents the oil after 24 hours of initital weathering. At this time the 38° constant temperature viscosity had increased to 360 centipoise, and the density had increased from 0.885 to 0.953 g/ml. Water content at this time was determined to be 18%. Significant bubble formation from air entrapment or degasing of low molecular weight hydrocarbons was noted in all of the slicks during these and other flow through oil weathering experiments where turbulence was induced by electric stirs (Figures 5-69 and 5-70).

After three days the oil viscosity was approaching 1000 centipose and water content in the water-in-oil emulsion was nearing 34%. At that time significant color alterations were noted in the slick, and the oil was thick enough to allow water droplets to accumulate on top of the oil surface due to breaking wave turbulence (Figure 5-71). After nine days (Figure 5-72) the oil

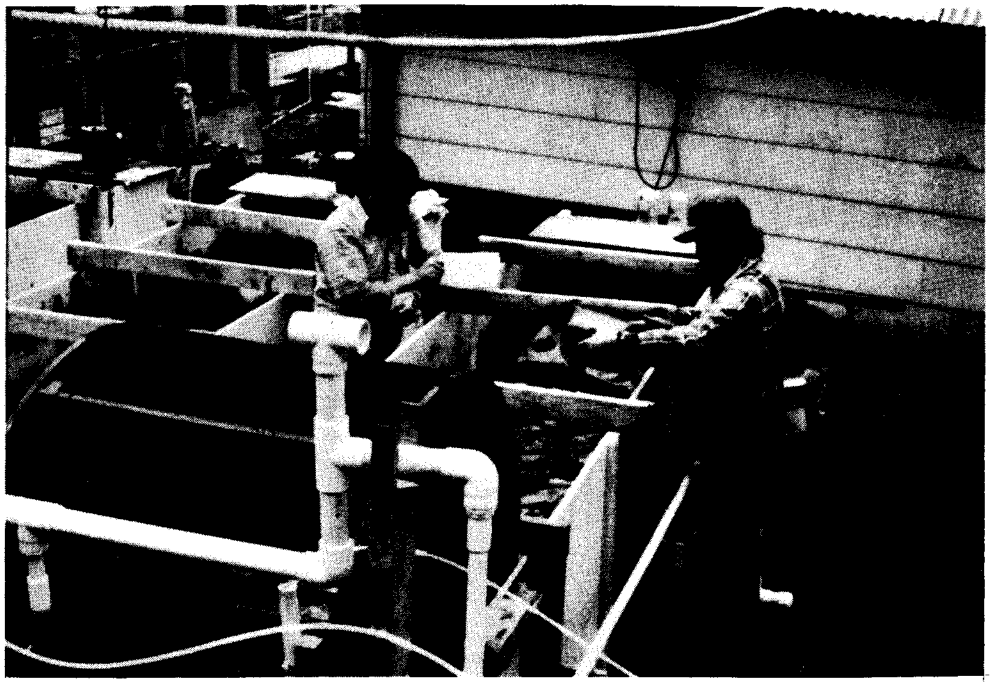

Figure 5-65. Wave tank 1 spill initiation, July 11, 1982.

Figure 5-66. Appearance of surface oil five minutes after the initiation of a spill of fresh Prudhoe Bay crude oil. Note: 4 to 6 inch standing wave appearance for height magnitude and lack of clearly defined surface oil/open water discontinuity.

Table 5-8. Water/Oil and Oil/Air Interfacial Tensions (dynes/cm) from Wave Tanks #1-3

	Time 0 Ave/SD[a]	1 hour Ave/SD	2 hours Ave/SD	12 hours Ave/SD	24 hours Ave/SD	2 days Ave/SD	6 days Ave/SD	9 days Ave/SD	12 days Ave/SD	4 months Ave/SD	9 months Ave/SD
Water/Oil	27.3	25.4/4.1	22.2/6.1	21.5/3.8	21.9/.60	15.4/3.0	14.4/2.4	12.7/1.9	11.9/.75	12.7/1.6	13.3/.92
Oil/Air	34.3	33.5/.42	33.8/.50	33.5/1.6	33.4/1.5	33.3/1.6	34.8/1.5	34.9/1.3	35.6/.30	37.8/.10	38.3/.07

a - Ave indicates the average value and SD indicates the standard deviation

Table 5-9. Physical Properties of Oil from Wave Tanks #1-4

	Time 0 Ave/SD[a]	4 hours Ave/SD	8 hours Ave/SD	12 hours Ave/SD	24 hours Ave/SD	2 days Ave/SD	6 days Ave/SD	9 days Ave/SD	12 days Ave/SD	4 months Ave/SD	9 months Ave/SD	12 months Ave/SD
Density (g/ml)	.885	.930/.008	.932/.017	.942/.010	.953/.006	.931/.029	.926/.018	.928	.932/.032	.986/.007	.987/.006	.986/.005
Water Content (%)	.054/.025	.15 -	.093 -	.22/.09	18.0/8.0	34.0/14.0	50.0/9.8	51.0/4.4	55.0/2.9	54.9/4.9	na[b]	na
Viscosity(dPas.s) @38°C	.30/.001	.55/.33	1.0/.60	1.6/.80	3.6/2.2	9.2/1.6	22.7/1.2	31.7/2.1	34.3/8.3	16,000/290	28,000/500	nd[c]

a - Ave indicates the average value and SD indicates the standard deviation

b - na indicates "not analyzed"

c - nd indicates "not determinable" due to the nonhomogeneity of the sample

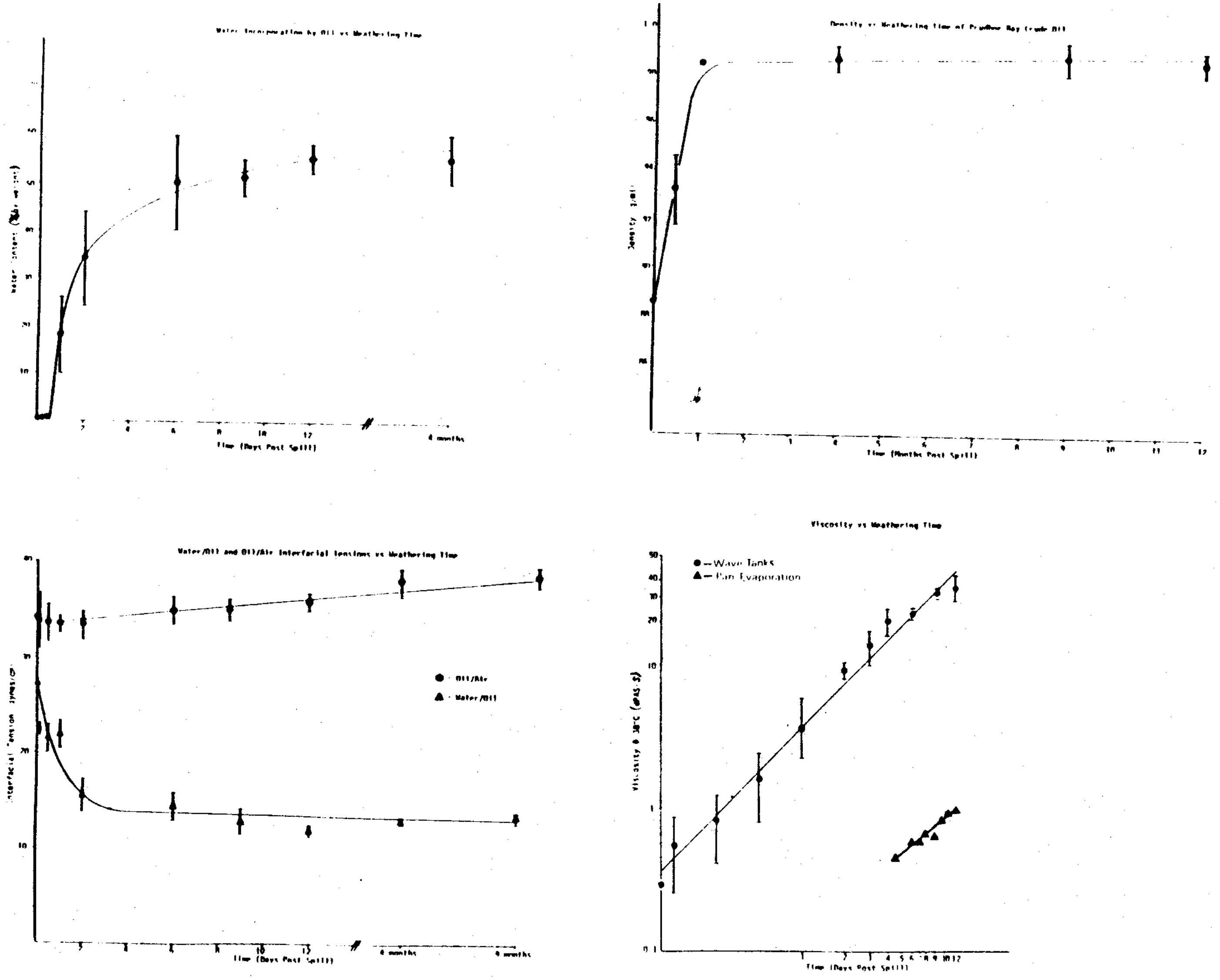

Figure 5-67. Physical properties data on Prudhoe Bay crude oil weathering in flow through Wave Tanks. Values are means from threetanks ± one standard deviation.

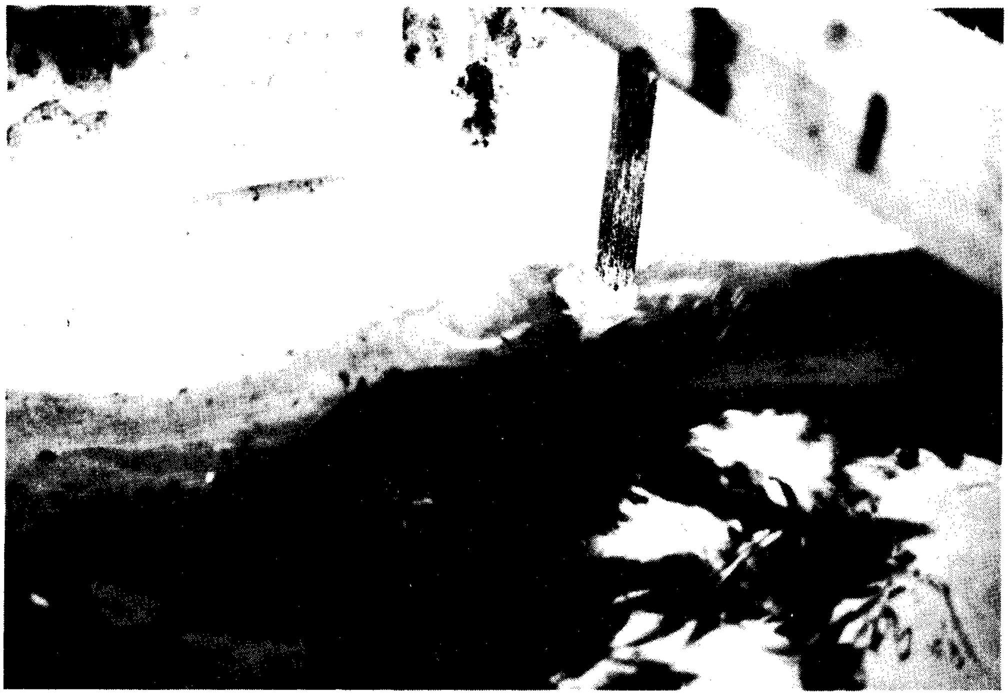

Figure 5-68. Appearance of the surface oil eight hours after the initiation of fresh Prudhoe Bay crude oil spill in wave tank 1 (7/11/82). The surface oil/open water discontinuity is becoming more defined although patches of oil were still noted to break away from the leading edge of the slick and approach the paddle wheel to within a distance of 0.7 meters.

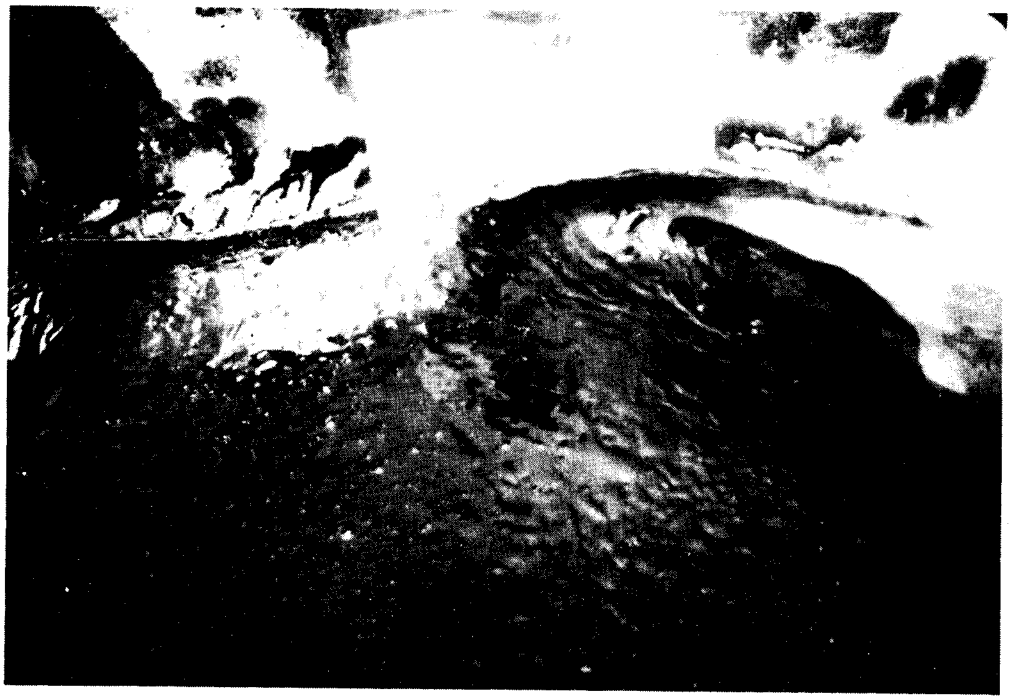

Figure 5-69. Appearance of the surface oil in wave tank 1 twenty-four hours after the spill. The surface oil/open water discontinuity is becoming well defined and significant quantities of air bubbles are noted in the surface slick.

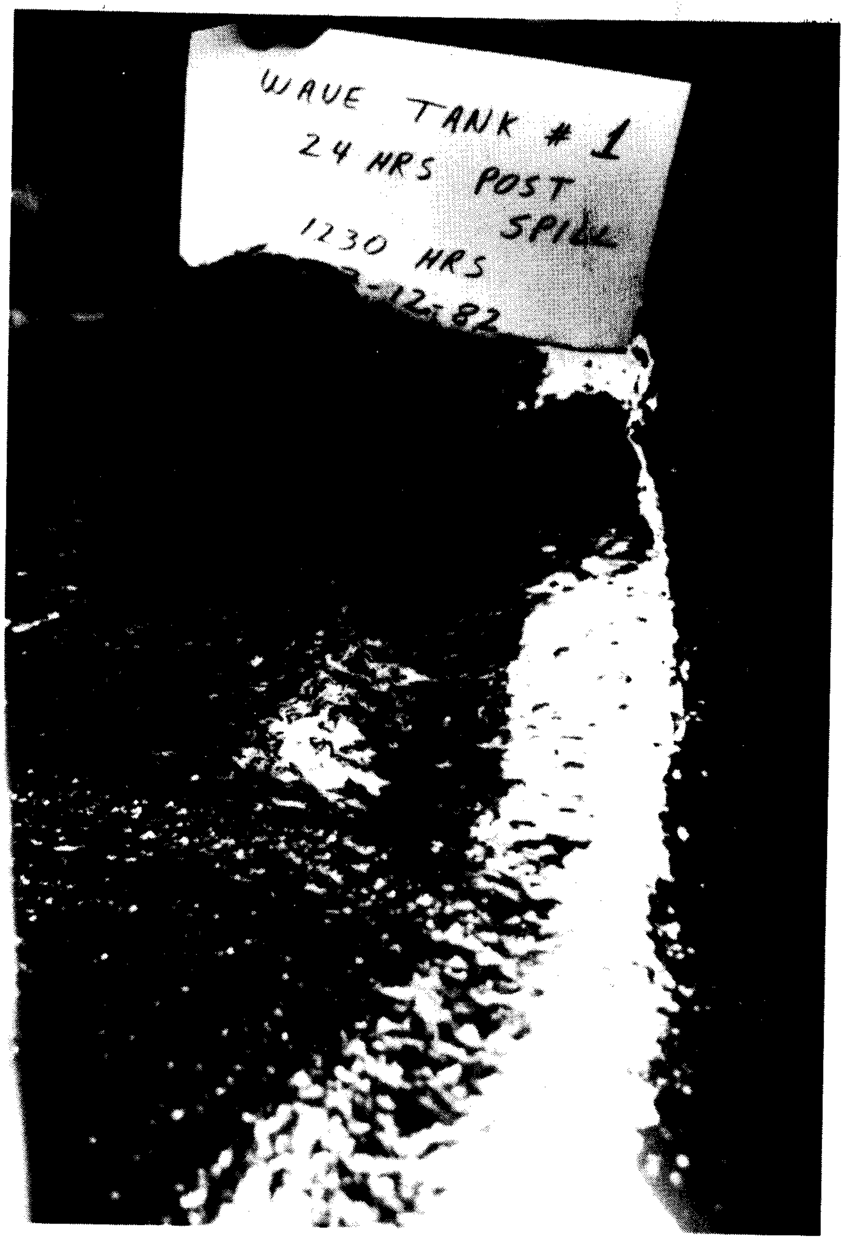

Figure 5-70. Closeup of thick surface slick at the quiescent end of the wave tank twenty-four hours post spill. Significant quantities of entrapped air are observed as bubbles cover the entire slick surface.

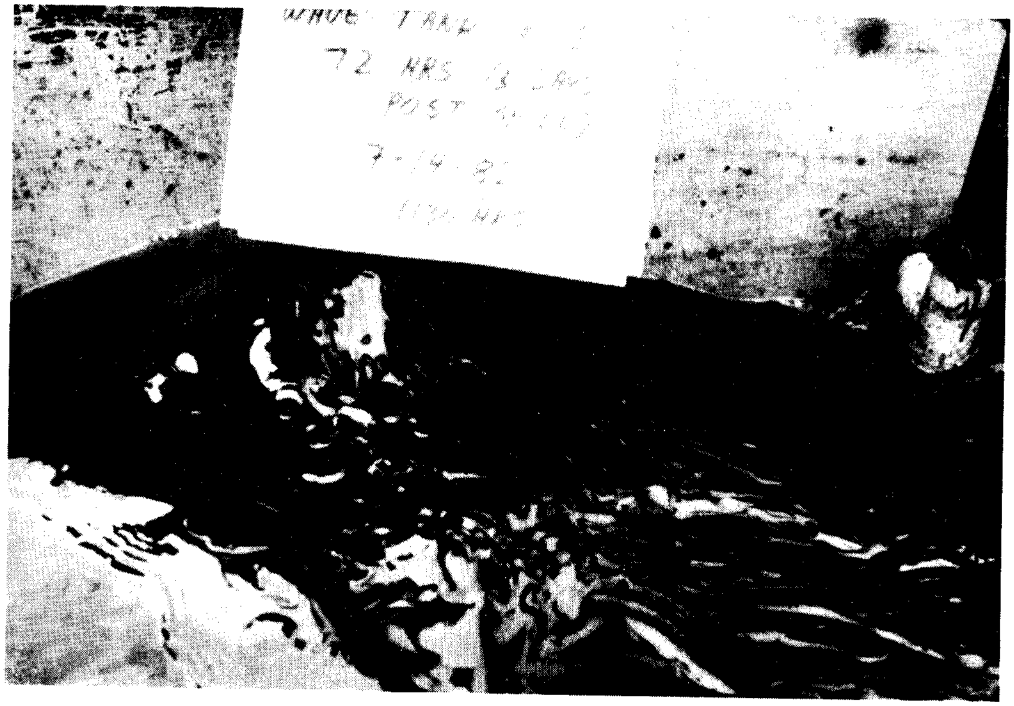

Figure 5-71. Surface oil 72 hours post spill. The viscosity has increased, allowing water droplets to stand on the surface oil for periods of up to 30 seconds before penetrating.

Figure 5-72. Appearance of the surface oil slick nine days post spill. A distinct surface oil/open water discontinuity can be observed along with a silver sheen emanating from the discontinuity. The oil at this time began to form a mosaic pattern with leads which opened and closed during each passing wave.

was observed to open and close in a mosaic pattern with the passing of each wave, and water content was observed to reach 51% in the water-in-oil emulsion. The constant temperature viscosity at 38° had increased to 3200 centipoise. After 12 days (Figures 5-73 and 5-74) the oil had turned a lighter brown, and significant leads were observed to open and close with each passing wave. During this entire weathering period a colored sheen was noted eminating from the leading edge of the slick, and this sheen continued to be observed for several months.

After the initial 12 days of the experiment, the wave tanks were allowed to run continuously until the laboratory was reoccupied in November 1982, approximately four months after the initiation of the spills. At that time the appearance of the oil in all three tanks was identical, as exemplified by the photographs in Figures 5-75, and 5-76. During the November field study, the air temperature was quite cold (generally between 0 and -5°C) and the water temperature was 3.5°C during all observations. At this time the oil was observed to have broken into discreet tarballs ranging in size from one to two cm to upwards of 10 cm in diameter. As shown in Figure 5-75 and 5-76, the tarballs had a saucer like appearance with a rounded center and flat saucer like ring around the center dome. Examination of the underside of these tarballs showed them to be smooth or bowl shaped such that it appeared that the tarballs were initially formed as small spherical objects with growth then attributed to bumping against one another and/or smaller floating oil patches. After four months the water content in the water-in-oil emulsion was still constant at approximately 55%, although the density of the water-in-oil emulsion had increased to 0.99 g/ml. The constant temperature (38°) viscosity was 1.6 million centipoise.

During the fall/winter field program, the experiment in wave tank 1 was terminated, and the tank was cleaned for initiation of a winter spill which will be discussed in the following section. The remaining two tanks (2 and 3) were allowed to continue to run however, and in March 1983, the laboratory was reoccupied and measurements were obtained on the oil and water in

Figure 5-73. Surface oil/open water discontinuity 12 days post spill. Note the sheen emanating from the oil surface and the mosaic pattern in the background of the figure.

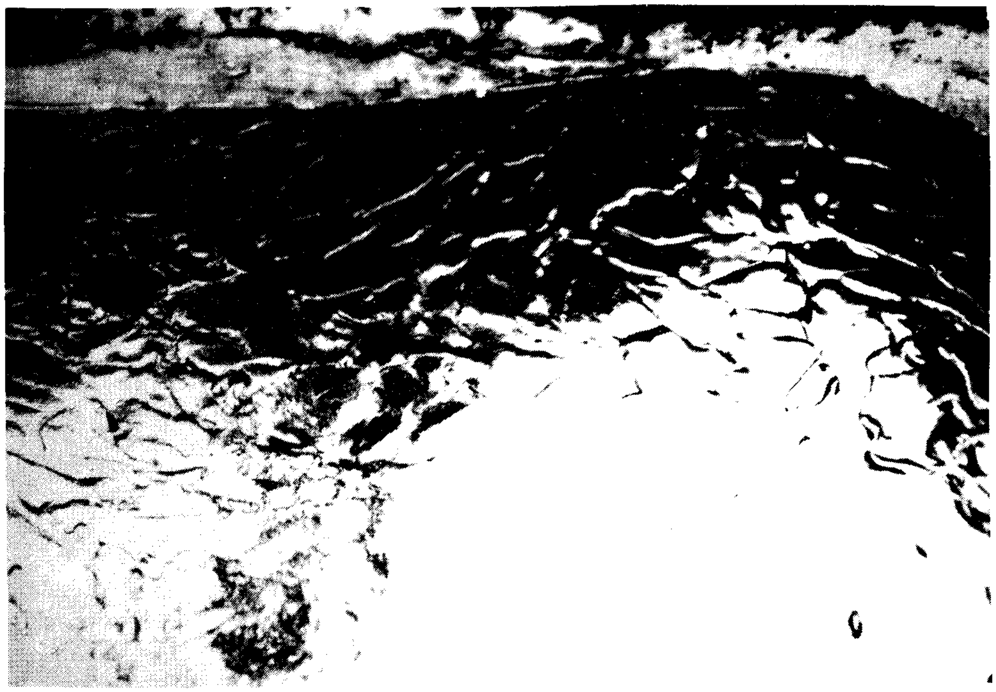

Figure 5-74. Mosaic pattern of oil patches at the quiescent end of the wave tank 12 days post spill.

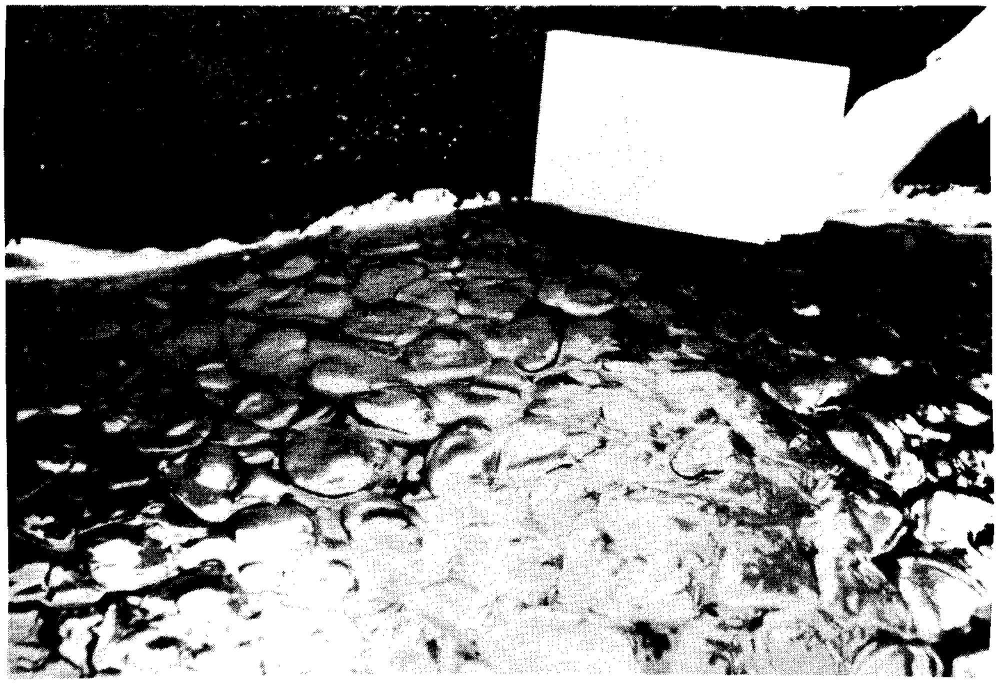

Figure 5-75. Appearance of tarballs in wave tank 2, approximately four months post spill. At this time wave tanks 1, 2, and 3 all exhibited similar tarball formation with the larger tarballs being surrounded by a Saturn-like ring suggesting the adherence of oil to the central site of nucleation during tarball growth.

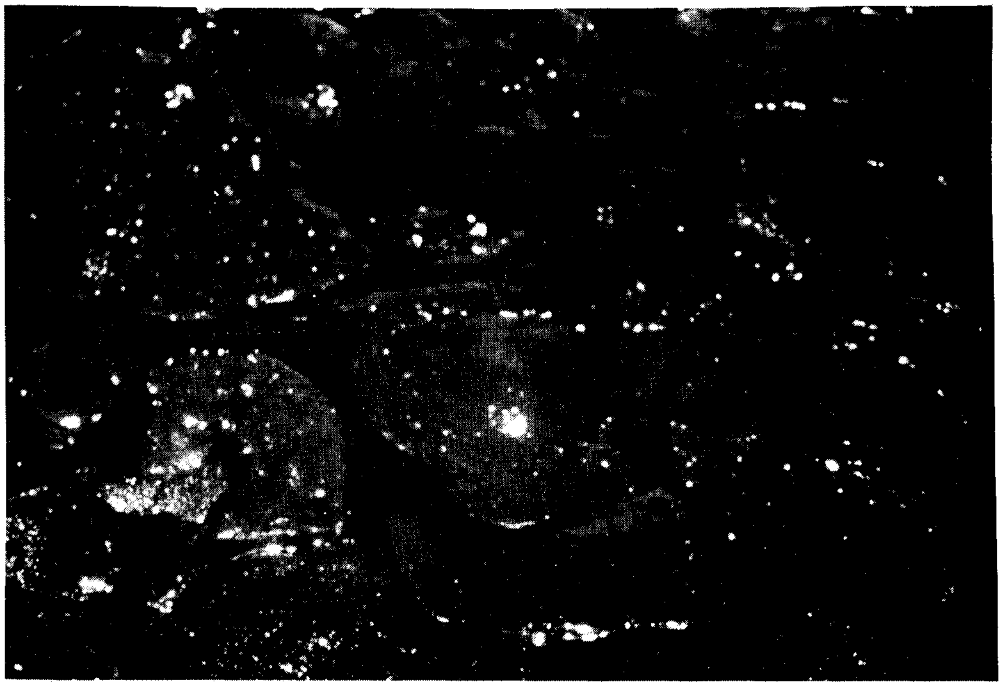

Figure 5-76. Closeup of tarballs in wave tank 1 at four months post spill.

tanks 2 and 3 after 8.5 months of ambient subarctic weathering. During March 1983, the ambient temperature was still quite cold (10°C) and there was considerable snow covering the area (Figure 5-77). After 8.5 months of weathering several significant differences were noted in the oil behavior in wave tanks 2 and 3. Wave tank 2 was characterized by discreet tarballs ranging in size from four to 10 cm (Figures 5-78 and 5-79) with only a slight amount of floating oil or flakes of oil-like material observed adjacent to the major oil tarballs. In tank 3 however, the tarballs were surrounded by a significant amount of a syrupy oil mat (Figures 5-80 and 5-81) which showed considerable evidence of microbial degradation after analysis by capillary flame ionization gas chromatography, as discussed in the following sections (5.4.7 and 7.0). At the nine month point in oil weathering, the density and percent water content of the water-in-oil emulsion (or mousse) generating the tarballs had not significantly changed from the four month values; however, the constant temperature (38°) viscosity had increased to 2.8 million centipoise. Interestingly, when tarballs were removed from the tank as shown by Figures 5-82 through 5-85, the tertiary structure of the tarballs was observed to be destroyed after approximately one hour, and the mousse appeared to melt into a continuous mass. No significant separation of oil and water was observed, however, even after standing at 38°C for over 24 hours.

Twelve months after initiation of the original spills in wave tanks 2 and 3, the Kasitsna Bay Laboratory was reoccupied, and additional measurements were made. Figure 5-86 shows an overview of the tanks at this time, and significant differences in the amount of oil present in wave tanks 2 and 3 can be observed. Substantial amounts of oil-covered algae were present in wave tank 2 (Figure 5-87), and these appeared as darker patches in the syrupy oil mat which still covered ~40-50 percent of the tank (Figure 5-88). No significant amount of visible sheen was observed at the surface oil/open water discontinuity (Figure 5-89), and the oil itself appeared to be extremely well weathered (as later determined by capillary gas chromatography). Darker patches were observed in the oil (Figures 5-87 and 5-90), and analysis of this material showed it to be primarily algae which had presumably been introduced by the

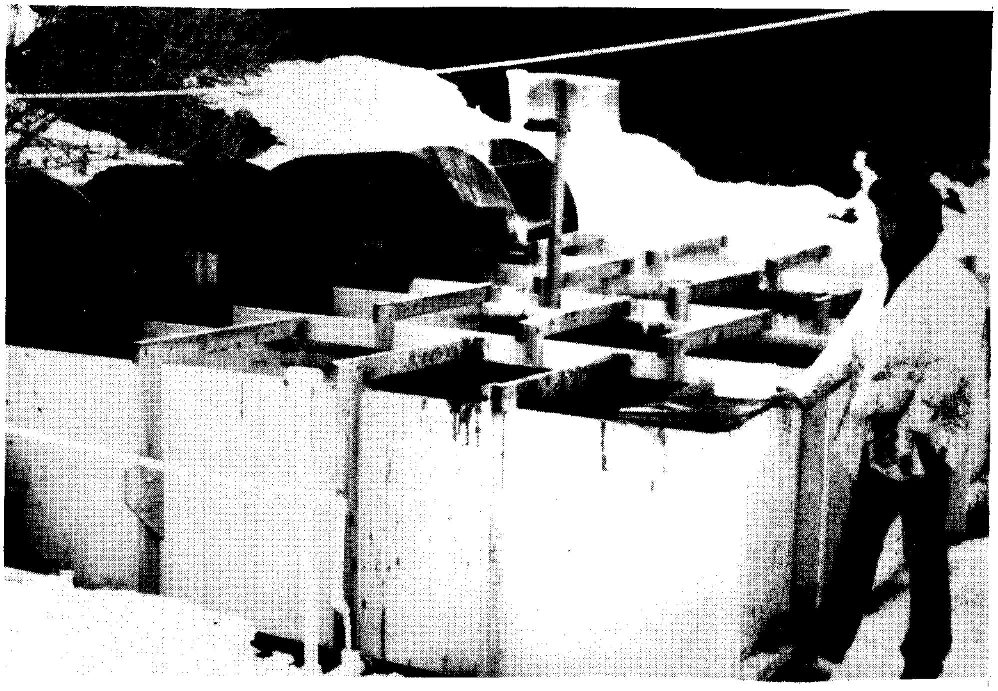

Figure 5-77. Overview of the wave tank systems in March, 1983.

Figure 5-78. Closeup of tarballs at the quiescent end of wave tank 2, 8.5 months post spill. Note the 5-10 millimeter size flakes adjacent to the larger balls.

Figure 5-79. Overview of wave tank 2, 8.5 months after spill initiation. Note the appearance of oil flakes sloughing at the main tarball surfaces and the lack of attached oil rings surrounding each tarball.

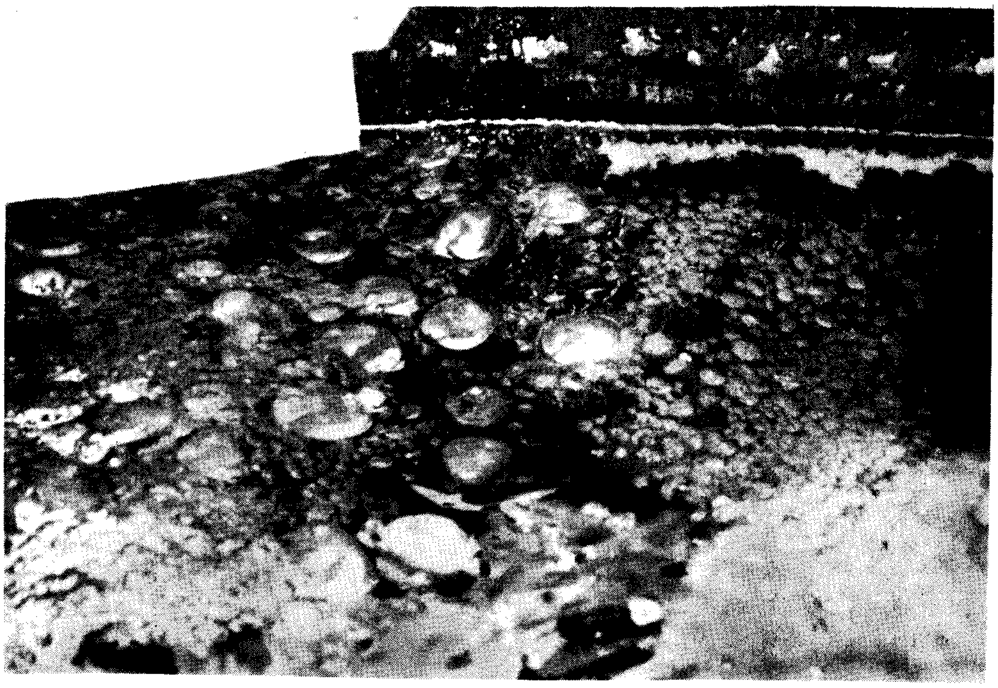

Figure 5-80. Tarballs and 1-2 cm flakes of more heavily weathered and microbially degraded oil in wave tank 3,.8.5 months post spill.

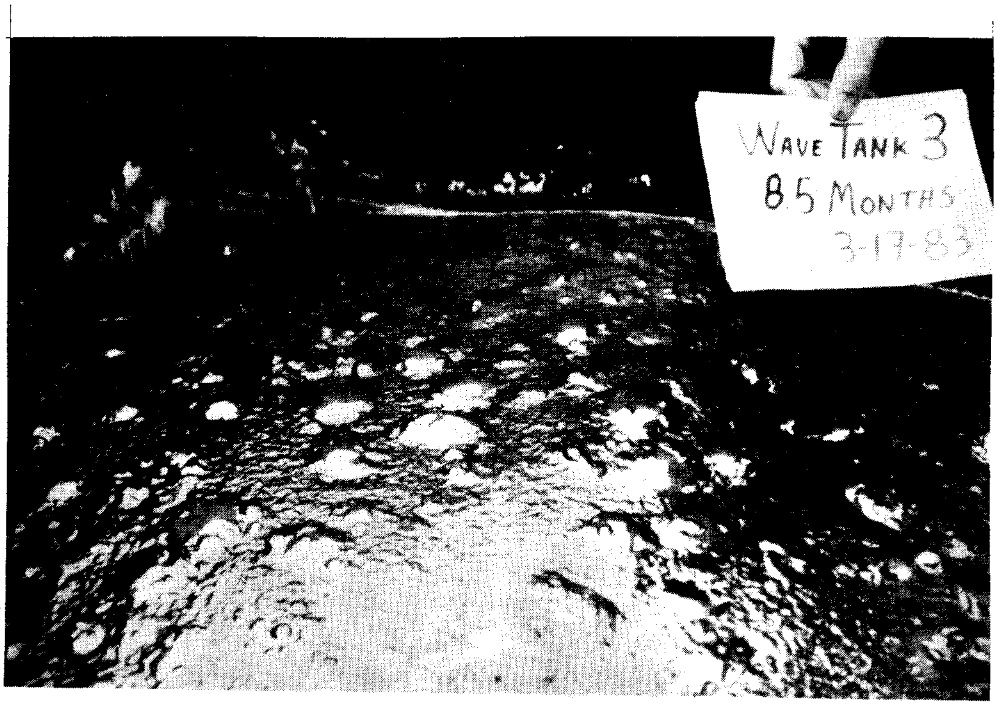

Figure 5-81. Appearance of the tarballs and oil/water sauce mixture surrounding tarballs at the quiescent end of wave tank 3, 8.5 months post spill.

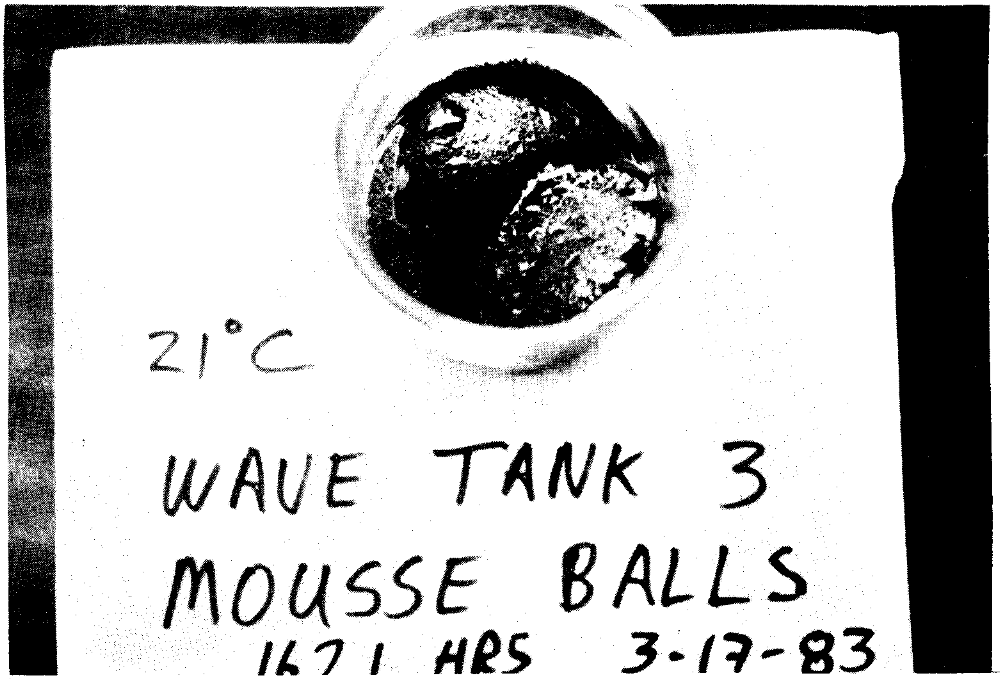

Figure 5-82. Observations of the behavior of tarballs isolated from wave tank 3 in March, 1983.

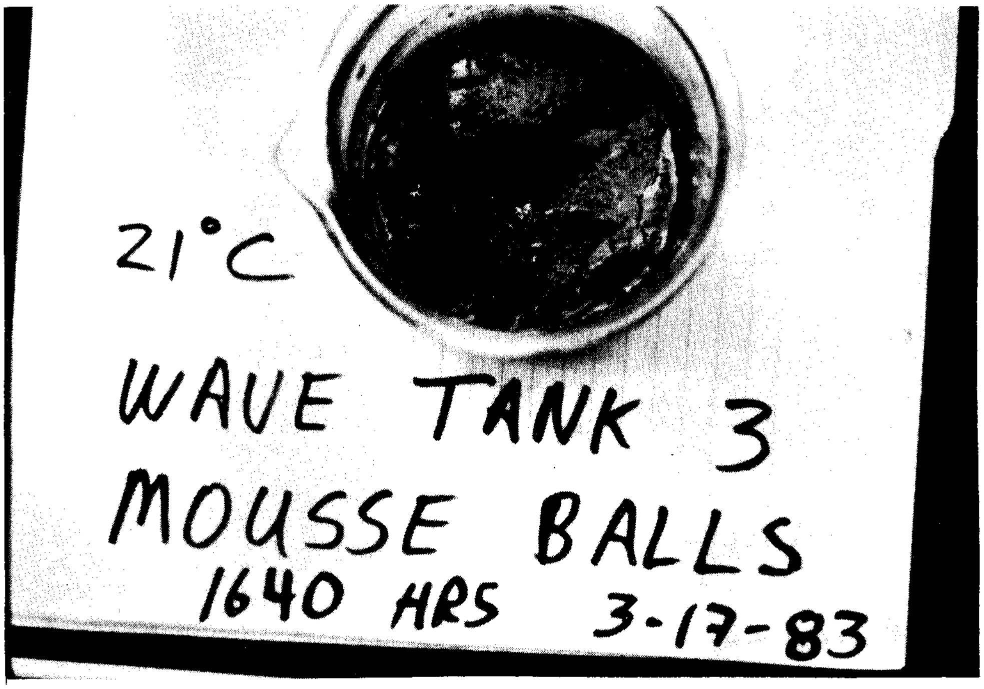

Figure 5-83. Significant thawing is noted over a 30-minute period.

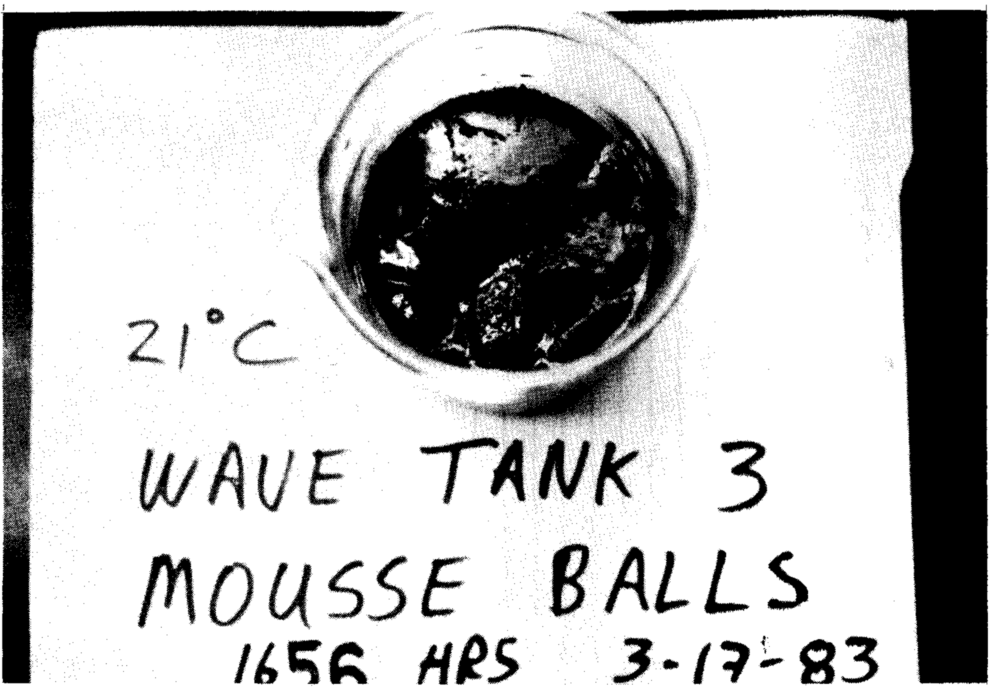

Figure 5-84. Thawing of tarballs at 21°C from wave tank 3 approximately 40 minutes after collection.

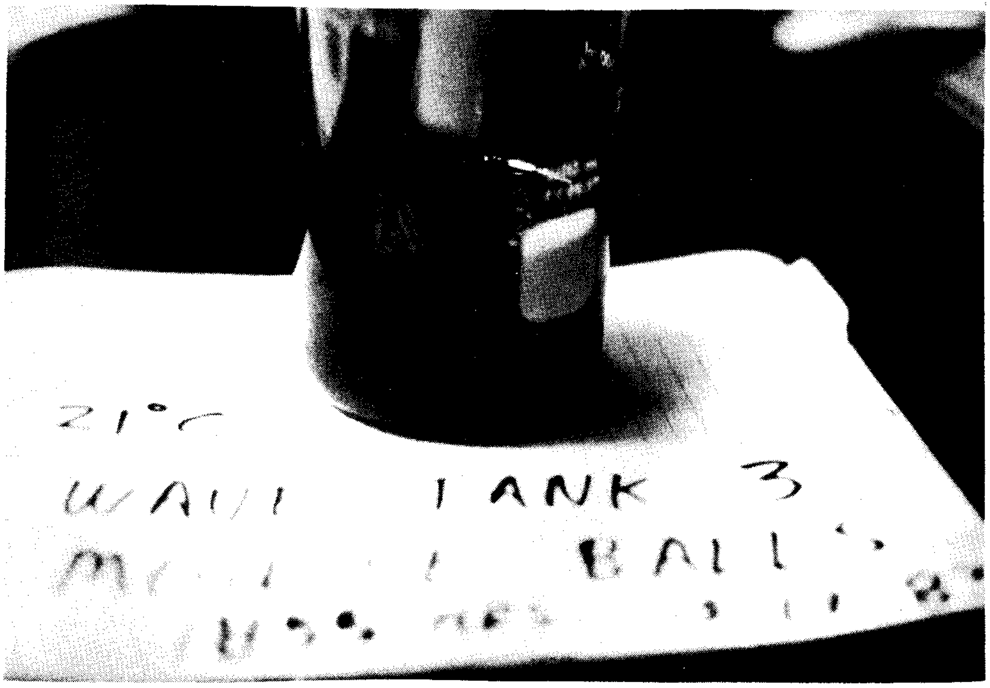

Figure 5-85. Tarballs approximately two hours after collection that had melted to form a continuous water-in-oil emulsion. No oil/water separation was noted; however, the physical structure of the tarball is clearly temperature controlled.

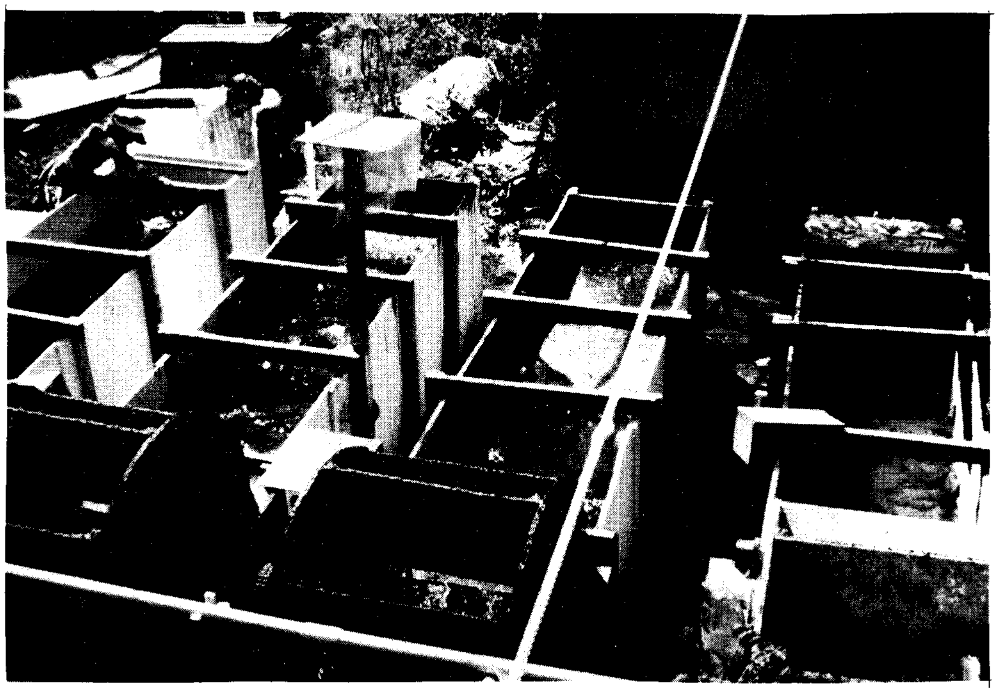

Figure 5-86. Overview of the wave tank system, 13 months after spill initiation. Significant differences in the amount of surface oil remaining can be observed in wave tanks 2 and 3. The wave tank 1 experiment had been terminated at the time of this photograph.

Figure 5-87. Closeup of oil entrained algae from wave tank 2, 13 months post spill.

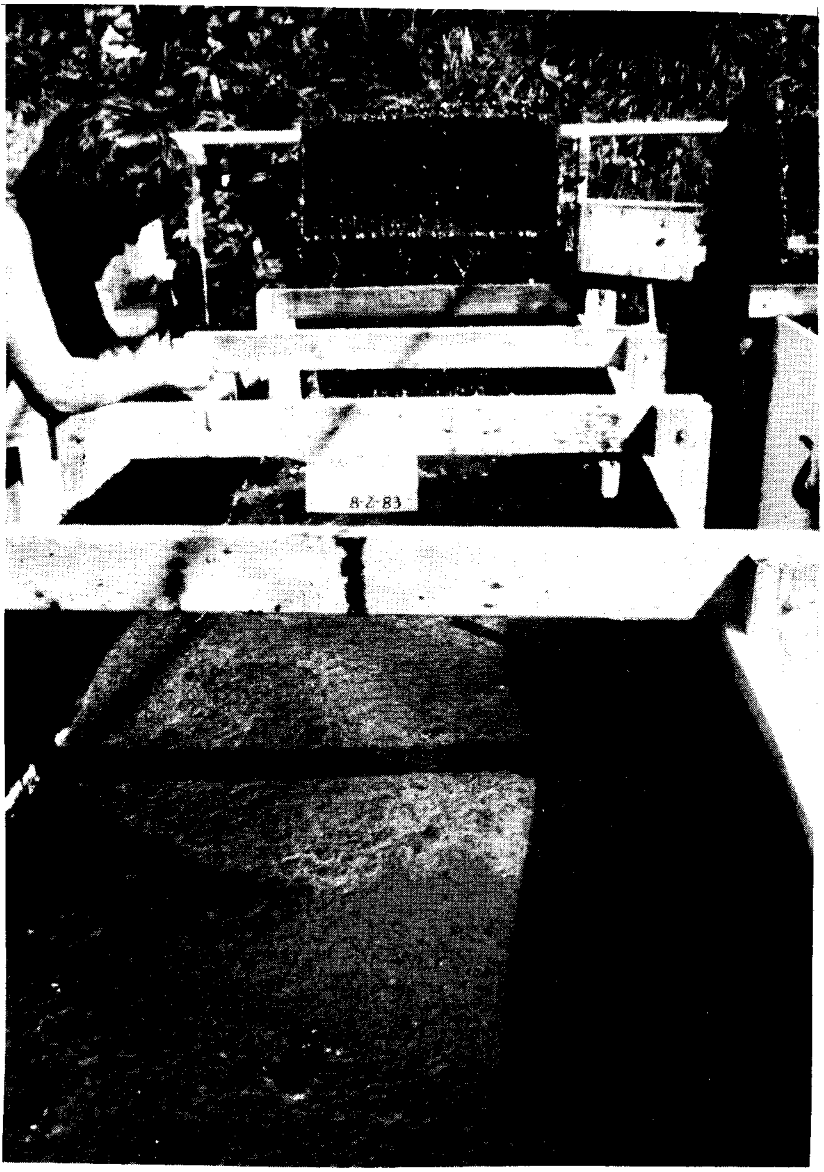

Figure 5-88. Appearance of the surface oil mat and algae in wave tank 2, 13 months after spill initiation. Note the significant absence of tarballs observed during the winter period and the continuous mat of heavily degraded oil.

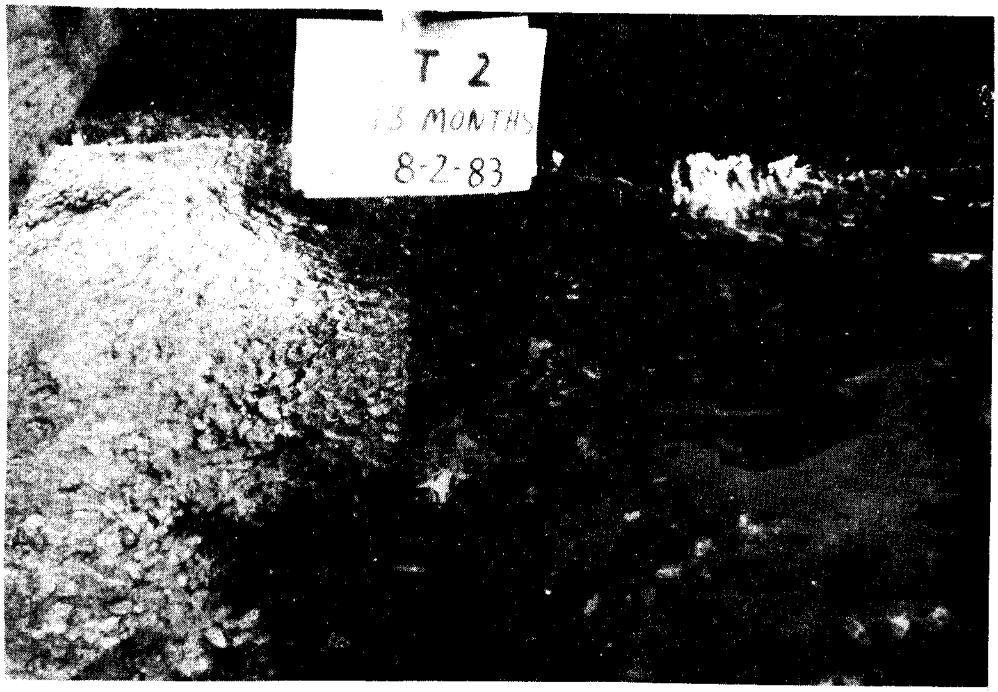

Figure 5-89. Surface oil mat/open water discontinuity in wave tank 2, 13 months post spill. The oil is characterized as discreet 1-2 cm flakes and oil droplets and significant sheen is no longer observed emanating from the material.

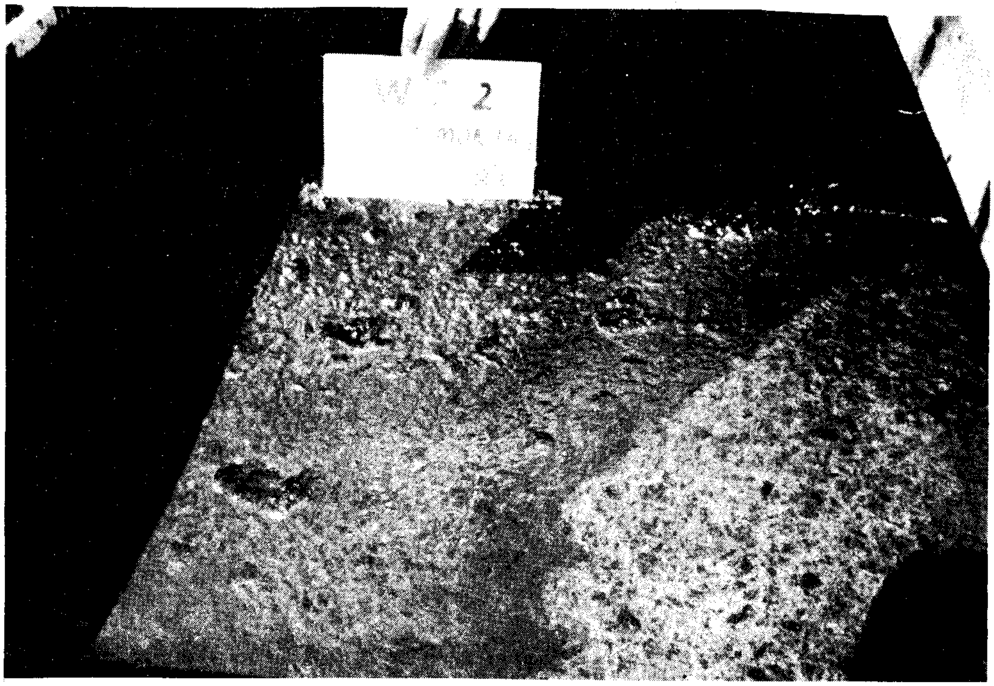

Figure 5-90. Closeup of the quiescent end of wave tank 2, 13 months post spill. Darker patches were found to be algae.

constant inflow of seawater or released from the algae growing on the tank sides and the paddle wheel. Wave tank 3, after 13 months of ambient weathering, showed significantly less oil, and what did remain, appeared to be discreet tarballs as shown in Figures 5-91 through 5-94. Note the appearance of significant amounts of green algae and other debris in the tank in addition to the 2-3 mm sized tarballs themselves. Viscosity measurements could not be obtained at this time due to limitations of the viscomiter and the fact that incorporation of water and air pockets (micelle) had rendered the sample to a non-Newtonian fluid (Figure 5-95). On standing in the sunlight, however, the tarballs were again observed to "melt" and flow readily.

WINTER SEASON WAVE TANK EXPERIMENTS

This section presents observations of oil weathering behavior during the spill initiated under winter conditions (air temperature -1 to -5°C, water temperature 3.5°C). As noted earlier, the wave tank 1 experiment initiated during July 1982 was terminated in November, and after cleaning the tank, a new spill herein designated as wave tank 4 was initiated on November 2, 1982. Note that in the following figures the notation Wave Tank 1 is used, as the tanks were numbered sequentially during construction. For discussion purposes, however, wave tank experiment 4 should be considered as the winter experiment.

The air temperature at the initiation of the spill was -2°C, and several significant differences were noted in comparison with the oil behavior during the warmer summer months. Initial dispersed oil concentrations were observed to rise during the first eight hours; however, the significantly higher viscosity of the oil inhibited dispersion of larger (cm sized) oil droplets. Viscosity increases to upwards of 2200 centipoise were noted after as little as eight hours and the formation of colored sheen appeared to be inhibited somewhat under the colder conditions (Figures 5-96 to 5-98). Twenty four hours post spill, a very clear discontinuity between the surface oil and open water phases could be noted as shown in Figure 5-99. The discontinuity was even more pronounced forty-eight hours after the spill (Figure 5-100).

Figure 5-91. Overview of wave tank 3, 13 months post spill. Most of the oil in this tank was removed at this point, and the oil was characterized as 10-20 cm tarballs with significant amounts of algae and a white, foamy material.

Figure 5-92. Closeup side view of tarballs and white, foamy degradation material and algae at the quiescent end of wave tank 3, 13 months after spill initiation.

Figure 5-93. Fifteen centimeter tarball isolated from wave tank 3.

Figure 5-94. Closeup of a tarball surrounded by algae in wave tank 3, 13 months post spill.

Figure 5-95. Closeup of a tarball from wave tank 3, 13 months post spill showing encapsulated air pockets and initiation of "melting" behavior during warming on surface plate.

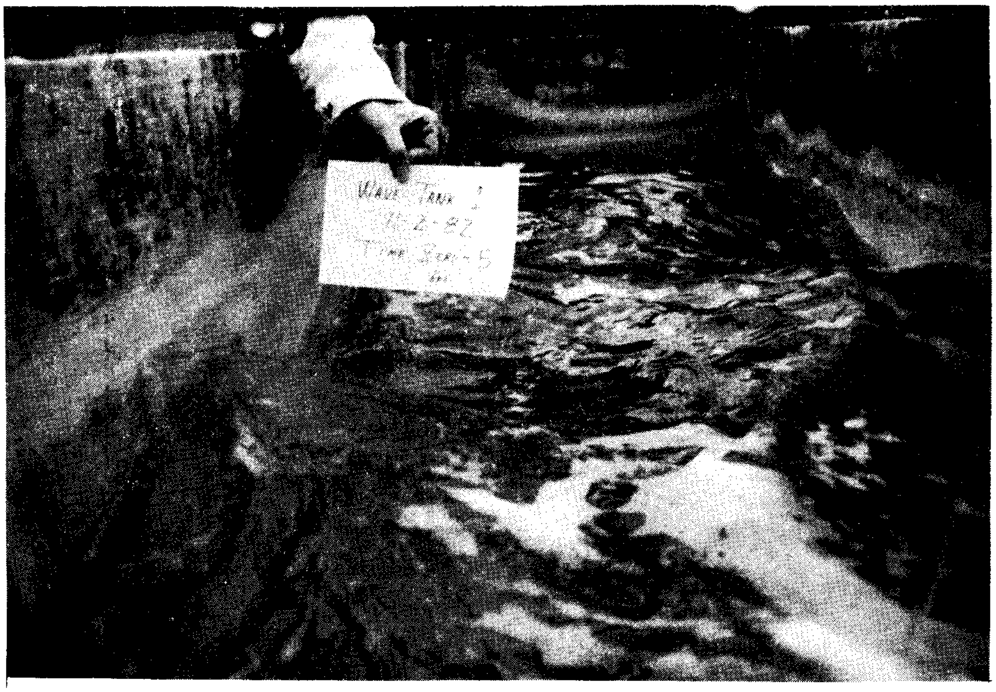

Figure 5-96. Initiation of the winter wave tank spill #4 in wave tank 1 in November, 1982. Wave tank turbulence before spill initiation.

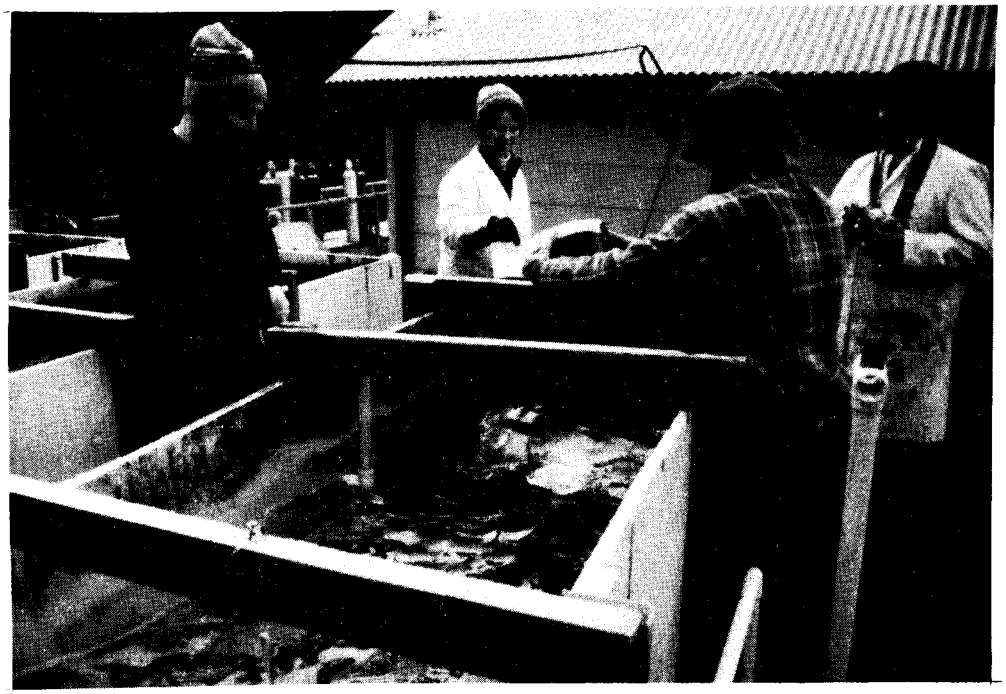

Figure 5-97. Addition of 16.0 l of Prudhoe Bay crude oil during spill initiation.

Figure 5-98. Appearance of the winter-spill surface slick five minutes post spill. A significantly greater discontinuity between the surface oil and open water was observed during the winter spill conditions compared to the summer spill conditions observed in July, 1982.

Figure 5-99. Surface oil/open water discontinuity 24 hours post spill.

Figure 5-100. Surface oil/open water discontinuity from winter wave tank spill experiment 4 (Wave tank 1) 48 hours post spill.

The oil viscosity four days into the spill was observed to be approximately 9000 centipoise, and water column dispersed and dissolved oil concentrations were observed to be significantly less than those observed during the summer period.

When the laboratory was reoccupied in March 1983, the oil in wave tank 1 had been undergoing open ocean subarctic weathering under winter conditions for 4.5 months. At that time, interestingly, there was no evidence of the discreet tarball formation as observed during the summer/fall weathering period Figures 5-101 and 5-102). More detailed analyses of the tarballs remaining in wave tanks 2 and 3 showed that many of them had formed around sites of nucleation such as leaves or other debris which may have blown into the tank in the fall. A similar nucleation phenomona was observed during the IXTOC I blowout in the Gulf of Mexico (PAYNE, 1981) where significant portions of mousse aggregates were noted to accumulate on sugar cane stock or other debris present at the time of that spill. Interestingly, Figure 5-103 shows significant amounts of silver and lightly colored sheen still eminating from the water-in-oil emulsion in wave tank 1 after 4.5 months, and the quiescient end of tank was characterized by a thick mat-like oil coating which was not subject to significant turbulence or mixing.

Under these conditions, it is quite probable that loss of materials in the oil due to either evaporation or dissolution would be diffusion controlled, thus contributing to their longer lifetime in the slick. As the ambient temperature started to increase in the spring, these materials were then slowly released causing the observed sheen long after it had disappeared in the summer spills after a similar time period. The lower temperature which concomitantly increases viscosity would also inhibit the more significant dispersion of cm sized whole oil droplets as noted during the summer period. These observations will be discussed further in the following sections wherein oil weathering model verification is undertaken using the observed chemical and rheological (physical) properties data and measurements of dispersed oil concentrations in the water in the four experimental systems.

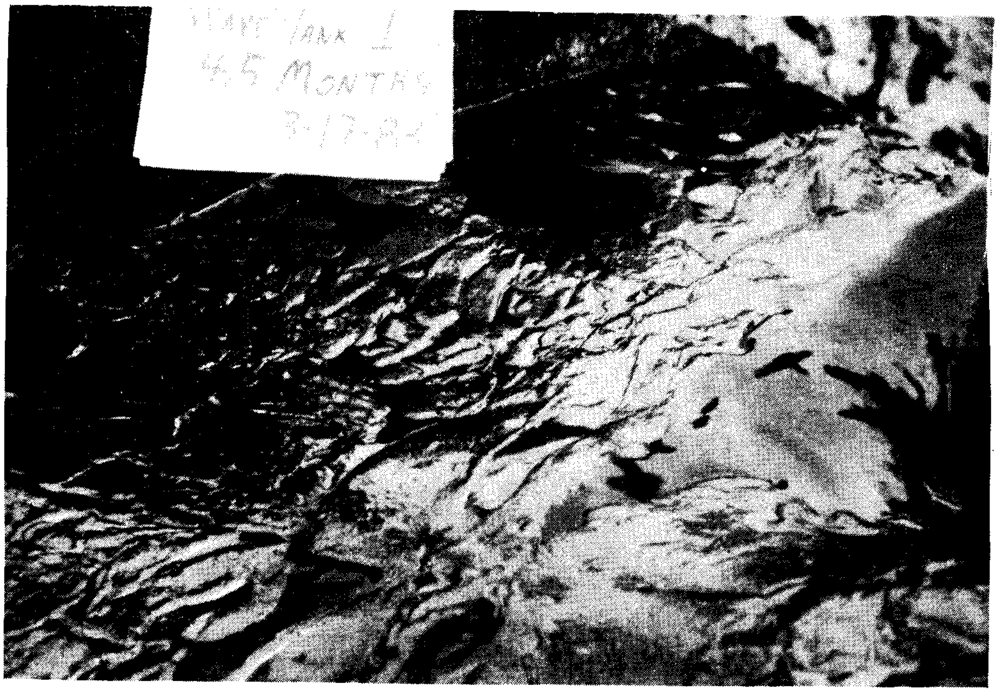

Figure 5-101. Appearance of spill #4 (wave tank 1) surface oil 4.5 months after spill initiation over winter period. Note the absence of tarball formation.

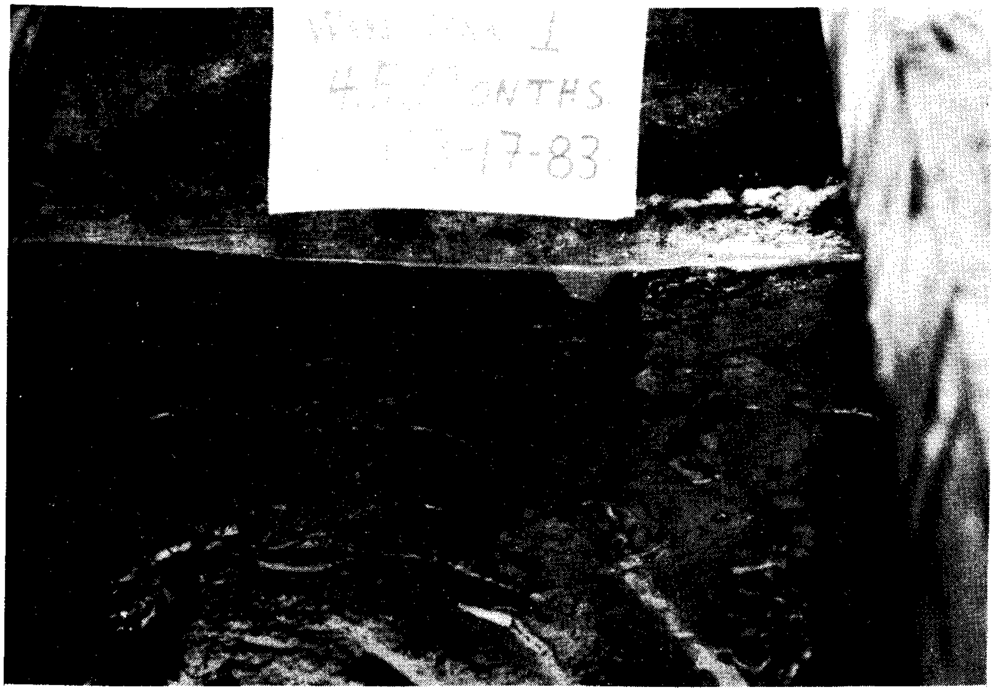

Figure 5-102. Appearance of the open and closing leads and oil mat at the quiescent end of the wave tank from the winter spill experiment.

Figure 5-103. Closeup of the surface oil/open water interface from the winter spill study, 4.5 months after spill initiation. Considerable sheen can still be observed emanating from the oil patches and this was not observed in the summer spill conditions after this time period. The presence of low molecular weight components was still indicated at this time by gas chromatographic analyses, and these components presumably contribute to the higher levels of observed sheen compared to the summer spill.

5.4.7 Oil Phase Chemical Alternations During Flow Through Wave Tank Experiments

During the triplicate wave tank experiments initiated in July 1982, surface oil samples were collected for chemical and physical properties determinations according to the following schedule: at 0 minutes, 5 minutes, 1 hour, 2 hours, 4 hours, 8 hours, 12 hours, 24 hours, 48 hours, 3 days, 6 days, 9 days, 12 days, 4 months, 9 months, and 12 months after spill initiation. Section 5.4.6 discussed changes in the rheological properties of the slicks and presented photographic documentation of the observed changes in oil slick appearance and behavior in the wave tanks. This section presents changes in the chemical properties of the slicks as determined by flame ionization detector gas chromatography and gas chromatography/mass spectrometry.

As noted in the previous sections, evaporation begins immediately upon release of the oil to the sea surface, and this is clearly illustrated in the chromatographic profiles shown in Figures 5-104 and 5-105. These samples were collected from wave tank 2 at the times indicated in the figure legends, and identical chromatographic profiles were obtained on samples from wave tanks 1 and 3 collected over the same time intervals. As shown by chromatogram B in Figure 5-104, compounds with molecular weights less than nC-9 are largely removed 8 hours after initiation of the spill. Loss of components in the KOVAT 900 to 1100 range is significantly delayed, and nC-10 is still clearly observed 9 days after spill initiation (chromatogram D). At the 7 month weathering point (Figure 5-105B) the first chromatographically observed peak is nC-13. After 12 months all components essentially below nC-14 have been removed from the slick, and at this point significant alterations in the nC-17/pristane and nC-18/phytane ratios can be observed suggesting microbial degradation. These observations will be discussed in greater detail later in this section and in Section 7.0.

To evaluate the chemical changes to surface oil due to weathering during the winter period, a fourth wave tank study was initiated in November 1982, and Figures 5-106 and 5-107 present the time-series chromatograms

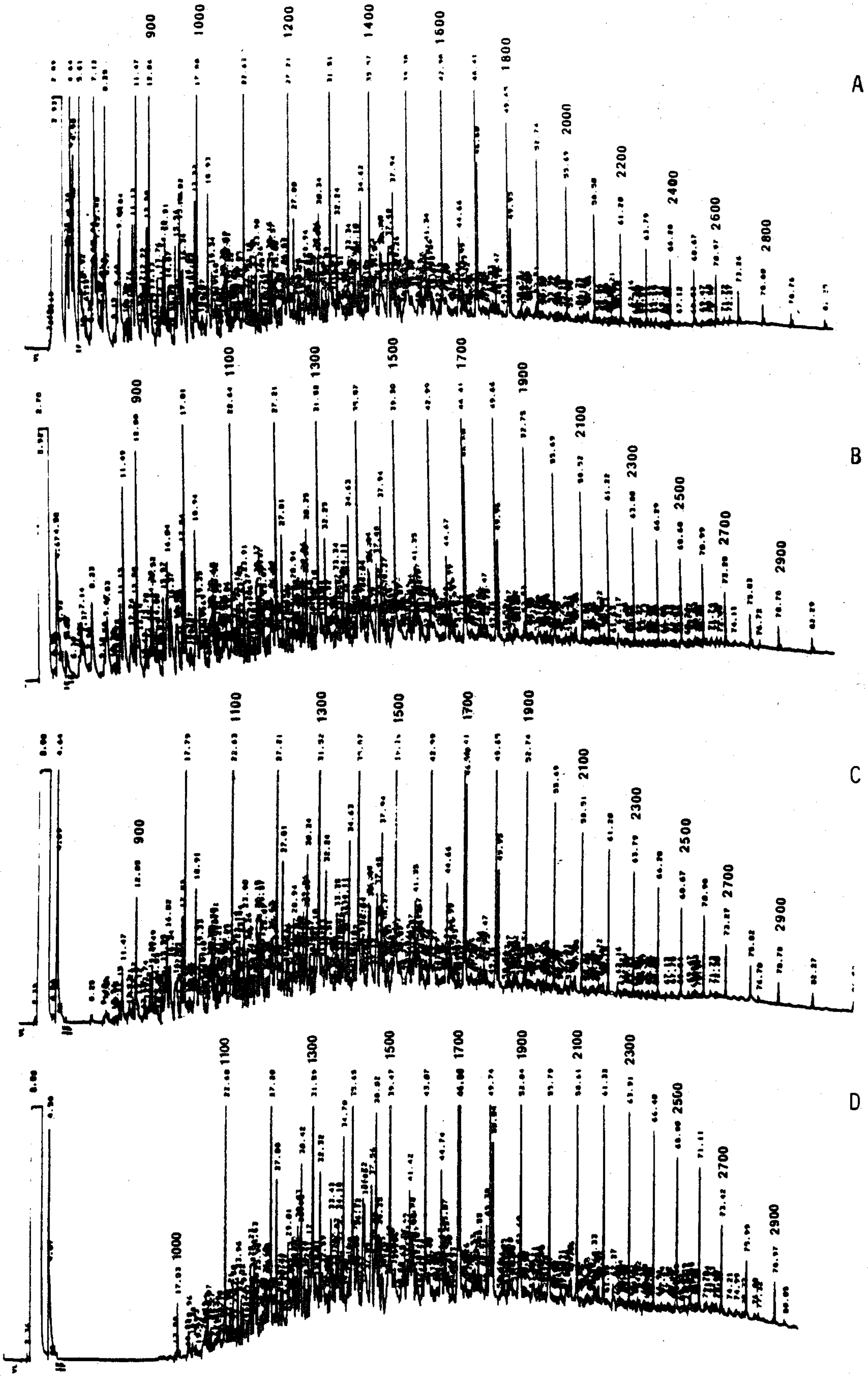

Figure 5-104. FID-GC chromatograms of oil samples obtained from Wave Tank #2 at: (A) 0 minutes, (B) 8 hours, (C) 48 hours, and (D) 9 days after a spill of 16 liters of Prudhoe Bay crude oil.

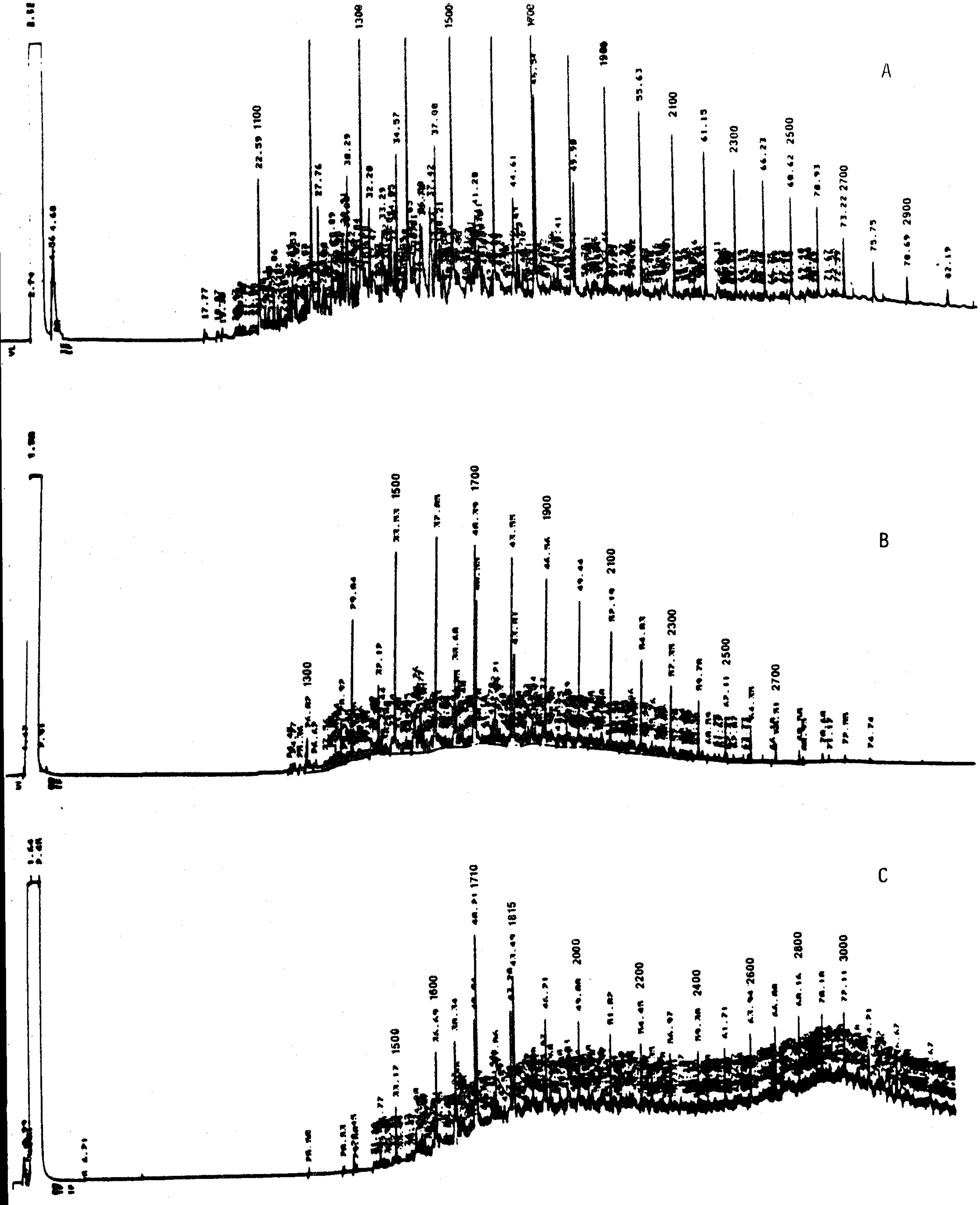

igure 5-105. FID-GC chromatograms of oil samples obtained from Wave Tank #2 at: (A) 12 days, (B) 7 months, and (C) 12 months after a spill of 16 liters of Prudhoe Bay crude oil.

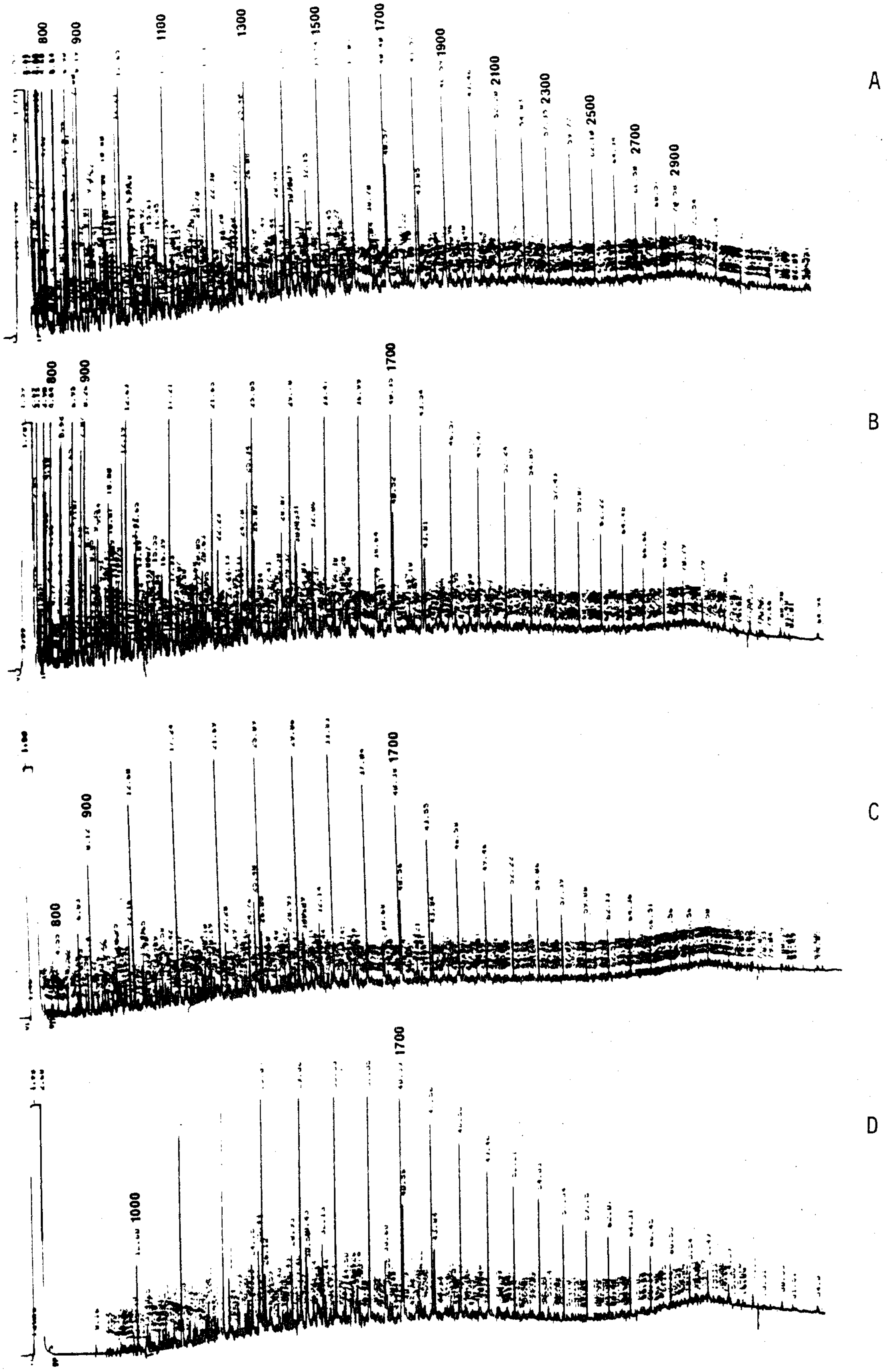

Figure 5-106. FID-GC chromatograms of oil samples obtained from Wave Tank #4 at:(A) 0 minutes, (B) 8 hours, (C) 48 hours, and (D) 10 days after a spill of 16 liters of Prudhoe Bay crude oil.

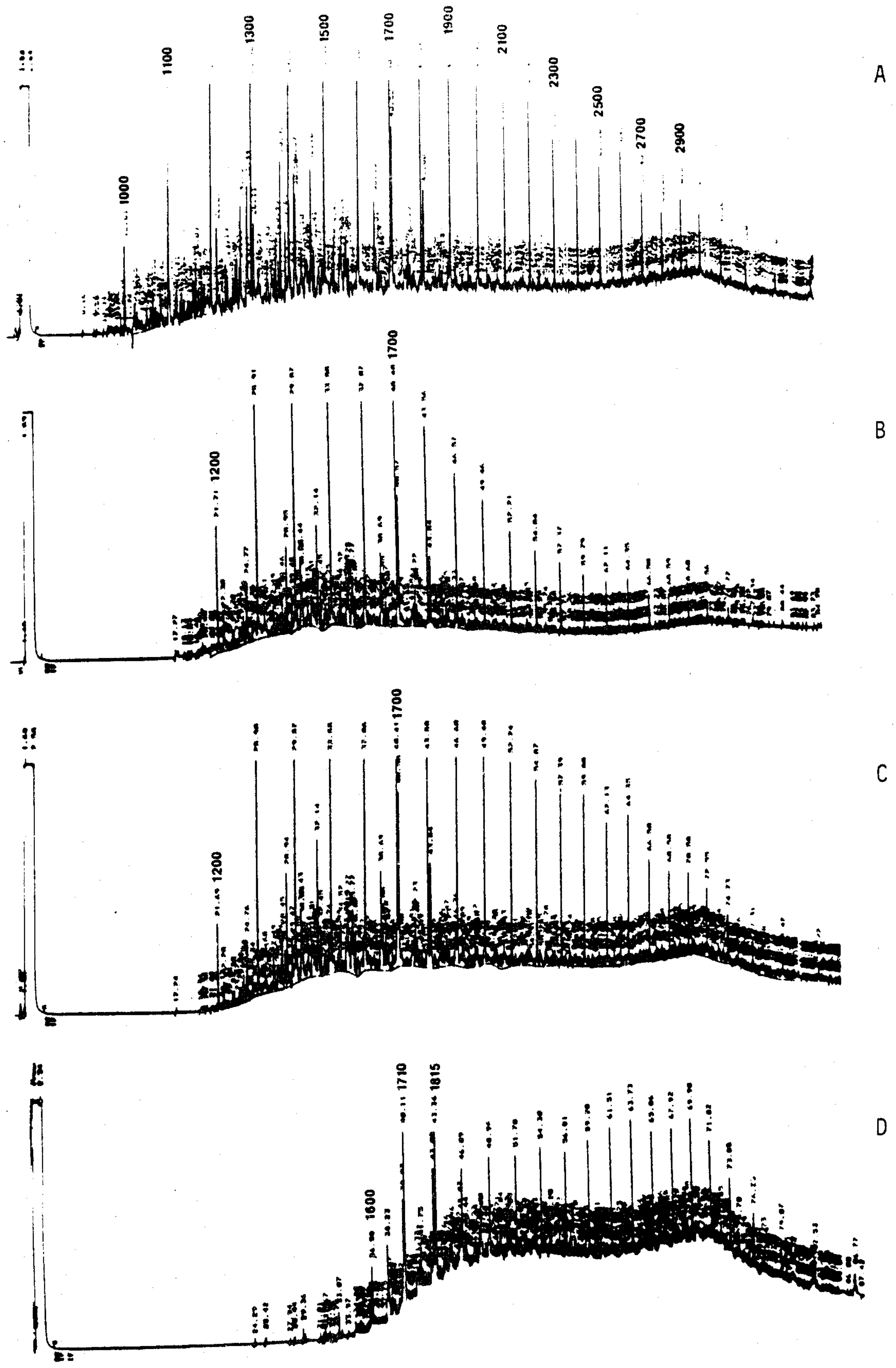

Figure 5-107. FID/GC chromatograms of oil samples obtained from Wave Tank #4 at: (A) 12 days, (B) 3 months, (C) 5 months, and (D) 9 months (stranded oil on tank side) after a spill of Prudhoe Bay crude oil.

obtained on oil from this experiment. Initial weathering appeared to be slightly delayed as evidenced by comparison of the 8 hour chromatogram for the winter spill (Figure 5-106B) versus the 8 hour chromatogram for the summer spill (Figure 5-104B). During the colder winter period, components in the KOVAT 800 to 900 range were clearly evident for a longer period, as would be predicted from temperature-dependent vapor pressure data for these components. Even after 48 hours (Figure 5-106C) there is still considerable evidence of n-alkanes and branched components in the KOVAT 800 to 900 range, and these were largely removed during the summer spills. After 10 days, however, the chromatographic profiles obtained during the winter period more closely matched those during the summer spill, with nC-10 being the first major resolved n-alkane in the surface oil. Longer term weathering over three to five months shows significant amounts of components with molecular weights greater than nC-12 remaining in the slick (Figure 5-107B and C), however, all components below nC-13 were removed from the slicks during the summer spills over a similar time frame. Chromatogram D in Figure 5-107 was obtained on an oil sample scrapped from the upper tank wall from wave tank 4 approximately 9 months after the initiation of the spill. As in the 12 month sample of surface oil from the summer spill, there is significant evidence of microbial degradation due to changes in the nC-17/pristane and nC-18/phytane ratios, although the winter-time stranded oil in wave tank 4 still contained significantly higher levels of n-alkanes in the nC-20 to nC-32 range compared to the surface oil from wave tank 2 after 12 months of simulated open ocean weathering.

The relative changes in total gas chromatographically resolved and unresolved complex mixture concentrations are presented graphically for the winter and summer spills in Figure 5-108. A rapid decrease in chromatographically resolved components is observed during both spill conditions during the first month; however, the rate of loss is clearly greater for the summer conditions, and continued loss of resolved components is suggested over the 12 months after spill initiation. During the winter spill the initial loss of chromatographically resolved components is somewhat slower, and there appears

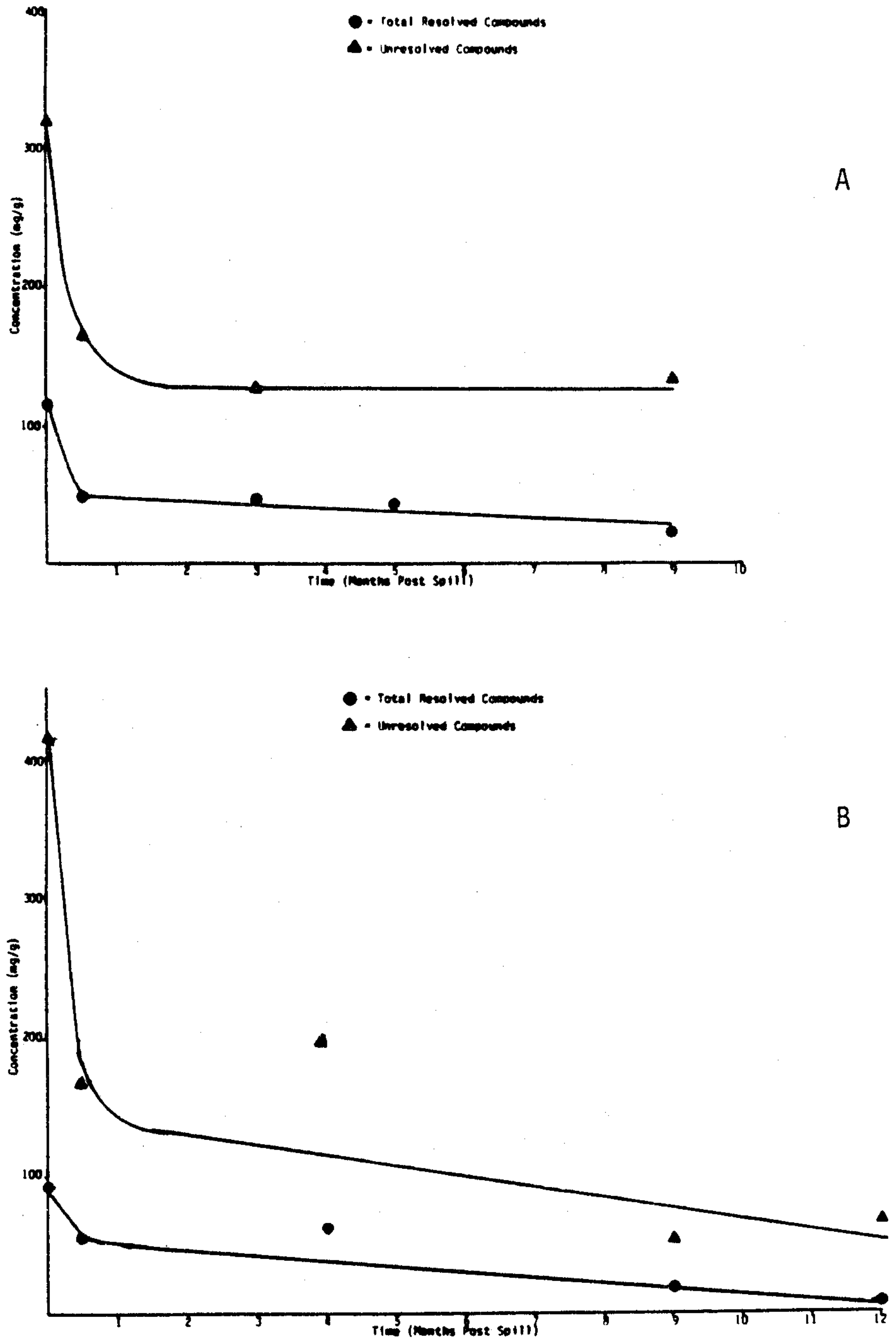

Figure 5-108. Total Resolved and Unresolved compounds remaining in the oil slick from (A) Wave Tank #4 and (B) Wave Tanks #1-3. Values are means.

to be a relatively constant level of chromatographically resolved peaks over a longer period for the spill started under the colder conditions. With regard to the unresolved complex mixture present in the oil from both the summer and winter experiments, a slightly greater decrease is also observed for the mean concentrations of components in the UCM for the summer spill compared to the winter conditions.

Table 5-10 presents individual n-alkane concentrations in the oil from wave tanks 1 through 3 initiated during the summer period. Concentrations are reported on a microgram/gram of oil basis, and they have been corrected for the incorporation of water. These data are perhaps illustrated better graphically, and Figure 5-109 presents selected time-series n-alkane concentrations (from nC-8 through nC-27) from wave tanks 1 through 3. Note the difference in time scales for the different molecular weight components illustrating complete loss of compounds up to nC-9 during the first 48 hour period. Traces of nC-11 were still observed (at an extremely low level) 4 months after initiation of the spill, and a slow, but steady, decrease in nC-16 and nC-27 concentrations in all three tanks is observed in Figure 5-109C. The data in Figure 5-109D show a similar rate for nC-15 compared to nC-16, however, phytane, a branched isoprenoid compound is lost at a significantly slower rate compared to the n-alkane of similar boiling point (nC-18). Differences in the rate of loss in these compounds can be used to evaluate the influence of microbial degradation as will be discussed below in Section 7.0.

Table 5-11 presents individual n-alkane concentrations in the oil slick from the winter spill (wave tank 4), and again the concentrations have been corrected for water incorporation. These data are also presented graphically in Figure 5-110, and the data in Figure 5-110A illustrate that nC-8 could be detected up to 6 days after initiation of the spill. Similar data presented in Figure 5-109A show complete loss of detectable nC-8after only 2 days during the summer conditions. Likewise, nC-9 was observed during the winter spill up to 12 days after initiation of the spill event, and during the summer conditions (Figure 5-109A) this component was largely removed after 48

Table 5-10. Individual n-alkane Concentrations (µg/g) in the Oil Slick from Wave Tanks #1-3 - **Corrected for Water Incorporation**

Compound	Time 0 Ave/SD[a]	12 hours Ave/SD	24 hours Ave/SD	48 hours Ave/SD	6 days Ave/SD	12 days Ave/SD	4 months Ave/SD	9 months Ave/SD	12 months Ave/SD
n-C_8	2490/615	680/99.0	290/5.0	nd[b]	nd	nd	nd	nd	nd
n-C_9	4290/830	2660/390	1650/28	450/54	nd	nd	nd	nd	nd
n-C_{10}	4640/933	3740/396	2670/320	1350/162	610/209	298	nd	nd	nd
n-C_{11}	4770/955	4210/382	3170/14.0	1960/236	1730/510	1030/358	nd	nd	nd
n-C_{12}	4700/990	4230/353	3270/21.0	2240/242	2580/830	2200/691	146/34.8	nd	nd
n-C_{13}	5790/1150	5290/262	4100/8.0	2960/376	3100/1040	2580/694	945/124	260/14.1	125
n-C_{14}	3890/700	3580/106	2870/63	2120/255	2150/721	2230/550	2090/197	810/36.8	263
n-C_{15}	3980/276	3420/99.0	2910/219	2270/218	2090/675	2170/508	2880/238	1100/16.3	340
n-C_{16}	3750/502	3260/77.0	2880/233	2390/315	2060/603	2060/503	2490/243	1240/1.41	333/155
n-C_{17}	3360/403	2970/42.0	2660/134	2500/217	1910/651	1960/517	2525/277	1070/32.5	403/118
Pristane	1990/283	1710/35.0	1560/212	1470/200	1080/367	1160/280	1870/214	1070/6.36	445/118
n-C_{18}	2870/480	2360/49.0	2260/28.0	2060/215	1630/547	1580/484	2250/282	953/19.1	365/146
Phytane	1280/210	1070/70.0	1030/63.0	1020/96.0	962/152	728/201	1670/216	688/24.7	400/73.5
n-C_{20}	2410/610	2120/10.0	2460/78.0	2560/192	2150/360	1570/436	1990/288	680/28.3	315/57.2
n-C_{24}	2360/57.0	1660/23.0	2060/304	2920/352	1090/230	1190/239	2630/715	470/113	370/61.5
n-C_{27}	2790/700	1620/147	2340/156	2780/198	980/195	996/277	1890/262	442/128	338/59.3
Total Resolved	92,300	102,000	88,000	67,000	65,000	58,000	83,800	19,300	9,200
Unresolved Compounds	-	-	416,000	385,000	227,000	170,000	203,000	56,500	68,100

a - Ave indicates the average value and SD indicates the standard deviation

b - **nd indicates "not detected"**

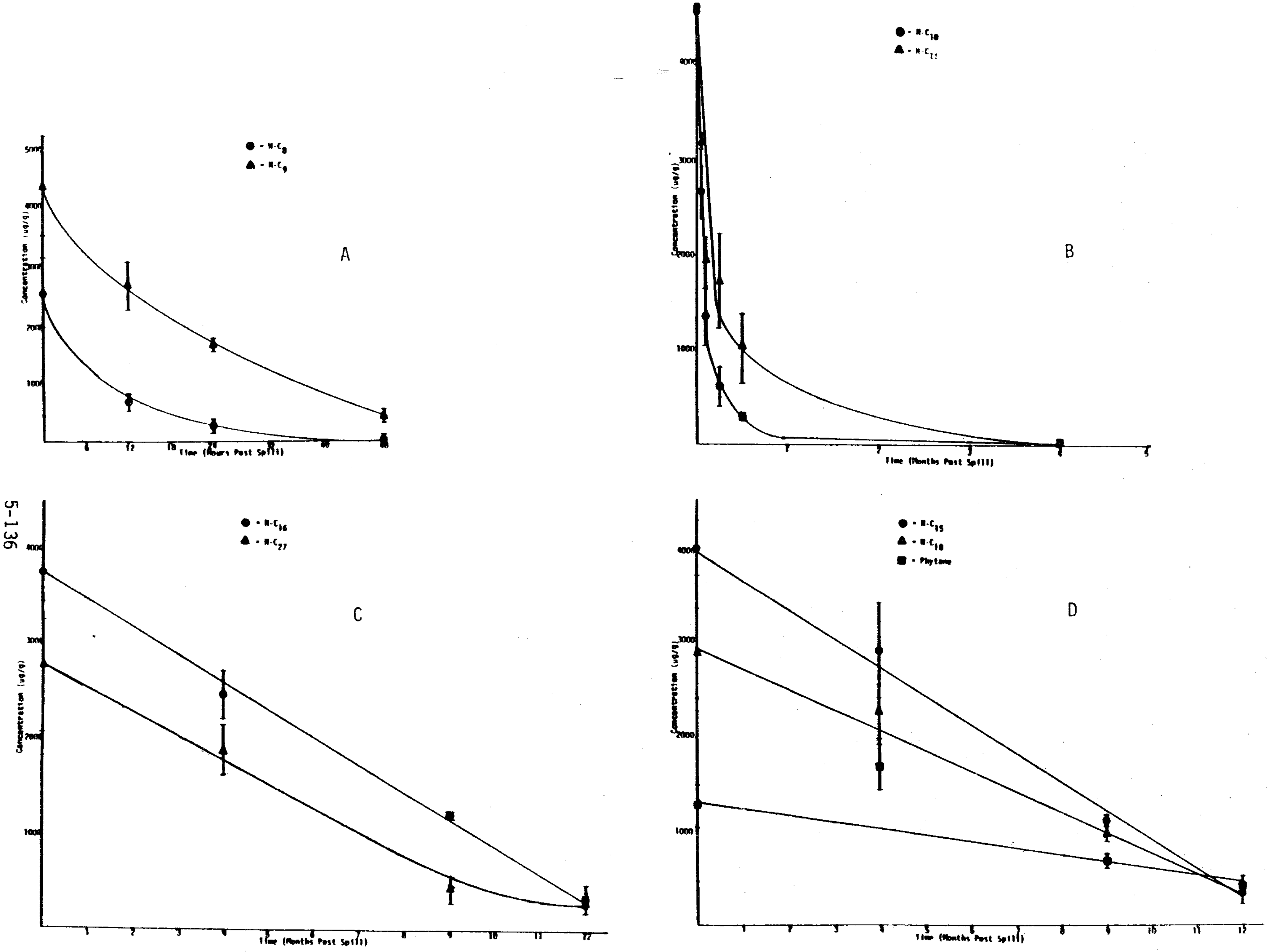

Figure 5-109. Time series concentrations of individual compounds remaining in the oil slick from Wave Tanks #1-3. Values are means ± one standard deviation.

Table 5-11. Individual n-alkane Concentrations (μg/g) in the Oil Slick from Wave Tank #4 - Corrected for Water Incorporation

Compound	Time 0	8 hours	24 hours	48 hours	6 days	12 days	3 months	5 months	9 months
n-C_8	2620	1560	329	84.5	nd[a]	nd	nd	nd	nd
n-C_9	3860	2910	1140	507	210	nd	nd	nd	nd
n-C_{10}	3690	2950	1380	834	860	515	nd	nd	nd
n-C_{11}	3600	2900	1440	973	1360	1420	110	nd	nd
n-C_{12}	3490	2360	1390	982	1520	2190	948	565	nd
n-C_{13}	3530	3060	1465	1030	1640	2300	1540	1540	nd
n-C_{15}	3200	2150	1830	1420	1390	2450	1940	2160	315
n-C_{17}	2360	1660	1090	823	1300	1740	1360	1570	530
Pristane	1210	850	504	472	660	939	893	995	1180
n-C_{18}	2076	1420	871	688	1050	1470	1100	1530	453
Phytane	1030	738	478	345	572	792	575	768	1000
n-C_{20}	1920	860	819	453	1060	1120	768	1300	298
n-C_{23}	2100	1160	669	486	977	1200	1180	1380	358
n-C_{26}	1890	877	542	296	736	962	975	1310	520
Total Resolved	115,000	76,200	38,400	23,300	37,500	49,800	46,750	43,300	21,000
Unresolved Compounds	320,000	158,000	86,800	62,400	81,400	166,000	128,000	175,000	134,000

a - nd inciates "not detected"

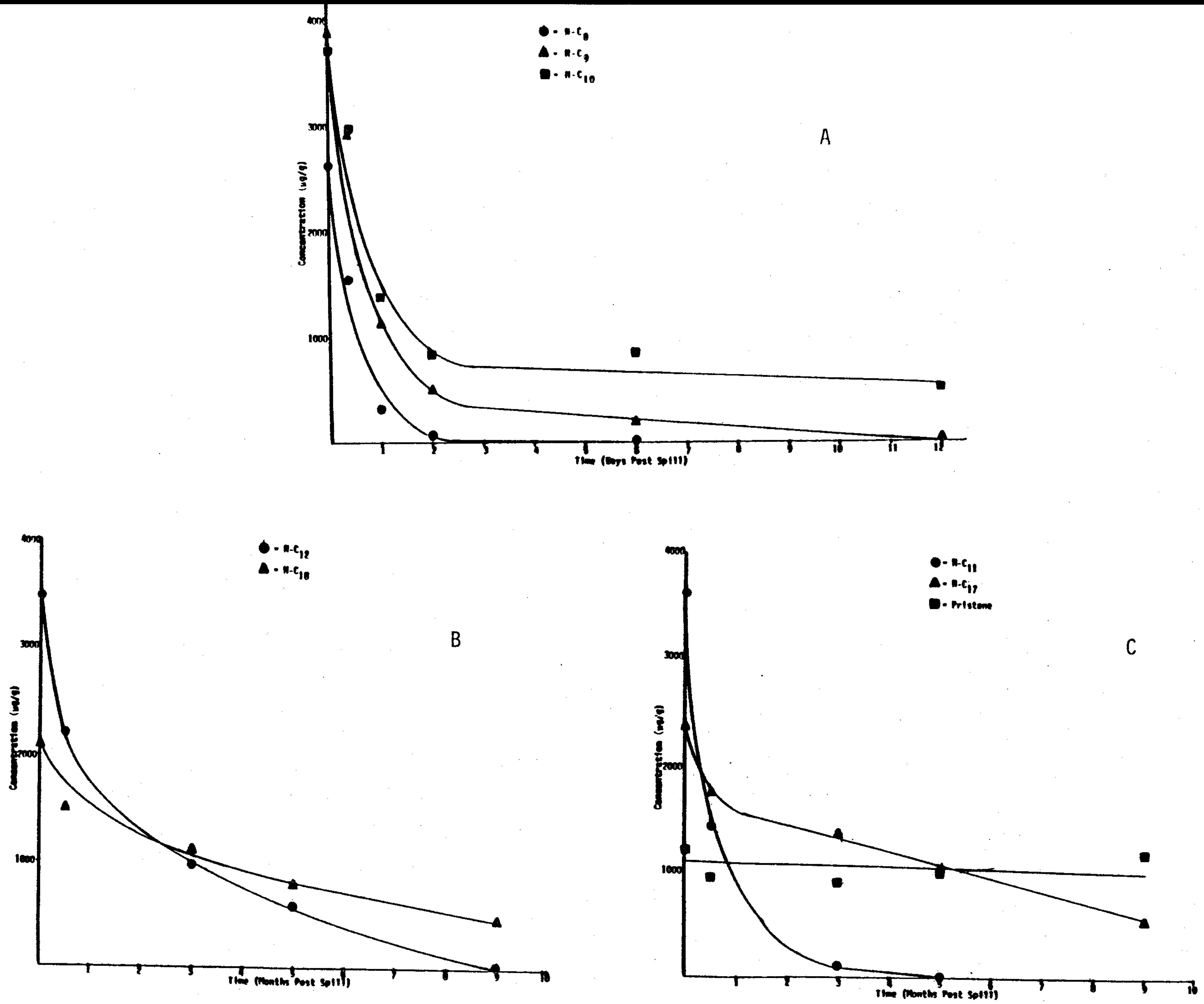

Figure 5-110. Time series concentrations of individual compounds remaining in the oil slick from Wave Tank #4.

hours. The data in these figures also demonstrate that nC-11 remained in the winter spill for up to 5 months (Figure 5-110C) whereas this compound was completely removed after the 4 month interval from July to November during the summer spill conditions (Figure 5-109B). During the winter conditions the concentration of nC-17 was observed to decrease slowly, however, the isoprenoid pristane was observed at relatively constant concentrations up to the 9 month sampling point.

Comparisons of the ratios of nC-17/pristane, nC-18/phytane and absolute concentrations of farnesane are presented in Table 5-12 and graphically in Figure 5-111. Ratios of nC-17/pristane for the oil in all four tanks are observed to decrease uniformly as shown in Figure 5-111A, and no significant differences in the winter versus summer spills are readily apparent. This may reflect the fact that the values shown are derived from ratios of individual component concentrations, and thus any expeprimental variance in concentration determinations would cause a larger spread in the ratio data as shown. Nevertheless, a relatively constant decrease in the nC-17/pristane ratio is observed for the 12 months of the experiment. Ratios of nC-18/phytane also decreased in a relatively constant fashion for all four tanks (Figure 5-111B), and from these data it is not possible to draw any definitive conclusions regarding summer vs winter microbial degradation rates. Farnesane concentrations in all four tanks drop quite quickly during the first 5 days of the experiment and then remain relatively constant throughout the remaining period of observation.

5.4.8 Time-Series Dissolution of Aromatic Hydrocarbons in the Water Column from the Wave Tank Systems

As described in Section 5.4.4, filtered water column samples were obtained from the flow-through wave tanks to determine time-series concentrations of dissolved and particulate (including dispersed) hydrocarbons in the water column beneath the slick. These filtered-water samples were extracted and analyzed at the Kasitsna Bay Laboratory, and Figures 5-112 and 5-113 present selected flame ionization detector gas chromatograms obtained on the

Table 5-12. Kasitsna Bay Wave Tanks nC_{17}/Pristane, nC_{18}/Phytane Ratios and Isoprenoid Concentrations in Oil

	WT#1 - Kasitsna Bay SPM			WT#2 - Seldovia Bay SPM			WT#3 - No SPM Addition			WT#4 - Glacial Till SPM		
	nC_{17}/Pristane	nC_{18}/Phytane	Farnesane(μg/g)	nC_{17}/Pristane	nC_{18}/Phytane	Farnesane(μg/g)	nC_{17}/Pristane	nC_{18}/Phytane	Farnesane(μg/g)	nC_{17}/Pristane	nC_{18}/Phytane	Farnesane(μg/g)
Time 0	1.84	1.84	1700	1.71	2.23	1180	1.66	2.26	1420	1.95	2.01	1170
8 hours	1.52	1.92	880	1.52	1.94	847	1.58	2.07	1430	1.96	1.93	762
24 hours	1.60	2.06	827	1.84	2.37	747	1.94	2.00	-	1.82	1.82	630
48 hours	1.69	2.01	512	1.55	2.00	613	1.53	2.08	629	1.75	1.99	435
8 days	1.56	2.10	327	1.56	2.33	366	1.52	1.90	494	1.87	1.85	564
12 days	1.44	1.84	186	1.67	2.00	300	1.75	2.29	385	1.85	1.86	474
4 months	1.53	1.67	289	1.60	1.58	302	1.26	1.47	151	1.58	1.99	383
6 months	-[a]	-	-	.804	1.17	128	1.16	1.34	342	na[b]	na	na
9 months	-	-	-	1.08	1.32	143	.801	1.10	218	.463	.510	78.8
12 months	-	-	-	.438	.520	26.7	.777	.876	171	-	-	-

a - Wave tank experiment terminated at this time

b - na indicates sample "not available" for analysis

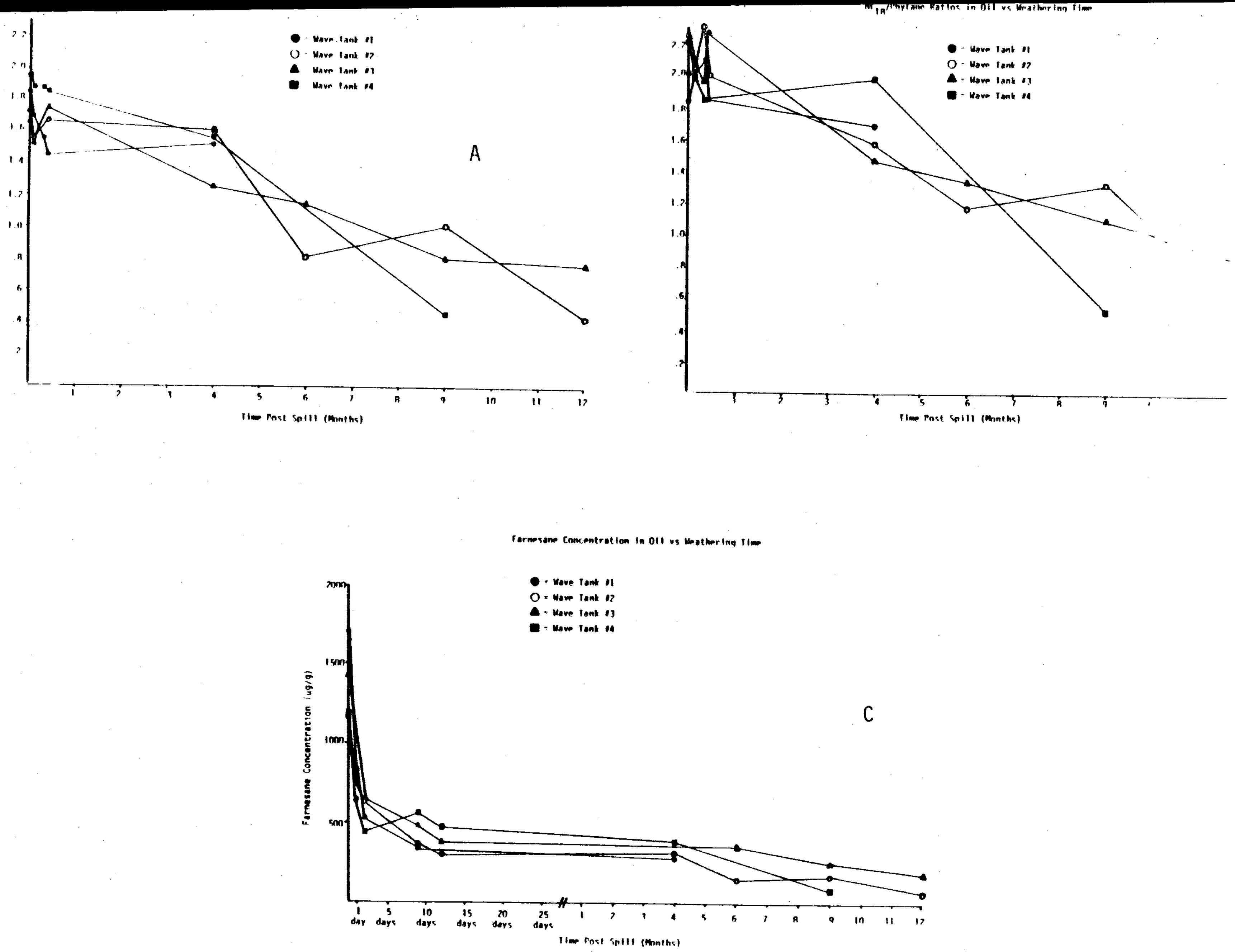

Figure 5-111. Time series ratios and isoprenoid (farnesane) concentrations in the oil slick from Wave Tanks #1-4.

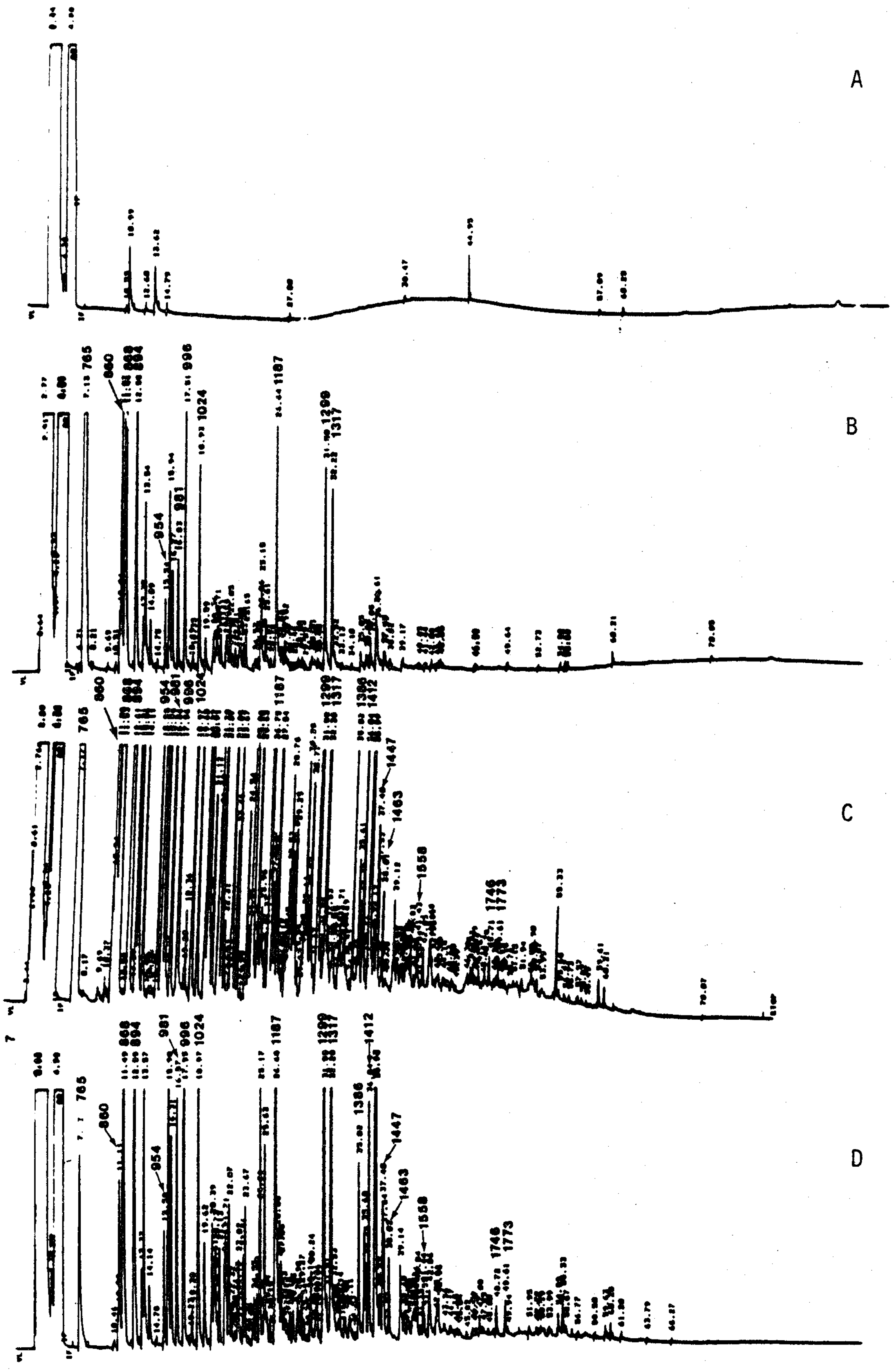

Figure 5-112. FID-GC chromatograms of filtered seawater extracts from Wave Tank #2 at: (A) Prespill Blank, (B) 5 minutes, (C) 8 hours, and (D) 48 hours after a spill of 16 liters of Prudhoe Bay crude oil.

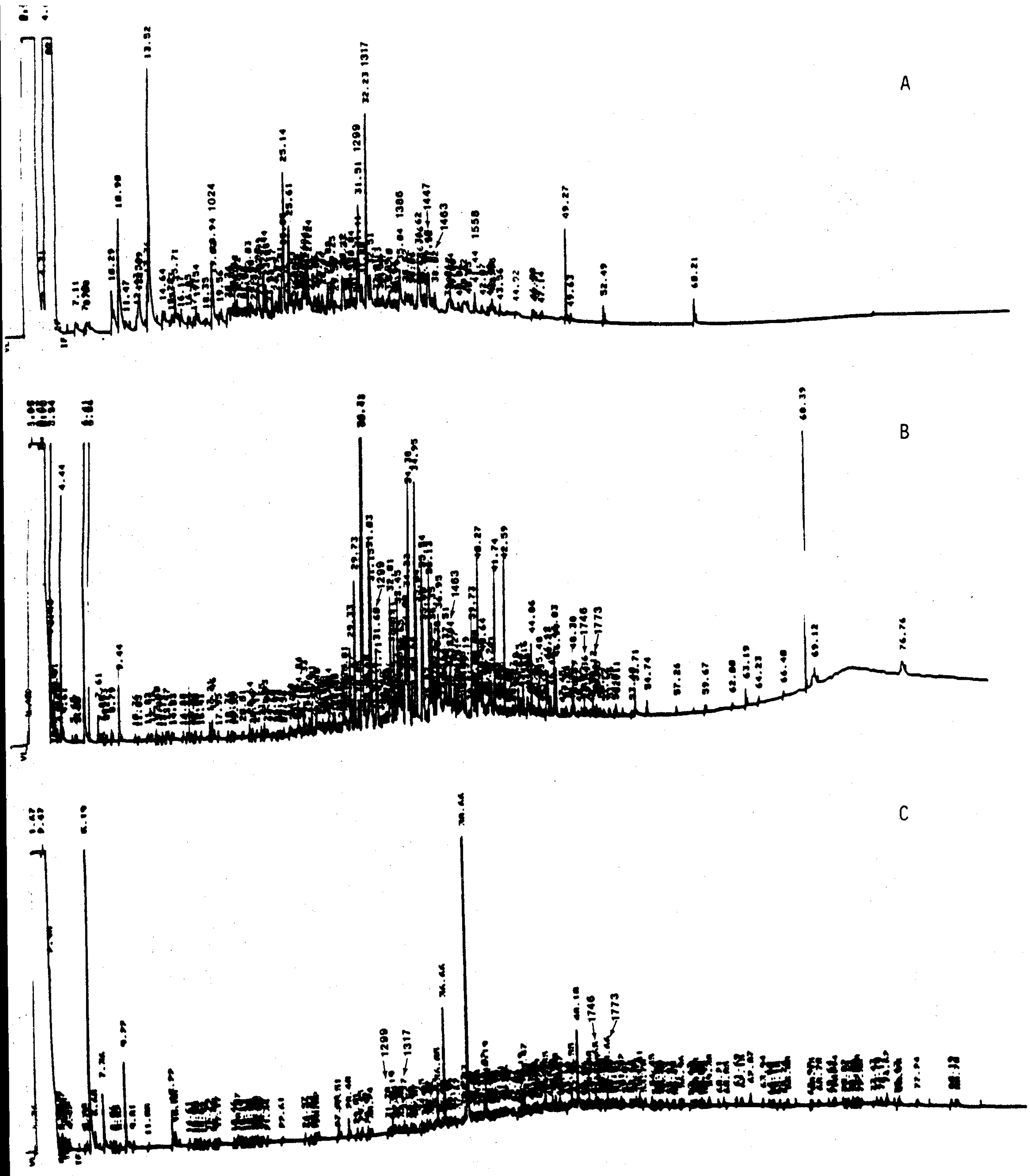

Figure 5-113. FID-GC chromatograms of filtered seawater extracts from Wave Tank #2 at: (A) 12 days, (B) 4 months, and (C) 12 months after a spill of 16 liters of Prudhoe Bay crude oil.

summer-spill water column samples from wave tank 2 at the time intervals shown. Chromatogram A in Figure 5-112 was obtained on a pre-spill blank and shows essentially no significant hydrocarbon contamination before initiation of the experiment. Chromatogram B obtained 5 minutes after initiation of the spill shows the immediate and significant buildup of lower molecular weight dissolved aromatic compounds which are identified by KOVAT retention indices. Specific compound identifications, listed by KOVAT index, and time-series concentrations of dissolved aromatic hydrocarbons in the water column from all three tanks are presented in Table 5-13. Dissolved aromatic hydrocarbon concentrations were observed to reach a maximum between 8 and 12 hours after spill initiation (Figure 5-112C). After 48 hours, significant loss of the lower molecular weight (below KOVAT index 868) compounds due to a combination of evaporative and advective processes is observed (Figure 5-112D). After as little as 12 days (Figure 5-113A) most of the lower molecular weight aromatic compounds are no longer present at high concentrations, with only the intermediate molecular weight naphthalenes, alkyl-substituted naphthalenes and phenanthrenes continuing to dissolve from the surface slick. This higher molecular weight aromatic compound dissolution is most prominant in Chromatogram B of Figure 5-113 which shows the water column extract 4 months after initiation of the spill. At that time the only significant aromatic hydrocarbons observed are in the C2-naphthalene to phenanthrene range, and even then, these concentrations were only present in the 50 to several hundred nanogram per liter range (see Table 5-13). Twelve months after initiation of the spill (Figure 5-113C) almost all evidence of any significant aromatic hydrocarbon dissolution from the slick is gone.

As during the summer spill experiments, water column samples were obtained for dissolved and dispersed hydrocarbon concentration measurements during the winter spill initiated in November, 1982. Figures 5-114 and 5-115 present the time-series chromatographic profiles obtained on those extracts. Again, the pre-spill blank (Figure 5-114A) shows no significant evidence of hydrocarbon contamination, and yet, significant (10 to 70 μg/liter) levels of aromatic hydrocarbons ranging from toluene to o-xylene are observed in the

Table 5-13. Dissolved Aromatic Hydrocarbon Concentrations (μg/l) from Wave Tanks #1-3.

Compound	KOVAT	Time 0 Ave/SD[a]	1 hour Ave/SD	2 hours Ave/SD	4 hours Ave/SD	8 hours Ave/SD	12 hours Ave/SD	2 days Ave/SD	6 days Ave/SD	12 days Ave/SD	4 months Ave/SD	9 months Ave/SD	12 months Ave/SD
Toluene	765	44.8/14	160/54	134/23	91.8/13	30.1/1.8	13.5/1.8	1.30/1.1	.122/.040	nd[b]	nd	nd	nd
Ethylbenzene	860	3.70/1.2	11.5/7.5	14.6/1.1	12.7/5.2	6.70/.88	4.31/1.3	.920/.21	.260/.10	.258/.27	nd	nd	nd
p-xylene	868	13.9/4.1	40.4/23	52.9/1.0	48.1/21	28.3/3.8	18.5/5.1	4.97/1.2	1.20/1.3	.039/.05	nd	nd	nd
o-xylene	894	7.74/2.4	23.0/12	23.0/11	27.6/10	16.5/2.1	11.4/2.7	2.89/1.7	.723/.89	.045/.04	nd	nd	nd
Isopropylbenzene	925	.521/.15	1.44/.87	1.50/.86	2.10/1.1	1.40/.35	.991/.39	.376/.008	.100/.061	nd	nd	nd	nd
n-propylbenzene	954	.862/.25	1.84/1.2	2.20/1.2	3.40/1.8	2.30/.62	1.70/.67	.765/.21	.181/.17	nd	nd	nd	nd
C_3-benzene	969	.780/.20	1.92/.95	2.10/1.1	3.50/2.2	2.80/.83	2.10/.72	1.23/.14	.333/.12	.077/.07	nd	nd	nd
1,3,5-trimethylbenzene	981	1.30/.35	3.40/1.6	4.60/.01	5.50/2.7	3.80/1.4	2.96/.94	1.81.06	.609/.11	.042/.008	nd	nd	nd
C_3-benzene	996	4.01/.75	8.80/4.3	12.2/.42	14.8/7.1	10.3/3.9	7.78/2.7	5.23/.14	2.00/.95	.136/.20	nd	nd	nd
C_4-benzene	1024	2.20/.41	6.30/2.9	8.60/.52	10.9/4.8	8.22/2.2	6.31/1.9	4.50/.40	1.61/.45	.087/.05	nd	nd	nd
n-buthylbenzene	1060	1.20/1.8	1.30/.55	1.40/2.1	2.50/.78	.380/.17	.382/.13	.301/.04	.120/.009	.049/.03	nd	nd	nd
Naphthalene	1187	2.96/.88	9.20/5.4	10.2/4.0	21.3/7.6	16.8/5.6	13.4/3.0	6.22/2.4	3.82/1.5	.111/.14	nd	nd	nd
2-methylnaphthalene	1299	2.88/.74	7.00/3.3	8.00/2.9	15.5/4.7	13.9/5.7	11.3/4.7	8.75/1.1	5.45/.88	1.35/1.5	.0705/.03	.0112/.0001	.00565/.00
1-methylnaphthalene	1317	200/.50	5.00/2.2	5.70/1.7	11.9/3.8	10.7/4.6	9.22/2.9	7.56/1.8	4.51/.68	1.27/1.3	.0642/.02	.0104/.008	.0433/.06
1,1'-biphenyl	1386	.180/.18	.450/.49	1.10/.65	1.90/.50	2.20/.035	1.63/.49	1.44/.42	.850/.13	.300/.26	.0359/.03	.0495/.02	.0424/.06
2,6-dimethylnaphthalene	1412	.290/.28	.990/.59	1.00/.34	2.20/.64	2.80/.06	2.29/.71	1.96/.45	1.32/.070	.314/.32	.266/.02	.0228/.008	nd
C_2-naphthalene	1428	nd	nd	.850/.82	3.60/1.0	4.40/.13	3.38/1.0	2.99/.78	1.63/.31	.413/.50	.583/.02	.0214/.005	nd
C_2-naphthalene	1447	nd	nd	.309/.01	.850/.26	1.04/.11	.732/.23	.610/.23	.344/.03	.117/.13	.153/.008	.00668/.001	nd
C_2-naphthalene	1463	nd	nd	.240/.08	.730/.17	.901/.04	.674/.21	.604/.19	.352/.04	.159/.14	.0890/.008	.00159/.002	nd
2,3,5-trimethylnaphthalene	1558	nd	nd	.133/.12	.259/.03	.211/.08	.221/.05	.214/.06	.181/.06	.047/.04	.105/.02	.0165/.0006	nd
Dibenzothiophene	1746	nd	nd	nd	.438/.04	.412/.12	.474/.006	.324/.04	.313/.09	.179/.15	.191/.06	.00687/.004	.00695/.00
Phenanthrene	1773	nd	nd	nd	.463/.18	.482/.29	.526/.17	.580/.22	.279/.07	.0360/.06	.175/.04	.0138/.0001	.0150/.02
Total Resolved	-	99.1/32	335/114	325/18	384/79	193/50	169/7.1	74.2/7.1	35.6/7.7	26.3/14	7.33/2.7	5.95/.03	5.33/.34
Unresolved Compounds	-	0	0	0	132/14	104/5.7	102/42	113/17	86.2/10	89.0/37	12.6/5.2	13.2/.01	5.04/.45

a - Ave indicates the average value for 3 wave tanks and SD indicates the standard deviation

b - nd indicates "not detected"

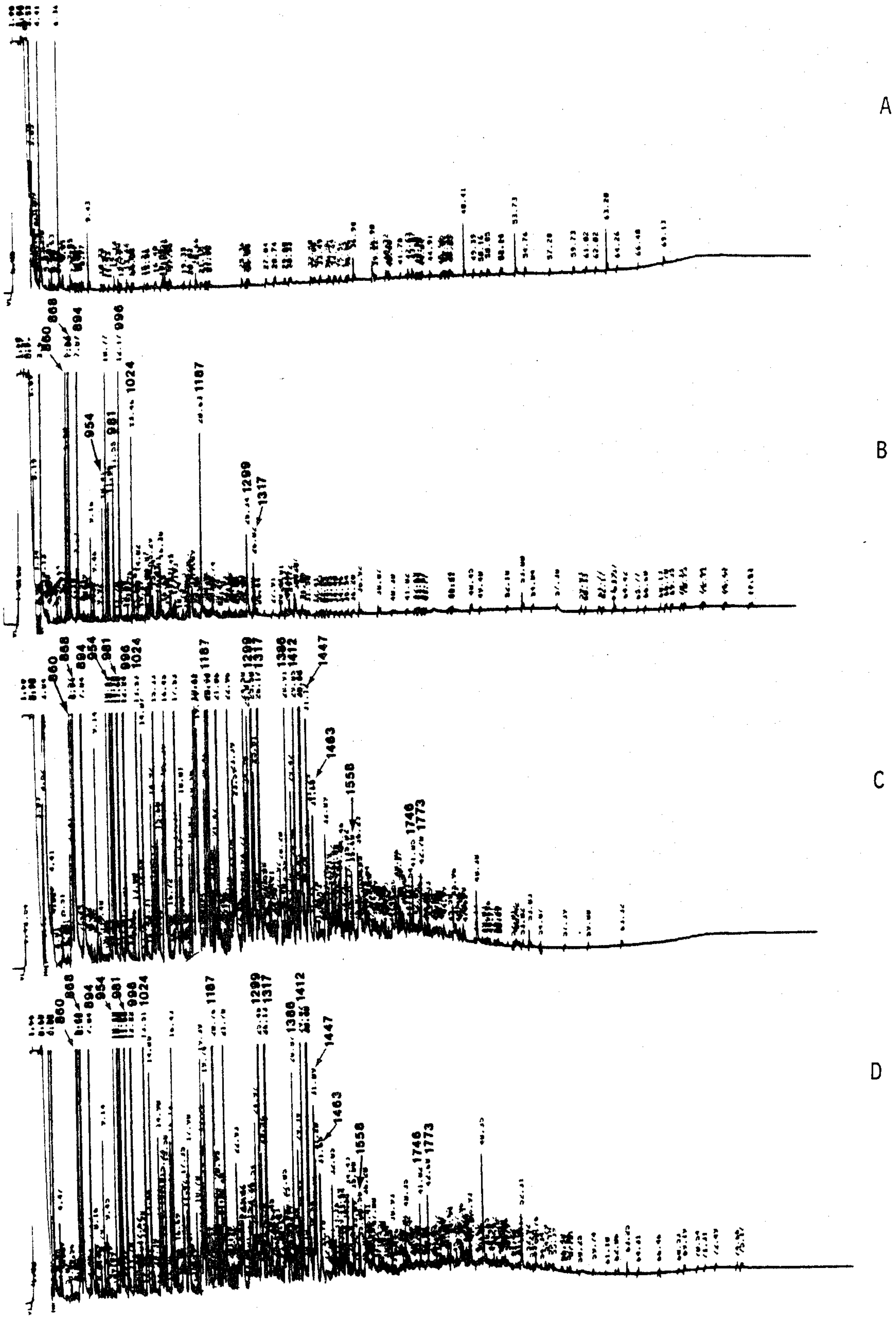

Figure 5-114. FID-GC chromatograms of filtered seawater extracts obtained from Wave Tank #4 at: (A) Prespill Blank, (B) 5 minutes, (C) 8 hours and (D) 48 hours after a spill of 16 liters of Prudhoe Bay crude oil.

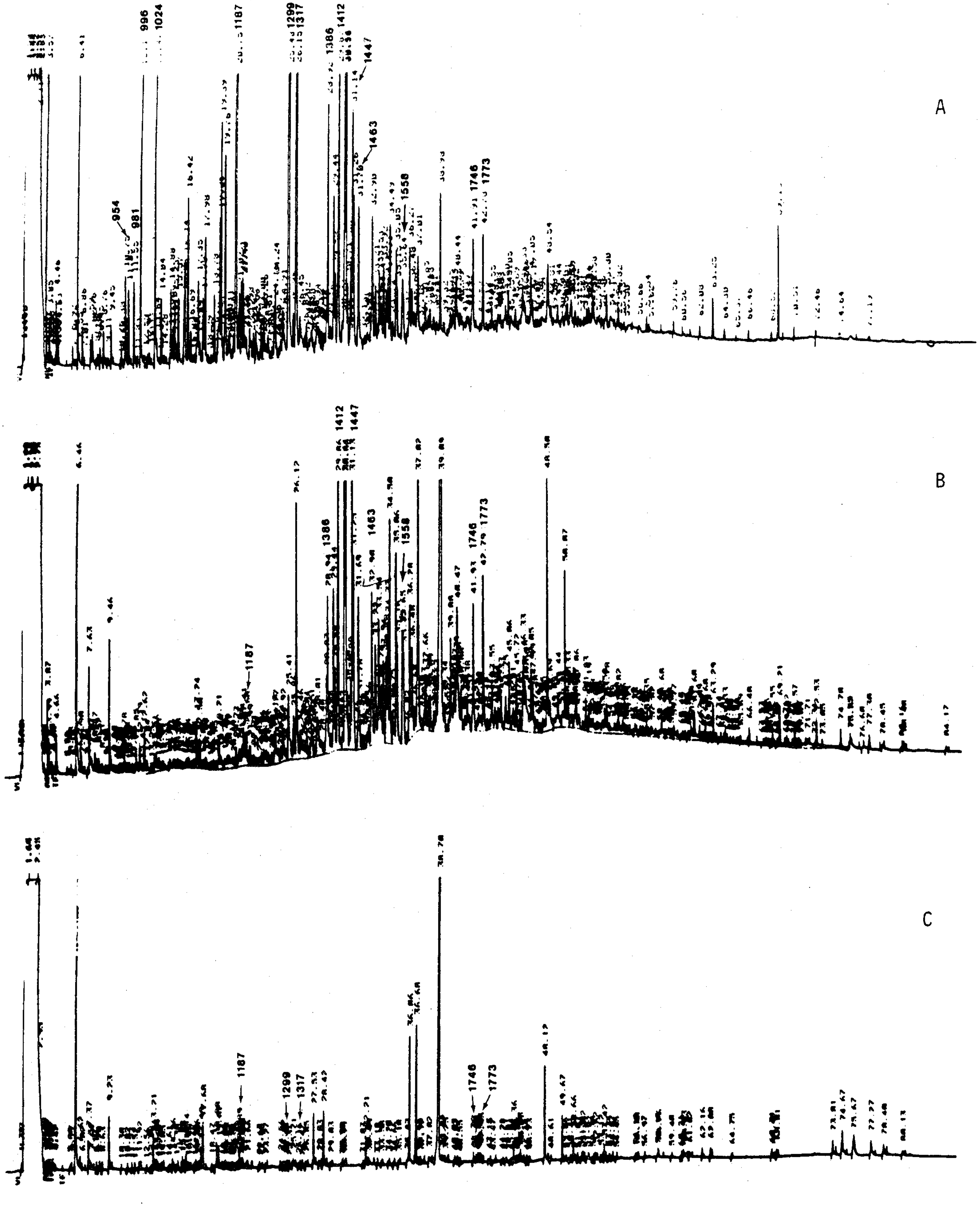

Figure 5-115. FID-GC chromatograms of filtered seawater extracts obtained from Wave Tank #4 at: (A) 12 days, (B) 5 months, and (C) 9 months after a spill of 16 liters of Prudhoe Bay crude oil.

water column as little as 5 minutes after spill initiation. Compound identifications by KOVAT index are labelled as in Figures 5-112 and 5-113 (and Table 5-13), and absolute hydrocarbon concentrations in the water column for the winter spill are presented separately in Table 5-14. As in the summer spill, the lower molecular weight aromatic hydrocarbon concentrations reach a maximum during the first 8 to 12 hours. They are gradually lost as shown by the chromatographic profiles in Figure 5-114 and the data in Table 5-14. This loss from the water column reflects the combination of advective removal due to water-column turnover, evaporation from the slick (e.g., the hydrocarbon source) and air/sea exchange (evaporation) from the open water portions of the wave tank. With extended time these lower molecular weight aromatics are continually removed; however, the chromatographic profile in Figure 5-115A still shows elevated levels of aromatics in the KOVAT index 900 to 1300 range after 12 days compared to the values observed during the summer spill. These significantly higher concentration and greater longevity in the water column during the winter conditions reflect two features. First, due to lower evaporation rates as effected by the specific component's vapor pressures at -5°C, their residence time in the slick is significantly longer, and as such, they continue to dissolve into the water column over an extended period. Second, as noted in Section 5.4.6 (oil slick rheological properties and wave tank observations) the winter spill did not form as significant a water-in-oil emulsion during the initial days of the spill compared to the summer experiments. The lower temperature did increase the viscosity, however, such that a loss due to evaporation may have been diffusion controlled. After approximately 5 months of weathering with continuous tank-volume turnover every 3 hours, the only components continuing to dissolve into the water column at significant rates were the alkyl-substituted naphthalenes as shown by the chromatogram in Figure 5-115B. At this time the chromatographic pprofile of the water column appeared to be very similar to those observed with the spills initiated during the summer months (after a similar time frame), and the absolute hydrocarbon concentrations are similar in magnitude to those observed during the 4 to 9 month interval for the summer spill (see Tables 5-13 and 5-14).

Table 5-14. Dissolved Aromatic Compound Concentrations (μg/l) - Wave Tank #4, Fall 1982

Compound	5 min.	½ hour	1 hour	2 hours	4 hours	8 hours	12 hours	48 hours	3 days	4 days	10 days	12 days	5 months	9 months
Toluene	66.7	57.1	65.7	126	141	10.9	16.4	1.81	.421	.164	nd[a]	nd	nd	nd
Ethylbenzene	8.07	6.46	6.44	12.1	19.6	3.03	3.34	.949	.564	.317	nd	nd	nd	nd
m & p - xylene	25.3	22.1	21.3	40.2	61.9	10.0	11.3	4.00	2.53	1.60	nd	nd	nd	nd
o - xylene	11.2	9.92	9.89	19.1	30.3	5.04	6.10	2.43	1.70	1.14	.133	nd	nd	nd
Isopropylbenzene	.931	.894	.697	1.28	2.11	.366	.428	.196	.149	.114	.0193	nd	nd	nd
n-propylbenzene	1.39	1.55	1.18	1.07	3.72	.587	.669	.353	.293	.231	.0776	.0262	nd	nd
C_3-benzene	1.45	1.69	1.38	2.51	3.47	.710	.885	.487	.466	.405	.246	.101	nd	
1,3,5-trimethylbenzene	1.83	2.15	1.93	3.19	5.12	.927	1.15	.654	.612	.525	.285	.118	nd	nd
C_3-benzene	4.42	5.24	4.35	7.98	13.9	2.41	2.99	1.84	1.80	1.57	1.14	.515	nd	nd
C_4-benzene	3.00	3.58	3.23	5.77	9.15	1.64	2.21	1.35	1.33	1.20	1.01	.503	nd	nd
Naphthalene	3.28	4.85	5.21	10.8	18.8	2.93	4.41	3.54	3.91	3.62	4.75	2.99	nd	nd
2-methylnaphthalene	1.95	3.65	4.23	7.84	12.8	3.01	4.29	2.25	2.51	2.44	4.66	3.01	.0449	.0246
1-methylnaphthalene	1.54	2.52	3.10	6.26	10.3	2.58	3.82	1.97	2.17	2.13	3.79	2.49	.109	.0311
1,1'-biphenyl	nd	.280	.468	1.10	1.79	.428	.604	.318	.339	.339	.553	.444	.0107	.0102
2,6-dimethylnaphthalene	.238	.785	1.13	1.67	3.57	.636	.918	.525	.521	.490	.722	.665	.124	nd
C_2-naphthalene	nd	.871	1.32	2.54	4.29	1.14	1.64	.774	.797	.741	1.17	.984	.0659	nd
C_2-naphthalene	nd	nd	.272	.629	1.13	.360	.520	.218	.187	.183	.282	.247	.0232	.00459
C_2-naphthalene	nd	nd	.255	.261	.789	.235	.373	.183	.141	.134	.184	.176	.0313	nd
2,3,5-trimethylnaphthalene	nd	.227	.287	.460	.790	.0955	.442	.0575	.0452	.144	.237	.0669	.0210	nd
Dibenzothiophene	nd	nd	nd	.303	.601	.126	.257	.126	.113	.120	.241	.237	.0366	.0292
Phenanthrene	nd	nd	nd	.314	.521	.123	.220	.122	.116	.134	.190	.191	.0523	.0380
Total Resolved	143	203	149	393	464	67.1	92.1	34.5	33.6	26.0	31.8	20.8	5.19	5.81
Unresolved Compounds	0	0	0	793	213	16.1	44.7	17.5	19.5	18.7	33.2	30.3	10.7	5.38

a - nd indicates "not detected"

Figure 5-116 presents time-series dissolved concentrations for the total resolved and unresolved components in the water column from wave tank 4 during the winter spill conditions along with the mean concentrations observed from wave tanks 1 through 3 during the summer spill. During the winter conditions, the total hydrocarbon concentration of chromatographically resolved components approached 460 µg/l compared to 390 µg/l for the resolved components during the summer spill. This presumably reflects the longer life time of the components in the slick due to inhibited evaporative loss. The concentration of components in the unresolved complex mixture during the winter spill is observed to rapidly increase to approximately 200 µg/l during the first 8 hours and then fall off rapidly to values below 20 µg/l within 12 hours after spill initiation. By contrast, the components in the unresolved complex mixtures remained relatively high (100 µg/l) and constant during the first 12 days of the summer experiment.

Individual dissolved aromatic hydrocarbon concentrations for the summer spills are presented in Figures 5-117 and 5-118. Similar time-series concentrations for individual dissolved aromatic hydrocarbons during the winter spill are presented in Figures 5-119 and 5-120. Detailed examination of the data in the figures shows nearly identical <u>absolute</u> concentrations for individual aromatic compounds in the water column during the summer and winter spills. The relative time lag in water column buildup during the colder winter conditions is clearly apparent, however, in comparing such individual compounds as toluene (Figure 5-117A and Figure 5-119A), ethylbenzene (Figure 5-117B and Figure 5-119B), C3-substituted benzenes (Figure 5-117C and Figure 5-119C), and other components presented in Figures 5-117 through 5-120. In particular, the greater number of sampling points on the increasing side of the concentration profiles (all samples from both summer and winter were obtained at times 5 minutes, 1 hour, 2 hours, 4 hours, 8 hours, 12 hours, 24 hours and 48 hours post spill) show this slower buildup in the water column concentrations during the winter conditions. Again, the compounds are present longer in the slick due to lowered component-specific vapor pressures at -5°C, and their buildup in the water column is presumably delayed due to diffusion

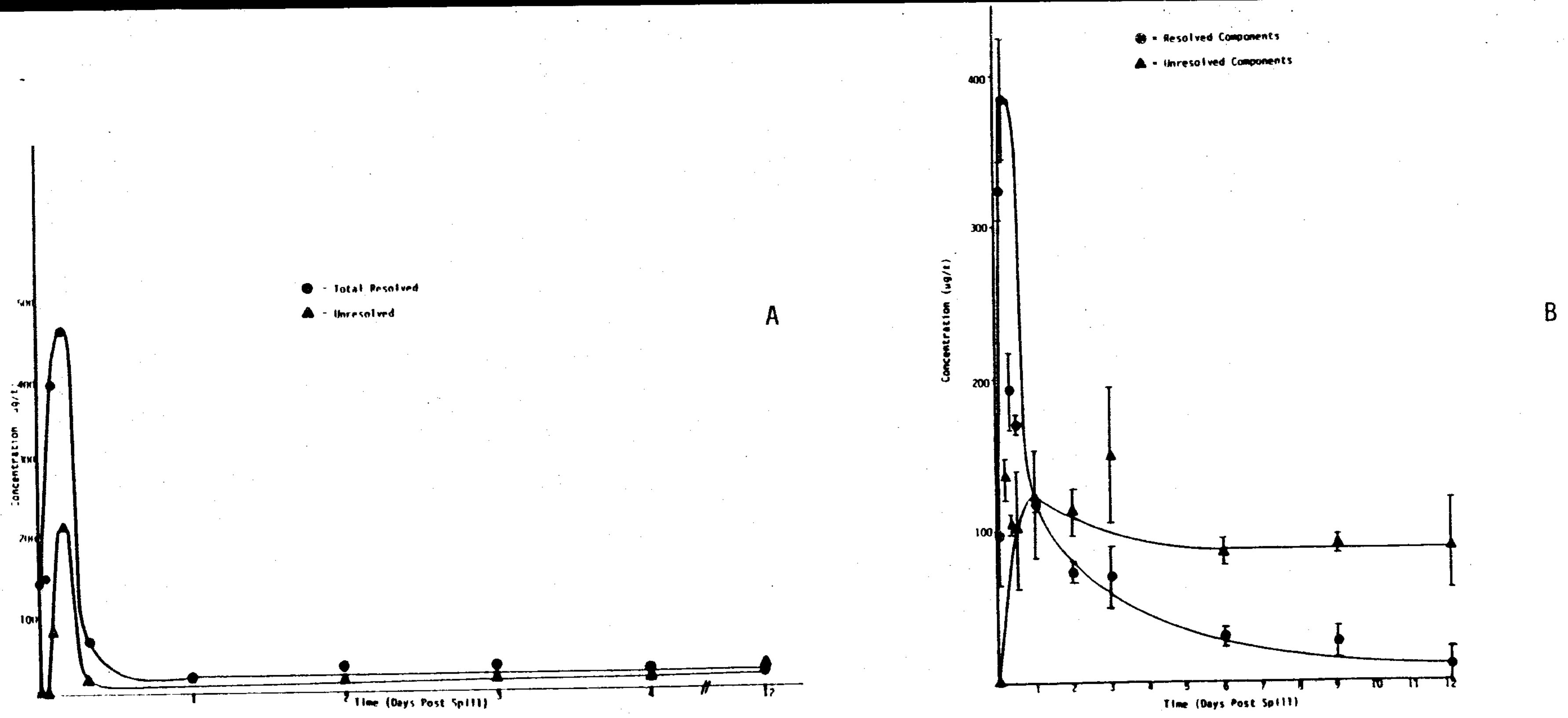

Figure 5-116. Time series concentrations for total Resolved and Unresolved compounds dissolved in the water column from (A) Wave Tank #4, and (B) Wave Tanks #1-3. Values are means ± one standard deviation.

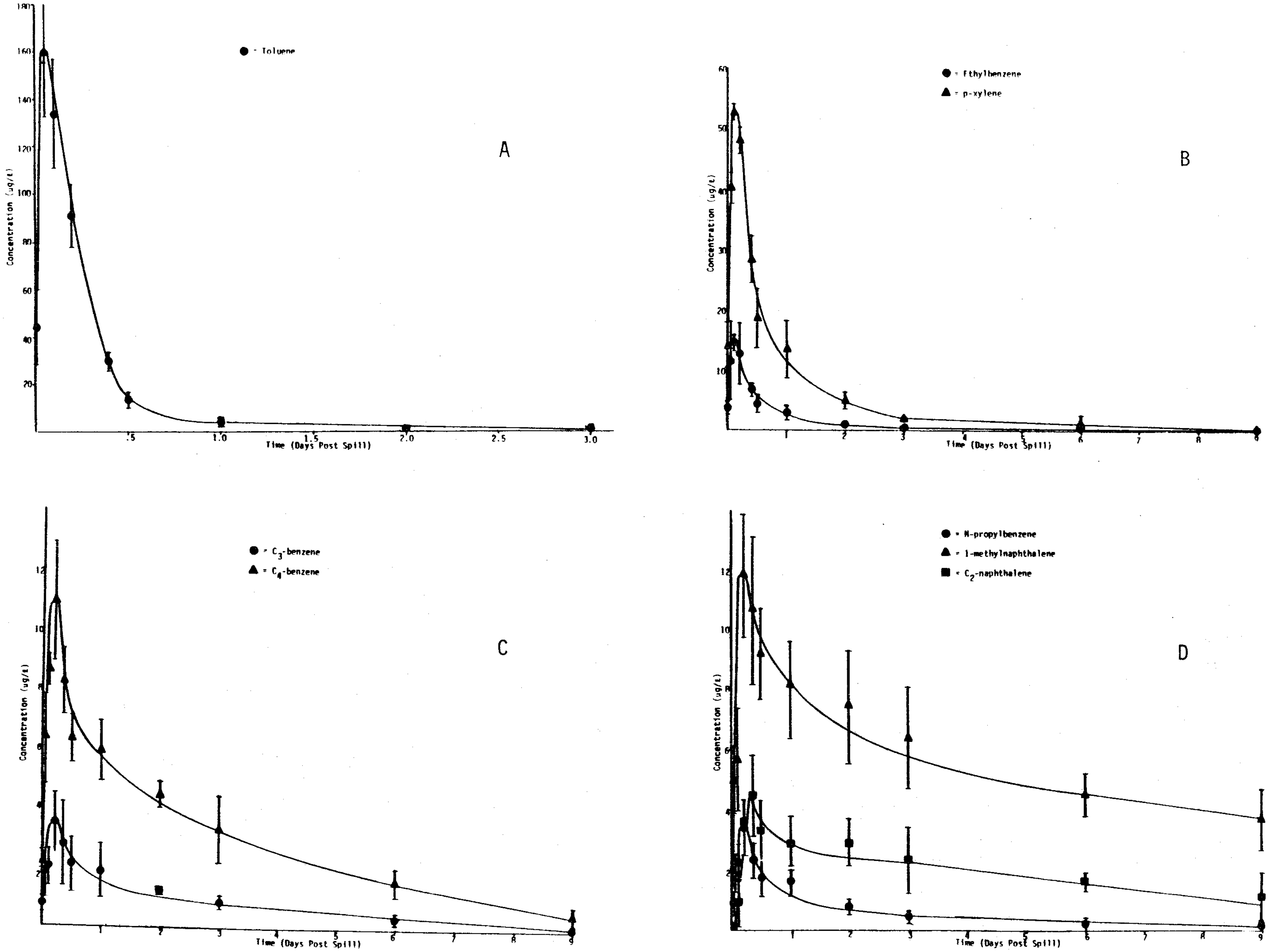

Figure 5-117. Time series concentrations of individual dissolved aromatic hydrocarbons measured in Wave Tanks #1-3. Values are means ± one standard deviation.

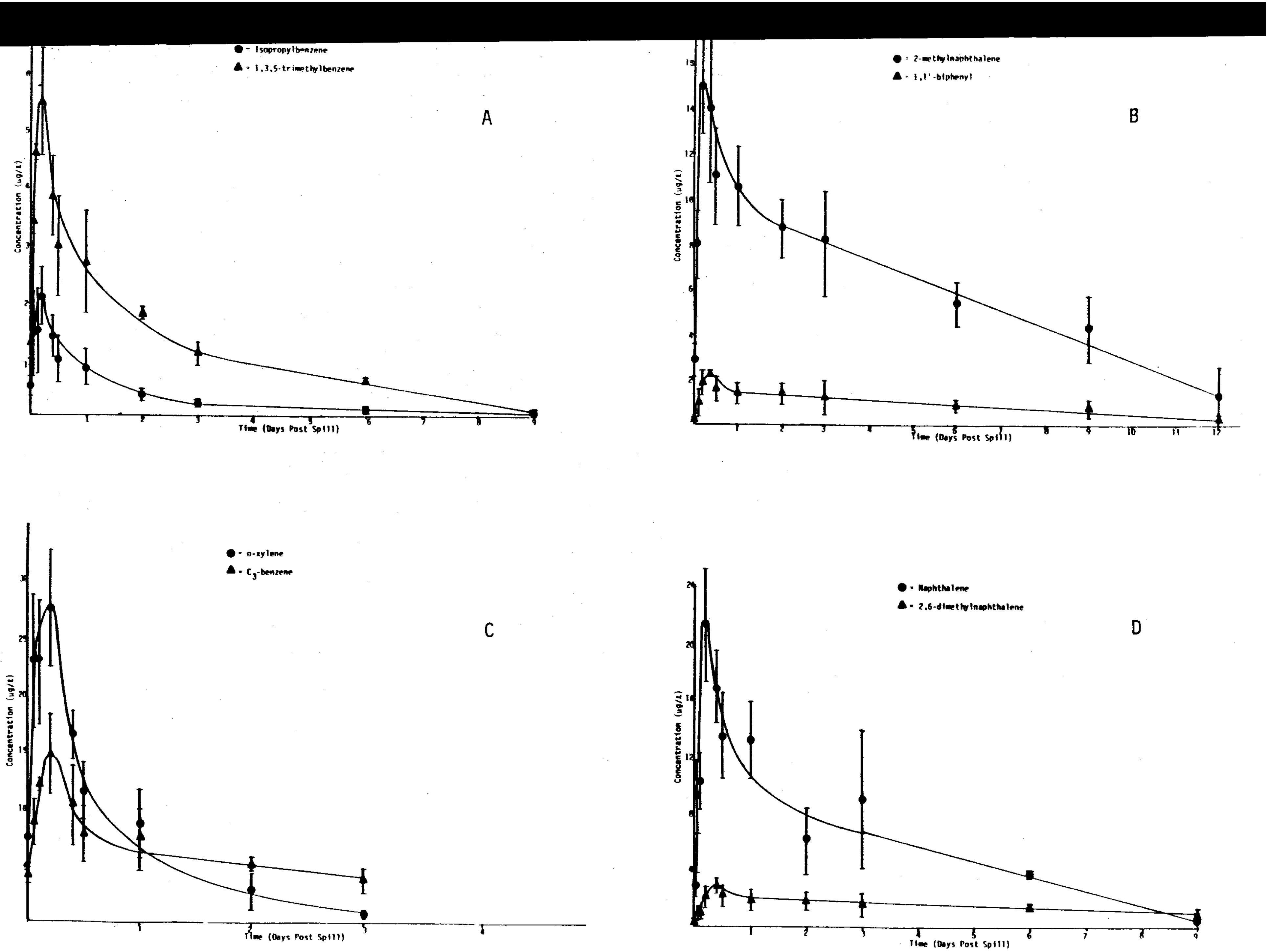

Figure 5-118. Time series concentrations of individual dissolved aromatic hydrocarbons measured in Wave Tanks #1-3. Values are means ± one standard deviation.

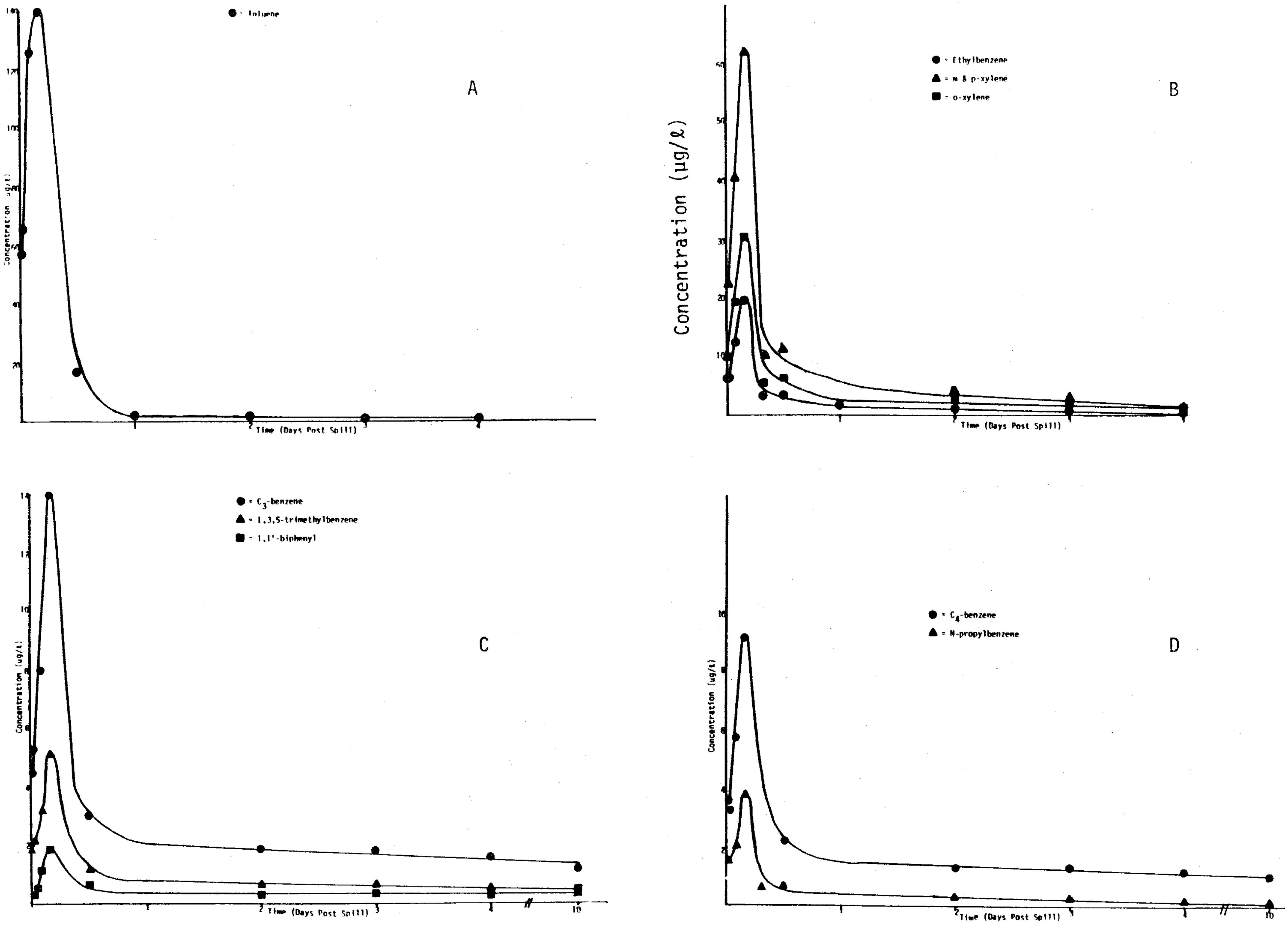

Figure 5-119. Time series concentrations of individual dissolved aromatic hydrocarbons measured in Wave Tank #4

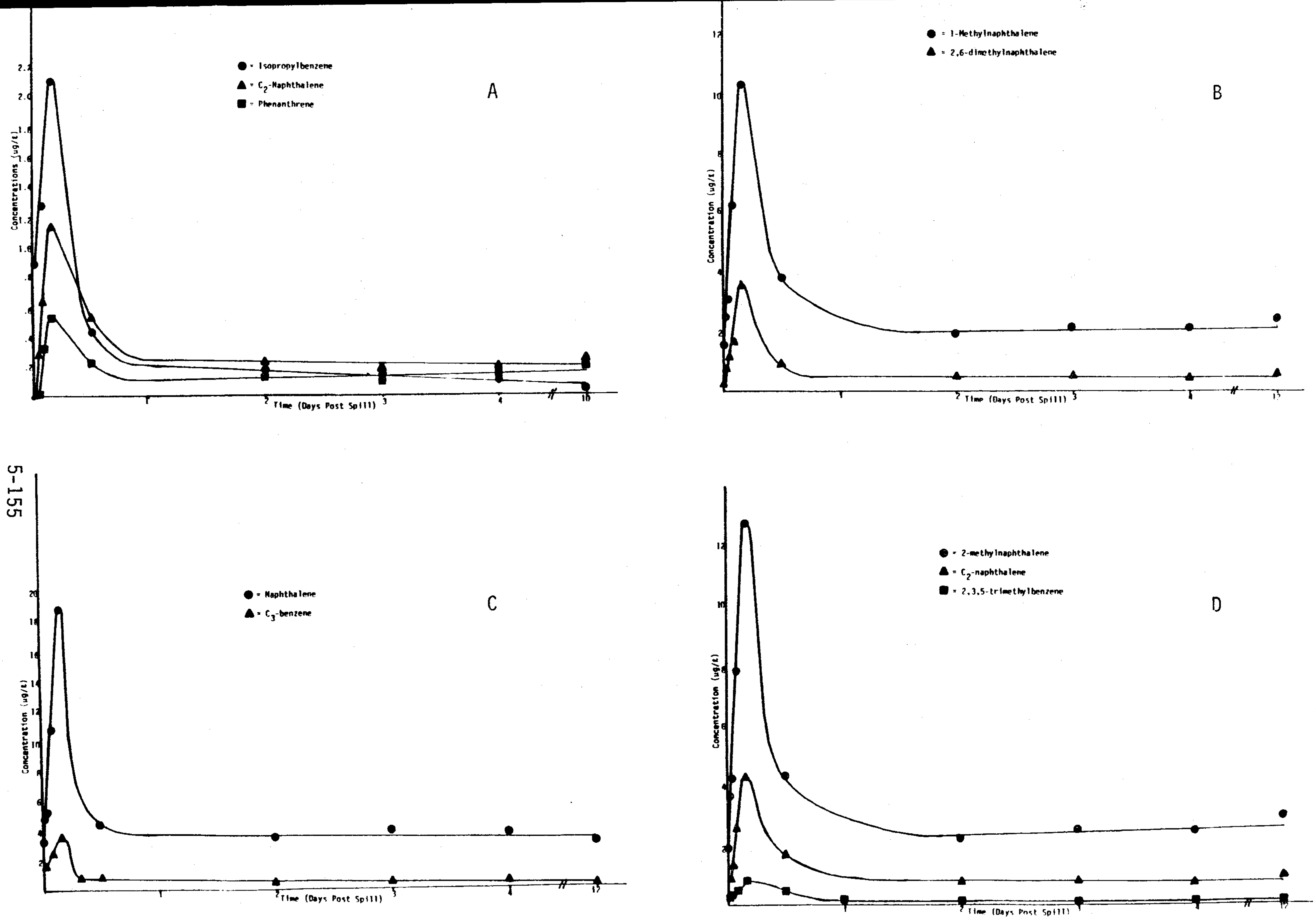

Figure 5-120. Time series concentrations of individual dissolved aromatic hydrocarbons measured in Wave Tank #4.

controlled mass transfer from the slick which was more viscous (due to lower temperatures). As such, it was not as well stirred, and these trends are clearly observed in the data presented in graphical form.

5.5 OIL WEATHERING MODEL VERIFICATION

5.5.1 Model Predicted vs Observed Evaporation/Dissolution Results from Controlled Chamber Experiments in La Jolla

As described in detail in the modeling section (4.0), two distinctly different modeling approaches are being taken in our efforts to predict oil weathering behavior. The component-specific model predicts individual compound concentrations in the slick or water column as a function of time, and the pseudo-compound (or fractional-distillation cut) approach allows predictions of overall oil mass balance. Output data from the component-specific approach predicts time series concentrations in the slick, air and water column based on thermodynamic properties such as Henry's Law constants, liquid-liquid partitioning coefficients and mass transfer coefficients.

Predicted vs observed water column concentrations for benzene, cyclohexane and toluene were generated using the data from evaporation/dissolution chamber experiments in La Jolla, California, and preliminary results from these studies were described in our November 1980 Interim Quarterly Report (PAYNE et al., 1980). A much more sophisticated evaporation-dissolution model has since been generated, allowing prediction of specific compound concentrations in the water column beneath an oil slick.

A significant improvement in the model has come from the utilization of Henry's law coefficients in the calculation of the mass-transfer coefficient at the oil-air interface. Previously, only benzene, toluene and cyclohexane were modeled, and since these compounds all have similar volatilities, they behave in a similar manner. However, when considering compounds which are much less volatile (e.g., naphthalane), water column concentrations will peak much later than the concentrations of benzene, toluene, and cyclohexane.

This is due to the fact that the less volatile compounds leave the oil-water phases much more slowly, allowing more time to transfer from the oil to the water phase. The equations being used to predict water and oil column concentrations are those presented in the November Quarterly (PAYNE et al., 1980), with changes being made only to the over-all mass transfer coefficient at the oil-air interface. Tables 5-15 through 5-26 present specific numerical output for six selected compounds examined in the evaporation and dissolution experiments at 3 and 21°C. The output presented in these tables is all the information needed to calculate the water and oil phase concentrations. The KW, KA, and KO values are individual-phase mass transfer coefficients; the M-value and Henry's law coefficient was derived from the Antoine vapor pressure equation and the constants, ANTA, ANTB, and ANTC are from REID et al. (1977). The quantities A through Z2 on the output are intermediate results used to calculate the final concentrations. For the water column concentrations:

$$Y = Z1*EXP(D1*TIME)+Z3*EXP(D2*TIME) \tag{5.1}$$

Figures 5-121 and 5-122 present the predicted water column concentrations at 21 and 3°C for the compounds presented in Tables 5-15 through 5-26. These figures clearly show the less volatile compounds persisting in the water column. This is what has been recently observed experimentally as shown in plots of observed component concentration (Figures 5-25 and 5-31). The experimental observations at 19°C indicate that the naphthalenes tail-off much faster than predicted; however, this rapid tail-off of dissolved naphthalene could be due to some other mechanism such as adsorption to the walls or stirring blades of the evaporation/dissolution chamber (high surface area to volume ratio).

In general, the predicted time of occurrence of the peak water concentrations is quite good, but the peak concentrations do not always agree well. The prediction of the peak concentration is directly dependent on the initial concentration and the M-value. While our M-value data represent first-of-a-kind measurements, future determinations will no doubt yield improvements.

TABLE 5-15. STIRRED TANK MODEL COMPUTER PREDICTED WATER COLUMN CONCENTRATIONS FROM EVAPORATION/DISSOLUTION EXPERIMENTS: KOVAT 854 ETHYLBENZENE.

```
STIRRED TANK MODEL FOR KOVAT  857, ETHYLBENZENE
FROM THE KEYBOARD, KW =  3.000E+00, KA =  1.500E+03, KO =  1.000E+00 CM/HR
M (OIL/WATER) =  2.660E+03, HENRYS LAW (AIR/OIL) =  4.048E-05 DIMENSIONLESS, AT  3.000E+00 DEG C
ANTA =  1.602E+01, ANTB =  3.298E+03, ANTC = -5.995E+01
MOLE WT OF OIL =  2.800E+02, DENSITY =  8.800E-01 GM/CC
VO =  2.000E+02 ML, VW =  3.000E+04 ML
XZERO =  4.740E+02 MICROGRAMS/GRAM OF OIL, AREA =  6.170E+02 CM*CM
OVER-ALL KW AT WATER-OIL =  2.997E+00 CM/HR
OVER-ALL KO AT OIL-AIR =  5.725E-02 CM/HR
A = -6.163E-02, B =  2.317E-05
C =  9.245E+00, D = -1.801E-01
H =  1.220E-01
D1 = -5.983E-02, D2 = -1.819E-01
C1 =  6.920E+00, C2 =  4.671E+02
Z1 =  9.001E-02, Z2 = -9.001E-02
WATER CONCENTRATION PEAKS AT  9.109E+00 HOURS
WHERE THE WATER CONCENTRATION =  3.501E-02, AND THE OIL CONCENTRATION =  9.312E+01
AND THE CONCENTRATION RATIO (OIL/WATER) =  2.660E+03

      HOUR      H2O        OIL

      0.20  2.144E-03  4.572E+02
      0.40  4.186E-03  4.411E+02
      0.60  6.130E-03  4.255E+02
      0.80  7.979E-03  4.104E+02
      1.00  9.738E-03  3.959E+02
      1.20  1.141E-02  3.819E+02
      1.40  1.300E-02  3.685E+02
      1.60  1.451E-02  3.554E+02
      1.80  1.594E-02  3.429E+02
      2.00  1.729E-02  3.308E+02
      2.25  1.889E-02  3.163E+02
      2.50  2.037E-02  3.024E+02
      2.75  2.176E-02  2.891E+02
      3.00  2.306E-02  2.765E+02
      3.25  2.426E-02  2.643E+02
      3.50  2.537E-02  2.528E+02
      3.75  2.640E-02  2.417E+02
      4.00  2.736E-02  2.311E+02
      4.25  2.824E-02  2.210E+02
      4.50  2.905E-02  2.113E+02
      6.00  3.263E-02  1.617E+02
      8.00  3.475E-02  1.133E+02
     10.00  3.487E-02  7.958E+01
     12.00  3.374E-02  5.605E+01
     14.00  3.188E-02  3.961E+01
     16.00  2.964E-02  2.810E+01
     18.00  2.724E-02  2.004E+01
     20.00  2.482E-02  1.439E+01
     22.00  2.248E-02  1.040E+01
     24.00  2.026E-02  7.585E+00
     26.00  1.819E-02  5.589E+00
     28.00  1.629E-02  4.165E+00
     30.00  1.456E-02  3.144E+00
     32.00  1.299E-02  2.406E+00
     34.00  1.158E-02  1.868E+00
     36.00  1.031E-02  1.472E+00
     38.00  9.169E-03  1.177E+00
     40.00  8.152E-03  9.552E-01
     42.00  7.244E-03  7.853E-01
     44.00  6.436E-03  6.535E-01
```

TABLE 5-16. STIRRED TANK MODEL COMPUTER PREDICTED WATER COLUMN CONCENTRATIONS FROM EVAPORATION/DISSOLUTION EXPERIMENTS: KOVAT 867, P-XYLENE.

```
STIRRED TANK MODEL FOR KOVAT  867, P-XYLENE
FROM THE KEYBOARD, KW =  3.000E+00, KA =  1.500E+03, KO =  1.000E+00 CM/HR
H (OIL/WATER) =  3.030E+03, HENRYS LAW (AIR/OIL) =  4.032E-05 DIMENSIONLESS, AT  3.000E+00 DEG C
ANTA =  1.609E+01, ANTB =  3.347E+03, ANTC = -5.780E+01
MOLE WT OF OIL =  2.800E+02, DENSITY =  8.800E-01 GM/CC
VO =  2.000E+02 ML, VW =  3.000E+04 ML
XZERO =  1.794E+03 MICROGRAMS/GRAM OF OIL, AREA =  6.170E+02 CM*CM
OVER-ALL KW AT WATER-OIL =  2.997E+00 CM/HR
OVER-ALL KO AT OIL-AIR =  5.702E-02 CM/HR
A = -6.164E-02, B =  2.034E-05
C =  9.246E+00, D = -1.790E-01
R =  1.205E-01
D1 = -6.006E-02, D2 = -1.806E-01
C1 =  2.355E+01, C2 =  1.770E+03
Z1 =  3.029E-01, Z2 = -3.029E-01
WATER CONCENTRATION PEAKS AT  9.135E+00 HOURS
WHERE THE WATER CONCENTRATION =  1.168E-01, AND THE OIL CONCENTRATION =  3.530E+02
AND THE CONCENTRATION RATIO (OIL/WATER) =  3.030E+03

      HOUR      H2O         OIL

      0.20  7.126E-03  1.731E+03
      0.40  1.391E-02  1.670E+03
      0.60  2.030E-02  1.611E+03
      0.80  2.653E-02  1.555E+03
      1.00  3.238E-02  1.500E+03
      1.20  3.794E-02  1.447E+03
      1.40  4.322E-02  1.397E+03
      1.60  4.824E-02  1.348E+03
      1.80  5.300E-02  1.300E+03
      2.00  5.752E-02  1.255E+03
      2.25  6.283E-02  1.200E+03
      2.50  6.779E-02  1.148E+03
      2.75  7.242E-02  1.098E+03
      3.00  7.673E-02  1.050E+03
      3.25  8.074E-02  1.004E+03
      3.50  8.446E-02  9.602E+02
      3.75  8.791E-02  9.184E+02
      4.00  9.110E-02  8.784E+02
      4.25  9.404E-02  8.402E+02
      4.50  9.675E-02  8.036E+02
      6.00  1.087E-01  6.157E+02
      8.00  1.159E-01  4.322E+02
     10.00  1.163E-01  3.040E+02
     12.00  1.126E-01  2.143E+02
     14.00  1.065E-01  1.515E+02
     16.00  9.901E-02  1.075E+02
     18.00  9.100E-02  7.664E+01
     20.00  8.294E-02  5.493E+01
     22.00  7.510E-02  3.962E+01
     24.00  6.769E-02  2.881E+01
     26.00  6.078E-02  2.113E+01
     28.00  5.443E-02  1.567E+01
     30.00  4.863E-02  1.175E+01
     32.00  4.338E-02  8.927E+00
     34.00  3.865E-02  6.876E+00
     36.00  3.440E-02  5.372E+00
     38.00  3.059E-02  4.259E+00
     40.00  2.719E-02  3.424E+00
     42.00  2.416E-02  2.791E+00
     44.00  2.145E-02  2.304E+00
```

TABLE 5-17. STIRRED TANK MODEL COMPUTER PREDICTED WATER COLUMN CONCENTRATIONS FROM EVAPORATION/DISSOLUTION EXPERIMENTS: KOVAT 1021, 1-METHYL-4-ISOPROPYLBENZENE.

```
STIRRED TANK MODEL FOR KOVAT 1021, 1-METHYL-4-ISOPROPYLB
FROM THE KEYBOARD, KW =  3.000E+00, KA =  1.500E+03, KO =  1.060E+00 CM/HR
M (OIL/WATER) =  1.480E+04, HENRYS LAW (AIR/OIL) =  5.463E-06 DIMENSIONLESS, AT  3.000E+00 DEG C
ANTA =  1.594E+01, ANTB =  3.539E+03, ANTC = -7.010E+01
MOLE WT OF OIL =  2.880E+02, DENSITY =  8.800E-01 GM/CC
VO =  2.000E+02 ML, VW =  3.000E+04 ML
XZERO =  4.530E+02 MICROGRAMS/GRAM OF OIL, AREA =  6.170E+02 CM*CM
OVER-ALL KW AT WATER-OIL =  2.999E+00 CM/HR
OVER-ALL KO AT OIL-AIR =  8.127E-03 CM/HR
A = -6.169E-02, B =  4.168E-06
C =  9.253E+00, D = -2.570E-02
R =  3.807E-02
D1 = -2.466E-02, D2 = -6.273E-02
C1 =  4.406E+02, C2 =  1.239E+01
Z1 =  4.959E-02, Z2 = -4.959E-02
WATER CONCENTRATION PEAKS AT  2.453E+01 HOURS
WHERE THE WATER CONCENTRATION =  1.644E-02, AND THE OIL CONCENTRATION =  2.433E+02
AND THE CONCENTRATION RATIO (OIL/WATER) =  1.480E+04

      HOUR      H20        OIL

      0.20  3.743E-04  4.507E+02
      0.40  7.422E-04  4.484E+02
      0.60  1.104E-03  4.461E+02
      0.80  1.459E-03  4.438E+02
      1.00  1.808E-03  4.416E+02
      1.20  2.150E-03  4.393E+02
      1.40  2.487E-03  4.370E+02
      1.60  2.817E-03  4.348E+02
      1.80  3.142E-03  4.325E+02
      2.00  3.461E-03  4.303E+02
      2.25  3.852E-03  4.276E+02
      2.50  4.233E-03  4.249E+02
      2.75  4.607E-03  4.222E+02
      3.00  4.971E-03  4.195E+02
      3.25  5.328E-03  4.168E+02
      3.50  5.676E-03  4.141E+02
      3.75  6.016E-03  4.115E+02
      4.00  6.348E-03  4.089E+02
      4.25  6.672E-03  4.063E+02
      4.50  6.989E-03  4.037E+02
      6.00  8.735E-03  3.885E+02
      8.00  1.069E-02  3.692E+02
     10.00  1.227E-02  3.509E+02
     12.00  1.353E-02  3.336E+02
     14.00  1.451E-02  3.171E+02
     16.00  1.525E-02  3.015E+02
     18.00  1.578E-02  2.867E+02
     20.00  1.614E-02  2.726E+02
     22.00  1.635E-02  2.593E+02
     24.00  1.644E-02  2.466E+02
     26.00  1.641E-02  2.345E+02
     28.00  1.630E-02  2.231E+02
     30.00  1.612E-02  2.122E+02
     32.00  1.587E-02  2.018E+02
     34.00  1.557E-02  1.920E+02
     36.00  1.523E-02  1.827E+02
     38.00  1.486E-02  1.738E+02
     40.00  1.446E-02  1.653E+02
     42.00  1.405E-02  1.573E+02
     44.00  1.362E-02  1.497E+02
```

TABLE 5-18. STIRRED TANK MODEL COMPUTER PREDICTED WATER COLUMN CONCENTRATIONS FROM EVAPORATION/DISSOLUTION EXPERIMENTS: KOVAT 1185, NAPHTHALENE.

```
STIRRED TANK MODEL FOR KOVAT 1185, NAPHTHALENE
FROM THE KEYBOARD, KW =  3.000E+00, KA =  1.500E+03, KO =  1.000E+00 CM/HR
M (OIL/WATER) =  5.570E+03, HENRYS LAW (AIR/OIL) =  6.590E-07 DIMENSIONLESS, AT  3.000E+00 DEG C
ANTA =  1.614E+01, ANTB =  3.992E+03, ANTC = -7.130E+01
MOLE WT OF OIL =  2.880E+02, DENSITY =  8.800E-01 GM/CC
VO =  2.000E+02 ML, VW =  3.000E+04 ML
XZERO =  5.200E+02 MICROGRAMS/GRAM OF OIL, AREA =  6.170E+02 CM*CM
OVER-ALL KW AT WATER-OIL =  2.998E+00 CM/HR
OVER-ALL KO AT OIL-AIR =  9.887E-04 CM/HR
A = -6.167E-02, B =  1.107E-05
C =  9.250E+00, D = -4.711E-03
R =  6.045E-02
D1 = -2.966E-03, D2 = -6.341E-02
C1 =  5.050E+02, C2 =  1.501E+01
Z1 =  9.524E-02, Z2 = -9.524E-02
WATER CONCENTRATION PEAKS AT  5.066E+01 HOURS
WHERE THE WATER CONCENTRATION =  7.812E-02, AND THE OIL CONCENTRATION =  4.361E+02
AND THE CONCENTRATION RATIO (OIL/WATER) =  5.570E+03

      HOUR       H20          OIL

      0.20  1.144E-03  5.195E+02
      0.40  2.273E-03  5.190E+02
      0.60  3.386E-03  5.185E+02
      0.80  4.485E-03  5.181E+02
      1.00  5.570E-03  5.176E+02
      1.20  6.640E-03  5.171E+02
      1.40  7.696E-03  5.166E+02
      1.60  8.738E-03  5.162E+02
      1.80  9.767E-03  5.157E+02
      2.00  1.078E-02  5.152E+02
      2.25  1.203E-02  5.146E+02
      2.50  1.326E-02  5.141E+02
      2.75  1.447E-02  5.135E+02
      3.00  1.566E-02  5.129E+02
      3.25  1.682E-02  5.124E+02
      3.50  1.797E-02  5.118E+02
      3.75  1.910E-02  5.112E+02
      4.00  2.021E-02  5.107E+02
      4.25  2.131E-02  5.101E+02
      4.50  2.238E-02  5.096E+02
      6.00  2.846E-02  5.063E+02
      8.00  3.566E-02  5.022E+02
     10.00  4.194E-02  4.982E+02
     12.00  4.741E-02  4.943E+02
     14.00  5.217E-02  4.906E+02
     16.00  5.630E-02  4.870E+02
     18.00  5.987E-02  4.835E+02
     20.00  6.296E-02  4.801E+02
     22.00  6.562E-02  4.768E+02
     24.00  6.791E-02  4.736E+02
     26.00  6.986E-02  4.704E+02
     28.00  7.152E-02  4.673E+02
     30.00  7.292E-02  4.642E+02
     32.00  7.410E-02  4.612E+02
     34.00  7.508E-02  4.583E+02
     36.00  7.588E-02  4.554E+02
     38.00  7.633E-02  4.525E+02
     40.00  7.705E-02  4.497E+02
     42.00  7.745E-02  4.469E+02
     44.00  7.774E-02  4.441E+02
```

TABLE 5-19. STIRRED TANK MODEL COMPUTER PREDICTED WATER COLUMN CONCENTRATIONS FROM EVAPORATION/DISSOLUTION EXPERIMENTS: KOVAT 1295, 2-METHYLNAPHTHALENE.

```
STIRRED TANK MODEL FOR KOVAT 1295, 2-METHYLNAPHTHALENE
FROM THE KEYBOARD, KW =  3.000E+00, KA =  1.500E+03, KO =  1.000E+00 CM/HR
M (OIL/WATER) =  3.580E+04, HENRYS LAW (AIR/OIL) =  1.592E-07 DIMENSIONLESS, AT  3.000E+00 DEG C
ANTA =  1.627E+01, ANTB =  4.237E+03, ANTC = -7.475E+01
MOLE WT OF OIL =  2.880E+02, DENSITY =  8.800E-01 GM/CC
VO =  2.000E+02 ML, VW =  3.000E+04 ML
XZERO =  1.260E+03 MICROGRAMS/GRAM OF OIL, AREA =  6.170E+02 CM*CM
OVER-ALL KW AT WATER-OIL =  3.000E+00 CM/HR
OVER-ALL KO AT OIL-AIR =  2.388E-04 CM/HR
A = -6.169E-02, B =  1.723E-06
C =  9.254E+00, D = -9.951E-04
R =  6.122E-02
D1 = -7.334E-04, D2 = -6.196E-02
C1 =  1.255E+03, C2 =  5.384E+00
Z1 =  3.547E-02, Z2 = -3.547E-02
WATER CONCENTRATION PEAKS AT  7.246E+01 HOURS
WHERE THE WATER CONCENTRATION =  3.323E-02, AND THE OIL CONCENTRATION =  1.190E+03
AND THE CONCENTRATION RATIO (OIL/WATER) =  3.580E+04

      HOUR      H2O         OIL

       0.20  4.316E-04  1.260E+03
       0.40  8.578E-04  1.259E+03
       0.60  1.279E-03  1.259E+03
       0.80  1.694E-03  1.259E+03
       1.00  2.105E-03  1.259E+03
       1.20  2.510E-03  1.259E+03
       1.40  2.910E-03  1.258E+03
       1.60  3.306E-03  1.258E+03
       1.80  3.696E-03  1.258E+03
       2.00  4.081E-03  1.258E+03
       2.25  4.557E-03  1.257E+03
       2.50  5.024E-03  1.257E+03
       2.75  5.485E-03  1.257E+03
       3.00  5.938E-03  1.256E+03
       3.25  6.384E-03  1.256E+03
       3.50  6.823E-03  1.256E+03
       3.75  7.256E-03  1.255E+03
       4.00  7.681E-03  1.255E+03
       4.25  8.100E-03  1.255E+03
       4.50  8.513E-03  1.255E+03
       6.00  1.086E-02  1.253E+03
       8.00  1.365E-02  1.251E+03
      10.00  1.612E-02  1.248E+03
      12.00  1.829E-02  1.246E+03
      14.00  2.021E-02  1.244E+03
      16.00  2.189E-02  1.242E+03
      18.00  2.337E-02  1.240E+03
      20.00  2.468E-02  1.238E+03
      22.00  2.582E-02  1.236E+03
      24.00  2.683E-02  1.234E+03
      26.00  2.771E-02  1.232E+03
      28.00  2.849E-02  1.230E+03
      30.00  2.917E-02  1.228E+03
      32.00  2.976E-02  1.226E+03
      34.00  3.028E-02  1.224E+03
      36.00  3.073E-02  1.223E+03
      38.00  3.112E-02  1.221E+03
      40.00  3.147E-02  1.219E+03
      42.00  3.176E-02  1.217E+03
      44.00  3.202E-02  1.215E+03
```

TABLE 5-20. STIRRED TANK MODEL COMPUTER PREDICTED WATER COLUMN CONCENTRATIONS FROM EVAPORATION/DISSOLUTION EXPERIMENTS: KOVAT 1317, 1-METHYLNAPHTHALENE.

```
STIRRED TANK MODEL FOR KOVAT 1317, 1-METHYLNAPHTHALENE
FROM THE KEYBOARD, KW =  3.000E+00, KA =  1.500E+03, KO =  1.000E+00 CM/HR
M (OIL/WATER) =  3.040E+04, HENRYS LAW (AIR/OIL) =  1.204E-07 DIMENSIONLESS, AT  3.000E+00 DEG C
ANTA =  1.620E+01, ANTB =  4.207E+03, ANTC = -7.814E+01
MOLE WT OF OIL =  2.880E+02, DENSITY =  8.800E-01 GM/CC
VO =  2.000E+02 ML, VW =  3.000E+04 ML
XZERO =  7.370E+02 MICROGRAMS/GRAM OF OIL, AREA =  6.170E+02 CM*CM
OVER-ALL KW AT WATER-OIL =  3.000E+00 CM/HR
OVER-ALL KO AT OIL-AIR =  1.806E-04 CM/HR
A = -6.169E-02, B =  2.029E-06
C =  9.254E+00, D = -8.616E-04
R =  6.145E-02
D1 = -5.545E-04, D2 = -6.200E-02
C1 =  7.333E+02, C2 =  3.684E+00
Z1 =  2.434E-02, Z2 = -2.434E-02
WATER CONCENTRATION PEAKS AT  7.676E+01 HOURS
WHERE THE WATER CONCENTRATION =  2.312E-02, AND THE OIL CONCENTRATION =  7.020E+02
AND THE CONCENTRATION RATIO (OIL/WATER) =  3.040E+04

      HOUR      H2O         OIL

      0.20   2.973E-04   7.369E+02
      0.40   5.909E-04   7.367E+02
      0.60   8.808E-04   7.366E+02
      0.80   1.167E-03   7.365E+02
      1.00   1.450E-03   7.364E+02
      1.20   1.729E-03   7.362E+02
      1.40   2.005E-03   7.361E+02
      1.60   2.277E-03   7.360E+02
      1.80   2.546E-03   7.359E+02
      2.00   2.812E-03   7.358E+02
      2.25   3.139E-03   7.356E+02
      2.50   3.461E-03   7.355E+02
      2.75   3.779E-03   7.353E+02
      3.00   4.091E-03   7.352E+02
      3.25   4.398E-03   7.350E+02
      3.50   4.701E-03   7.349E+02
      3.75   4.999E-03   7.347E+02
      4.00   5.292E-03   7.346E+02
      4.25   5.581E-03   7.344E+02
      4.50   5.866E-03   7.343E+02
      6.00   7.401E-03   7.334E+02
      8.00   9.411E-03   7.323E+02
     10.00   1.111E-02   7.312E+02
     12.00   1.261E-02   7.302E+02
     14.00   1.393E-02   7.292E+02
     16.00   1.510E-02   7.282E+02
     18.00   1.613E-02   7.272E+02
     20.00   1.703E-02   7.263E+02
     22.00   1.782E-02   7.254E+02
     24.00   1.852E-02   7.245E+02
     26.00   1.914E-02   7.236E+02
     28.00   1.968E-02   7.227E+02
     30.00   2.015E-02   7.218E+02
     32.00   2.057E-02   7.209E+02
     34.00   2.093E-02   7.201E+02
     36.00   2.125E-02   7.192E+02
     38.00   2.153E-02   7.184E+02
     40.00   2.177E-02   7.175E+02
     42.00   2.198E-02   7.167E+02
     44.00   2.216E-02   7.159E+02
```

TABLE 5-21. STIRRED TANK MODEL COMPUTER PREDICTED WATER COLUMN CONCENTRATIONS FROM EVAPORATION/DISSOLUTION EXPERIMENTS: KOVAT 857, ETHYLBENZENE.

```
STIRRED TANK MODEL FOR KOVAT  857, ETHYLBENZENE
FROM THE KEYBOARD, KW =  3.000E+00, KA =  1.500E+03, KO =  1.000E+00 CM/HR
H (OIL/WATER) =  2.400E+03, HENRYS LAW (AIR/OIL) =  1.232E-04 DIMENSIONLESS, AT  2.100E+01 DEG C
ANTA =  1.602E+01, ANTB =  3.298E+03, ANTC = -5.995E+01
MOLE WT OF OIL =  2.000E+02, DENSITY =  8.800E-01 CM/CC
VO =  2.000E+02 ML, VW =  3.000E+04 ML
XZERO =  4.740E+02 MICROGRAMS/GRAM OF OIL, AREA =  6.170E+02 CM*CM
OVER-ALL KW AT WATER-OIL =  2.996E+00 CM/HR
OVER-ALL KO AT OIL-AIR =  1.560E-01 CM/HR
A = -6.162E-02, B =  2.568E-05
C =  9.243E+00, D = -4.850E-01
R =  4.245E-01
D1 = -6.106E-02, D2 = -4.856E-01
C1 =  6.250E-01, C2 =  4.734E+02
Z1 =  2.867E-02, Z2 = -2.867E-02
WATER CONCENTRATION PEAKS AT  4.804E+00 HOURS
WHERE THE WATER CONCENTRATION =  1.860E-02, AND THE OIL CONCENTRATION =  4.464E+01
AND THE CONCENTRATION RATIO (OIL/WATER) =  2.400E+03

      HOUR      H2O        OIL

      0.20  2.305E-03  4.302E+02
      0.40  4.369E-03  3.904E+02
      0.60  6.215E-03  3.543E+02
      0.80  7.862E-03  3.216E+02
      1.00  9.329E-03  2.919E+02
      1.20  1.063E-02  2.649E+02
      1.40  1.179E-02  2.404E+02
      1.60  1.282E-02  2.182E+02
      1.80  1.372E-02  1.981E+02
      2.00  1.452E-02  1.798E+02
      2.25  1.537E-02  1.593E+02
      2.50  1.609E-02  1.411E+02
      2.75  1.670E-02  1.251E+02
      3.00  1.719E-02  1.108E+02
      3.25  1.759E-02  9.819E+01
      3.50  1.791E-02  8.702E+01
      3.75  1.816E-02  7.712E+01
      4.00  1.835E-02  6.835E+01
      4.25  1.848E-02  6.059E+01
      4.50  1.856E-02  5.371E+01
      6.00  1.832E-02  2.613E+01
      8.00  1.700E-02  1.011E+01
     10.00  1.534E-02  4.023E+00
     12.00  1.369E-02  1.695E+00
     14.00  1.216E-02  7.939E-01
     16.00  1.078E-02  4.352E-01
     18.00  9.546E-03  2.839E-01
     20.00  8.451E-03  2.130E-01
     22.00  7.480E-03  1.740E-01
     24.00  6.621E-03  1.485E-01
     26.00  5.860E-03  1.293E-01
     28.00  5.186E-03  1.137E-01
     30.00  4.590E-03  1.003E-01
     32.00  4.062E-03  8.865E-02
     34.00  3.595E-03  7.842E-02
     36.00  3.182E-03  6.938E-02
     38.00  2.816E-03  6.140E-02
     40.00  2.492E-03  5.434E-02
     42.00  2.206E-03  4.809E-02
     44.00  1.952E-03  4.256E-02
```

TABLE 5-22. STIRRED TANK MODEL COMPUTER PREDICTED WATER COLUMN CONCENTRATIONS FROM EVAPORATION/DISSOLUTION EXPERIMENTS: KOVAT 867, P-XYLENE.

```
STIRRED TANK MODEL FOR KOVAT  867, P-XYLENE
FROM THE KEYBOARD, KW =  3.000E+00, KA =  1.500E+03, KO =  1.000E+00 CM/HR
M (OIL/WATER) =  2.800E+03, HENRYS LAW (AIR/OIL) =  1.220E-04 DIMENSIONLESS, AT  2.100E+01 DEG C
ANTA =  1.609E+01, ANTB =  3.347E+03, ANTC = -5.780E+01
MOLE WT OF OIL =  2.880E+02, DENSITY =  8.800E-01 GM/CC
VO =  2.000E+02 ML, VW =  3.000E+04 ML
XZERO =  1.794E+03 MICROGRAMS/GRAM OF OIL, AREA =  6.170E+02 CM*CM
OVER-ALL KW AT WATER-OIL =  2.997E+00 CM/HR
OVER-ALL KO AT OIL-AIR =  1.547E-01 CM/HR
A = -6.163E-02, B =  2.201E-05
C =  9.245E+00, D = -4.806E-01
R =  4.199E-01
D1 = -6.115E-02, D2 = -4.811E-01
C1 =  2.073E+00, C2 =  1.792E+03
Z1 =  9.404E-02, Z2 = -9.404E-02
WATER CONCENTRATION PEAKS AT  4.912E+00 HOURS
WHERE THE WATER CONCENTRATION =  6.079E-02, AND THE OIL CONCENTRATION =  1.702E+02
AND THE CONCENTRATION RATIO (OIL/WATER) =  2.800E+03

      HOUR      H2O         OIL

      0.20  7.483E-03  1.630E+03
      0.40  1.419E-02  1.480E+03
      0.60  2.019E-02  1.345E+03
      0.80  2.555E-02  1.221E+03
      1.00  3.033E-02  1.110E+03
      1.20  3.459E-02  1.008E+03
      1.40  3.837E-02  9.156E+02
      1.60  4.172E-02  8.318E+02
      1.80  4.468E-02  7.556E+02
      2.00  4.728E-02  6.865E+02
      2.25  5.009E-02  6.089E+02
      2.50  5.246E-02  5.400E+02
      2.75  5.444E-02  4.790E+02
      3.00  5.607E-02  4.249E+02
      3.25  5.740E-02  3.769E+02
      3.50  5.846E-02  3.344E+02
      3.75  5.929E-02  2.967E+02
      4.00  5.991E-02  2.632E+02
      4.25  6.035E-02  2.335E+02
      4.50  6.062E-02  2.072E+02
      6.00  5.991E-02  1.014E+02
      8.00  5.565E-02  3.946E+01
     10.00  5.025E-02  1.571E+01
     12.00  4.485E-02  6.569E+00
     14.00  3.984E-02  3.010E+00
     16.00  3.531E-02  1.593E+00
     18.00  3.127E-02  1.000E+00
     20.00  2.767E-02  7.289E-01
     22.00  2.449E-02  5.853E-01
     24.00  2.167E-02  4.951E-01
     26.00  1.918E-02  4.294E-01
     28.00  1.697E-02  3.766E-01
     30.00  1.502E-02  3.320E-01
     32.00  1.329E-02  2.933E-01
     34.00  1.176E-02  2.593E-01
     36.00  1.041E-02  2.294E-01
     38.00  9.208E-03  2.030E-01
     40.00  8.148E-03  1.796E-01
     42.00  7.210E-03  1.589E-01
     44.00  6.380E-03  1.406E-01
```

TABLE 5-23. STIRRED TANK MODEL COMPUTER PREDICTED WATER COLUMN CONCENTRATIONS FROM EVAPORATION/DISSOLUTION EXPERIMENTS. KOVAT 1021, 1-METHYL-4-ISOPROPYLBENZENE.

```
STIRRED TANK MODEL FOR KOVAT 1021, 1-METHYL-4-ISOPROPYLB
FROM THE KEYBOARD, KW =  3.000E+00, KA =  1.500E+03, KO =  1.000E+00 CM/HR
M (OIL/WATER) =  7.500E+03, HENRYS LAW (AIR/OIL) =  2.040E-05 DIMENSIONLESS, AT  2.100E+01 DEG C
ANTA =  1.594E+01, ANTB =  3.539E+03, ANTC = -7.010E+01
MOLE WT OF OIL =  2.880E+02, DENSITY =  8.800E-01 CM/CC
VO =  2.000E+02 ML, VW =  3.000E+04 ML
XZERO =  4.530E+02 MICROGRAMS/GRAM OF OIL, AREA =  6.170E+02 CM*CM
OVER-ALL KW AT WATER-OIL =  2.999E+00 CM/HR
OVER-ALL KO AT OIL-AIR =  2.969E-02 CM/HR
A = -6.168E-02, B =  8.223E-06
C =  9.251E+00, D = -9.284E-02
H =  3.571E-02
D1 = -5.940E-02, D2 = -9.512E-02
C1 =  2.886E+01, C2 =  4.241E+02
Z1 =  1.043E-01, Z2 = -1.043E-01
WATER CONCENTRATION PEAKS AT  1.318E+01 HOURS
WHERE THE WATER CONCENTRATION =  1.790E-02, AND THE OIL CONCENTRATION =  1.342E+02
AND THE CONCENTRATION RATIO (OIL/WATER) =  7.500E+03

      HOUR      H2O         OIL

      0.20   7.336E-04   4.447E+02
      0.40   1.445E-03   4.365E+02
      0.60   2.134E-03   4.285E+02
      0.80   2.802E-03   4.206E+02
      1.00   3.448E-03   4.129E+02
      1.20   4.075E-03   4.053E+02
      1.40   4.681E-03   3.978E+02
      1.60   5.268E-03   3.905E+02
      1.80   5.836E-03   3.833E+02
      2.00   6.385E-03   3.763E+02
      2.25   7.046E-03   3.677E+02
      2.50   7.680E-03   3.593E+02
      2.75   8.287E-03   3.510E+02
      3.00   8.868E-03   3.430E+02
      3.25   9.424E-03   3.351E+02
      3.50   9.956E-03   3.275E+02
      3.75   1.046E-02   3.200E+02
      4.00   1.095E-02   3.127E+02
      4.25   1.141E-02   3.055E+02
      4.50   1.186E-02   2.985E+02
      6.00   1.409E-02   2.599E+02
      8.00   1.612E-02   2.161E+02
     10.00   1.730E-02   1.798E+02
     12.00   1.782E-02   1.496E+02
     14.00   1.787E-02   1.246E+02
     16.00   1.755E-02   1.037E+02
     18.00   1.698E-02   8.646E+01
     20.00   1.623E-02   7.209E+01
     22.00   1.536E-02   6.014E+01
     24.00   1.443E-02   5.026E+01
     26.00   1.347E-02   4.193E+01
     28.00   1.250E-02   3.504E+01
     30.00   1.154E-02   2.931E+01
     32.00   1.062E-02   2.453E+01
     34.00   9.732E-03   2.054E+01
     36.00   8.893E-03   1.722E+01
     38.00   8.105E-03   1.444E+01
     40.00   7.369E-03   1.213E+01
     42.00   6.686E-03   1.019E+01
     44.00   6.055E-03   8.570E+00
```

TABLE 5-24. STIRRED TANK MODEL COMPUTER PREDICTED WATER COLUMN CONCENTRATIONS FROM EVAPORATION/DISSOLUTION EXPERIMENTS: KOVAT 1185, NAPHTHALENE.

```
STIRRED TANK MODEL FOR KOVAT 1185, NAPHTHALENE
FROM THE KEYBOARD, KW =  3.000E+00, KA =  1.500E+03, KO =  1.000E+00 CM/HR
N (OIL/WATER) =  6.800E+03, HENRYS LAW (AIR/OIL) =  2.996E-06 DIMENSIONLESS, AT  2.100E+01 DEG C
ANTA =  1.614E+01, ANTB =  3.992E+03, ANTC = -7.130E+01
MOLE WT OF OIL =  2.880E+02, DENSITY =  8.800E-01 GM/CC
VO =  2.000E+02 ML, VW =  3.000E+04 ML
XZERO =  5.200E+02 MICROGRAMS/GRAM OF OIL, AREA =  6.170E+02 CM*CM
OVER-ALL KW AT WATER-OIL =  2.999E+00 CM/HR
OVER-ALL KO AT OIL-AIR =  4.474E-03 CM/HR
A = -6.167E-02, B =  9.070E-06
C =  9.251E+00, D = -1.516E-02
R =  4.999E-02
D1 = -1.342E-02, D2 = -6.341E-02
C1 =  5.019E+02, C2 =  1.809E+01
Z1 =  9.434E-02, Z2 = -9.434E-02
WATER CONCENTRATION PEAKS AT  3.106E+01 HOURS
WHERE THE WATER CONCENTRATION =  4.902E-02, AND THE OIL CONCENTRATION =  3.333E+02
AND THE CONCENTRATION RATIO (OIL/WATER) =  6.800E+03

      HOUR     H20        OIL

      0.20  9.860E-04  5.184E+02
      0.40  1.850E-03  5.169E+02
      0.60  2.765E-03  5.153E+02
      0.80  3.659E-03  5.137E+02
      1.00  4.539E-03  5.122E+02
      1.20  5.405E-03  5.107E+02
      1.40  6.258E-03  5.091E+02
      1.60  7.098E-03  5.076E+02
      1.80  7.925E-03  5.061E+02
      2.00  8.738E-03  5.046E+02
      2.25  9.738E-03  5.027E+02
      2.50  1.072E-02  5.008E+02
      2.75  1.168E-02  4.989E+02
      3.00  1.262E-02  4.971E+02
      3.25  1.354E-02  4.952E+02
      3.50  1.445E-02  4.934E+02
      3.75  1.534E-02  4.915E+02
      4.00  1.620E-02  4.897E+02
      4.25  1.706E-02  4.879E+02
      4.50  1.789E-02  4.861E+02
      6.00  2.256E-02  4.754E+02
      8.00  2.793E-02  4.617E+02
     10.00  3.245E-02  4.485E+02
     12.00  3.623E-02  4.357E+02
     14.00  3.935E-02  4.234E+02
     16.00  4.191E-02  4.115E+02
     18.00  4.396E-02  4.000E+02
     20.00  4.559E-02  3.888E+02
     22.00  4.684E-02  3.781E+02
     24.00  4.777E-02  3.676E+02
     26.00  4.841E-02  3.575E+02
     28.00  4.881E-02  3.477E+02
     30.00  4.899E-02  3.382E+02
     32.00  4.900E-02  3.290E+02
     34.00  4.885E-02  3.201E+02
     36.00  4.857E-02  3.114E+02
     38.00  4.817E-02  3.030E+02
     40.00  4.768E-02  2.948E+02
     42.00  4.711E-02  2.869E+02
     44.00  4.647E-02  2.792E+02
```

TABLE 5-25. STIRRED TANK MODEL COMPUTER PREDICTED WATER COLUMN CONCENTRATIONS FROM EVAPORATION/DISSOLUTION EXPERIMENTS. KOVAT 1295, 2-METHYLNAPHTHALENE.

```
STIRRED TANK MODEL FOR KOVAT 1295, 2-METHYLNAPHTHALENE
FROM THE KEYBOARD, KW =  3.000E+00, KA =  1.500E+03, KO =  1.000E+00 CM/HR
H (OIL/WATER) =  1.300E+04, HENRYS LAW (AIR/OIL) =  8.402E-07 DIMENSIONLESS, AT  2.100E+01 DEG C
ANTA =  1.627E+01, ANTB =  4.237E+03, ANTC = -7.475E+01
MOLE WT OF OIL =  2.880E+02, DENSITY =  8.800E-01 GM/CC
VO =  2.000E+02 ML, VW =  3.000E+04 ML
XZERO =  1.260E+03 MICROGRAMS/GRAM OF OIL, AREA =  6.170E+02 CM*CM
OVER-ALL KW AT WATER-OIL =  2.999E+00 CM/HR
OVER-ALL KO AT OIL-AIR =  1.259E-03 CM/HR
A = -6.169E-02, B =  4.745E-06
C =  9.253E+00, D = -4.595E-03
R =  5.861E-02
D1 = -3.836E-03, D2 = -6.244E-02
C1 =  1.244E+03, C2 =  1.632E+01
Z1 =  1.020E-01, Z2 = -1.020E-01
WATER CONCENTRATION PEAKS AT  4.760E+01 HOURS
WHERE THE WATER CONCENTRATION =  7.977E-02, AND THE OIL CONCENTRATION =  1.037E+03
AND THE CONCENTRATION RATIO (OIL/WATER) =  1.300E+04

      HOUR      H2O         OIL

      0.20  1.108E-03  1.259E+03
      0.40  2.360E-03  1.258E+03
      0.60  3.517E-03  1.257E+03
      0.80  4.658E-03  1.255E+03
      1.00  5.785E-03  1.254E+03
      1.20  6.896E-03  1.253E+03
      1.40  7.993E-03  1.252E+03
      1.60  9.075E-03  1.251E+03
      1.80  1.014E-02  1.250E+03
      2.00  1.120E-02  1.249E+03
      2.25  1.249E-02  1.247E+03
      2.50  1.377E-02  1.246E+03
      2.75  1.503E-02  1.244E+03
      3.00  1.626E-02  1.243E+03
      3.25  1.747E-02  1.242E+03
      3.50  1.867E-02  1.240E+03
      3.75  1.984E-02  1.239E+03
      4.00  2.099E-02  1.237E+03
      4.25  2.213E-02  1.236E+03
      4.50  2.324E-02  1.235E+03
      6.00  2.956E-02  1.227E+03
      8.00  3.703E-02  1.216E+03
     10.00  4.354E-02  1.206E+03
     12.00  4.920E-02  1.195E+03
     14.00  5.412E-02  1.185E+03
     16.00  5.888E-02  1.176E+03
     18.00  6.205E-02  1.166E+03
     20.00  6.522E-02  1.157E+03
     22.00  6.793E-02  1.147E+03
     24.00  7.025E-02  1.138E+03
     26.00  7.221E-02  1.129E+03
     28.00  7.387E-02  1.120E+03
     30.00  7.525E-02  1.111E+03
     32.00  7.640E-02  1.102E+03
     34.00  7.733E-02  1.094E+03
     36.00  7.808E-02  1.085E+03
     38.00  7.867E-02  1.077E+03
     40.00  7.911E-02  1.068E+03
     42.00  7.943E-02  1.060E+03
     44.00  7.963E-02  1.052E+03
```

TABLE 5-26. STIRRED TANK MODEL COMPUTER PREDICTED WATER COLUMN CONCENTRATIONS FROM EVAPORATION/DISSOLUTION EXPERIMENTS: KOVAT 1317, 1-METHYLNAPHTHALENE.

```
STIRRED TANK MODEL FOR KOVAT 1317, 1-METHYLNAPHTHALENE
FROM THE KEYBOARD, KW =  3.000E+00, KA =  1.500E+03, KO =  1.000E+00 CM/HR
M (OIL/WATER) =  5.000E+03, HENRYS LAW (AIR/OIL) =  6.661E-07 DIMENSIONLESS, AT  2.100E+01 DEG C
ANTA =  1.620E+01, ANTB =  4.207E+03, ANTC = -7.815E+01
MOLE WT OF OIL =  2.880E+02, DENSITY =  8.800E-01 GM/CC
VO =  2.000E+02 ML, VW =  3.000E+04 ML
XZERO =  7.370E+02 MICROGRAMS/GRAM OF OIL, AREA =  6.170E+02 CM*CM
OVER-ALL KW AT WATER-OIL =  2.998E+00 CM/HR
OVER-ALL KO AT OIL-AIR =  9.982E-04 CM/HR
A = -6.166E-02, B =  1.233E-05
C =  9.249E+00, D = -4.929E-03
R =  6.062E-02
D1 = -2.985E-03, D2 = -6.361E-02
C1 =  7.134E+02, C2 =  2.363E+01
Z1 =  1.499E-01, Z2 = -1.499E-01
WATER CONCENTRATION PEAKS AT  5.046E+01 HOURS
WHERE THE WATER CONCENTRATION =  1.229E-01, AND THE OIL CONCENTRATION =  6.146E+02
AND THE CONCENTRATION RATIO (OIL/WATER) =  5.000E+03

       HOUR     H2O        OIL

       0.20  1.806E-03  7.363E+02
       0.40  3.588E-03  7.356E+02
       0.60  5.346E-03  7.348E+02
       0.80  7.081E-03  7.341E+02
       1.00  8.793E-03  7.334E+02
       1.20  1.048E-02  7.327E+02
       1.40  1.215E-02  7.320E+02
       1.60  1.379E-02  7.313E+02
       1.80  1.542E-02  7.306E+02
       2.00  1.702E-02  7.299E+02
       2.25  1.899E-02  7.291E+02
       2.50  2.093E-02  7.282E+02
       2.75  2.283E-02  7.274E+02
       3.00  2.471E-02  7.265E+02
       3.25  2.655E-02  7.257E+02
       3.50  2.837E-02  7.249E+02
       3.75  3.015E-02  7.240E+02
       4.00  3.190E-02  7.232E+02
       4.25  3.362E-02  7.224E+02
       4.50  3.532E-02  7.216E+02
       6.00  4.491E-02  7.168E+02
       8.00  5.626E-02  7.107E+02
      10.00  6.615E-02  7.049E+02
      12.00  7.477E-02  6.993E+02
      14.00  8.226E-02  6.939E+02
      16.00  8.875E-02  6.886E+02
      18.00  9.437E-02  6.836E+02
      20.00  9.923E-02  6.786E+02
      22.00  1.034E-01  6.739E+02
      24.00  1.070E-01  6.692E+02
      26.00  1.100E-01  6.646E+02
      28.00  1.126E-01  6.601E+02
      30.00  1.148E-01  6.558E+02
      32.00  1.167E-01  6.515E+02
      34.00  1.182E-01  6.472E+02
      36.00  1.195E-01  6.431E+02
      38.00  1.205E-01  6.390E+02
      40.00  1.213E-01  6.349E+02
      42.00  1.219E-01  6.309E+02
      44.00  1.223E-01  6.270E+02
```

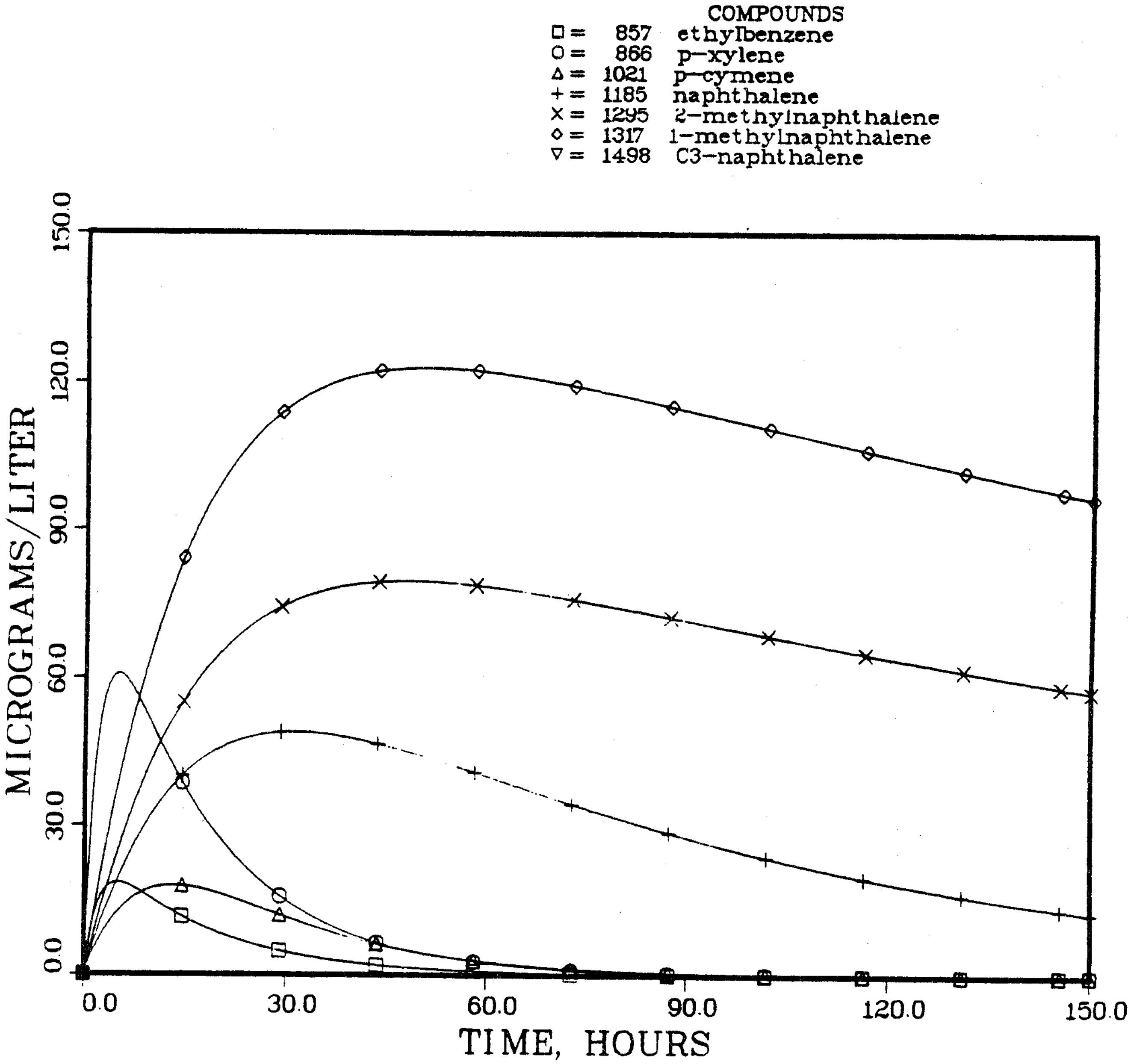

FIGURE 5-121. PREDICTED WATER COLUMN CONCENTRATIONS, STIRRED TANK MODEL AT 19°C.

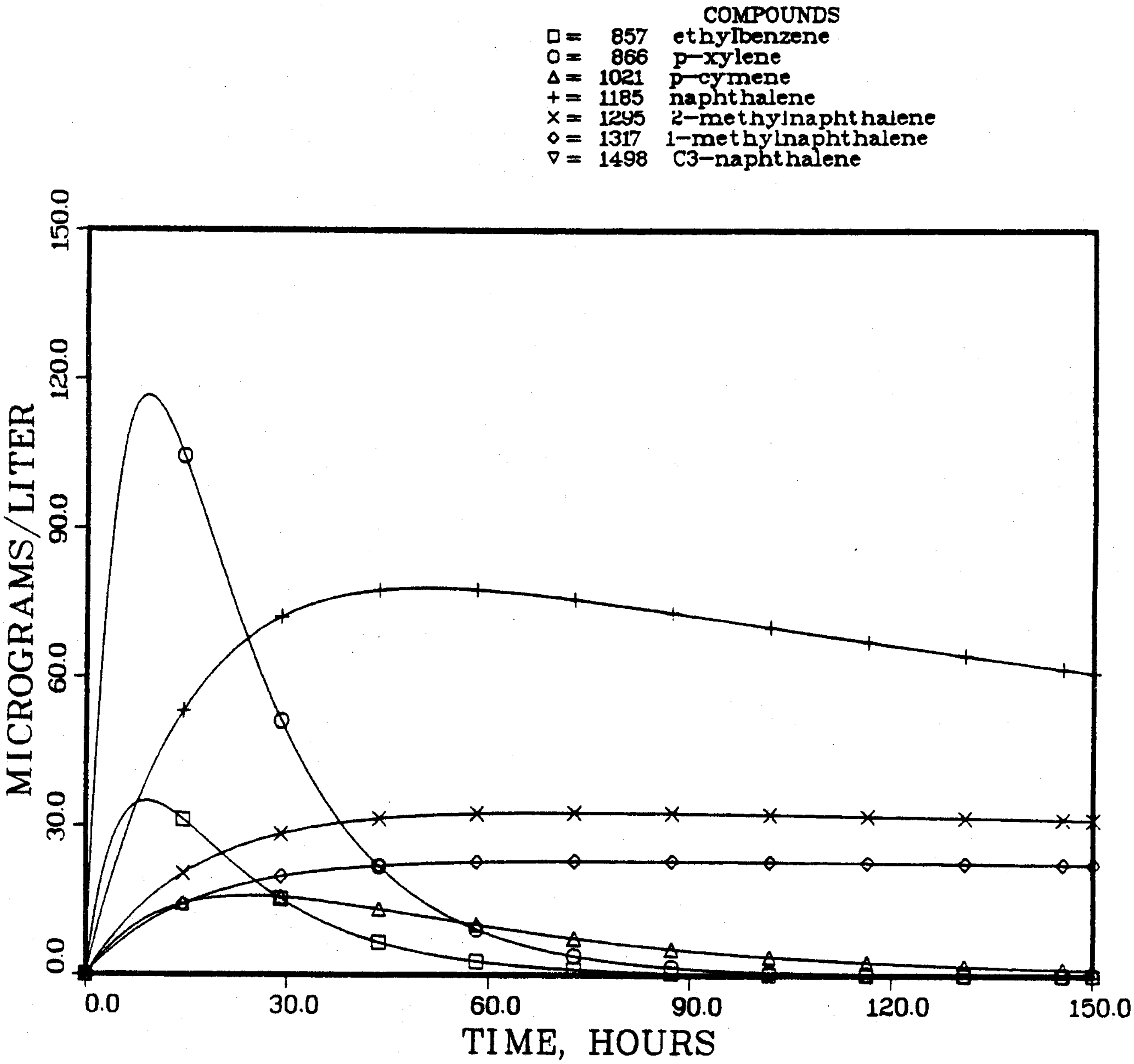

FIGURE 5-122. PREDICATED WATER COLUMN CONCENTRATIONS, STIRRED TANK MODEL AT 3°C.

5.5.2 Model Predicted vs Observed Oil Weathering Behavoir from Flow-through Seawater Wave Tank Experiments at Kasitsna Bay

In order to further access the reliability and accuracy of the oil weathering model, it was also applied to the experimental spill conditions of the Kasitsna Bay wave tanks. The flexibility of the program allowed for minor adjustments of various constants as well as initial spill condition input. For example, a better agreement between observed and predicted viscosity was obtained by changing one of the mousse formation constants from a default value of 10.5 to 12.5 (see Appendix B--Oil Weathering Users Manual). The different equations contained in the program are empirical in nature, and not to be seen as absolute; thus minor modifications by the users are not only allowable but encouraged.

5.5.2.1 Verification at 55°F

Listed below are the input parameters, dictated solely by initial spill conditions, for the three wave tank spills in the summer of 1982.

Temperature in degrees F = 55
Spill size in barrels = .1 (16 l)
Wind speed in knots = 2
Slick spreading = OFF
Slick thickness in cm = 1

Better agreement between observed and predicted oil behavior was obtained by slight adjustment of certain optional user specified constants. Following are the suggested (default) values and the modifications that were applied to modeling wave tank spills.

Constant	Suggested Value	Value Used
Maximum Weight Fraction H_2O	.55	.6
Mousse-Viscosity	.65	.67
Water Incorporation Rate	.001	.01
Oil/Water Interfacial Tension	30	27
Viscosity-Fraction-Oil-Weathered	10.5	12.5
Wind Speed Constant (K_a)	.1	.075

Using the input parameters listed above, the oil weathering model was applied to the spill situations in the three Kasitsna Bay wave tanks initiated in July 1982. For comparison purposes, and to eliminate data spread, experimental (observed) data are expressed as the average for all three wave tanks. Four output parameters were monitored - namely, % mass distilled, weight fraction of water-in-oil, viscosity, and dispersion flux. A discussion concerning each of these parameters and how they related to experimental data follows.

Viscosity (Experimental Results in Sec. 5.4.6)

Table 5-27 presents observed versus predicted values for oil viscosity at ambient temperatures, in this case approximately 55°F. A graphical representation of these data can be found in Figure 5-123. As shown, there is excellent agreement between observed and predicted viscosity for the first 100 hours of weathering. After 100 hours, the predicted viscosity is approximately 25% higher than observed. While this deviation is acceptable, there is a notable difference between the model's method of calculation and the actual method of measurement. Whereas, at the later times, ambient temperature viscosity measurements were made on whole mousse (water included), the model predicts the viscosity of the parent oil (water excluded). Taking this difference into account, and understanding that viscosity (while being a relatively important physical property) is one of the most difficult parameters to model; overall agreement between observed and predicted viscosity is quite good.

Weight Fraction Water-in-Oil (Experimental Results in Sec. 5.4.6)

Table 5-27 also shows observed and predicted values for water incorporation by oil, and Figure 5-123 presents the data in a graphical fashion. Note that output data from the model lists this parameter as mass fraction, however it is presented here as % water (by weight). Generally, agreement between experimental and predicted values is good, especially after 24 hours of weathering, where the deviation is less 20% for all data points. In many cases the standard deviation of the experimental data (presented in Table 5-8

DM/WTS.TAB

Table 5-27. Observed [a] vs Model Predicted Data from the Summer Wave Tank Spills

	Viscosity[b] (centipoise)		Water Incorporation (% by weight)		Dispersion Flux (g/m^2/hr)	
Time (hours)	Observed	Predicted	Observed	Predicted	Observed	Predicted
1	68.0	160	<.10	.96	1.1	1.2
2	130	190	<.10	1.9	1.1	1.1
4	220	240	.15	3.7	1.0	.99
8	340	320	<.10	7.4	.91	.86
12	620	410	.22	10.0	.80	.79
24	690	630	18.0	19.0	.55	.62
48	1080	1300	34.0	33.0	.28	.43
72	2350	2000	49.0	44.0	.16	.35
144	5400	6500	50.0	58.0	.070	.19
216	6200	8450	51.0	60.0	.050	.17

a - Based on the average values from three wave tanks

b - Observed viscosity data were obtained at ambient temperature (averaging 58°F) while predicted values were calculated using a temperature of 55°F.

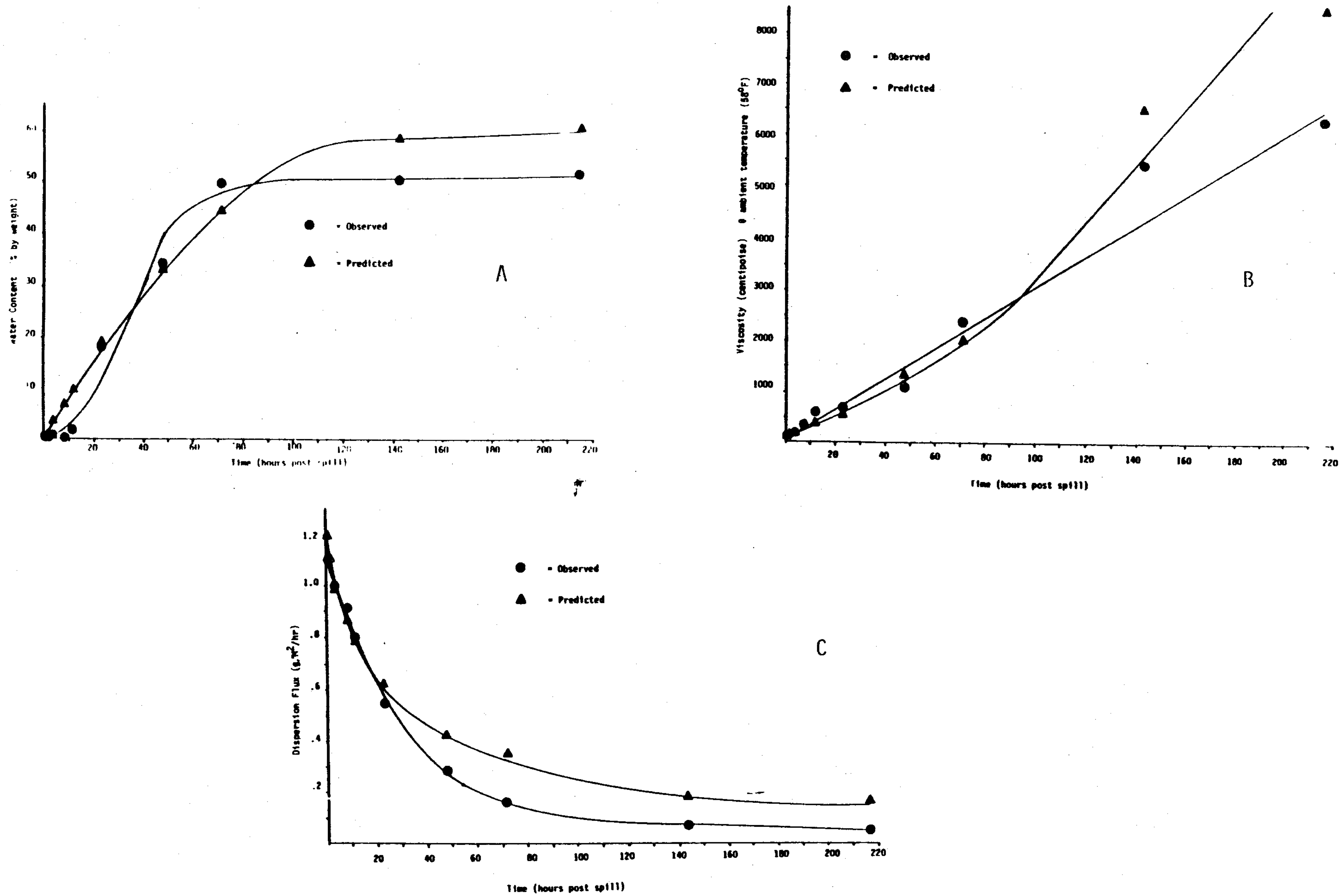

Figure 5-123. Observed vs Model Predicted data for the Summer Spills in Wave Tanks #1-3 for (A) Water Incorporation, (B) Viscosity, and (C) Dispersion Flux.

in Section 5.4.6) would include the predicted value. Initially, however, the predicted rate of water incorporation is greater than actually observed. In this case, however, stable mousse was not generally formed prior to 24 hours of weathering (required for removal of low viscosity distillate cuts up to n-C_9), and as such, the higher predicted rate of initial water incorporation is not considered to be terribly significant. Additional modifications to the water incorporation rate constants might provide better fit initially, but the overall fit out to 200 hrs is nevertheless quite good.

Dispersion Flux (Experimental Results in Sec. 6.2)

Dispersed oil was measured in the wave tanks as concentration (i.e., μg/l) of discreet oil droplets in the water column. In order to convert dispersed oil concentration (sum of the total resolved and UCM) to dispersion flux the following mathematical calculations were employed.

$$\text{Assuming } V\frac{dc}{dt} = -vc + ae^{-bt} \tag{5.2}$$

where V = tank volume = 2800 l

dc/dt = the change in concentration as a function of time

v = the tank flow = 0.26 l/sec

c = concentration of dispersed oil in g/l

a & b = constants to be determined

and t = time in seconds

the mass in the tanks at any given time ($V\frac{dc}{dt}$), equals the mass removed due to water column turn over (-vc) plus the contribution due to dispersion flux (ae^{-bt}).

Rearrangement yields:

$$\frac{dc}{dt} + \frac{v}{V}c = \frac{a}{V}e^{-bt} \tag{5.3}$$

Multiplying through by the integration factor $e^{\frac{v}{V}t}$ gives

$$e^{\frac{v}{V}t} \frac{dc}{dt} + \frac{v}{V} ce^{\frac{v}{V}\,t} = \frac{a}{V} e^{(-b + \frac{v}{V})t} \tag{5.4}$$

which is

$$\frac{d \quad ce^{\frac{v}{V}t}}{dt} = \frac{a}{V} e^{(-b + \frac{v}{V})t} \tag{5.5}$$

Integration yields

$$ce^{\frac{v}{V}t} = \frac{a/V}{\substack{v-b\\ V}} e^{(-b + \frac{v}{V})t} + \text{constant} \tag{5.6}$$

At $t = 0$, $c = 0$ so

$$0 = \frac{a/V}{\frac{v}{V} -b} + \text{constant} \tag{5.7}$$

$$\text{or constant} = - \frac{a/V}{\frac{v}{V} -b} \tag{5.9}$$

Substituting the constant into (5.6) yields

$$ce^{\frac{v}{V}t} = \frac{a/V}{\frac{v}{V} -b} e^{(-b + \frac{v}{V})t} - \frac{a/V}{\frac{v}{V} -b} \tag{5.9}$$

or

$$c = \frac{a/V}{\frac{v}{V} -b} e^{-bt} \quad V \quad - \frac{a/V}{\frac{v}{V} -b} e^{-\frac{v}{V}t} \tag{5.10}$$

which yields $c = \frac{a}{v-bV} \quad e^{-bt} - e^{\frac{v}{V}t}$ (5.11)

Attempts were made to choose constants a and b such that the experimental concentration values could be matched for any given time. Success using this single exponential decay equation was limited, therefore a double exponential decay equation, present below, was used.

$$c_{total} = c_1 + c_2 = \frac{a_1}{v - b_1 V} e^{-b_1 t} - e^{-\frac{v}{V}t} + \frac{a_2}{v - b_2 V} e^{-b_2 t} - e^{-\frac{v}{V}t} \qquad (5.12)$$

Where, as before, values for constants a_1, b_1, a_2 and b_2 were chosen in order to match experimental concentration data.

The table below presents the observed and calculated dispersed oil concentration values using $a_1 = 3 \times 10^{-4}$, $b_1 = 10^{-5}$, $a_2 = 3 \times 10^{-5}$ and $b_2 = 10^{-6}$

Time (Hours)	Concentration (mg/l) Experimental	Concentration (mg/l) Calculated
2	1.7	.60
4	2.2	.86
8	2.3	1.0
12	1.1	.92
24	1.2	.65
48	.63	.33
72	.32	.19
216	.14	.054

Once the proper values for the constant were determined, the dispersion flux ($g/m^2/hr$) can be calculated by:

$$\text{Flux} = a_1 e^{-b_1 t} + a_2 e^{-b_2 t} \quad \text{(from the initial assumption)}$$

Numerical values and a graphical representation of observed versus model predicted flux can be found in Table 5-27 and Figure 5-123 respectively. As can be seen, excellent agreement between observed and predicted flux is observed, especially during the first 24 hours following the spill. Although predicted flux values are generally a factor of two higher than the observed dispersion rates after 48 hours, these comparisons show that the model is indeed in the correct range for dispersion predictions. In all likelihood, further adjustments of the constants a_1, b_1, a_2, and b_2 or the use of a triple exponential decay equation, would facilitate even better agreement between experimental and predicted dispersed oil rates.

% Mass Distillable

Experimentally, the mass of the slick evaporated was converted to % distillable by utilizing FID-GC chromatographic data from the weathered oil characterization (Section 5.4.7). Assuming that only 60% of the fresh Prudhoe Bay crude is chromatographable, time zero percentages were normalized from 100% to 60%. Knowledge of n-alkane boiling points coupled with normalized percents of mass evaporated from the slick yields temperature versus % distilled plots like the ones presented in Figures 5-124 and 5-125. Likewise, Figures 5-126 and 5-127 show similar curves for total distillable hydrocarbons (disregarding non-chromatographable oil components).

Figures 5-124 and 5-126 present the observed (calculated from GC data) mass balance and total distillable curves for wave-tank weathered oil at 58°F with a 2 knot wind. Figures 5-125 and 5-127 show similar curves, predicted by the model, for the same spill. A comparison of Figure 5-124 (observed mass balance distillation) with Figure 5-125 (predicted mass balance distillation) shows reasonable agreement from curve to curve. The most notable discrepancy between the observed and predicted curves is that the model predicts that approximately 52% of the oil weathered for 293 hours could be distilled at 800°F whereas observed data for 288 hours gives a value of approximately 47%. Also, the general shape of the curves is slightly different--in the mid-range temperatures the model constantly predicts 10 to 20% less mass distilled than shown by observation (i.e., more oil has already been lost to evaporation during environmental weathering as predicted by the model).

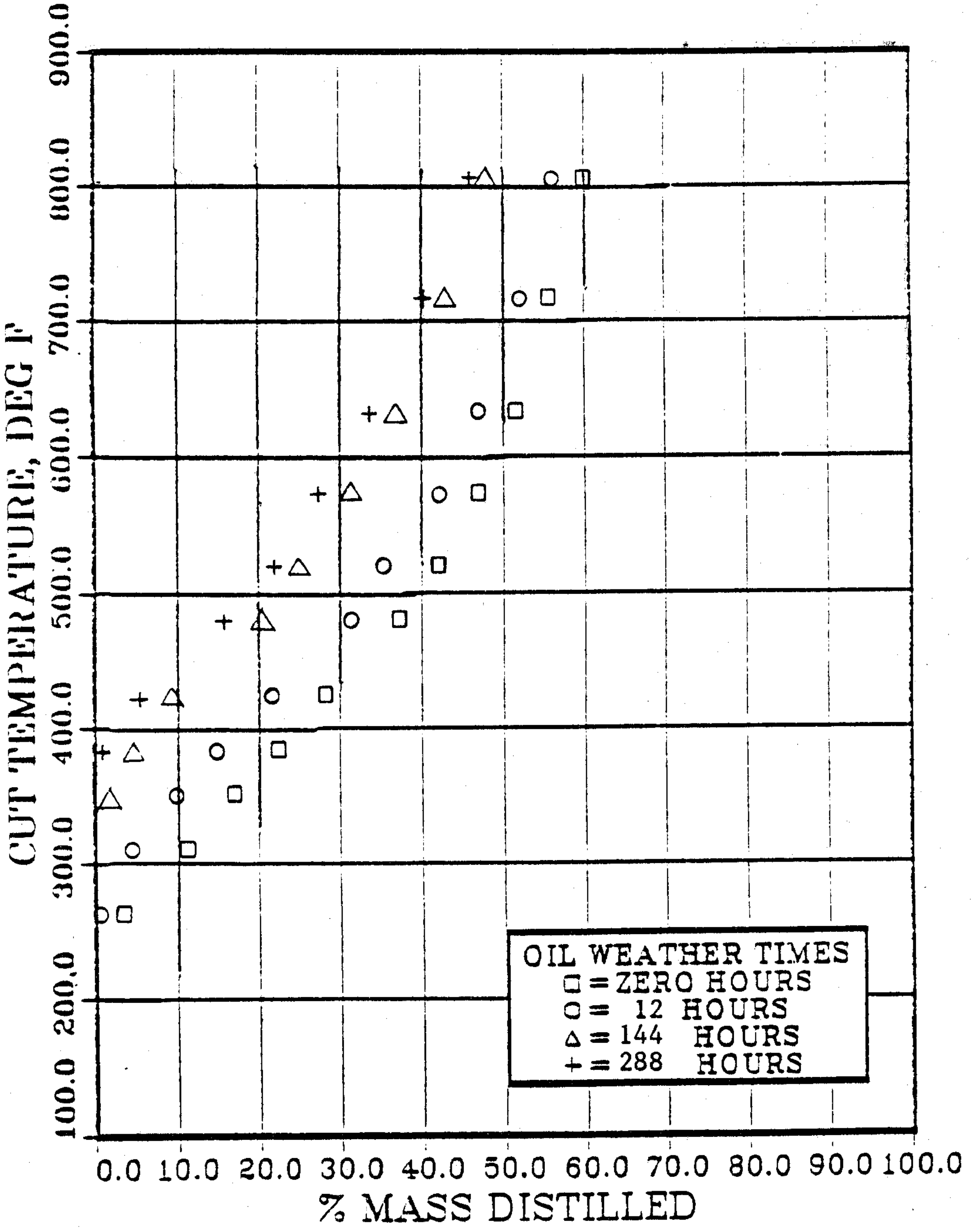

Figure 5-124. Observed Mass Balance Distillation Curves for Oil Weathering in the Wave Tank Experiment at 58°F with a 2 Knot Wind.

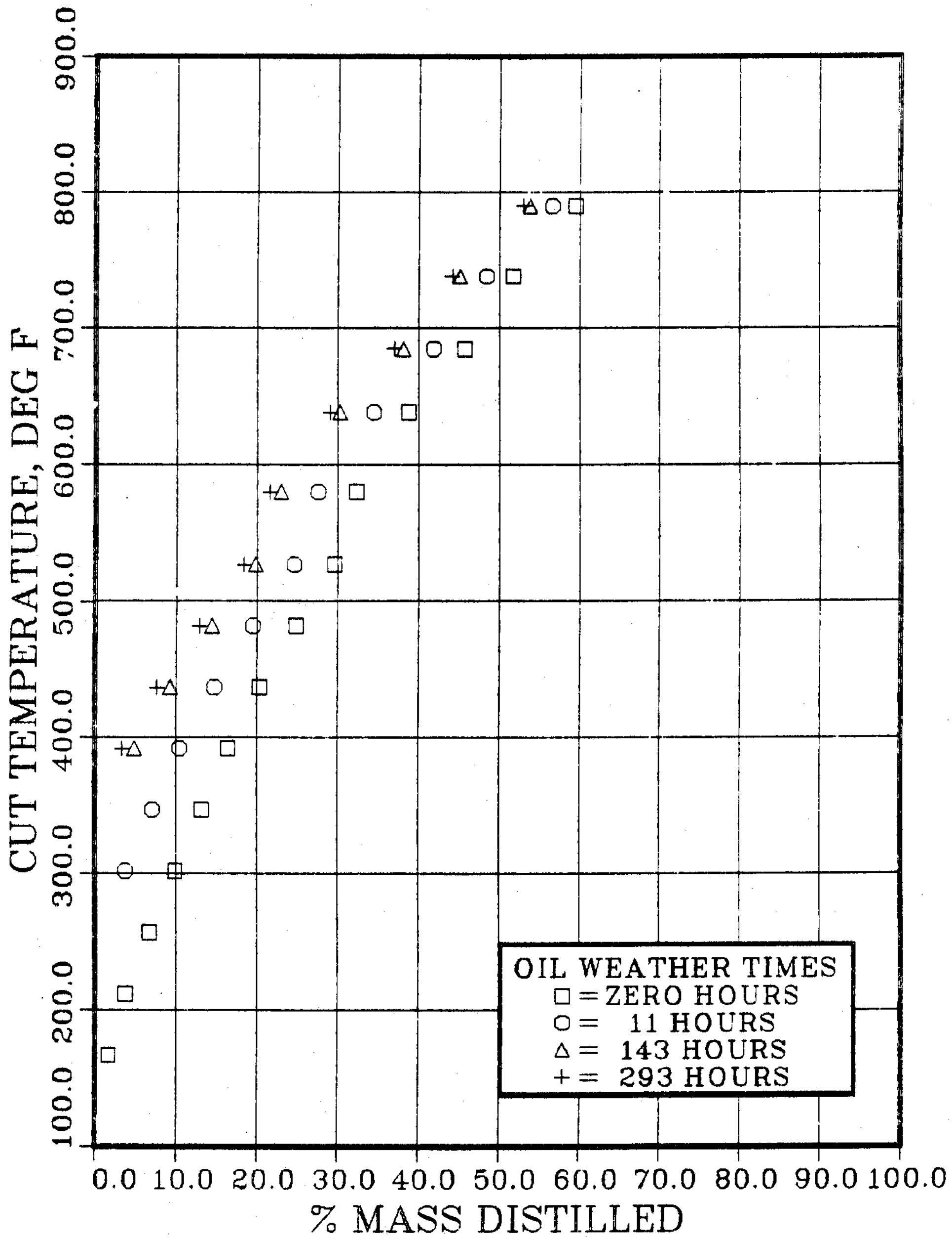

Figure 5-125. Predicted Mass Balance Distillation Curves for Oil Weathering in the Wave Tank Experiment at 55°F with a 2 knot wind.

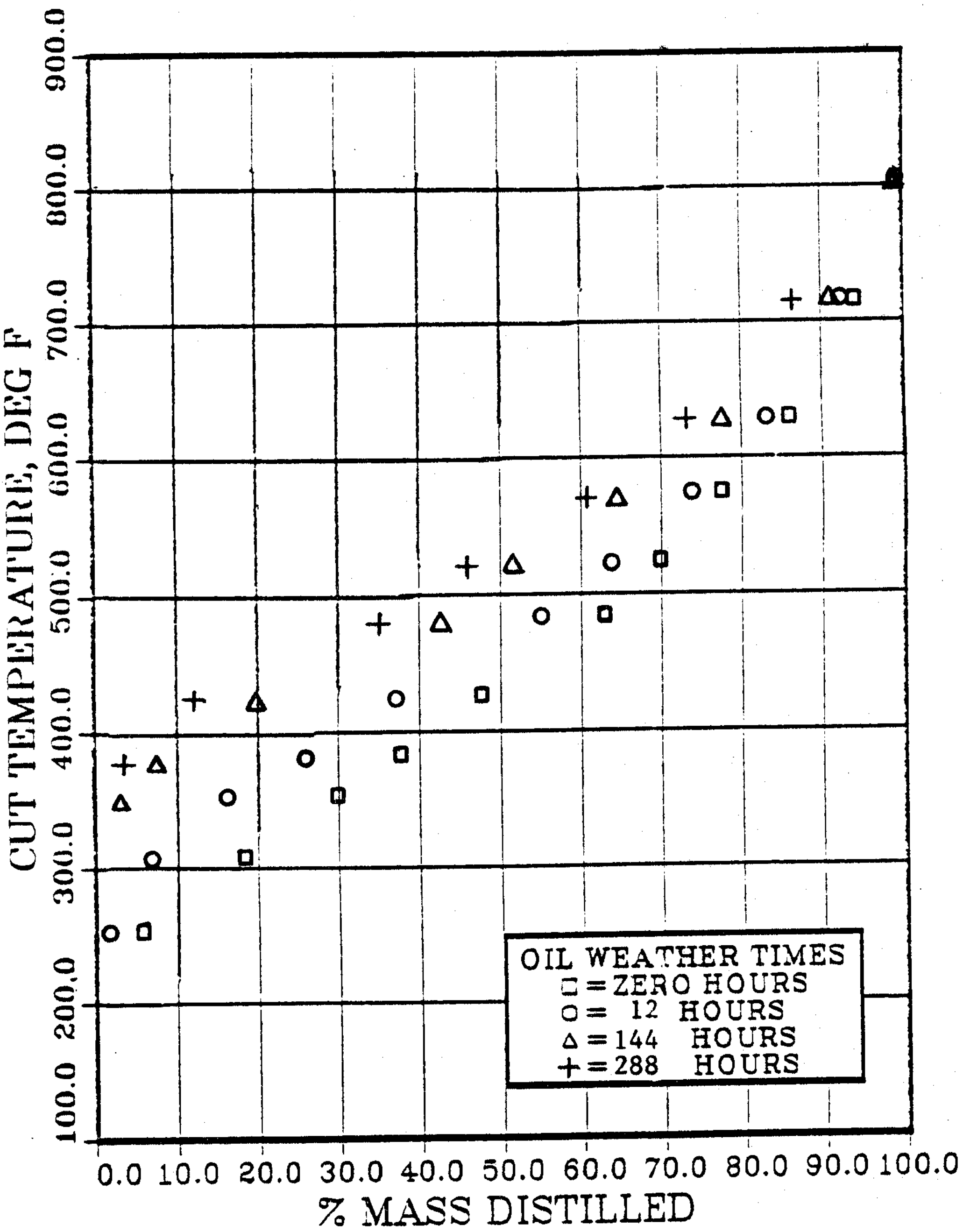

Figure 5-126. Observed Total Distillable Boiling Point Distribution Curves for Oil Weathering in the Wave Tank Experiment at 58°F with a 2 Knot Wind.

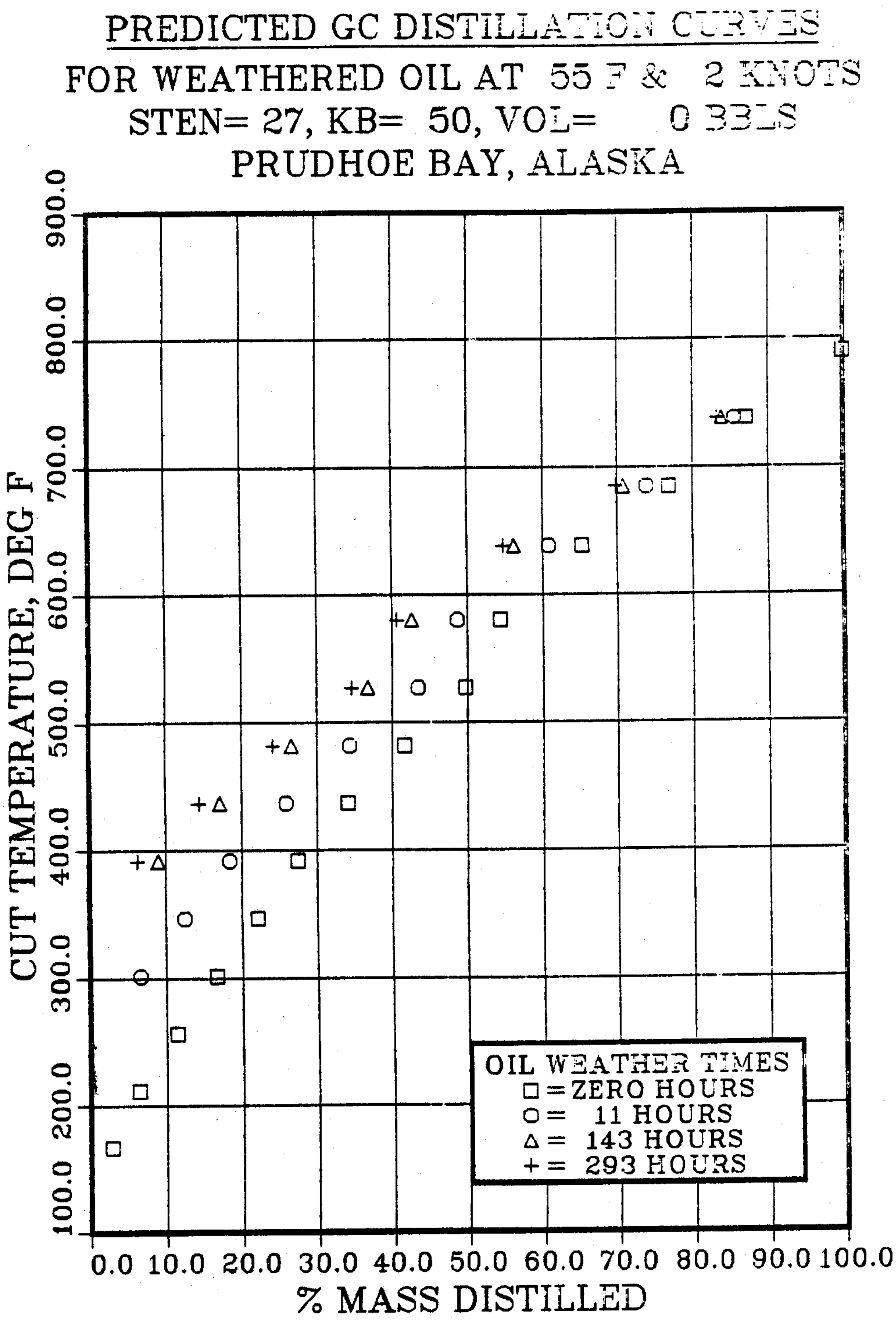

Figure 5-127. Predicted Total Distillable Boiling Point Distribution Curves for Oil Weathering in the Wave Tank Experiment at 55°F with a 2 knot wind.

Inspection of Figures 5-126 and 5-127 show similar differences between observed and predicted total distillation curves. As in the mass balance distillation curves, the predicted % mass distilled for total distillables is 10-20% less than the observed % total distilled at any given temperature.

A possible explanation for the above mentioned differences may lie in the method of calculating % mass distilled from GC data. Whereas, the model prediction is based on true distillate cut characterizations, supplied by Coleman (1978), the calculation from raw GC data to % mass distilled involves a necessary conversion that treats hydrocarbons heavier than n-C_{28} as non-chromatographable. The data must be treated this way in order to adjust non-chromatographable mass % to match % non-distillable (pot residue). This procedure may not be totally accurate, and could possibly be the cause of variations between observed and predicted temperature vs. % mass distilled curves.

5.5.2.2 Verification at 30°F

Further verification of the oil weathering model was undertaken by applying it to the fall/winter wave tank experiment, where the average air temperature was approximately 30°F. Again, minor modifications in the program were used to facilitate better agreement. The initial spill conditions in this case were:

Temperatures in degrees F = 30
Spill size in barrel = 0.1 (16 l)
Wind speed in knots = 2
Slick spreading = OFF
Slick thickness in cm = 1

Slight adjustments of some optional user specified constants were again useful and those changes are noted below, along with the models suggested values.

Constant	Suggested Value	Value Used
Maximum Weight Fraction H_2O	.55	.5
Water Incorporation Rate	.001	.003
Oil/Water Interfacial Tension	30	27
Viscosity-Fraction-Oil-Weathered	10.5	14

Using these input parameters the model was applied to the wave tank spill initiated in November 1982 at Kasitsna Bay, Alaska. Output predictions are again compared to experimental data, as with the summer spills, with one exception - no experimental data were obtained for water incorporation. Therefore, only viscosity, dispersion flux and % distilled (evaporation) are addressed.

Viscosity at 30°F

Table 5-28 presents experimental ambient temperature viscosity data and model predicted values for wave tank oil as it weathers at approximately 30°F. A graphical presentation of these numbers can be found in Figure 5-128. Clearly, the agreement between predicted and observed viscosity is not as good as in the summer spill (Figure 5-123). Initially, the predicted viscosities at 30° are two to three times higher than measured values; however, after 8 hours the observed viscosity increases rapidly and predicted values tend to be quite depressed. Nevertheless, the final time point at 288 hours gives reasonable agreement with the observed viscosity at 11,500 centipoise and the predicted viscosity at 16,000 centipoise. While the same arguments, regarding differences in model calculation vs. actual measurement, apply to the fall spill as well as the summer spills, another factor must also be taken into consideration. Experimental varience in the data was accounted for in the summer spills by having triplicate viscosity measurements available; because only one wave tank spill was iniated in the fall, these data are somewhat less reliable. Also, in both cases, the model predicts spill behavior based solely on one temperature input and, naturally, there is a wide daily temperature range during field measurements of viscosity. For example, the time zero

Table 5-28. **Observed vs Model Predicted Data from the Fall/Winter Wave Tank Spill**

	Viscosity (centipoise)		Dispersion Flux (g/m^2/hr)	
Time (Hours)	Observed	Predicted	Observed	Predicted
1	270	730	—	—
2	280	830	.96	.71
4	580	980	.90	.65
8	2200	1200	.78	.59
12	2900	1300	.68	.56
24	5600	1800	.45	.49
75	8700	3400	.097	.36
144	9800	6400	.035	.26
288	11,500	16,000	.030	.17

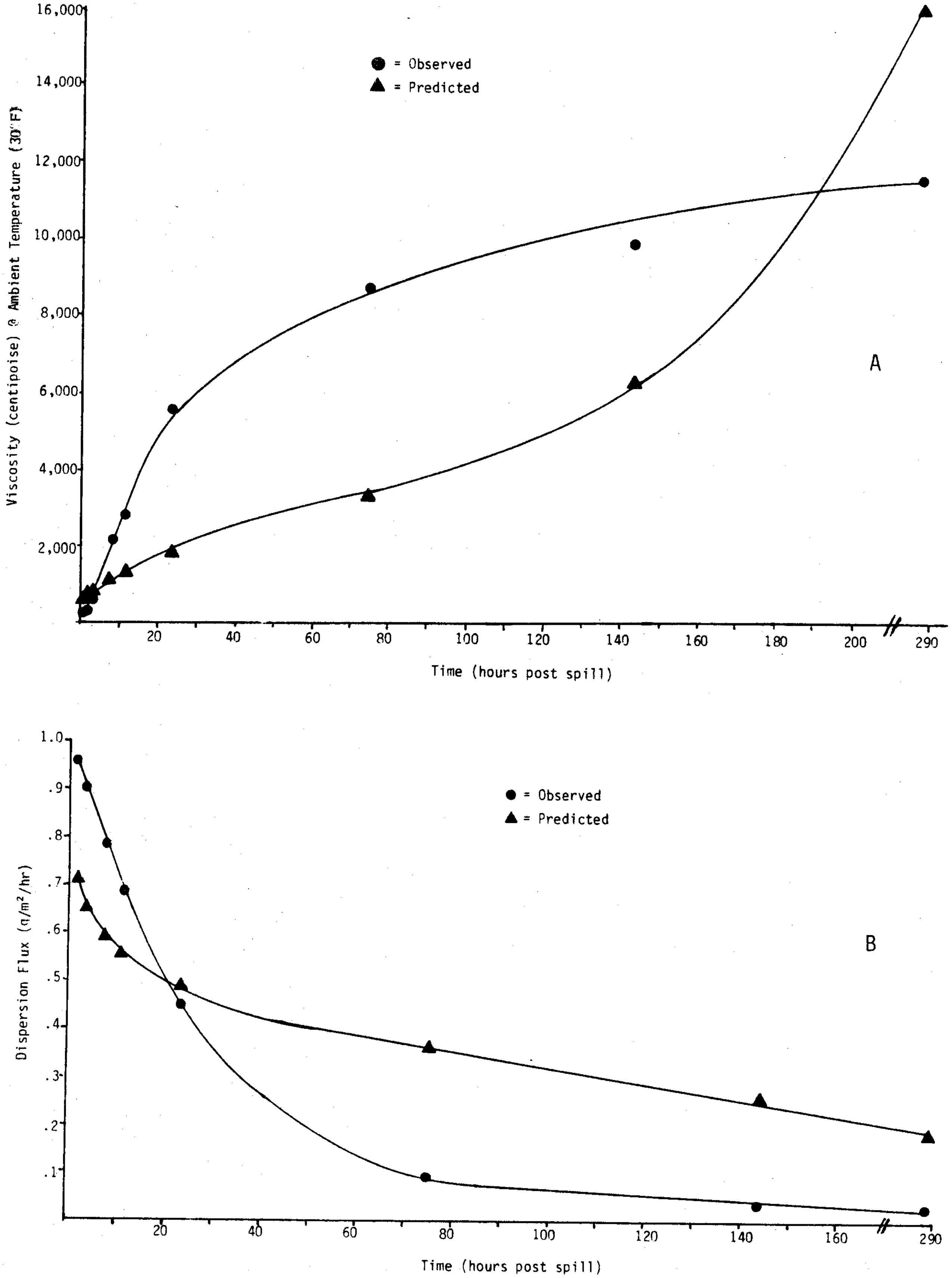

Figure 5-128. Observed Vs Model Predicted Data for the Fall/Winter Spill in Wave Tank #4 for (A) Viscosity, and (B) Dispersion Flux.

observed viscosity was taken at noon while the temperature was approximately 40°C but the 12-hour measurement was taken at midnight with a temperature of 29°C. Since viscosity is so very temperature dependent, temperature fluctuations such as these are reflected in the actual measurements, but not in predicted values. Taking these arguments into account, the agreement between observed and predicted viscosities at 30° is reasonable.

Dispersion Flux

Dispersed oil flux for the fall spill was calculated from concentration data in the same manner as described for the summer tanks. Values for the constants a_1, b_2, a_2 and b_2 were chosen to make the calculated dispersed oil concentration match the measured concentration as closely as possible. The table below presents the observed and calculated dispersed oil concentrations using $a_1 = 10^{-3}$, $b_1 = 10^{-5}$, $a_2 = 3 \times 10^{-5}$, and $b_2 = 10^{-8}$

	Concentration (mg/l)	
Time (Hours)	Experimental	Calculated
1	1.5	1.1
2	2.2	1.9
4	2.1	2.7
8	3.7	3.0
12	.47	2.8
24	.36	1.9
144	.14	.14

Table 5-28 and Figure 5-128 present the "calculated observed" and model predicted flux data. The agreement seen between predicted and experimental flux values seems quite reasonable. Again, refinements in the calculations of flux from measured concentrations could possibly provide a better fit.

% Mass Distillable

GC data, for oil weathered in the fall wave tank spill, were treated in the same fashion as described previously for comparisons of observed and predicted % mass distilled. Figures 5-129 through 5-132 present temperature vs. % mass distilled curves for the fall spill at Kasitsna Bay. Inspection of the graphs reveals differences in "GC observed" and predicted distillation behavior similar to those found in the summer spill case. At 30° the curve shape of the observed data is skewed in the same fashion as at 55°, compared to the respective model predicted curves. Likewise, the total % mass distilled at 800°F after 288 hours of weathering (Figure 5-129) is somewhat less than the model predicts (i.e., 47% observed compared to 53% predicted). One similarity worth noting can be seen by comparing observed data at 55° and 30° (Figures 5-124 and 5-129) with model predicted data at 55° and 30° (Figures 5-125 and 5-130). Note that in both observed and predected cases the curve for the % mass distilled after eight hours is shifted further to the left of the time zero curve at 55° when compared to 30°. This means that at 55° more of the predicted and observed oil mass has evaporated than at 30°, and that on distillation, a higher temperature would be required for the oil weathered at 55° before the first drop of the weathered oil could be distillled.

Considering the inherent problems, such as experimental error, boundary conditions and changing weather conditions, overall agreement between observed and model predicted weathering phenomona is quite reasonable for the wave tank spill scenarios. In particular, the agreement in observed and predicted time series changes in viscosity, % water incorporation, dispersion flux and distillation trends for the ambient temperatures studied, adds further credence to the applicability of the oil weathering model towards predecting oil weathering behavior in a variety of subarctic conditions.

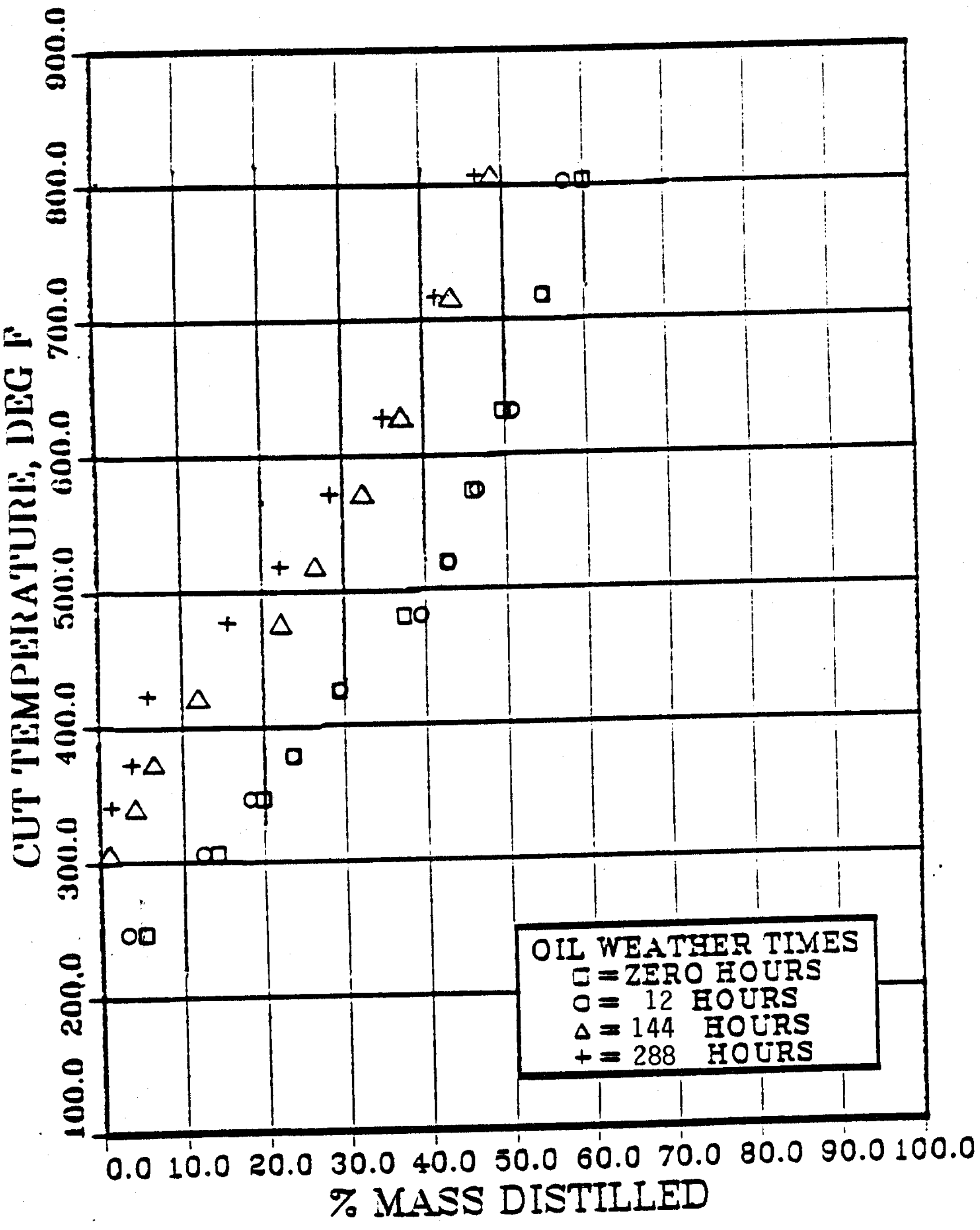

Figure 5-129. Observed Mass Balance Distillation Curves for Oil Weathering in the Wave Tank Experiment at 30°F with a 2 knot wind.

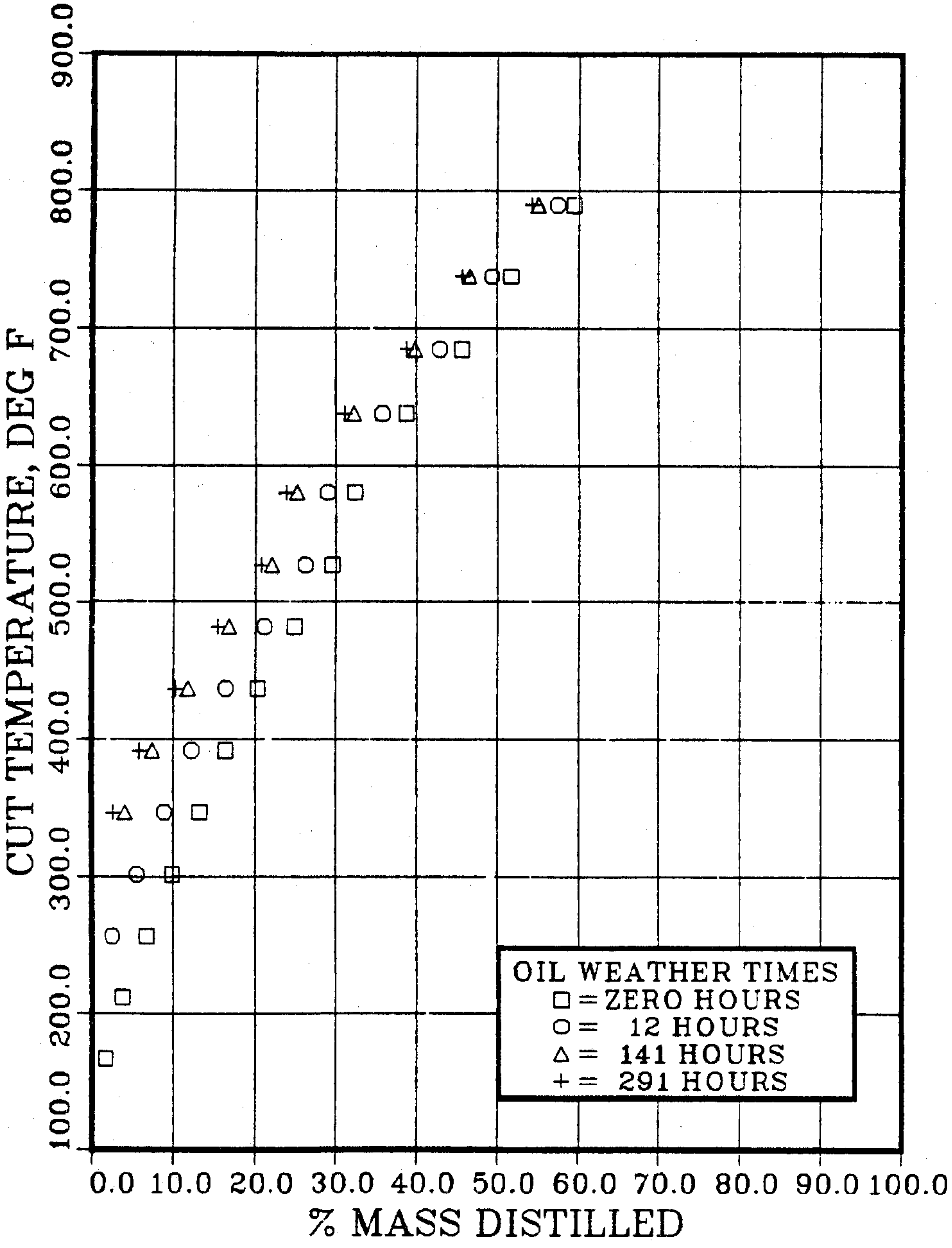

Figure 5-130. Predicted Mass Balance Distillation Curves for Oil Weathering in the Wave Tank Experiment at 30°F with a 2 Knot Wind.

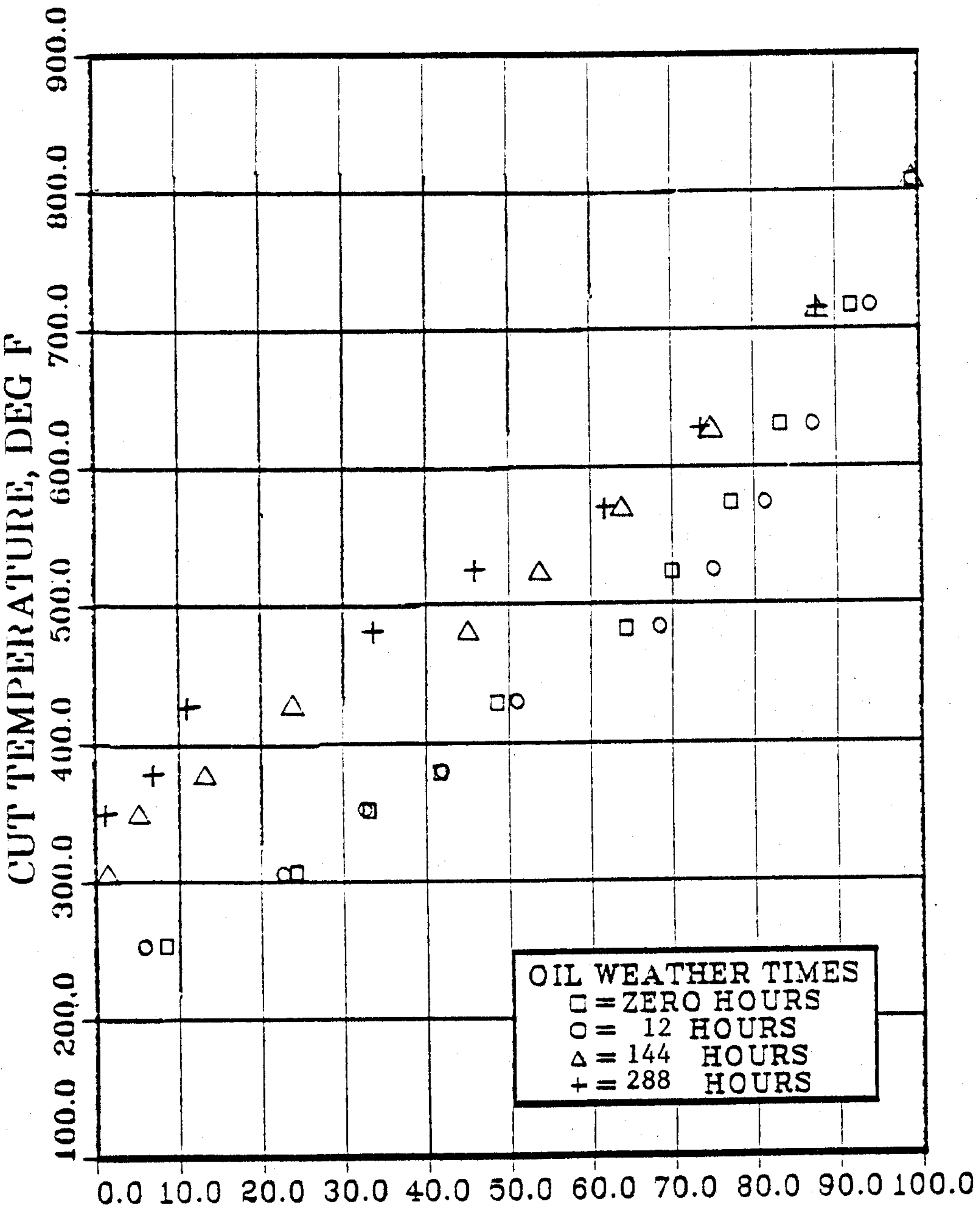

Figure 5-131. Observed Total Distillable Boiling Point Distribution Curves for Oil Weathering in the Wave Tank Experiment at 30^{o}F with a 2 Knot Wind.

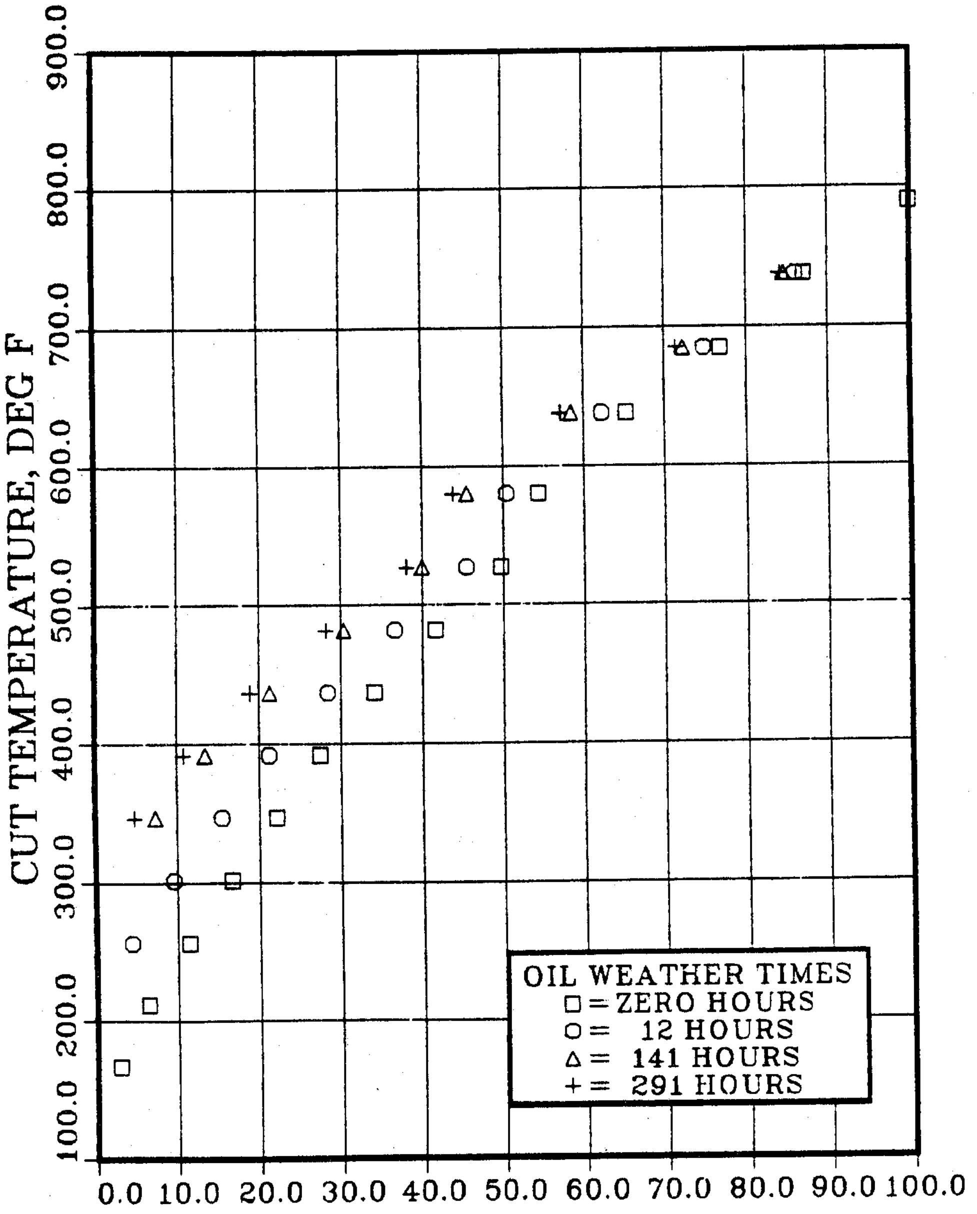

Figure 5-132. Predicted Total Distillable Boiling Point Distribution Curves for Oil Weathering in the Wave Tank Experiment at 30°F with a 2 Knot Wind.

6.0 OIL/SUSPENDED PARTICULATE MATERIAL INTERACTIONS

6.1 Effects of Oil on SPM Settling Rates - La Jolla Studies

During the first half of this program, oil/suspended particulate material interactions were studied to determine adsorption/desorption rates at different temperatures and to determine the affects of these processes on sedimentation rates with various types of particulate material. These studies were undertaken with fresh Prudhoe Bay crude oil and Prudhoe Bay crude which had undergone evaporation/dissolution weathering for 48 hours. The presence and absence of the dispersant Corexit 9527 (10 parts oil to 1 part dispersant) were also incorporated as experimental variables, and three types of relatively pure sediments were utilized (carbonate, silica and deep basin clay; Table 6-1). Sedimentation rate determinations were made using a Cahn 2000 series sediment balance, and a particle size range of 4.0 ϕ to 9.0 ϕ (62 μm to 2 μm) was used.

The sediment material being analyzed was added to the stirred chamber shown in Figure 6-1, and aliquots were taken at times 0, 3 hours, 24 hours and 48 hours for analyses on the sediment balance. The data were then analyzed to yield final wet and dry weights of (settled) particulates and according to the Waddell settling equations to yield mean, median, skewness and kurtosis data on the grain size distribution.

Waddel Settling formula

$$T = \frac{K}{D^2} \tag{6.1}$$

where T = time (minutes)
D = diameter (micrometers)

and

$$K = \frac{0.3\ h\ v\ 10^8}{(d_s - d_1)\ g} \tag{6.2}$$

where h = height of column of water
v = viscosity (poises)
d_s = density (solid) g/ml
d_1 = density (liquid) g/ml
g = gravity in cm/sec

TABLE 6-1. GRAIN SIZE AND MAJOR METALLIC CATION ABUNDANCES FOR INITIAL OIL/SUSPENDED PARTICULATE MATERIAL EXPERIMENTS.

Dispersive X-ray Analysis (SEM)

Sample	Relative Atom % Mg	Al	Si	K	Ca	Fe
Commercial Diatomite	-	-	93	-	6	1
Milled Foram Sand	2	2	12	-	85	1
San Nicolas Basin Clay	2	6	48	3	35	6

Grain Size Information

Sample	Median	Mean	Skewness	Kurtosis
Commercial Diatomite	5.5	5.5	+ .03	1.0
Milled Foram Sand	5.4	5.9	+ .25	.8
San Nicolas Basin Clay	5.5	5.8	+ .19	0.8

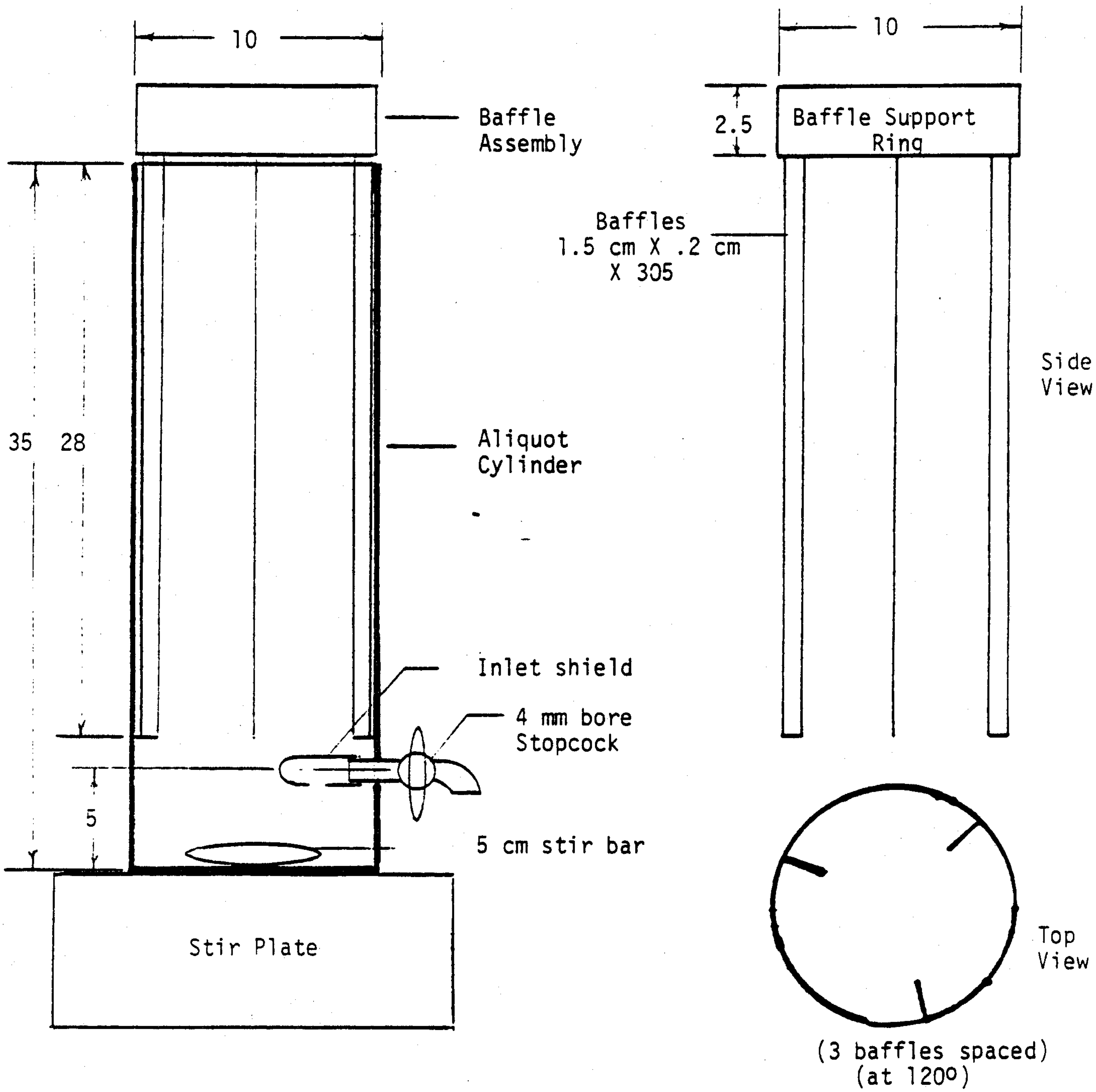

Note: All dimensions in cm.

FIGURE 6-1. ALIQUOT CYLINDER ASSEMBLY FOR INITIAL OIL/SPM INTERACTION STUDIES

GRAPHICAL STATISTICS

$$\text{Skewness} = \frac{\phi16 + \phi84 - 2\phi50}{2\ (\phi84 - \phi16)} + \frac{\phi5 + \phi95 - 2\phi50}{2(\phi95 - \ \phi5} \qquad (6.3)$$

$$\text{Kurtosis} = \frac{\phi95 - \phi5}{2.44\ (\phi75 - \phi75)} \qquad (6.4)$$

$$\text{Mean} = \frac{\phi84 + \phi16}{2} \qquad (6.5)$$

$$\text{Median} = \phi \text{ size at 50\% cumulative weight} \qquad (6.6)$$

Results from these initial studies were presented in detail in the September 1980 Interim Report (PAYNE et al., 1980). Essentially only very slight perturbations in SPM settling characteristics were observed as a result of oil, oil plus Corexit, and mousse interactions. Tables 6-2 and 6-3 present the results from initial interaction studies completed with diatomite powder and deep basin clay (San Nicolas), respectively. From these results some subtle changes in the median and mean sediment size characteristics with both substrate types were observed for the oil-Corexit mixtures; however, oil alone did not have as significant an effect on these parameters. Table 6-4 presents a summary of the settling experiments using San Nicolas Basin sediment and oil and oil plus Corexit. Results of the first two runs with oil and the Corexit-oil mixture indicated minor interactions which can be detected in the settling rate data. The small increase in phi size (decrease in grain size) for both the median and mean and the decrease in settled weight percent are indicative of some buoyant force at work and/or of adsorption of oil, decreasing the effective density of the particles below a critical size (FEELY et al., 1978; BASSIN and ICHIYE, 1977). The largest settled weight differences occur in the oil/Corexit sediment experiments; however, the median, mean, skewness and kurtosis were not as drastically affected by the oil or oil plus Corexit interaction. Time-series changes in the phi size, skewness and final weight settled as a result of oil exposure are shown in Figure 6-2, and while the affect of exposure on all three parameters is statistically significant, their overall perturbation to SPM characteristics were considered to be minor.

TABLE 6-2. INITIAL INTERACTION, STATISTICAL EFFECTS OF DENSITY, DISPERSANT, AND SAMPLE WEIGHT ON DIATOMITE POWDER AT 23°C.

Sample	Addition	ρ	Method of Injection	Dry Weight	Wet wt.* Dry wt.	Median	Mean	Shewness	Kurtosis
A	.01N Calgon	.997	30cc in cent. tube	200 mg	.57	5.50	5.49	+.03	1.04
Run #4	---	1.025	30cc in cent. tube	200 mg	.51	5.37	5.41	+.11	1.13
Run #5	---	.997	40cc in cent. tube	300 mg	.56	5.57	5.49	-.38	1.06
Run #6	---	1.025	6cc in 10cc syringe	160 mg	.50	5.47	5.50	+.13	1.27
Run #7	Oil only	1.025	30cc in cent. tube	205 mg	.51	5.42	5.50	+.98	1.11
Run #8	Oil-Corexit	1.024	30cc in cent. tube	200.2 mg	.35	5.59	5.84	+.16	.78
Run #9	Oil-Corexit	.997	30cc in cent. tube	204 mg	.52	5.50	5.50	+.03	1.05
Run #10	Oil-Corexit	.997	30cc in cent. tube	208 mg	.56	5.70	5.70	+.03	.98
Run #11	Oil-Corexit	.997	separate addition of sediment and oil	211 mg	.54	5.69	5.73	+.08	1.05

* Ratio of sedimentation balance weight (weight of sediment in water)/dry weight of added sediment.

TABLE 6-3. STATISTICAL SUMMARY OF DEEP BASIN CLAY (SAN NICOLAS) AMBIENT TEMP (23°C), SEAWATER, MIXING TIME = 15 min.

Date	Oil	10:1 Corexit	(0-4) Run Rating	Median	Mean	Skewness	Kurtosis	Final Wt.	% Sett
7/22/80	---	---	4.0	5.53	5.80	+.19	.75	108.9	100%
7/23/80	---	---	4.0	5.32	5.51	+.21	.89	105.5	100%
7/21/80	X	X	2.5	4.89	5.31	+.37	.98	72.5	68%
7/28/80	X	X	3.5	4.92	5.35	+.35	.95	71.9	67%
7/24/80	X	---	4.0	5.36	5.75	+.26	.87	91.7	86%

Run Reproducibility

	Mean	Skewness	Kurtosis	Final Wt.
Sediment	5.66± 0.2	.21 ± .01	.82 ± .1	107 ± 2.4
Sediment-oil-Corexit	5.33± 0.03	.36 ± 0.1	.97 ± .02	72.2 ± 0.4

TABLE 6-4. SUMMARY OF SAN NICOLAS BASIN SUSPENDED PARTICULATE MATERIAL AND FRESH PRUDHOE BAY CRUDE OIL INTERACTIONS.

	CONDITIONS			STATISTICS				
	Additive	temp.	time	median	mean	skewness	kurtosis	final weight recovered (wet)
1.	none	23°C	0	5.25	5.47	+ .21	.91	78.4
2.	oil	"	3 hrs.	5.50	5.69	+ .17	.87	77.5
3.	oil	"	24 hrs	5.79	5.91	+ .11	.94	74.3
4.	oil	"	48 hrs.	6.03	6.02	+ .005	.90	71.5
5.	oil & corexit	"	0	5.25	5.28	+ .90	.75	44.70
6.	" "	"	3 hrs.	5.13	5.39	+ .28	1.05	26.32
7.	" "	"	24 hrs.	5.30	5.30	+ .08	.85	34.05
8.	" "	"	48 hrs.	5.91	6.13	+ .12	.81	31.15

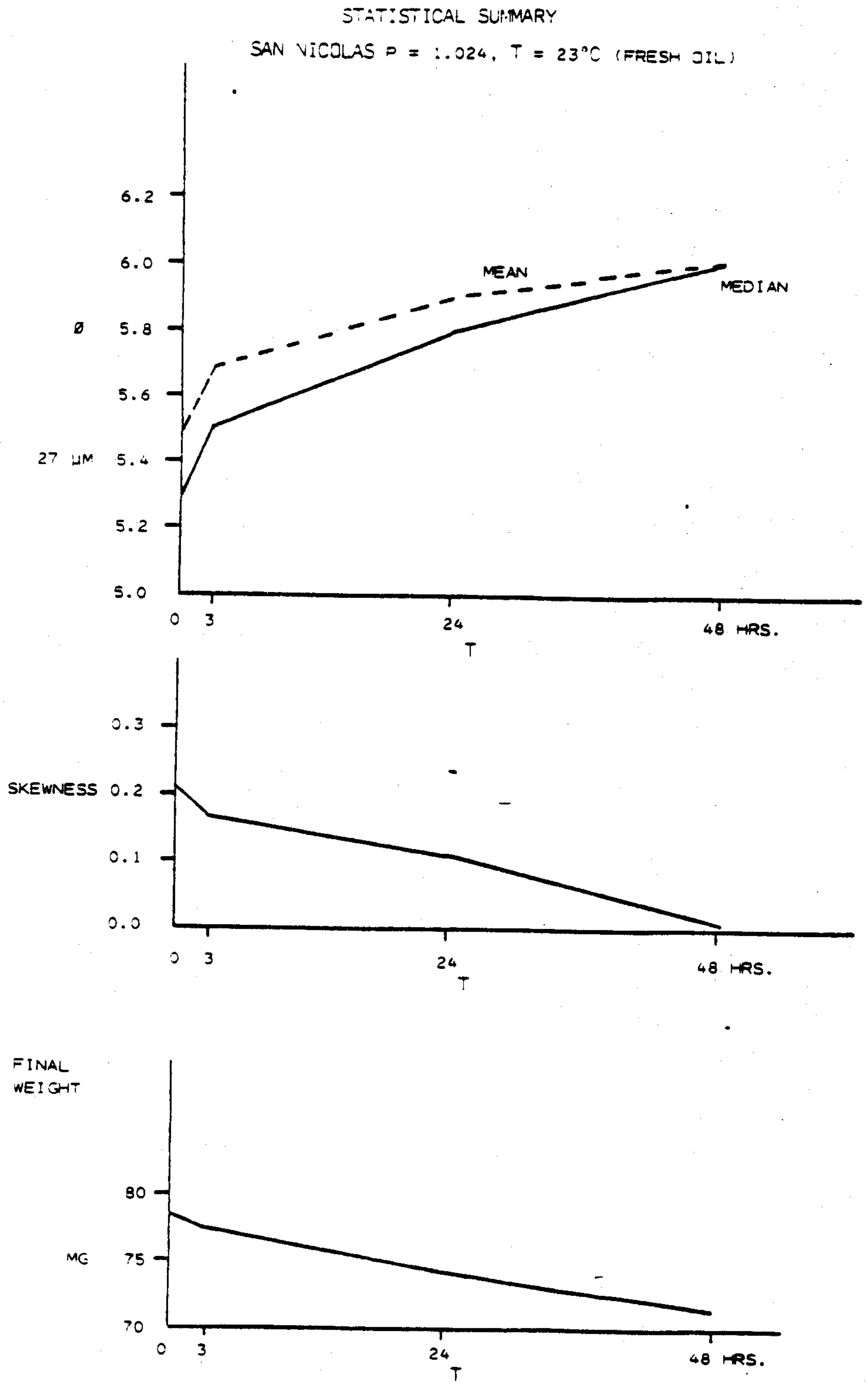

FIGURE 6-2. GRAPHICAL DISPLAY OF THE AFFECTS OF THE INTERACTION TIME FOR SAN NICOLAS BASIN SEDIMENT AND FRESH PRUDHOE BAY CRUDE OIL ON MAJOR STATISTICAL PARAMETERS (SEE TABLE 6-4). THE EFFECT OF TIME ON ALL THREE PARAMETERS IS STATISTICALLY SIGNIFICANT BUT NOT CONSIDERED TO BE MINOR.

6.2 DETAILED ANALYSES OF SUSPENDED PARTICULATE MATERIALS CHARACTERISTIC OF LOWER COOK INLET ALASKAN WATERS

6.2.1 Selection of Representative SPM Sources for Extended Oil Adsorption Studies

As a result of the above findings, examinations of phi size and settling characteristics of oil/SPM mixtures were discontinued, and attention was directed instead towards the compound specific nature of the oil suspended particulate material interactions. Further, in an effort to satisfy environmental manager's needs with regard to oil/SPM interactions in Alaskan waters, attention was focused on the compound specific adsoprtion of petroleum hydrocarbon components onto sediments and fines representative of Lower Cook Inlet suspended particulate material.

Thus, during the Spring 1981 Kasitsna Bay program, studies were initiated to locate intertidal sites having significant deposits of sediment fines representative of Lower Cook Inlet suspended particulate material, and samples of these sediments were characterized as to their physical and compound specific oil retention properties. From the results of these initial investigations, three intertidal sites were selected as sources of divergent but representative samples of Lower Cook Inlet SPM. These sediments were then used for outdoor flow-through oil/SPM interaction experiments during the summer 1981 and 1982 programs at Kasitsna Bay.

Figure 6-3 presents a navigational chart for the Lower Cook Inlet/Shelikof Strait area, and Figure 6-4 shows expanded detail of the Kachemak Bay region. Sampling sites for initial SPM characterizations were selected using "Cook Inlet-southern part, navigational chart (1:200,000)-NOAA, C&GS 8554"; and the unpublished Environmental Sensitivity Index (ESI) for Lower Cook Inlet (RUBY and MAIERO, 1979).

Suspended particulate material in Kachemak Bay was considered to have four primary sources:

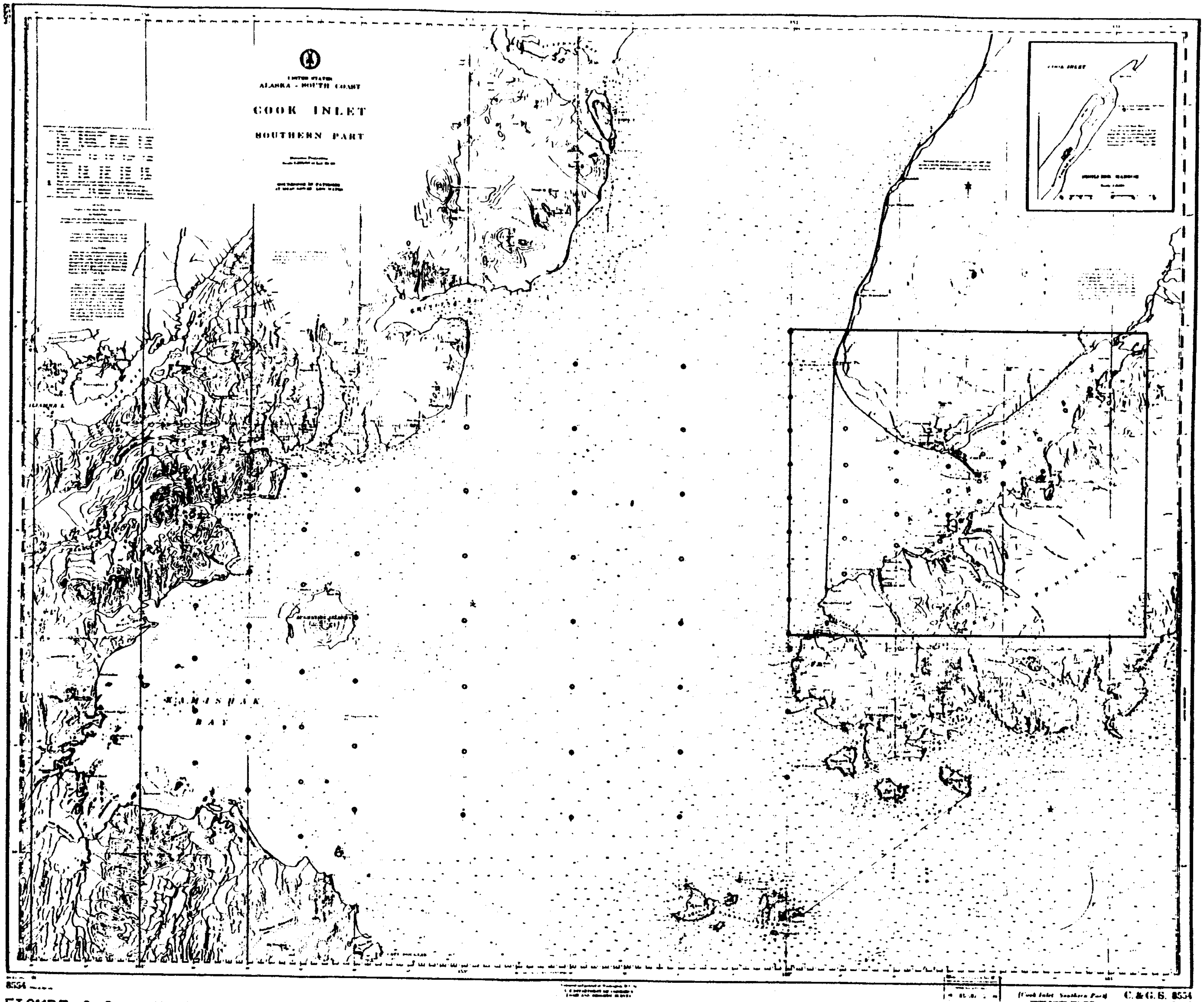

FIGURE 6-3. US DEPARTMENT OF COMMERCE COAST AND GEODETIC SURVEY, CHART #8554 OF THE LOWER COOK INLET REGION.

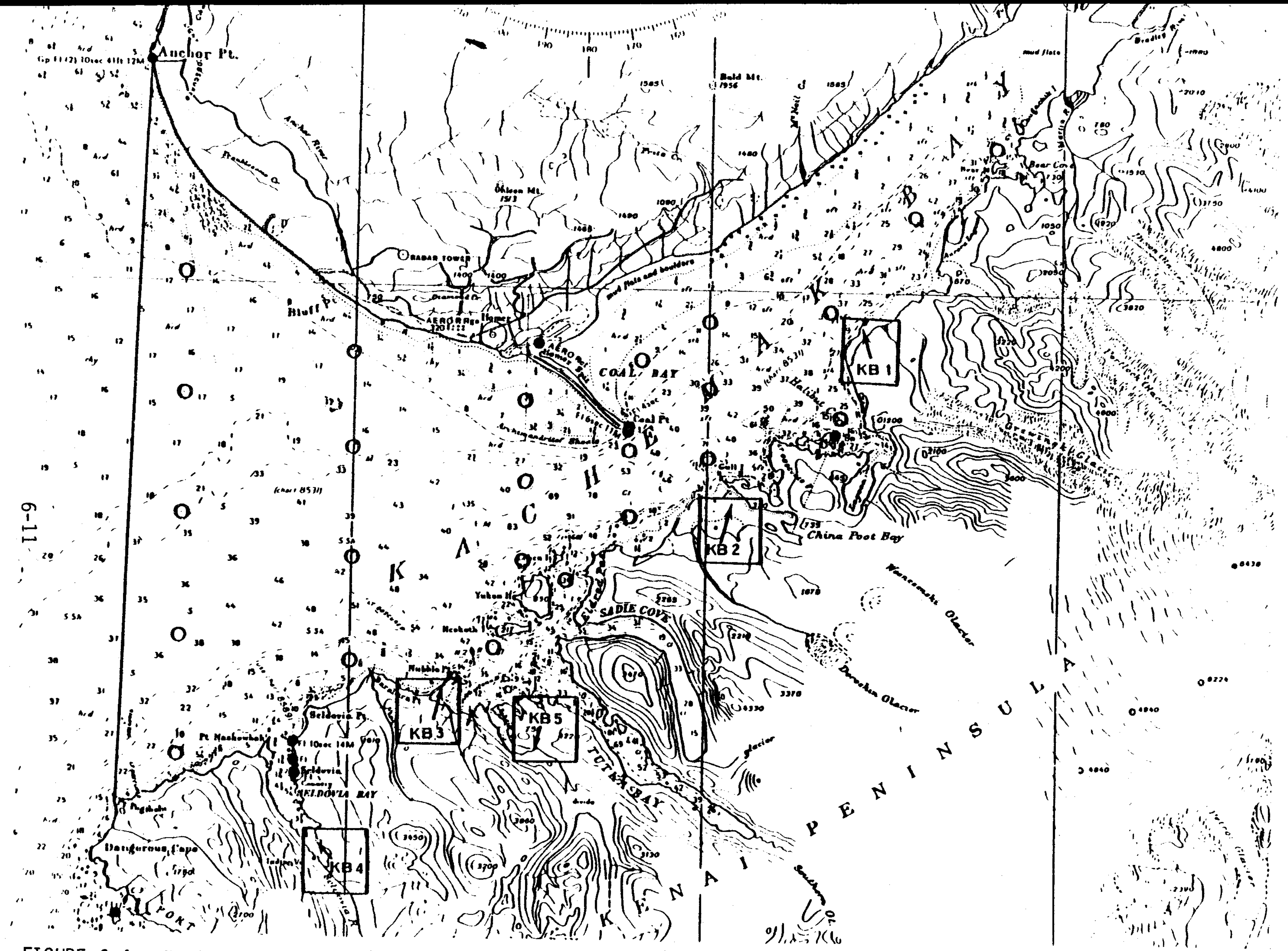

FIGURE 6-4. EXPANDED VIEW OF THE KACHEMAK BAY, KASITSNA BAY REGION (FROM C.&G.S. CHART 8554). SAMPLING SITES FOR OIL/SPM INTERACTION STUDIES AND INTERTIDAL OILED-CORRAL EXPERIMENTS ARE DENOTED AS: KB-1 GREWINGK GLACIER DELTA; KB-2 CHINA POOT BAY MUD FLATS; KB-3 KASITSNA BAY COMPOSITE SEDIMENT; KB-4 SELDOV RIVER SALT MARSH DETRITAL SEDIMENTS; KB-5 JAKOLOF INTERTIDAL MUD FLATS

- Marine waters introduced to Kachemak Bay by tides and currents from Lower Cook Inlet (Gulf of Alaska and Shelikof Straits)
- Glacial melt waters
- Terrestrial sources-runoff
- Marsh detritus

A secondary source to any site was also considered to be resuspension of sediment through wind and wave scour and transport of sediments by tidal actions and long-shore and bottom currents.

The Spring 1981 sampling program was designed such that 3 sediment types which were representative of Lower Cook Inlet suspended particulate material could be obtained, and these included: pure glacial till, tidal flats supported primarily by marine deposits and tidal flats supported by marsh detritus and terrestrial runoff. To represent these sediment types, four primary sites were selected for sampling and these are shown on Figure 6-4 as KB-1, KB-2, KB-3 and KB-4. At each site, fine particulates and sediment floc were obtained from the upper 1 to 2 cm of deposits exposed during lower tidal excursions. Detailed descriptions of each site follow.

KB-1: Grewingk Glacier Delta and Melt Stream

This site is characterized as a large, protected, delta subject to tidal marine flushing and fresh water input from the Grewingk Glacier melt stream. The glacier is central and 3 to 4 miles southeast of the tidal flat which is bounded on the west by a wide gravel spit oriented southwest to northeast as formed by northeasterly moving tides and longshore currents in Kachemak Bay (Figure 6-4). Glacial sediments were found directly behind the tip of the gravel spit at the point that the glacial waters met the marine waters which were draining from the southern section of the flat. These deposits of glacial silt (2-5 mm thick) formed a mat which could be removed from underlying sediment, and samples of this material were obtained for oil/SPM characterization studies. The exposed surfaces of small to medium cobble in the area were also covered with a similar mat of glacial silt, but quantitative sampling of this material was not possible. The richest glacial deposits were restricted to an area of approximately 800 meters^2 out of approximately 20,000 meters^2 inspected.

The influence of glacial melt waters served to increase biological productivity as evidenced by large stands of Ulva sp. accompanied by significant numbers of amphipods. Filamentous brown algae were ubiquitous to the flat. Bird use of the area appeared moderate - evidence of bird tracks was lower than expected.

The glacial melt water was "milky" (bluish white) and had a fresh-bitter taste. The mouth of the delta (interface of drainage and receiving waters) was subject to erosion due to the meandering of the delta channel, and as such, the site at which samples were taken is considered to be geologically active. Little perburbation of the area was noted on re-occupying the station during the Summer 1981 field program; however, it was apparent that the sampling site may not remain in its present state for extended periods of time. Overall energy is low; however, localized disturbances may affect the subject sediment when incoming or outgoing tidal waters covering the flat are a few centimeters to a 1/3 meter deep (or depth equaling fetch height) so that wind driven waves can scour the bottom. Further discussions of the results of oil/SPM interaction studies using the substrate from KB-1 are presented in Section 6.3.

KB-2/China Poot Bay - Mud Flats

The area at which samples were taken is common to protected tidal flats in Lower Cook Inlet and Prince William Sound (RUBY and MAIERO, 1979). The sampling site is located on the southwest section of the flats, and this site is protected from wave energy by a long, curved gravel spit forming the boundary between China Poot and Kachemak Bay (Figure 6-4). There is no source of fresh water immediately adjacent to the sampling site. The sources of sediment at this site are expected to be primarily of marine (i.e., outer bay) origin. The flat is very high in biological productivity - clams, polycheates and amphipods were abundant. It is apparent that benthic organisms are constantly reworking these sediments - fecal pellets and burrows were in profusion, and for the most part, the sediments appeared to be well oxidized with little or no evidence of H_2S.

The sampling area included "random" surficial samples taken from the sloping face of the flat (slope of 1:12 on the lower face to 1:23 on the upper face) and the flat itself (average slope along transect of 1:75). The sediments on the slope face (to a depth of approximately 10 cm) consisted of a thin veneer of brown organic sediments in a consolidated mat having a thickness of 2 - 5 mm overlying black silt/sand homogeneous, well oxidized sediments. These sediments were well packed and did not yield to any degree to foot pressure. In comparison, the sediment composition on the flat proper was visually alike the sediments of the slope; however, the underlying black sediments were in a moderately reduced state (moderate H_2S noted). Sample KB-2B was obtained from these reduced sediments while KB-2 was obtained on the 0-1 cm subsection from the slope face. Biological activity was higher on the flats compared to the slope face (evidence of siphon holes, etc.) and interstitial water was observed in each cross-section of sediment. The upper flat sediments were not as firm as those of the slope so that foot pressure could easily cause a depression. The reduced state (notable H_2S present) may be a function of the ability of the flats to: drain quickly, increasing retention of organics (as opposed to wave action gently scouring the somewhat steeper slope with each tidal cycle), heating of the flats by solar energy (slope would be subject to direct sunlight during a limited portion of the sun's arc), and increased bacterial activity.

KB-3, Kasitsna Bay - Composite Shell Fragments, Sand and Mud

The Kasitsna Bay sediment sample was taken from the interior of the bay along a tidal flat adjacent to Nubble Pt. (see Figure 6-4). The mud flats are located on the east side of a small spit located in the western interior of the Bay. Wave energy is minimized in this portion of the bay because of the short distance between spits; however, tidally generated currents appear significant. The sampling station lies at the foot of a sand/gravel beach having a moderate slope (1:17) to the high tide wrach and a steep slope (1:9) from the high tide to the maximum storm tide wrach on Nubble Pt.

The sediments on the protected flats consist of an unsorted matrix of sand, gravel and shell fragments bound tightly together with silts and organic materials. The nature of the components in the sediments indicate that material is transported to this area as a result of bottom scour (tidal) and longshore transport. Biological productivity is high. The flats were populated with vegetation stands of *Ulva*, *Fucus* and *Enteromorpha* accompanied by *Mytilus*, *Balanus* and numerous polycheates and amphipods. The holdfasts of the plants and byssal threads of the mussels appear to play a significant role in trapping sediments on the flats.

The sediments at this station were unique to the sediment samples collected during the spring season. Sediments sampled at other sites were fairly well sorted and somewhat homogeneous. Bottom scour did not seem to contribute to the sediment at the other stations and shell fragments were not as abundant. This station appears to contain representative composite of the components of the other stations sampled.

KB-4, Seldovia Bay - Salt Marsh in Upper Bay

The sample from this station was taken in a submerged tidal channel in the *Spartina sp.* marsh at the head of Seldovia Bay. The marsh lies to the north of Seldovia River (Figure 6-4).

The sediments of the marsh are composed primarily of organic, decomposing detritus originating from the *Spartina* marsh. The normal cycle of the marsh is to die back in early winter and regrow in spring of the following year. When the marsh plants die back, the dead vegetative material is matted down, by wind and snow to form a thick vegetative cover over the flat. New shoots sprout from the rhizome mat in the spring pushing through the decomposing vegetative mat. In spring, the old vegetative mat decomposes introducing a significant amount of organic material to the marsh channels and flats in the vicinity of the marsh. Our sampling effort occurred during the stage of regrowth/decomposition.

The sampling station is adjacent to the mouth of Seldovia River. Incoming tides transport the fresh water runoff (overlying the denser marine wedge) onto the marsh so that terrestrial sediments may be deposited with marsh detritus. The transport of fresh water onto the marsh was confirmed during sampling as incoming tidal waters tasted totally fresh.

The marsh was rich in invertebrates and showed signs of heavy bird use (tracks).

Table 6-5 presents an overall description of the sediment/SPM samples collected at each site, and Table 6-6 presents size-compositional data derived from visual and microscopic observations of the samples collected from the four sites. From these examinations a pure form compositional diagram for the samples was prepared and is presented in Figure 6-5A. Figure 6-5B characterizes the sediments as far as suspected sediment source.

Immediately after these samples were collected, they were extracted and analyzed at the Kasitsna Bay facility for background biological and potential petroleum hydrocarbon content (from previous spill events). These analyses were completed at that time such that <u>if</u> the results had then indicated previous petroleum hydrocarbon contamination, alternative sampling sites could have been selected and sampled during the spring 1981 program before returning to La Jolla. Particular attention was paid to the sediments from KB-4, the Seldovia River salt marsh, because of a Bunker C spill which occurred in Seldovia Bay (down stream) during 1978. Observations were completed during

TABLE 6-5. OBSERVED CHARACTERISTICS AND OVERALL DESCRIPTIONS OF SEDIMENT/SPM SAMPLES COLLECTED DURING THE SPRING 1981 KASITSNA BAY FIELD PROGRAM.

	1	2	2B	3	4
Sediment Component	Glacial Silts Fine sand Gravel	Silt Fine sand	Silt Fine sand	Organics, Silt Fine-medium sand Gravel, shell frag.	Organics, Silt
Sediment Classification	Sandy Silt	Sandy Silt	Silty Sand	Conglomerate	Detritus/Silt
^{0}/oo	0-5	15-30	15-30	15-30	0-5
	Wet: Gray brown color. Very fine sediments, easy to suspend - remain in suspension easily. Silts gray when in suspension-settle portion brown. Dry: Blue gray color - Sample cements together when dry. Sufficient pressure needed to break sample apart.	Wet: Green brown color. Muddy-suspended easily, heavier fraction forms a "clay" on the bottom of the trap - Remains in suspension easily. Dry: Green gray color fragments easily but needs sufficient pressure to reduce it all the way to powdered form.	Wet: Brown black color. Silt suspended easily and sand (black) settles quickly. Sand forms the majority of the sample, silts remain in suspension easily. Dry: Gray black color. Very fine sand is black in color. Drying causes clumping rather than laying powder easily.	Wet: Brown color. Silt and organics suspend easily. Organics appear to be a flock or mucoid sand, gravel and shell fragments settle easily. Organics approx. 50% of sample. Dry: Brown gray color. Sample cements together-difficult to break apart. Silt and organics act as a strong bonding agent.	Wet: Brown color. Silt and plant fiber suspend easily. Fibers settle first followed by the very small sandy silt-a small fraction of the silt remains in suspension over 8 hours. Dry: Brown color. Drys as silt/fiber matrix. Flakes when broken. Easy to powder.

TABLE 6-6. SIZE COMPOSITIONAL DATA DERIVED FROM VISUAL AND MICROSCOPIC OBSERVATIONS OF SPM SAMPLES COLLECTED FROM INTERTIDAL SAMPLING SITES KB-1, KB-2, KB-2B, KB-3 AND KB-4 (SPRING 1981 KASITSNA BAY PROGRAM).

	1	2	2B	3	4
Cobble				X	
Heavy Gravel				X	
Medium Gravel	X			X	
Heavy Sand				X	
Medium Sand			X	X	
Light Sand	X	X	X	X	
Silt	X	X	X	X	X
Glacial Silt	X	?	?	?	
Organics		X	X	X	X

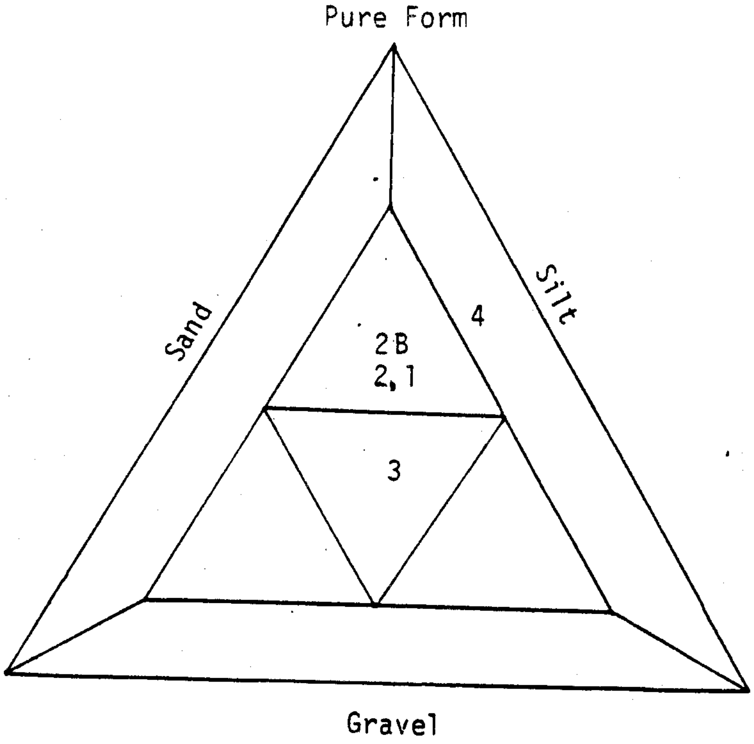

1 - silts, sand - sandy silt (glacial)
2 - sand, silts - sandy silt (marine)
2B - silts, sand - silty sand (marine)
3 - organics, silt, sand, gravel - conglomerate (marine)
4 - organics, silt - silt (organic)

Glacial	Marine	Terrest.	Marsh
Glacial	1	1	
	Marine	2,2B,3	4
		Terrest.	4
			Marsh

FIGURE 6-5. (A) FIELD ESTIMATED SIZE COMPOSITIONAL DIAGRAM FOR SEDIMENT/SPM SAMPLES COLLECTED DURING THE SPRING 1981 PROGRAM; (B) SEDIMENTARY SOURCE DIAGRAM DERIVED FROM FIELD OBSERVATION DATA.

that spill event from vessels, aircraft and through the use of drift cards (MAIERO and MAYNARD, November 1978), and the results of those studies had indicated that the oil did not enter the upper end of the Bay. Fortunately, the capillary column gas chromatographic data confirmed that no prior contamination of that area (or any of the other sites) had occurred, and only trace levels of biogenic compounds were detected in most of the analyses. As a result, no additional field sampling was required during the spring program, and the frozen sediment samples were then shipped to La Jolla for additional characterization and initial oil/SPM interaction studies.

6.2.2 Additional Suspended Particulate Material Sample Characterization by Scanning Electron Microscopy and X-ray Diffraction

Upon returning to our laboratories in La Jolla, CA additional characterizations of the sediment/SPM samples were undertaken and these included: specific surface area determinations, scanning electron microscopy (SEM), dispersive X-ray compositional analyses and diffractive X-ray mineralogical analyses.

Each sample for SEM analyses was prepared by transferring a 55 to 57-mg sediment sample into 35 ml of deionized water. The sample was then shaken for 15 min on a wrist action shaker; this water was then transferred to a 50-cc plastic polyethylene centrifuge tube with a side arm to withdraw subsamples using a 3-cc syringe.

After bubbling with N_2 to insure SPM suspension, the sediment/water mixture was diluted twice and filtered through a 0.2 m pore size nuclepore filter to yield 135 to 139 g per filter. This filter was then sputter coated with gold for scanning electron microscopy analyses on a model ISI Super IIIA SEM. Figures 6-6 through 6-15 present two selected fields from each SPM sample as shown below.

Figure 6-6 - KB-1 Grewingk Glacial Till
Upper 0-5 mm of deposits removed from Glacier Delta

Figure 6-8 - KB-2A China Poot Bay
Upper 0-1 cm of deposits from intertidal mud flats

Figure 6-10 - KB-2B China Poot Bay
Lower 1-8 cm composite from intertidal mud flats

Figure 6-12 - KB-3 Kasitsna Bay
Upper 0-1 cm composite of sediment floc from protected mud flats

Figure 6-14 - KB-4 Seldovia River Estuary
Upper 0-1 cm composite of sediment/detrital floc from channel in Spartina sp. salt marsh

Following each set of SEM photomicrographs, a schematic diagram is presented which identifies the major components present.

Because the μg loading on each filter represents the same overall mass/filter area, direct compositional comparisons can be made for all the SPM samples. Thus, in Figure 6-6 it can be seen that diatoms and several larger clay fragments make up the majority of the sample by weight, while the majority of the surface is covered by less than 5-μm clay fragments.

In Figure 6-8 of the surface 0 to 1-cm sample from China Poot Bay, the upper photographs show several plant fragments, and large clay fragments while a significantly reduced level of less than 5 μm clay fragments compared to the sample from the Grewingk Glacier delta is observed. In the lower photograph for the 0 to 1-cm sample (Figure 6-8), a large diatom and a smaller fragment of what appears to be a diatom are present in addition to two larger clay flake fragments as shown in the schematics in Figure 6-9. The 1 to 8-cm depth sample from China Poot (Figure 6-10) shows a higher relative composition of clay <5 μm fragments compared to the surface 0 to 1-cm sample, although the 1 to 8-cm sample is also characterized by several diatoms and clay fragments.

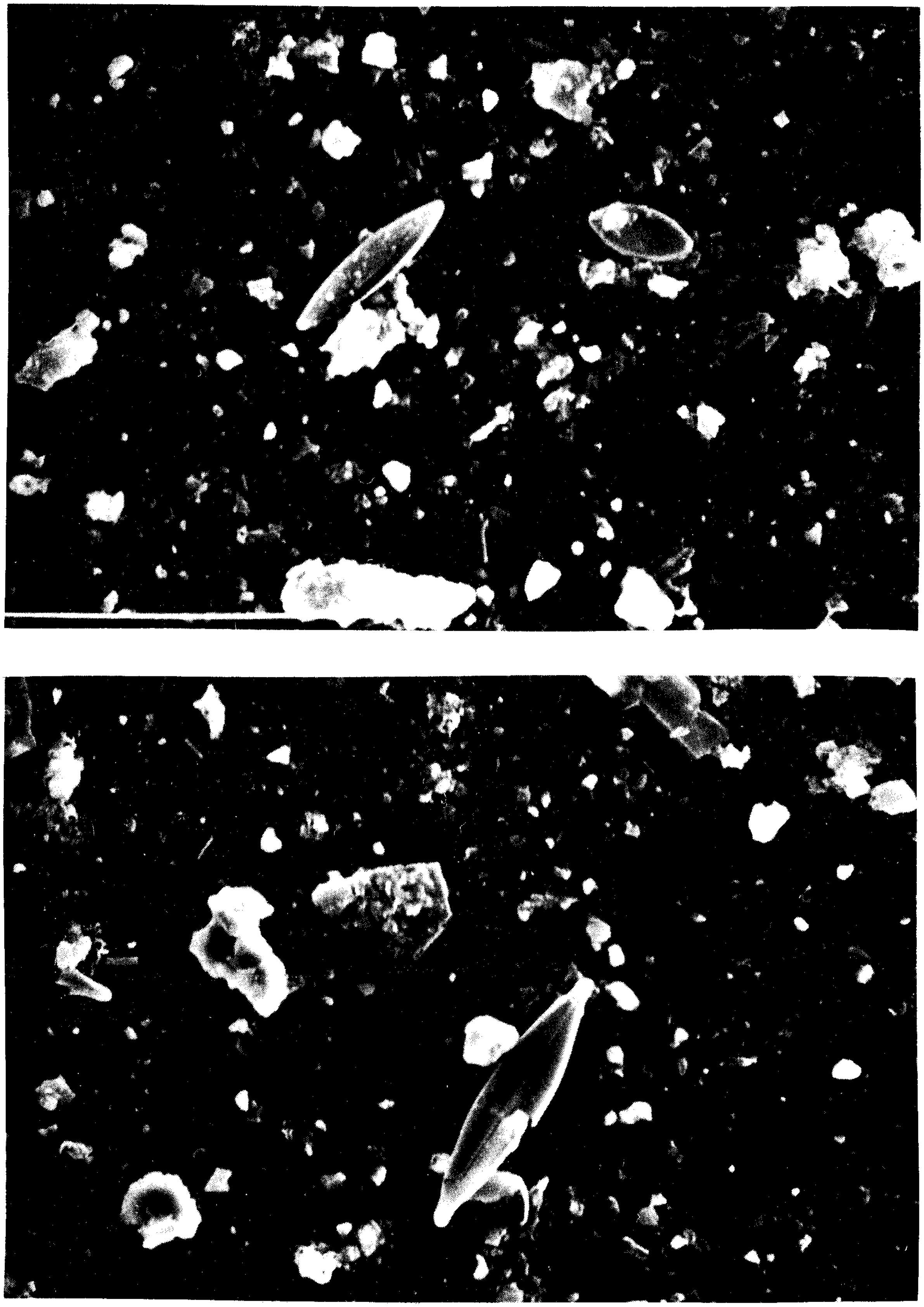

FIGURE 6-6. SCANNING ELECTRON MICROGRAPHS (1400X) OF KB-1-81 (Grewingk Glacier).

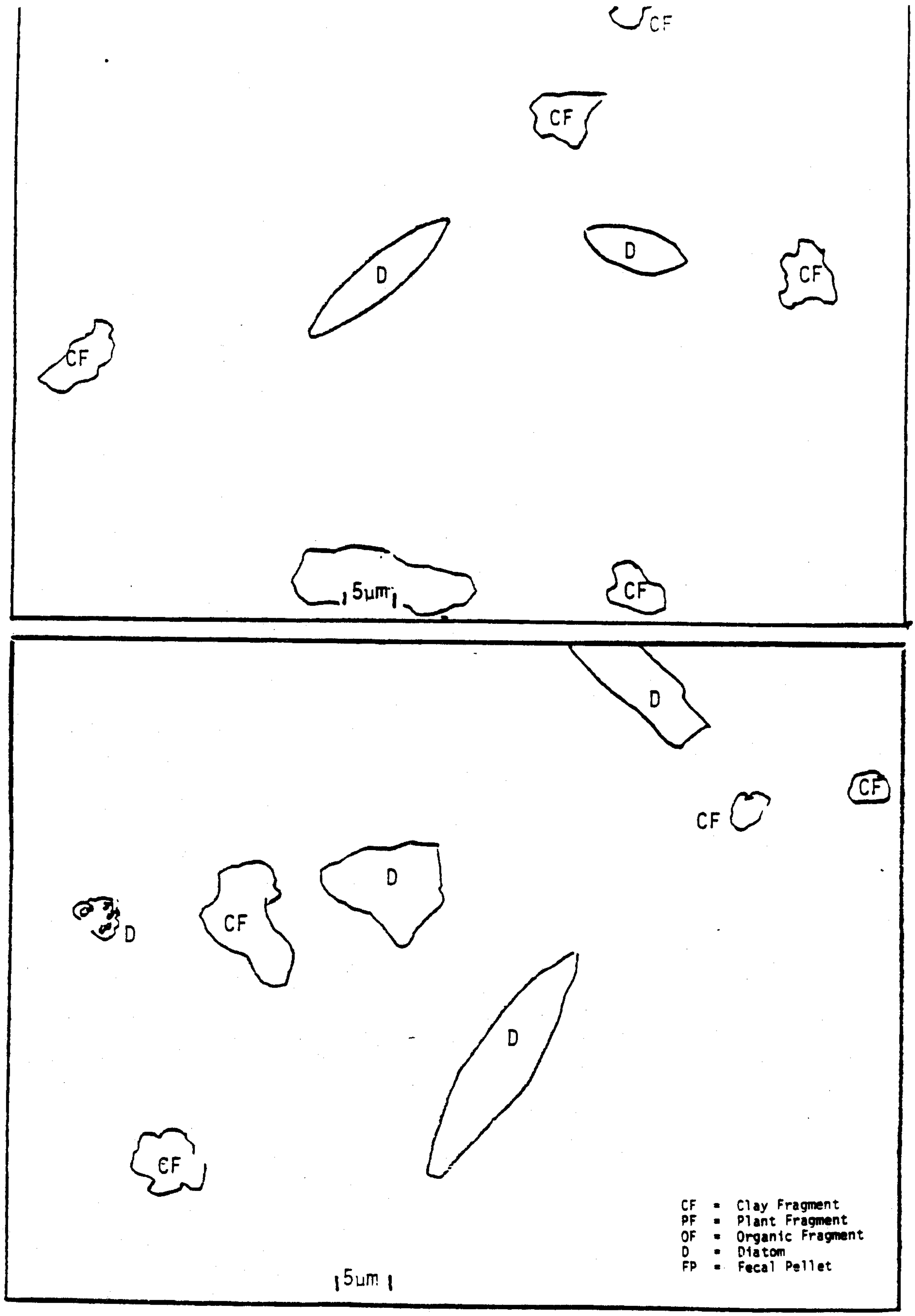

FIGURE 6-7. IDENTIFICATION OF MAJOR COMPONENTS IN SEM PHOTO-MICROGRAPH OF KB-1-81 (Grewingk Glacier).

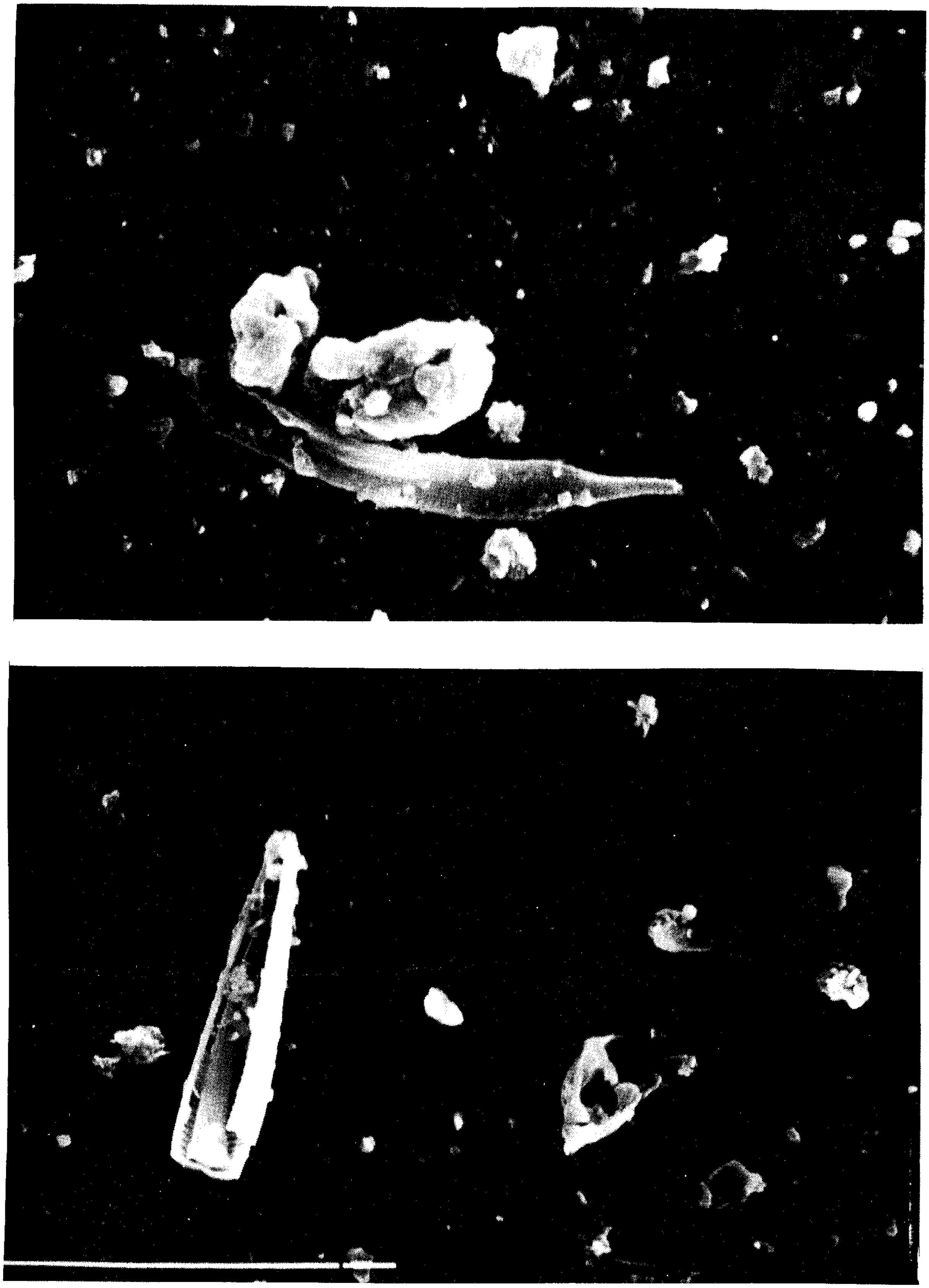

FIGURE 6-8. SCANNING ELECTRON MICROGRAPHS (1400X) OF KB-2-81A (China Poot Bay 0-1 cm).

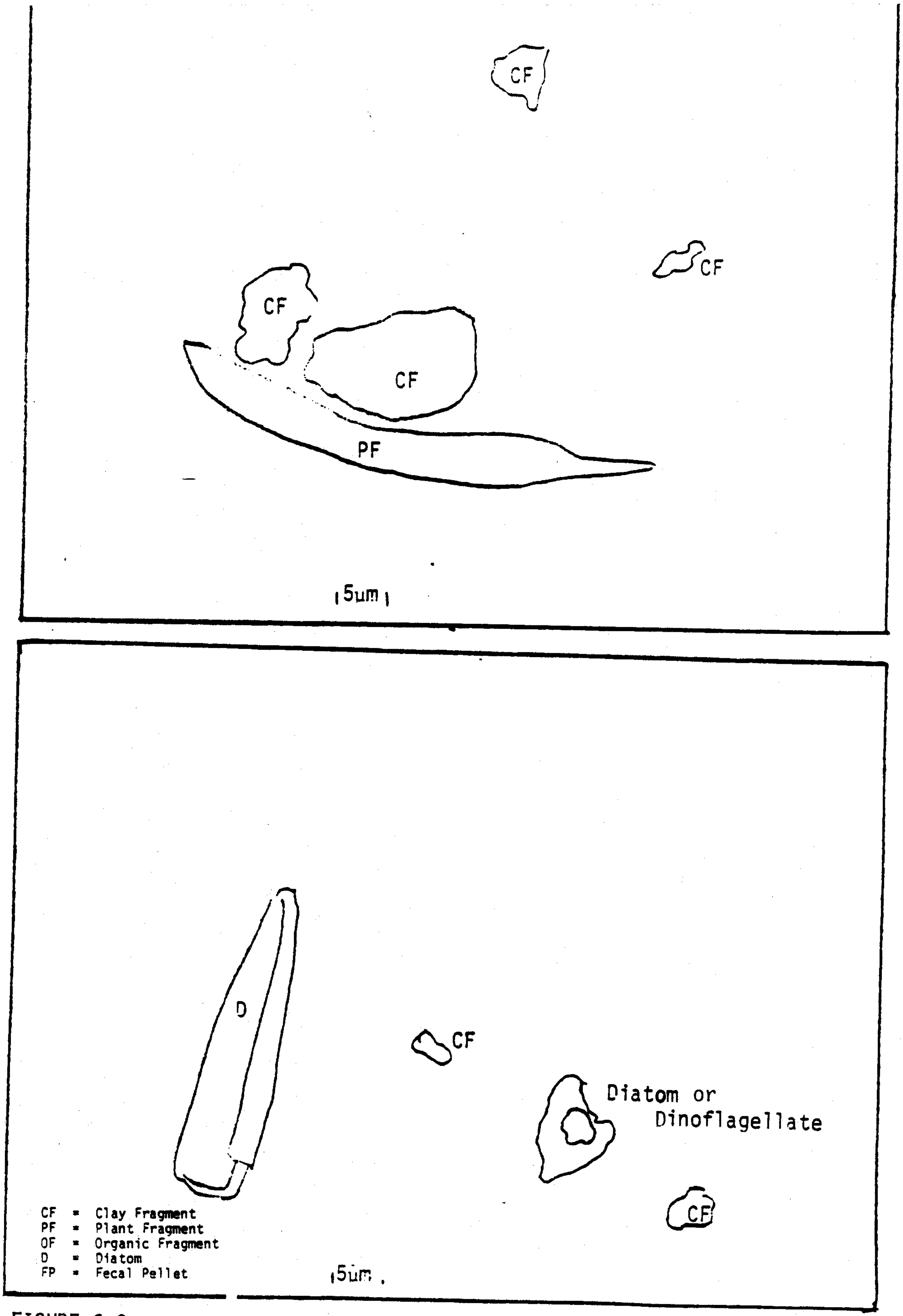

FIGURE 6-9. IDENTIFICATION OF MAJOR COMPONENTS IN SEM PHOTO-MICROGRAM OF KB-2-81A (China Poot Bay 0-1 cm).

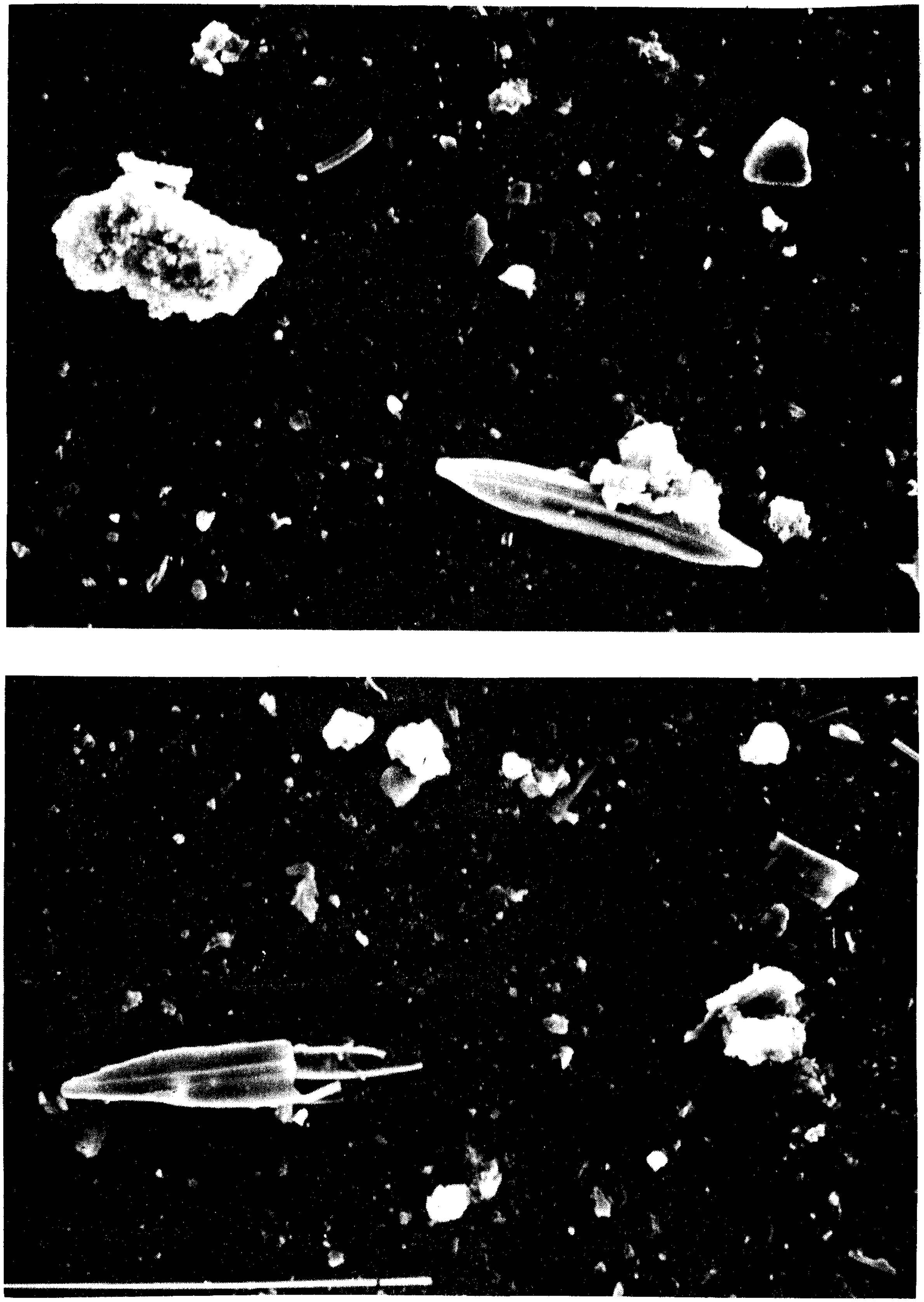

FIGURE 6-10. SCANNING ELECTRON MICROGRAPHS (1400X) OF KB-2-81B (China Poot Bay 1-8 cm).

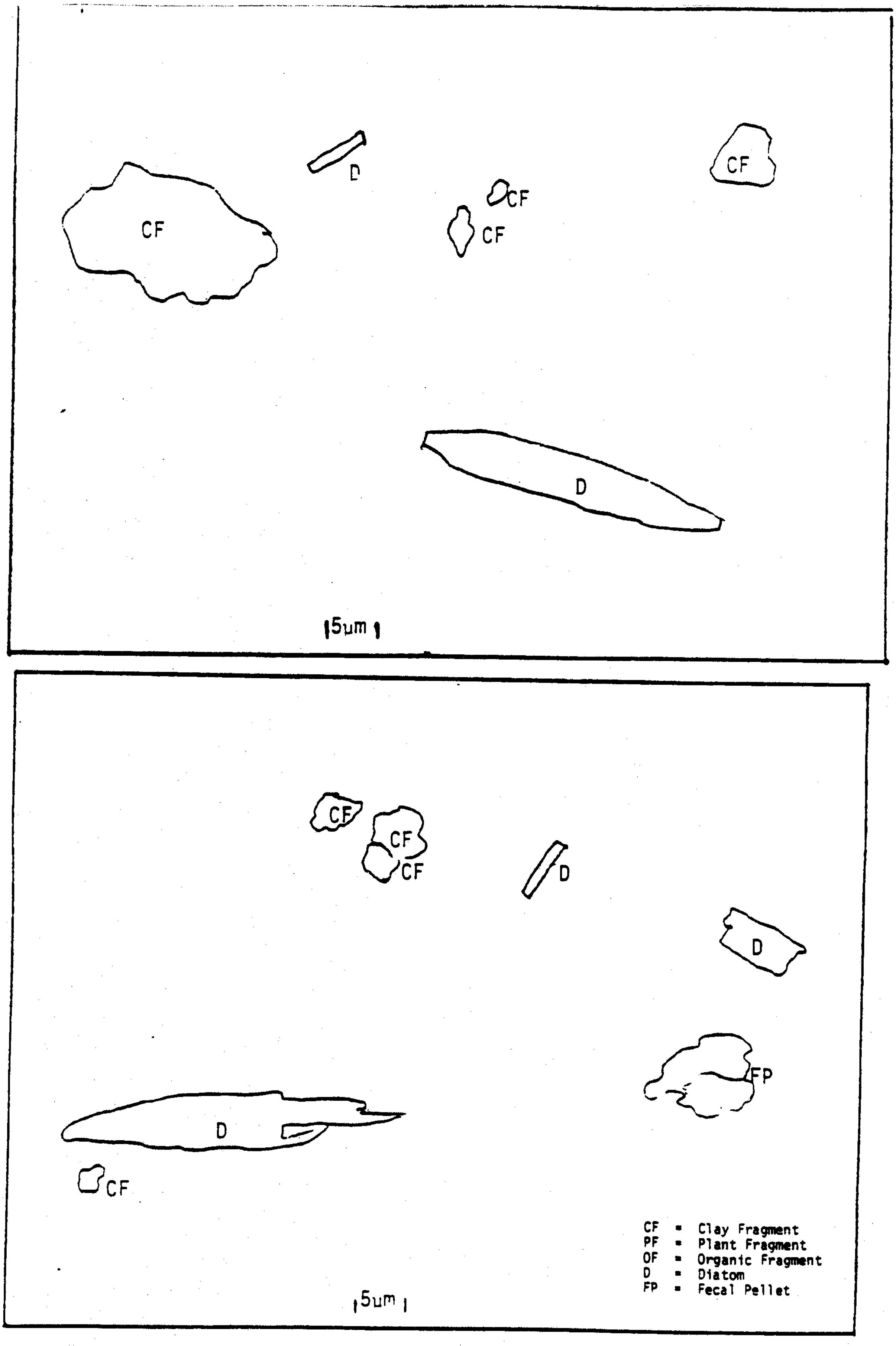

FIGURE 6-11. IDENTIFICATION OF MAJOR COMPONENTS IN SEM PHOTO-MICROGRAM OF KB-2-81B (China Poot Bay 1-8 cm).

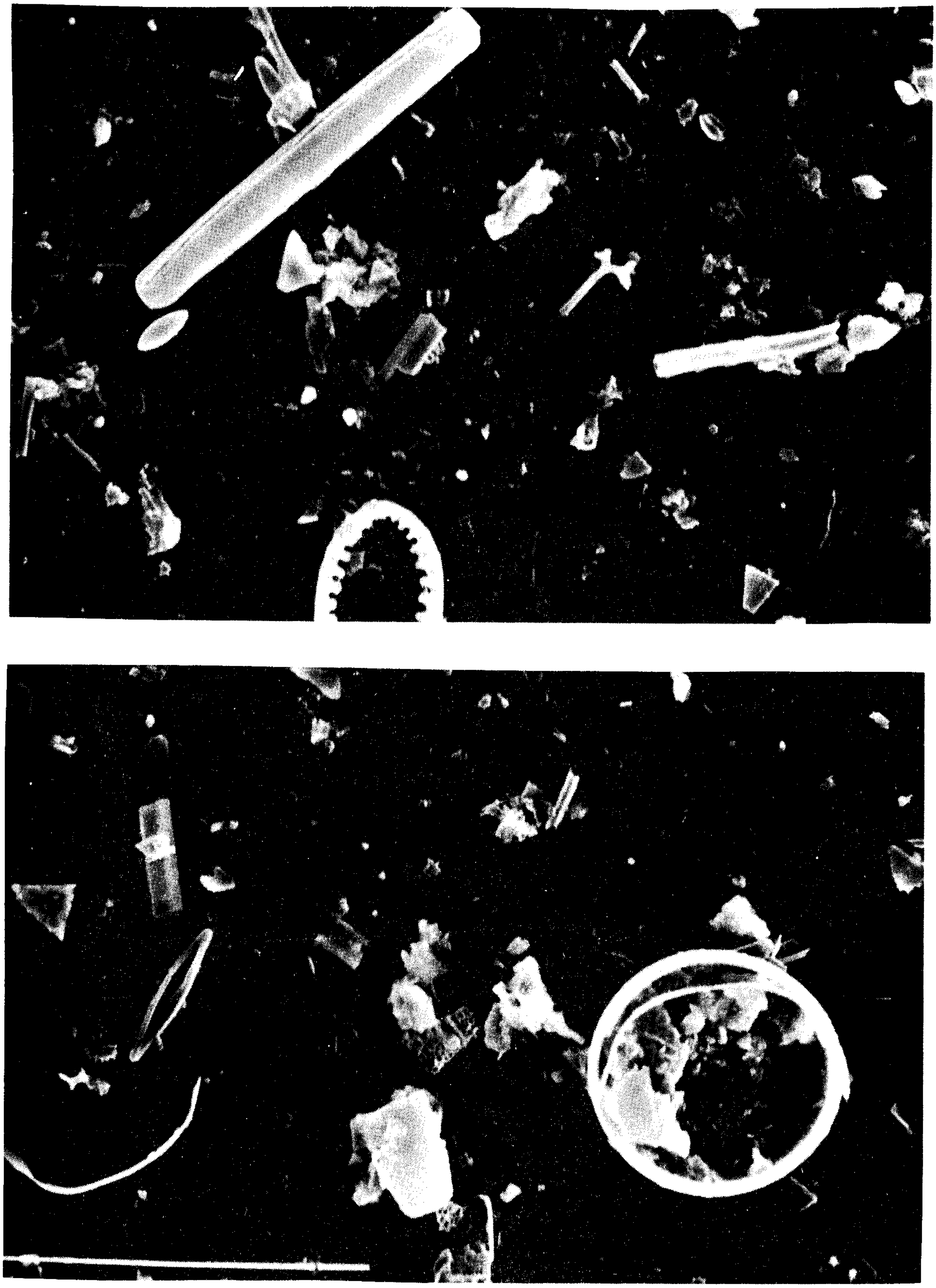

FIGURE 6-12. SCANNING ELECTRON MICROGRAPHS (1400X) OF KB-3-81 (Kasitsna Bay).

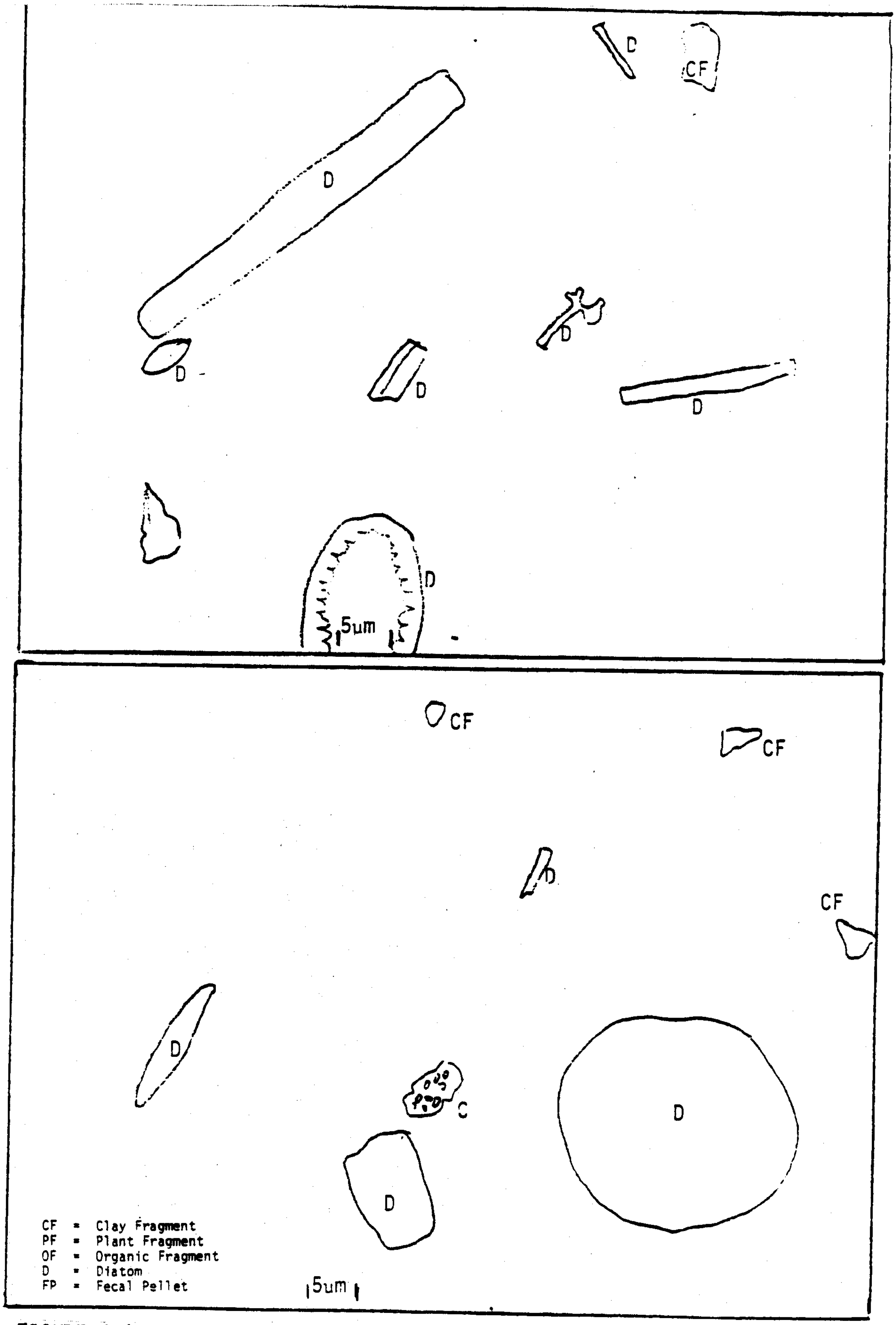

FIGURE 6-13. IDENTIFICATION OF MAJOR COMPONENTS IN SEM PHOTO-MICROGRAM OF KB-3-81 (Kasitsna Bay).

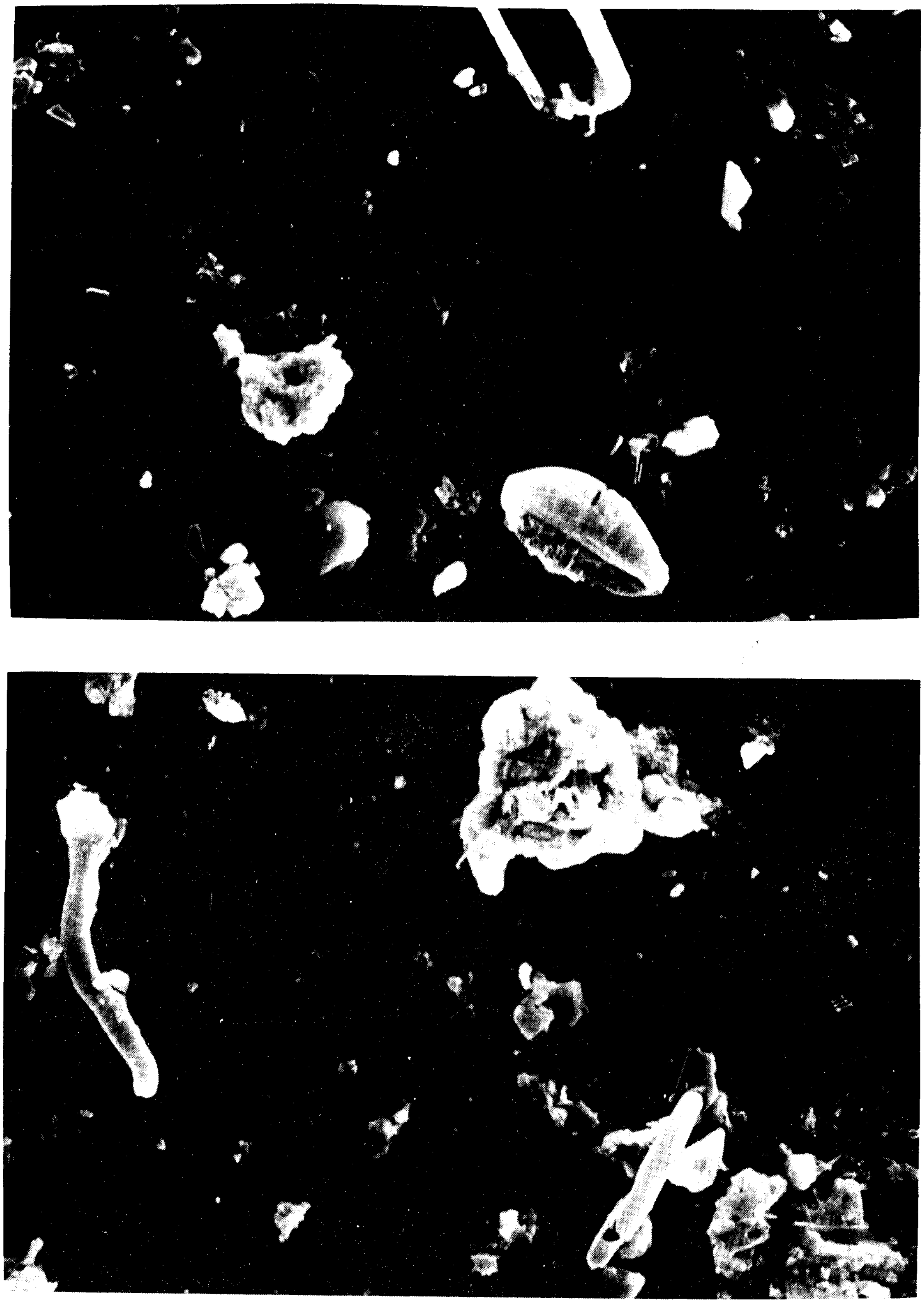

FIGURE 6-14. SCANNING ELECTRON MICROGRAPHS (1400X) OF KB-4-81 (Seldovia River Estuary).

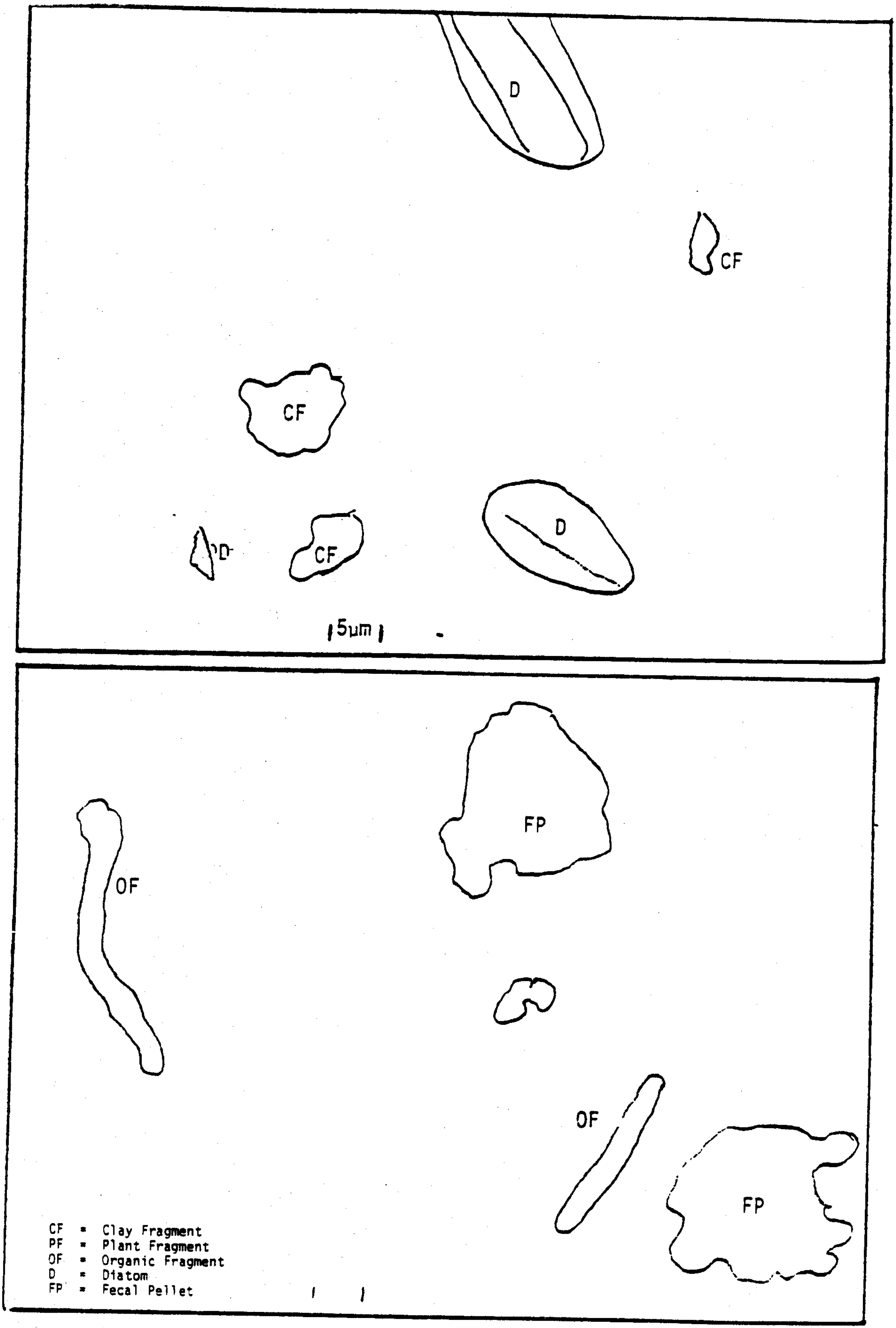

FIGURE 6-15. IDENTIFICATION OF MAJOR COMPONENTS IN SEM PHOTO-MICROGRAM OF KB-4-81 (Seldovia River Estuary).

In the second field from the 1 to 8-mm sample, another large diatom can be observed along with several fecal pellets and smaller diatom fragments mixed in with the less than 5-µm clay fragments.

In Figure 6-12 for KB-3 (Kasitsna Bay) the photographs show exceedingly high levels of diatom fragments and several clay fragments. In comparison to other sites sampled, there are significantly more diatom fragments at KB-3, however, here too several clay fragments in the 5 micron range can be observed.

The SEM photographs from KB-4 (Seldovia River Estuary) show very few clay fragments (Figures 6-14 and 6-15), and in general the samples are characterized by several large organic fragments, fecal pellets and a few diatoms.

Additional discussions of how the SEM characterizations correlate with hydrocarbon adsorption potential follow the next section on oil/SPM interactions (6.3), however, from the initial examination it is apparent that from a minerological standpoint, all five SPM types are basically from the same source which is believed to be terrestrial rock flour generated by glacial action, melting snow and river runoff. This is also reflected in Table 6-7 which presents the results of X-ray diffraction analyses (completed by Technology of Minerals Co.--see Appendix G) on these and other SPM samples. Additional discussion is presented in Section 6.3.2 on Wave Tank Oil/SPM Interactions; however, it should be noted that quartz is the primary mineral in the majority of the samples with dilution by other minerals (kaolinite and feldspar) depending on the sampling site. This "dilution" is also represented by the SEM characterications of the rock flour from the Grewingk Glacier (KB-1). The other sites selected then show various degrees of dilution of this rock flour material with other components. KB-3 (Kasitsna Bay) SPM was primarily diluted by silica tests from diatoms and the mud flat SPM contained elevated kaolinite. KB-4 (Seldovia River Estuary) exhibited evidence of the basic mineralogical material (quartz) and was diluted by kaolinite and high levels of decaying organic plant material which was primarily

Table 6-7. Sediment Minerology as Determined by X-ray Diffraction[a]

Sediment Source	Composition (%)						
	-Quartz	Kaolinite	Feldspar	Calcite	Mica	Sodium Chloride	Other
KB-1 (Grewingk Glacier Spit)	>50	20-40	20-40	None	<2	None	—
KB-3 (Kasitsna Bay)	>50	5-10	20-40	None	None	2-5	Gypsum <2
KB-4 (Seldovia Salt Marsh)	>50	5-10	20-40	None	None	2-5	—
KB-5 (Jakalof Bay)	>50	10-20	20-40	<2	None	2-5	—
Wave Tank #1 SPM (Kasitsna Bay)	>50	40-50	5-10	None	<2	None	—
Wave Tank #2 SPM (Seldovia Bay)	5-10	>50	2-5	<2	2-5	None	Huntite <2
Wave Tank #4 SPM (Glacial Till)	>50	20-40	20-40	None	<2	None	—

a - Analyses completed by Technology of Minerals - 2030 Alameda Padre Serra, Santa Barbara, California 93103 derived from the Spartina salt marsh. The two sediment samples from China Poot Bay (KB-2 and KB-2B) exhibited intermediate results in that the lower (1 to 8-cm subsection) showed extensive concentrations of terrestrial clay flakes with silution by plant fragments and diatom skeletons. Interestingly, in this instance, the upper 0 to 1-cm sample contained fewer less than 5 m sized clay flakes by weight and larger contributions from plant fragments and diatoms compared to the 1 to 8-cm samples.

6.3 COMPOUND SPECIFIC OIL/SPM PARTITIONING EXPERIMENTS

6.3.1 Static System Equilibrations of Fresh Prudhoe Bay Crude Oil and Representative Lower Cook Inlet SPM Types

After the various sediment samples were characterized with regard to compositional makeup, a series of static equilibrium partitioning experiments were undertaken to evaluate their relative adsorption potential for individual components in Prudhoe Bay crude oil. From these results, three representative sediment samples encompassing the greatest range in affinity for crude oil adsorption were then selected for extended flow-through outdoor wave tank experiments at Kasitsna Bay during the Summer, 1982 program. Specifically, the Summer, 1982 experiments were designed to examine partitioning of oil components onto suspended particulate material as a function of the degree of sub-arctic evaporation and dissolution weathering (see Section 6.3.2).

For the initial oil/SPM static equilibrium partitioning experiments, 20 grams of each sediment type were added to filtered seawater and the mixtures were agitated at 23° with magnetic stir bars. Care was taken in adjusting the stirring motors to insure that vortexing in the samples did not occur, and 3.5 ml of fresh Prudhoe Bay crude oil were added to each beaker. The beakers were covered (watch glass) and the mixtures were allowed to stir for 4 days and then allowed to settle over an additional 12-hr period. At that time the sedimentary material from the bottom of each beaker was carefully siphoned under vacuum taking care to ensure that none of the sediment came into direct contact with the oil during removal. Similarly, 300-ml aliquots of the water beneath the oil slicks were removed for determination of water column burdens. The respective sediment and water column samples from each experiment were then extracted and analyzed for petroleum hydrocarbon contamination along with unexposed sediment samples to determine background level hydrocarbon components present at each site.

Table 6-8 presents the total resolved component and UCM concentrations for the aliphatic and aromatic fractions from the sediment and water column extracts. Specific aromatic compound concentration burdens are also listed for the two phases examined in each experiment. From the data in the Table 6-8, it is possible to rank the sediments according to their overall adsorption efficiency for total and specific petroleum hydrocarbon components, and in the order of decreasing adsorption potential they are: KB-4 (Seldovia River salt marsh detritus); KB-1 (Grewingk Glacial till); KB-2A (China Poot Bay surface sediment); KB-2B (China Poot Bay 1 to 8-cm sediment) and KB-3 (Kasitsna Bay composite sediments). These rankings were generated by examining the cumulative sum of the n-alkanes and total resolved and UCM component concentrations in the aliphatic fractions and the total resolved and UCM component concentrations observed in the aromatic fractions for each sediment type. Numerical rankings in the order of 1 through 5 were given to each sediment for each parameter described above, and these rankings were then summed to arrive at an overall total to reflect each sediment type's affinity for oil. Specific compound concentrations were also considered in this ranking, as were the relative water column concentrations above each sediment. That is, an inverse relationship was observed between particulate adsorption potential and the levels of hydrocarbons observed in the water above each sediment type, and this relationship was also used in the overall rankings.

Figures 6-16 and 6-17 present the capillary gas chromatograms obtained on the sediment and water samples from the most adsorptive (Bay-4, Seldovia River salt marsh) and least adsorptive (Bay-3, Kasitsna Bay composite sediment) samples, respectively. Each figure is arranged as follows: Chromatogram "A" represents the aliphatic hydrocarbons in the oil-exposed

TABLE 6-8. RESULTS OF EQUILIBRIUM PARTITIONING OIL/SPM INTERACTION STUDIES (STATIC SYSTEM, 19°C).

	ALIPHATIC FRACTION**				AROMATIC FRACTION***											
							Benzenes		Naphthalenes						Phenanthrenes	
Sample*	Total Res	Total UCM	Σn-alk	Σn-alk/Branched	Total Res	Total UCM	1,4&1,3-dimethyl (884)	ethyl (874)	naphthalene (1196)	2-methyl (1305)	1-methyl (1322)	2-ethyl (1404)	2,3-dimethyl (1430)	1,6,7-trimethyl (1542)	phenanthrene (1788)	2-methyl (1904)
K. Bay-1																
Sediment	340,000	73,000	26,000	0.08	46,000	42,000	15	62	40	630	400	103	440	290	570	390
Aqueous Phase	4,760	0	33	0.007	601	75	2.9	0.56	1.3	7.4	7.4	9.8	3.1	1.0	0.23	-
K. Bay-2A																
Sediment	795,000	18,000	16,000	0.02	385,000	7,100	46	270	90	550	310	96	240	143	200	83
Aqueous Phase	3,380	0	11	0.003	1,907	0	3.4	1.4	3.3	7.2	6.8	0.7	2.2	1.0	-	-
K. Bay-2B																
Sediment	647,000	51,000	14,000	0.02	9,600	22,000										
Aqueous Phase	170	0	17	0.1	2,720	0										
K. Bay-3																
Sediment	85,000	10,000	5,000	0.06	12,000	10,000	33	130	4	91	83	25	89	35	44	-
Aqueous Phase	5,840	0	8	0.001	512	0	2.0	0.74	-	0.63	4.4	0.28	2.3	0.28	0.53	-
K. Bay-4																
Sediment	253,000	262,000	60,000	0.3	44,000	75,000	12	200	29	48	370	125	337	210	71	-
Aqueous Phase	Not reduced very low		-	-	2,180	0	2.9	0.46	0.16	0.49	1.3	0.12	2.2	0.34	-	-

*K. Bay-1--Grewingh Glacier Till - fine grained terrestrial plus diatoms, many flakes 5 μm and less - Specific Surface Area 9.1
K. Bay-2A-China Poot Bay surface 1 cm - mostly > 5 μm terr plus some plant " 8.2
K. Bay-2B-China Poot Bay depth 1-8 cm - most material < 5 μm " 15.2
K. Bay-3--Kasitsna Bay consolidated sediment - 90% diatoms > 5 μm, some terr. ≤ 5 μm " 9.1
K. Bay-4--Seldovia River salt marsh - organic plus fecal pellets " 11.1

**Sediment concentration in μg/kg, water concentration in μg/l

***Sediment concentration in μg/kg, water concentration in μg/l; numbers in parentheses are compound Kovat indices.

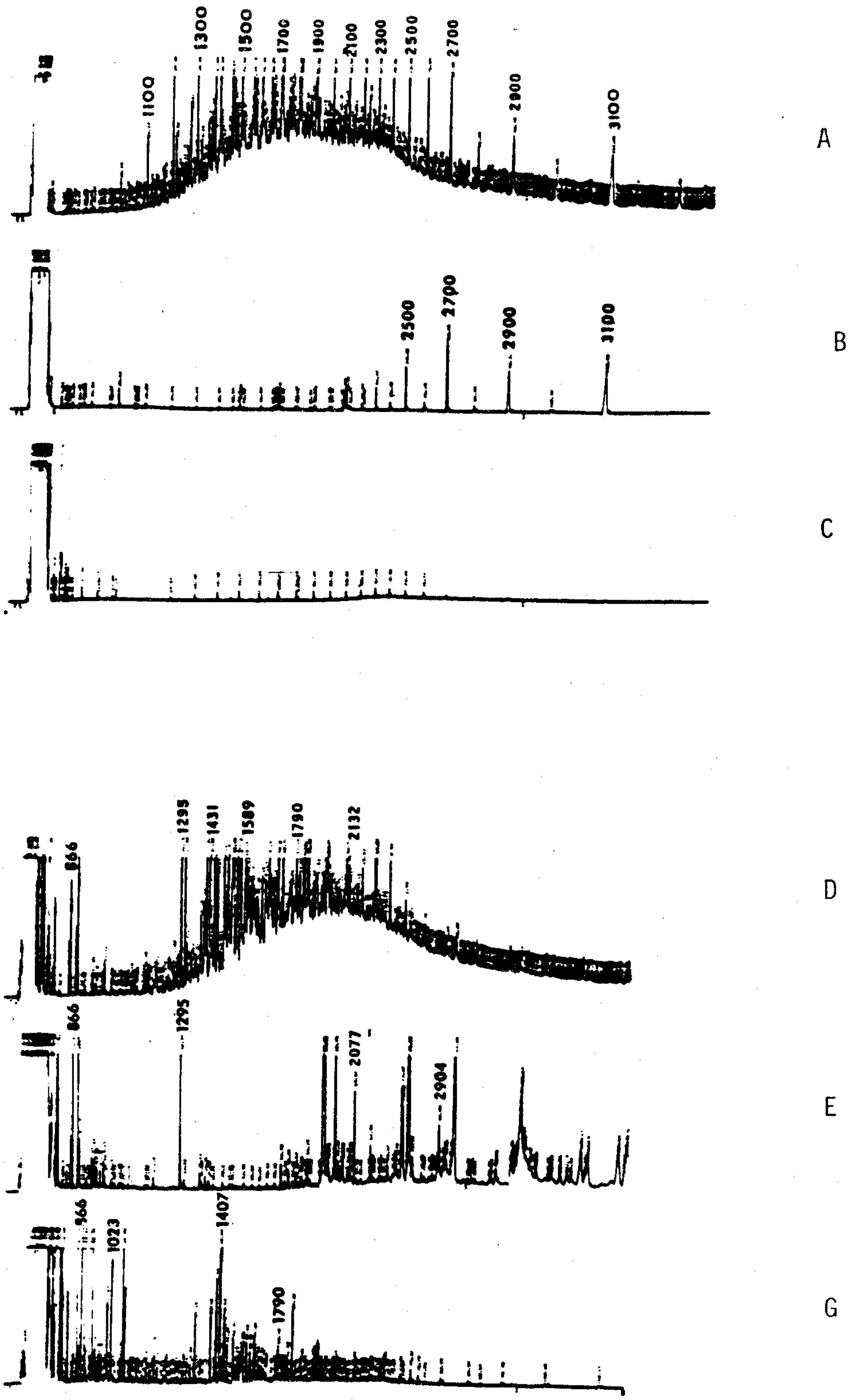

FIGURE 6-16. FLAME IONIZATION DETECTOR CAPILLARY GAS CHROMATOGRAMS FROM KB-4 (SELDOVIA RIVER SALT MARSH) OIL/SPM INTERACTION STUDIES: (A) ALIPHATIC HYDROCARBONS IN THE OIL EXPOSED SEDIMENTS; (B) BACKGROUND LEVEL ALIPHATIC HYDROCARBONS MEASURED IN UNEXPOSED SEDIMENT; (C) ALIPHATIC HYDROCARBONS IN THE WATER COLUMN EXTRACT; (D) AROMATIC HYDROCARBONS IN THE OIL EXPOSED SEDIMENTS; (E) BACKGROUND LEVEL AROMATIC HYDROCARBON COMPONENTS MEASURED IN THE UNEXPOSED SAMPLE; AND (G) AROMATIC-HYDROCARBONS IN THE WATER COLUMN EXTRACT.

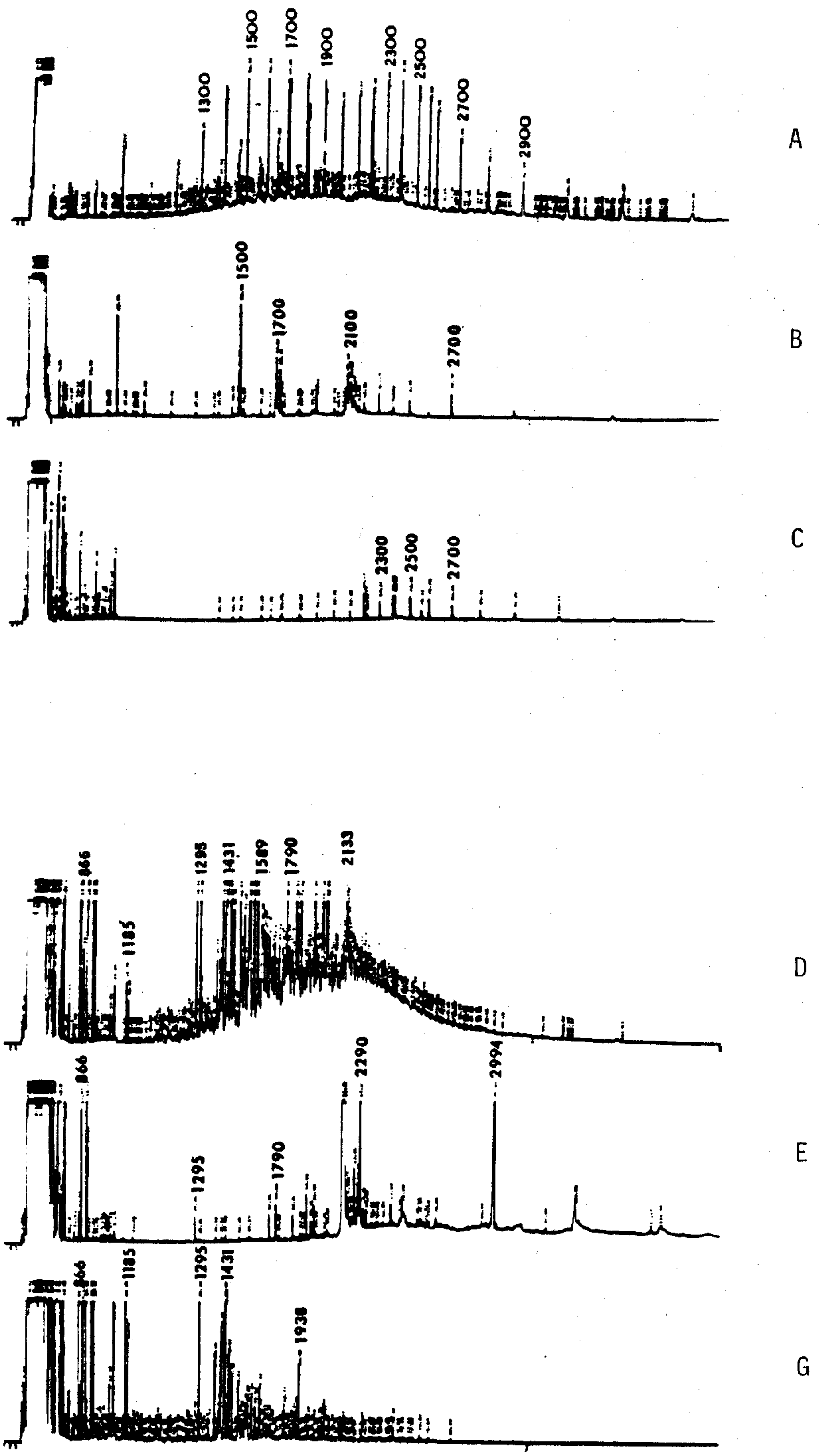

FIGURE 6-17. FLAME IONIZATION DETECTOR CAPILLARY GAS CHROMATOGRAMS FROM KB-3 (KASITSNA BAY COMPOSITE SEDIMENT) OIL/SPM INTERACTION STUDIES: (A) ALIPHATIC HYDROCARBONS IN THE OIL EXPOSED SEDIMENTS; (B) BACKGROUND LEVEL ALIPHATIC HYDROCARBONS MEASURED IN UNEXPOSED SEDIMENT; (C) ALIPHATIC HYDROCARBONS IN THE WATER COLUMN EXTRACT; (D) AROMATIC HYDROCARBONS IN THE OIL EXPOSED SEDIMENTS; (E) BACKGROUND LEVEL AROMATIC HYDROCARBON COMPONENTS MEASURED IN THE UNEXPOSED SAMPLE; AND (G) AROMATIC HYDROCARBONS IN THE WATER COLUMN EXTRACT.

sediments; Chromatogram "B" represents the background level of aliphatic hydrocarbons measured in the unexposed sample; Chromatogram "C" represents the aliphatic hydrocarbons in the water column extract; Chromatogram "D" represents the aromatic hydrocarbons in the oil-exposed sediments; Chromatogram "E" represents the background level aromatic hydrocarbon components measured in the unexposed sample; and Chromatogram "G" represents aromatic hydrocarbons in the water column extract. Clearly, the most significant differences appear in considering the aliphatic fractions for the oil-exposed sediments, (Chromatograms A in Figures 6-16 and 6-17). The Seldovia River salt marsh sample shows a significant unresolved complex mixture and a suite of normal and branched hydrocarbons extending from nC-10 through nC-31. While this same suite of compounds is observed in the Kasitsna Bay sediments, the unresolved complex mixture is significantly smaller as is reflected in the reduced UCM data in Table 6-8. The aliphatic fraction chromatograms on the unexposed sediments showed some differences, with higher molecular weight odd numbered n-alkanes clearly predominating in the Seldovia River salt marsh sample. Specifically, nC-23, nC-25, nC-27 and nC-29 from plant wax components are clearly the most predominant feature in Figure 6-16B. Slightly higher aliphatic water column concentrations are observed in the samples from KB-3 compared to KB-4, and this reflects the inverse relationship noted above for SPM adsorption potential and water column hydrocarbon burdens.

The aromatic fractions of the contaminated sediments appear to be very similar, however, here again the unresolved complex mixture in the Seldovia River salt marsh sample is significantly larger, and higher levels of individual aromatic components with KOVAT indices extending from 1400 to 1788 are noted with the organic-rich Seldovia River salt marsh SPM. The data in Table 6-8 also illustrate that a factor of 7 increase in total aromatic unresolved component concentrations is noted in comparing the Seldovia River and Kasitsna Bay sediment samples. The aromatic fractions of the uncontaminated sediments (Chromatograms E in Figures 6-16 and 6-17) show several significant differences, and in particular more higher molecular weight components can be observed in the sediment sample from the salt marsh. The large peaks near

KOVAT index 1900 to 2200 in the middle of both chromatograms are believed to be due to polyunsaturated components of biogenic origin; as determined by GC/MS analyses.

Interestingly, the aromatic fraction of the water column components appear very similar for both samples. This largely reflects the higher compound-specific seawater solubilities for the lower molecular weight alkyl-substituted benzenes in the Kovat indices range of 700 to 874 and the limited solubilities of the alkyl-substituted naphthalenes in the Kovat index range of 1305 through 1542. It should be noted, in general, that the lower molecular weight aromatics do not specifically adsorb onto the particulate material, but that they instead reside in the water column beneath the slick. Several lower molecular weight aromatics are suggested by the chromatogram in Figure 6-17D of the aromatic fraction of the sediment sample from KB-3; however, their presence may simply reflect inclusion of slightly greater volumes of water collected during siphoning off the sediment sample.

In terms of the overall oil affinity of the five selected SPM samples, several interesting correlations can be made between the composition data of the SPM as determined by scanning electron microscopy and the results from the glass capillary/gas chromatographic analyses. Specifically, the Seldovia Bay estuary SPM had the highest overall affinity for oil, and the SEM photos illustrate that this material was primarily composed of diatoms and larger (greater than 30 m) organic fragments and fecal pellets. It also contains a few clay fragments which, as will be shown below, also have a very high affinity for oil.

The fine glacial rock flower or till from the Grewingk Glacial delta exhibited the next highest affinity for hydrocarbons, and in many instances, showed an equal or greater affinity for specific aromatic compounds compared to the organic rich detrital sediments from the Seldovia Bay estuary. The SEM photographs of this material show that the sample is primarily very small clay fragments plus a relatively limited number of diatoms, which no doubt came from the marine input and flushing of the intertidal zone. The high affinity for oil in this instance, is believed to be due to the high surface area (on a surface area per weight basis) due to the profusion of fine clay fragments. Because of this material's high affinity for oil and the fact that the nearshore waters in many areas in Alaska receive significant contributions of SPM from glacial till, this sample was considered to be ideal for extended long-term studies, and additional wave tank studies were undertaken at Kasitsna Bay (see Section 6.3.2) with kg quantities of silt/rock flour collected from the melt lake at the base of the Grewingk Glacier.

The SPM sample with the next highest affinity for oil was the surface 0 to 1-cm mat from China Poot Bay (K Bay-2A). The SEM photographs of this sample showed it to be primarily made up of clay and plant fragments with an occasional diatom skeleton. The 1 to 8-cm depth sample from this site also showed high affinities for aliphatic and aromatic components; and the SEM photographs in this case showed a higher concentration of the less than 5 m sized clay fragments with additional input and/or dilution from diatoms. The SPM sample from K Bay-3 (Kasitsna Bay) which showed the lowest affinity for adsorption, consisted almost exclusively of diatom fragments (by weight) with a few clay fragments in the less than 5 micrometer size range appearing in the background of the SEM photos.

The results of these initial oil/SPM interaction studies are in good agreement with the work of several other authors who have investigated oil/SPM (sediment) interactions. Several of these similarities and one striking difference (dealing with a previous study on Glacial till) are considered in the following discussion.

With regard to similarities, GEARING et al. (1979) also reported the fractionation or partitioning of lower molecular weight aromatic compounds (including up to 3-ring aromatics) into the dissolved phase before adsorption of the oil onto suspended particulate material and subsequent sinking. In test tank studies completed at the Marine Ecosystem Research Laboratory at the

University of Rhode Island, they found that the aromatic/aliphatic ratio in the sediment was much lower than that in the parent oil suggesting that preferential dissolution of lower molecular weight aromatic compounds may be occurring. Specifically, 2-34% of the higher molecular weight aliphatic, acyclic and greater than 3-ring hydrocarbons were absorbed onto the suspended particulates and sediments in contrast to 0.1% of the more water soluble naphthalene and methylnaphthalene components which were the predominant aromatic materials in the No. 2 fuel oils used in their studies.

WINTERS (1978) also observed similar partitioning in studying two simulated oil spills and one mixture of aromatic compounds added to a test tank. The petroleum derived alkanes were approximately 10 times greater in the particulate fraction, and the lower molecular weight aromatics were at least 5 times more concentrated in the dissolved phase.

In samples of suspended particulate material collected along transects perpendicular to the South Texas OCS near Corpus Christi, PARKER and MACKO (1978) noted that the concentrations of higher molecular weight (nC-28 through nC-30) compounds remained relatively constant with distance from the shore while the total particulate hydrocarbon burdens decreased with increasing distance. These authors attributed this to the introduction and sorption of the hydrocarbons near the shore with subsequent movement of particulate bound oil with preferential retention of the higher molecular weight compounds during weathering. Several higher molecular weight polynuclear aromatic hydrocarbons were also identified on the particulate material, and these included alkyl-substituted naphthalenes, phenanthrenes, dibenzothiophenes, fluoranthrene and pyrene. Concentrations of these materials were too low for quantitation; however, they could be detected by selected ion monitoring GC/MS. Similar partitioning of lower and higher molecular weight compounds have been observed by DELAPPE et al. (1979) in a study designed to measure the partitioning of petroleum hydrocarbons among seawater, particulates and the filter feeting *Mytilus californianus*.

PAYNE et al. (1980) and BOEHM and FIEST (1980) also observed a similar partitioning between lower and higher molecular weight compounds in the dissolved phase and suspended particulate material samples removed by filtration of large volume water samples obtained in the vicinity of the IXTOC-I blowout in the Gulf of Mexico.

In a laboratory study, MEYERS and QUINN (1973) found that the hydrocarbon adsorption efficiency (for the less than 44 m particle sized fractions) decreased in the order of bentonite > kaolinite > illite > monmorillinite. Interestingly, when Meyers and Quinn treated sediment samples from Narragansette Bay with 30% peroxide to remove indigenous organic material, an increase in absorption potential was noted. These authors concluded that the organic material (which was presumably humic substances) presumably masked the sorption sites on the sediment thereby reducing the available surface area for adsorption of the organic compounds. SEUSS (1968), on the other hand, has suggested that a 3 to 4% organic material coating on clay will enhance sorption processes by providing, in effect, a lipophillic layer to enhance non-polar hydrophobic binding. These findings would be more in line with the results presented here in comparing the adsorption potential of the organic rich materials from the Seldovia River estuary (KB-4) to the composite diatom rich sediment samples from Kasitsna Bay (KB-3).

In a laboratory study, ZURCHER et al. (1978) considered the dissolution, suspension, aglomeration and adsorption of fuel oil onto pure kaolinite. In their studies, as in ours, the dissolved water column samples showed significant levels of lower molecular aromatics in the benzene to methylnaphthalene range, and the adsorbed fraction contained n-alkanes and aromatics from Kovat indices 1400 through 3200. The clay minerals in this experiment were shown to adsorb about 200 mg of hydrocarbons per kilogram of dry material. MEYERS and QUINN (1973) reported a similar value of 162 mg/kilogram for dry kaolinite. Our data, in Table 6-8, suggest values in line with these earlier determinations with a low of 122 mg/kilogram (total resolved and UCM from both the aliphatic and aromatic fractions) from the SPM samples from Kasitsna Bay

(KB-3) to a high of 1.2 g/kilogram for the 0 to 1-cm subsample from the tidal mud flats from China Poot Bay (KB-2A).

While the results of these most recent oil/SPM interaction studies using representative samples from the lower Cook Inlet parallel the findings reported by previous investigators, they are somewhat contradictory to recent results reported by MALINKY and SHAW (1979). These authors examined the association of two lower molecular weight petroleum components and suspended sediments (primarily gracially derived sediments from the south central Alaska region) and concluded that sedimentation of oil by the adsorption to suspended mineral particles may not be a major pathway for the dispersion of petroleum in the marine environment. In that study, however, they used ^{14}C-labelled decane and biphenyl at near saturation levels. In these experiments, the concentrations of the two hydrocarbons associated with the sediments was approximately 30% of the original aqueous concentration in parts per million. From loadings of permitted discharges in Port Valdez and measured sediments loads, the authors calculated that less than 3% of the oil released into the harbor could be associated with the sediment. Thus, the authors concluded that adsorption of hydrocarbons to suspended particulate material was not that significant, and that the role of suspended mineral particulate material may be far less significant in adsorption of polynuclear aromatic hydrocarbons in natural waters than is the role of total suspended matter. The applicability of their findings to real oil spills situations in natural environments may be limited, however, in light of the fact that they did not use a natural oil or even a water accommodated fraction of a natural oil, and by the fact that the compounds which were utilized have significantly higher water solubilities that the more toxic polynuclear aromatic hydrocarbons of interest. Clearly, the results of our studies on the glacially derived till from the Grewingk Glacier show that it does have a high affinity for polynuclear aromatic hydrocarbons (see Table 6-8) and that the high surface area of the glacial till can provide an active site for oil adsorption and ultimate sedimentation.

6.3.2 Extension of Dispersed and Dissolved Oil/SPM Interaction Studies During Summer/Fall Wave Tank Experiments at Kasitsna Bay

6.3.2.1 Introduction

After the initial characterization of the component specific affinity of the five representative SPM types, extended oil/SPM interaction studies were undertaken at Kasitsna Bay, Alaska during the Summer 1982 program. Unlike the previously described experiments where oil was allowed to interact with suspended particulate material in a closed system, the more recent Alaska experiments were designed to look at the time-dependent partitioning of selected hydrocarbons onto SPM as other evaporation, dispersion and dissolution processes were simultaneously occurring. That is, an overall SPM load was established in the flow-through seawater system in two of the outdoor wave tanks, and oil was then added to the three tanks under simulated 2 knot wind/wave turbulence (see Section 5.4 for general description of Wave Tank Experiments).

6.3.2.2 Experimental Design for Dispersed/Particle-Bound Oil Concentration Measurements

In order to better comprehend (and ultimately predict) the effects of dispersion and oil/SPM interactions, three different types of sediment indigenous to the coastal areas of south central Alaska were introduced into the flow-through wave tanks at the Kasitsna Bay laboratory. Basically, the types of sediment were chosen according to: their measured static equilibrium affinity for oil, their abundance in the coastal waters of Cook Inlet, their accessibility to collection (in kg quantities), and the differences in their geological origins. The three types of sediment used were glacial till, from the Grewingk glacier melt lake at the base of the glacier, Seldovia Bay salt marsh sediment, and Kasitsna Bay (MacDonald Spit) sediment. Characterization regarding mineralogy, grain size, surface area, and organic content can be found in the previous Section 6.2.

Information concerning the construction, dimensions, and flow scheme of the wave tanks and SPM master reservoirs, as well as sampling and experimental procedures are presented in Section 5.4.

To introduce the SPM into the wave tanks a bifurcated master reservoir was constructed as described in Section 5.4.3. Initially, a weighed amount of each sediment type was added to a known volume of seawater in the reservoir, and, with the stir motor (used to suspend the fines) at a set position, a 100 ml aliquot of water was filtered in order to determine the percent of sediment suspension on a mg per liter basis. Using this percentage, weights of sediment added and flow from the master reservoir into the wave tanks were adjusted to achieve a particulate load of approximately 10 mg/l in the wave tanks. SPM load was monitored daily by filtering a 200 ml aliquot of wave tank water through 0.45 µm Type HA filters, using a 12-port Millipore head (Figures 6-18 through 6-21). Prior to an actual oil spill it was necessary to "shock" the tanks up to these levels, which was done by addition of calculated amounts of sediment to the wave tank itself. Shocking the tanks was required because, owing to the three hour turnover volume in the wave tanks, calculations showed that it would take weeks to build up to the desired levels by solely using the master reservoir addition method. The SPM levels for each tank, monitored during the experiments, are presented in Table 6-9; and as seen, they are fairly constant at approximately 10 ppm.

Once the desired levels of SPM were obtained and deemed stablized, 16 liters of Prudhoe Bay crude oil were added to each wave tank. Sampling times and procedures are presented in Sections 5.4.4 and 5.4.5.

Due to the inherent difficulty in separating dispersed oil droplets from suspended particles in the water column, both were collected on 0.45 µm glass fiber filters for extraction and analysis. A control tank, with no SPM addition, was also monitored, whereby only dispersed oil concentrations were measured. In this way, it was hoped that the amount of adsorption of hydrocarbons by various SPM types as a function of weathering time could be determined.

Figure 6-18. Sampling wave tank discharge for SPM particle loading determinations.

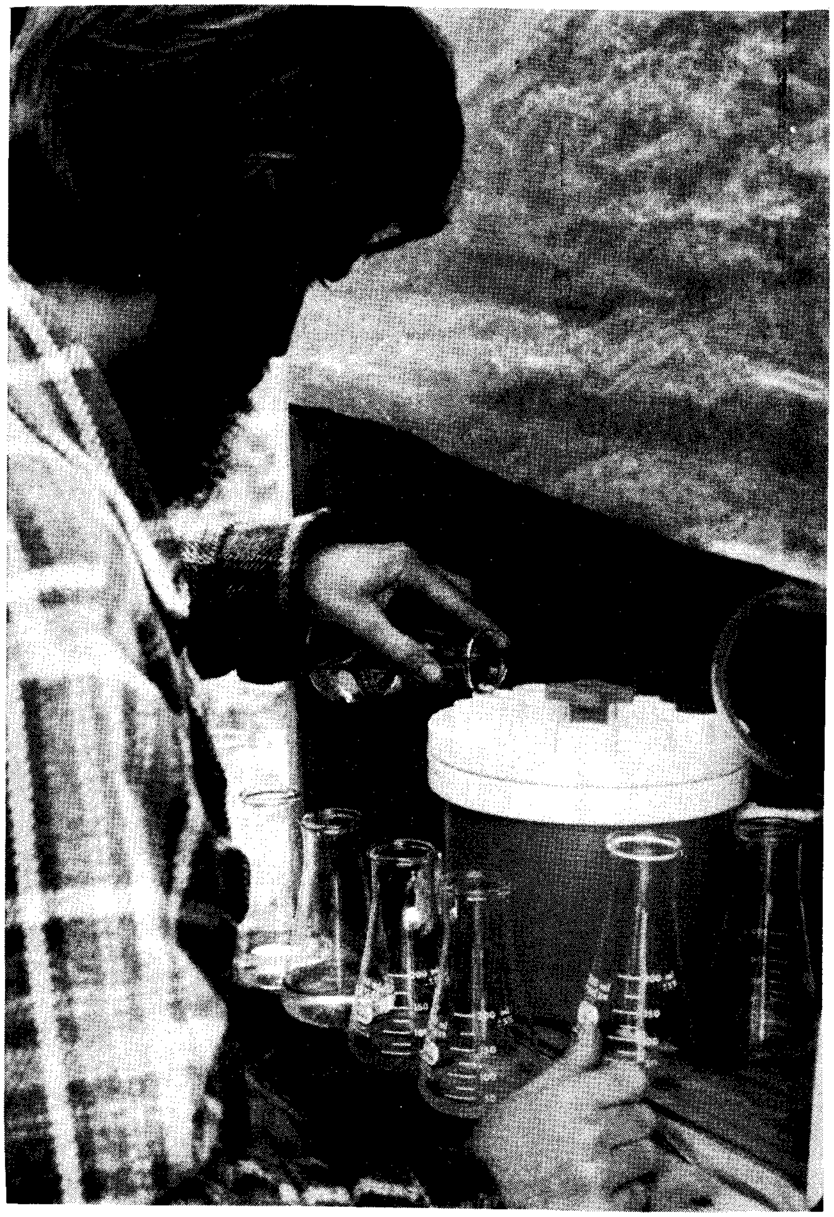

Figure 6-19. Filtration of wave tank water for SPM loading measurements before spill initiation.

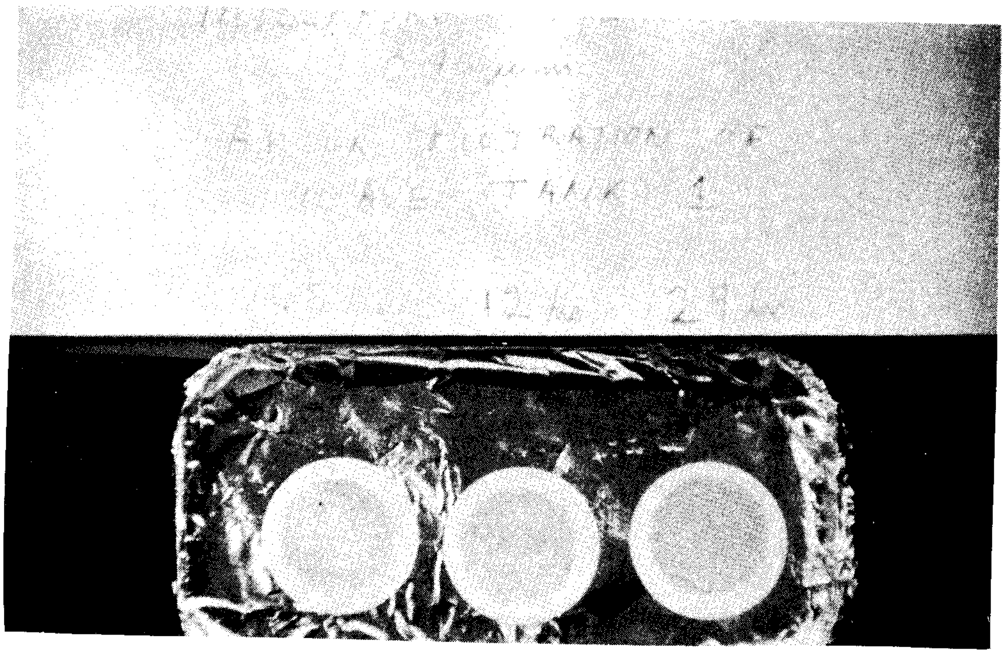

Figure 6-20. 0.45 micrometer Millipore filters (after drying) for gravimetric determination of SPM levels.

Figure 6-21. Closeup of particle filters used for SPM concentration determinations.

TABLE 6-9. Suspended Particulate Matter Load Monitoring for Wave Tanks #1-4

Sample #[a]	Kasitnsa Bay Sediment (ppm)	Seldovia Bay Sediment (ppm)	Glacial Till Sediment (ppm)	Control Tank (ppm)
1	15.1	7.5	6.8	1.9
2	7.2	6.3	12.9	3.9
3	8.9	10.0	9.7	3.1
4	6.4	9.1	8.4	3.8
5	15.7	9.5	8.9	4.8
6	9.1	10.3	12.1	3.6
7	5.2	6.6	6.8	3.7
8	11.4	9.4	7.9	3.9
9	9.6	10.0	7.2	3.1
10	9.7	10.8	7.8	4.1
Average	9.8	9.0	8.9	3.6

a - Samples were collected approximately once a day

Bottom Sediments

Settling of oil laden particles and incorporation by bottom sediments was also monitored by collecting and analyzing sediments from the bottom of each wave tank at various times. To insure that bottom sediments did not contact the oil slick during sampling, the following method of collection was utilized. A Teflon tube was inserted into the wave tank at the paddle wheel end (where the slick was not present) and extended to the bottom of the tank. The tube was then moved to the other end of the tank, where bottom sediments tended to accumulate, and a siphon was started. Bottom sediment was siphoned into glass jars, and the accompanying water was decanted off after the sediment had settled. Weighed amounts of bottom sediments were then extracted by shaker table extraction methods, fractionated by silica gel chromatography (see Appendix F for analytical procedures). Resulting samples were then analyzed by FID-GC and GC/MS.

Bottom sediments were obtained from the tanks 13 days, 5 months, 9 months, and 12 months after initiation of the spills, and, for comparative purposes, glass fiber filter samples of SPM in the water column were collected at these times as well. The filters were extracted as before, however selected filter extracts were fractionated and subjected to GC/MS analysis.

6.3.2.3 Experimental Results from the Continuous-Flowing Wave-Tank Experiments

Kasitsna Bay SPM

The oil/SPM interaction experiment using Kasitsna Bay sediment was initiated during the summer of 1982 in wave tank #1. Although a more complete characterization of Kasitna Bay SPM is presented in Section 6.2, the following description is useful in evaluating the results of the oil adsorption experiments. X-ray diffraction analyses shows that this sediment is primarily composed of quartz (<50%) and kaolinite (40-50%), with some feldspar (5-10%). Identification of physical constituents, by electron microscopy, indicates this sediment to have numerous diatoms and clay fragments present, and a specific surface area of 9.1 was determined by nitrogen absorption techniques. Naturally occurring hydrocarbons present were identified by extraction and fractionation, followed with analysis by FID-GC. The chromatograms obtained on the aliphatic fractions and aromatic fraction of "background" Kasitsna Bay sediment extracts are presented in Figure 6-22 (A and B, respectively). As seen, the aliphatic fraction contains only small to intermediate sized peaks with KOVAT indices of 1500, 1700, and 2100; this odd carbon preference is indicative of imput from marine algae. The aromatic fraction contains some large peaks between KOVAT 1900 and 2300, with another large peak at KOVAT 2994. These compounds are primarily derived from polyunsaturated molecules of biogenic origin. This sediment is fairly "clean" regarding naturally occurring hydrocarbon loads, and interferences with adsorbed hydrocarbons during wave tank experiments were therefore at a minimum.

Figures 6-23 and 6-24 show time series FID-GC chromatograms of glass fiber filter extracts, and Table 6-10 presents dispersed/particle bound n-alkane concentrations up to 9 days after initiation of the spill. Figure 6-23A is of a prespill particulate phase blank, and several trace level lower and intermediate molecular weight compounds are observed to be present. The lower molecular weight peaks are possibly due to residual epoxy resin or sealant used during wave tank construction; while the intermediate weight compounds are presumably biogenic in origin as similar components were observed in background Kasitsna Bay sediments. This assumption is also based on the physical appearance of the glass fiber filter prior to extraction. During the summer spills at Kasitsna Bay there was a massive algae bloom occurring in all four wave tanks. Hair-like strands of green/brown algae - up to six inches long - covered the bottom and sides of the tanks, as well as the paddle wheels used to generate waves. Fragments of this algae tended to clog the filters and gave them a light brown/green color. In any event, there is no evidence of any particulate/dispersed phase petroleum hydrocarbons in the pre-spill blank.

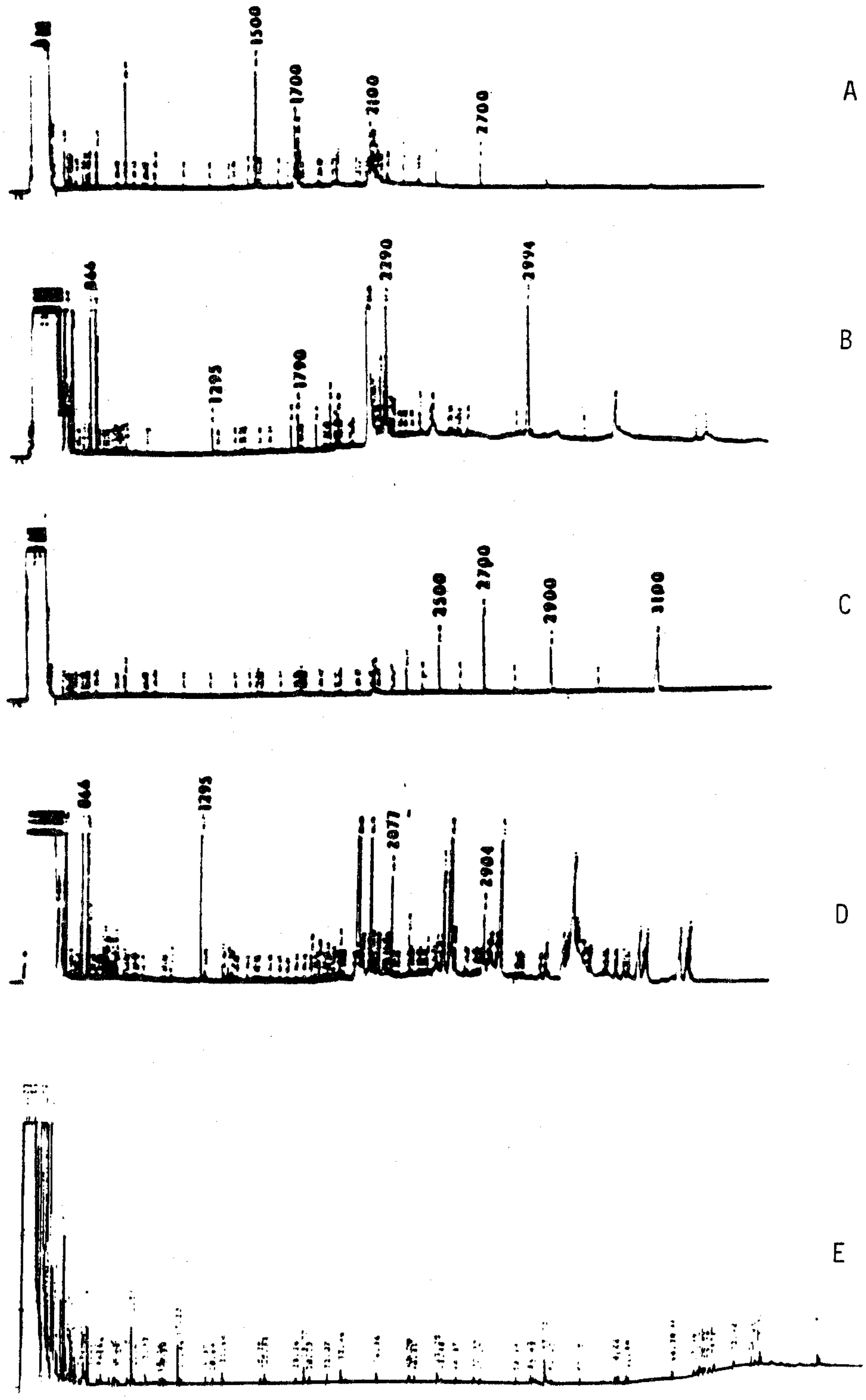

FIGURE 6-22. FID-GC chromatograms showing background hydrocarbons in sediments used for oil/SPM interaction experiments in wave tanks at Kasitsna. (A) Aliphatic fraction of Kasitsna Bay sediment, (B) Aromatic fraction of Kasitsna Bay sediment, (C) Aliphatic fraction of Seldovia Bay sediment, (D) Aromatic fraction of Seldovia Bay sediment, and (E) whole extract of Grewingk glacial till.

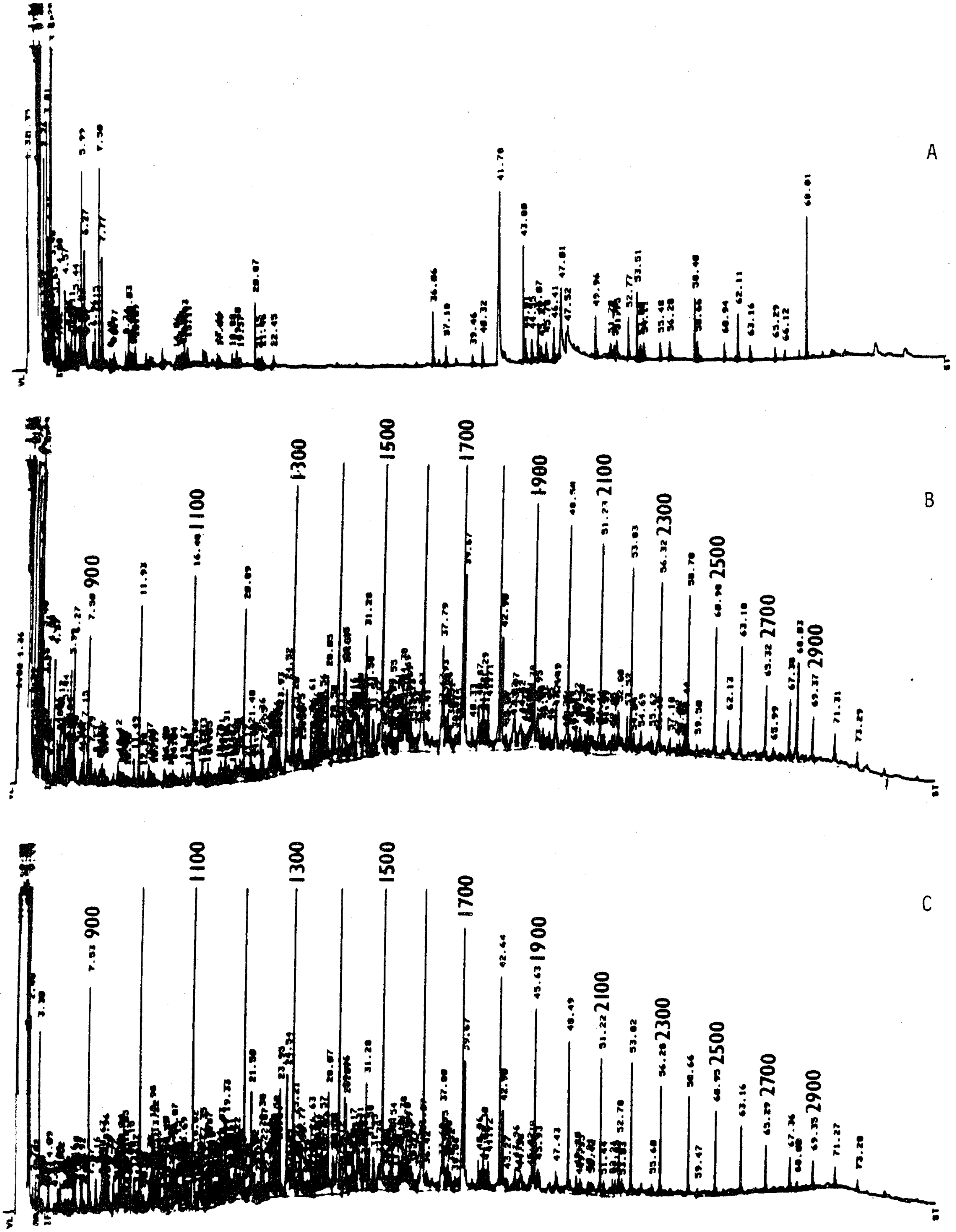

FIGURE 6-23. FID-GC chromatograms of filter extracts from Wave Tank #1 showing Dispersed/Particle Bound Oil at: (A) Prespill Blank, (B) 5 minutes, and (C) 8 hours after a spill of 16 liters of Prudhoe Bay crude oil.

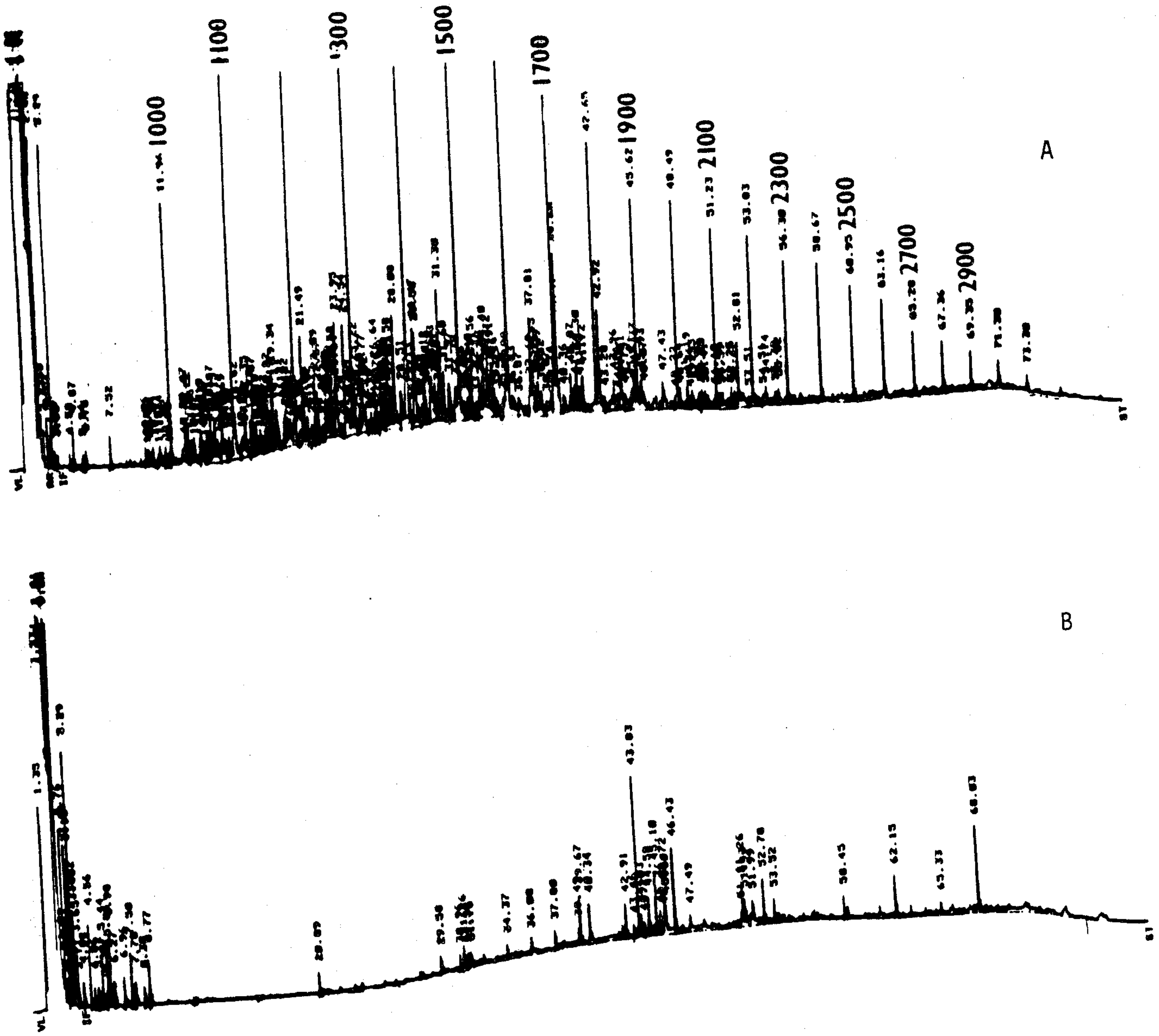

FIGURE 6-24. FID-GC chromatograms of filter extracts from Wave Tank #1 showing Dispersed /Particle Bound Oil at: (A) 48 hours, and (B) 12 days after a spill of 16 liters of Prudhoe Bay crude oil.

TABLE 6-10. Dispersed/Particle Bound Oil Concentrations(μg/l) from Wave Tank #1 (Kasitsna Bay SPM)

Compound	5 min.	1 hour	2 hours	4 hours	8 hours	12 hours	24 hours	48 hours	3 days	9 days
n-C_{10}	1.60	9.70	39.7	25.4	22.1	-	13.6	4.99	1.72	nd[a]
n-C_{11}	2.96	23.6	26.1	27.8	24.9	2.51	17.0	9.55	1.03	nd
n-C_{12}	2.43	23.7	10.[illegible]	26.5	23.5	6.76	17.6	9.98	.427	nd
n-C_{13}	4.52	25.1	11.[illegible]	27.5	25.9	13.5	18.5	12.3	nd	nd
n-C_{15}	7.37	25.2	12.9	23.9	23.6	19.1	16.7	12.0	nd	nd
n-C_{17}	6.33	19.0	9.69	17.2	18.1	16.1	12.3	9.70	nd	nd
Pristane	3.11	5.92	4.32	8.48	8.73	8.24	5.50	4.68	1.26	.0452
n-C_{18}	5.28	17.3	8.00	13.6	13.9	12.7	9.35	7.57	nd	nd
Phytane	3.01	9.24	4.34	8.02	7.02	7.32	5.45	4.49	1.00	.272
n-C_{20}	4.52	16.8	6.37	12.5	12.1	11.2	8.78	7.40	nd	nd
n-C_{23}	3.94	14.9	5.26	10.2	9.95	9.41	7.40	5.76	nd	nd
n-C_{26}	3.00	11.4	4.76	7.30	6.32	5.96	5.35	3.56	nd	nd
Total Resolved	144	603	343	573	515	323	377	238	16.0	10.0
Unresolved Compounds	658	2380	1090	2820	3190	1580	1520	1050	589	54.6

a - nd indicates "not detected"

Figure 6-23B shows a chromatographic profile of filter extract five minutes after initiation of the spill. This chromatogram is characterized by n-alkanes ranging from n-C_8 to n-C_{32}. The fact that the n-C_8 through n-C_{12} peaks are relatively smaller than the peaks of the remaining n-alkanes may suggest some selective partitioning of higher molecular weight alkanes onto the SPM; however, Figure 6-23C presents a profile of filter extract eight hours after the spill, and it resembles the parent oil slick at that time (Figure 5-104B) quite markedly. These data indicate that what was measured in the "particulate" phase was primarily dispersed oil.

A slight molecular weight dependent partitioning may again be occurring as suggested by comparison of Figure 6-24A (filter extract) with Figure 5-104C (parent oil) - both obtained after 48 hours of weathering. In this case, evaporation has removed compounds lighter than n-C_9 from the parent oil, however, the first major component observed in the dispersed/particulate phase is nC_{10}. Also there is not near the complexity of branched and/or cyclic components between nC_9 and nC_{10} in the dispersed/particle phase (Figure 6-24A) compared to the surface oil (Figure 5-104C). Nevertheless, the similarity of higher molecular weight components in the filter extract and the parent oil at these times suggests that discreet dispersed oil droplets are the primary source of hydrocarbons in the water column.

Figure 6-24B presents the chromatographic profile from the wave tank #1 particulate phase sample 12 days after the spill. It resembles the profile in Figure 6-23A, of the prespill blank and, as such, indicates that the dispersion detected earlier has essentially terminated due to concomitant increases in oil viscosity after as little as 12 days.

The dispersed/Kasitsna Bay SPM bound oil concentration data presented in Table 6-10 show a general trend of total resolved and unresolved component concentrations climbing rapidly and peaking between four and eight hours, with a subsequent decline in both the resolved and UCM components after 48 hours of weathering. After three days most petrogenic compounds are absent, as seen in the concentration data listed for three and nine days in Table 6-10. Indeed, chromatographic evidence and GC/MS data indicate that the compounds, found in filter extracts obtained after three days and all those subsequently taken, are strictly biogenic in origin.

Seldovia Salt Marsh SPM

The oil/SPM interaction experiment using Seldovia Salt Marsh sediment (added to wave tank #2), was also begun in the summer of 1982. X-ray diffraction analyses of Seldovia Salt Marsh sediment (Table 6-7) shows that its mineralogical composition is significantly different than that of Kasitna Bay sediment. Specifically, this sediment is composed principally of kaolinite (>50%), with some quartz (5-10%), feldspare (2-5%) and trace amounts of calcite (<2%). Electron microscopy showed this sediment to be rich with organic fragments with some fecal pellets and diatoms present, but relatively lower amounts clay fragments were found compared to Kasitsna Bay. The specific surface area of this sediment was determined to be 11.1. Background hydrocarbons present in Seldovia Bay sediment are shown in Figure 6-22C (Aliphatic fraction) and Figure 6-22D (Aromatic fraction), respectively. The aliphatic fraction contains only four small peaks, with KOVAT indices of 2500, 2700, 2900 and 3100. Again, these profiles are different from Kasitsna Bay "background" sediment, and these higher molecular weight odd-carbon alkanes are primarily representative of plant waxes. The aromatic fraction shows the presence of quite a few more peaks; specifically, several clusters occurring from the middle to the end of the chromatogram. However, the use of Selected Ion Monitoring (during GC/MS analysis) made it possible to distinguish between these peaks of biological origin and adsorbed petroleum derived aromatic compounds.

Time series FID-GC chromatograms of filter extracts obtained with Seldovia SPM are presented in Figure 6-25 and 6-26, and Table 6-11 presents the dispersed/particle bound oil concentrations observed out to 6 days post spill. The prespill filter blank (Figure 6-25A) shows similar residual epoxy

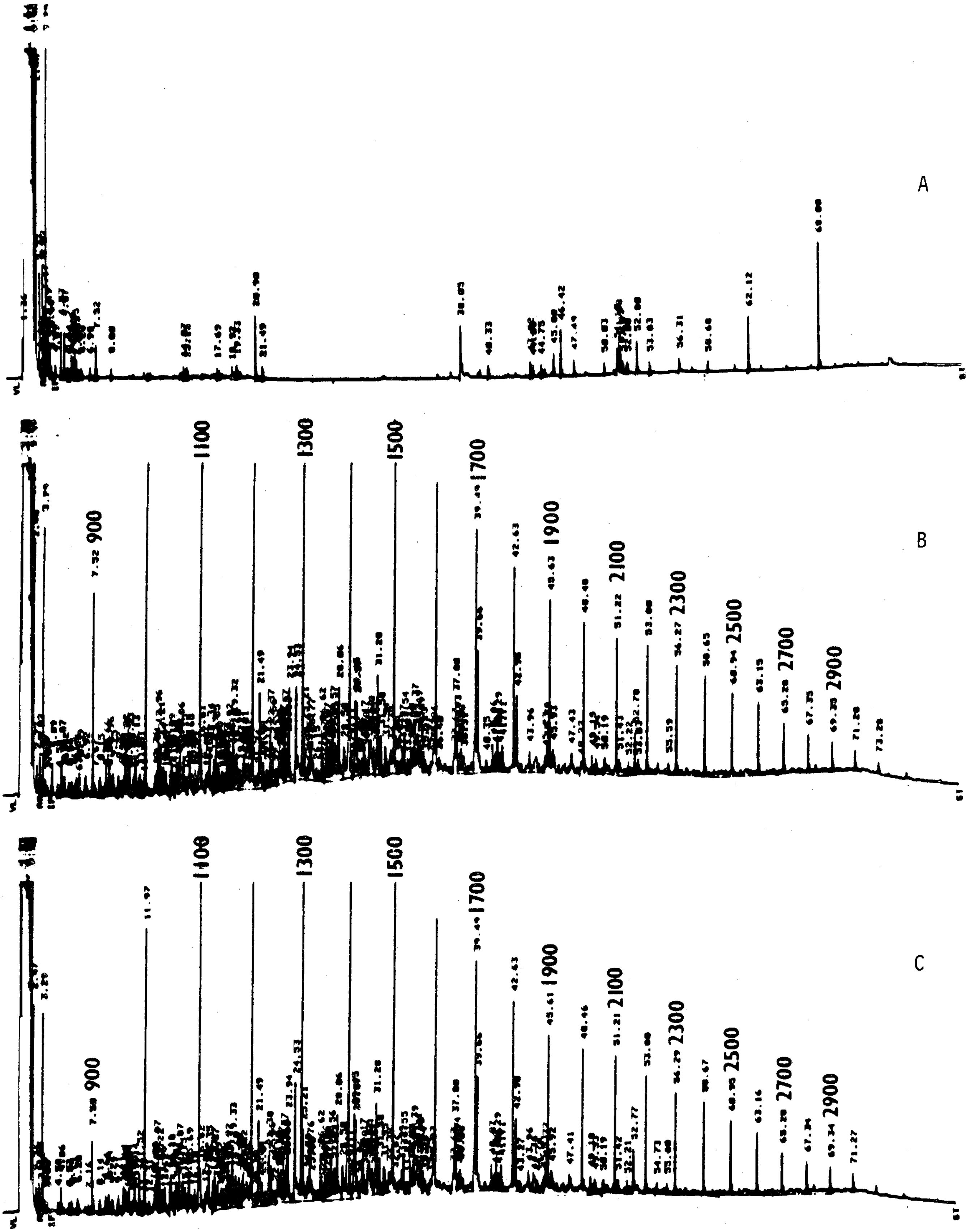

FIGURE 6-25. FID-GC chromatograms of filter extracts from Wave Tank #2 showing Dispersed/Particle Bound Oil at: (A) Prespill Blank, (B) 1 hour, and (C) 8 hours after a spill of 16 liters of Prudhoe Bay crude oil.

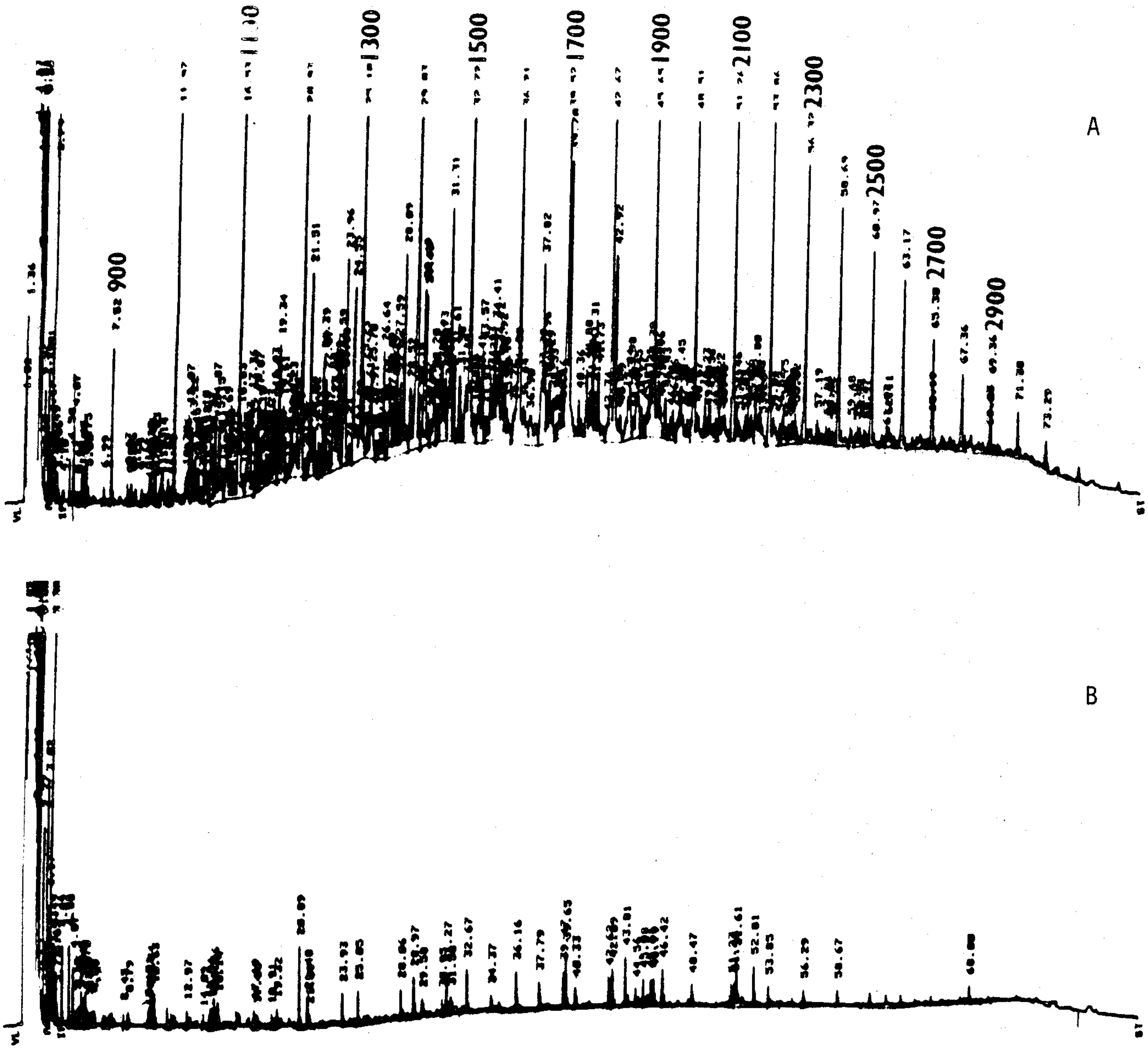

FIGURE 6-26. FID-GC chromatograms of filter extracts from Wave Tank #2 showing Dispersed/Particle Bound oil at: (A) 48 hours, and (B) 12 days.

TABLE 6-11. Dispersed/Particle Bound Oil Concentrations (μg/l) from Wave Tank #2 (Seldovia Bay SPM)

Compound	5 min.	1 hour	2 hours	4 hours	8 hours	12 hours	24 hours	48 hours	6 days
n-C_{10}	nd[a]	nd	nd	9.28	7.71	7.00	3.28	1.74	.981
n-C_{11}	13.3	nd	nd	10.7	9.49	9.10	7.75	2.32	.573
n-C_{12}	36.7	1.30	1.46	10.1	9.98	10.1	8.74	2.81	nd
n-C_{13}	75.2	4.60	3.93	11.5	11.6	11.7	10.5	3.46	nd
n-C_{15}	93.7	11.0	5.95	10.2	10.4	10.7	9.11	3.40	nd
n-C_{17}	74.4	8.86	[illegible].96	7.78	8.47	8.85	7.92	2.45	nd
Pristane	36.9	3.98	[illegible].53	3.73	4.26	4.28	3.95	1.02	.262
n-C_{18}	55.5	7.19	3.93	6.02	6.43	6.80	6.05	2.07	nd
Phytane	32.7	3.95	1.92	2.96	3.15	3.21	3.07	1.12	nd
n-C_{20}	45.2	6.37	3.16	4.84	5.17	5.35	5.14	1.75	nd
n-C_{23}	36.6	4.02	2.60	3.85	4.04	4.18	4.24	1.54	nd
n-C_{26}	25.2	3.31	1.70	2.67	2.64	2.85	2.86	.957	nd
Total Resolved	1350	172	92.6	197	201	194	171	66.5	7.73
Unresolved Compounds	5780	778	384	651	635	664	637	231	116

a - nd indicates "not detected"

resin (applied during wave tank construction) and biogenic compounds as did the prespill blank from wave tank #1. Their concentrations, however, are orders of magnitude lower than the dispersed oil loads introduced as little as 5 minutes after initiation of the spill.

Chromatograms of filter extracts after one hour, eight hours, and 48 hours (Figures 6-25B, 6-25C and 6-26A, respectively) resemble chromatograms of parent Prudhoe Bay crude oil sampled from the slick at the same times (Figures 5-104A through 5-104C). The profiles of filter extracts have the predominance of n-alkanes (ranging from n-c_9 to n-c_{32}) characteristic of Prudhoe Bay crude oil, although there may be a little evidence of slightly greater complexity in the KOVAT index 800-1000 range in the surface oil compared to the dispersed/particle bound phase. Nevertheless, significant removal of lighter molecular weight compounds is seen after eight hours of weathering in both the surface and dispersed oil phases. The chromatographic profile obtained from a filter extract 12 days after the spill (Figure 6-26B) still shows a little evidence of oil derived hydrocarbons (primarily n-alkanes) with the SPM from the Seldovia Salt marsh while these dispersed components were not observed to as great an extent after that time period with Kasitsna Bay SPM (see Figures 6-24B and 6-26B). It is extremely interesting to note, however, that close examination of the chromatogram of dispersed/particle bound oil in Figure 6-26B shows the resolved components to be dominated by several branched (isoprenoid) compounds, including pristane (RT 37.65) and phytane (RT 42.89). Thus, the dispersed oil phase components remaining in the water column after 12 days in the tank spiked with the organic rich sediment from Seldovia Salt marsh showed evidence of extensive microbial degradation.

With regard to the individual, total resolved and UCM component concentration data presented in Table 6-11, the extremely high (order of magnitude greater than wave tank 1) concentrations found after five minutes are believed to be most likely due to one or more larger (possibly >1 cm) random oil drops entrained into the sampling system. Drops this size would normally return to the slick, and therefore cannot be regarded as truly dispersed oil over a longer time frame. Disregarding the five minute concentrations, the trend seen here is an increase in concentration over the first hour; the hydrocarbon levels remain relatively constant (171 μg/l to 201 μg/l total resolved components) over the next 24 hours and the concentrations then begin to drop at 48 hours with less than 1 μg/l levels of dispersed oil-related compounds present at six days after the spill.

No SPM

In an attempt to separate dispersion processes from oil/particulate interactions, a control tank spill (with no SPM addition) was also initiated and monitored in the summer of 1982. Table 6-9 shows that, although there was no supplemental SPM addition, a naturally occurring load of approximately 3.6 mg/ℓ was present. This loading is presumably due to suspended sediments in Kasitsna Bay which get introduced to the wave tank by way of the seawater delivery system and to the weight associated with the algae fragments present in the tank. The control tank was designated as wave tank #3 and time series FID-GC chromatographic profiles of filter extracts, from this tank, are shown in Figures 6-27 and 6-28. Table 6-12 presents the time-series dispersed oil concentrations derived from the gas chromatographic measurements.

Figure 6-27A shows the same profile, for a prespill blank, as do the tanks to which SPM was added. Comparison of Figures 6-27C and 6-28A, (filter extracts after eight hours and 48 hours, respectively) with Figures 5-104B and 5-104C, (parent oil sampled at the same times) again shows very similar profiles (except that the parent surface oil exhibits slightly greater complexity in the KOVAT index 800 to 1000 range. A filter extract obtained one hour after the spill (Figure 6-27B) shows n-alkanes ranging from n-C_8 to n-C_{32}. Evaporative losses and dissolution of selected lower molecular weight components from the parent oil slick are reflected by the filter extract profile at eight hours (Figure 6-27C) where the lowest molecular weight n-alkane detected is n-C_9. As with the tanks to which SPM was added, chromatographic evidence, presented in Figure 6-28B, shows very little evidence of particulate bound or dispersed oil 12 days after the spill.

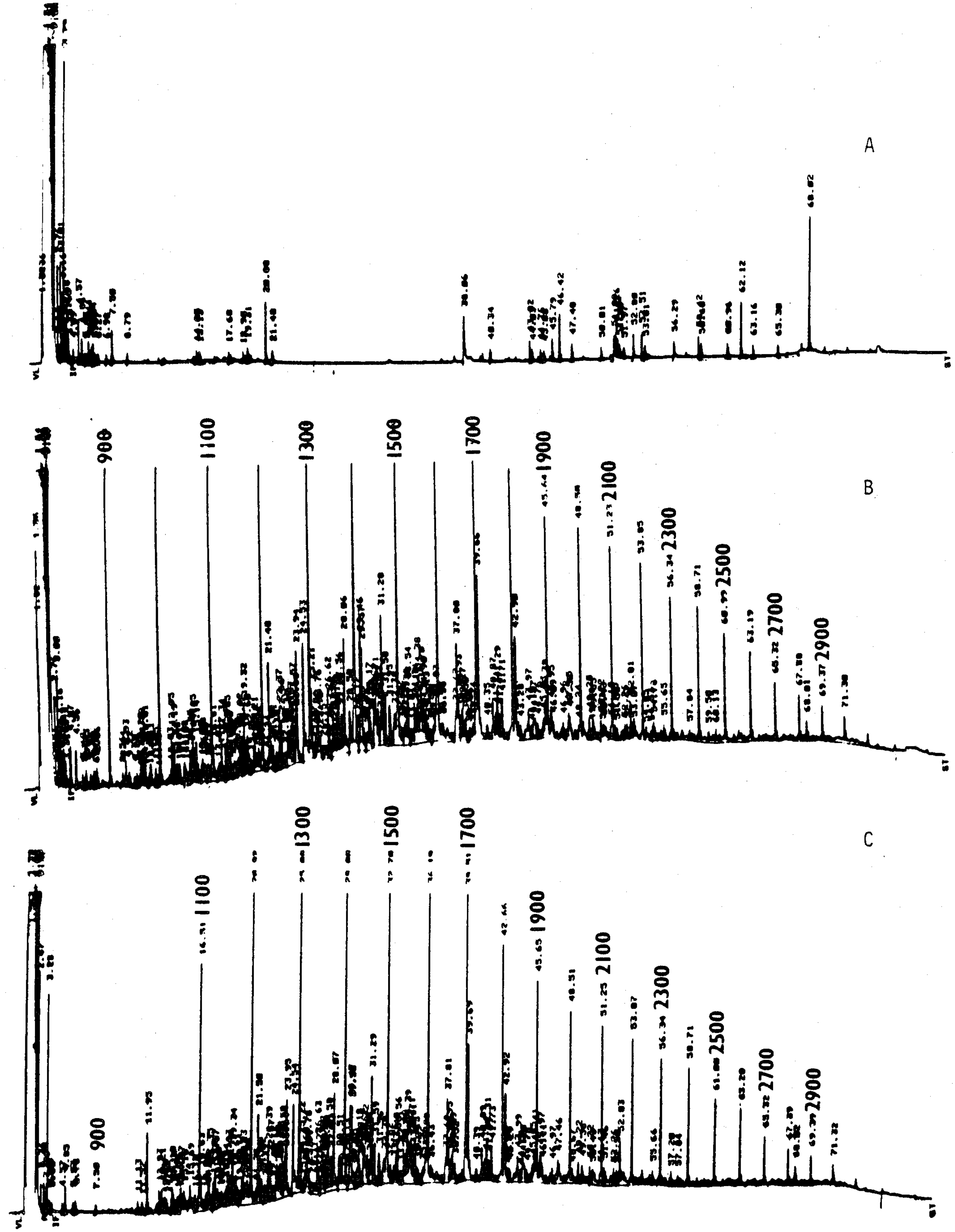

FIGURE 6-27. FID-GC chromatograms of filter extracts from Wave Tank #3 showing Dispersed/Particle Bound oil at: (A) Prespill Blank, (B) 1 hour, and (C) 8 hours after a spill of 16 liters of Prudhoe Bay crude oil.

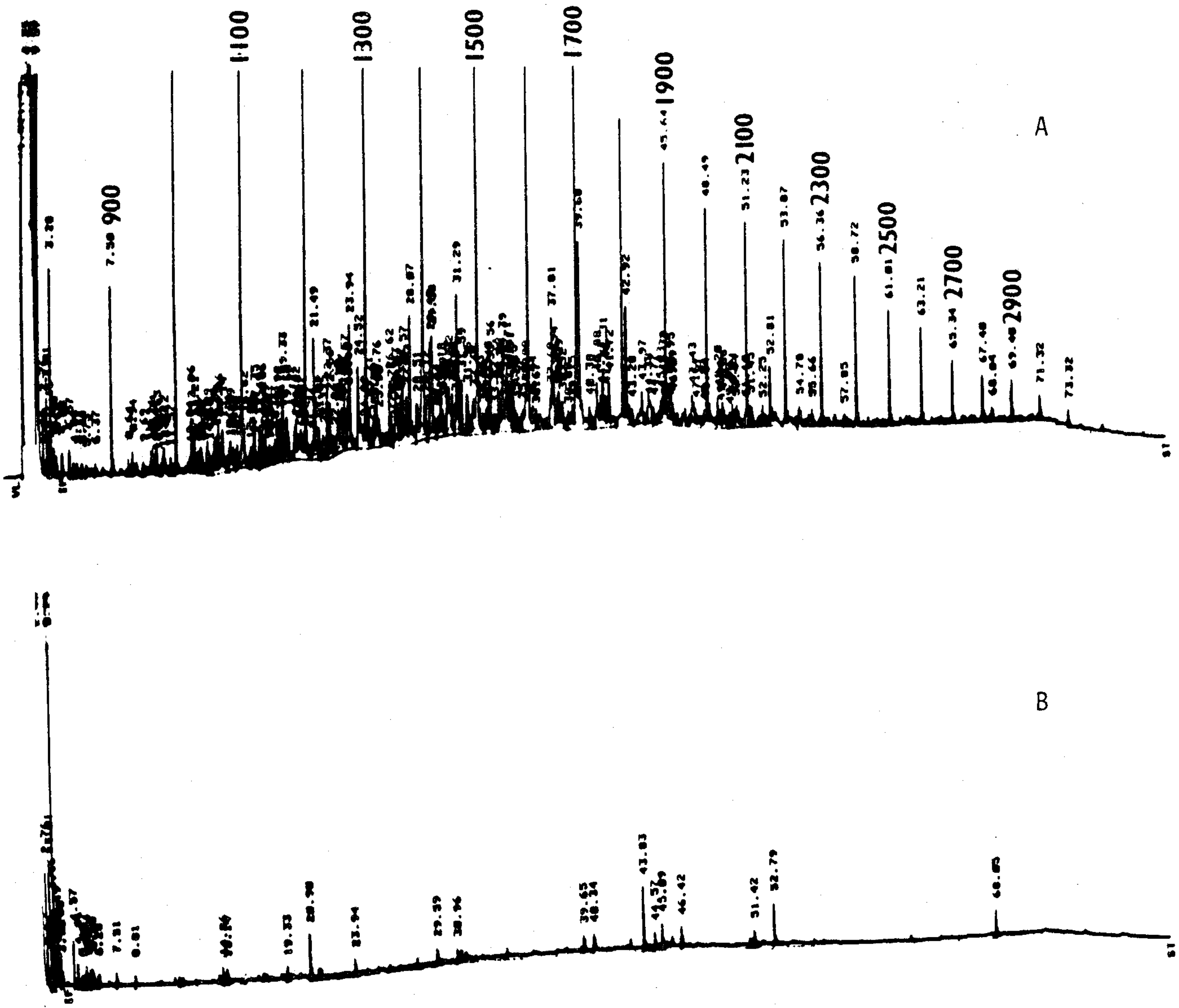

FIGURE 6-28. FID-GC chromatograms of filter extracts from Wave Tank #3 showing Dispersed/Particle Bound oil at: (A) 48 hours, and (B) 12 days after a spill of 16 liters of Prudhoe Bay crude oil.

TABLE 6-12. Dispersed/Particle Bound Oil Concentrations (µg/l) from Wave Tank #3 (no SPM addition)

Compound	5 min.	1 hour	2 hours	4 hours	8 hours	12 hours	24 hours	48 hours	3 days	6 days	9 days	12 days
n-C_{10}	nd[a]	41.5	20.5	.290	1.41	7.93	1.54	4.15	.231	3.72	1.98	nd
n-C_{11}	25.7	33.2	27.2	3.75	5.75	10.1	8.83	4.46	1.09	2.31	.989	nd
n-C_{12}	58.4	26.0	25.4	11.2	9.05	11.3	15.1	4.70	1.63	1.46	nd	nd
n-C_{13}	106	32.0	32.0	21.5	11.8	14.1	17.9	5.88	2.48	1.98	nd	nd
n-C_{15}	116	31.6	31.3	27.3	11.4	13.6	17.0	5.75	2.90	2.35	nd	nd
n-C_{17}	92.9	23.3	25.8	21.7	8.88	10.9	12.3	4.61	2.67	2.07	nd	nd
Pristane	46.9	11.0	12.6	9.28	4.60	5.33	5.94	2.37	1.43	1.16	nd	nd
n-C_{18}	71.2	17.7	19.7	18.8	6.92	8.45	9.48	3.62	2.18	1.70	nd	nd
Phytane	33.1	8.41	9.63	10.4	3.00	4.97	5.40	2.09	1.11	.886	.421	.269
n-C_{20}	60.0	15.2	16.2	16.4	5.97	8.13	8.14	3.12	1.91	1.51	nd	nd
n-C_{23}	51.1	12.5	13.0	14.5	4.79	5.95	6.75	2.50	1.52	1.25	nd	nd
n-C_{26}	33.2	8.07	8.22	10.1	2.93	3.77	4.88	1.61	.974	.812	nd	nd
Total Resolved	1810	609	548	466	191	254	313	107	47.3	46.6	5.86	3.97
Unresolved Compounds	7610	2270	2340	2050	816	1070	1360	464	264	228	159	83.7

a - nd indicates "not detected"

The data in Table 6-12 show that as in the case with wave tank #2, the five minute sample had significantly higher levels of hydrocarbons than the remaining samples. Again, this is believed to be due to a random large drop of oil entrained into the sample port, and it must be disregarded. The trend, indicated by the concentrations of total resolved compounds, shows a rapid increase in hydrocarbon levels (to 609 μg/l) within the first hour, with a gradual decrease in concentration (to 107 μg/l) over 48 hours, followed by a more rapid decrease in concentration (to approximately 4 μg/l) between three and 12 days following the spill. All evidence of dispersed petroleum hydrocarbons is gone by nine days, and this suggests that dispersion of oil into the water column has ceased. Nevertheless, in the absence of added SPM under the summer spill conditions, the dispersed oil phase concentrations in wave tank #3 appear to remain elevated longer in the water column than in tanks 1 and 2 where the ambient SPM load was increased.

Grewingk Glacial Till SPM

This spill was initiated in the Fall/Winter period of 1982 in wave tank #4, and the water column was augmented with measured amounts of glacial till SPM collected from the base of Grewingk Glacier. The minerological composition of Grewingk glacial fines, as determined by X-ray diffraction, is somewhat similar to Kasitsna Bay sediment. The majority of the sediment is comprised of quartz (>50%), with roughly equal amounts of kaolinite and feldsar present (both 20-40%). The major components of this sediment, as observed by electron microscope, are clay fragments and diatoms. The specific surface area of Grewingk glacial till is identical to that of Kasitsna Bay sediment at 9.1. A chromatogram of an unfractionated extract of this sediment can be found in Figure 6-22E, and it is noticeably devoid of any hydrocarbon peaks. It might be noted here that this sediment is indeed extremely pristine - the extract presented in Figure 6-22E represents over 250 grams of sediment extracted and concentrated to less than 400 μl before analysis. As such, any adsorption of petroleum hydrocarbons would be easily detected.

Actually, the summer-spill wave-tank #1 experiment was terminated in late October 1982 (as described in Section 5.4.6), and the tank was then emptied, cleaned and allowed to flush for one week before the Fall/Winter experiment described here was initiated. Nevertheless, the Fall/Winter spill was conducted in wave tank #1, but it has been designated as wave tank #4 to avoid confusion.

Similar time series FID-GC chromatographic profiles of glass fiber filter extracts were obtained from this spill, and these are presented in Figures 6-29 and 6-30. Table 6-13 presents the time-series concentrations of selected dispersed/particulate hydrocarbons derived from the GC data. The prespill blank profile, found in Figure 6-29A, shows some evidence of residual hydrocarbons, presumably from the previous spill, and some peaks characteristic of biogenic origin. However, it should be noted that, at this time, the algae bloom that occurred during the summer had ended - there was, however, evidence of other biogenic material input into the tank. Namely, a large number of decaying leaves could be seen on the tank bottom.

Comparisons of chromatograms of filter extracts obtained at times eight hours and 48 hours, Figures 6-29C and 6-30A, respectively, with chromatograms of parent oil obtained at the same time, Figures 5-106B and 5-106C, show nearly identical profiles. Note that, owing to the colder air temperature (~-5 to 0°C) in the Fall, evaporative losses by the parent stick are retarded when compared to the summer evaporation losses. Specifically, Figure 5-106B of parent oil after eight hours of weathering shows essentially no indication of evaporation. Figure 5-106C, of parent oil sampled after 48 hours of weathering, still contains some compounds with KOVAT indices less than 900. During the summer experiments, the oil had generally reached this state by 8 hours. The slower rate of evaporation during the winter is reflected by the chromatograms of dispersed oil as well, where a similar trend in elevated levels of lower molecular weight components is observed. After 8 hours, the filter extract presented in Figure 6-29C shows no sign of evaporative loss, with compounds as volatile as n-C_8 still present. After 48 hours the chromatogram

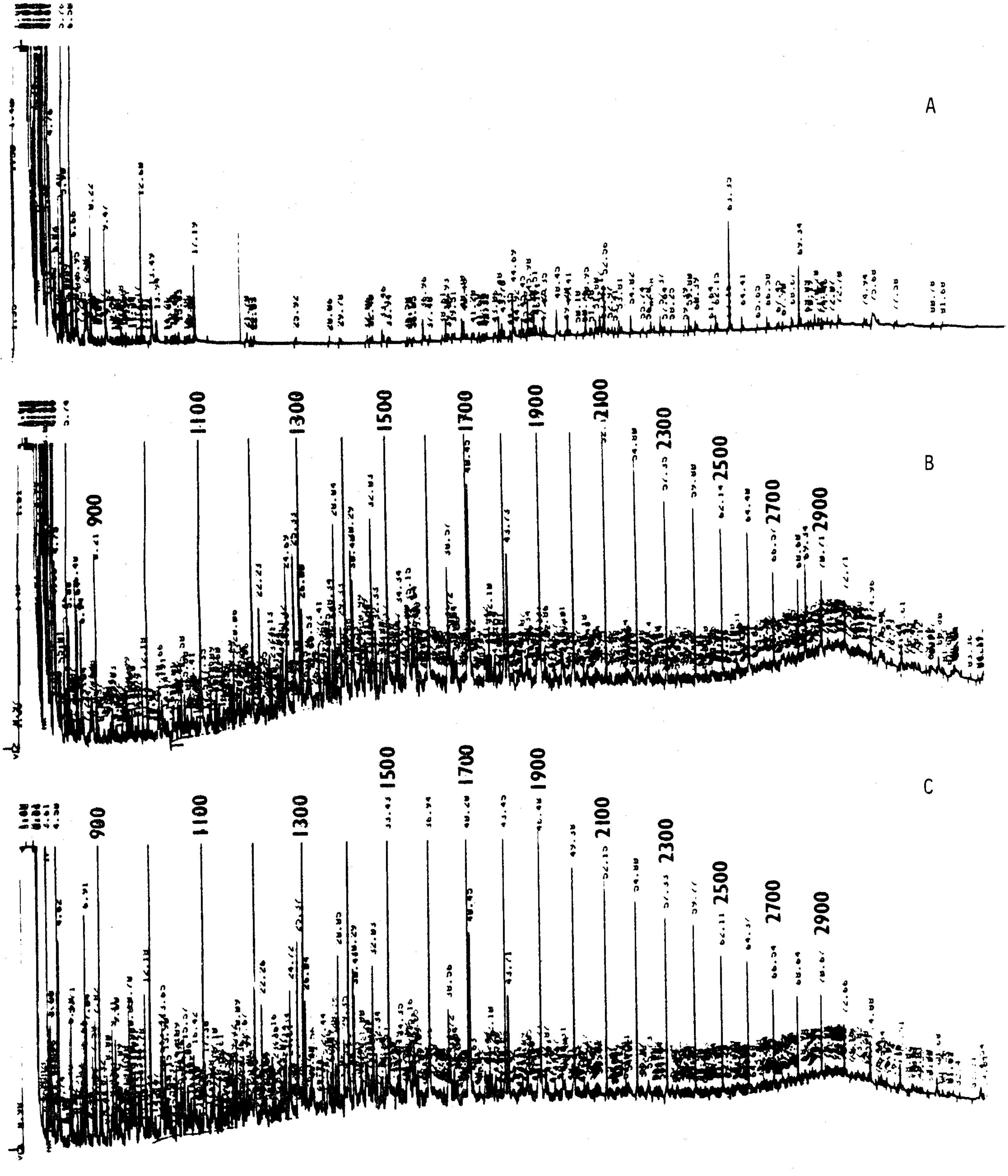

FIGURE 6-29. FID-GC chromatograms of filter extracts from Wave Tank #4 showing Dispersed/Particle Bound oil at: (A) Prespill Blank, (B) 2 hours, and (C) 8 hours after a spill of 16 liters of Prudhoe Bay crude oil.

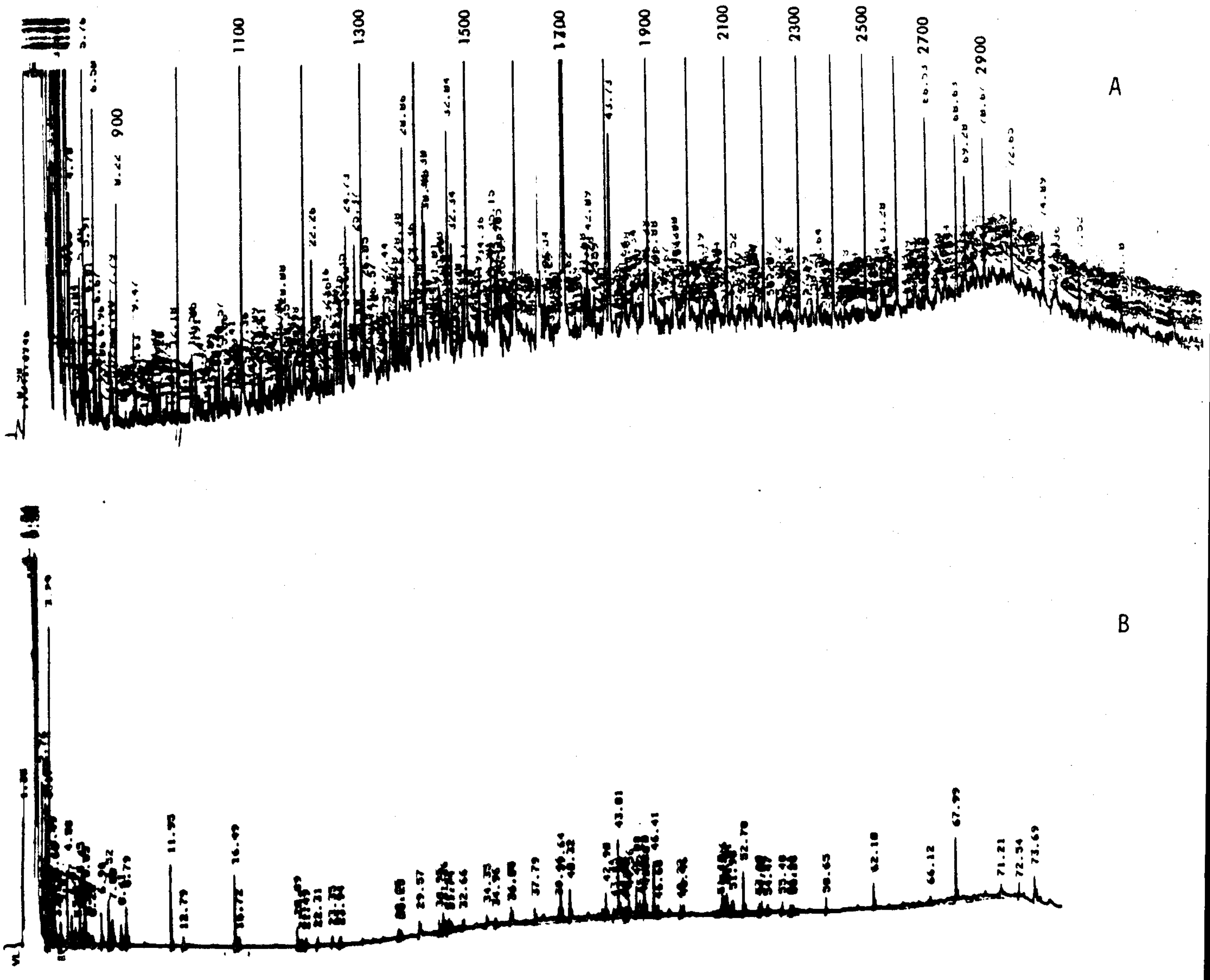

FIGURE 6-30. FID-GC chromatograms of filter extracts from Wave Tank #4 showing Dispersed/Particle Bound oil at: (A) 48 hours, and (B) 12 days after a spill of 16 liters of Prudhoe Bay crude oil.

TABLE 6-13. Dispersed/Particle Bound Oil Concentrations (μg/l) from Wave Tank #4 Fall 1982 (Glacial Till SPM)

Compound	5 min.	½ hours	1 hour	2 hours	4 hours	8 hours	12 hours	24 hours	48 hours	3 days	6 days	8 days
n-C_9	1.67	-	1.58	3.27	-	25.4	.989	.688	.459	.173	.157	.152
n-C_{10}	2.37	-	3.09	6.37	1.08	33.1	2.38	1.26	1.05	.401	.285	.323
n-C_{11}	1.33	.485	6.12	10.3	4.03	36.3	3.44	1.55	1.44	.610	.469	.579
n-C_{12}	.668	1.17	4.99	10.9	8.82	30.5	3.52	1.51	1.55	.715	.752	.950
n-C_{13}	1.75	2.50	6.62	13.7	11.9	45.5	5.82	2.70	2.48	1.54	.996	1.26
n-C_{15}	3.47	4.49	8.98	13.8	17.2	29.5	4.12	2.33	2.20	1.33	1.29	1.59
n-C_{17}	3.30	5.00	7.21	12.1	12.6	24.1	2.84	1.85	1.69	1.23	1.11	1.26
Pristane	1.87	2.85	3.73	6.24	6.40	12.8	1.55	.952	.862	.640	.595	.636
n-C_{18}	2.71	4.32	6.73	9.15	11.1	19.7	2.27	1.65	1.49	1.08	.966	.868
Phytane	1.45	2.31	3.48	5.06	6.12	10.3	1.19	.794	.773	.559	.463	.562
n-C_{20}	2.47	3.27	5.98	8.94	10.9	16.8	1.97	1.52	1.46	1.06	.791	.751
n-C_{23}	2.22	3.80	6.20	7.94	12.5	20.9	2.16	1.54	1.49	1.06	.844	.941
n-C_{26}	1.63	2.40	4.65	6.49	9.28	16.8	1.77	1.26	1.27	.895	.573	.637
Total Resolved	432	278	553	744	346	1030	146	137	125	74.6	57.8	66.8
Unresolved Compounds	345	563	907	1430	1767	2620	322	228	225	156	87.0	110.

of the filter extract (shown in Figure 6-30A) still contains many of the lighter hydrocarbon components, with n-C_9 easily detectable. Because the dispersed/particulate phase so closely parallels the composition of the parent oil slick, the data suggest that dispersion, not SPM adsorption, is the primary mechanism whereby hydrocarbons are introduced to the water column. Again, 12 days following the spill, the chromatographic profile of filter extract (Figure 6-30B) shows virtually no petroleum related hydrocarbons present.

As seen by the reduced data in Table 6-13, the dispersed oil concentrations rise rapidly and peak at eight hours with a total resolved compound concentration of 1,030 µg/l. An extremely rapid decrease, to 146 µg/l follows at 12 hours where concentrations remain fairly stable for the next 36 hours and finally decrease gradually to approximately 60 µg/l after eight days. This rapid decay in dispersed water column concentrations presumably can be attributed to the colder winter conditions and the SPM load added to the wave tank system.

Bottom Sediments

Because addition of SPM was terminated two weeks following the spill in each tank, the accumulation of bottom sediment (after a few months) must be attributed primarily to sediment introduced to the tanks from the seawater delivery system which pumps seawater from Kasitsna Bay. As such, there should be no inherent differences concerning the nature of the bottom sediment from one tank to another. However, accumulated bottom sediment collected from wave tank #4 after 13 days, must be considered to be primarily composed of the glacial till that had been added via the SPM master reservoir.

Figure 6-31A presents a chromatographic profile of extract from sediment collected off the bottom of wave tank #4 13 days after the spill, while Figures 6-31B and 6-31C show aliphatic and aromatic fraction extracts of bottom sediment collected from wave tank #3 12 months after the spill. Aliphatic

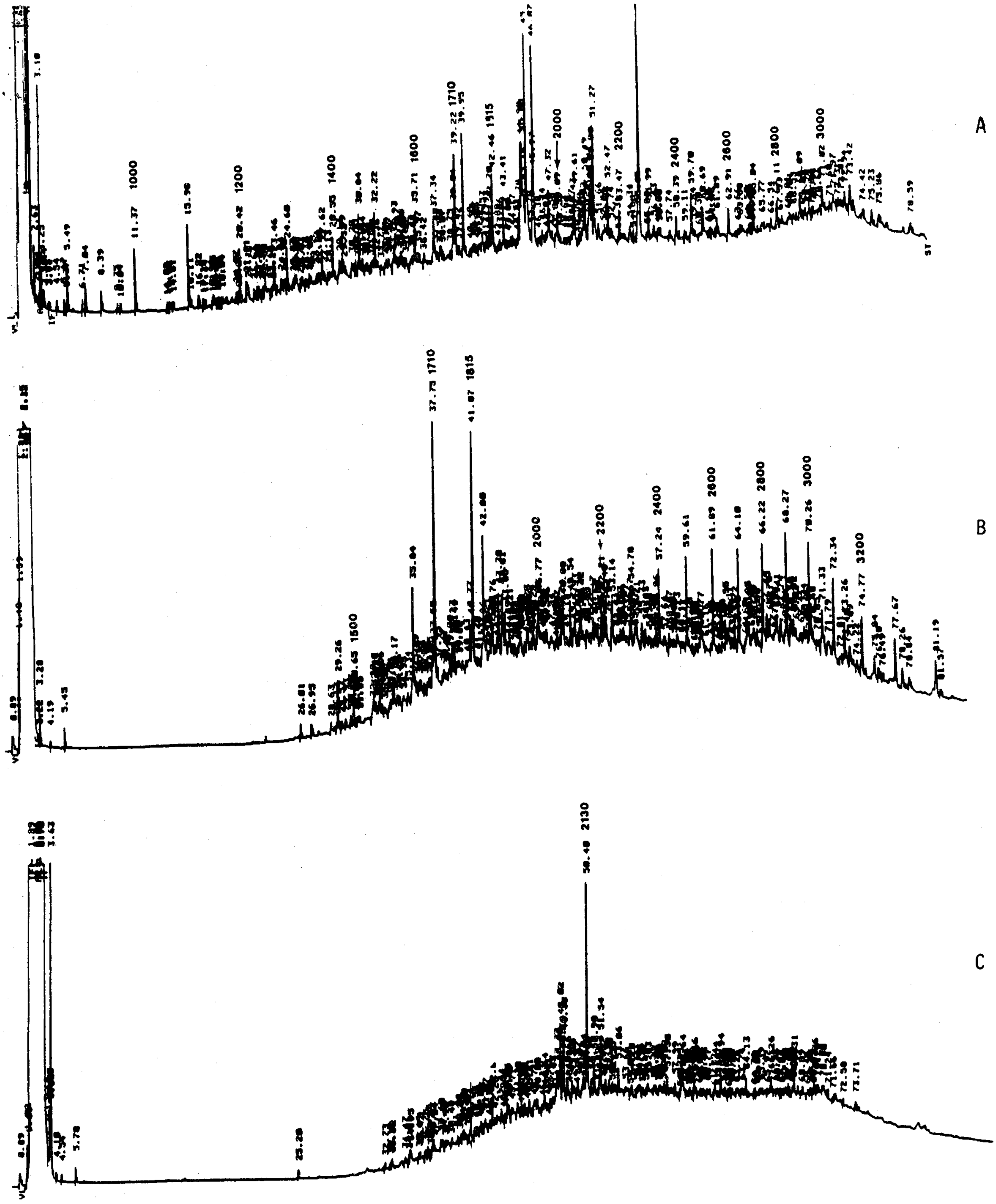

FIGURE 6-31. FID-GC Chromatograms of Sediment Extracts collected off the bottom of Wave Tanks. (A) Whole Extract from Wave Tank #1 after 13 days, (B) Aliphatic fraction from Wave #3 after 12 months, and (C) Aromatic fraction from Wave Tank #3 after 12 months.

and aromatic fractions of bottom sediments extracts, from wave tank #2 after 9 months are shown in Figure 6-32. Individual compounds, total resolved compounds, and UCM concentration values of hydrocarbons incorporated into bottom sediments are presented in Table 6-14 (aliphatic fractions) and Table 6-15 (aromatic fractions).

The profile of extracted bottom sediment from wave tank #4, after 13 days of weathering, is characterized by a series of small homologous peaks extending from retention time 11 minutes to 73 minutes and two clusters of larger peaks from retention time 43 to 46 minutes and again from 50 to 52 minutes. GC/MS analysis indicated that the homologous series of peaks are n-alkanes, ranging from n-C_9 to n-C_{32}, while the clusters of peaks between KOVAT indices 1900 and 2200 are most likely intermediate molecular weight carboxcylic acids, presumably of biological origin. A cluster of carboxcylic acids can also be seen in the aromatic fraction of the bottom sediment obtained from wave tank #3 after 12 months (Figure 6-31C). GC/MS analysis, with Selected Ion Monitoring (SIM), showed no evidence of any petroleum derived <u>aromatic</u> compounds in either of these samples.

Evidence of hydrocarbon contamination was seen in the aliphatic fraction of all bottom sediments extracted. Table 6-14 shows that after 13 days, the bottom sediment from the Grewingk Glacier SPM contained n-alkanes ranging from n-C_9 to n-C_{32}, while samples collected after longer periods from wave tanks #2 and #3 showed n-alkanes from n-C_{15} to n-C_{32}. Clear indication of this higher molecular weight aliphatic fraction contamination of the bottom sediments is presented in Figure 6-31B (bottom sediment from tank #3 after 12 months), where n-alkanes, ranging from n-C_{20} to n-C_{32}, are easily detected. The most predominant components in these sediments are pristane (KOVAT 1710) and phytane (KOVAT 1815) suggesting more extensive microbial degradation in the sediments over time. Concentrations of aliphatic hydrocarbons, present in bottom sediments, given in Table 6-14, are highest (161 μg/g total resolved compounds) after 13 days, and decrease (to between 20 to 85 μg/g) in samples obtained months later.

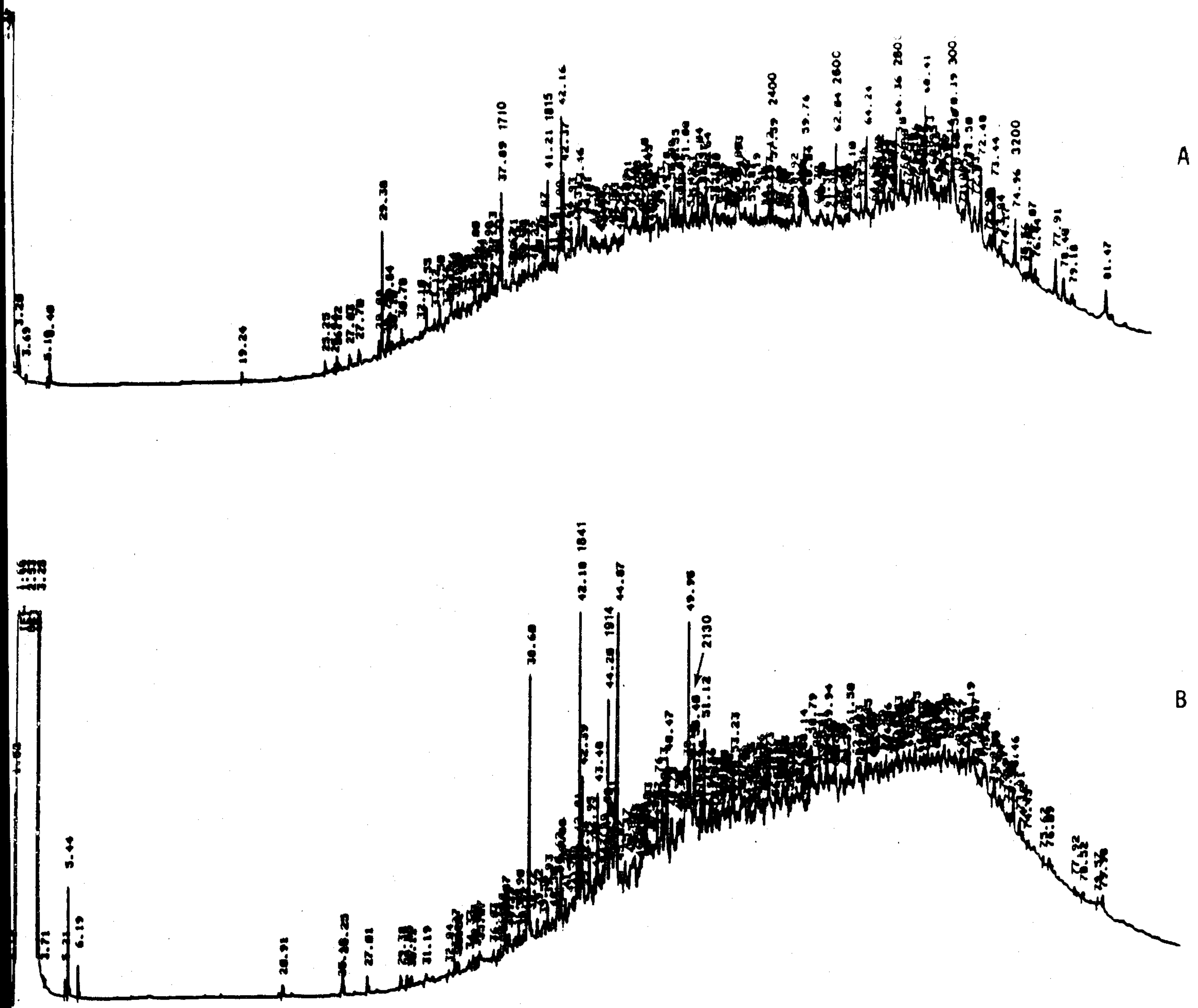

FIGURE 6-32. FID-GC chromatograms of extracts from sediment collected off the bottom of Wave Tank #2-9 months after a spill of 16 liters of Prudhoe Bay crude oil. (A) Aliphatic fraction (B) Aromatic fraction.

Table 6-14. Aliphatic Concentrations (ug/g) of Oil Incorporated in the Bottom Sediments from Wave Tanks #1-4

Compound	Concentration (ug/g)				
	Wave Tank #4 13 days	Wave Tank #4 5 months	Wave Tank #2 9 months	Wave Tank #3 9 months	Wave Tank #3 12 months
N-C_9	.745	nd[a]	nd	nd	nd
N-C_{10}	2.15	nd	nd	nd	nd
N-C_{11}	2.98	nd	nd	nd	nd
N-C_{13}	1.89	nd	nd	nd	nd
N-C_{15}	2.07	nd	.120	nd	.536
N-C_{17}	1.67	nd	.141	nd	.595
Pristane	5.08	.882	.688	1.57	6.74
N-C_{18}	1.68	nd	.289	nd	.834
Phytane	4.49	.793	.828	1.73	6.94
N-C_{20}	1.38	.278	.114	.263	.336
N-C_{23}	.956	.894	.0977	.418	.609
N-C_{25}	1.25	1.53	.365	.378	1.64
N-C_{29}	2.01	.955	.566	.805	2.19
Total Resolved	161	22.1	29.6	29.8	86.3
Unresolved Compounds	167	210	547	877	825

a- nd indicates "not detected"

Table 6-15. Aromatic Concentrations (ug/g) of Oil Incorporated in the Bottom Sediments from Wave Tanks #1-4

	Concentration (ug/g)			
Compound	Wave Tank #4 5 months	Wave Tank #2 9 months	Wave Tank #3 9 months	Wave Tank 3 12 months
C_{18} - carboxcylic acids	.321	1.02	.0674	1.94
ID Unknown (base m/e = 64)	.0330	.352	.0348	2.10
C_{20} - carboxcylic acids	nd[a]	nd	nd	.831
Total Resolved	1.25	2.17	10.3	11.5
Unresolved Compounds	4.67	68.3	187	388

a- nd indicates "not detected"

Representative chromatographic profiles of corresponding long-term filter extracts, showing particulate hydrocarbons in the water column five and nine months after the spills, can be seen in Figure 6-33. These three chromatograms are very similar in nature - all show the cluster of peaks between retention times 42 and 46 minutes, with very few resolved peaks elsewhere. GC/MS analysis, with SIM, suggests that, as with the bottom sediments, the cluster of peaks are primarily composed of intermediate molecular weight carboxcylic acids, with no evidence of any oil related hydrocarbons. The concentrations - not presented in tabular form - for the total resolved compounds in the particulate phase (principally due to the cluster of carboxcylic acids) ranges from 5 to 10 μg/l of water filtered.

6.3.2.4 Summary Comparisons of Winter vs Summer Dispersed/Particulate Bound Oil

Several notable similarities and differences were observed during the wave tank experiments completed at Kasitsna Bay. A graphical representation of comparative concentration data is presented in Figure 6-34. This figure shows concentrations vs time data for total resolved compounds and UCM's of glass fiber filter particulate/dispersed oil extracts, for all four wave tanks for the first two days following the spills.

One similarity worth noting is that the shape of the curve (for each tank) of the total resolved compound concentrations over time is matched by the shape of the curve of UCM concentrations over time. Also, the relative magnitude and position of the resolved and UCM curves is the same, except that wave tank #4 (Glacial till SPM) shows the most total resolved compounds, while UCM concentrations are highest in wave tank #1 (Kasitsna Bay SPM). Except for this perplexing difference, the two graphs shown are quite similar in appearance. Considering the chromatographic profiles, discussed in the previous section, this should not be unexpected. In all four wave tanks the GC profiles of the dispersed/particulate phase in the water column, are nearly identical to the GC profile of the parent oil. This strongly implies dispersion of discreet whole oil droplets into the water column, and as such, the

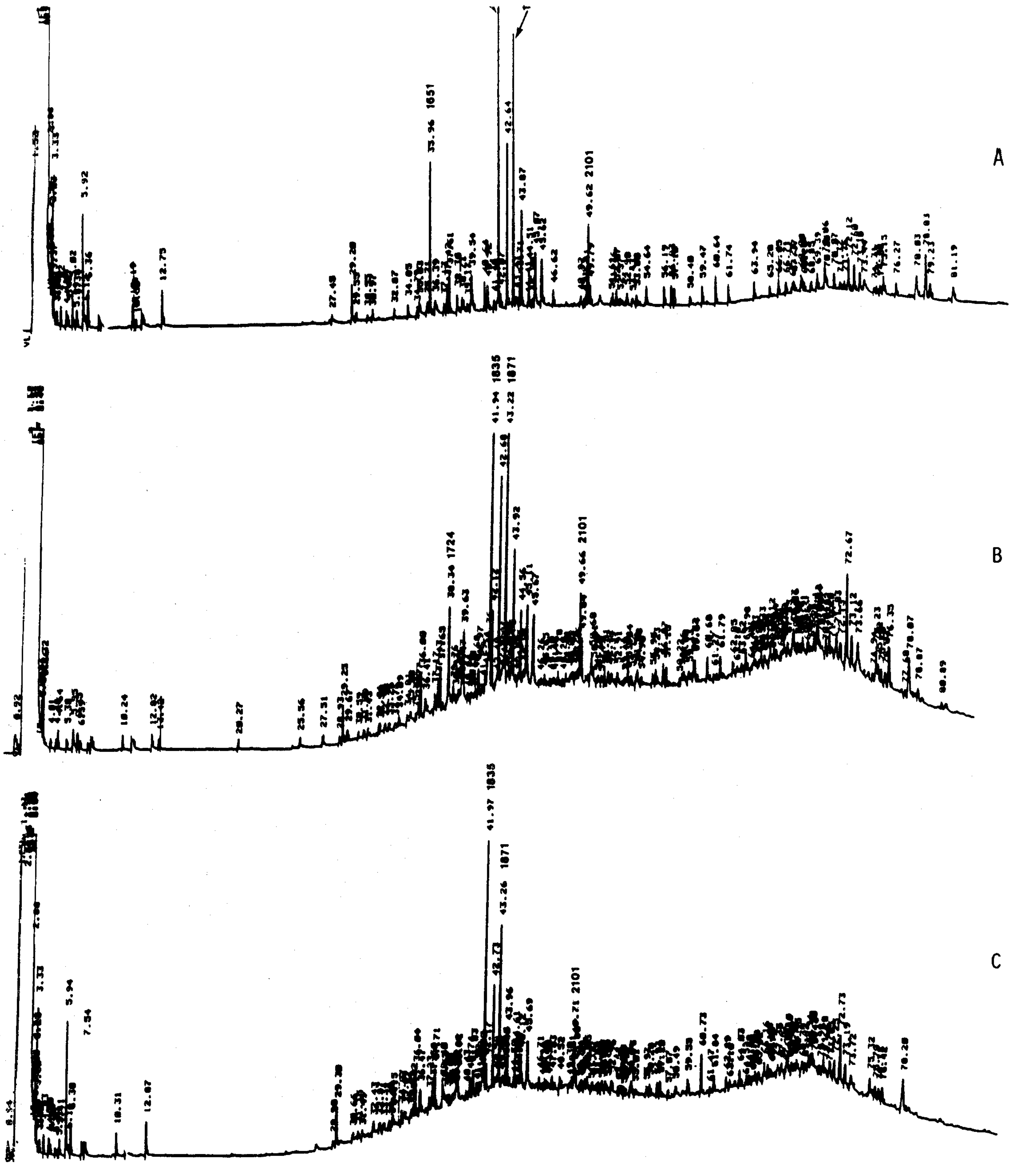

FIGURE 6-33. FID-GC Chromatograms of Filter Extracts from (A) Wave Tank #1 after 5 months, (B) Wave Tank #2 after 9 months, and (C) Wave Tank #3 after 9 months.

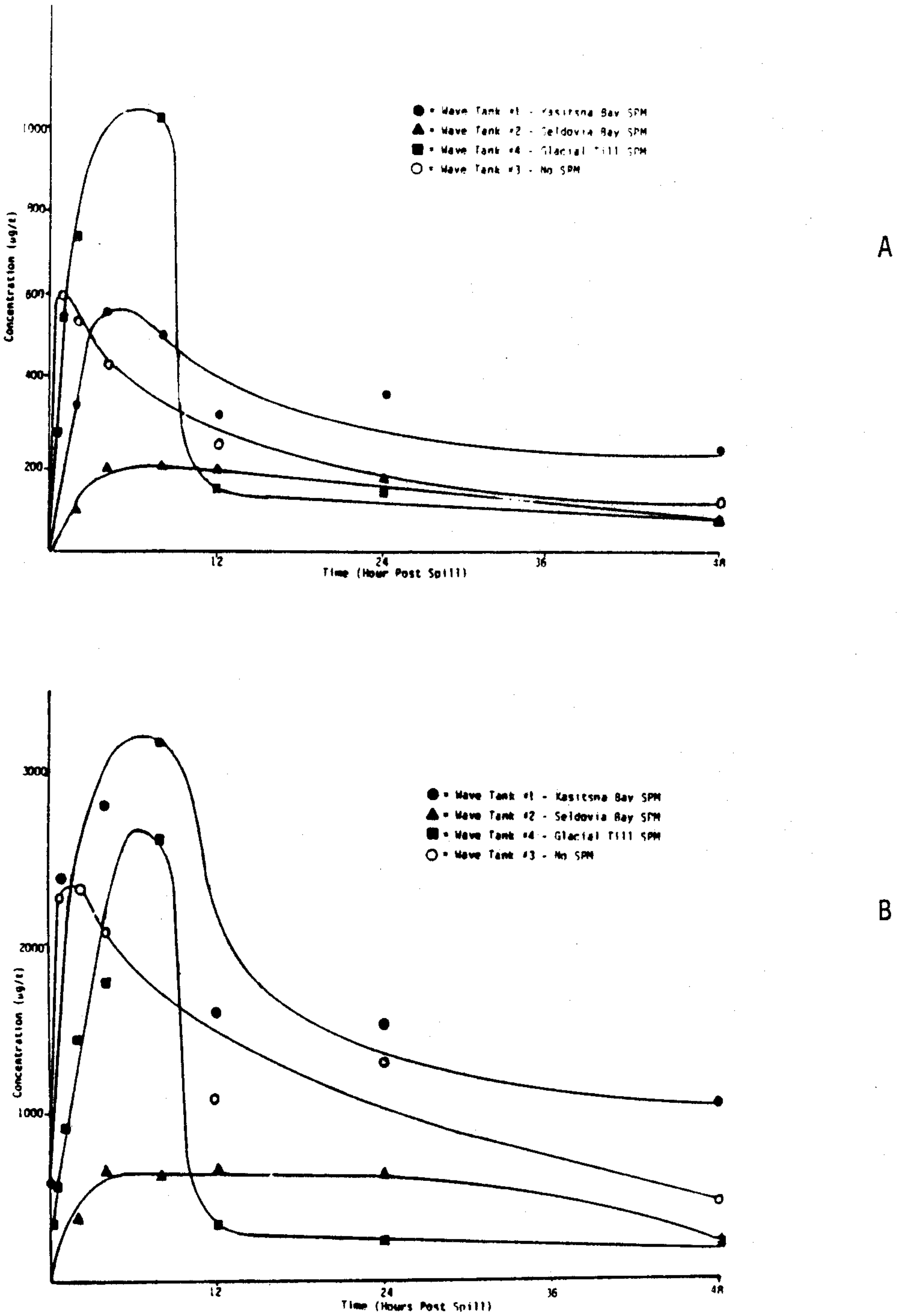

FIGURE 6-34. Time series concentrations of Dispersed/Particle Bound Oil from Wave Tanks #1-4. (A) Total Resolved Compound, and (B) Unresolved Compound Mixture.

unresolved and total resolved oil components would be expected to behave similarly.

With the exception of the control tank (no SPM added), the general trend of dispersed/particle bound oil concentrations is a rapid increase over the first four hours, with a peak concentration reached between four and eight hours after the spill. The concentration in the control tank peaks after only one hour and this is possible evidence that elevated levels of SPM may actually occlude dispersed oil and prevent its rapid return to the surface initially following the start of the spill. In all cases, the level of hydrocarbons associated with the particulate phase, drops from the maximum at about eight hours until, by nine to twelve days, there is little or no evidence of dispersed/particle bound petroleum related compounds present. It should be remembered, however, that dissolution of aromatic components -- although at lower absolute concentrations -- continues for months after the initial dispersion process has ceased (see Section 5.4.8). Indeed, comparison of Tables 6-10 through 6-13 (dispersed/particulate bound oil concentrations) with Tables 5-13 and 5-14 (dissolved hydrocarbon concentrations) shows that dispersed oil concentrations are roughly two to three times greater than dissolved oil concentrations in the water column during the first few days. Apparently, once the slick has weathered to a certain physical state (i.e., increased viscosity), dispersion is markedly reduced while dissolution can continue at compound-specific diffusion controlled rates.

Inspection of the total resolved compound concentrations, found in Tables 6-10 through 6-13, shows that wave tank #4 (glacial till SPM) contained the highest initial levels of hydrocarbons associated with dispersed/particle bound oil; wave #1 (Kasitsna Bay SPM) and wave tank #3 (no added SPM) showed approximately equal levels, and wave tank #2 (Seldovia Bay SPM) contained the lowest levels.

One possible explanation of these results would be that under the colder Fall/Winter spill conditions, evaporation of the less viscous, lower molecular weight components was initially inhibited, and as such, the early process as of dissolution, dispersion and spontaneous (microscale) oil-into-water emulsification would predominate (as observed). Then with the high levels of added glacial till SPM, oil-particle adsorption and increased slick viscosity (due to the lowered temperatures) resulted in the rapid decay in dispersed oil concentrations. That is, the oil that had initially dispersed was adsorbed and removed due to sedimentation, and at the colder temperatures, continued dispersion after 8-10 hours was inhibited. In comparing the three summer conditions, the Kasitsna Bay SPM (tank 1) and control (tank 3) which had no manually added SPM but ambient (3-4 mg/l) levels of SPM from the Kasitsna Bay seawater source behaved similarly. In these tanks, 200-300 μg/l levels of resolved components in the dispersed phase were observed out to 48 hours. In the presence of Seldovia Salt Marsh SPM (tank 2), the dispersed oil resolved component concentrations were depressed. This may be due to the dispersed oil being adsorbed by the added SPM (in static tank tests -- Section 6.2 -- Seldovia SPM had the highest oil affinity), and the then occluded material was removed by sedimentation. Because the control tank exhibited hydrocarbon levels similar, to the other tanks, we believe that dispersion, not direct SPM interaction with the surface oil slick, is the primary mechanism whereby petroleum hydrocarbons are introduced to the water column beneath a spill.

An inherent difficulty encountered, when measuring the amount of dispersion occurring in a wave tank experiment, is the randomness of oil drop sizes residing at any given depth below the slick. While small droplets (below the critical droplet size) can and do remain permanently associated with the water column, larger plunging drops will return to and coalesce with the slick, and these cannot be counted as truly dispersed oil. The amount of oil, sampled onto glass fiber filter, that might otherwise have returned to the slick is a factor of this randomness. Thus, the random nature of dispersion - and the problem it presents in experimental design, sampling and data interpretation - must be acknowledged.

Thus, regarding the concentration values presented, for the three types of SPM used, it cannot be said that Seldovia Salt Marsh SPM has the highest affinity for petroleum hydrocarbons, or that Kasitsna Bay SPM has the lowest affinity - rather, it can be said that dispersion processes overpower whatever adsorption potential a SPM has (at least as far as interaction with the surface slick is concerned).

The conclusions from the dispersed/particle bound oil portion of the Kasitsna Bay wave tank experiments can be summarized as follows:

- Dispersion processes overpower the SPM adsorption potential for surface oil using the three sediments examined.
- Dispersion is primarily operative initially following a spill and accounts for the majority of the petroleum derived hydrocarbons present in the water column; dispersed oil being responsible for two to three times more oil in the water column that present due to dissolution.
- Elevated levels of SPM may actually occlude dispersed oil during the first few hours following a spill resulting in enhanced removal (sedimentation) from the water column, and this process appears to be SPM source dependent.
- Dispersed or particulate bound oil does not contribute significant amounts of hydrocarbons to the water column once a stable mousse has been formed.

Hydrocarbon Incorporation into Bottom Sediments

Although the results of the experiments, presented above, show that dispersed/particulate bound oil entrainment into the water column decreases significantly as the surface slick viscosity increases, this does not imply that these mechanisms are not going to impact marine life. The fate of dispersed/particle bound oil is of extreme importance. Once introduced into the water column, dispersed and particulate bound oil can ultimately sink and become incorporated into the benthic sediment, as observed in all three wave tank systems. Because of the relative solubilities of aliphatic and aromatic hydrocarbons, however, the more toxic aromatics are preferentially removed during the SPM/dispersed oil interaction and sedimentation (particularly in well oxygenated and well mixed sediments where interstitial water exchange with bottom water can occur).

Thus, while evidence of petroleum derived hydrocarbon contamination of bottom sediments was found after just 13 days following the spill, and after periods of 5, 9, and 12 months; this contamination was primarily limited to aliphatic hydrocarbons, as essentially no oil related aromatic compounds were detected. The particulate phase of the water column was essentially clean 12 days following the spill in all tanks (see Figures 6-24, 6-26, 6-28, and 6-30), and subsequent long term sampling showed only the presence of biogenic material (see Figure 6-33).

The total resolved compound concentrations for incorporated aliphatic hydrocarbons in bottom sediments were highest when sampled 13 days after the spill. As noted previously, collected bottom sediments from wave tank #4 must be considered to be composed mostly of glacial till, whereas sediments collected at 5, 9 and 12 months from the other tanks are most likely comprised primarily of Kasitsna Bay sediment. Beaker oil/SPM experiments, conducted earlier, showed a concentration of 340 μg/g total resolved aliphatic hydrocarbon incorporation by glacial till compared to 161 μg/g after 13 days in the wave tank experiments. This lower value in the wave tank is no doubt due to the flow through nature of the tank, which (when considering the turnover time of one tank volume every three hours) would be expected to advect large amounts of oil-in-water before possible impact on bottom sediments. Comparison of beaker oil/SPM experimental results, using Kasitsna Bay SPM, with bottom sediments obtained from wave tanks months after the spill, are also useful. Beaker oil/SPM data shows that Kasitsna Bay SPM adsorbed 85 μg/g of aliphatic hydrocarbons per gram of sediment; and, wave tank bottom sediments showed values averaging approximately 40 μg/g. In both cases, partitioning of the lower molecular weight aliphatics and aromatics into the water column, with adsorption by SPM primarily limited to higher molecular weight aliphatics, was noted. However, bottom sediments collected months after the spill are expected to show lower values of total resolved hydrocarbons owing to dilution by uncontaminated sediments introduced into the tanks by the seawater system, biodegradation after incorporation, and advective removal of bottom sediments due to wave induced turbulence in the tanks.

Because GC/MS analysis showed no evidence of any petroleum derived aromatic compounds present in the bottom sediments and, because of evidence from particulate phase analysis - indicating no further addition of hydrocarbons via dispersion or SPM adsorption after 12 days - the following mechanism for incorporation of hydrocarbons by the bottom sediment is suggested. When the slick is fairly fresh, dispersion and SPM interactions occur; oil laden particles sink and become incorporated, while purely dispersed oil may possibly become entrained directly into the bottom sediments. As evidenced by data presented in Section 6.3.2.3, this process will occur only until the slick becomes weathered enough to form a stable water-in-oil emulsion. Once a stable mousse is formed there is very little additional input of hydrocarbons to the water column due to dispersion or SPM adsorption. Once assimilated into the bottom sediments, or concurrently during the sinking process, the highly soluble aromatic compounds and the more volatile aliphatic compounds become partitioned into the water column leaving the intermediate and higher molecular weight aliphatic compounds behind. Also, the aliphatic fraction makes up 4 to 5 times more mass in the starting oil, and any aromatics which did partition onto the SPM may have simply been below our detection limit. Microbial action with straight chain hydrocarbon preference, will then further degrade the incorporated oil.

Although we found that dissolution from the slick continued long after dispersion and particulate interactions had ceased, dissolution was principally restricted to aromatic compounds. Because no aromatic hydrocarbon contamination of bottom sediments was detected, these compounds were presumably advected away before possible impact with bottom sediments. This is not to say that aromatic compounds cannot be incorporated by bottom sediments. Indeed, the beaker oil/SPM partitioning experiments (discussed in Section

6.3.1) showed total resolved aromatic compound concentrations in the sediments tested, ranged from 9.6 µg/g to 385 µg/g. Therefore, important considerations regarding subsurface currents and depth to the bottom, among others, must be taken into account before a reliable forecast concerning possible hydrocarbon impact on the benthic sediments and organisms can be made.

The preferential partitioning of the higher molecular weight aliphatics into the wave tank bottom sediments and the observed absence of aromatic compounds in those sediments agrees well with the studies done by GEARING et al. (1979) and WINTERS (1978). Also, levels of oil adsorbed by bottom sediments are in reasonable agreement with levels determined in the small scale laboratory study completed by ZURCHER and THUER (1978).

6.4 LONG TERM FATE OF STRANDED OIL IN SELECTED REGIMES REPRESENTATIVE OF THE LOWER COOK INLET AREA

As another related aspect of the oil weathering program, SAI scientists participated in a collaborative effort with Drs. Griffiths and Morita of Oregon State University to evaluate long-term weathering trends in sub-tidal sediments which had been artificially contaminated with fresh and artificially weathered Cook Inlet crude oil. Because the results of these analyses detailed the long-term (up to 1 year) chemical weathering of sedimented oil, and are therefore relevant to the overall goals of this program, a copy of our report on the chemical analyses of the subtidal sediments has been included as Appendix G of this report. However, the results will be reviewed briefly below.

6.4.1 Long Term Fate of Stranded Oil in Sub-tidal Regimes

In the Griffiths and Morita program, fresh and artificially weathered* Cook Inlet crude oil samples were spiked into subtidal sediment quadrants, and these quadrants were then placed back into the subtidal regime in Kasitsna Bay and Sadie Cove (see Figure 6-4). Three levels of spiking were utilized: 50 parts per thousand (ppt), 1 ppt and 0.1 ppt (using both fresh and artificially weathered crude), and samples from these experiments were analyzed chemically at time 0 and after 1 year of natural weathering in the subtidal regime.

After one year, essentially no measurable hydrocarbon biodegradation took place in the sediments which had been spiked at the 50 ppt level with either fresh or previously weathered Cook Inlet crude oil. Additionally, GRIFFITHS and MORITA (1980) reported that from time-series experiments using sediments spiked at the 50 part per thousand level with fresh crude oil, the affects of the crude oil on glucose uptake would continue for 3 to 5 years and the effects on nitrogen fixation would continue for an estimated 2 to 8 years.

---

*Oil allowed to stand on seawater in static tanks for one week.

At 1 ppt extensive degradation of the lower molecular weight aliphatic fraction was noted, but many of the aromatic components were not degraded. Statistically significant reductions in glucose uptake rates, nitrogen fixation rates, and redox potentials and a significant increase in respiration percentages were also noted. Interestingly, the effects on nitrogen fixation in the 1 to 50 ppt oil range were limited to fresh Cook Inlet crude. The weathered crude oil did not produce the same effects at these concentrations.

In the sediments treated with 0.1 ppt crude oil there was essentially 100% degradation of both the aliphatic and aromatic components after one year. No significant changes in glucose uptake or respiration rates were noted, and methane concentrations, CO_2 production rates, nitrogen fixation and denitrification rates were not significantly affected. There was, however, an 89% reduction in redox potential in the quadrants at this level, and this finding was deemed to be important since redox potential is depressed after the crude oil has been degraded. It was suggested that the added carbon source plus the toxic effects of the oil itself caused an increased BOD in the system, and that this then further altered the sediment chemistry after the crude oil degraded.

Thus, while considerable data have been generated on the long-term fate and chemical weathering in oil in subtidal regimes in the Alaskan subarctic, no parallel set of data as yet exist on the rates and extents of the chemical weathering processes on stranded oil in sub-arctic intertidal zones. As part of this program then, a series of controlled intertidal oil-degradation experiments were initiated during the summer 1981 field study. The previously characterized sites, KB-1 through KB-4, plus an additional site (KB-5) at the head of Jakolof Bay (Figure 6-4), were thus revisited and a series of "controlled" intertidal sediment "oilings" were initiated.

6.4.2 Long Term Fate of Stranded Oil in Selected Intertidal Regimes

At each of the sites a series of three 1 m^2 vented corrals were buried in the intertidal sediments as the tide receded, and then each corral was "oiled" with 1.0 liters of fresh Prudhoe Bay crude oil. A corral was placed in the upper intertidal zone at an elevation such that tidal flooding was expected to occur only every 10 to 16 days during maximum tidal excursions. A second corral was then placed in the middle intertidal zone such that tidal action would be encountered daily, and finally, a third corral was buried in the lower intertidal zone such that during neep tides, the sediments would be continuously covered by seawater for several days. Table 6-16 shows the number of times each intertidal zone from each site was flooded per month.

The plywood corrals were prefabricated at Kasitsna Bay and then transported to each intertidal site by Boston Whaler. They were bolted together at each site as shown in Figures 6-35 and 6-36, and a narrow trench was then excavated taking care not to disturb the intertidal sediment surface in the center of the corral. The corrals were then lowered into place, and excavated sediment was repacked around the walls. Again, every effort was taken not to disturb the center portion of the corral where the oil penetration/weathering experiments were to be completed (Figures 6-37 and 6-38). No attempt was made to artificially mix the oil into the intertidal sediment, as the experiments were intended to simulate, as closely as possible, the effects of oil stranding after contamination during maximum tidal periods. Jakolof Bay was added to the other previously characterized sites; it is a location which experiences permanent shore-fast ice during several of the winter months. In this manner, it was hoped that the effects of this ice cover on intertidal oil weathering behavior could be examined. As shown by the scanning electron microscope data and oil adsorption potential results from these sites, significantly different intertidal substrates representative of several low energy intertidal regimes were encompassed in this study.

Initially, three intertidal areas were selected to represent three environments of significantly different long-range oil vulnerability as indicated by the associated Hayes/Gundlach Environmental Susceptability Index (ESI) (GUNDLACH and HAYES, 1978; HAYES et al., 1976). This approach was modified, however, to examine the long-term weathering rates of oil in selectively

Table 6-16 Intertidal Corral Sites - Number of Floodings per Month

	Number of Floodings per Month[a]		
Site Location	Lower	Middle	Upper
KB-1 (Grewingk Glacier)	58	58	.2[b]
KB-3 (Kasitsna Bay)	58	58	1
KB-4 (Seldovia Bay)	58	51	15
KB-5 (Jakalof Bay)	58	47	5

[a] - based on 30 days per month, averaged over one year

[b] - this corral (at 22.8 ft.) was flooded only two times in one year

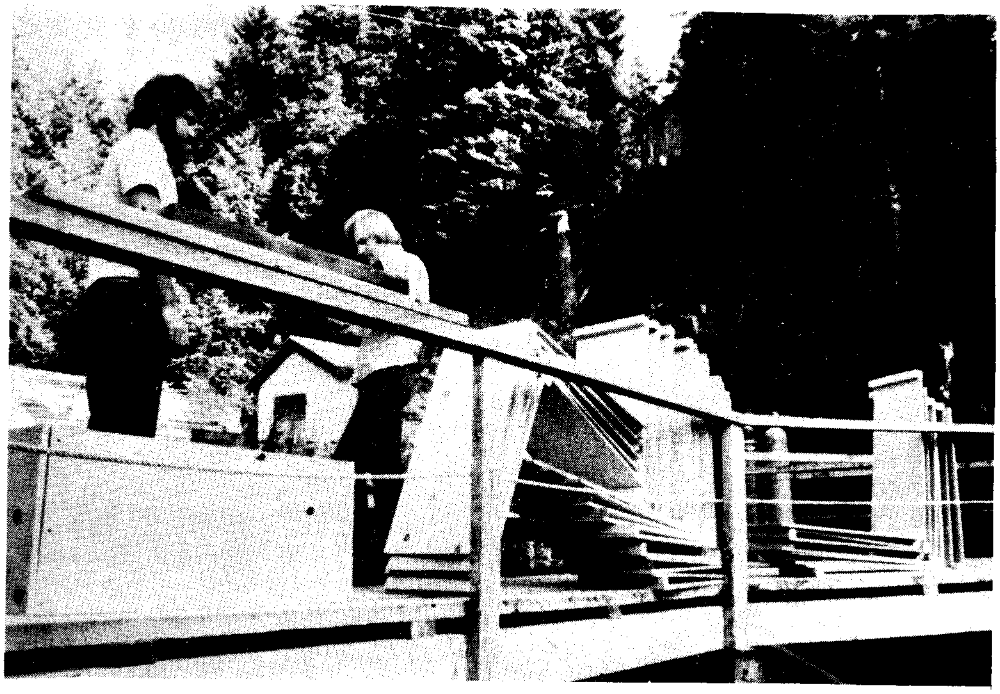

Figure 6-35. Prefabrication of intertidal plywood corrals at the Kasitsna Bay Laboratory.

Figure 6-36. Final construction of intertidal corrals at the site prior to placement.

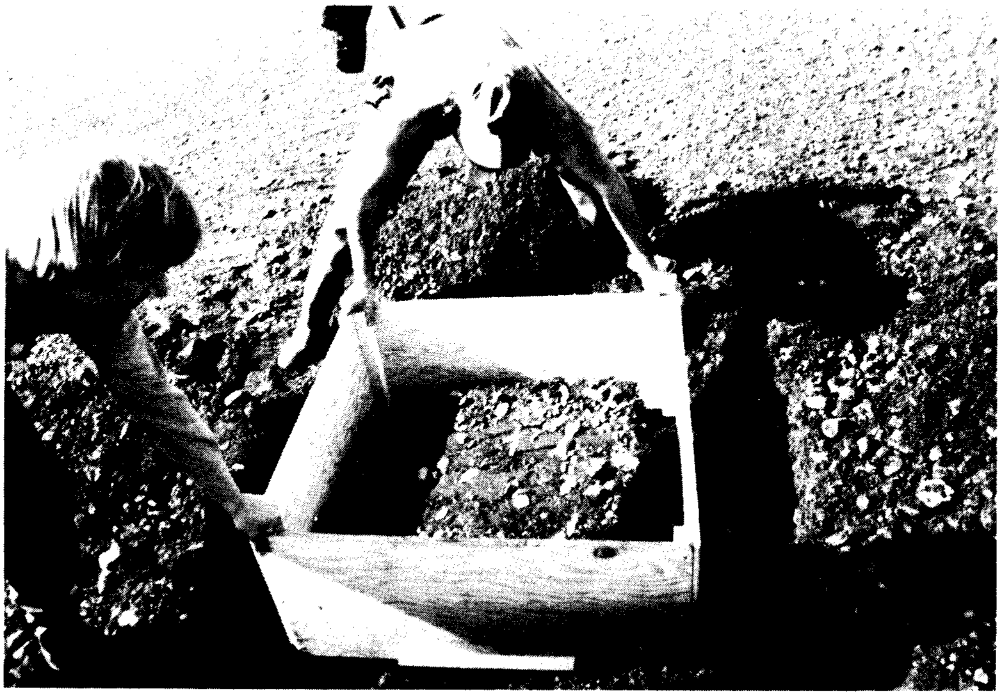

Figure 6-37. Placement of the corral in a trench surrounding an undisturbed area.

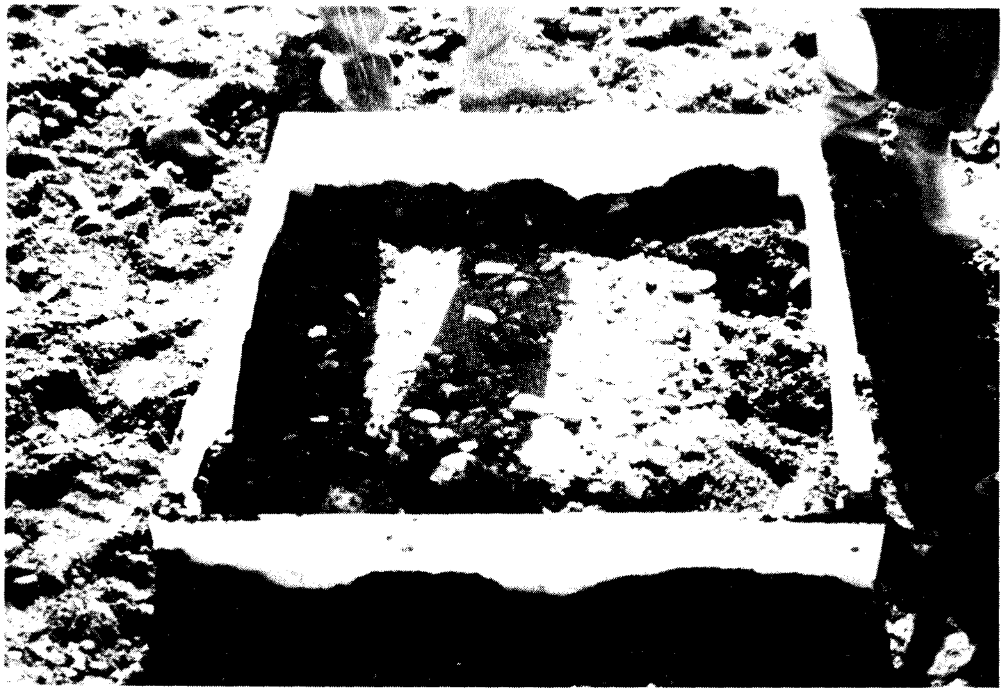

Figure 6-38. Excavated sediment is packed around the edges of the corral to secure it into place.

different low-energy intertidal regimes as a function of sediment type, detrital input, fresh water availability and tidal exposure. Thus, while each of the intertidal sites selected could be classified with ESI indices values of 9 and 10 (sheltered tidal flats and/or marshes) subtle differences due to the topography at the selected sites (including fresh water input, extensive *spartina* covering, possibility of wave scour, etc.) were included in the experimental design. Also, since the ESI ranges in value from 1 through 10, with 1 being the least vulnerable to oil spill impacts and 10 being the most vulnerable, it was believed that by only addressing sites with ESI indices of 9 and 10, those intertidal regimes which would be most problematic in the event of a "real" spill would be addressed.

The purpose benhind evaluation of differential hydrocarbon removal and oxygenated product formation is to determine if impact profiles can be generated as a function of the sub-arctic intertidal environment. These data will be useful to managers in oil spill predictions to assess long-term affects on different sub-arctic intertidal zones as a function of the energy regime and the sediment matrix. Correlation of these degradation rates with further refinement of numerical values (such as the Hayes/Gundlach index) might then be helpful in prediction and mapping ultimate long-term impacts for different intertidal zones. If oiled sediments from a particulate intertidal regime were removed by storm activities and then redeposited in the nearshore subtidal region, potential re-release of lower molecular weight aromatic compounds to the water column and/or inhibition of biotic activity as demonstrated by GRIFFITHS and MORITA (1980) in many of these sediments can take place. Knowledge of this potential behavior is felt to be important for long-term environmental impact assessment.

As noted above, data on longer term intertidal weathering of stranded oil was obtained by reoccupying the field sites during the ensuing Alaskan programs. Immediately after sampling the sediment from one of these sites, the sample was either extracted and analyzed at the Kasitsna Bay facility or shipped frozen to the La Jolla laboratory facility for extraction and analysis (Methods are presented in Appenidx G).

Several processes occur within the selected intertidal regimes that influence the rate at which oil is removed from the environment. They include: physical lifting of the surface oil with incoming tides; evaporation during exposed periods and dissolution during flooded periods; scouring and/or shifting of the sediment by tidal currents or storm-generated wave action; in-situ biodegradation of the oil as it remains trapped in the sediment; and sunlight induced photo-oxidation of oil in the surface sediments.

These processes all occur to varying degrees in a given setting depending on the specific intertidal regime and the location of the oil (corral placement) within that regime. The first process of oil removal (physical lifting with incoming tides) was a very important factor in the lower and middle intertidal corrals at all five sites. Typically, after initial oiling, the oil from the lower and middle corrals was observed to lift off the sediment with the incoming tide and wash out to sea. At the intertidal sites where this phenomenon wasn't observed visually, physical evidence of its occurrence was discerned by oil stains on the inner sides of the corrals. This observation was similar to the findings of Hayes et al., 1979 during the Amoco Cadiz oil spill. They reported that during the first week of grounding, oil lifted off the beach with each incoming tide and was redeposited on the ebb. During their second study period, one month later, they found the oil to be sediment bound. In contrast, the upper corrals weren't flooded until several days or weeks after oiling, so the oil had a much greater time to penetrate into the sediment and become more thoroughly entrained into the sediment matrix.

However, frequency and extent of tidal flooding influences other oil removal processes rather than just physical lifting of the oil. Tidal flooding enhances dissolution of lower molecular weight compounds into the water column, shifting and scouring of the sediment -- especially important if the corral is located in a tidal drainage channel, and microbial degradation -- because the seawater percolates through the sediment replenishing nutrients and dissolved oxygen that are utilized during biodegradation.

Another important factor influencing which processes are active in oil removal is the sediment type. The grain size and extent of sorting influence oil penetration (both the depth of penetration and the surface area of exposed oil), while the organic content and permeability influence absorbtive and adsorptive properties of the sediment and whether an oxidizing (or reducing) environment will prevail at a given site. Oil introduced into a reducing environment undergoes very few if any biodegradational changes with time (Bailey et al., 1973; Ward and Brock, 1978; DeLaune et al., 1980; and Ward et al., 1980).

As discussed previously in this section, these experiments were intended to simulate, as closely as possible, the effects of fresh oil stranding during maximum tidal periods. Since no attempt was made to artificially mix the oil into the intertidal sediment, homogeneous oil concentrations within the corrals were not expected. As such, a general decrease in oil concentrations with time was expected (and seen), but this decrease was only expected to be qualitatively significant. The majority of data from these intertidal corral studies lies in differences noted between and within sites during field observations. For instance, the timing and extent of regrowth (or absence of) for various plants, algae, mussel colonies, burrowing animals, etc. at each corral gave valuable information on the toxicity lifetime of oil contamination in a particular environment and the toxicity threshold of the resident biota. Depth observations revealed concentrated bands or pools of oil due to preferential penetration caused by sediment discontinuities and/or layering.

The presence of oil in the field was estimated visually, by smell (due to the characteristic odor of crude oil), or by feel (rubbing sediment between the fingers leaves a black, oily residue). Selected samples were then collected to support these field observations, and after chemical analysis, valuable data on the absolute concentration of oil in the sediments and qualitative differences in the individual components (i.e., ratios which indicate overall weathering and biodegradative processes) were obtained. These data were then the most useful in assessing the longevity of oil within the environment.

Although the five sites selected for corral placement had similar ESI vulnerability indices of 9 or 10, they were all different and characteristic of unique environments that would be encountered in the Lower Cook Inlet area. Detailed descriptions of each site are presented in Section 6.2. Briefly, Site KB-1 (Grewingk Glacier Spit) is characterized by a large, protected delta subject to tidal marine flushing and glacial meltwater input; KB-2 (China Poot Bay) is a protected tidal mudflat; KB-3 (Kasitsna Bay) is a tidal flat subject to significant tidal currents; KB-4 (Seldovia Salt Marsh) is in estuarine surroundings near the mouth of Seldovia River and is subject to fresh water (terrestrial) runoff and marine tidal waters; KB-5 (Jakolof Bay) is at the mouth of Jakolof River and subject to freshwater runoff and marine tidal waters (similar to Seldovia Salt Marsh but on a more sloping surface and without the heavy plant growth). Unfortunately, the logistics of reaching KB-2 (China Poot Bay) made frequent sampling visits difficult, and this intertidal site was abandoned shortly after its inception. Data and observations from each of the other sites are discussed in the following sections and figures of the intertidal profiles, generated using water-level transects, are presented. In addition, a combination of photographs, summary tables, bar graph illustrations, and gas chromatographic profiles from the sites are presented to support the observations.

6.4.2.1 KB-1 Grewingk Glacier Spit

This site was characterized by a significant gravel berm originating from glacial and marine deposits with a meandering stream containing glacial-melt waters running parallel to the coastline (Figure 6-39) and through extensive mud flats inshore of the gravel berm (Figure 6-40). Figure 6-41 shows the two dimensional profile of this intertidal site. This profile, and profiles of other intertidal sites, was generated in five meter increments using the water transect method illustrated in Figure 6-42. Measurements were begun at water level during a low tide, and height differences between ends of the five-meter tube were referenced to the known low tide height as transects progressed up the intertidal zone. The profile (Figure 6-41) shows that a

Figure 6-39. Site KB-1 (Grewingk Glacier Spit) - Transect data being obtained where the middle corral will be placed.

Figure 6-40. Site KB-1 (Grewingk Glacier Spit) - Glacier water stream that runs through the mud flats where the lowest corral will be placed.

Figure 6-41. Profile of Intertidal Corral Site KB-1 (Grewingk Glacier Spit)

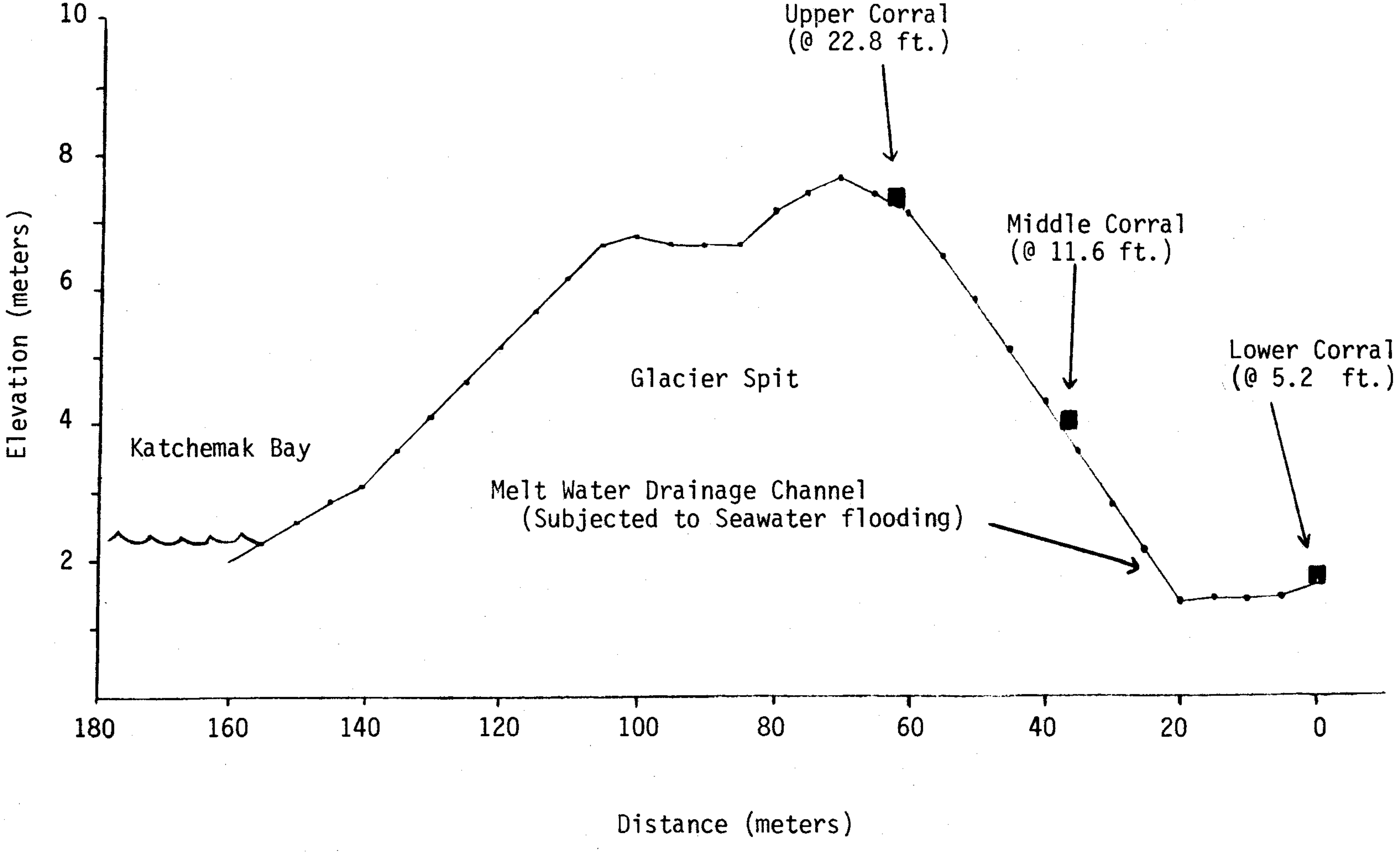

Figure 6-42. Example of the Water Level Transect Method used to obtain Profiles at the Intertidal Corral Sites.

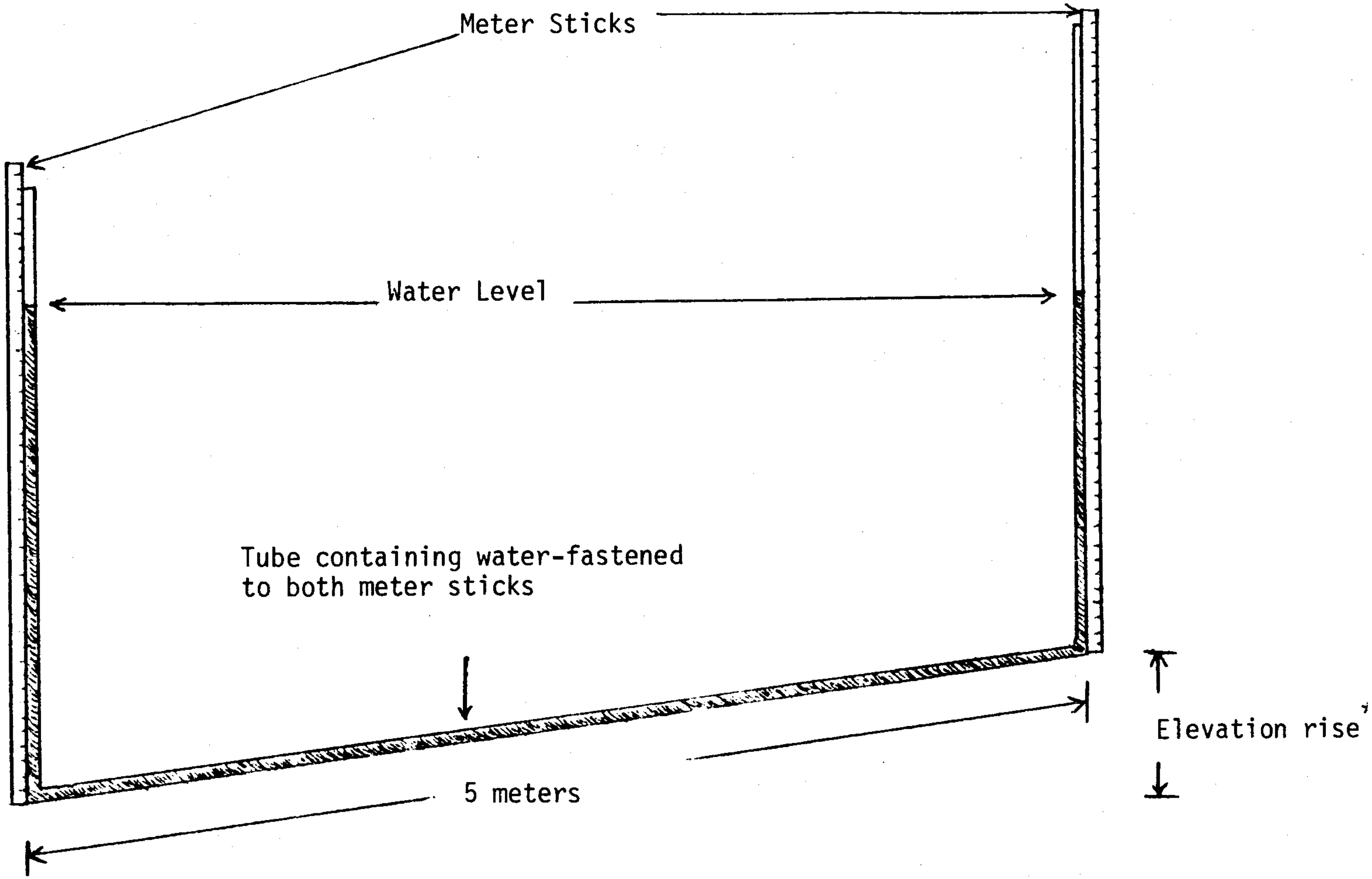

* The elevation rise is determined by difference (in cm) of readings on meter sticks at the water level

fairly steep slope of approximately 12% exists between the upper and middle corrals and continues on down to the meltwater drainage channel. The sediment levels out at this point and the lower corral is located on the other side of the channel on fairly level terrian. Figure 6-43 shows the relative distance and tidal height variation in the three intertidal corrals placed at this site. The corral in the foreground of the figure is in the lowest intertidal zone in the mudflats, and the corral in the center of the picture is in the mid-tide zone. The upper tidal corral is located just inshore of the crest of the berm near the scientists standing in the background.

The upper corral (buried near the top of the semi-permanent sand-gravel berm) was approximately 10 meters away from the highest high tide mark. The sediment was a fine, dark sand interspersed with rocks ranging from 3-20 cm in diameter. A number of green plants were also present, suggesting that this area is only occasionally inundated by seawater. The sediment at the middle corral was similar to the upper, except the sand was coarser and the rocks were a bit larger. The lower corral sediment was characterized by a very fine mud/silt of glacially and marine-derived materials. Significant amounts of stranded algae and mussels were present, and the mud was extremely soft to foot pressure (in some areas personnel to sank to mid-calf). The surface sediments at the lower corral were a light gray, but the mud was black at depths greater than ~ 1 cm. The odor of hydrogen sulfide in disturbed areas suggested a reducing environment in the subsurface sediments.

The corrals were oiled with 1.0 liters of fresh Prudhoe Bay crude oil and then allowed to undergo natural weathering processes for up to 17 months. Oil was spilled on September 1, 1981 during a receding low tide. The oil that was spilled into the lower corral formed pools and didn't appear to sink into the sediment to any great degree, although some was observed to percolate into the sediment through worm boreholes. At the middle and upper corrals, however, the oil sank in quickly (within 30 to 60 seconds) and only minimal pooling was observed. This site was occupied long enough for the tide to come in and cover the lowest corral. The oil which was still pooled on the surface

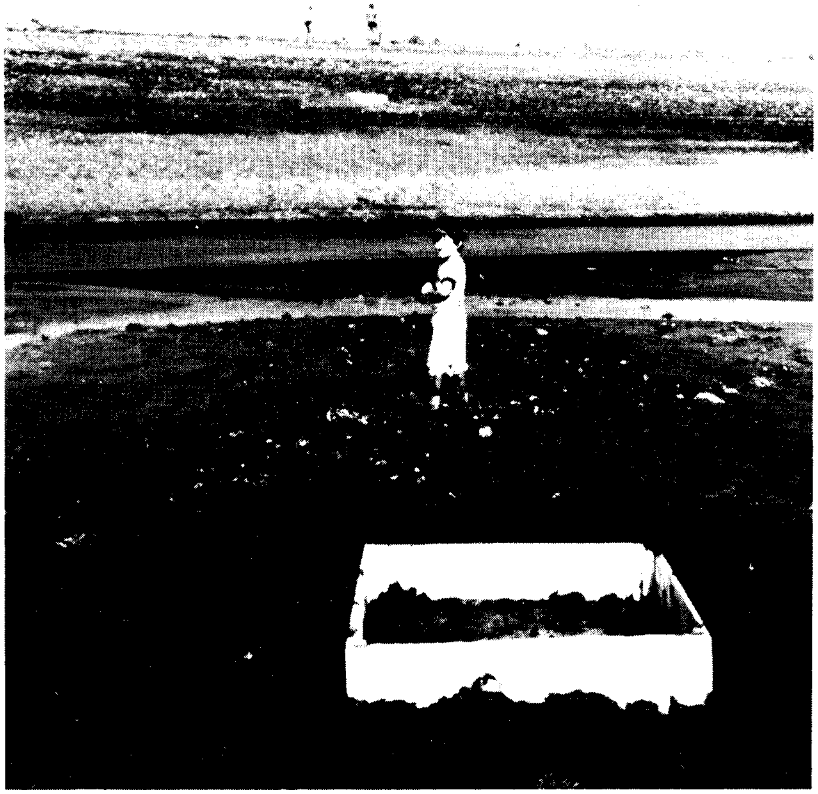

Figure 6-43. Relative distance and height variation for all three corrals placed at site KB-1 (Grewingk Glacier Spit).

was observed to lift off the sediment and float away on the water, while much of the oil that had soaked into the sediment was forced out hydrostatically, and it too floated away on the water surface. Figure 6-44 shows the aliphatic and aromatic FID-GC chromatograms of sediment from the middle corral, sampled immediately after the spill of 1 liter of Prudhoe Bay crude oil. Both fractions are characteristic of "fresh" Prudhoe Bay crude oil, i.e., an oil which hasn't undergone any alteration or weathering.

Returning to this site after 10 months, the lowest corral was found to be covered with algae and fucus. Figures 6-45 and 6-46 show the status of the low tide corral after 10 months. Deposits of fine, silty material were observed within the corral and on all the surrounding sediments. Although the tide was out beyond the corral, some standing water was still noted in the wet sediment. The drainage on this nearly level tidal flat appears quite poor. Sampling of the corral caused considerable amounts of silver and slightly colored sheen to form on the standing water, and a strong hydrogen sulfide odor was again noted. Figure 6-47 and 6-48 show the sheen formation at 10 and 17 months after initial oiling. Obviously, not all the oil at this lowest site was lifted out of the sediment on incoming tides.

The photographs in Figures 6-49 and 6-50 show the status of the middle and upper corrals after 10 months. The middle corral was observed to have filled with coarse sand and gravel to the upper limits of its wooden boundaries. Apparently, this intertidal area is subject to strong tidal and/or longshore currents causing significant sediment movement (shifting, slumping, etc.). When the new sediment was scraped away to its original level at the time of oiling, no observable evidence of oil contamination was seen. However, at a depth of 12 to 16 inches below the original level, a distinct oil smell was noted in the sediment. The upper corral, unfortunately, was observed to have been used as a fire-ring sometime between the one month and 10 month sampling periods. As such, all surface and near-surface samples were suspect due to pyrogenic input and/or alteration of existing oil. At eight inches below the sediment surface a sand layer was encountered which still had a very distinctive oil smell.

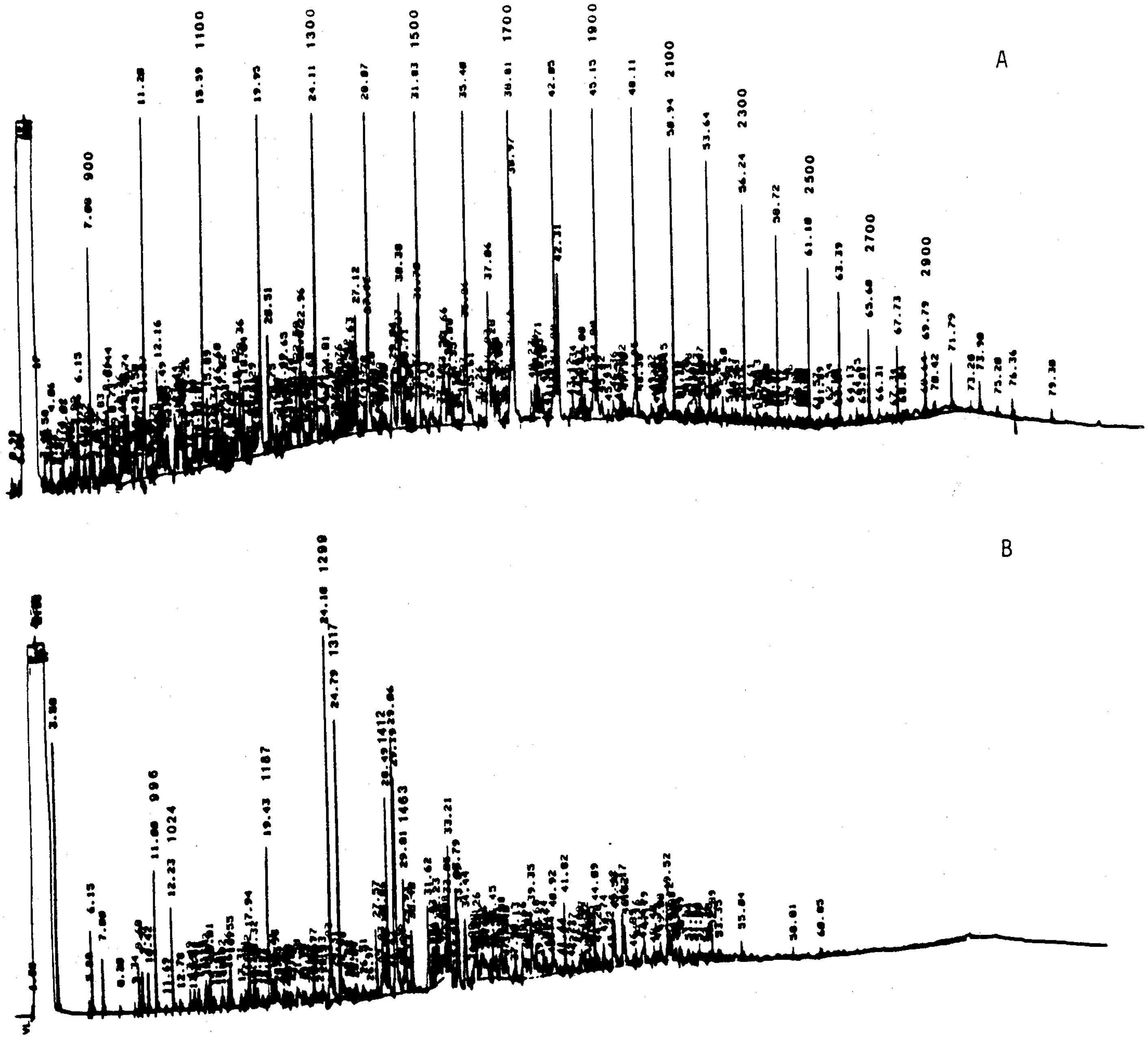

Figure 6-44. FID-GC chromatograms of sediment extracts from Grewingk Glacier (site KB-1). Middle corral immediately following a spill of 1 liter of Prudhoe Bay crude oil. (A) Aliphatic fraction, and (B) Aromatic fraction.

Figure 6-45. Site KB-1 (Grewingk Glacier Spit) - Appearance of the lowest corral after 10 months.

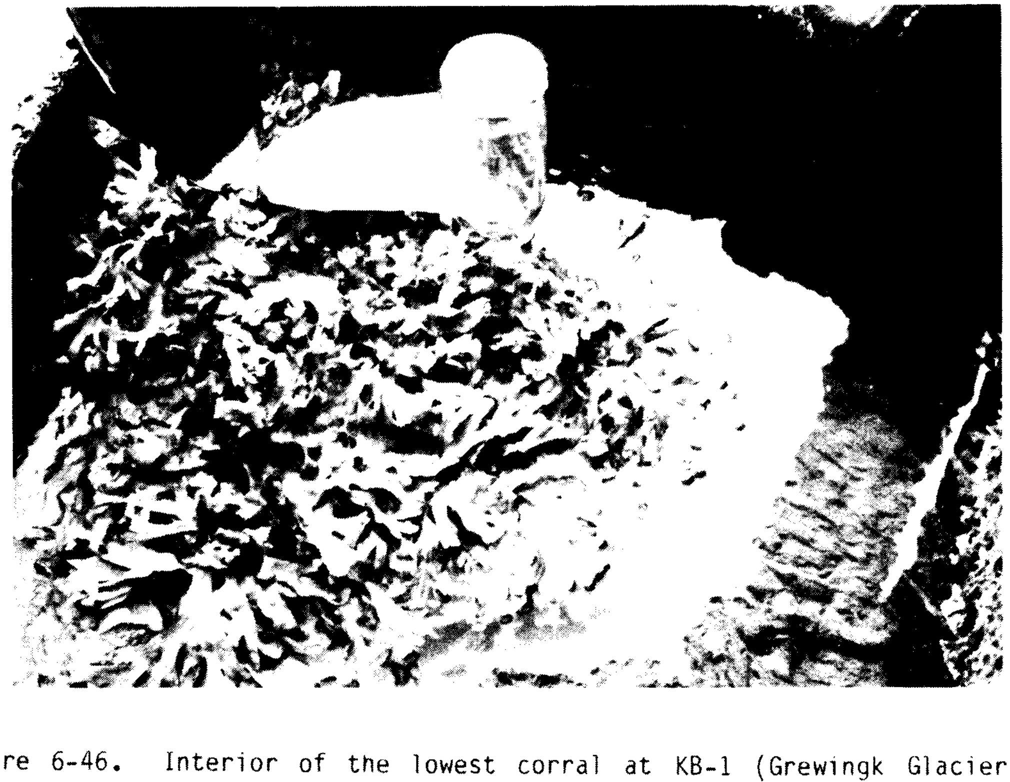

Figure 6-46. Interior of the lowest corral at KB-1 (Grewingk Glacier Spit) after 10 months of weathering.

Figure 6-47. Sampling at the lower corral at KB-1 (Grewingk Glacier Spit) after 10 months of weathering.

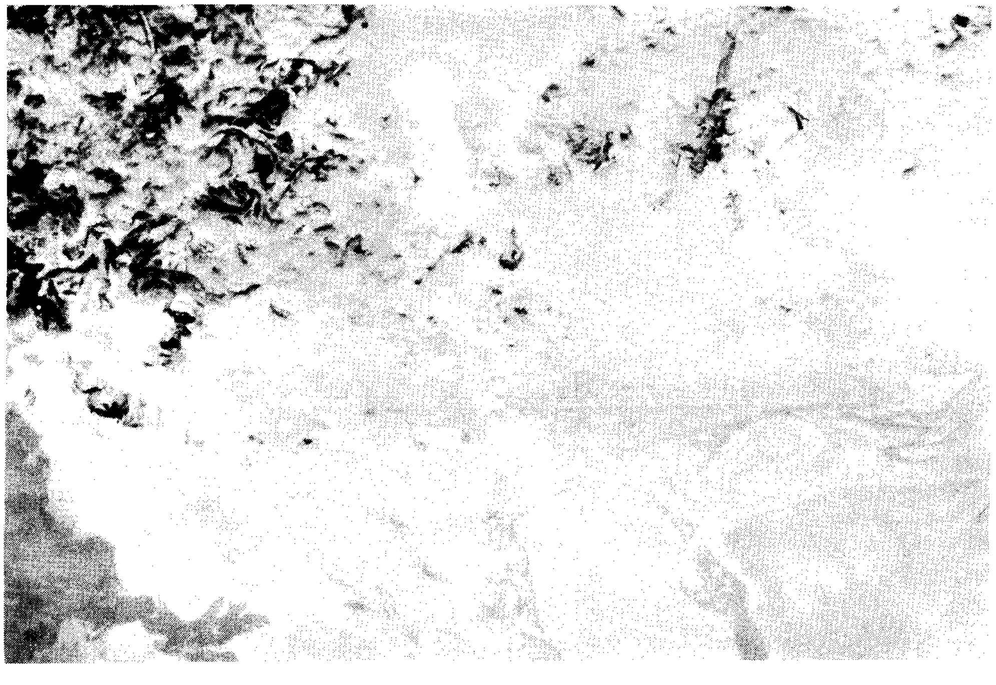

Figure 6-48. Sampling at the site of the lower corral at KB-1 (Grewingk Glacier Spit) after 17 months of weathering.

Figure 6-49. Site KB-1 (Grewingk Glacier Spit) Middle corral after 10 months of weathering.

Figure 6-50. Site KB-1 (Grewingk Glacier Spit) Middle corral prior to sampling after 10 months of exposure.

Figures 6-51 and 6-52 show chromatograms of sediment extracts from the corrals after 12 months of weathering. Comparing the aliphatic fractions from all three corrals in Figure 6-51 shows a distinct difference between the lower corral and the other two. Except for the branched isoprenoids pristane, phytane, and farnesane, the lower corral sediment had very few resolved peaks of consequence. Some of the higher molecular weight n-alkanes (ranging from nC-24 to nC-32) were present, but they too were only present at very low concentrations. The middle and upper corrals, on the other hand, contained oil which had been altered very little (except for loss of light ends) from the "fresh" parent oil that was spilled 12 months earlier. Evidently, the oil at the lower corral was largely removed by initial tidal flushing and it had undergone more extensive degradation than at the other two corrals. The aromatic fractions for the middle and upper corrals in Figure 6-52 show the upper to have more resolved compounds. This possibly suggests less weathering at the upper corral, and presumably reflects the infrequency of tidal flushing and the porosity of the sediment which allowed signficant oil penetration on initial oiling.

At 17 months a depth profile of the upper corral was completed. The chromatograms in Figure 6-53 show aliphatic and aromatic fractions from depths of 10 inches and 24 inches, respectively. Table 6-17 compares total resolved and unresolved concentrations for the two, and various ratios that indicate weathering and biodegradation. The chromatograms and the table are remarkable in that they show very little alteration of the oil over the 17 month period. This is probably a reflection of the limited tidal flooding at the upper corral and, owing to the depth of sinking, limited evaporative losses. The sediment-bound oil contains n-alkanes down to nC-11 (as compared to oil from a wave tank experiment of similar duration which shows total loss of n-alkanes up to nC-15). The sediment from the upper (and middle) corrals is a porous sand-gravel mixture having very little interstitial water. This type of substrate allows the oil to sink very quickly, and to a greater depth, than it would at a fine-grained site like the lower corral.

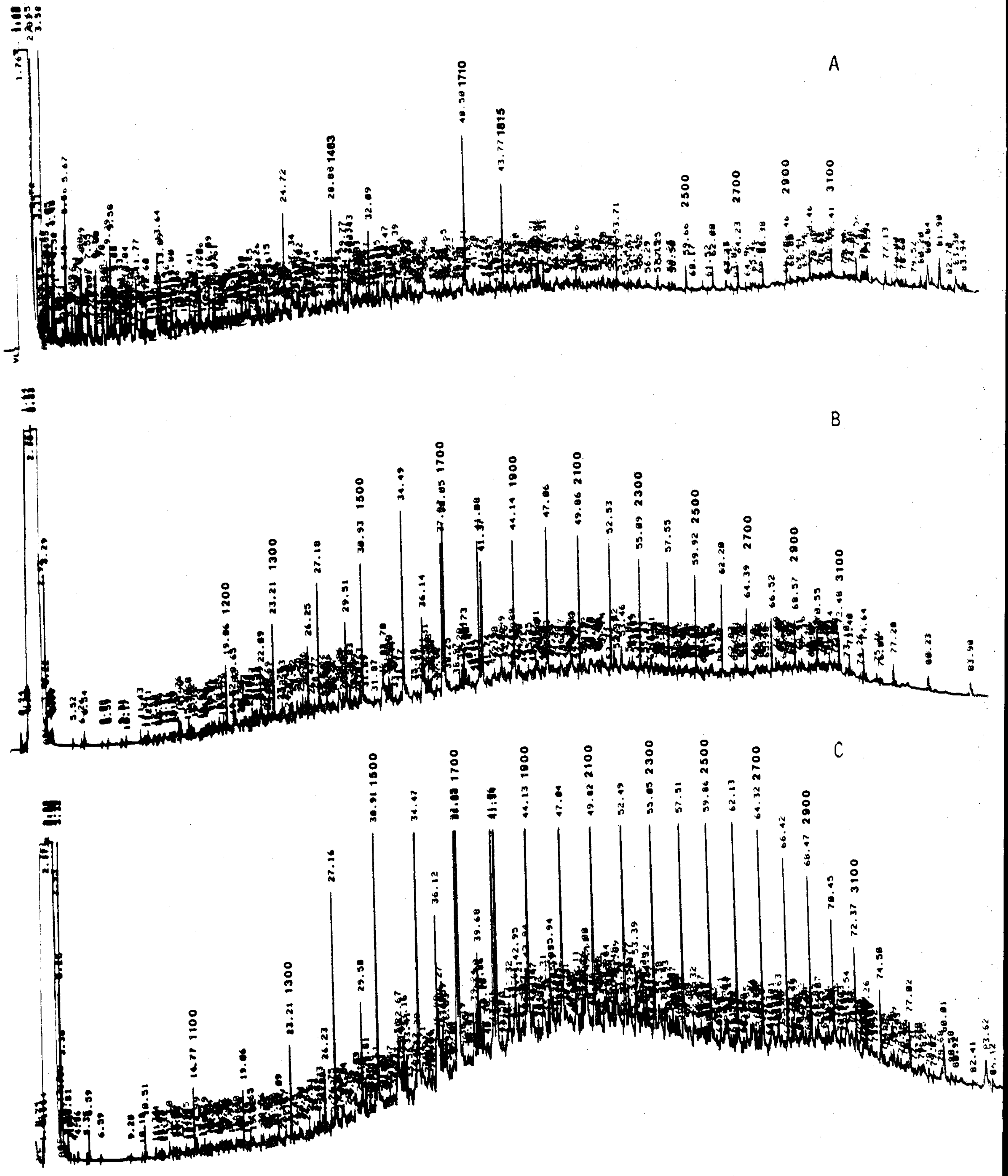

Figure 6-51. FID-GC chromatograms of sediment extracts from Grewingk Glacier (site KB-1). Aliphatic fraction 12 months after a spill of 1 liter of Prudhoe Bay crude oil. (A) Lower, (B) Middle, and (C) Upper Intertidal corral sites.

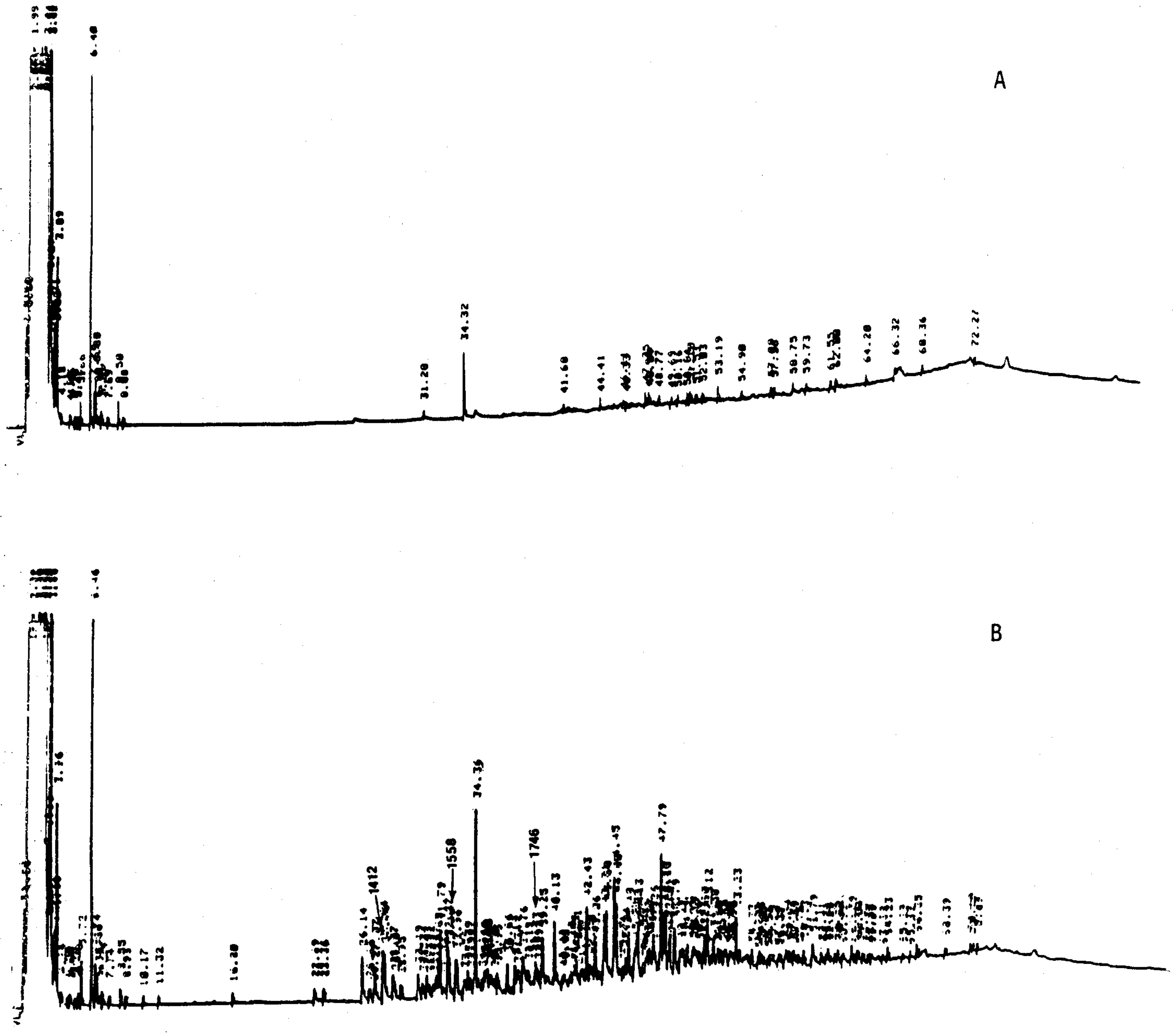

Figure 6-52. FID-GC chromatgrams of sediment extracts from Grewingk Glacier (site KB-1). Aromatic fraction 12 months after a spill of 1 liter of Prudhoe Bay crude oil. (A) Middle, (B) Upper Intertidal corral sites.

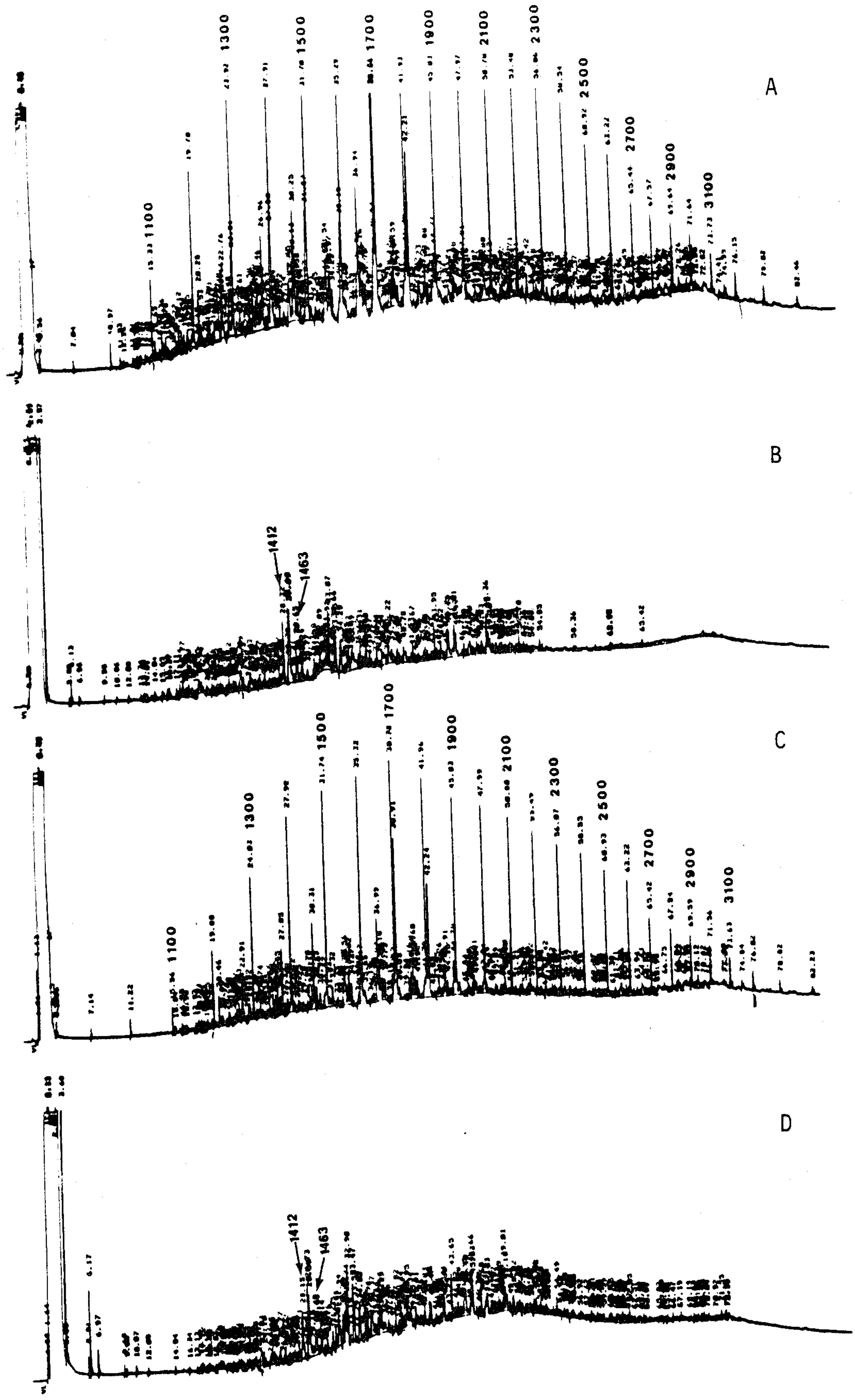

Figure 6-53. FID-GC chromatograms of sediment extracts from Grewingk Glacier (site KB-1). Upper corral site 17 months after a spill of 1 liter of Prudhoe Bay crude oil. (A) Aliphatic fraction from a depth of 10", (B) Aromatic fraction from a depth of 10", (C) Aliphatic fraction from a depth of 24", and (D) Aromatic fraction from a depth of 24".

TABLE 6-17. KB-1 GREWINGK GLACIER SPIT

Depth Profile of Hydrocarbon Concentrations and Weathering Ratios in the Upper Intertidal Corral at 17 Months Post-Spill

Sample depth (inches)	Total Resolved Concentration	Total Unresolved Concentration	nC-17/ pristane	nC-18/ phytane	Total Resolved/ Total Unresolved
10"	221 ug/g	887 ug/g	1.5	2.1	0.25
24"	48 ug/g	187 ug/g	1.3	1.7	0.26
Reference [a]	—	—	1.8	2.1	0.35

a - The Reference values were calculated by multiple FID-GC analyses of "fresh" unaltered Prudhoe Bay crude oil.

After 17 months, the low tide corral had been washed away by ice scour and excessive run off from the Grewingk Glacier and surrounding water sheds. The former location of the corral could be determined, however, by triangulation with stable landmarks and the positions of the upper and middle intertidal corrals. Digging in the general area where the corral had been located caused oil droplets to come to the surface, emitting considerable sheen as shown in Figure 6-48. Figure 6-54 shows chromatograms from the lower corral after 17 months. Again, these chromatograms emphasize the extensive alteration that has taken place at the lower corral. Similar to the 12 month sample, the branched isoprenoids pristane, phytane, and farnesane clearly predominate over the other resolved peaks, although a suite of n-alkanes from nC-23 to nC-31 is seen. Except for one very large unidentified peak at Kovat 1638 in the aliphatic fraction, these chromatograms are nearly identical to those generated from the 12-month sediments.

A summary of absolute concentrations in the sediments over time is presented in Table 6-18, and illustrated with bar graphs in Figures 6-55 and 6-56. (When more than one depth sample was analyzed these concentrations represent an average value.) As expected, the concentration of oil in the sediment diminishes with time. However, when comparing the two bar graph illustrations, the total resolved components generally show a greater rate of reduction than the total unresolved complex mixture. This indicates that the oil is not only experiencing physical removal, but undergoing alteration processes such as evaporation, dissolution, and biodegradation. The apparent increases in relative concentrations at selected locations (e.g., Middle Corral at 1 and 10 months) also reflect the heterogeneity in the sediments due to slightly different percolation rates and the experimental difficulties in always obtaining a "representative" sample.

Although Table 6-18 and the bar graph illustrations show the general trend of diminishing oil concentration with time, they are somewhat misleading for the lower corral. As was noted in the field observations, most of the oil at the lower corral was lifted from the sediment on the first incoming tide.

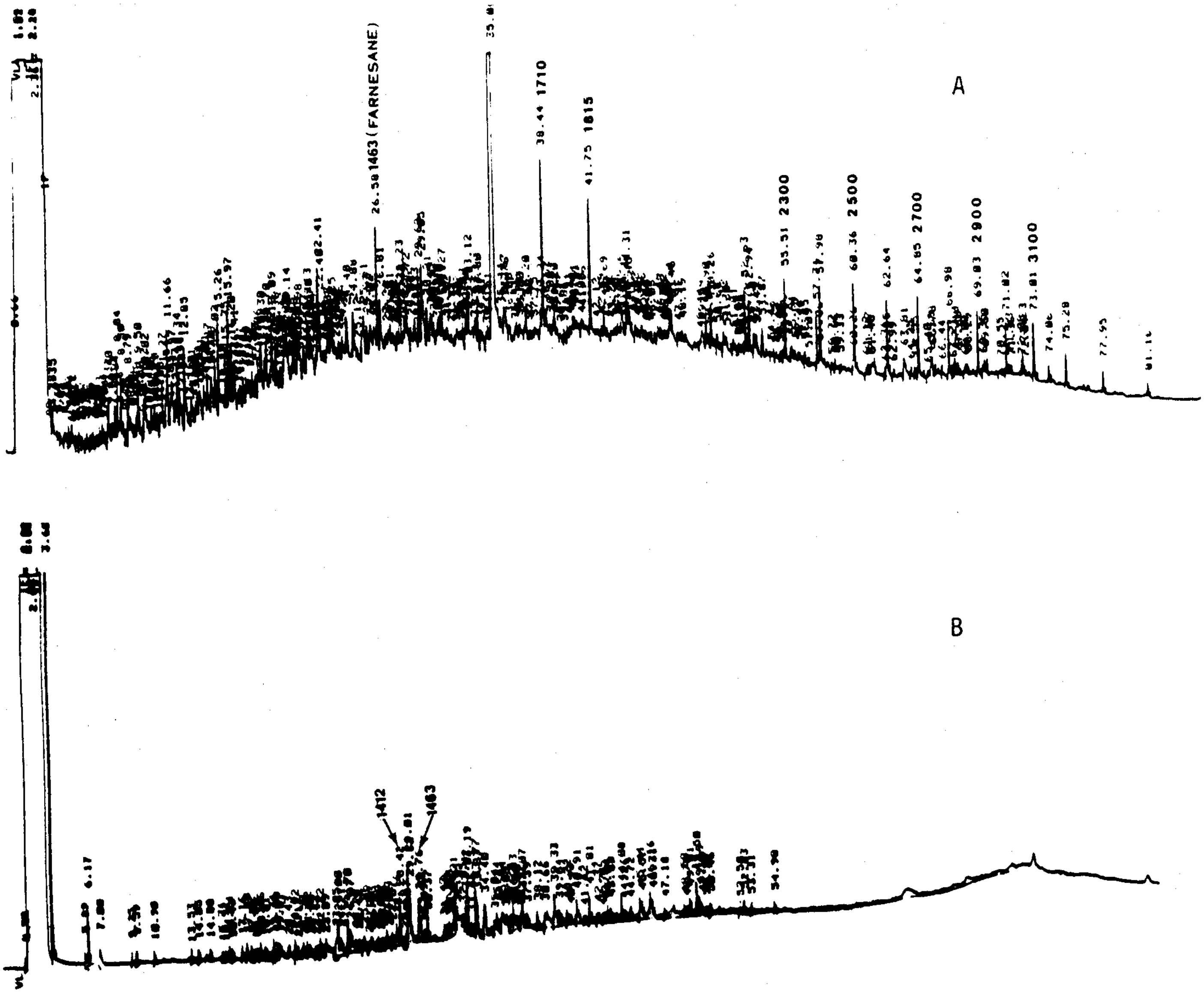

Figure 6-54. FID-GC chromatograms of sediment extracts from Grewingk Glacier (site KB-1). Lower corral site 17 months after a spill of 1 liter of Prudhoe Bay crude oil. (A) Aliphatic fraction, and (B) Aromatic fraction.

TABLE 6-18. KB-1 GREWINGK GLACIER SPIT

Concentration of Total Resolved and Unresolved Compounds in the Intertidal Sediments at Various Times Post-Spill (all concentrations in ug/g)[a]

		Day 0	Day 4	1 Month	10 Months	12 Months	17 Months
UPPER CORRAL	Total resolved (ug/g)	2,588	1,060	1,169	891	122	135
	Total unresolved (ug/g)	8,112	4,615	5,092	1,797	607	537
MIDDLE CORRAL	Total resolved (ug/g)	7,507	1,878	230	590	251	43
	Total unresolved (ug/g)	27,228	9,151	2,102	9,635	3,717	658
LOWER CORRAL	Total resolved (ug/g)	618	NA[b]	137	NA	18	42
	Total unresolved (ug/g)	2,934	NA	435	NA	188	713

a - When more than one sample was analyzed for a specific time point these numbers represent average values.

b - NA indicates sample not analyzed or not available.

KB-1 GREWINGK GLACIER SPIT

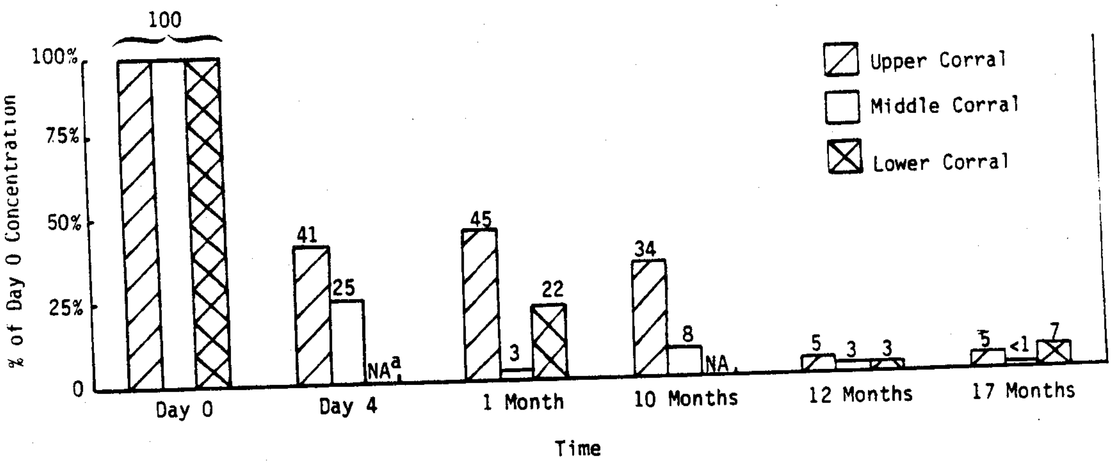

FIGURE 6-55. Relative Abundance of Resolved Compounds Remaining in the Sediment at Various Times Post-Spill.

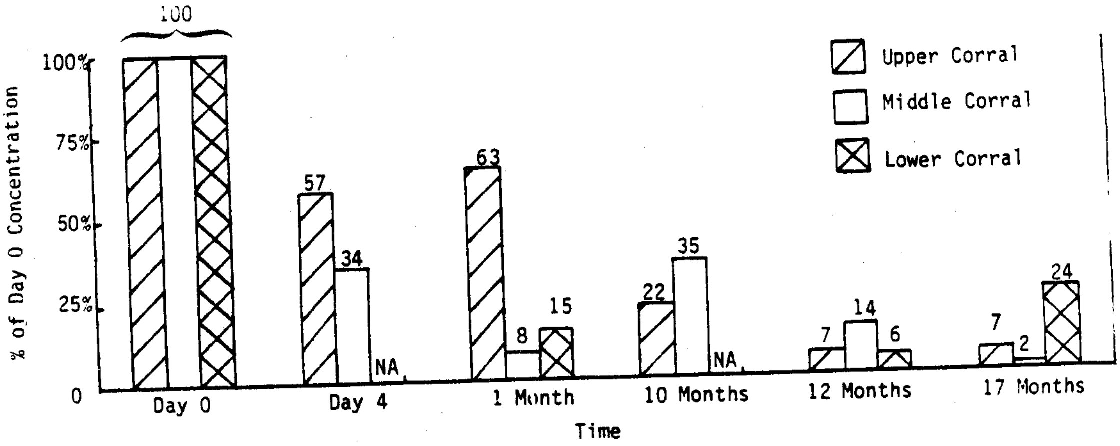

FIGURE 6-56. Relative Abundance of Unresolved Compounds Remaining in the Sediment at Various Times Post-Spill.

[a] NA indicates sample not analyzed or not available.

The Day 0 concentration of oil in the sediment reflects this phenomenon since it is nearly an order of magnitude less than the middle and upper levels. Consequently, the oil concentrations at the lower corral don't drop as quickly as one would expect, but this is simply an artifact of the Day 0 lifting. When this factor is taken into account, the oil seems to be most persistent at the upper corral. It had the highest absolute concentration of oil in the sediment after 17 months, and showed the slowest rate of removal.

The bio-toxicity lifetime of the oil at the lowest intertidal corral appeared quite short; after only 10 months the corral had a mussel community growing within its boundaries and numerous algal growths and Fucus attached to the sediment and on the corral borders (previously stained with oil). Bio-toxicity interpretations at the middle and upper corrals were not as easily made since there was very little pre-spill bio-growth at these locations. The middle corral was located on a steeply sloping sand-gravel substrate. Observations showed it to be filling with sand and gravel, indicating that this intertidal area is subject to moderate sediment shifting, slumping, etc. The upper corral was located near the permanent berm which had a variety of green plants and other growth, but because it had been used as a fire-ring it was difficult to make conclusive plant growth observations. Any plants which were growing in the corral would have been burned by this fire, and dormant seeds would have been destroyed as a result of the intense heat.

One other important consideration in reviewing these data is that the absolute concentrations in Table 6-18 represent selective samplings of the corrals. Sediment from each corral was carefully inspected and only those patches where oil was observed were sampled. After 17 months of weathering, oil was not observed at the upper corral until 10 inches of surface sediments had been removed. In actuality, the concentrations in Table 6-18 represent a worst case. A large, homogeneous sample of the sediment would probably have shown far lower concentrations of the oil with time.

6.4.2.2 KB-3 Kasitsna Bay

Much of Kasitsna Bay is a tidal mud flat characterized by dense mussel beds (Mytilus edulis) and intense algal growth (mostly Fucus). The water transect of this intertidal site is shown in Figure 6-57. As the profile shows, both the upper and middle corrals were located on a tidal slope of approximately 7%. About halfway between the middle and lower corrals the sedimments leveled out to a tidal flat where the lowest corral was located. Figures 6-58 and 6-59 show photographs of this intertidal site. These mudflats are protected from erosion into Kachemak Bay by MacDonald Spit (terminating at Nubble Point) as shown in the chart in Figure 6-4. The spit is well above the highest high tide level and supports a significant growth of pine and other needleleaf evergreens (see Figure 6-59).

The upper intertidal zone of MacDonald Spit received considerable amounts of beach wrack (logs, timber, and other debris) from occasional storms. The Upper corral was placed about 1 meter away from the kelp line (indicating the limit of the most recent high tides). A large log was located about 1 meter seaward of the corral and probably shielded it from some water-wave exposure and tidal currents (see Figure 6-60). The sediment at this site was homogeneous down to at least 18 inches (depth of corral placement) and primarily contained sand with some cobble sized rocks ranging from 1 to 3 cm in diameter. The sediment at the middle corral (Figure 6-61) was the same type of unconsolidated sand and gravel mixture, however, it was covered with a thin 1-2 mm coating of very fine sedimentary ooze. Below this ooze the sediment was homogeneous and appeared to be well oxidized. Numerous shell fragments, barnacles and some marine algae were also present; probably deposited by receding tides. During burial of the corral, water was encountered at a depth of about 12 inches, and this could affect the depth of maximum oil penetration. The lowest intertidal corral was located in the tidal mudflats (Figure 6-62). Similar to the middle corral, the surface of the sediment at this site was covered with a thin layer of gray sedimentary ooze. Below the ooze, the sediment was black and smelled anoxic. It was very wet and quite soft to

Figure 6-57. Profile of Intertidal Corral Site KB-3 (Kasitsna Bay)

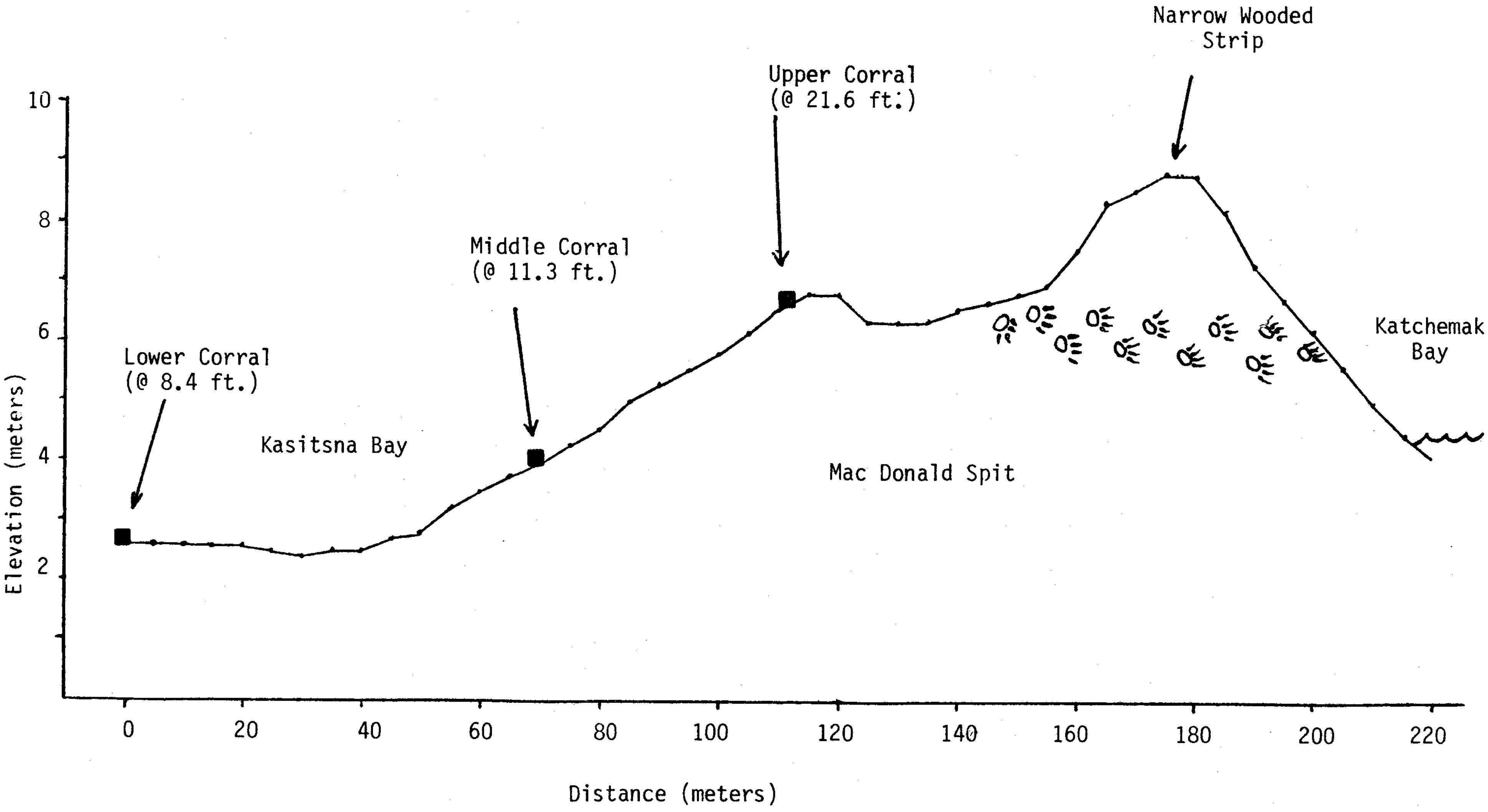

Figure 6-58. Site KB-3 (Kasitsna Bay) Collection of sediment for characterization purposes.

Figure 6-59. Site KB-3 (Kasitsna Bay) mud flats where the lower corral will be placed.

Figure 6-60. Position of the upper corral at site KB-3 (Kasitsna Bay).

Figure 6-61. Position of the middle corral at site KB-3 (Kasitsna Bay)

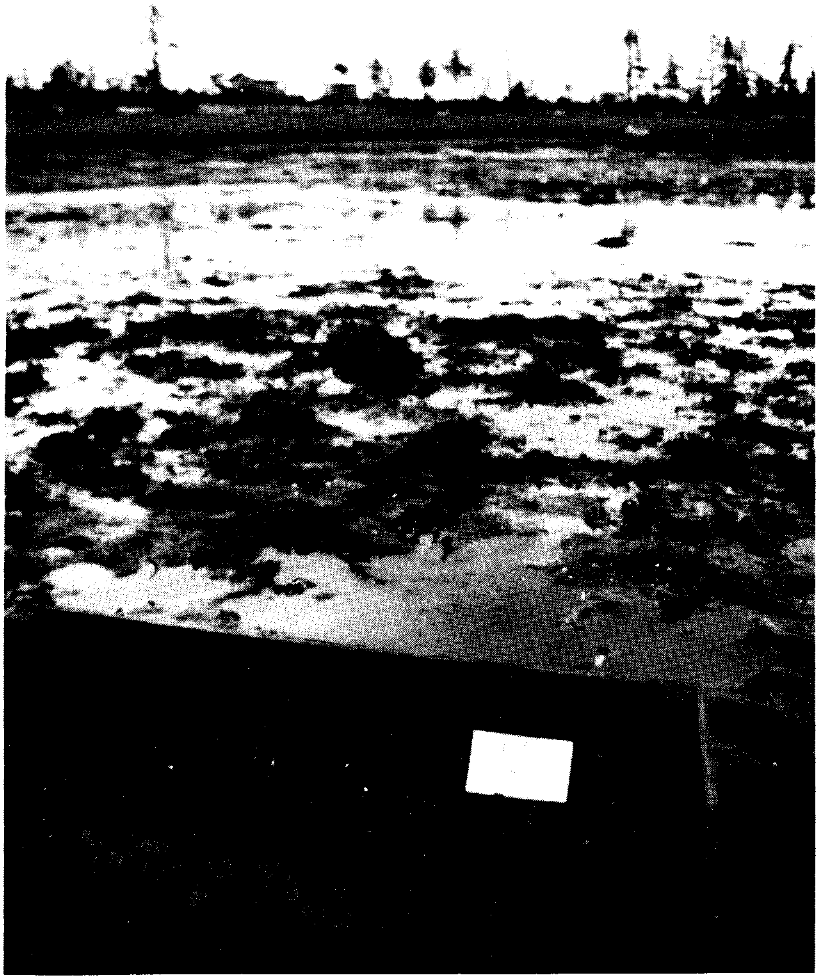

Figure 6-62. Appearance of the lower corral at site KB-3 (Kasitsna Bay) immediately after oil addition on September 12, 1981.

foot pressure. Numerous clam burrows, mussel communities, and various algal growths were noted at this locale. This site was inundated by tides on a daily basis and standing pools of water were present during all but the lowest tides (Figure 6-62). Sediments from all three corral sites were analyzed prior to oiling and the chromatograms from these samples are presented in Figure 6-63. As the figure shows, very few resolved peaks were detected in these background samples.

The oil was spilled on September 4, 1981, thirty minutes before a four foot low tide. At the low corral, very little of the oil was observed to sink into the sediment. Most of it pooled in depressions caused by corral placement, or floated on the standing water present in some of the depressions. As oil was spilled at the middle corral, the sloping surface within the corral caused much of the oil to flow towards the seaward corral wall. The oil pooled into depressions near the edge of the corral and sank within 2 to 3 minutes. However, the undisturbed quadrant in the middle of the corral still had small standing pools of oil (approximately 8 mm thick) on the ooze surface. Apparently, the surfacial flocculate material hindered the oil from penetrating into the coarser-grained sediment below. In an effort to correct for the slope, oil at the upper site was spilled onto the uppermost part of the corral, giving it more time to penetrate the sediment before flowing to the downhill edge of the corral. The oil sank quickly into this coarse-grained sediment matrix, and no pooling was observed. Before leaving MacDonald Spit, the low intertidal corral was re-occupied for further observations. Thirty minutes after addition, most of the oil was still observed in standing pools. As such, penetration was limited at this corral.

Returning to the lowest corral after 7 days, oil sheen was still observed on the standing water within the corral. The sides of the corral were oil-stained, suggesting that the incoming tide had lifted oil off of (and out of) the sediment. At the middle corral there was no visible evidence of oil on the sediment surface, but underlying rocks were stained. The uppermost site still hadn't been covered by the tides and oil was visibly evident. The sediment within the corral looked like dark coffee grounds.

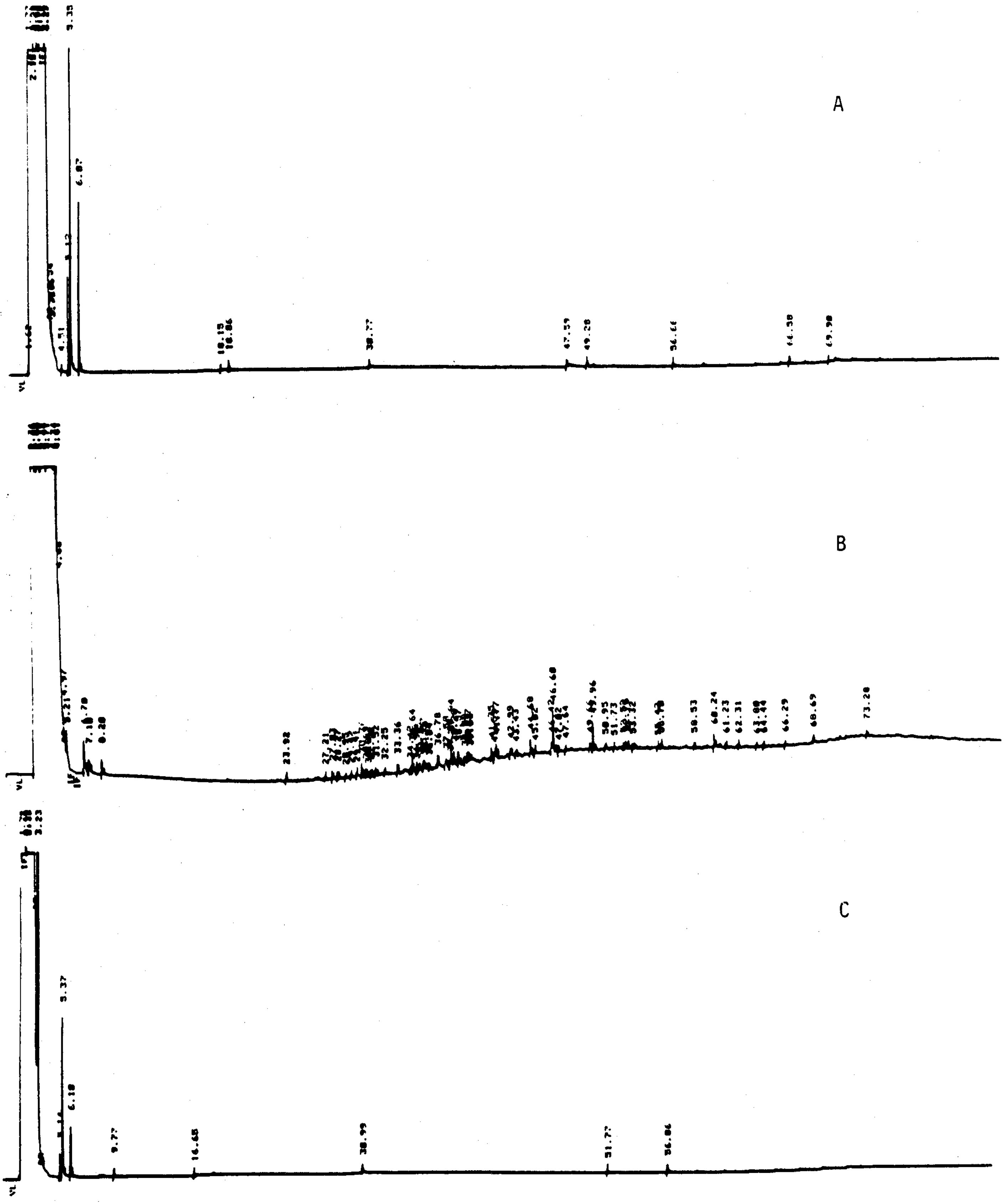

Figure 6-63. FID-GC chromatograms of backround sediment extracts from Kasitsna Bay (site KB-3). (A) Lower, (B) Middle, and (C) Upper Intertidal corral sites.

After 10 months of weathering the intertidal corrals were revisited. The lower intertidal site had the familiar 5-10 mm covering of light brown ooze with dark black mud underneath. The distinct odor of hydrogen sulfide was very evident when the sediment was disturbed. A small Fucus colony was growing in the corral and the corral structure itself was covered with green-colored algae. The sediment sample from this site consisted of an oily layer at 2 to 3 inches depth. Some oil sheen was observed on the water during sample collection, and a few dark, shiny patches of oil were observed at in the 2 to 3 inch depth. The middle intertidal sediment and corral were covered with Fucus and juvenile barnacles. Fine sedimentary particles, which apparently settle out with each receding tide, blanketed the sediment. The sample collected at this site consisted of sediment from just below the surface down to about 4 inches depth. At 2 to 3 inches a distinct oil layer was encountered with a characteristic crude oil odor and sediment discoloration. The corral structure at the upper intertidal site was pretty banged up and worn. Presumably, this was caused by collisions with rocks and other beach wrack during storm events. Contaminated sediment wasn't encountered until a depth of approximately 8 inches at this site. At 12 to 14 inches a discrete band of oil, or extremely oily sand, was encountered.

FID-GC chromatograms of all three corrals after 10 months of weathering are shown in Figure 6-64. Compositionally, the oil at all three sites is quite different. The middle corral exhibits enhanced biodegradation relative to the other two, oil in the lower corral opens to contain more low molecular weight hydrocarbons than the others. Lower molecular weight hydrocarbons are normally removed by a combination of evaporative and dissolutive processes. However, these oil removal processes are severely hindered at the lowest intertidal site because the fine, muddy sediments have very little mixing energy (limited dissolution) and they retain so much water that even during exposed periods they remain wet (limited evaporation). What oil did penetrate this site through worm and clam vent holes, apparently did not undergo extensive weathering within this time frame.

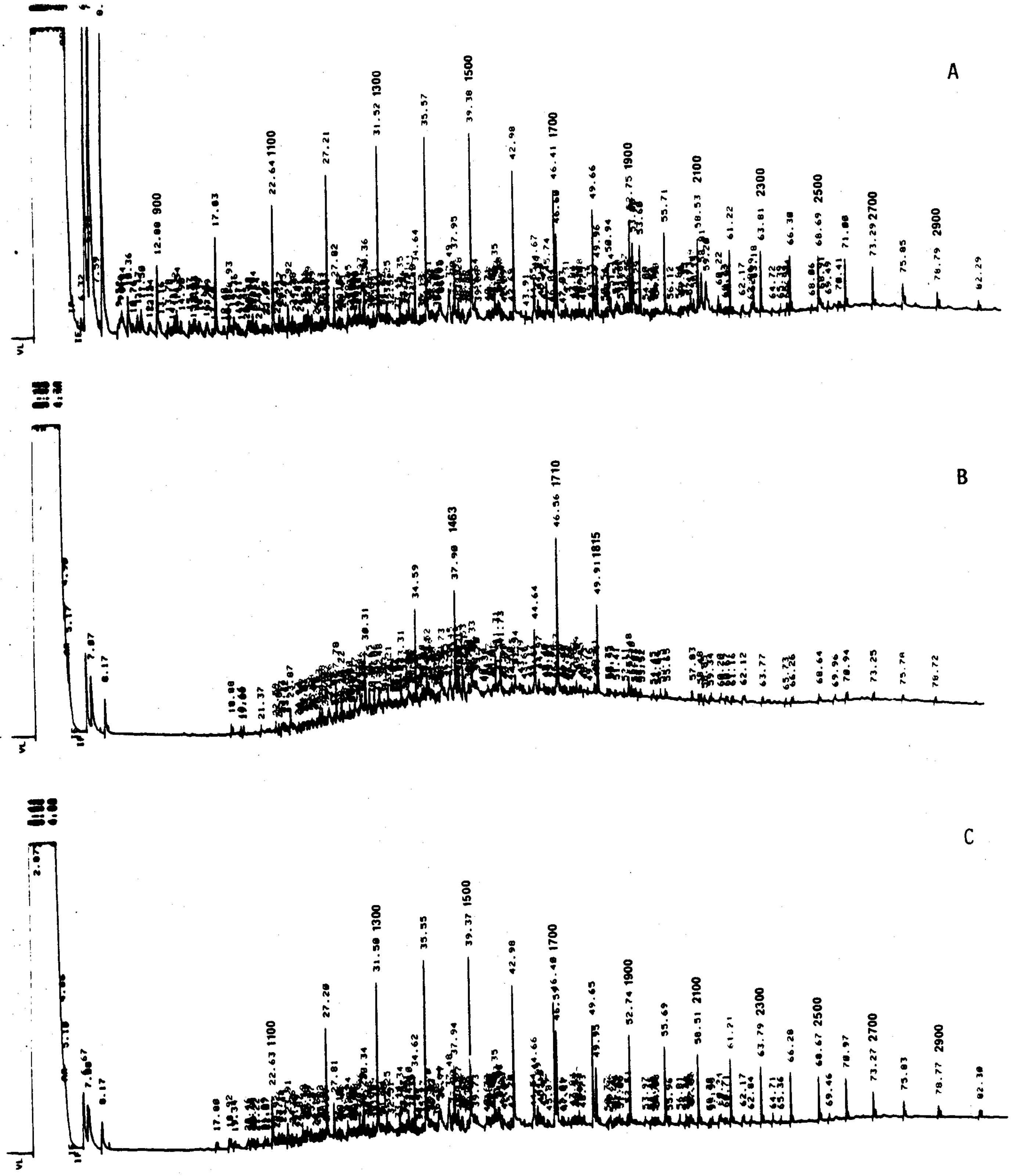

Figure 6-64. FID-GC chromatograms of sediment extracts from Kasitsna Bay (site KB-3) 10 months after a spill of 1 liter of Prudhoe Bay crude oil. (A) Lower, (B) Middle, and (C) Upper Intertidal corral sites. Note - the PIV for the chromatogram in Figure A is approximately 10 times less than that of Figure B or Figure C.

Two months later MacDonald Spit (Kasitsna Bay) was reoccupied to allow collection of 12 month post-spill samples and field observations. At the middle corral samples were taken from the 1 to 2 inch range and 4 to 8 inch depths. Figure 6-65 shows chromatograms of the aliphatic and aromatic fractions from these samples and Table 6-18 presents the reduced data along with various weathering ratios. The surface sediment had a large, bimodal UCM and was devoid of the usual suite of n-alkanes. Except for the isoprenoids pristane, phytane, and farnesane, there were very few resolved peaks of consequence. The oil at 4 to 8 inches also experienced degradation, but not to nearly the same extent. Ratios of nC-17/pristane, nC-18/phytane, and total resolved/total unresolved were significantly lower than for the parent oil, but n-alkanes still dominate the resolved peaks in the chromatogram. The aromatic fractions are not concentrated enough to allow detailed descriptions of differences, but the 4 to 8 inch sample does appear to contain more resolved compounds. Unfortunately, a seawall was built near the high tide mark between the 10 month and 12 month sampling periods. The upper intertidal site was destroyed during the construction and no more samples or observations were possible.

During the Spring 1983 field effort (17 months post-spill) observations of the lower intertidal site showed significant algal growth and several clam burrows within the corral. Figure 6-66 and 6-67 show the appearance of the lowest intertidal corral 17 months after initiation of the experiment. Also shown in Figure 6-66 is the seawall built against the timberline on MacDonald's spit approximately ten to eleven months after initiation of the experiment. As shown by Figure 6-67, the lower intertidal corral had considerable overgrowth of algae and fucus, and the corral itself was covered by significant layers of marine algae. In addition, the sediment appeared to be a lighter color and more oxygenated than during previous observations. While sampling, various worms and other infaunal organisms were noted. Sediment with the characteristic crude oil odor was not discovered until 14 inches depth. At this depth, sampling caused formation of a slight sheen on the water.

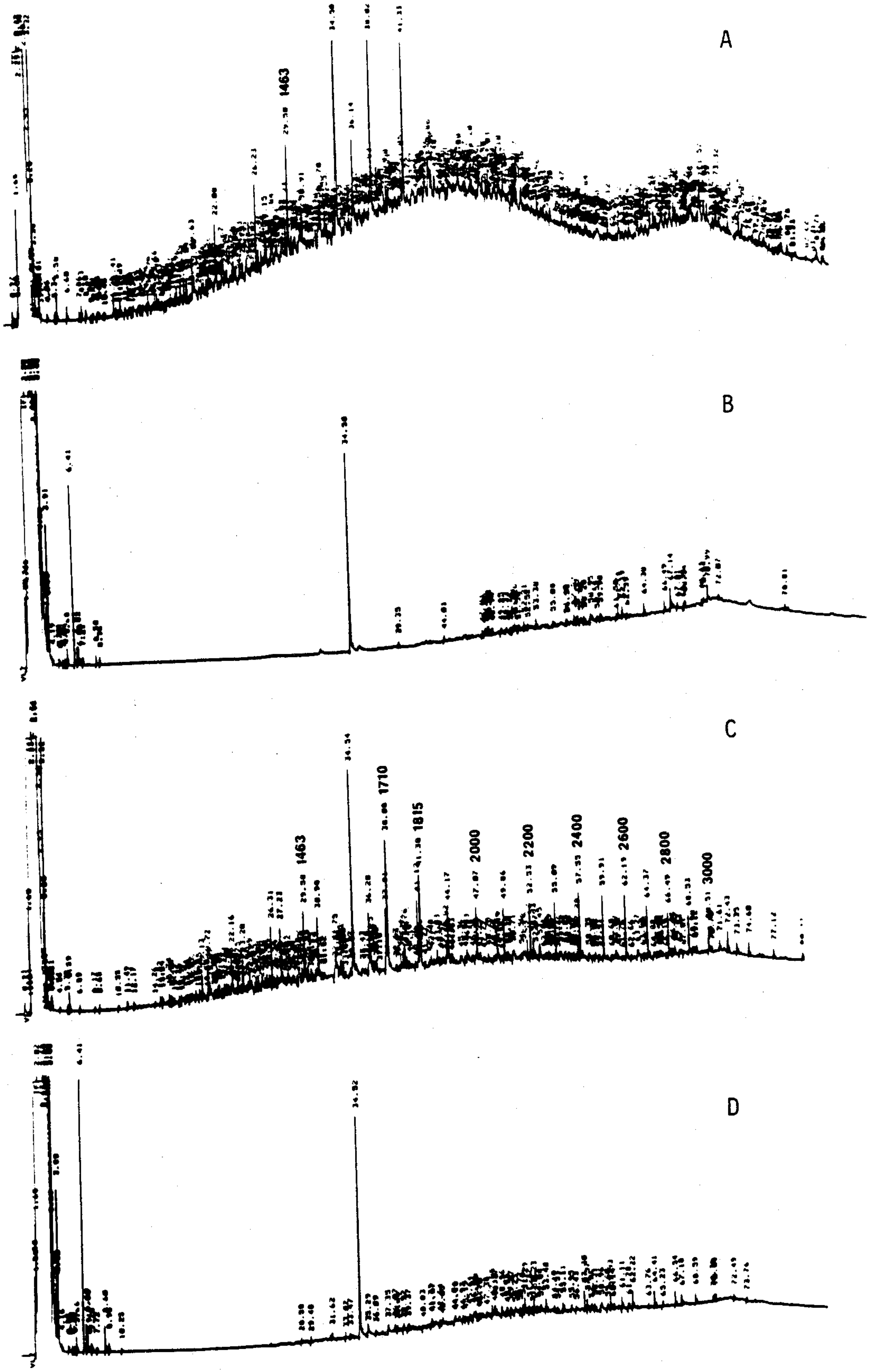

Figure 6-65. FID-GC chromatograms of sediment extracts from Kasitsna Bay (site KB-3) 12 months after a spill of 1 liter of Prudhoe Bay crude oil at the Middle corral site. (A) Aliphatic fraction at a depth of 1-2", (B) Aromatic fraction at a depth of 1-2", (C) Aliphatic fraction at a depth of 4-8", and (D) Aromatic fraction at a depth of 4-8".

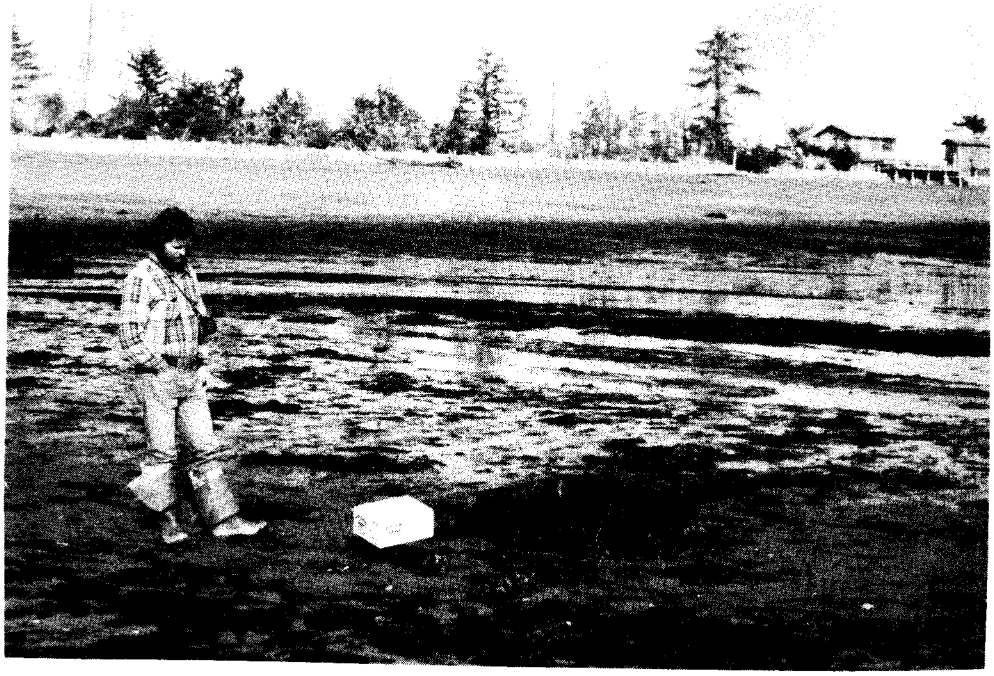

Figure 6-66. Site KB-3 (Kasitsna Bay) Lowest Corral after 17 months of weathering.

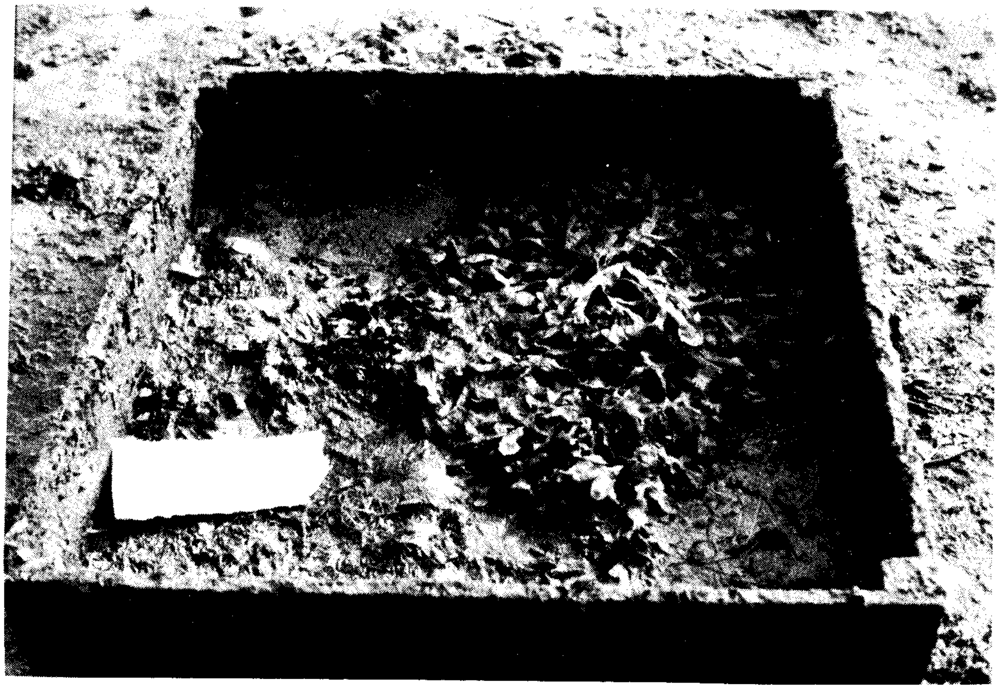

Figure 6-67. Site KB-3 (Kasitsna Bay) Interior of the lower corral prior to sampling after 17 months of weathering.

TABLE 6-19. KB-3 KASITSNA BAY

Depth Profile of Hydrocarbon Concentrations and Weathering Ratios in the Middle Intertidal Corral at 12 Months Post-Spill

Sample depth (inches)	Total Resolved Concentration	Total Unresolved Concentration	nC-17/ pristane	nC-18/ phytane	Total Resolved/ Total Unresolved
1 to 2"	62.5 ug/g	1,244 ug/g	—	—	0.05
4 to 8"	137 ug/g	643 ug/g	0.2	0.4	0.49
Reference[a]	—	—	1.8	2.1	0.35

a - The Reference values were calculated by multiple FID-GC analyses of "fresh" unaltered Prudhoe Bay crude oil.

Figure 6-68 shows the middle intertidal corral 17 months after initiation of the experiment. The surface of the sediment for both the lower and middle intertidal corrals appeared identical to the sediment in each adjacent surrounding area and there appeared to be no obvious reduction in barnacle growth or algae (as seen in the photographs).

Table 6-20 documents the changes in oil concentrations at the three intertidal sites over time. (When more than one depth sample was analyzed these concentrations represent an average value.) The lower corral had a much lower Day 0 concentration than the other corrals. This is due to poor oil penetration and subsequent lifting with the incoming tide (similar to other lower corral intertidal sites). Figures 6-69 and 6-70 are visual illustrations of the relative abundance of oil at various times post-spill. In general, the bar graphs show that the concentration of oil in the sediments diminished with time, radically at first and then at a reduced rate after several months. The total chromatographical resolved components tended to drop further than the total unresolved compounds, indicating that the oil was being compositionally altered over time. Initial oil removal at the upper corral was slower than at the other two; presumably this was due to its infrequent tidal coverage. After 10 months, however, oil concentrations in the middle and upper corrals were very similar, but seawall construction made further comparisons impossible. The most recent sampling of the corrals (17 months post-spill) showed the middle corral to have a somewhat higher oil concentration than the lower. But, in any case, it is only 3% of the Day 0 unresolved concentration and 1% of the Day 0 resolved concentration, showing that oil removal has been almost complete.

Bio-toxicity at the lower corral appeared to be negligible after 17 months. Numerous epifaunal and infaunal biota were observed in the sediment and on the corral. Visual bio-toxicity interpretations at the middle corral are limited since it was located in a more sparsely populated zone of the intertidal regime. However, as Table 6-20 shows, the concentration of oil in this sediment after 17 months was quite low and comparable to the concentration found at the lower corral.

Figure 6-68. Site KB-3 (Kasitsna Bay) Middle corral prior to sampling after 17 months of weathering.

TABLE 6-20. KB-3 KASITSNA BAY

Concentration of Total Resolved and Unresolved Compounds in the Intertidal Sediments at Various Times Post-Spill (all concentrations in ug/g)[a]

		Day 0	Day 17	5 Months	10 Months	12 Months	17 Months
UPPER CORRAL	Total resolved (ug/g) Total unresolved (ug/g)	2,249 4,098	1,117 2,350	490 1,090	86 506	NA[b] NA	NA NA
MIDDLE CORRAL	Total resolved (ug/g) Total unresolved (ug/g)	1,198 5,660	NA NA	20.1 275	66 681	100 944	10.2 70.1
LOWER CORRAL	Total resolved (ug/g) Total unresolved (ug/g)	590 658	NA NA	NA NA	21.8 89.8	NA NA	8.24 18.5

a - When more than one sample was analyzed for a specific time point these numbers represent average values.

b - NA indicates sample not analyzed or not available.

KB-3 KASITSNA BAY

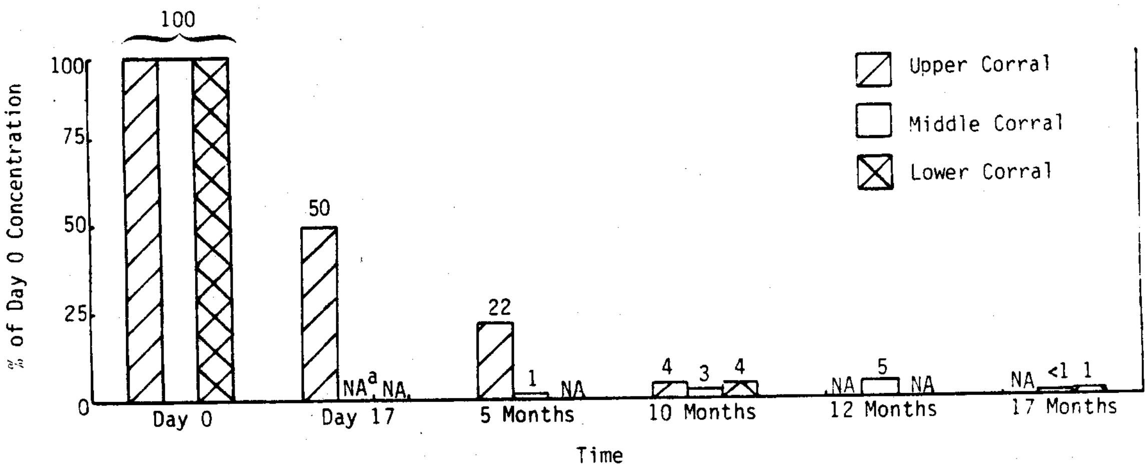

FIGURE 6-69. Relative Abundance of Resolved Compounds Remaining in the Sediment at Various Times Post-Spill.

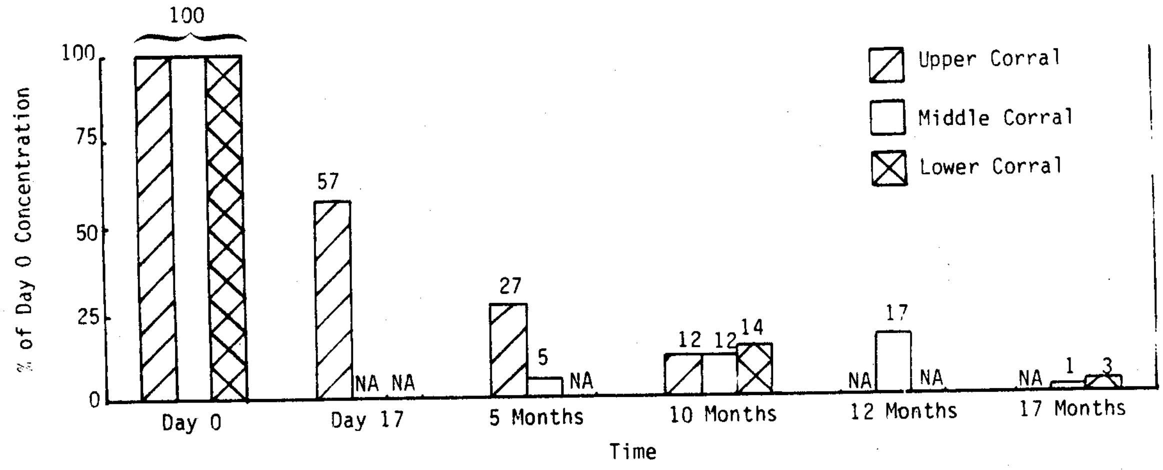

FIGURE 6-70. Relative Abundance of Unresolved Compounds Remaining in the Sediment at Various Times Post-Spill.

[a]NA indicates sample not analyzed or not available.

In conclusion, the most remarkable observations at the Kasitsna Bay intertidal sites were the drastic differences noted between surface and subsurface sediments at the middle corral after 12 months of weathering. Apparently, the processes which enhance oil degradation are more active in the surface sediments within this particular regime.

6.4.2.3 KB-4 Seldovia Salt Marsh

The Seldovia Salt Marsh is characteristic of a classic estuary and is covered by extensive mudflats and Spartina growth. The tidal range at this site is very large, and during the daily tidal range extensive areas are alternately submerged and exposed (Figures 6-71 and 6-72).

In preparation for the experiment, vertical water transects were taken, and an intertidal vertical profile was generated. Figure 6-73 shows the two-dimensional intertidal profile at this site. The placement of intertidal corrals and their height above mean low tide is also indicated in the figure. The sediment at the upper corral was characterized by a thin (approx. 1") layer of organic material comprised mostly of decomposing Spartina, and assorted twigs and branches. The upper intertidal site was located adjacent to the timberline at the uppermost edge of the Spartina zone (Figure 6-74). The corral was placed in an area where Spartina growth was still evident but significantly less dense than at the mid tide site (Figures 6-75 and 6-76). The soil in the upper intertidal corral had very little plant growth present at the time of oiling (Figure 6-76). The underlying material was mostly coarse sand with quite a bit of cobble-sized rock. The middle corral was located about 50 meters seaward from the upper intertidal site in the middle of a tidal drainage channel. Figures 6-77 and 6-78 show the channel during a floodstage and at low tide, respectively. The channel was characterized by low marsh grass growing on 1-1/2 to 2 inches of topsoil, consisting primarily of marsh grass roots and other decaying organic material. The area was very rocky and the sediment itself was a coarse sand. Installation of the middle corral was completed, as at the other sites, where a trench was dug taking

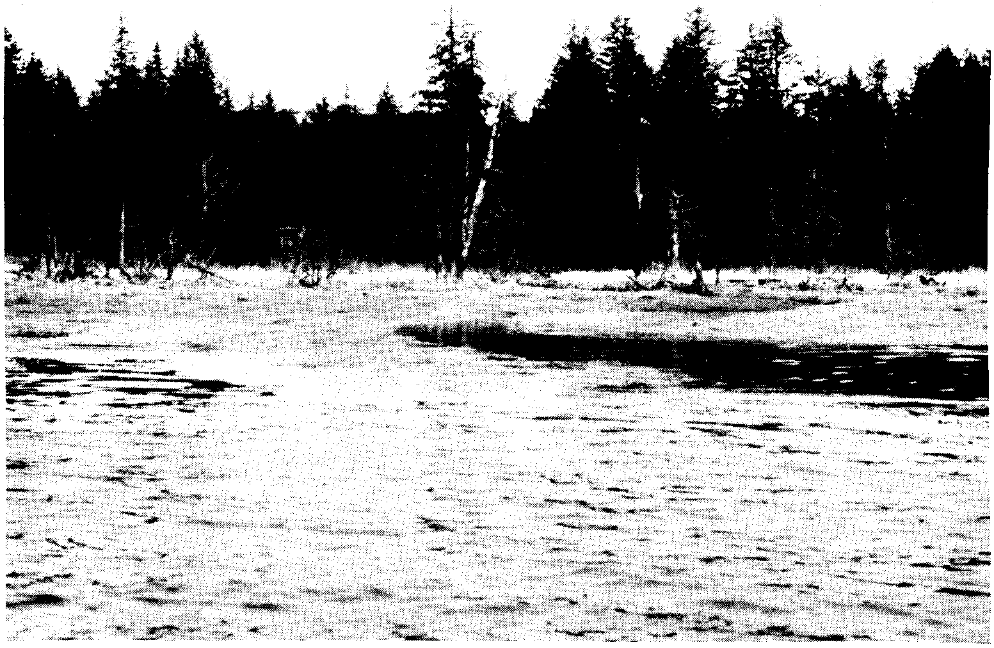

Figure 6-71. Site KB-4 (Seldovia Salt Marsh) at high tide.

Figure 6-72. Site KB-4 (Seldovia Salt Marsh) at low tide.

Figure 6-73. Profile Of Intertidal Corral Site KB-4 (Seldovia Bay)

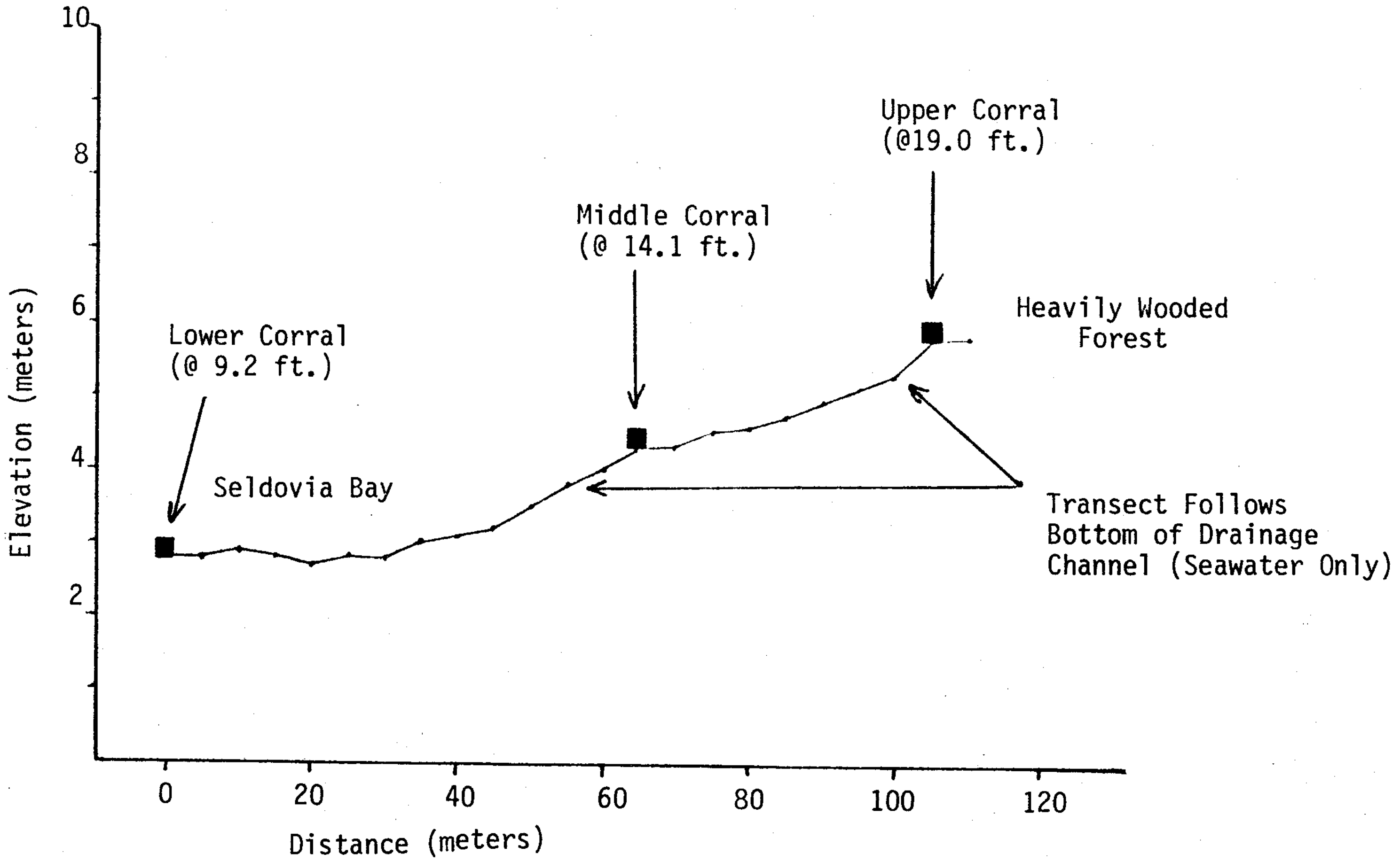

Figure 6-74. Location of the upper corral site at KB-4 (Seldovia Salt Marsh) prior to corral installation.

Figure 6-75. Site KB-4 (Seldovia Salt Marsh) position of the uppermost corral.

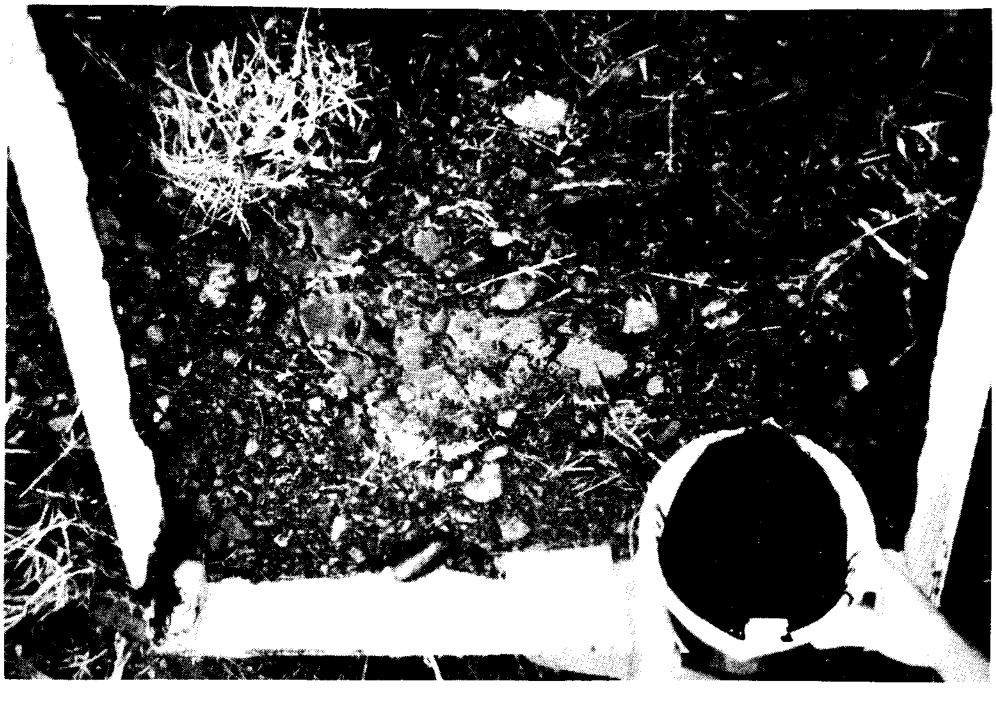

Figure 6-76. Addition of crude oil to the upper corral at site KB-4 (Seldovia Salt Marsh).

Figure 6-77. Transect data collection at KB-4 (Seldovia Salt Marsh) where the middle corral will be placed).

Figure 6-78. Position of the middle corral at site KB-4 (Seldovia Salt Marsh) shown at low tide.

care not to disturb the Spartina growth as shown in Figures 6-79 and 6-80. The lower corral was placed on a tidal flat about 60 meters seaward of the middle intertidal corral. The sediment was rocky on the surface with attached marine algae and kelp. There was also a substantial amount of shell and barnacle growth at this lowest intertidal zone. A light veneer of brown flocculate material blanketed the surface of the sediment. Underneath this brown skin was a layer of gray material which extended down to about 1/2 inch. During corral installation there was very little evidence of hydrogen sulfide, suggesting that the native area is reasonably well oyidized. Figure 6-81 presents the FID-GC profiles obtained on the sediments from these station locations before initiation of the intertidal oil weathering experiments. Fey few if any components were observed at any of the tide heights.

Oil was spilled during a receding 19.6 ft. tide on September 1, 1981. Figure 6-82 shows oil as it was applied to the middle corral. Similar to the other intertidal locations, oil from the middle and lower intertidal corrals was visually observed to lift off the sediment with the incoming tide. Oil stains on the corral walls gave further evidence of this occurrence. The upper corral was not flooded by the tides until September 26, approximately one month after oiling. Thus, the oil at the upper corral had a much greater time to sink in and become thoroughly entrained into the sediment matrix. The organic material (decomposing Spartina, twigs, branches etc.) which blankets the sediment at the upper and middle corrals was noted to trap a fair amount of oil. Visible drops were noted throughout this layer during the day 3 and 1 month sampling trips.

Figure 6-83 compares chromatograms of unfractionated sediment extracts from the upper and middle corrals after 10 months of weathering. The middle corral sample was collected from a depth of approximately 2 inches and showed a considerable loss of resolved components over the 10 month weathering period. The most abundant resolved compounds were the isoprenoids pristane, phytane, and farnesane. A large UCM occurring in the latter part of the chromatogram was the predominant feature of this chromatogram. In comparison, the

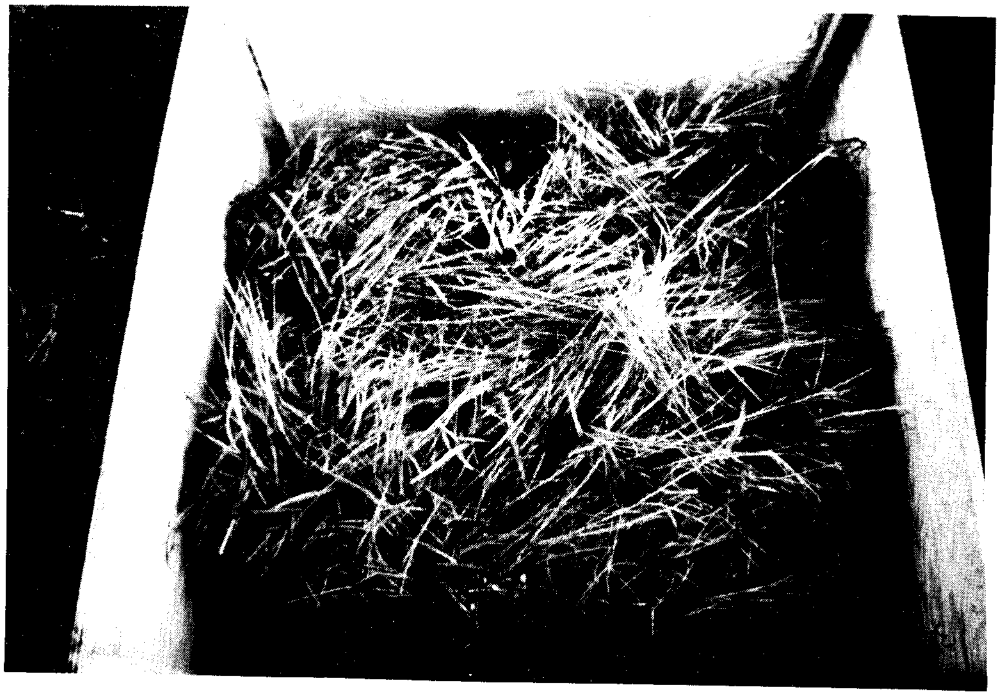

Figure 6-79. Preparation for placement of the middle corral at site KB-4 (Seldovia Salt Marsh).

Figure 6-80. Installation of middle corral at site KB-4 (Seldovia Salt Marsh) around undisturbed sediment.

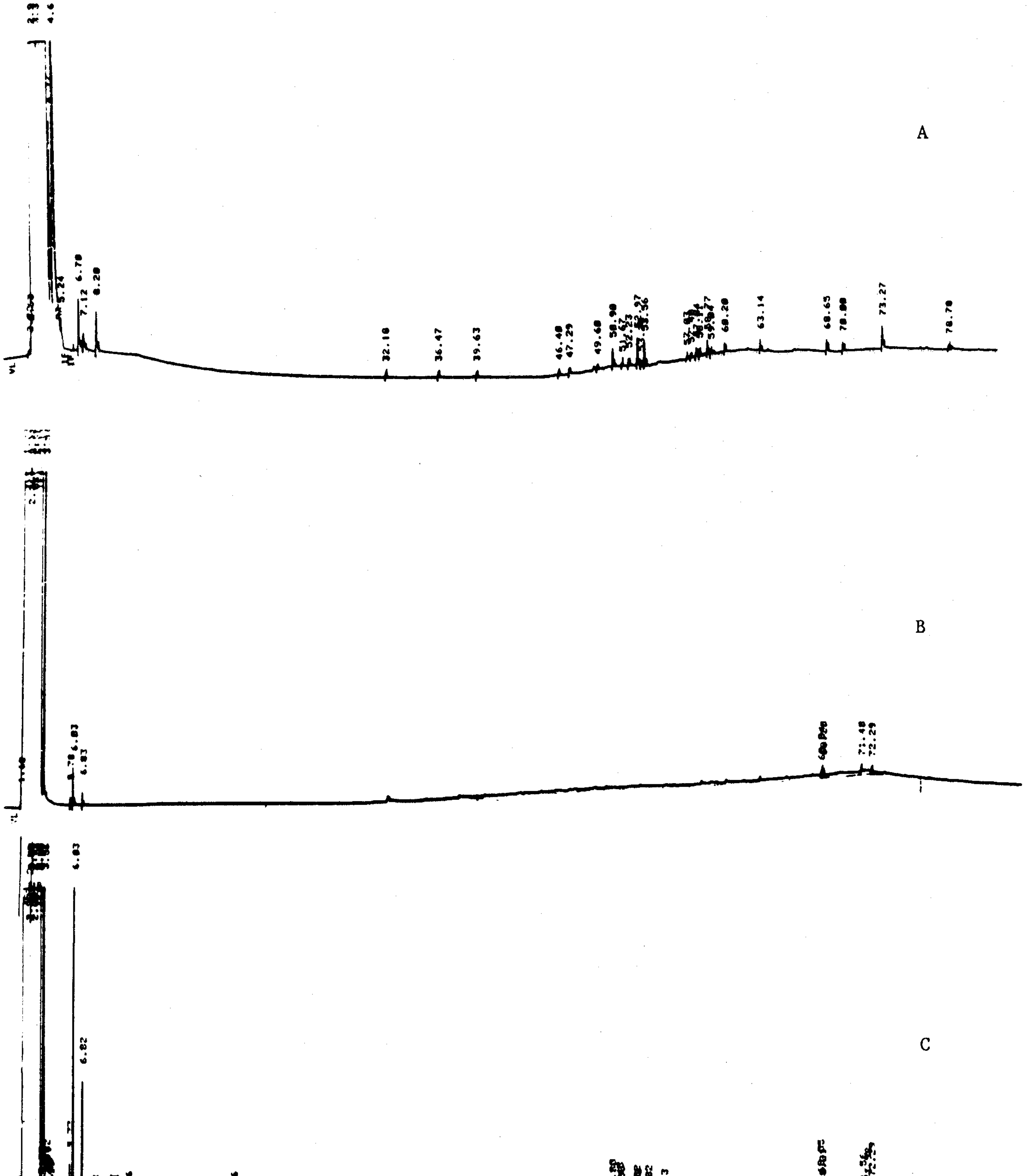

Figure 6-81. FID-GC chromatograms of background sediment extracts from Seldovia Bay (site KB-4). (A) Lower, (B) Middle, and (C) Upper Intertidal corral sites.

Figure 6-82. Application of crude oil to the middle corral at site KB-4 (Seldovia Salt Marsh).

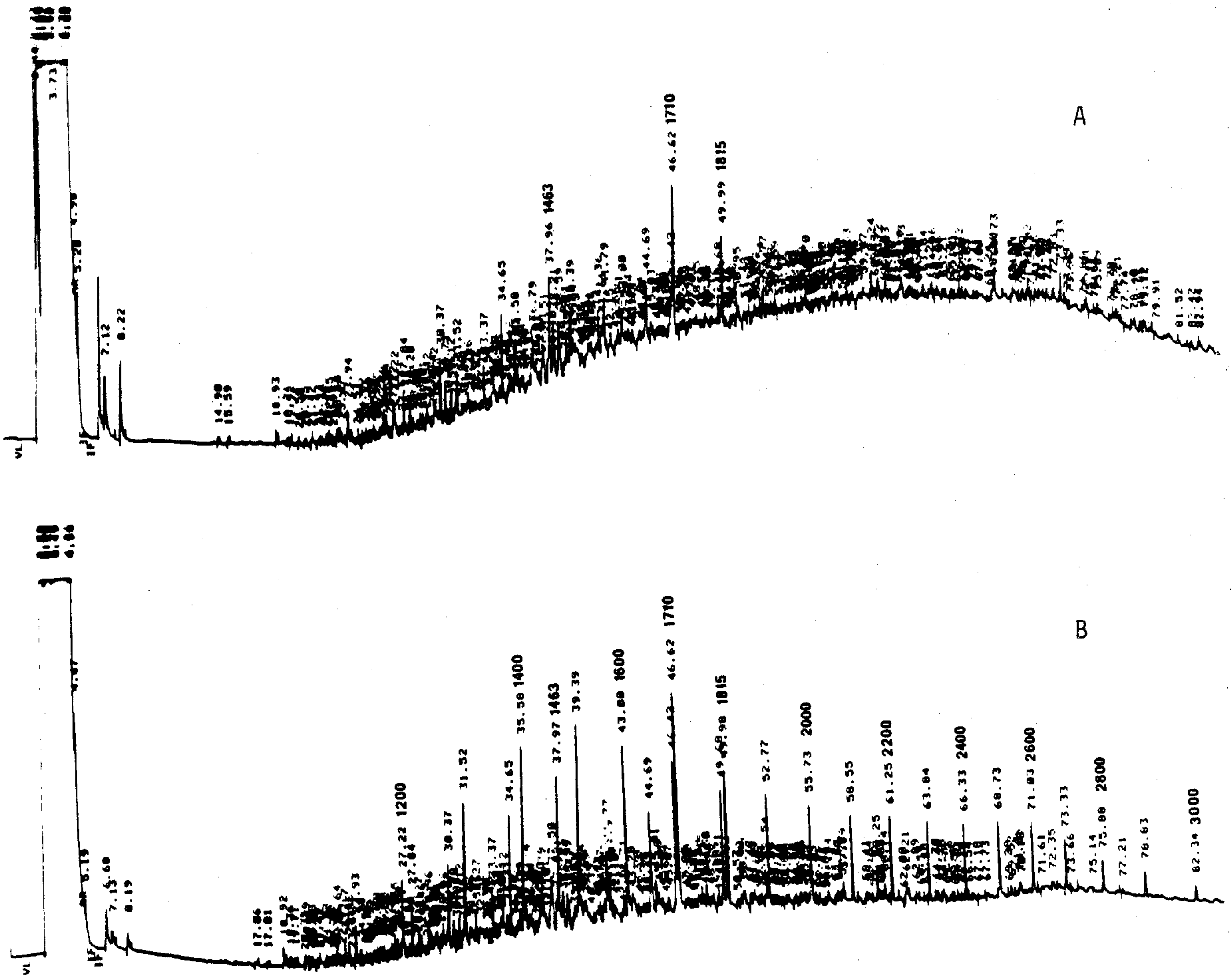

Figure 6-83. FID-GC chromatograms of sediment extracts from Seldovia Bay (site KB-4) 10 months after a spill of 1 liter of Prudhoe Bay crude oil. (A) Middle, and (B) Upper Intertidal corral sites.

chromatogram from the upper corral had a distinctive suite of n-alkanes ranging from nC-12 to nC-30. It also exhibited a moderate UCM, but not enhanced at the higher molecular weight end, as in the chromatogram from the middle corral. Unfortunately, the lower corral could not be located during the July, 1982 (10 month post-spill) sampling effort, making further sampling of this site impossible. Presumably, it was lost to storm activity.

Figure 6-84 shows the upper intertidal corral 17 months after the initiation of the experiment. This photograph was taken during March 1983 and, as such, the *Spartina* within the corral and surrounding area was still dead from winter kill (Figure 6-85). Most of the *Spartina* in the area had just been washed onto the site and was not firmly rooted. Removal of the upper layer of *Spartina* and depth profile sampling then yielded the hydrocarbon data presented in Table 6-21. The various ratios displayed in the table were selected as indicators of the extent of oil alteration or weathering. Figures 6-86 and 6-87 show chromatograms from the aliphatic and aromatic fractions, respectively, at depths of 1 to 2 inches, 6 to 8 inches, and 10 to 12 inches. Qualitatively, the chromatograms from the aliphatic fractions are similar in appearance to the chromatogram from the upper corral in Figure 6-83B after 10 months of weathering. The sediment at 6 to 8 inches had an approximately 4-fold greater hydrocarbon concentration than the other depths sampled, indicating a concentrated band of oil in the sediment. Also, the ratios which were selected as indicators of oil alteration indicated that the oil at this depth hadn't been degraded as extensively as other depths. This result was possibly due to the toxic effect oil has on microrganisms when it is at higher concentrations.

The similarities in the samples from 6-12' depth suggested that the same degradative processes which occurred at the sediment surface were also occurring to depths of at least 12 inches (although possibly at slightly slower rates). For most marine *subtidal* sediments hydrocarbon biodegradation is restricted to the upper 5 cm. (Bertha and Atlas, 1983). The thickness of this oxygenated layer is dependent on the organic content and the degree of

Figure 6-84. Site KB-4 (Seldovia Salt Marsh) Appearance of the upper corral after 17 months of weathering.

Figure 6-85. Interior of the upper corral at site KB-4 prior to sampling after 17 months of exposure.

TABLE 6-21. KB-4 SELDOVIA SALT MARSH

Depth Profile of Hydrocarbon Concentrations and Weathering Ratios in the Upper Intertidal Corral at 17 Months Post-Spill

Sample depth (inches)	Total Resolved Concentration	Total Unresolved Concentration	nC-17/ pristane	nC-18/ phytane	Total Resolved/ Total Unresolved
1 to 2"	28 ug/g	336 ug/g	0.4	0.5	0.09
2 to 4"	32 ug/g	259 ug/g	0.4	0.6	0.12
6 to 8"	135 ug/g	368 ug/g	0.9	1.0	0.37
10 to 12"	30 ug/g	270 ug/g	0.4	0.5	0.11
Reference[a]	---	---	1.8	2.1	0.35

a - The Reference values were calculated by multiple FID-GC analyses of "fresh" unaltered Prudhoe Bay crude oil.

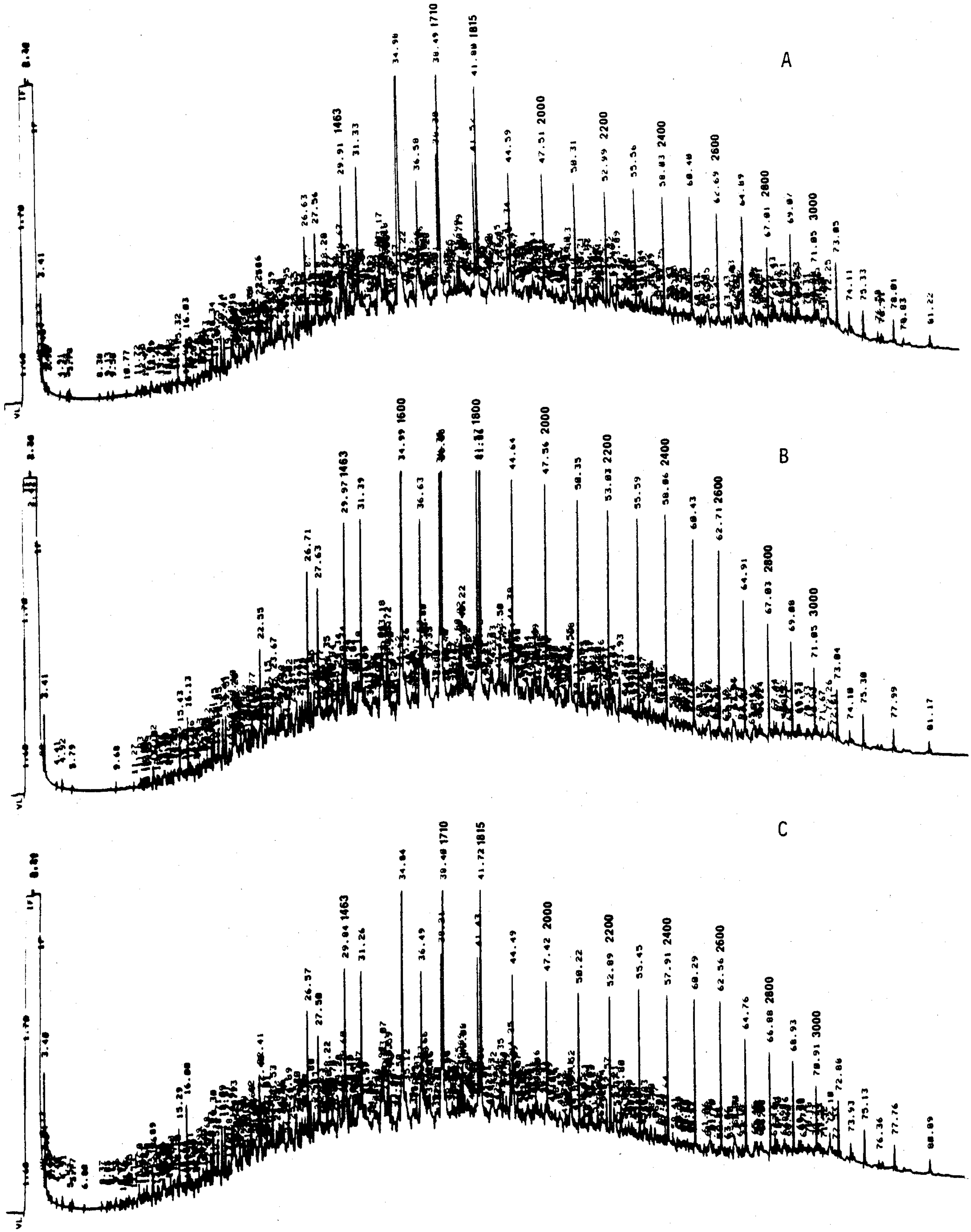

Figure 6-86. FID-GC chromatograms of sediment extracts from Seldovia Bay (site KB-4) 17 months after a spill of 1 liter of Prudhoe Bay crude oil. Aliphatic fraction from the Upper corral site at: (A) 1-2" depth, (B) 6-8" depth, and (C) 10-12" depth.

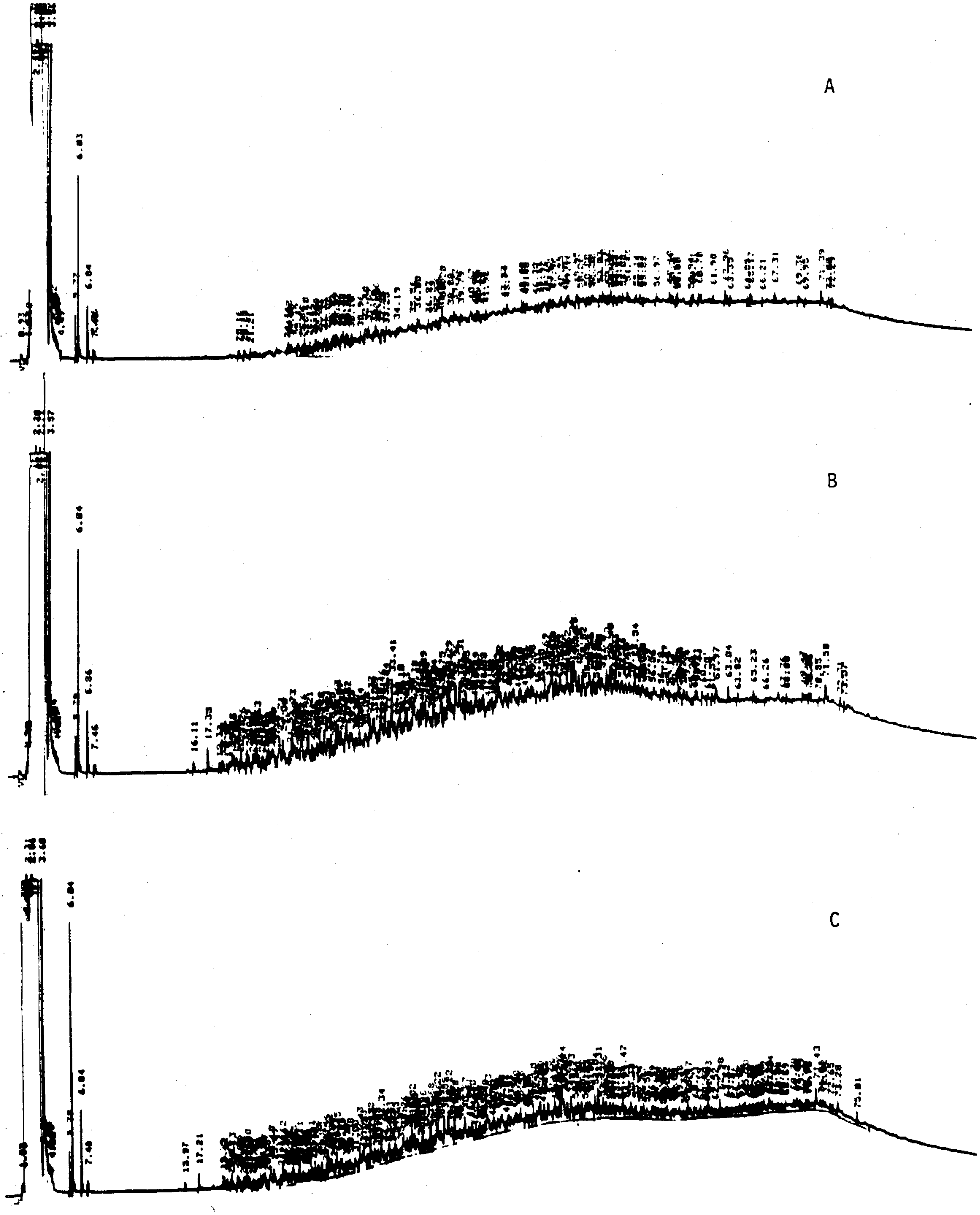

Figure 6-87. FID-GC chromatograms of sediment extracts from Seldovia Bay (site KB-4) 17 months after a spill of 1 liter of Prudhoe Bay crude oil. Aromatic fraction from the upper corral site at: (A) 1-2"depth, (B) 6-8" depth, and 10-12" depth.

physical or biological disturbances in the sediment. Apparently, the increased energy and oxygen availability in the Seldovia intertidal system extends this layer down to at least one foot.

Interestingly, the chromatograms show that many lower molecular weight compounds down to nC-11 still exist in the oil-laden sediments from the upper corral after 17 months of weathering. Wave tank experiments run for a similar period of time showed almost a complete loss of resolved compounds up to nC-15 in the oil. This suggests that evaporative processes are somewhat limited in sediment-bound oil.

Table 6-22 presents the absolute concentrations of oil remaining in the sediment, while Figures 6-88 and 6-89 show the abundance of resolved and unresolved compounds relative to the Day 0 reference value. When more than one depth sample was analyzed these concentations represent an average value. A qualitative examination of the two figures shows that, as expected, the relative concentration of hydrocarbons in the sediment dropped as a function of time in both the upper and middle corrals. A certain amount of variability in these values was expected, because in an effort to reproduce a "real" spill situation the oil was simply poured onto the sediment with no efforts at homogenization throughout the corral and/or at depth. As such, concentrated bands of oil within the corral would be expected and were, in fact, observed throughout the conduct of the field study portion of this project. However, some interesting differences do exist between the upper and middle intertidal corrals.

Given that the sediment types in these two zones are similar, i.e., a coarse, rocky sand; the main difference between these two sites appears to be the extent and frequency of floading. The middle corral is flooded twice daily, while the upper corral only gets submerged a few days each month. As seen by the chromatograms in Figure 6-83, the additional tidal coverage causes oil at the middle corral to degrade at a faster rate than at the upper corral. The ratio of resolved/unresolved tends to drop more quickly at the middle corral also, lending quantitative evidence to the differences noted between the two chromatograms.

KB-4 SELDOVIA SALT MARSH

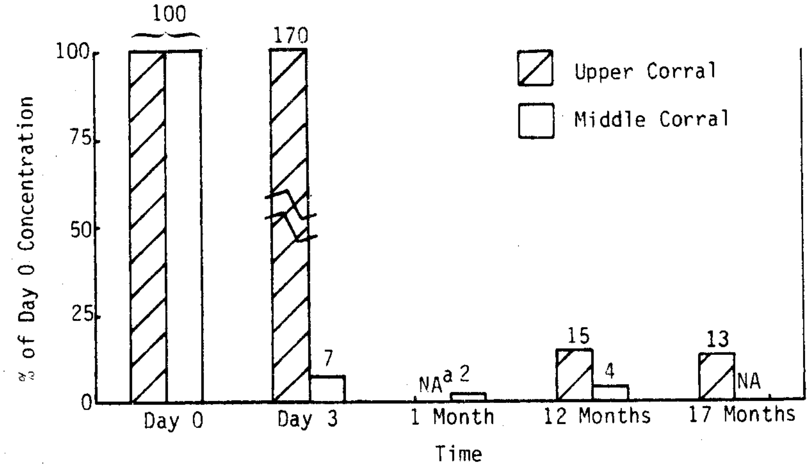

FIGURE 6-88. Relative Abundance of Resolved Compounds Remaining in the Sediment at Various Times Post-Spill.

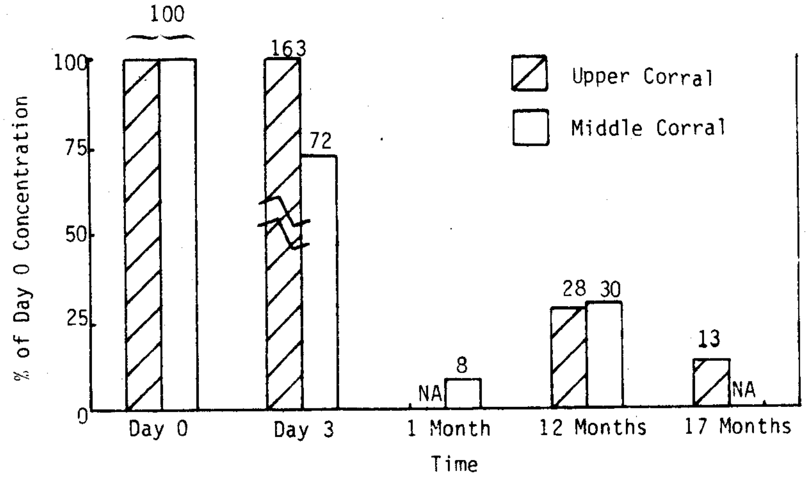

FIGURE 6-89. Relative Abundance of Unresolved Compounds Remaining in the Sediment at Various Times Post-Spill.

[a] NA indicates sample not analyzed or not available.

TABLE 6-22. KB-4 SELDOVIA SALT MARSH

Concentration of Total Resolved and Unresolved Compounds
in the Intertidal Sediments at Various Times Post-Spill
(all concentrations in ug/g)[a]

		Day 0	Day 3	1 Month	12 Months	17 Months
UPPER CORRAL	Total resolved (ug/g)	440	750	NA	67	56
	Total unresolved (ug/g)	2,374	3,875	NA	663	308
MIDDLE CORRAL	Total resolved (ug/g)	585	39	13	23	NA[b]
	Total unresolved (ug/g)	3,064	2,192	247	906	NA
LOWER CORRAL	Total resolved (ug/g)	NA	30	17	NA	NA
	Total unresolved (ug/g)	NA	450	377	NA	NA

a - When more than one sample was analyzed for a specific time point these numbers represent average values.

b - NA indicates sample not analyzed or not available.

Bio-toxicity observations of the corrals over the same 17 month sampling period also gave some interesting results. While collecting the 10 month samples in July, 1982, it was noted that the middle corral had experienced a summary regrowth of vegetation (Figure 6-90), although it was reduced compared to the growth of adjacent areas. However, the upper corral had not experienced regrowth to the same extent, indicating that levels of oil toxic to Spartina may still have existed in the surface sediments.

6.4.2.4 KB-5 Jakalof Bay

Like KB-4 (Seldovia Salt Marsh), Jakolof Bay is an estuarine area receiving freshwater from the Jakalof Creek. Unlike Seldovia Salt Marsh, however, Jakolof Bay does not have extensive Spartina growth, and it is characterized by a broad gently sloping well-drained area (Figure 6-91) and a grassy headland area at the end of the bay (Figure 6-92). Figures 6-91 and 6-92 were taken from approximately the same location, however, Figure 6-92 shows the location of the uppermost intertidal corral relative to the well-drained flats and mussel beds. There are numerous ponds of brackish water behind the grassy headland area (Figure 6-93), and the middled intertidal corral was located adjacent to one of these drainage ponds in an area that would be flooded on medium tides. The upper intertidal corral site (Figure 6-94) was on a grassy plain which was only covered by extreme high tides (approximately three or four days in a row per month). The two-dimensional Jakalof Bay intertidal profile is shown in Figure 6-95.

The soil at this site was well oxidized and contained a high percentage of organic material. The upper intertidal surface material was spongy and highly organic, like a peat. The middle corral was located on the backside of a gravel berm and was somewhat protected from the tidal currents. The mid-tide corral can be seen in the background of Figure 6-94, adjacent to the backwater pond and drainage channel. The sediment at this corral was characterized by a fine clay interspersed with gravel. There wasn't much organic growth at the middle intertidal site and the surface of the sediment was

Figure 6-90. Interior of the middle corral at site KB-4 (Seldovia Salt Marsh) prior to sampling after 10 months of exposure.

Figure 6-91. Overview of site KB-5 (Jakalof Bay) prior to intertidal corral placement.

Figure 6-92. Position of the upper corral at site KB-5 (Jakalof Bay).

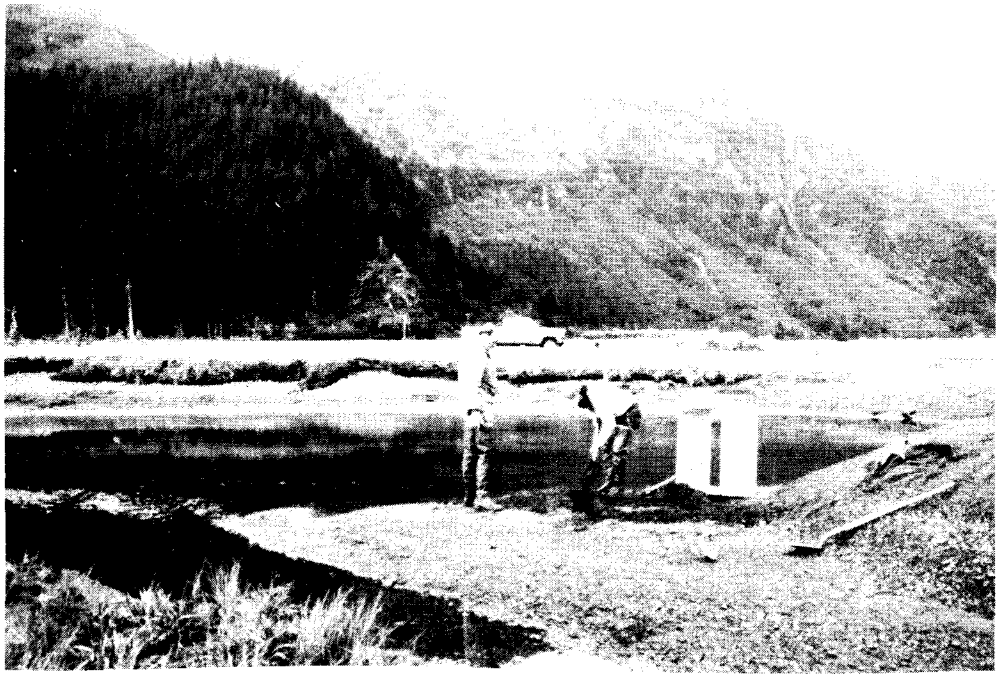

Figure 6-93. Installation of the middle corral at site KB-5 (Jakalof Bay).

Figure 6-94. Relative positions of the upper and middle corrals of site KB-5 (Jakalof Bay).

Figure 6-95. Profile of Intertidal Corral Site KB-5 (Jakalof Bay)

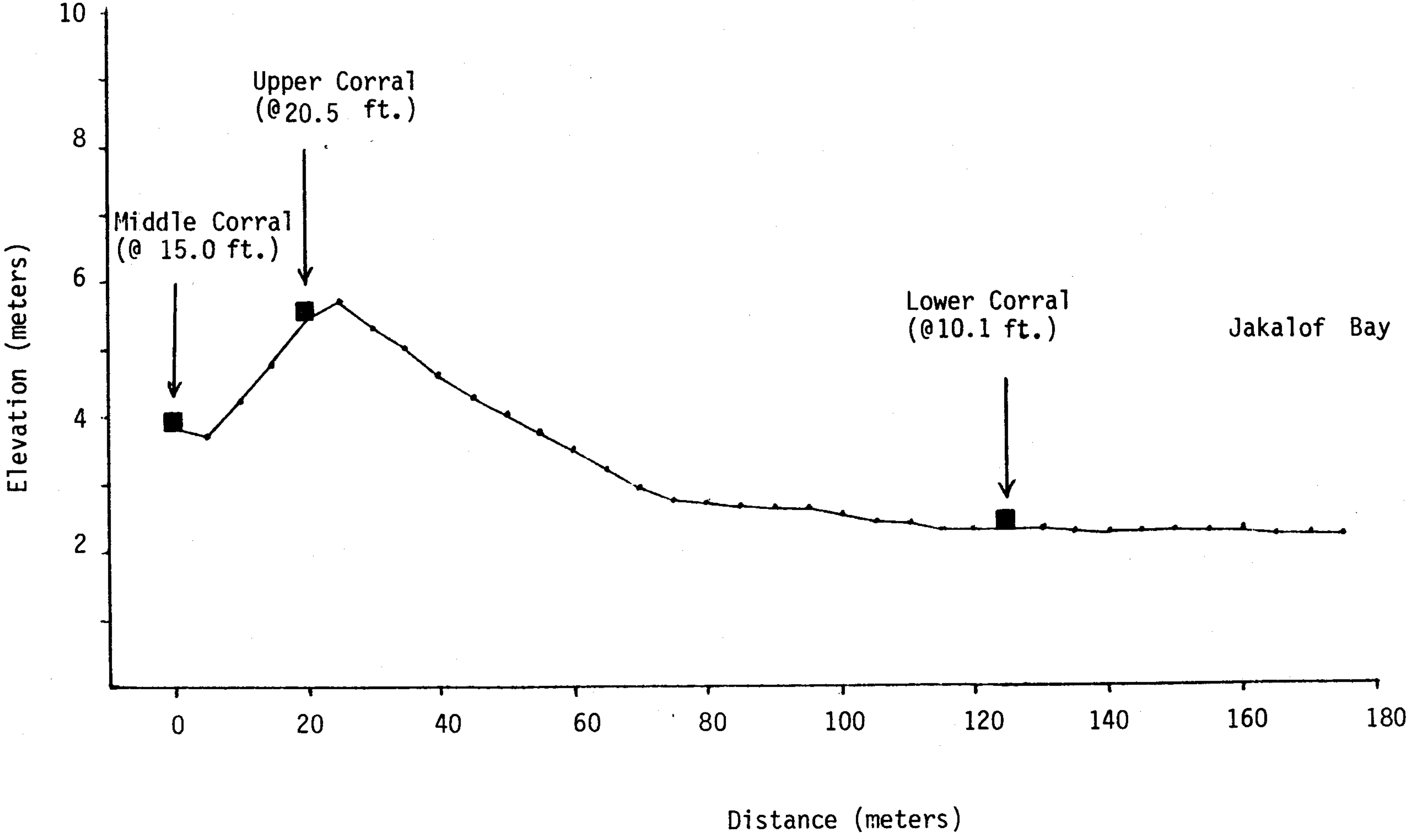

coated with a thin layer of fine filamentous silt. The low-tide corral was located in the middle of the smooth drainage flat shown in Figure 6-91. The sediment was well-oxidized and no hydrogen sulfide was detected during corral placement. The sediment consisted of a clay-gravel conglomerate which was fairly well compacted. Background samples from the middle and upper intertidal corrals were collected and analyzed by FID-GC for hydrocarbon content. The chromatograms from these sites are presented in Figure 6-96. As the figure shows, this was a relatively pristine environment with no evidence of petrogenic hydrocarbons. Some resolved components are seen in the middle intertidal sediment, but these peaks are believed to be biogenic and primarily marine in origin. Extremely low (<1 ng/g dry weight) levels of several higher molecular weight alkanes were present in the upper intertidal sediments (Figure 6-96B), and these presumably reflect terrestrial impact from decaying greens covering the area.

Oil was spilled on September 2, 1981, during a receding 19.6 foot tide. At the low corral the oil did not penetrate the sediment to a significant extent. Thirty minutes after addition, there were still 1 to 2 cm deep pools of oil on the intertidal sediment surface and visible oil sheen on the standing water. Even though the lower corral was well exposed at this tide, it was poorly drained and there were still numerous pools of standing water in and around the corral. At the middle corral the oil penetration rate was also slower than at most other sites. It was postulated that the fine filamentous silt layer which covered the sediment posed a barrier to sinking. At the upper corral, however, the oil sank into the sediment/soil readily. Figure 6-97 shows a closeup of the grassy upper-intertidal corral immediately after application of 1 liter of fresh Prudhoe Bay crude oil. The oil was observed to percolate rapidly (within two minutes) into the soil, although the grass within the corral retained oil film for up to two weeks after oil addition (i.e. until the area was inundated by extreme high tides).

Further observations of the intertidal corrals at Jakolof Bay three days later showed that the lower corral still had oil sheen on its standing

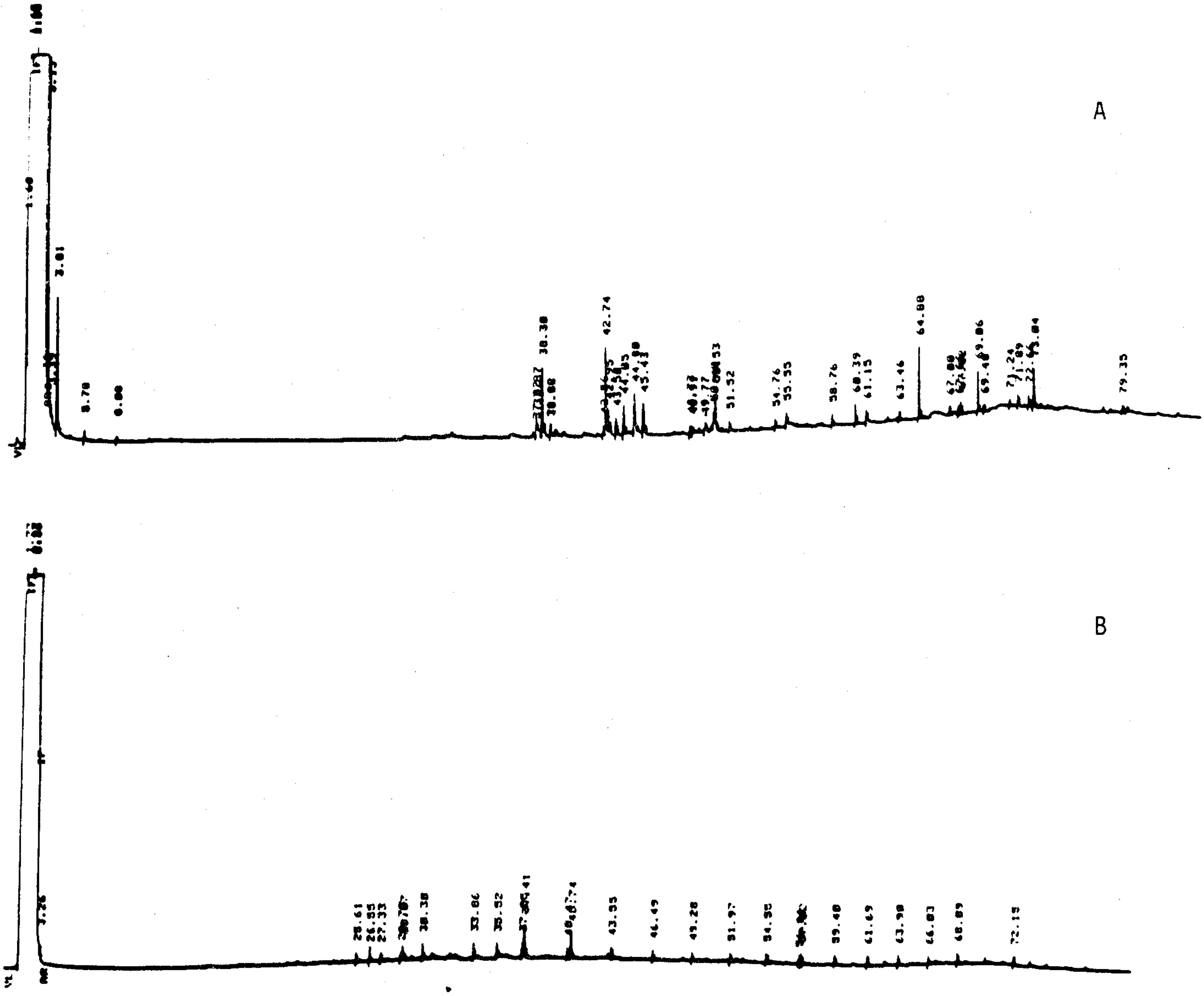

Figure 6-96. FID-GC chromatograms of background sediment extracts from Jakalof Bay (site KB-5). (A) Middle, and (B) Upper Intertidal corral sites.

Figure 6-97. Interior of the upper corral at site KB-5 (Jakalof Bay) immediately following application of 1 liter of crude oil.

waters. The corral sides were oil-stained, suggesting that lifting of the oil had occurred. The sides of the middle corral were also stained with oil, and there was no visible evidence of oil anywhere else within the corral. After three days, the upper corral site still hadn't been flooded, and oil was observed in abundance on the surfacial grass and peat-like material which covered the soil. Sometime between the three-day and 10-day site visits the low tide corral washed away, and no further efforts at making observations or collecting samples at that tide height were undertaken.

Figures 6-98 and 6-99 show the upper intertidal corral in July 1982, approximately 10 months after initiation of the spill. At that time there was considerable grass growth in the upper intertidal region, and the area had been used for limited cattle grazing. Figure 6-99 presents a closeup of the interior of the corral, and shows that there was considerably less regrowth within the corral compared to the surrounding area. Figure 6-100 shows the mid-tide corral approximately 10 months after initiation of the spill. Figure 6-100 is an overview of the area showing the position of the corral next to the backwater pond; Jakolof Creek can be observed in the background of the figure. Figure 6-101 presents a closeup of the mid-tide corral, and from this figure the sediment appears to be very similar in the interior of the corral to the surrounding area.

Additional samples and observations were taken 12 months after the initial spill. At the middle corral, oil wasn't apparent until a depth of approximately 4 to 8 inches; at this depth the sediment exhibited a slight oil odor. At the upper intertidal site, there was no evidence of oil on the attached plant growth or surface sediments. The grass within the corral had been cropped and there was evidence of cattle grazing. A dark band of sediment, presumably oil-laden, was encountered at a depth of 4 to 7 inches. Several depth samples were collected from each corral and analyzed at that time. The concentrations of total resolved and unresolved compounds and selected weathering ratios for these samples are displayed in Table 6-23. Chromotograms of the alphatic and aromatic fractions from the upper intertidal

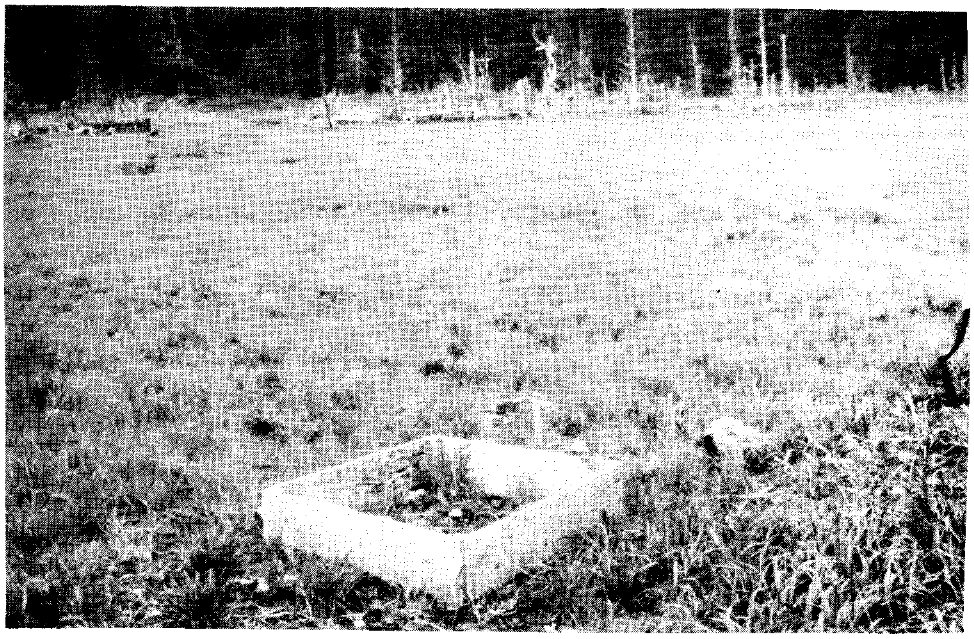

Figure 6-98. Appearance of the upper corral at site KB-5 (Jakalof Bay) after 10 months of weathering.

Figure 5-99. Interior of the upper corral at site KB-5 (Jakalof Bay) prior to sampling after 10 months of weathering.

Figure 6-100. Appearance of the mid-tide corral at site KB-5 (Jakalof Bay) 10 months after initiation of the experiment.

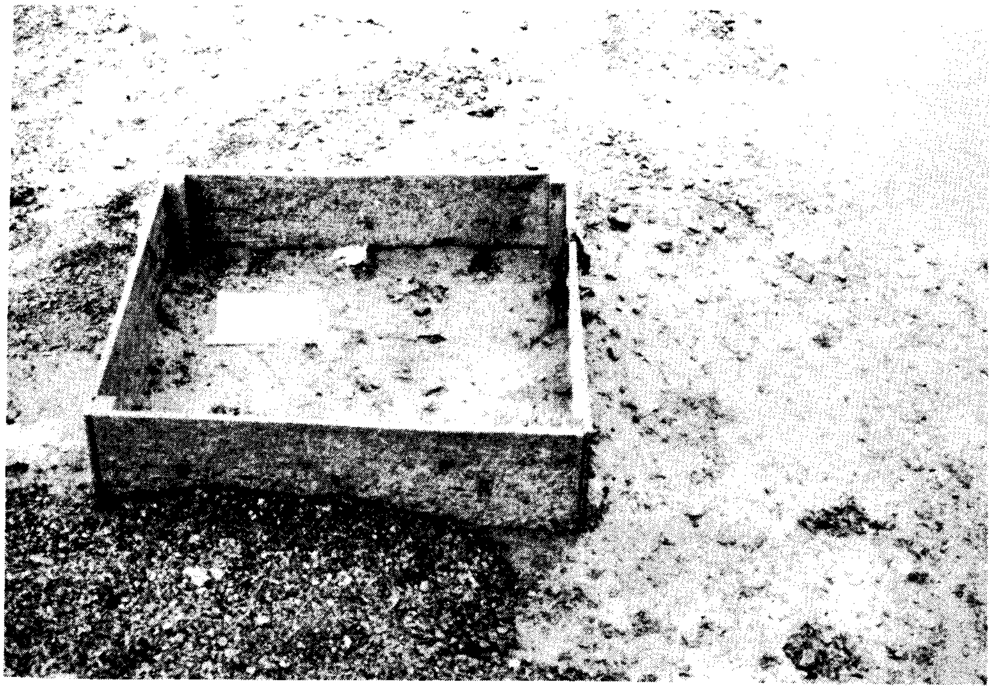

Figure 6-101. Interior of the middle corral at site KB-5 (Jakalof Bay) prior to sampling after 10 months after initiation of the experiment.

TABLE 6-23. KB-5 JAKALOF BAY

Depth Profile of Hydrocarbon Concentrations and Weathering Ratios in the Upper and Middle Intertidal Corral at 12 Months Post-Spill

Sample depth (inches)	Total Resolved Concentration	Total Unresolved Concentration	nC-17/ pristane	nC-18/ phytane	Total Resolved/ Total Unresolved
<u>UPPER CORRAL</u>					
1 to 2"	695 ug/g	11,373 ug/g	0.06	0.4	0.5
2 to 4"	1,252 ug/g	8,666 ug/g	0.14	0.9	1.2
4 to 8"	299 ug/g	2,144 ug/g	0.14	0.9	1.0
<u>MIDDLE CORRAL</u>					
1 to 2"	63 ug/g	175 ug/g	0.39	—	—
2 to 4"	2.1 ug/g	129 ug/g	0.02	—	—
4 to 8"	7.2 ug/g	76 ug/g	0.10	2.6	0.5
Reference[a]	—	—	1.8	2.1	0.35

[a] - The Reference values were calculated by multiple FID-GC analyses of "fresh" unaltered Prudhoe Bay crude oil.

area are presented (for three depths) in Figures 6-102 and 6-103, respectively. Chromatograms of the aliphatic and aromatic fractions from three depths within the middle intertidal corral are presented in Figure 6-104.

As expected, after 12 months of weathering the upper corral was much more heavily contaminated with oil than the middle corral. The oil was most concentrated in the 2 to 4 inch sediment sample, and least concentrated in the 4 to 12 inch sample. The surface sediment sample at 1 to 2 inches was similar in concentration to the 2 to 4 inch segment, however, the oil was altered more extensively. Ratios of nC17/pristane and nC-18/phytane for the 1 to 2 inch sample are half again as low as the other two depths. In addition, the ratio of resolved/unresolved compounds is less for the 1 to 2 inch sample than the others. Compared to the other depth samples, the 1 to 2 inch sample has also experienced a greater loss of the more volatile low-end components. These data illustrate that the evaporative and biodegradative processes which influence the rate of oil weathering become less active at depth for this intertidal environment. All three depth samples show an odd-carbon predominance starting at around nC-25 (see Figure 6-104A). This is evidence that biogenic hydrocarbon input was occurring at each depth tested. The aromatic fractions in Figures 6-104C and D for the 1 to 2 inch and 4 to 8 inch samples were quite similar, although the 1 to 2 inch sample exhibited a slightly enhanced UCM, indicating enhanced oil alteration.

Oil alteration and removal after 12 months was far more extensive at the middle corral. Although the results in Table 6-22 show the top 1 to 2 inch segment had the highest concentration of resolved compounds, examination of the chromatograms in Figure 6-104 shows that these peaks were not characteristic of petrogenic input. In fact, many of these same peaks were seen in a background sediment extract from the middle corral (see Figure 6-96A). These peaks were not present in the two deeper samples, however, indicating that the source of their input was only present at (or near) the sediment surface. The unfractionated extracts of sediments at 2 to 4 inches and 4 to 8 inches were quite similar; both exhibited an almost complete loss of any

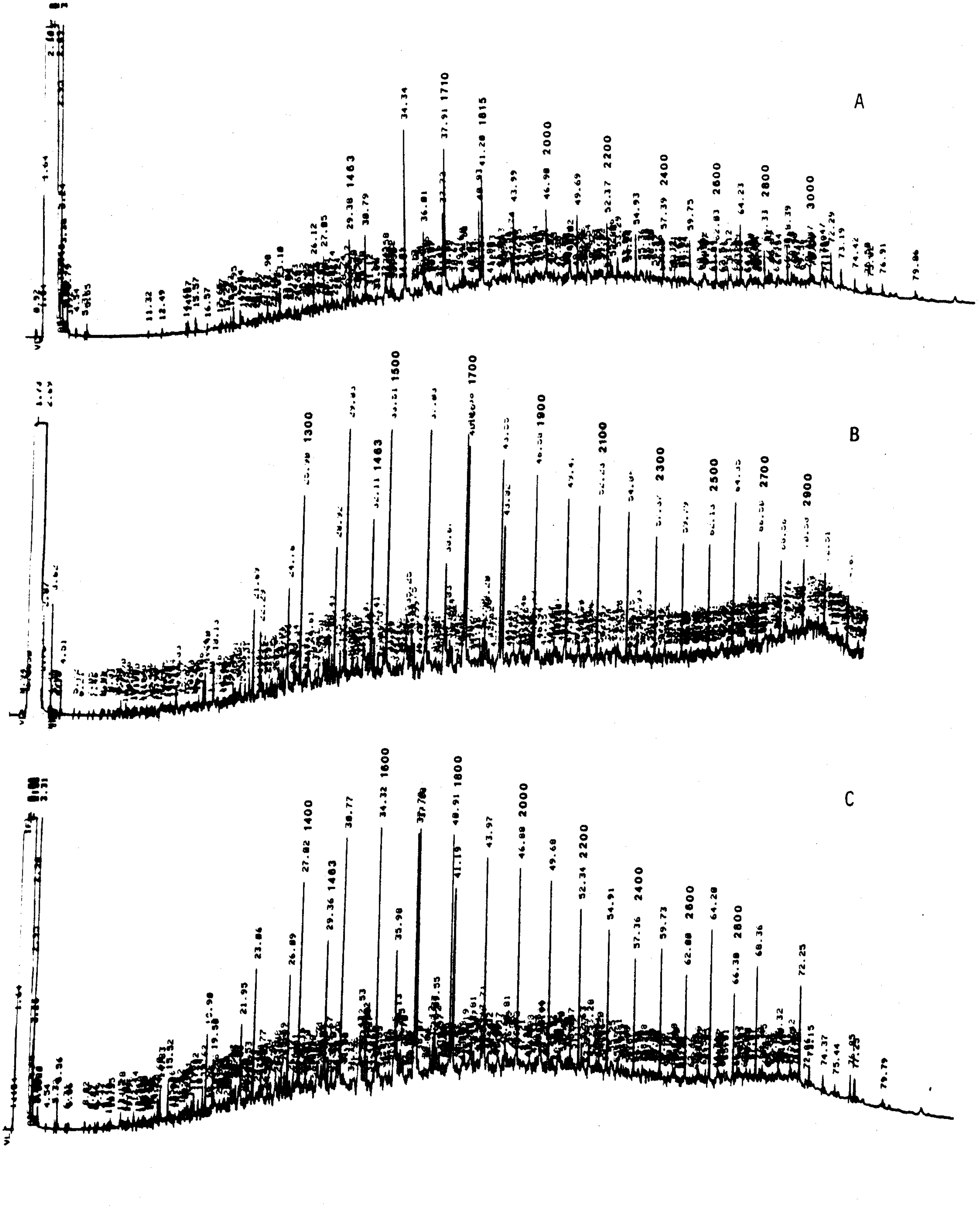

Figure 6-102. FID-GC chromatograms of sediment extracts from Jakalof Bay (site KB-5) 12 months after a spill of 1 liter of Prudhoe Bay crude oil at the Upper corral site. (A) Aliphatic fraction at a depth of 1-2", (B) whole extract at a depth of 2-4", and (C) Aliphatic fraction at a depth of 4-8".

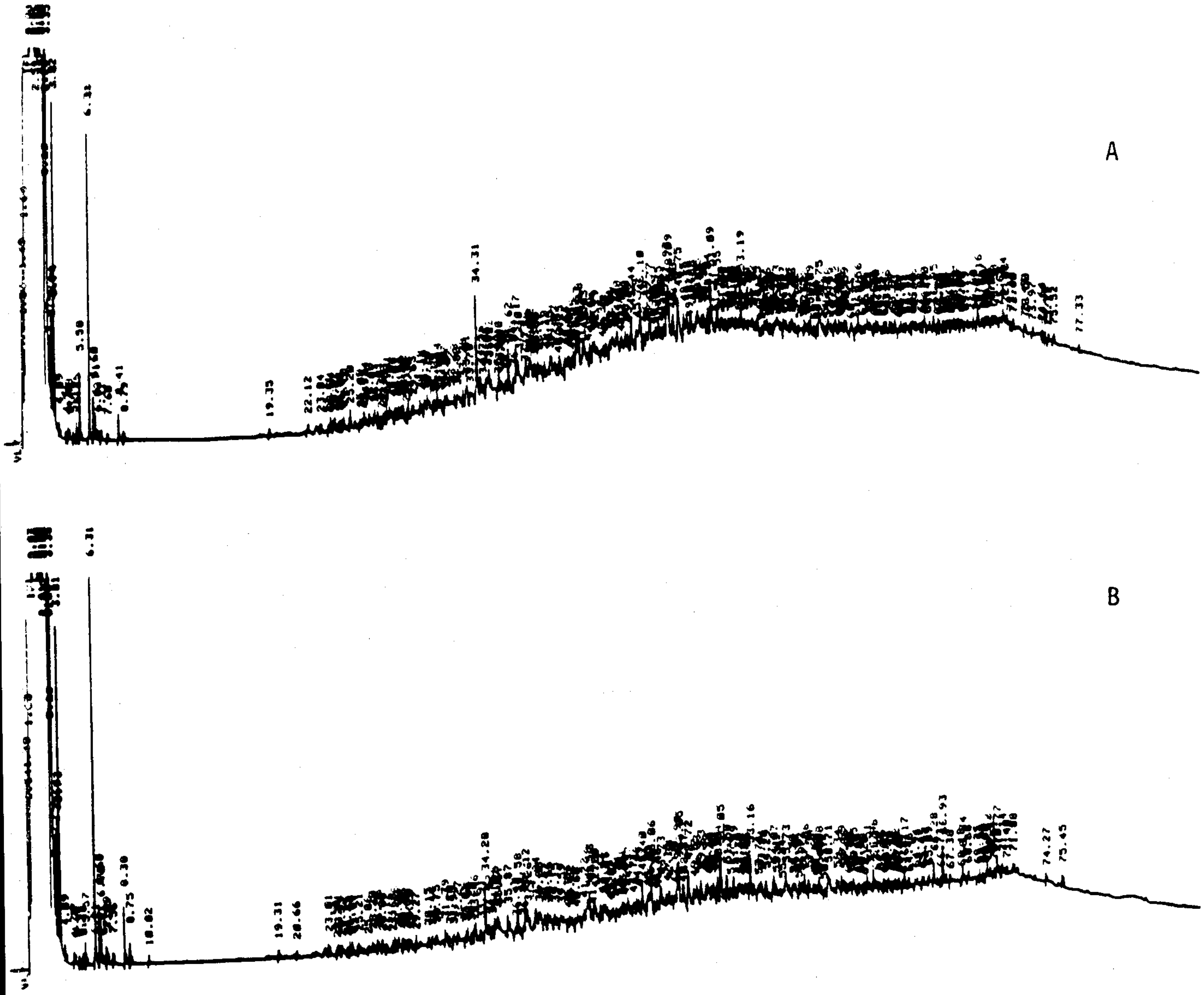

igure 6-103. FID-GC chromatograms of sediment extracts from Jakalof Bay (site KB-5) 12 months after a spill of 1 liter of Prudhoe Bay crude oil at the Upper corral site. Aromatic fraction at: (A) 1-2" depth, and (B) 4-8" depth.

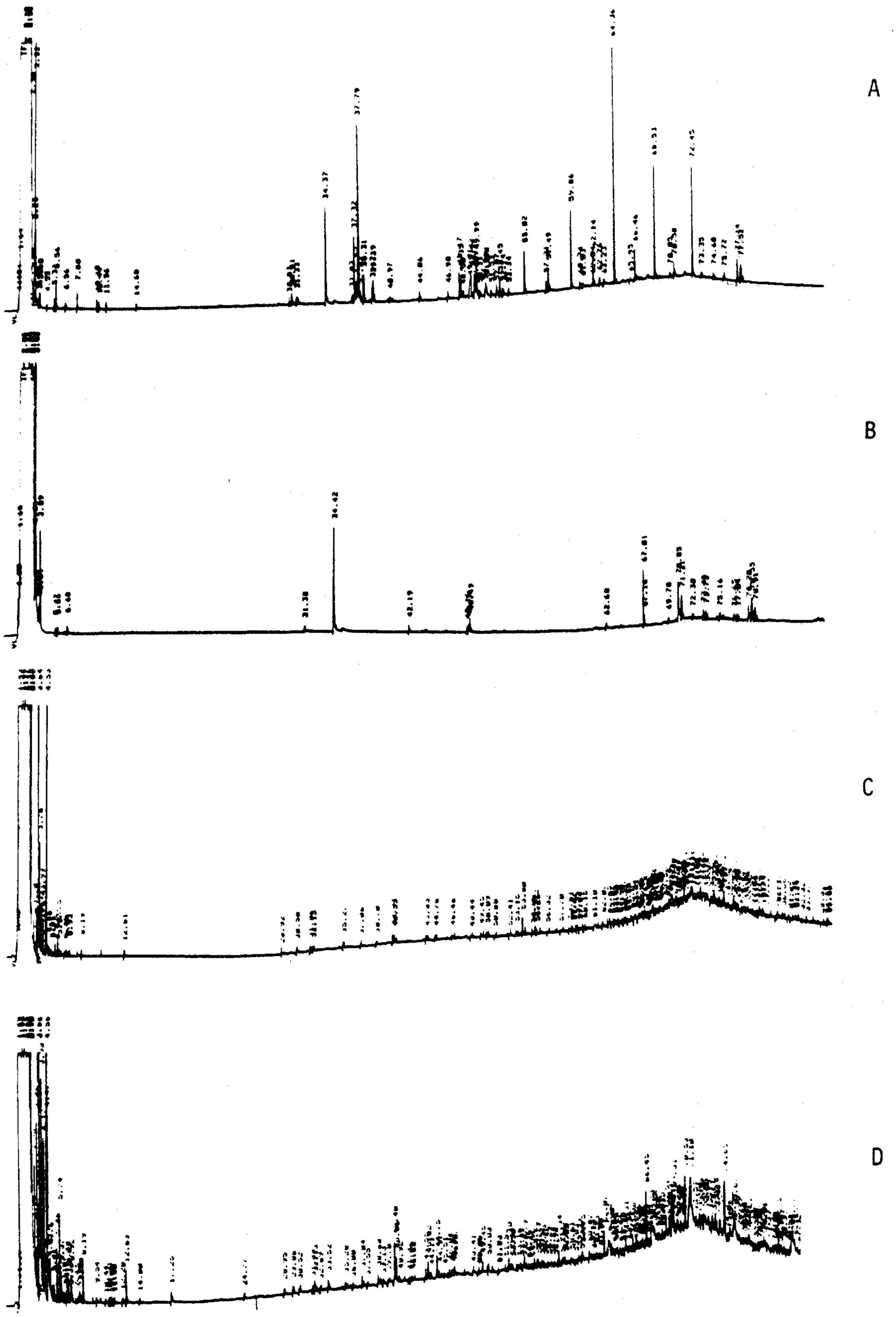

Figure 6-104. FID-GC chromatograms of sediment extracts from Jakalof Bay (site KB-5) 12 months after a spill of 1 liter of Prudhoe Bay crude oil at the Middle corral site. (A) Aliphatic fraction at a depth of 1-2", (B) Aromatic fraction at a depth of 1-2", (C) whole extract at a depth of 2-4", and (D) whole extract at a depth of 4-8".

resolved compounds before Kovat 2500, and an enhanced UCM at the latter part of the chromatogram. The 4 to 8 inch sample had more resolved peaks than the 2 to 4 inch sample, however, and this implies that comparatively less weathering occurred at the 4 to 8 inch depth.

The corrals were revisited in March 1983 (17 months post-spill). Again, numerous cattle tracks were present in and around the upper corral. Figure 6-105 shows the status of the upper intertidal corral after 17 months. All of the grass in the surrounding area of the upper corral had been killed by the winter temperatures, and extensive snow and ice cover, and there was only very limited regrowth during this early spring period. Visual observations showed no differences between the upper intertidal quadrant and adjacent areas. Figure 6-106 is a closeup of the corral interior 17 months after initiation of the spill, showing that there was no evidence of surface oil within the corral. Soil was excavated down to a depth of 10 inches, and a cross-sectional view of the hole showed that a distinct darker band of sediment extended between the 3 and 6 inch depths. This band of sediment had the characteristic Prudhoe Bay crude oil smell. Above and below this band the sediment returned to its original light brown color.

The middle corral was also similar in appearance to its adjacent intertidal area. There was very little plant growth at this site. Figures 6-107 and 6-108 show the status of the corral in March 1983 (17 months post-spill). Figure 27B is a closeup of the corral showing that it served to trap slightly higher levels of clay and silt-sized particulate material compared to the adjacent sediment. This light brown silty clay extended down to a depth of about 0.5 cm. Below this depth, the substrate consisted of a clay-gravel conglomerate identical to that in the surrounding regions. At three inches a darkened sediment layer with a faint crude oil odor was encountered. No other oil was observed until 10 inches depth. From 10 to 14 inches the sediment was heavily contaminated with oil. The majority of the oil seemed to be associated with the fine sedimentary material interspersed between the gravel. However, some discrete oil droplets (1-3 mm in diameter) were encountered on

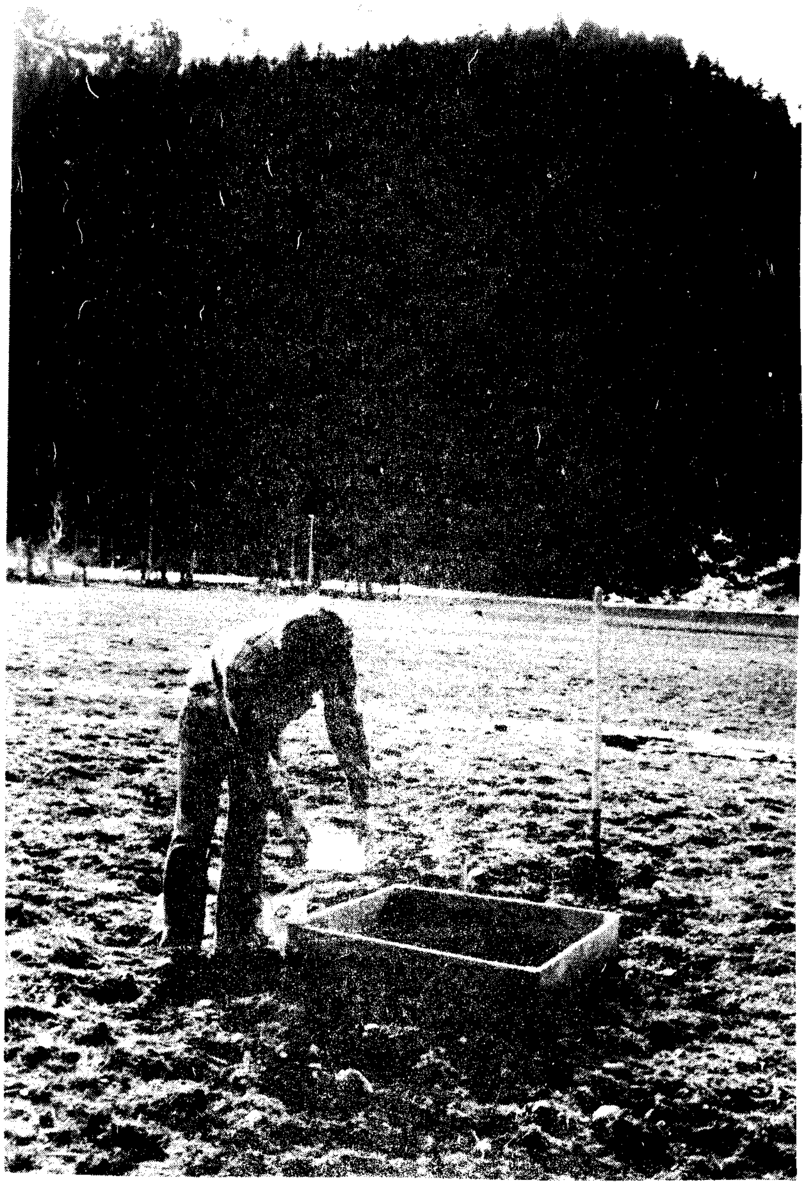

Figure 6-105. Appearance of the upper corral at site KB-5 (Jakalof Bay) after 17 months of exposure.

Figure 6-106. Interior of the upper corral at site KB-5 (Jakalof Bay) prior to sampling after 17 months of weathering.

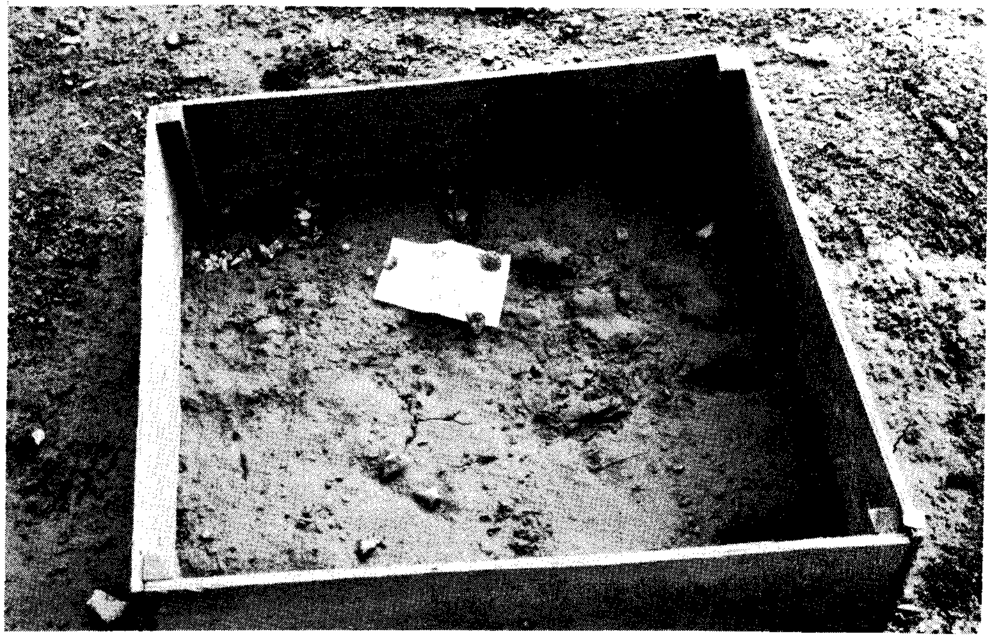

Figure 6-107. Interior of the mid-tide corral at site KB-5 (Jakalof Bay) prior to sampling after 17 months of weathering.

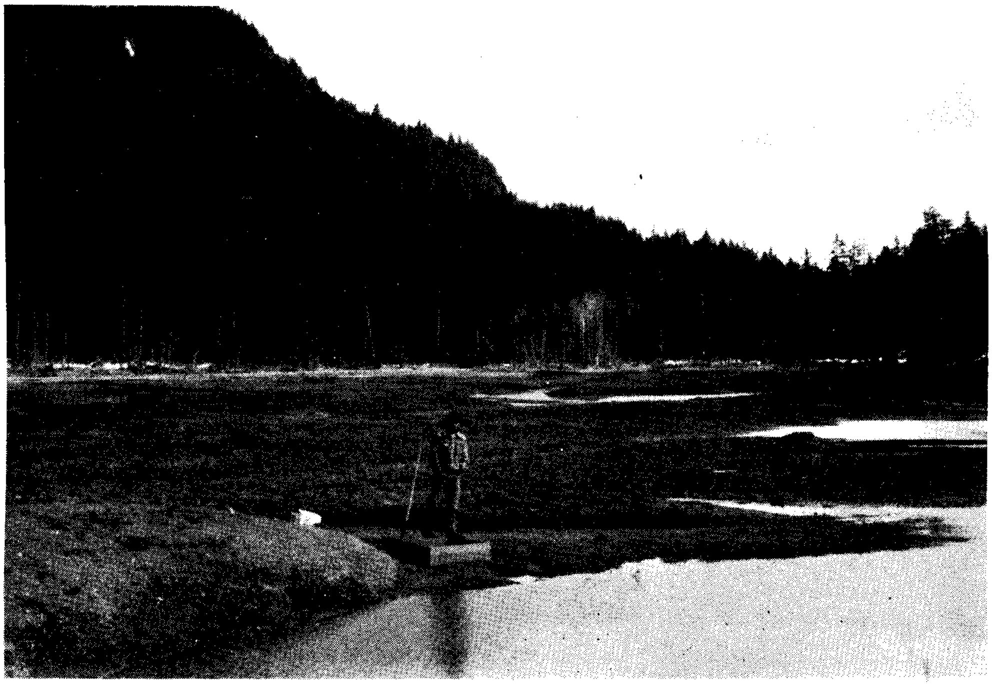

Figure 6-108. Appearance of the middle corral at site KB-5 (Jakolof Bay) after 17 months of exposure.

the gravel surface. At 18 inches depth the interstitial waters began to fill in the hole and some oil sheen was observed in the standing waters. Below this depth the hole tended to cave in so no observations of deeper sediments were attempted.

A summary of resolved and unresolved compound concentrations for the sediments which were analyzed at Jakolof Bay is presented in Table 6-24. (When more than one depth sample was analyzed for a particular sampling time these values represent average concentrations.) Bar graph illustrations were not included for this site since Day 0 data was inadequate. Except for the values at 12 months, the upper corral showed the general trend of decreasing with time. The middle corral also exhibits this trend, although the one month sample had a somewhat higher oil concentration than the 10 day sample.

Bio-toxicity observations of the middle corral were difficult because of the sparse biological presence at this site. However, the upper corral didn't seem to be affected adversely even though a fairly high concentration of oil was present. The grass within the corral grew to a similar length as that at adjacent areas, and the cattle didn't seem to show any preference in grazing.

TABLE 6-24. KB-5 Jakolof Bay

Concentration of Total Resolved and Unresolved Compounds
in the Intertidal Sediments at Various Times Post-Spill
(all concentrations in ug/g)[a]

		Day 2	Day 10	5 MonthS	12 Months	17 Months
UPPER CORRAL	Total resolved (ug/g)	965	NA[b]	182	749	19.6
	Total unresolved (ug/g)	3,968	NA	766	7,394	12.2
MIDDLE CORRAL	Total resolved (ug/g)	NA	46.9	39.4	24.1	12.2
	Total unresolved (ug/g)	NA	600	327	127	41.2

a - When more than one sample was analyzed for a specific time point these numbers represent average values.

b - NA indicates sample not analyzed or not available.

7.0 MICROBIAL DEGRADATION STUDIES

7.1 INTRODUCTION

The major themes of microbial degradation studies completed in this program were to: 1) examine the degradation of petroleum components in terms of specific compound susceptibility and microbial population dynamics, 2) isolate and characterize the stable oxidized products of catabolic processes, and 3) quantify the degree and rates of partitioning of these products into the air (CO_2), oil, and seawater phases (i.e., away from the slick-seawater interface.

Microbial degradation studies were performed in conjunction with Drs. Holm-Hansen and Azam at Scripps Institution of Oceanography (SIO) in La Jolla, while field studies were executed at NOAA's Sub-Arctic Research Station in Kasitsna Bay, Alaska. Continuous-flow experimental seawater aquarium systems were designed and fabricated at both locations (SIO and Kasitsna Bay) to facilitate comparisons of microbial interactions with Prudhoe Bay crude petroleum between a temperate and a sub-arctic marine environment.

The continuous-flow experimental approach was utilized with the intent of providing a dynamic characterization of marine microbial populations and their inherent metabolic capacity for degrading petroleum components as a function of the time of interaction with petroleum. This time-dependent response within the indigenous heterotrophic population, towards a greater relative abundance of hydrocarbonoclastic (hydrocarbon-degrading) microbes, is indicated by a concomitant increase in degradation potential of the system, which can be measured by increased ^{14}C-labeled compound degradation. This has been empirically demonstrated by increases in the rates of mineralization of selected ^{14}C-labeled hydrocarbons to $^{14}CO_2$ as a function of continued exposure to crude oil within the experimental aquariums. Additional components of the "response time" include: determinations of heterotrophic bacterioplankton growth rates both from incorporation of tritium-labeled thymidine into deoxyribonucleic acid (DNA) and from enumeration of bacterial cells by epifluorescence microscopy; and determinations of overall metabolic activity by uptake of tritium-labeled leucine and glucose.

It was also of interest to examine the influence of concentration levels of available dissolved inorganic nutrients (PO_4^{-3}, NO_2^-, NO_3^-) and dissolved oxygen upon microbial metabolic activities. Phosphorous requirements of bacterial cells are generally supplied by assimilation of inorganic phosphate for incorporation into organic phosphorous containing components, such as nucleic acids, ATP, and membrane phospholipids. Nitrate and nitrite ions can be assimilated into amino acids by assimilatory nitrate enzymes, and molecular oxygen incorporation is required for the metabolism of various hydrocarbons (Atlas and Bartha, 1981). To facilitate the comparison, a nutrient solution was introduced (via a peristaltic pump system) into one of the two experimental aquariums to maintain elevated levels (with respect to incoming seawater) and aeration of the seawater supplying this tank was also provided.

The continuous-flow experimental aquarium systems at Scripps Institution of Oceanography and NOAA's Kasitsna Bay, Alaska facility were set up (Summer 1981) and run for at least one week prior to initiation of each experiment to allow sufficient time for bacterial fouling, population buildup and stabilization of the microbial community within the aquariums.

The experimental aquaria and the incoming seawater were sampled for the radiolabeled substrate assays (^{14}C-hexadecane, ^{14}C-methylnaphthalene, ^{14}C-naphthalene; ^{3}H-glucose, ^{3}H-leucine, ^{3}H-thymidine) on Days 0, 1, 2, 4, 5, 6, 7, 9, 12, 14, 16, 19, 21, 23, 26, 28, 30, 35, 42, 49, and 56 at SIO and on the same schedule up to Day 30 at Kasitsna Bay. Samples for nutrients, and epifluorescence assays were taken on Days 0, 1, 2, 4, 7, 14,, 21, and 28 for both experiments. Seawater samples (20 to 30 liters) for petroleum hydrocarbon and metabolic product analyses were taken on Days 1, 2, 5, 9, 16, 23, 30, 43 and 58 at SIO, and up to Day 30 at Kasitsna Bay. To initiate each experiment, approximately 200 ml of Prudhoe Bay crude oil was added to each experimental aquarium shortly after sampling for the Day 0 assays listed above. Flow rates through the tanks were maintained by peristaltic pumps (Masterflex, Cole-Palmer Corp.) to provide a seawater throughput of about one tank volume (~ 20 liters) per day. A schematic representation of the aquarium system is depicted in Figure 7-1. Although not shown in the figure, both the master reservoirs and the experimental tanks were situated in continuous flow seawater baths to maintain ambient temperatures.

7.1.1 ^{14}C-Hydrocarbon Degradation

One of the important "components" of the overall microbial response to input of crude oil into the marine environment relates to the ability of the naturally occurring heterotrophic microbes to utilize the petroleum as a food (organic carbon) source. This capacity is referred to as "degradation potential", and can be inferred from the relative degree of mineralization (metabolism to CO_2) of representative petroleum hydrocarbons. Should selection within the heterotrophic fraction of the indigenous population favor an increase in relative abundance of hydrocarbonoclastic bacteria, this should be reflected by a concomitant increase in degradation potential. One approach to empirically define this potential, that is sensitive and reproducible, involves exposing the microbes to a ^{14}C-labeled petroleum hydrocarbon substrate, allowing sufficient time for degradation to occur, with subsequent trapping of evolved $^{14}CO_2$ and quantification by liquid scintillation spectrometry. This approach has been taken in various forms in past studies (Harrison et al. (1971); Caparello and La Rock (1975); Walker and Colwell (1976); Hodson et al. (1977)), however experimental conditions in most cases have made it difficult or totally infeasible to extrapolate results to a real spill situation. We have attempted to utilize the degradation potential approach, with the continuously flowing seawater aquaria systems at SIO and Kasitsna Bay, with the intention of providing empirical information which would be useful in characterizing the impact of microbial degradation upon spilled petroleum. Although caution must be taken in extrapolating results from a study utilizing such "controlled ecosystems" to open ocean spills, it is believed that this

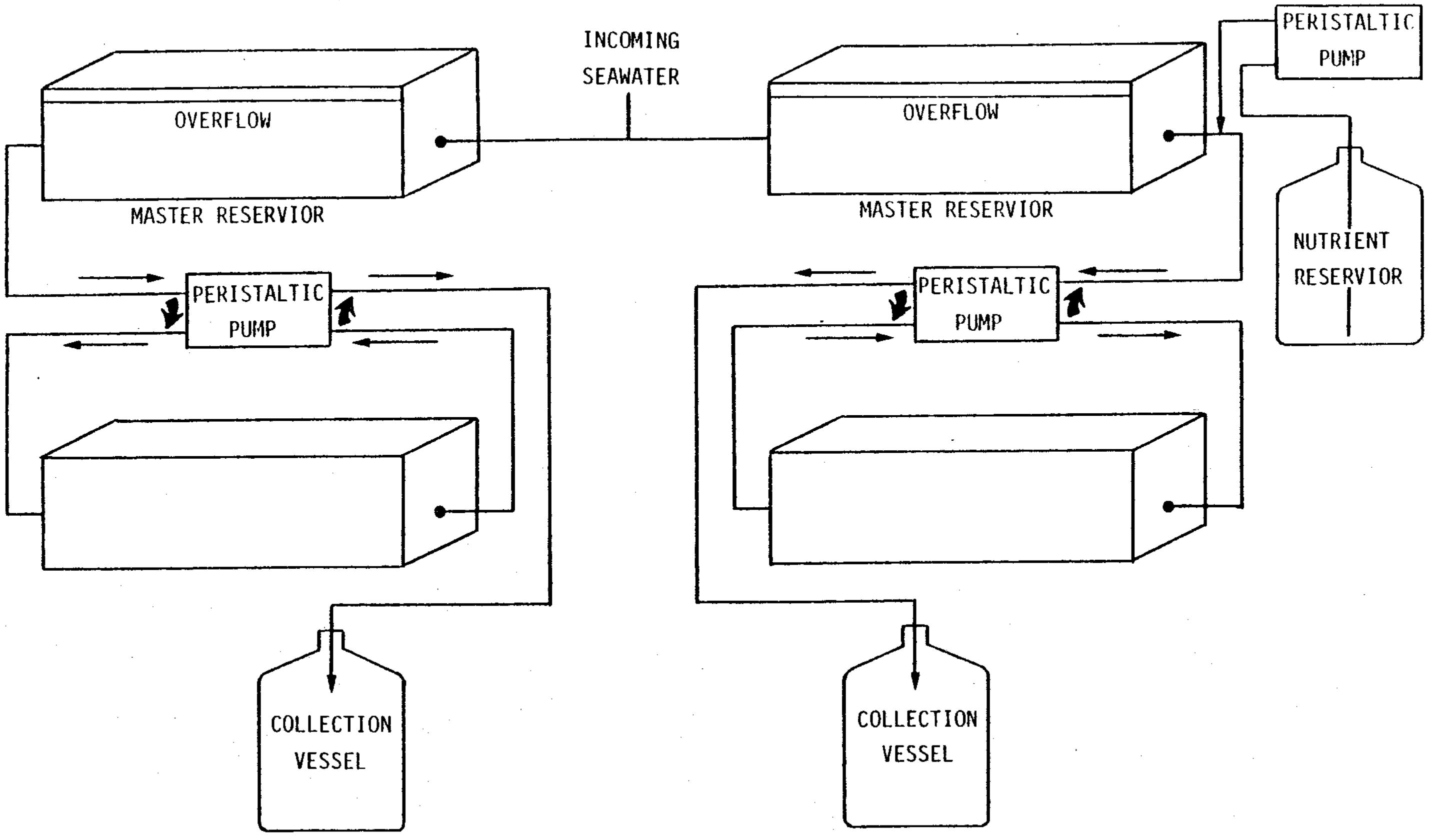

FIGURE 7-1. Diagram of the Continuous-Flow Experimental Aquarium Systems utilized at Scripps Institution of Oceanography and NOAA's Kasitsna Bay, Alaska Research Station

approach optimizes the ability to empirically describe the impact of oil upon various microbiological metabolic processes, and conversely, the impact of microbial degradation upon the disposition of the oil itself.

The degradation potential assay involves addition of a ^{14}C-labeled hydrocarbon substrate to seawater samples from the experimental aquaria and incoming seawater, incubation in stoppered vials for 24 hrs. at in situ temperatures, trapping of $^{14}CO_2$, and quantification by liquid scintillation spectrometry (details presented in Materials and Methods). The labeled substrates selected were ^{14}C-hexadecane, ^{14}C-methylnaphthalene, and ^{14}C-naphthalene. The selection was based upon both availability and representation within the compounds and class types found in Prudhoe Bay crude, as well as other crude petroleums.

7.1.2 ^{3}H-Labeled Substrate Uptake/Incorporation

To further assess the impact of spilled petroleum on microbial heterotrophic activity, it is necessary to determine influences on heterotrophic production (growth rates), microbial biomass, and general metabolic activity. The utilization of radiolabeled organic substrates at near ambient concentrations, for determining rates of uptake and/or incorporation into cell biomass, is a viable and sensitive empirical approach and has been pursued in past studies (Azam and Holm-Hansen, 1973; Hodson et al., 1977; Fuhrman et al., 1980; Fuhrman and Azam, 1980; Griffiths and Morita, 1981). The use of tritium-labeled organic compounds (sugars, amino acids, etc.) of high specific activities allows for direct measurement of uptake at near ambient concentrations (10^{-8} to 10^{-9} M) and precludes extrapolation using the Michaelis-Menten equation (as is needed when substrate concentrations are greater than those normally found in the marine environment).

The incorporation of ^{3}H-thymidine into bacterial DNA serves as a reasonable measure of DNA synthesis and cell production, although several assumptions and measurements are required for conversion of thymidine incorporation data into production estimates (Fuhrman and Azam, 1980). The level or rate of uptake (nmoles/liter-day) is converted to bacterial cell production rates (cells/liter-day) with an estimation of the DNA content of natural marine bacteria. This conversion has been recently refined by Fuhrman and Azam (1981) into separate coefficients for the nearshore and offshore (> 10 km) waters studied (Southern California Bight). Estimations of average cell biomass by epifluorescence photomicroscopy allow for further data conversion from production rates (cells/liter-day) to organic carbon production (gC/liter-day). This is accomplished by determining cell size (volume) distributions and by correlating the data to the amount of carbon per cell with a conversion factor developed by Watson et al. (1977).

General metabolic activities have been determined by uptake of ^{3}H-glucose and ^{3}H-leucine. The specific techniques utilized do not differentiate between substrate respired from that incorporated (assimilated) into cell biomass, and therefore, the overall uptake cannot be used to estimate cellular production. However, Fuhrman et al. (1980) found significant rank correlations between thymidine incorporation (mol/liter-day), thymidine turnover rates (%/hr), bacterial abundance or biomass (from epifluorescence microscopy), and glucose turnover rates (%/hr) in the euphotic zone of the Southern California Bight. Their results suggest that these methods may be comparable for assaying relative total bacterial activity between water samples.

7.2 MATERIALS AND METHODS

^{14}C-Hydrocarbon Mineralization Assay

The ^{14}C-hydrocarbon mineralization assay utilized in this study was based upon previous work by Watson et al. (1971), Caparello and La Rock (1975), Walker and Colwell (1976) and Hodson et al. (1977).

Three ^{14}C-labeled hydrocarbon substrates were utilized for the determination of hydrocarbon degradation potential, defined here as the percent mineralization to $^{14}CO_2$: n(1-^{14}C) hexadecane (53.6 mCi/mmol, Amersham), (1(4,5,8)-^{14}C) naphthalene (5 mCi/mmol, Amersham), and (1(4,5,8)-^{14}C) methylnaphthalene (5 mCi/mmol, Bionuclear). Working solutions were prepared with hexane or benzene as solvents to give 0.1μCi/μl activities, stored at 4°C, and assayed weekly for radioactivity to insure consistency in the concentrations of substrates. Seawater aliquots (50 ml) from each of the experimental tanks and the incoming seawater were transferred to 100 ml sterile serum bottles and spiked with 0.5μCi of the ^{14}C-labeled hydrocarbons, one compound per sample with each sample prepared in duplicate. Controls were killed with 1μM $HgCl_2$ prior to spiking with the labeled compound.

The spiked seawater samples were capped with sleeve stoppers and incubated in the dark for 24 hours at <u>in situ</u> temperatures in a water bath. After the incubation period the stoppers were replaced with identical stoppers fitted with a polypropylene "center well", containing a 25-mm by 30-mm rectangle of Whatman No. 1 filter paper folded into an accordian-pleated array and wetted with 0.2 ml of 1N NaOH. The samples were then acidified to pH 1.0-2.0 by injection of 0.5ml of 1N H_2SO_4 (through the sleeve stopper) with a hypodermic syringe. After 2 hours the filter paper was transferred to a second 100 ml serum bottle containing 1 ml of 1N H_2SO_4, which was quickly capped with a sleeve stopper fitted with a center well (as before) and a wick that had been wetted with 0.2ml of phenethylamine.

After 12-14 hours the phenethylamine-saturated wicks were transferred to a scintillation vial containing 10 ml of Beta-Phase cocktail (West Chem Products) and assayed for radioactivity on a Beckman LS100C scintillation counter. The resulting counts for duplicates were averaged and corrected for the control counts prior to further data treatment. The data (in counts per minute) were converted to μg/liter day by the following equation.

$$\mu g/\ell \cdot day = (cpm)\left(\frac{1\ dpm}{0.9\ cpm}\right)\left(\frac{1\ \mu Ci}{2.22 \times 10^6\ dpm}\right)\left(S.A.^{-1}\right)\left(m.w.\right)\left(\frac{1000\ ml}{1\ \ell}\right)\left(\frac{1}{50\ ml}\right)\left(\frac{1}{day}\right)$$

where a counting efficiency of 90% was utilized, S.A. is the specific activity in µCi/µ mole, and M.W. is the molecular weight of the particular labeled substrate.

^{3}H-Thymidine Incorporation

The ^{3}H-thymidine incorporation assay utilized in this study was based upon previous work by Fuhrman and Azam (1980), Fuhrman et al. (1980) and Fuhrman and Azam (1981).

Thymidine (methyl-^{3}H) solutions were stored as supplied (20 Ci/mmol, New England Nuclear) in 70% aqueous ethanol for maximum stability. Working solutions were prepared by evaporating to dryness the appropriate volume under a stream of dry, filtered air and reconstituting with distilled water. These solutions were stored at 4°C and checked weekly for radioactivity.

Duplicate seawater aliquots (10 ml) from each experimental aquarium and the incoming seawater were spiked with 5nM of labeled thymidine and incubated in the dark at in situ temperatures for 1 hour. Incubation uptake was terminated by filtration through a 25-mm dia. type HA membrane (0.45µm nominal pore size, Millipore Corp.). After filtration, the vacuum was stopped and 10 ml of ice-cold (< 5°C) filtered (sterile) seawater was added to cool the filter. This was filtered through, and the vacuum was stopped prior to addition of 15 ml ice-cold (< 5°C) 5% trichloroacetic acid (TCA) to extract the soluble thymidine pools from the cells. Temperature control is critical during the extraction as a temperature rise above 10°C for TCA will hydrolyse DNA and allow incorporated label to solubilize and pass through the filter. After 3 min. the vacuum was applied and the filter was rinsed twice with 5 ml ice-cold 5% TCA and then placed in a scintillation vial. Ethyl acetate (1 ml) was added, to dissolve the filter, followed by addition of 10 ml of Beta-Phase cocktail prior to radioactivity assay by liquid scintillation spectrometry.

The resulting counts for duplicates were averaged and corrected for poisoned controls (1μM $HgCl_2$) and a counting efficiency of 35%. The data were converted to nmoles/liter day of incorporation by the formula:

$$\text{n moles}/\ell\cdot\text{day} = (\text{cpm})\left(\frac{1\ \text{dpm}}{0.35\ \text{cpm}}\right)\left(\frac{1\ \text{Ci}}{2.22 \times 10^{12}\ \text{dpm}}\right)\left(\frac{1\ \text{m mol}}{20\ \text{Ci}}\right)\left(\frac{10^{6}\ \text{n mol}}{\text{m mol}}\right)\left(\frac{24\ \text{hr}}{\text{day}}\right)\left(\frac{1}{0.015\,\ell}\right)\left(\frac{1}{1\ \text{hr}}\right)$$

^{3}H-Leucine and ^{3}H-Glucose Uptake

The ^{3}H-leucine and ^{3}H-glucose assays utilized in this study were after Azam and Holm-Hansen (1973) and Fuhrman et al. (1980).

Working solutions of ^{3}H-leucine (60 Ci/mmol, New England Nuclear) were prepared by diluting an aliquot of the stock solution into distilled water. The ^{3}H-glucose solutions (30 Ci/mmol, New England Nuclear) were prepared by evaporating an aliquot under a stream of dry, filtered air followed by reconstitution in distilled water. All solutions were stored at 4°C and assayed weekly to check for radioactivity stability.

Each experimental aquarium and the incoming seawater was sampled in duplicate, and controls were killed with 1μM $HgCl_2$ prior to addition of radiolabeled substrate. 50μl. (1.5μCi) of radiolabeled compound was added to each sample (10 ml for ^{3}H-glucose; 15 ml for ^{3}H-leucine), followed by incubation for 2 hr. in the dark at *in situ* temperature.

The incubation was terminated by sample filtration through a HA membrane (0.45μm nominal pore size, Millipore Corp.), followed by several washes with filter-sterilized seawater, to remove any nonincorporated label. After filtration, each filter was placed in a scintillation vial, and 1 ml Ethyl acetate added to dissolve the membrane. After approximately 10 min., 10 ml of Beta-Phase cocktail was added and the sample assayed for radioactivity by liquid scintillation spectrometry. Duplicates were averaged and corrected for control blanks, and the resulting counts were converted to uptake in nmoles/liter day with the formula:

$$\text{n moles}/\ell\cdot\text{day} = (\text{cpm})\left(\frac{1\ \text{dpm}}{0.35\ \text{cpm}}\right)\left(\frac{1\ \text{Ci}}{2.22 \times 10^{12}\ \text{dpm}}\right)\left(\text{S.A.}^{-1}\right)\left(\frac{10^{6}\ \text{n mol}}{\text{m mol}}\right)\left(\frac{24\ \text{hr}}{\text{day}}\right)\left(\frac{1}{2\ \text{hr}}\right)\left(\frac{1}{0.015\,\ell}\right)$$

where a counting efficiency of 35% was utilized and S.A. is the specific activity (in Ci/mmol) for the labeled substrate.

Epifluorescence Enumeration

The epifluoriscence assay utilized in this study was based upon the methods of Hobbie et al. (1977) and Fuhrman and Azam (1980).

Seawater samples (10-15 ml) from each experimental aquarium and the incoming seawater were immediately preserved with 4% filter-sterilized formalin (buffered with $Na_2B_4O_7$), and the cellular DNA was stained with Acridine orange (0.01%, 2 min.) prior to filtration. The Nucleopore polycarbonate filters were stained prior to use with Irgalan black (to eliminate autofluorescence), and a type AA (0.8µm, Millipore) membrane was used as a back filter to distribute the vacuum evenly. After filtration, the filter was mounted on a microscope slide, with a cover slip affixed with paraffin oil. Blanks were prepared in a similar fashion except that filter-sterilized seawater (type GS, 0.2µm, Millipore Corp.) was preserved and stained.

The slides were examined by epifluorescence microscopy and counted in a random fashion by grids. All counts for each grid were averaged (10 grids per slide) for duplicate slides and the data converted to cells x 10^6/ml seawater. In addition to visual counts, each slide was photographed on Ilford HP5 35mm film for subsequent cell size distribution determinations. The photographs were enlarged and cell sizes were measured with a micrometer magnifier.

Cells were classified as rods or spheres and the volume distribution data were analyzed with the aid of a computer program.

7.3 RESULTS

7.3.1 ^{14}C-Hydrocarbon Degradation

As indicated previously, the sampling points were concentrated at the beginning of each experiment to best detect and describe any degradation potential increase following input of Prudhoe Bay crude into the two experimental aquariums. The incoming seawater (from the master reservoirs) was also sampled at each time point and assayed to check for "background" hydrocarbon degradation potential.

The data for the ^{14}C-hydrocarbon degradation studies have been converted to µg/liter-day and are presented graphically in Figure 7-2 for SIO results and Figure 7-3 for Kasitsna Bay, Alaska. The assumption made for data conversion is that trapping and detection of the ^{14}C carbon indicates a loss of parent compound molecular structure even though total mineralization (to CO_2) cannot be deduced. The results from the SIO experiment demonstrate a dramatic increase in the amount of labeled substrate for all three hydrocarbons mineralized to $^{14}CO_2$ within 48 hrs after introduction of oil. At Day 0, hexadecane was slightly degraded, although no capacity was apparent for degrading the methylnaphthalene and naphthalene substrates for any of the samples. The incoming seawater did not demonstrate any degradation capacity for the aromatic compounds until Day 56, although the hexadecane was degraded to some extent with similar patterns (note Figure) between the two experimental systems. Both tanks demonstrated slightly greater utilization of hexadecane over the course of the experiment, with a peak utilization for the nutrient supplemented system of approximately 5% of the added labeled substrate (again note that percent degradation is based upon the label itself and not the entire compound). All experimental systems followed similar trends (incoming seawater included) with time with an overall degradation rate of roughly 1.5% of the added substrate during any given 24 hr incubation period.

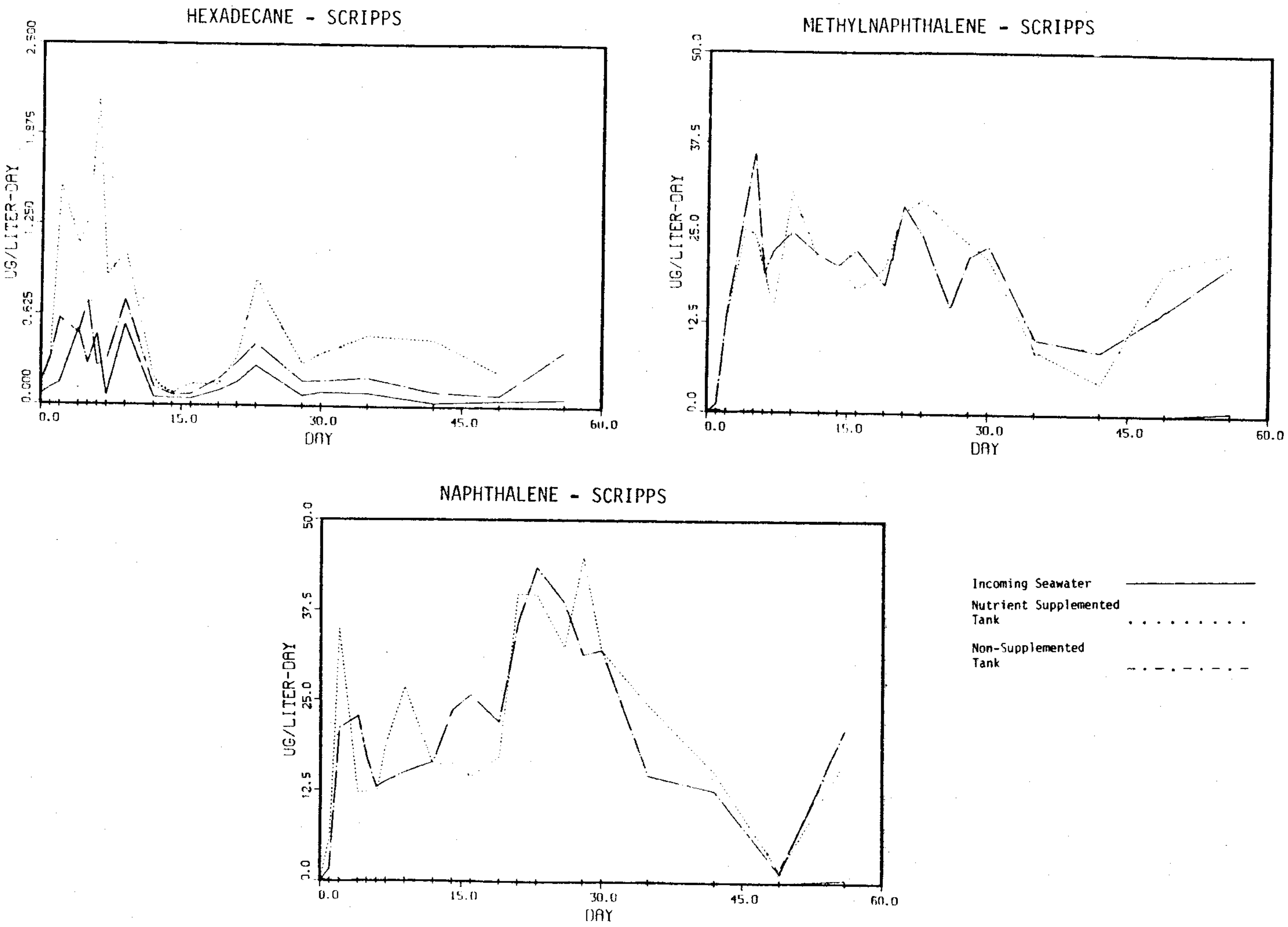

FIGURE 7-2. ^{14}C-HYDROCARBON DEGRADATION DATA, SCRIPPS INSTITUTION OF OCEANOGRAPHY, SUMMER 1981. DATA FOR EACH SUBSTRATE ARE DEPICTED FOR ALL EXPERIMENTAL AQUARIA AND INCOMING SEAWATER, VERTICAL LINES ON ABSCISSA INDICATE SAMPLING POINTS.

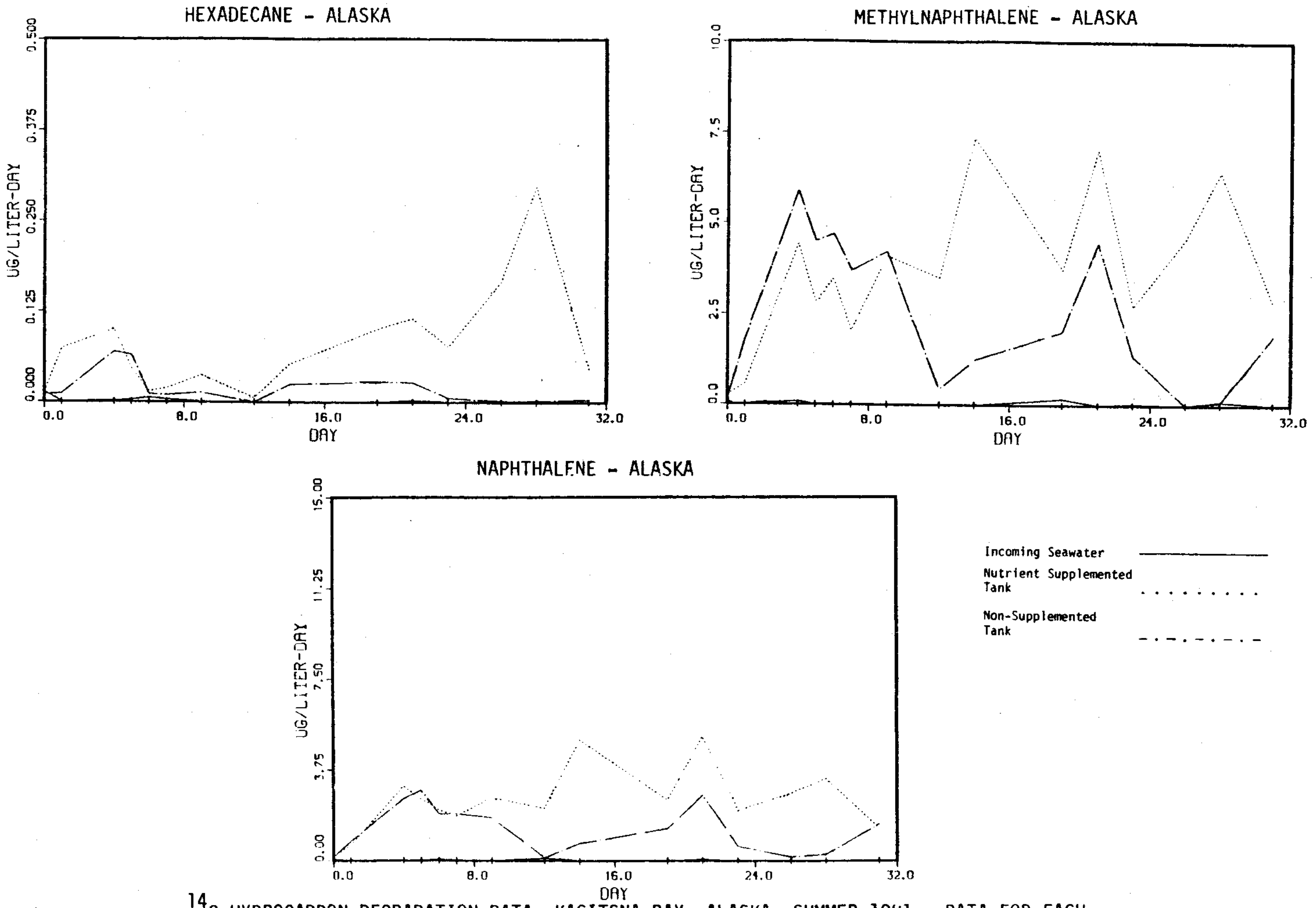

FIGURE 7-3. ^{14}C-HYDROCARBON DEGRADATION DATA, KASITSNA BAY, ALASKA, SUMMER 1981. DATA FOR EACH SUBSTRATE ARE DEPICTED FOR ALL EXPERIMENTAL AQUARIA AND INCOMING SEAWATER. VERTICAL LINES ON ABSCISSA INDICATE SAMPLING POINTS.

In comparing the relative rates of degradation for radiolabeled hydrocarbon substrates, it must be emphasized that the loss of label (^{14}C) from the parent molecule does not necessarily imply an "upper limit" on the amount of substrate which has been oxidized by microbes. In other words, certain metabolic conversions of the parent compound to other stable forms may occur <u>without</u> loss of the label. In this case, the degradation rate, as based upon detection and quantification of the lost ^{14}C label, would be an underestimation of the actual amount of the original parent substrate "attacked" by the microbial enzymatic systems. As will be noted below, the degradation data suggest that the hexadecane substrate was degraded at much lower rates than for either of the aromatic compounds. However, it is entirely possible that the mode of metabolic conversion for the aliphatic substrate renders the parent compound into stable forms (e.g., carboxylic acids, acetates), which may or may not undergo further mineralization during the 24-hr period of incubation.

Both of the labeled aromatic hydrocarbon substrates were degraded at substantially higher rates (based on $^{14}CO_2$ production) compared to hexadecane for the SIO experiment. The experimental seawater aquaria exhibited quite similar patterns for methylnaphthalene, with dramatic increases in the rate of substrate mineralization within 48 to 72 hrs to approximately 11% (of the amounts added for the 24 hour incubation), with an average rate of roughly 6% per day over the 56 days of monitoring. Less consistency between experimental systems is apparent for the naphthalene utilization data, although average degradation rates are comparable to those for methylnaphthalene.

The ^{14}C-hydrocarbon data for the Kasitsna Bay experiment (Figure 7-3) demonstrated several similarities to the results from SIO: (1) hexadecane was apparently utilized to a lesser extent than either methylnaphthalene or naphthalene; (2) the incoming seawater demonstrated very little capacity for degrading any of the substrates; and (3) some similarities exist between experimental tanks for the two aromatic hydrocarbons, although to a lesser extent than with the SIO systems. Only in the case of methylnaphthalene was a definite increase apparent in rate of mineralization for both tanks after introduction of Prudhoe Bay crude. Two additional trends which contrast the results from the SIO experiment are: (1) greater methylnaphthalene utilization for the inorganic nutrient supplemented tank where nutrient supplementation had no apparent effect in SIO mineralization rate data; and (2) rates of substrate degradation were substantially lower in the Kasitsna Bay systems for all three hydrocarbons relative to the SIO experiment. This could be attributable to generally lower metabolic activities due to colder water temperatures, as they averaged 19 to 21°C during the course of the SIO study, and 9 to 11°C for the Alaska study.

7.3.2 ^{3}H-Labeled Substrate Uptake/Incorporation

The ^{3}H-thymidine incorporation, ^{3}H-leucine uptake, and ^{3}H-glucose uptake data for the SIO and Kasitsna Bay experiments are presented graphically in Figures 7-4 and 7-5, respectively. All data have been converted to uptake rates in nmoles/liter-day and have been normalized to uptake on a per bacterial cell basis for the SIO data, Day 0 to Day 7 (Table 7-1).

In the SIO thymidine incorporation experiments, all experimental aquaria demonstrated similar patterns in terms of an initial increase in incorporation rates after introduction of oil, followed by a general decline and periodic fluctuations during the 56 days of monitoring. The incoming seawater remained relatively inactive during the course of the experiment, and this may also be attributable to the relative abundance of bacteria (abundance data will be discussed below).

The leucine uptake data from the SIO experiment are difficult to interpret due to the large fluctuations with time and between experimental systems. After introduction of Prudhoe Bay crude, both aquaria exhibited a sharp rise in uptake rates followed by declines. Some stability in trends among the systems is apparent after two weeks which, in some cases, paralleled trends of the incoming seawater.

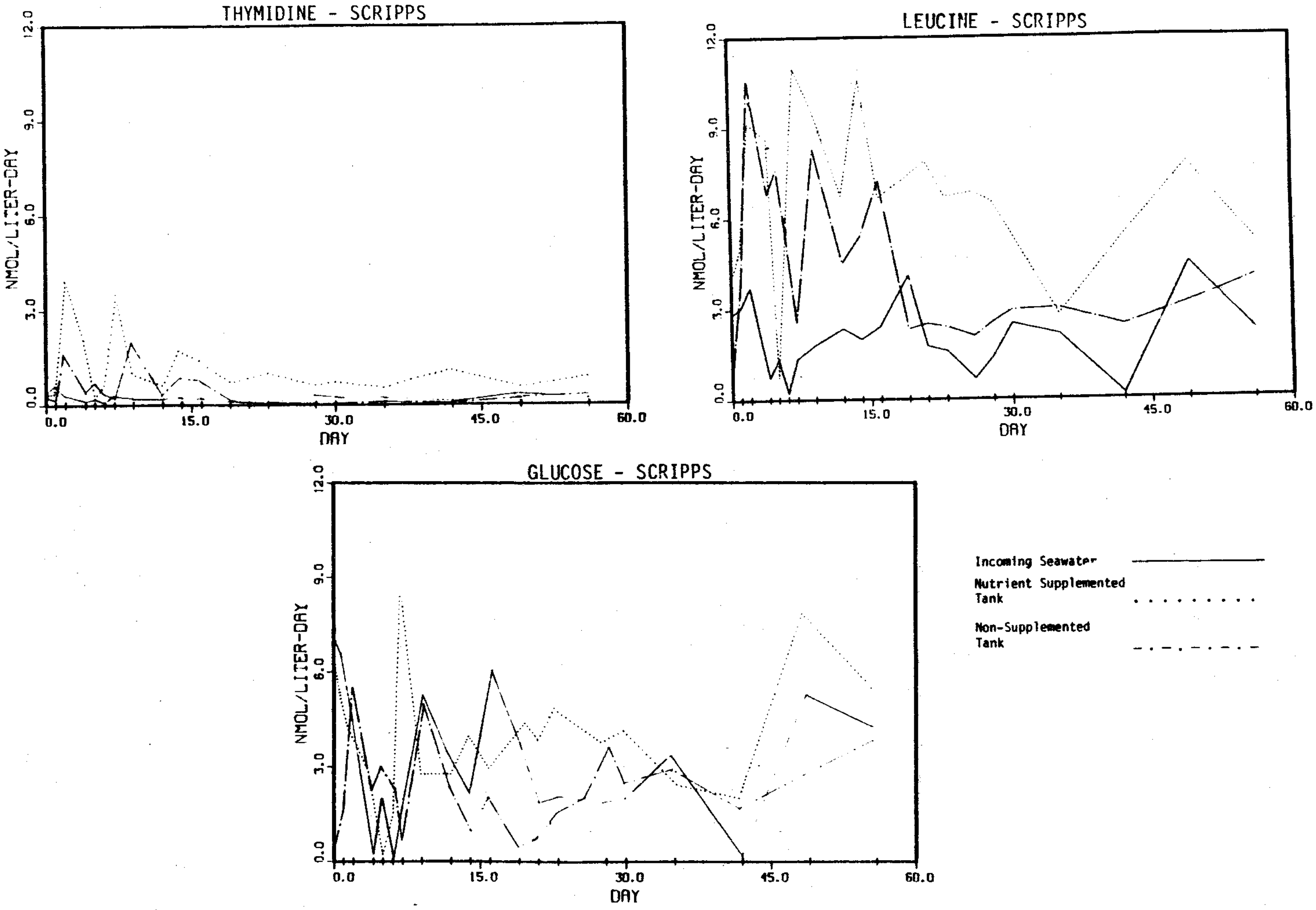

FIGURE 7-4. ^{3}H-Thymidine Incorpoation, ^{3}H-Leucine and ^{3}H-Glucose Uptake Data, Scripps Institution of Oceanography, Summer 1981. Data for each substrate is depicted for all experimental aquariums and incoming seawater. Vertical lines on absicissa indicate sampling points.

7-16

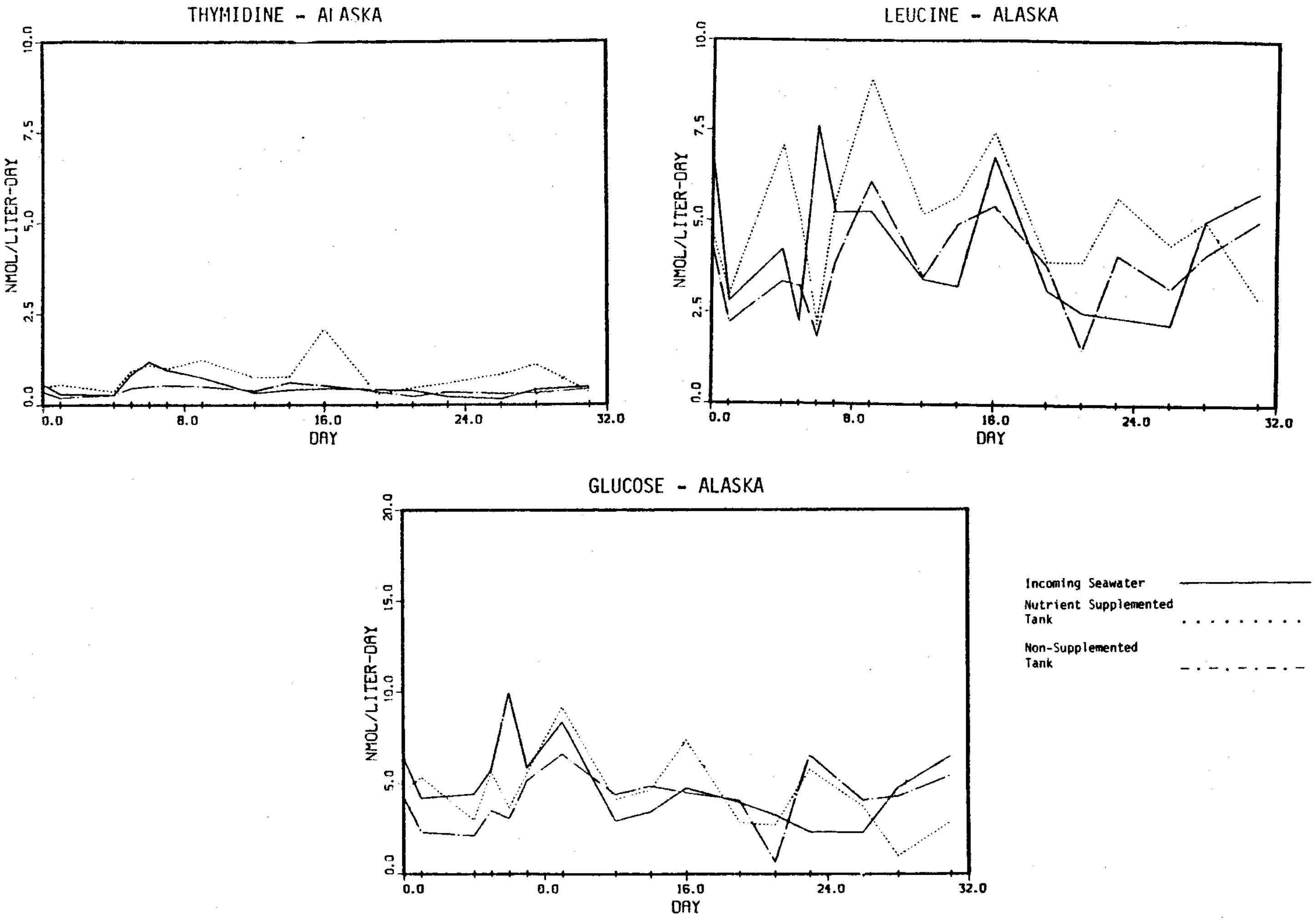

FIGURE 7-5. ^{3}H-THYMIDINE INCORPORATION, ^{3}H-LEUCINE AND ^{3}H-GLUCOSE UPTAKE DATA, KASITSNA BAY, ALASKA SUMMER 1981. DATA FOR EACH SUBSTRATE IS DEPICTED FOR ALL EXPERIMENTAL AQUARIUMS AND INCOMING SEAWATER, VERTICAL LINES ON ABSCISSA INDICATE SAMPLING POINTS.

The thymidine incorporation data for the Kasitsna Bay experiment bear resemblances to the SIO results in that a general increase in thymidine incorporation is apparent after oil introduction with roughly the same period of response. The SIO data have been converted to various forms of growth and production estimates for the first seven days following introduction of Prudhoe Bay crude (discussion below).

The leucine uptake data for Kasitsna Bay are difficult to interpret, as were the corresponding SIO data, due to variance between systems. The tanks exhibited a drop in uptake after oil introduction, however this drop was also apparent for the incoming seawater which supposedly had never been exposed to spilled petroleum.

The glucose uptake data from Kasitsna Bay bear resemblance to those from SIO in that most systems demonstrated some decline in uptake and somewhat followed trends of the incoming seawater.

7.3.3 Epifluorescence Enumeration and Photomicroscopy - Applications to Thymidine Uptake

With the aid of the epifluorescence enumeration and photomicroscopy results from the SIO study (Day 0 - Day 7), the thymidine uptake data have been connected into estimates of bacterioplankton production and biomass. As indicated in Table 7-1, both experimental tanks exhibited higher overall rates of thymidine uptake (nmoles.liter^{-1}.day^{-1}), incorporation into cellular DNA (moles x 10^{-19}.cell^{-1}.day^{-1}), and cell production (cells x 10^{9}.liter^{-1}.day^{-1}), relative to the incoming seawater, with the nutrient supplemented tank having higher overall rates than the non-supplemented (natural seawater) tank for the first seven days. Production estimates (μC.liter^{-1}.day^{-1} and fgC.cell^{-1}.-day^{-1}) followed the same trends, as would be expected, although biomass estimates were similar between the incoming seawater and the non-supplemented tank and higher for the nutrient supplemented system. The epifluorescence microscopy data, for the SIO study, is partially summarized in Table 7-2, and it is evident that both experimental aquariums exhibited greater concentrations of

TABLE 7-1. PRODUCTION ESTIMATES DERIVED FROM EPIFLUORESCENCE ENUMERATION AND THYMIDINE INCORPORATION RATE DATA

	Epifluorescence	^{3}H - Thymidine Incorporation			Production[c]		BIOMASS[d]
	cells · liter^{-1} (x10^9)	n moles · liter^{-1} · day^{-1}	moles · cell^{-1} · day^{-1} (x10^{-19})	cells · liter^{-1} · day^{-1} (x10^9)[b]	µg C · liter^{-1} · day^{-1}	fg C · cell · day^{-1}	fg C · cell^{-1}
Incoming Seawater - Day 0	1.05	0.27	2.57	0.46	0.7	0.74	3.1
Day 1	1.21	0.71	5.87	1.21	2.10	1.7	
Day 2	0.81	0.28	3.46	0.48	0.81	1.0	2.1
Day 4	0.77	0.06	0.78	0.10	0.17	0.23	
Day 5	(0.82)[a]	0.17	2.07	0.29	0.49	0.6	
Day 6	(0.82)[a]	0.02	0.24	0.03	0.06	0.07	
Day 7	0.87	0.09	1.03	0.15	0.26	0.3	2.0
x̄ ± SD		0.23±0.24	2.29±1.93	0.39±0.40	0.66±0.68	0.66±0.56	
Nutrient Supplemented Tank - Day 0	1.19	0.42	3.53	0.71	1.2	1.0	2.3
Day 1	1.32	0.35	2.65	0.60	1.0	0.8	
Day 2	2.93	4.14	14.13	7.04	12.0	4.1	4.7
Day 4	2.24	1.88	8.39	3.20	5.4	2.4	
Day 5	(1.93)[a]	0.39	2.02	0.66	1.1	0.6	
Day 6	(1.93)[a]	0.96	4.97	1.63	2.8	1.4	
Day 7	1.62	3.57	22.04	6.07	10.3	6.4	8.4
x̄ + SD		1.67±1.59	8.25±7.39	2.84±2.71	4.8±4.6	2.4±2.2	
Non Supplemented Tank - Day 0	1.62	0.34	2.10	0.58	0.98	0.6	2.2
Day 1	1.64	0.11	0.67	0.19	0.32	0.2	
Day 2	1.83	1.45	7.92	2.47	4.19	2.3	3.2
Day 4	2.34	0.68	2.91	1.16	1.97	0.8	
Day 5	(2.23)[a]	0.81	3.63	1.38	2.34	1.1	
Day 6	(2.23)[a]	0.60	2.69	1.02	1.73	0.8	
Day 7	2.12	0.33	1.56	0.56	4.51	2.1	1.6
x̄ + SD		0.62+0.44	3.07±2.34	1.05±0.75	2.29±1.56	1.1+0.8	

---

[a] Interpolated between Day 4 and 7

[b] Calculated with conversion factor from Fuhrman and Azam (1981) for average DNA content for nearshore bacteria (1.7×10^{18} moles Thymidine incorporated per cell produced).

[c] Calculated from thymidine incorporation data with above mentioned conversion factor and one from Watson et al. (1977) for average cellular carbon content (1.7×10^{-15} g C · cell^{-1}).

[d] Calculated from weighted average volumes of rods and spheres with conversion factor from Watson et al. (1977) for cell volume to biomas (1.21×10^{-13} g C · µm^{-3}).

TABLE 7-2. Epifluorescence Microscopy Data from SIO Continuous-flow Study

Source	Day	Mean Volume of Rods (μm^3)	Mean Volume of Spheres (μm^3)	Weighted Mean Volume (μm^3)*	Cells · liter^{-1} (x10^9)
Incoming Seawater	0	0.0214	0.0284	0.0258	1.05
	2	0.0168	0.0180	0.0173	0.81
	7	0.0239	0.0131	0.0165	0.87
	21	0.0296	0.0128	0.0179	0.42
Nutrient Supplemented Tank	0	0.0163	0.0216	0.0190	1.19
	2	0.0444	0.0190	0.0360	2.93
	7	0.0469	0.0081	0.0661	1.62
	21	0.0340	0.0149	0.0241	1.95
Non-Supplemented Tank	0	0.0222	0.0167	0.0185	1.62
	2	0.0353	0.0146	0.0264	1.83
	7	0.0161	0.0106	0.0135	2.12
	21	0.0264	0.0109	0.0178	1.31

* Determined as follows: $\frac{\text{(Number of Rods Counted) } (\bar{x} \text{ Volume}) + \text{(Number Spheres Counted) } (\bar{x} \text{ Volume})}{\text{Total Number of Rods \& Spheres Counted}}$

bacterioplankton relative to the incoming seawater. The mean cell volume data for the nutrient supplemented system are larger in magnitude relative to the natural seawater system and the incoming seawater, although this difference may not be significant.

Table 7-3 depicts the inorganic nutrient analyses data for the SIO study for available phosphorous (PO_3^{-4}, EPA Method 365) and nitrogen (NO_2^-, NO_3^-. EPA Method 353.3). Although most values fall below the detection limit for the colorimetric techniques utilized, it is evident that the nitrite/nitrate levels in the nutrient supplemented tank were higher than for both the incoming seawater and the non-supplemented tank. Levels of available inorganic nitrogen were generally higher for the Kasitsna Bay study (Table 7-4), and the nutrient supplementation maintained higher levels relative to the natural seawater.

7.4 DISCUSSION

7.4.1 Relations Between ^{14}C and ^{3}H Substrate Assays

To determine if any relationships exist between the degradation of the ^{14}C-labeled hydrocarbons and uptake/incorporation of the ^{3}H-labeled organic substrates, the data for each experimental system were plotted individually to include all substrates for the given experiment. The results from the SIO study are depicted in Figures 7-6 and 7-8, and for the Kasitsna Bay study in Figures 7-8 and 7-9. The ^{3}H-labeled substrate data is compared between the incoming seawater of the SIO and Kasitsna Bay studies in Figure 7-10.

As noted previously, a dramatic difference in degradation rates of hexadecane vs methylnaphthalene and naphthalene exists for the experimental systems for both the SIO and Kasitsna Bay studies. The aromatic hydrocarbon substrates were degraded at significantly higher levels than the aliphatic compound, which seems to be in contrast to trends arising in many past studies

TABLE 7-3. Nutrient Analysis Data for the Flow-through Aquaria at NOAA's Kasitsna Bay Facility for Available Nitrogen (NO_2^- and NO_3^-)

DAY	INCOMING SEAWATER	NUTRIENT SUPPLEMENTED	NON-SUPPLEMENTED
0	5.0μM	13.3μM	5.1μM
1	6.2	11.4	3.5
2	4.7	7.6	4.1
4	4.6	9.9	3.4
7	<2.0	8.9	<2.0
14	7.1	13.9	4.5
21	7.4	8.9	6.1
28	6.8	4.9	8.3

TABLE 7-4. Nutrient Analysis Data for the Flow-through Aquaria at NOAA's Kasitsna Bay Facility for Available Nitrogen (NO_2^- and NO_3^-)

DAY	INCOMING SEAWATER	NUTRIENT SUPPLEMENTED	NON-SUPPLEMENTED
0	5.0μM	13.3μM	5.1μM
1	6.2	11.4	3.5
2	4.7	7.6	4.1
4	4.6	9.9	3.4
7	<2.0	8.9	<2.0
14	7.1	13.9	4.5
21	7.4	8.9	6.1
28	6.8	4.9	8.3

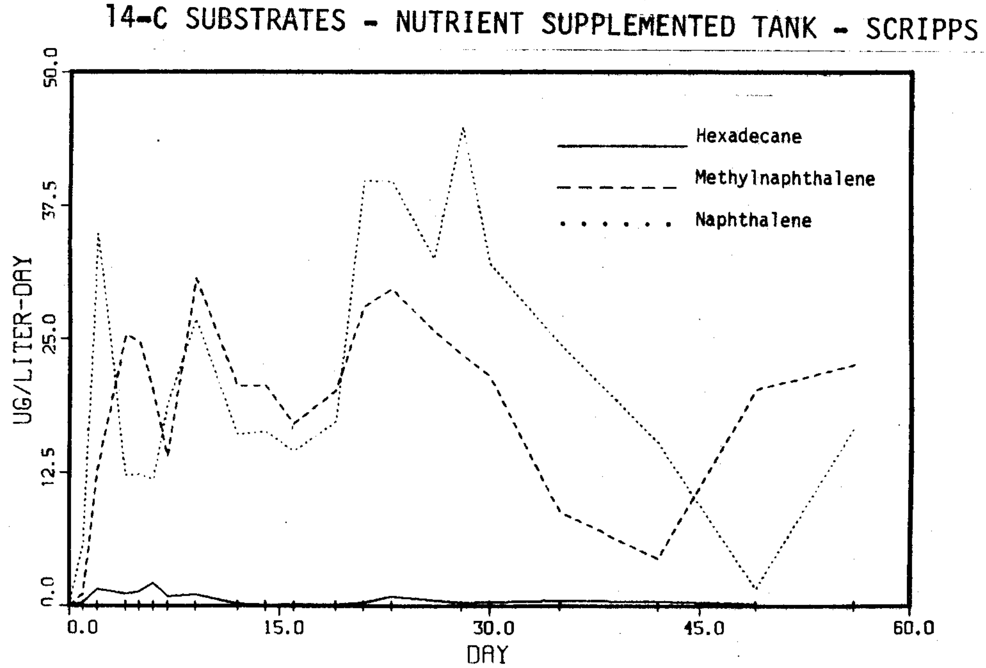

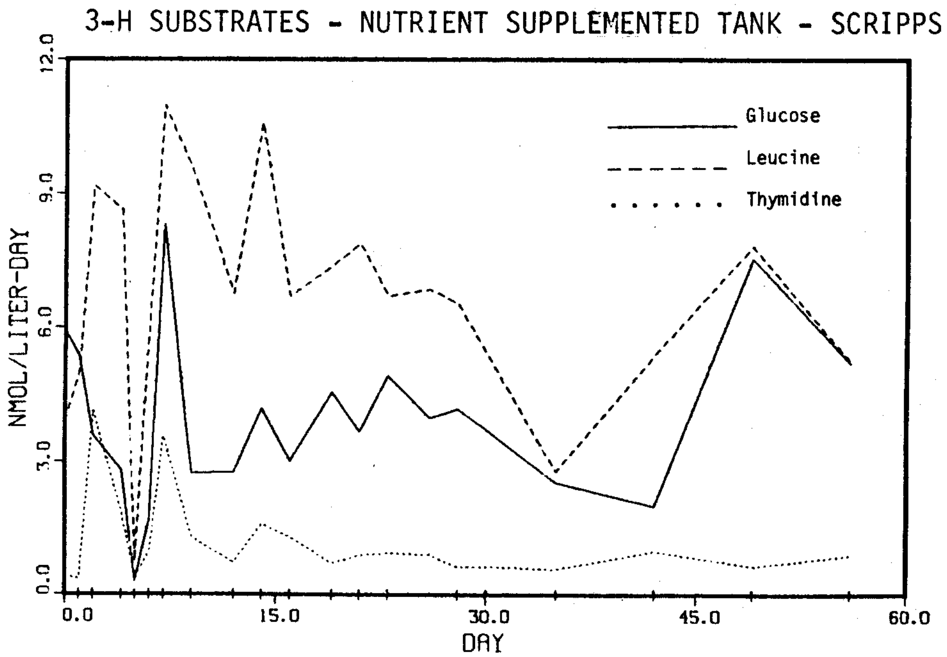

FIGURE 7-6. ^{14}C-HYDROCARBON DEGRADATION AND ^{3}H-SUBSTRATE INCORPORATION/UPTAKE DATA FOR THE NUTRIENT SUPPLEMENTED EXPERIMENTAL AQUARIUM, SCRIPPS INSTITUTION OF OCEANOGRAPHY, SUMMER 1981. VERTICAL LINES ON ABSCISSA INDICATE SAMPLING POINTS.

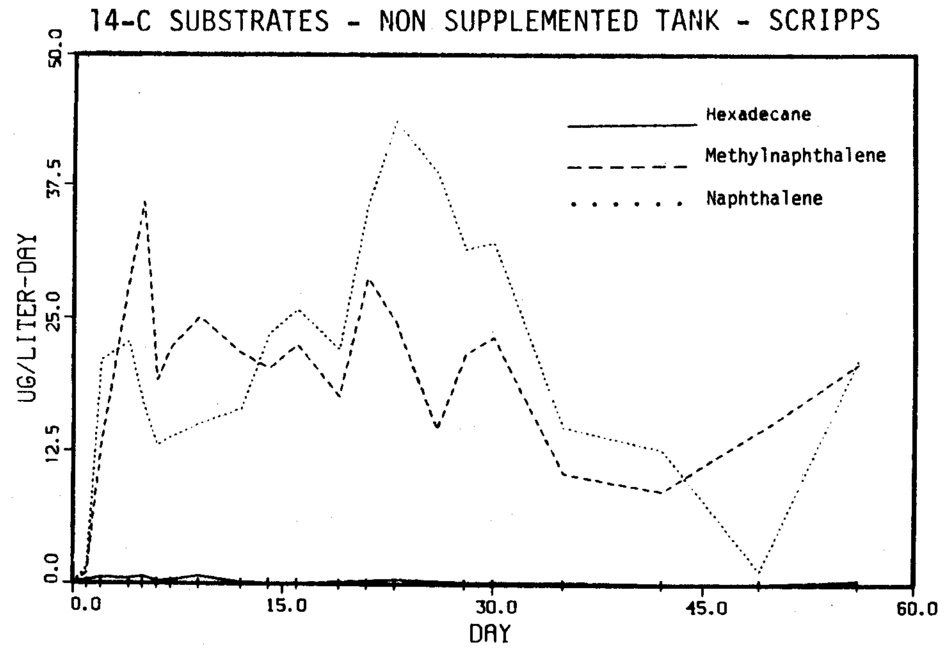

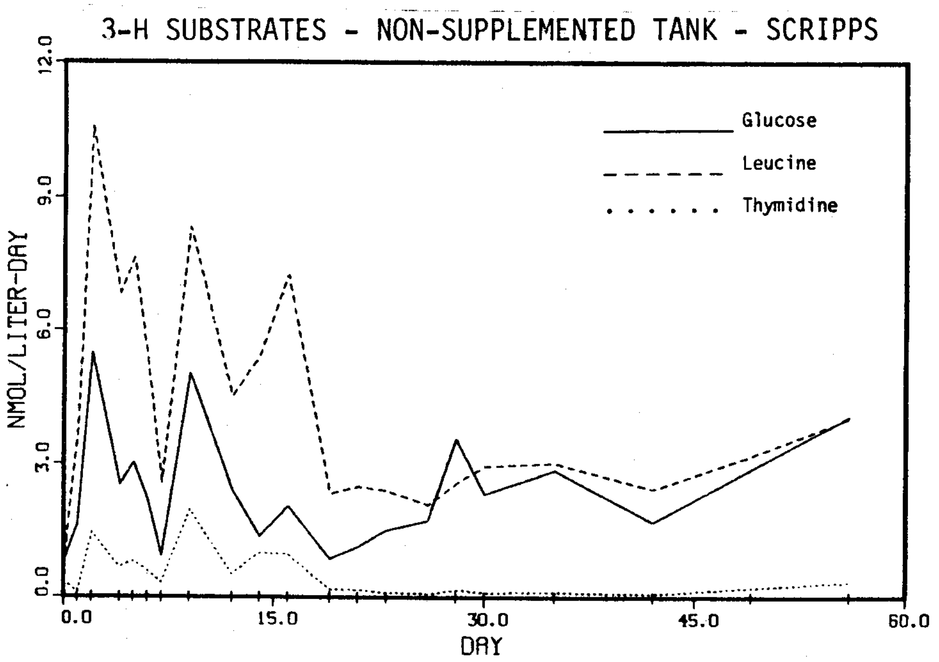

FIGURE 7-7. ^{14}C-HYDROCARBON DEGRADATION AND ^{3}H-SUBSTRATE INCORPORATION/ UPTAKE DATA FOR THE NATURAL SEAWATER (NON-SUPPLEMENTED) EXPERIMENTAL AQUARIUM, SCRIPPS INSTITUTION OF OCEANOGRAPHY SUMMER 1981. VERTICAL LINES ON ABSCISSA INDICATE SAMPLING POINT.

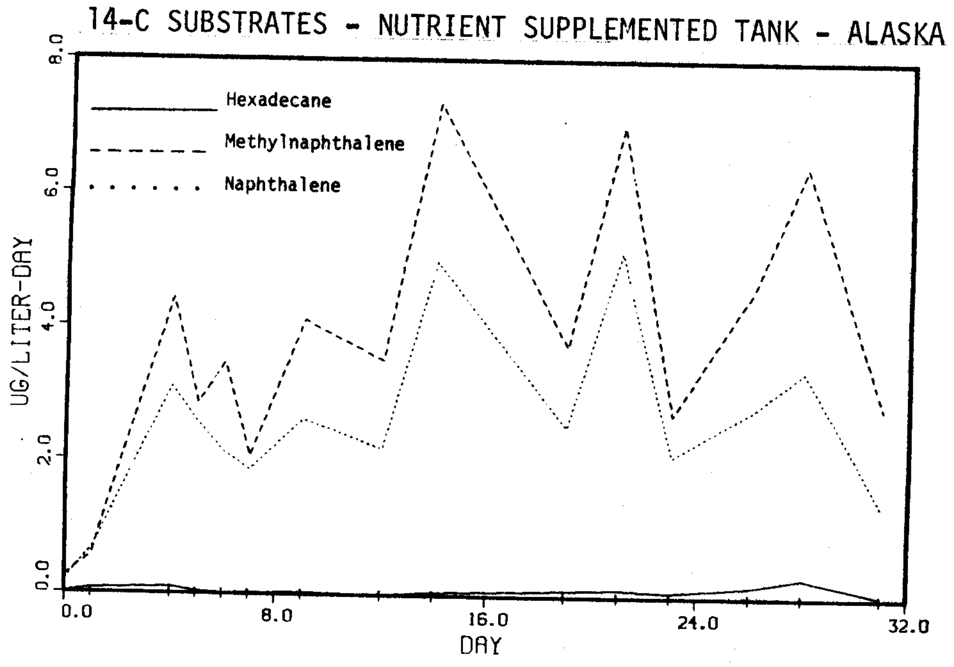

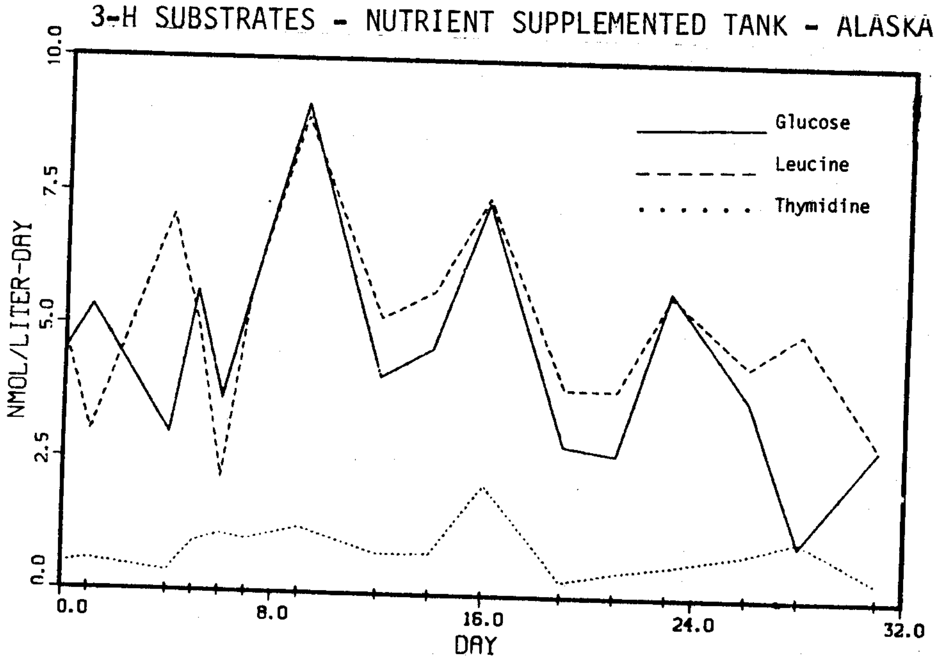

FIGURE 7-8. ^{14}C-HYDROCARBON DEGRADATION AND ^{3}H-SUBSTRATE INCORPORATION/ UPTAKE DATA FOR THE NUTRIENT SUPPLEMENTED EXPERIMENTAL AQUARIUM, KASITSNA BAY, ALASKA, SUMMER, 1981. VERTICAL LINES ON ABSCISSA INDICATE SAMPLING POINTS.

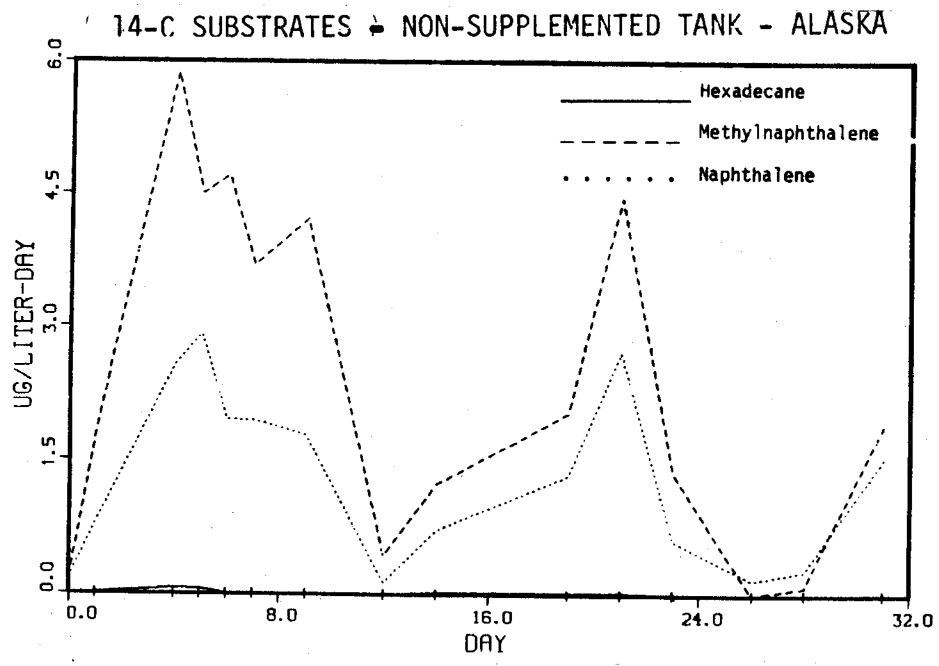

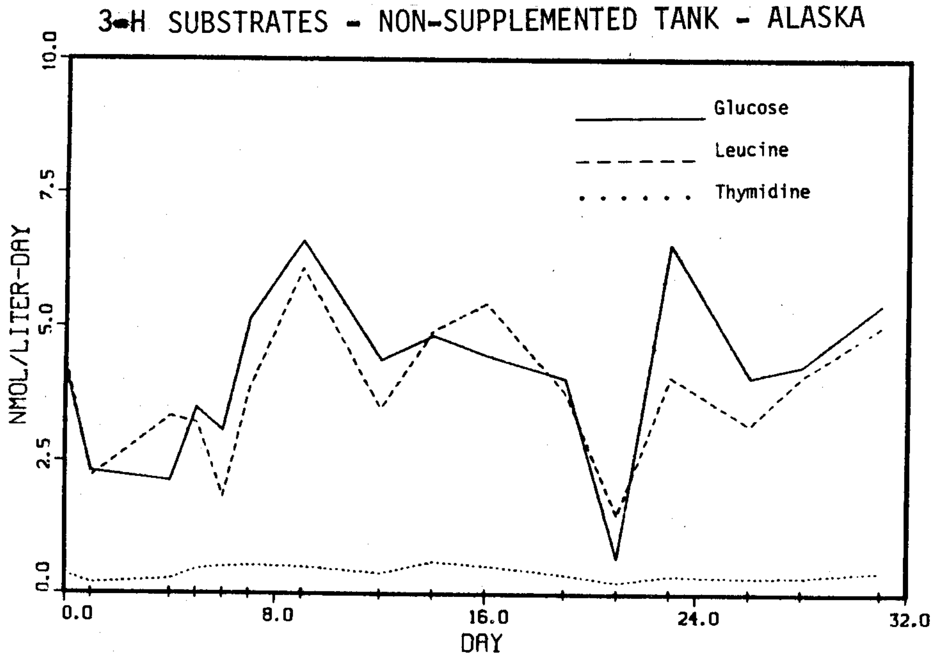

FIGURE 7-9. ^{14}C-HYDROCARBON DEGRADATION AND ^{3}H-SUBSTRATE INCORPORATION/UPTAKE DATA FOR THE NATURAL SEAWATER (NON-SUPPLEMENTED) EXPERIMENTAL AQUARIUM, KASITSNA BAY, ALASKA, SUMMER 1981. VERTICAL LINES ON ABSCISSA INDICATE SAMPLING POINTS.

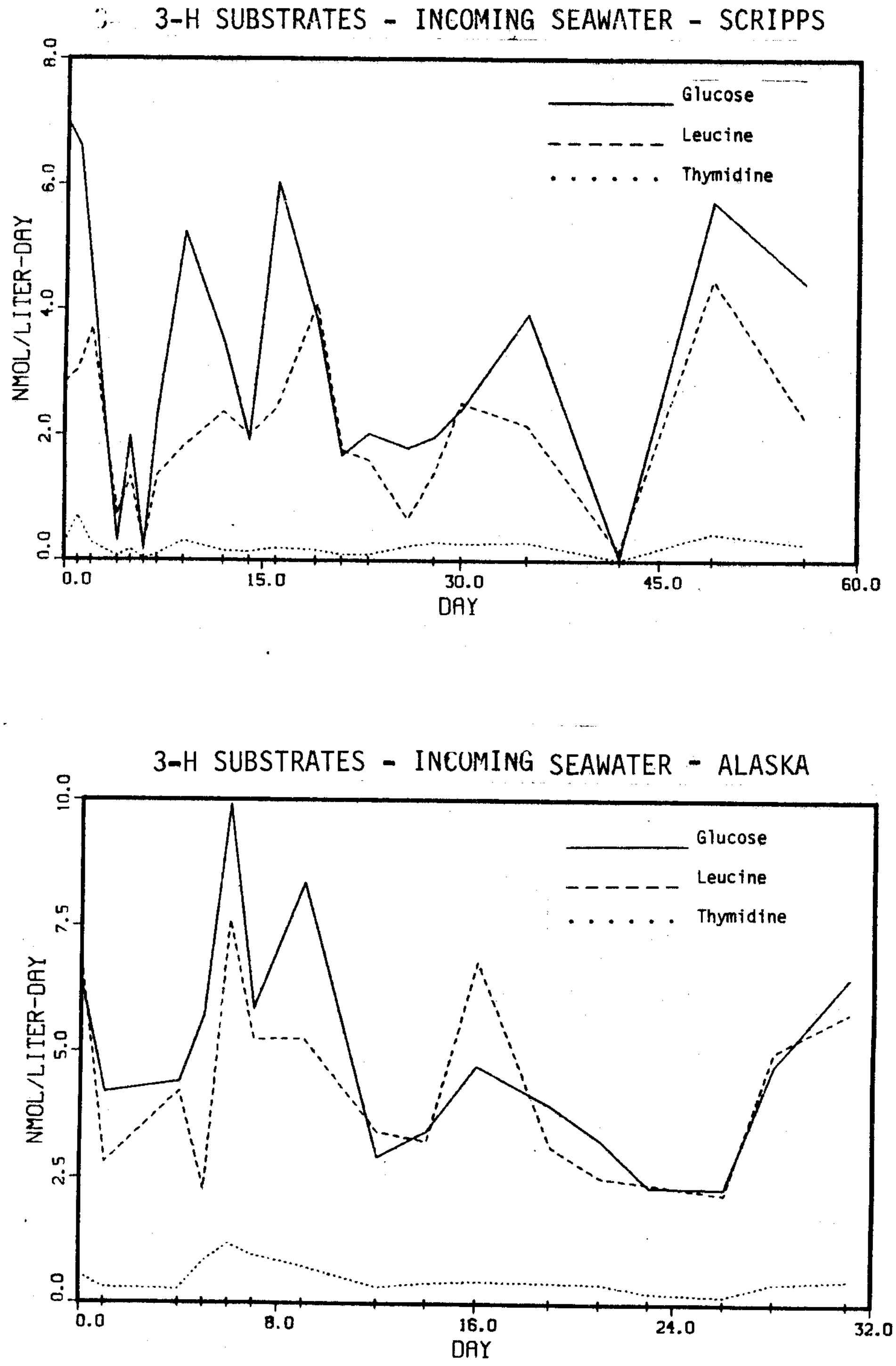
3-H SUBSTRATES - INCOMING SEAWATER - SCRIPPS

3-H SUBSTRATES - INCOMING SEAWATER - ALASKA

FIGURE 7-10. ^{3}H-THYMIDINE INCORPORATION, ^{3}H-GLUCOSE AND ^{3}H-LEUCINE UPTAKE DATA FOR INCOMING SEAWATER (SCRIPPS INST. OF OCEANOGRAPHY AND KASITSNA BAY, ALASKA, SUMMER 1981). VERTICAL LINES ON ABSCISSA INDICATE SAMPLING POINTS.

(Jordan and Payne, 1980). Both aromatic hydrocarbon substrates were degraded at comparable rates for all systems in each experiment, and the patterns (relative rates) were also similar, in most cases, between the two substrates. However, it must be emphasized that the relative rates of degradation between labeled substrates, as based upon loss of the ^{14}C label, does not imply an upper limit on the actual amount of parent substrate undergoing metabolic conversion during the given period of incubation. This consideration could certainly negate the apparent contrast in rates of degradation between the aliphatic and aromatic substances.

In terms of relations between the ^{14}C and ^{3}H-labeled substrate trends, only in the nutrient supplemented tank (for the SIO study) was a definite increase in hydrocarbon substrate degradation present which paralled increases in rates of both thymidine incorporation, and glucose and leucine uptake after introduction of oil (Figure 7-1). In most cases, no apparent impacts on the ^{3}H-labeled substrate incorporation/uptake rates following oil introduction are obvious from the data. It should be noted, however, that the experimental aquaria in the Kasitsna Bay study demonstrated generally lower rates of ^{14}C- and ^{3}H-labeled substrate utilization (relative to the SIO study), and that "experimental noise" from variance inherent in the techniques may tend to obscure general trends unless they are highly prominant.

In summary, the trends which are most apparent in the data for the continuously-flowing experiments conducted at SIO and Kasitsna Bay are the following:

- the ^{14}C-hexadecane appeared to be degraded at much slower rates than either ^{14}C-methylnaphthalene or ^{14}C-naphthalene (note previous statements on interpretation of relative rates).
- both aromatic hydrocarbon substrates were utilized at comparable rates, with similar patterns (relative rates over time) in most systems.
- generally lower rates of degradation were apparent for the Kasitsna Bay study relative to the SIO experiment.

- in most cases, dramatic increases in degradation rates for the ^{14}C-hydrocarbon substrates occurred within 48 hrs. of oil introduction.

- nutrient supplementation had no apparent influence on degradation rates except for some slight evidence in the Kasitsna Bay study (note Figures 7-6 to 7-9), where levels of available inorganic nitrogen (NO_2^-, NO_3^-) were somewhat higher than in the SIO study.

- Increases in ^{3}H-thymidine incorporation into cellular DNA after oil introduction were apparent for the SIO data and, to a much lesser extent, for the Kasitsna Bay study.

- high variance in the ^{3}H-glucose and ^{3}H-leucine data exists for most experimental systems in both studies, with no apparent impact from oil introduction except for some initial trends.

- in only one of the experimental aquaria (SIO) was there a concomitant increase in both ^{14}C-labeled and ^{3}H-labeled substrate utilization after introduction of Prudhoe Bay crude.

7.4.2 Longer-term Microbial Degradation Analyses -- Kasitsna Bay (Summer 1981)

As noted in Section 5.3 of the Evaporation Dissolution chapter, several long-term (6 months to 1 year) sub-arctic microbial degradation experiments were inititated in the outdoor tanks at the Kasitsna Bay laboratory in October, 1980. At that time, the tank configurations were set-up as shown below:

Tank 7	Flow-through condition	Fresh oil
Tank 3	Flow-through condition	Fresh oil + Corexit (20:1)
Tank 2	Static condition	Fresh oil
Tank 5	Static condition	Fresh oil + Corexit (20:1)

During the Spring 1981 program, after six months of weathering, oil and water column samples were obtained from all four tanks; flow-through tanks 3 and 7 were maintained to continue longer term weathering studies. All of the remaining oil from the static tanks (2 and 5) was then removed and frozen for future analysis (if desired), and 40-L seawater samples were obtained, acidified (to pH 2.0), extracted with CH_2Cl_2, and analyzed.

This section describes results of chemical analyses of the oil and water samples from these longer-term studies and presents additional results obtained from the 6 month to 1 year sampling period in the flow-through tanks 3 and 7. In addition, results are presented on summer (May through October) microbial degradation studies undertaken on fresh crude and artificially generated mousse in the presence and absence of turbulence and Corexit (as shown by the matrix diagram presented earlier in Section 5.3, Figure 5-34).

Two of the more significant findings of these longer term microbial degradation studies relate to the appearance of clear seasonal trends in bacterial utilization and differential microbial degradation with dependence on the status of the oil slick itself (i.e., stranded oil, mousse patches, surface slicks, oil droplets). As noted below, the chromatograms of samples collected after six months of ambient static tank weathering during the winter period from October 1980 through April 1981, showed only limited microbial degradation.

The significance of chromatographic analyses depicted in Figures 7-11 and 7-12 relates to a demonstration of the type of overall weathering which may occur during the subarctic winter season for oil stranded in an aquatic environment that experiences little flushing. This may be the case for an estuarine situation, where the water column beneath the slick is relatively stagnant. Limited evaporation would be expected due to the cold temperatures, and a "buildup" of the more water-soluble petroleum components in the underlying water column may occur. Microbial degradation of the oil slick and solubilized petroleum components in the water might also be limited due to cold water temperatures as well as limitations in nutrient supplies from lack of water column flushing and subsequent nutrient replenishment.

Figure 7-11 depicts the aliphatic and aromatic fraction chromatograms obtained from oil samples which had weathered over the six month winter period. In this experiment, both the oil and water (in tank 2) were maintained in a static condition from October 1980 to April 1981. In the aliphatic fraction (Figure 7-11A), n-alkanes are present down to nC-12, and the nC-17/pristane and nC-18/phytane ratios are 1.79 and 1.85, respectively. These values are nearly identical to the corresponding ratios obtained from analysis of the starting oil, and suggest limited microbial degradation during that time interval in that isoprenoids are generally thought to be less biodegradable than their straight-chain counterparts (BLUMER et al., 1973). Furthermore, during the winter months, it is clear that loss of lower molecular weight components by evaporation processes was inhibited due to the colder subarctic temeperatures (water temperatures were near 4°C when the experiments were initiated, and periodic freezing and thawing occurred during January and February, 1981.) Figure 7-11B shows the aromatic fraction of the oil, and this also shows that evaporation and dissolution of compounds with Kovat indices less than 1200 has occurred from the surface oil slick. These more water

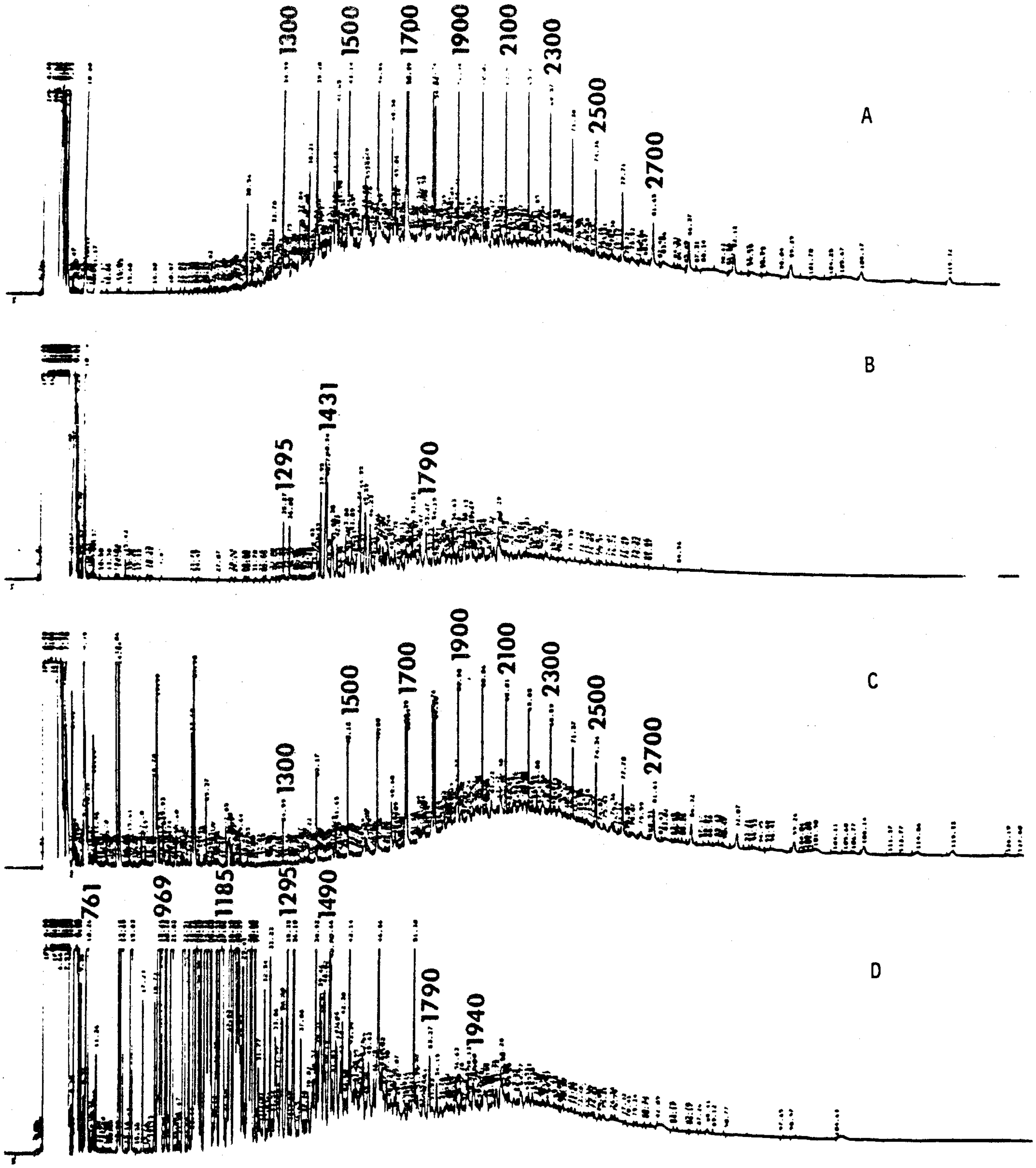

FIGURE 7-11. FLAME IONIZATION DETECTOR CAPILLARY GAS CHROMATOGRAMS OF PRUDHOE BAY CRUDE OIL AND SEAWATER SAMPLES OBTAINED AFTER 6 MONTHS OF SUB-AMBIENT WEATHERING FROM OCTOBER TO APRIL 1981 UNDER STATIC (NO-FLOW) CONDITIONS (TANK 2). A AND B REPRESENT THE ALIPHATIC AND AROMATIC FRACTIONS OF THE OIL, RESPECTIVELY, AND C AND D REPRESENT THE ALIPHATIC AND AROMATIC FRACTIONS OF THE WATER COLUMN, RESPECTIVELY.

obtained from the water beneath the slick; Figures 7-11C and 7-11D depict the aliphatic and aromatic fractions, respectively, of the acidified water column extract from the outdoor tank 2. While the capillary column is clearly overloaded, the presence of exceedingly high levels of aromatic compounds in the water can be observed. Aromatic compounds present include benzene, toluene, xylenes, alkyl-substituted naphthalenes, and phenanthrenes. The exceedingly high levels in the aromatic fraction also help to explain the limited breakthrough of some of these components into the aliphatic fraction (Figure 7-11C) during the liquid column chromatography.

Because the outdoor tank was stagnant during the six month period between October to April of 1981, these lower molecular components were not readily removed by advection. However, they might be expected a priori to be lost due to evaporative processes. One hypotheses to explain the lack of this anticipated loss is that the oil on the surface of the water formed a skin or cap which then prevented additional loss of these more water soluble aromatic compounds from the water column via evaporative processes. Similar observations were made by PAYNE, et al. (1980) during the sub-surface IXTOC-I blowout in the Gulf of Mexico in 1979, where elevated levels of benzene, tuolene, and xylenes were found in the water column. In that instance it was also believed that the oil coating on the water acted as a cap to inhibit efficient air-sea exchange and that removal of the compounds by evaporation would only occur after advection of the water away from the slick (or wind driven movement of the slick itself).

Figure 7-12 presents the chromatograms of oil samples from the static tank experiment of oil plus Corexit (tank 5) after the same period of weathering. Qualitatively the chromatograms appear very similar to those in Figure 7-11, and it can be seen that during the winter months, most of the volatile components with molecular weights less than nC-12 (Kovat Index 1200) were lost (Figure 7-12). Figure 7-12B shows that the aromatic compounds with molecular weights less than the methylnaphthalenes were lost by evaporative and dissolution processes.

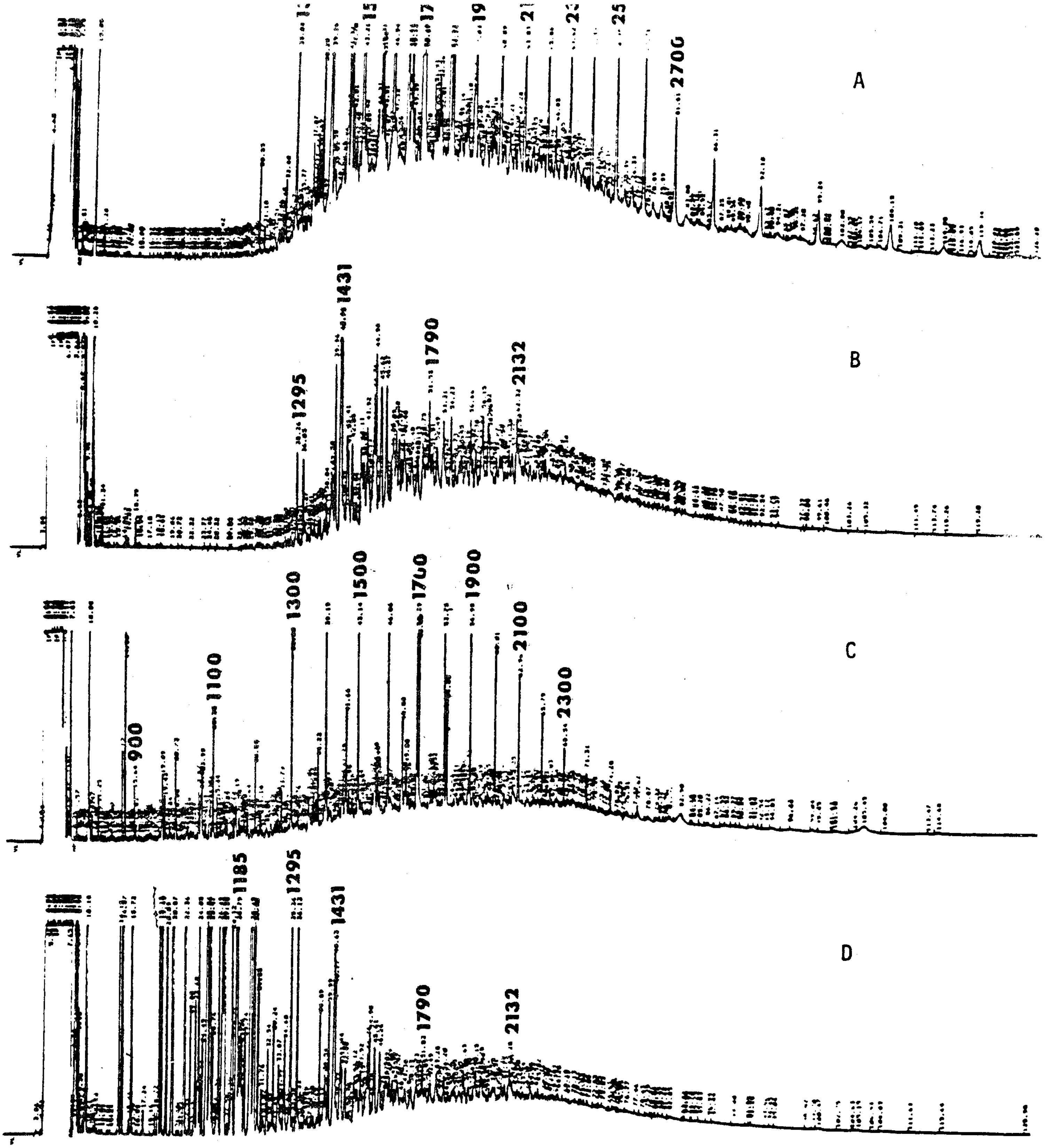

FIGURE 7-12. FLAME IONIZATION DETECTOR CAPILLARY GAS CHROMATOGRAMS OF PRUDHOE BAY CRUDE OIL PLUS COREXIT AND SEAWATER SAMPLES OBTAINED AFTER 6 MONTHS OF SUB-AMBIENT WEATHERING FROM OCTOBER TO APRIL 1981 UNDER STATIC (NO-FLOW) CONDITIONS (TANK 5). A AND B REPRESENT THE ALIPHATIC AND AROMATIC FRACTIONS OF THE OIL, RESPECTIVELY, AND C AND D REPRESENT THE ALIPHATIC AND AROMATIC FRACTIONS OF THE WATER COLUMN, RESPECTIVELY.

The aliphatic fraction of the acidified water column extract (Figure 7-12C) has higher levels of aliphatic compounds compared to the aliphatic fraction for the tank 2 water (Figure 7-11C), and this is presumably due to the influence of the dispersant.

Figure 5-11D shows the chromatogram obtained on the aromatic fraction of the water column extract from this tank, and as in the other case from the winter experiments, high levels of aromatic hydrocarbons are observed to remain in the water after six months of subarctic weathering. As noted before, this presumably reflects diffusion controlled processes limiting loss of these components through the viscous oil slick cover.

As noted above, outdoor tanks 3 and 7 were maintained in the flowing condition during the period of April through October 1981. During this period significant increases in microbial degradation of the oil in the tanks were noted. Further, while examining the oil from the different tanks, longer term oil weathering processes were observed to be clearly dependent on the status of the stranded or floating oil. Specifically, microbial degradation appeared to be primarily a surface phenomenon, and evidence of extenisve microbial processes was limited to surface films emanating from larger oil/mousse patches.

Evidence of the differential weathering patterns observed in oil droplets versus surface film are presented in Figure 7-13. Figure 7-13A presents the capillary column gas chromatogram (non-fractionated) obtained on oil droplets observed in outside tank 3 after eleven months of continuous weathering in the flow-through system. Interestingly, compounds are present down to Kovat indices 1100 showing limited evaporation from the interior of the droplet. In this instance, formation of a surface crust on the oil during the winter months presumably limited further evaporation/dissolution losses and microbial activity over the summer.

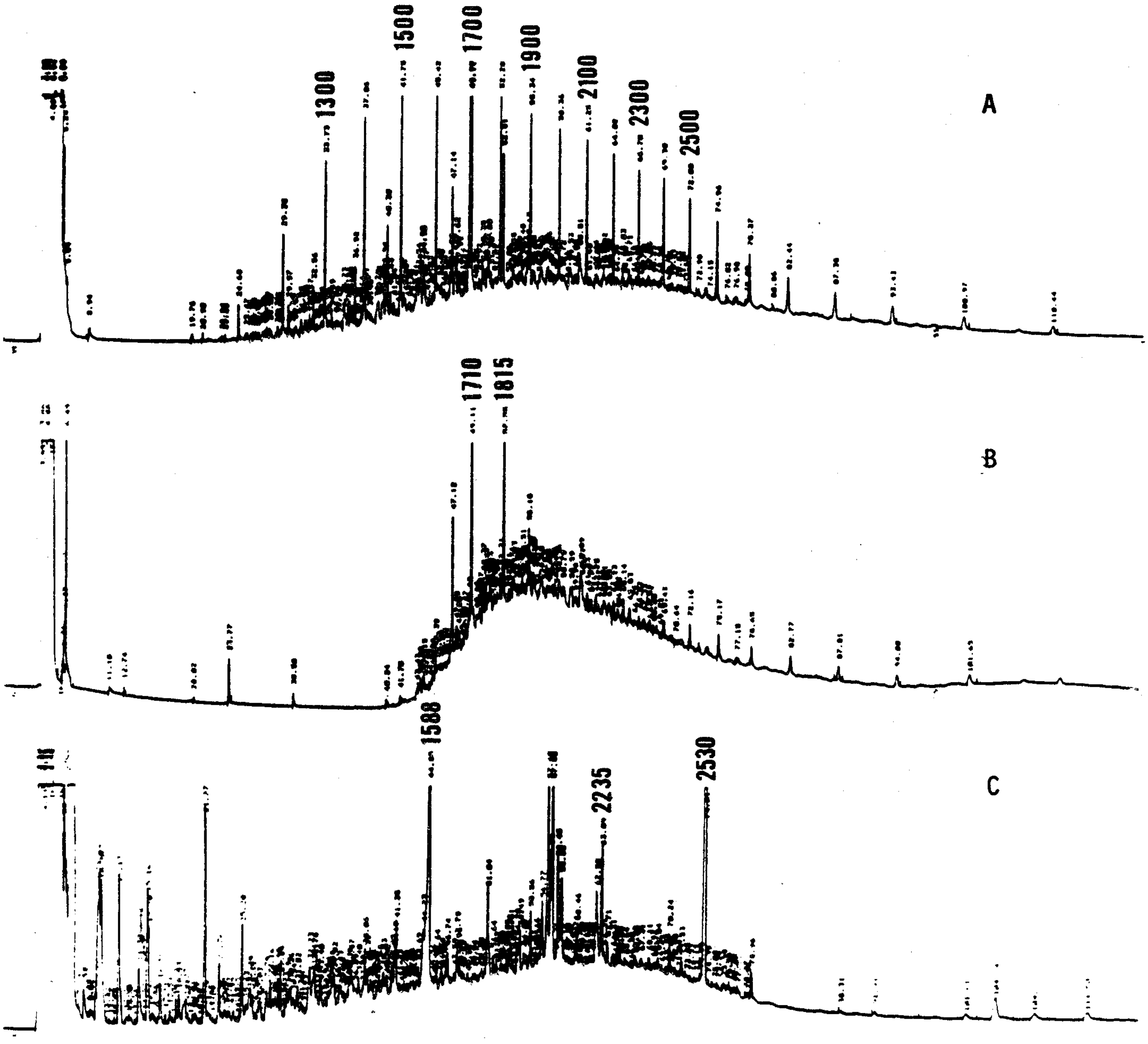

FIGURE 7-13. FLAME IONIZATION DETECTOR CAPILLARY GAS CHROMATOGRAMS OF WEATHERED OIL AND WATER COLUMN SAMPLES AFTER 11 MONTHS OF CONTINUOUS SUB-ARCTIC WEATHERING (OCTOBER 1980 TO SEPTEMBER 1981) IN THE OUTDOOR FLOW-THROUGH AQUARIA (TANK 3): (A) OIL DROPLETS (ENTIRE EXTRACT); (B) SURFACE FILM EMINENTING FROM OIL PATCHES (ENTIRE EXTRACT); AND (C) ACIDIFIED SEAWATER EXTRACT.

Figure 7-13B, however, shows extensive evaporative and microbial degradation losses in the translucent film emanating from the large patches of the oil in the outdoor tank. In this instance, the only major resolved components remaining in the chromatogram are those of pristane and phytane and other isoprenoid compounds. The chromatogram is also characterized by a relatively large unresolved complex mixture and higher molecular weight n-alkanes ranging from nC-23 through nC-29.

Figure 7-13B presents the chromatogram obtained from the acidified water extract after eleven months of natural weathering under the subarctic conditions. Clearly there are a number of polar compounds present in the sample extract.

Figure 7-14A presents the FID capillary gas chromatogram for a large patch of floating mousse from tank 2 (artificial mousse and Corexit) after five months of weathering (May to September). Essentially complete loss of compounds below nC-13, due to evaporation and dissolution, can be observed. However, microbial degradation is not readily evident in this sample from the appearance of the chromatogram. This is believed to be due to the fact that the higher concentrations of relatively unweathered components (making up the interior of the patch) mask any selective microbial utilization of specific alkanes that might have occurred on the lower surface which was exposed to the water column.

Figure 7-14B presents the chromatogram obtained on a sample of stranded mousse collected in September from the sides of tank 2. This also shows only limited microbial degradation, although a slight increase in loss of compounds below Kovat index 1400 is noted. This presumably reflects elevated temperatures encountered during summer-time exposure.

Figure 7-14C shows the chromatogram obtained from a translucent film extending from the bulk of the mousse patch from tank 2. In this instance a loss of aliphatic and aromatic compounds below 1500 is evident and enhanced microbial degradation is suggested by the nC-17/pristane and nC-18/phytane ratios of 0.61 and 0.73, respectively.

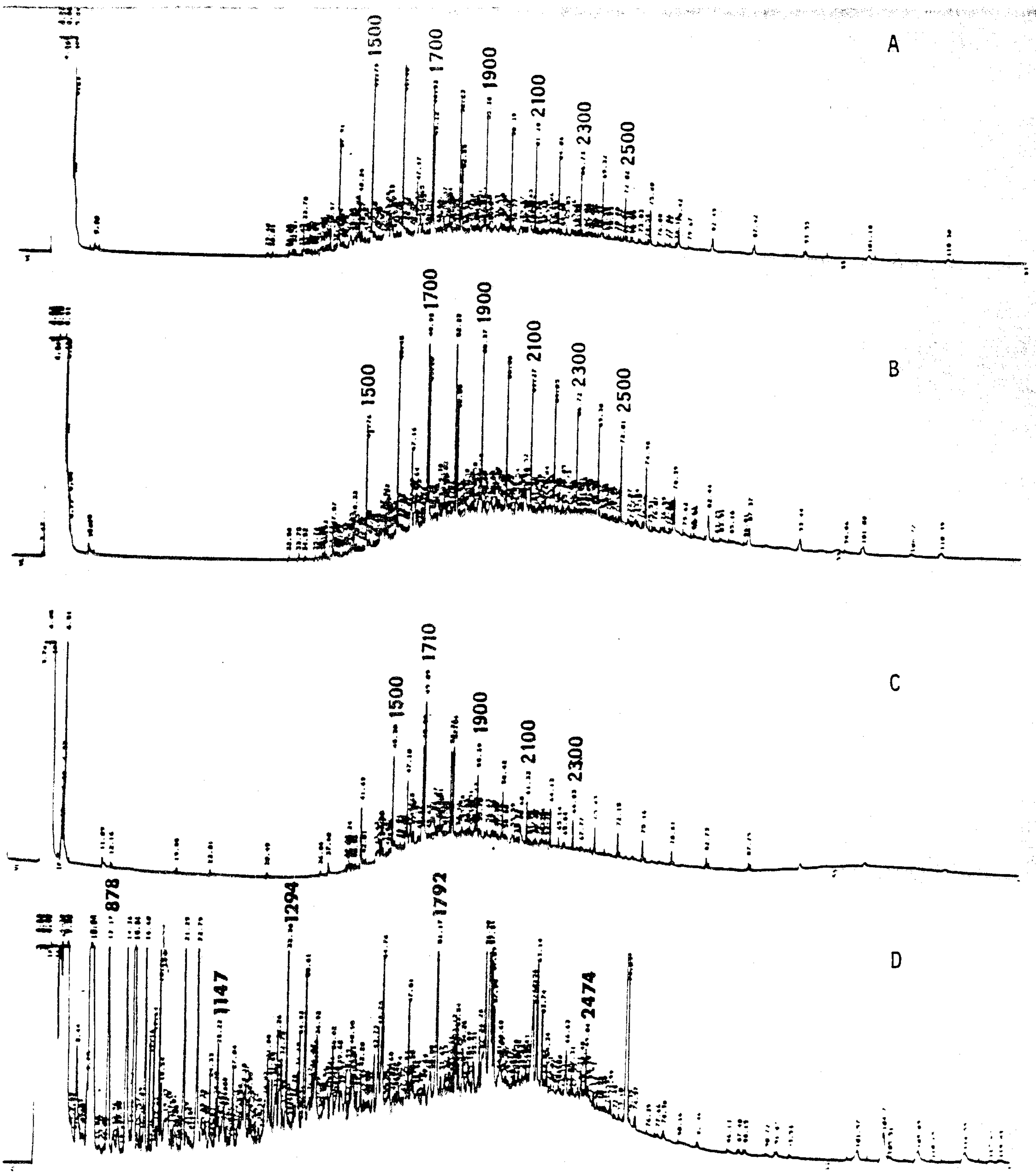

FIGURE 7-14. FLAME IONIZATION DETECTOR CAPILLARY GAS CHROMATOGRAMS OF ARTIFICALLY GENERATED PRUDHOE BAY MOUSSE PLUS COREXIT AFTER 5 MONTHS OF WEATHERING (MAY TO SEPTEMBER 1981) IN THE OUTDOOR FLOW-THROUGH AQUARIA (TANK 2) AT KASITSNA BAY, ALASKA: (A) ARTIFICIAL MOUSSE FLOATING ON THE WATER COLUMN; (B) STRANDED MOUSSE FROM THE SIDE OF THE CORRAL; (C) SURFACE FILM EMINENTING FROM MOUSSE PATCHES; AND (D) ACIDIFIED SEAWATER EXTRACTS.

Figure 7-14D shows the acidified water extract obtained from a 31.7 liter water sample obtained four months after the mousse was initially spilled in the flow-through water system. This extract has been submitted to GC/MS analysis and Figure 5-41D (in Section 5.3) presents the reconstructed ion chromatogram obtained on that sample. The disparity in the appearance of the chromatogram in Figure 5-41D compared to Figure 7-14D can be attributed to inadevertent loss of lower molecular components before GC/MS analysis during transport to our La Jolla facility.

7.4.3 Observations of Microbial Degradation in the Flow-Through Wavetank Studies - Kasitsna Bay (Summer 1982 - 1983)

In Section 5.4.5 we discussed the changes in realogic properties and chemical composition of the slick due to physical/chemical weathering in the wave tank experiments. In support of the microbiological oil degradation work presented in this section, additional chromatographic data were interpreted to provide information on the microbial degradation processes occurring in the wave tanks.

The summer experiments were begun in June, 1982, and we returned in October to further monitor the weathering process. After four months of ambient subarctic weathering over the summer and early fall period, significant changes in the oil were observed. Figure 5-75 in Section 5.4.6 presents a photograph of the tarballs and rather fluid sauce-like material observed in the tanks. To determine if microbial degradation was selectively different on the exterior versus interior of the tarballs shown in the figure, aliquots were obtained on several tarballs. The surface skin of the material was compared to the interior of the tarball. Figures 7-15A and 7-15B present the flame ionization detector gas chromatograms obtained on the surface skin and interior, respectively, of a tarball from wave tank #2 sampled in October, 1982. Sixty milligram aliquot subsamples of the surface and interior were removed and dissolved in 2000 microliters of methylene chloride. The number of resolved peaks in the surface skin is significantly lower than the resolved peaks observed in the interior. The first major component observed in both

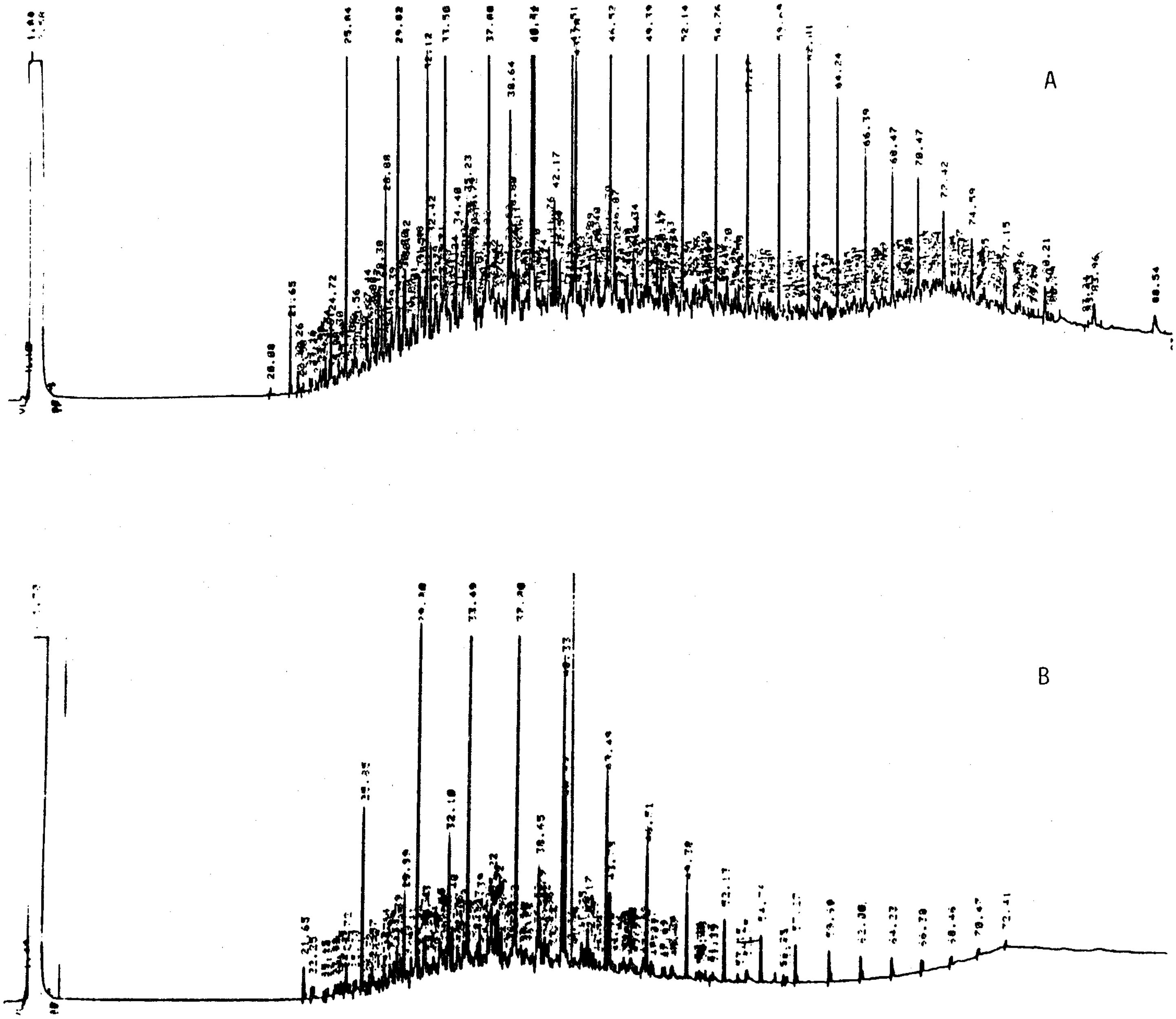

FIGURE 7-15. Flame Ionization Detector Gas Chromatograms of A) Surface Skin and B) Interior of Tar Balls from Tank #2 (October 1982).

samples is n-C_{12} which suggests that evaporative processes had dominated prior to tarball formation. The lower number of resolved components in the surface skin versus the interior, for the same mass of oil, reflects the extremely high water content in the oil on the surface of the tarball. The ratios of n-C_{17} to pristane and n-C_{18} to phytane (Table 7-5) indicate that, after this weathering period, no significant changes in the ratios of straight chain to branched chain components or straight chain to selected aromatic components were observed in the surface versus interior. This suggests that there was only limited microbial degradation up to that time.

Table 7-5

Ratios of Selected Components in Tarball Surface and Interior Samples

	Center of Tarball	Outer Surface of Tarball
n-C_{17}/pristane	1.49	1.39
n-C_{18}/phytane	1.76	1.85
n-C_{14}/biphenyl	4.62	4.54
n-C_{16}/2,3,5-trimethyl-naphthalene	8.21	8.17
n-C_{16}/dibenzothiophene	5.64	7.08

When the wave tanks were again examined in March, 1983, after nine months of "open ocean" weathering, there were several significant differences among the tanks. The tarballs had, in a number of instances, been reduced in size and volume. This produced a very sloppy, foamy type oil-water emulsion that was observed to float adjacent to the limited number of tarballs remaining. Figure 7-16 presents the flame ionization detector chromatograms obtained on the foamy oil-water emulsion surrounding the tarballs. Interestingly, the scummy, foamy oil mat and the exterior surface of the tarball produce chromatographic profiles which are nearly identical. From this we believe that the materials observed in the tank simply slough off of the exterior surface of the tarballs.

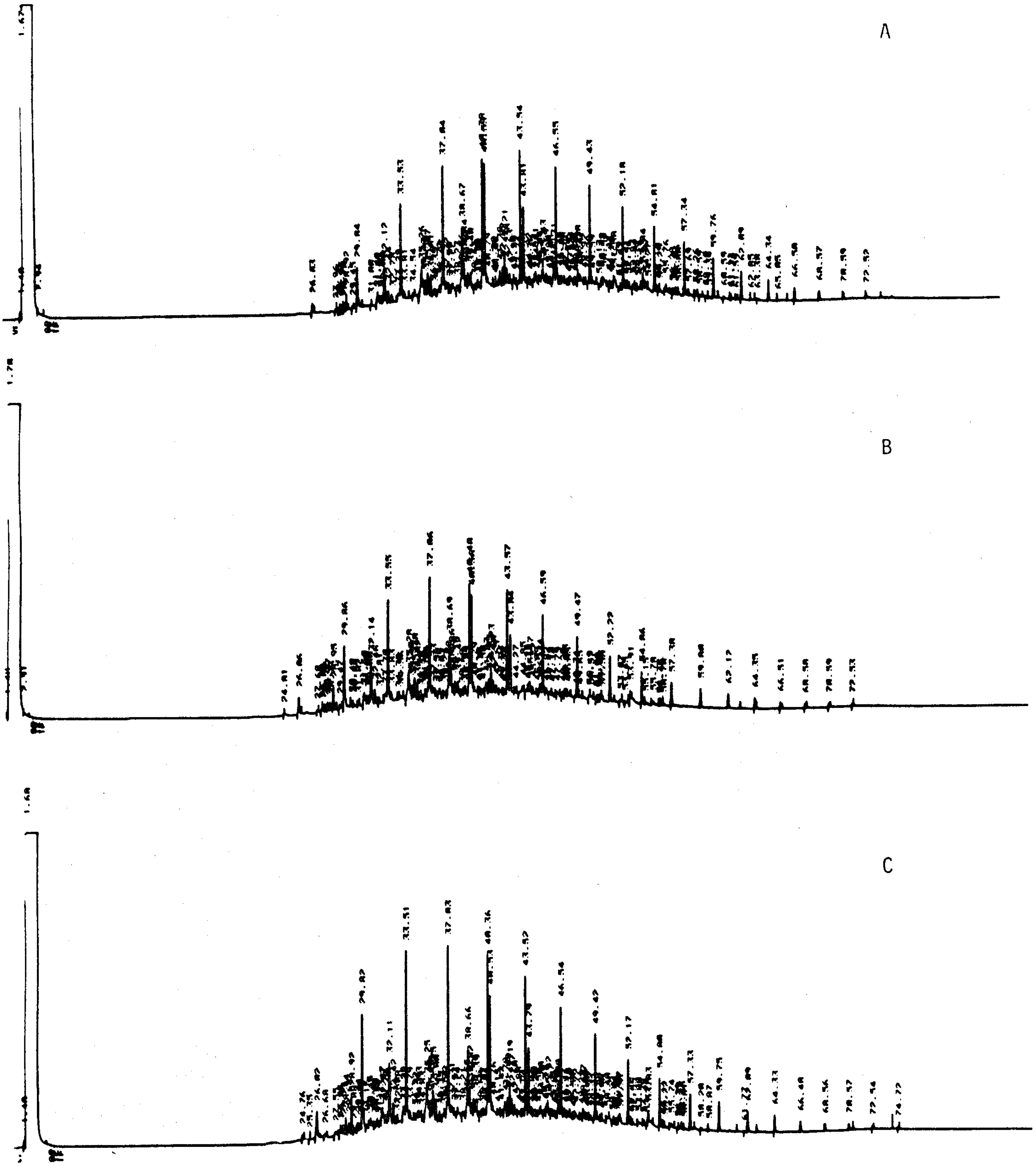

FIGURE 7-16. FID Gas Chromatograms of A) the Foamy Oil/Water Emulsion Surrounding the Tarballs, B) the Outside Surface of Discrete Tarballs, and C) the Interior Material Obtained from Tarballs from Wave Tank 2.

With continued weathering in the spring and summer season, microbial degradation of the oil appeared to be accelerated. Figures 5-88 through 5-90 in Section 5.4.6 present a photograph of the tarballs and foamy surface material observed in the wave tanks after one year of weathering at Kasitsna Bay. Figure 7-17 presents flame ionization detector gas chromatograms obtained on the white foamy material observed in the photograph, the whole oil obtained from several of the smaller sized (less than one centimeter) tarballs, and oil from the lower swash zone of wave tank #2. At this time, the n-C_{17}/pristane and n-C_{18}/phytane ratios have continued to decrease and, in the small tarballs most of the other n-alkanes have been completely removed. In the chromatogram (Figure 7-17C), all of the n-alkanes have been removed from the oil material, and the only components remaining are the isoprenoid compounds farnesene, pristane, and phytane.

In evaluating the data presented for time series concentrations of individual components under Section 5.4.7, rates of evaporative/dissolution and microbial degradation can be obtained for several of the components of interest. In particular, the rate of loss of n-C_{17} appears to be approximately 100 micrograms per month from two months to nine months following the spill. During the same time interval, the degradation rate for pristane is less than 25 micrograms per month. Slightly higher molecular weight components show a similar removal rate, which is assumed to be due solely to microbial degradation and ultimate dissolution of the oxidation products. Figure 5-109 depicts the data for n-C_{16} and n-C_{27} and their respective loss rates of 300 and 250 micrograms per month. The similarity of these rates suggests that n-C_{16} is not being removed by evaporative processes (as the boiling points of n-C_{16} and n-C_{27} are 287°C and 422°C, respectively). Rate loss data for n-C_{15}, n-C_{18}, and phytane are also shown in Figure 5-109. Pentadecane (n-C_{15}) is lost to a slight extent by evaporative processes, and an overall rate constant of 275 micrograms per month is estimated from the data. The n-C_{18} loss rate over the 12 months of the experiment was 200 micrograms per month; however, the branched isoprenoid, phytane, is estimated to be removed at a rate of only 50 micrograms per month.

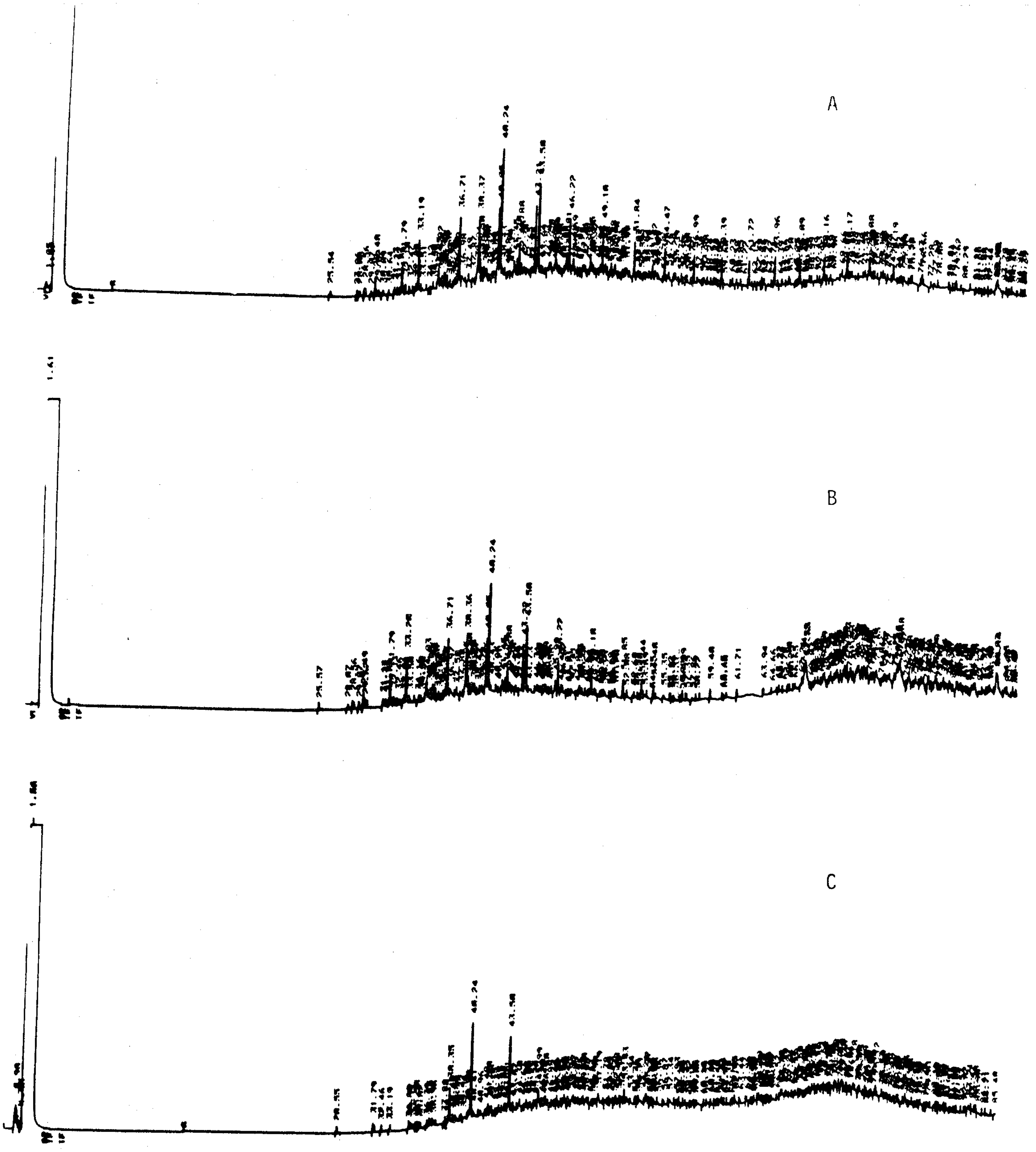

FIGURE 7-17. FID Gas Chromatograms of Samples of A) White Foamy Material, B) Whole Oil from Small Tarballs, and C) Oil from Lower Swash Zone of Tank #2.

A time-series representation of petroleum hydrocarbon component losses from the oil slick in the wavetanks at Kasitsna Bay is seen in Table 5-10. Evaporative loss of the lower molecular weight aliphatics occurred within the first twelve days of weathering such that only n-alkanes of molecular weight n-C_{11} and greater remained in the oil. Drastic reductions in the n-C_{17}/pristane and n-C_{18}/phytane ratios are evident over longer periods of weathering (Figure 5-111A versus 5-111B).

Similar time-series FID chromatograms for wave tank seawater extracts are presented in Figures 5-112 to 5-113. The lighter aromatic components quickly disperse into the water column, but this flux appears to begin falling off within 48 hours of the spill (Figure 5-112C versus 5-112D).

Over longer periods of weathering, the chromatograms of the seawater extracts no longer resemble the continued dissolution of "parent" petroleum components, suggesting biodegradation as an important mechanism for continued dissolution. Figure 5-113 depicts the filtered seawater extracts (nonfractionated) from wavetank #2 at Kasitsna Bay; it is apparent from the chromatograms that dissolution falls off between four and twelve months of weathering.

It is of interest to compare the behavior of petroleum components (parent and degradation products) in the Kasitsna Bay wave tanks to the dissolution behavior which occurred during the Summer 1981 continuous-flow weathering study performed at Scripps Institution of Oceanography. In this study the seawater extracts were fractionated by silica gel, liquid-solid chromatography to facilitate isolation of polar components resulting from microbial degradation. From the chromatograms in Figure 7-18 it is evident that microbial degradation does become an important mechanism for component dissolution in that the flux of polar components increases for both tanks between nine and 23 days. The corresponding chromatograms of the incoming seawater polar fractions (not shown), as well as those for the parent (unweathered) Prudhoe Bay crude polar fraction extracts (see Figure 3-6, Oil Characterization, Section 3.0) are void of FID-sensitive components.

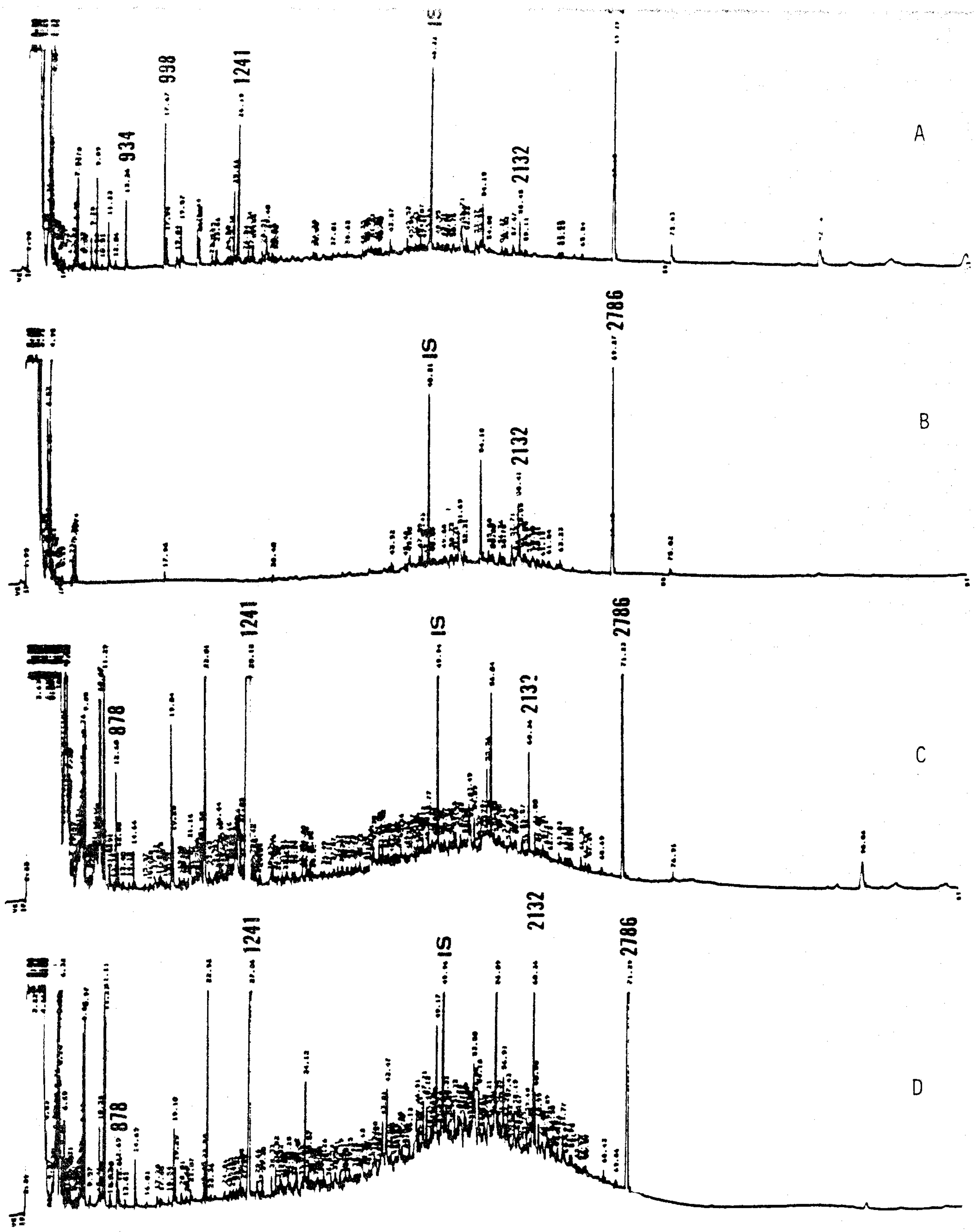

FIGURE 7-18. FID-GC Chromatograms of the Polar Seawater extract fractions from the SIO Summer 1981 continuous-flow weathering study: (A) and (B) two experimental tanks at day 9; (C) and (D) at day 23 post-spill time. (IS= Internal Standard).

Further support of the role of biodegradation as an important mechanism for continued dissolution, by altering parent petroleum components to more polar (and therefore more water-soluble) components, is offered by GC/MS analyses of polar fraction extracts from the SIO study. The polar fraction of a water column extract from one continuous-flow experimental tank after 30 days of weathering was subjected to FID-GC and GC/MS characterization. The FID-GC chromatogram (not shown) bears strong resemblance to that of the 23 day extract (Figure 7-18). Tentative component identifications by GC/MS indicate the presence of aromatic species containing hydroxyl, dihydroxyl (diols), polyhydroxyl, ketone, aldehyde, and carboxylic functions. Aliphatic derivatives which could arise from microbial degradation, such as fatty acids, esters and long-chain alcohols, were also present, although in relatively small quantities.

In an attempt to assess the relative impacts of dissolution and microbial degradation rates upon removal of petroleum components from an oil slick, the dissolved concentrations of selected components from the Kasitsna Bay wavetank studies have been compared to the results of the ^{14}C-labeled hydrocarbon degradation rate studies performed in the summer of 1981.

Although caution must be taken when trying to compare results from two different experimental systems operated under different turbulence and seawater throughput conditions during different summer seasons, this approach can, at least in a semi-quantitative fashion, determine which process (physical dissolution versus biodegradation) is the dominant mechanism. The indoor aquaria utilized for the ^{14}C-labeled hydrocarbon degradation studies were operated under relatively "static" conditions; there was no induced turbulence and tank volume turnover rates were slower (approximately one per day as compared to about eight volumes per day for the wavetanks). However, since it is generally believed that microbial degradative activity is primarily centered at the oil-seawater interface (JORDAN and PAYNE, 1980), the lower turbulence and longer residence time for water soluble petroleum components in the indoor aquaria should allow for more degradation to occur if nutrient availability and dissolved oxygen levels do not become limiting.

From the wave tank studies, the average dissolved concentrations over the first 12 days (post spill) were about 9 μg/l for naphthalene and 7 μg/l for 1- and 2-methylnaphthalenes. From the ^{14}C-substrate work, average degradation rates for ^{14}C-naphthalene and ^{14}C-methylnaphthalene were 2 μg/l-day and 4 μg/l day, respectively. It is of interest to note that the corresponding rates from the SIO study (performed during the same time period) were about 25 μg/l-day for both compounds. This is most likely attributable to higher water temperatures for the SIO study. The high flux of these aromatics, as well as other soluble components, due to the high wave tank volume turnovers (which is most likely more realistic for a real open-ocean spill situation), indicate that dissolution by far dominates biodegradation. From the chromatograms presented earlier, however, continued dissolution appears to be due both to the creation of polar metabolic products as well as polar photochemical degradation products.

8.0 RECENT INTERLABORATORY INTERCALIBRATION PROGRAMS

SAI's laboratory has routinely participated in intercalibration programs: (1) an intercalibration program among the participating hydrocarbon laboratories in the Southern California OCS BLM program (Payne et al., 1979a); (2) a water column extract and mousse intercalibration among the major laboratories involved in the NOAA RESEARCHER cruise to study the IXTOC-I blowout (Payne et al., 1980a); and (3) the NOAA/OCSEAP sediment intercalibration program using Duwamish River sediment samples (Payne et al., 1979b). As part of the Multivariant Analysis of Petroleum Weathering Program, more recent NOAA/OCSEAP intercalibration programs were completed in January 1981 (Duwamish II), November 1982 (Sinclair Inlet sediment), and December 1983 (Test Extract-1 and its associated standard, vial A).

In the BLM program, several different methods were utilized by the participating laboratories, but excellent interlaboratory accuracy and precision were obtained. In the first OCSEAP intercalibration program, our own laboratory evaluated three separate methods for sediment analyses: Soxhlet extraction; shaker table extraction; and Soxhlet extraction using solvents recommended by Dr. William MacLeod of NOAA/NMFS-Seattle. As in the previous intercalibration exercises, very good intermethod precision was obtained, and examination of our data and MacLeod's showed that essentially identical results were obtained in both laboratories.

In the Duwamish II intercalibration program a shaker table procedure for sediment extraction was used; however, the solvent systems were those which are typically utilized in our laboratory for hydrocarbon analyses. The results of our Duwamish II intercalibration analysis are presented in Table 8-1. As the data indicate, fairly good precision was obtained, with coefficients of variations generally less than 20 percent for both the aliphatic and aromatic fractions. Figure 8-1 presents the relative concentrations of the polynuclear aromatic hydrocarbons obtained by our laboratory and by the NOAA/NMFS-Seattle laboratory. The profiles are nearly identical over a wide

TABLE 8-1. NOAA/NMFS INTERCALIBRATION RESULTS - DUWAMISH II, SCIENCE APPLICATIONS, INC.

Concentration of areas (μg/g dry wt)
Replicate No.

Sample #:	1	2	3		$\bar{X}$ $\bar{x}$	CV* s
Naphthalene	57.5	37.4	49.8		48.2	21
Benzothiophene	0	0	0		0	--
2-Methylnapthalene	41.2	45.2	60.9		49.1	21
1-Methylnaphthalene	16.6	15.8	19.5		17.3	11
Biphenyl	7.14	4.3	6.7		6.0	25
2,6-Dimethylnaphthalene	46.0	59.2	76.7		60.6	25
2,3,5-Trimethylnaphthalene	10.2	8.0	16.6		11.6	39
Fluorene	93.2	105.	115.		104.	10
Dibenzothiophene	93.0	85.6	91.2		89.9	4
Phenanthrene	536.	572.	471.		526.	10
Anthracene	168.	251.	310.		243.	29
1-Methylphenanthrene	29.8	29.9	29.1		29.6	1
Fluoranthene	1159.	1127.	1255.		1180.	6
Pyrene	731.	771.	941.		814.	14
Benz [a] anthracene	395.	467.	648		503.	26
Chrysene	722.	791.	1076.		863.	22
Benz [e] pyrene	328.	349.	574.		417.	33
Benz [a] pyrene	311.	412.	566.		430.	30
Perylene	263.	284.	355.		300.	16
Aliquot Weight	119.7	122.8	113.9		118.8	3.8
Percent Dry Weight	48.0	47.7	48.4		48.0	.73

Concentration of n-alkanes (μg/g dry wt)
Replicate No.

	1	2	3		$\bar{X}$	CV*
C_{14}	152	138	242		177	32
C_{15}	143	157	221		174	24
C_{16}	146	147	213		167	23
C_{17}	465	439	476		460	4
Pristane	433	438	466		446	4
C_{18}	141	149	214		168	24
Phytane	191	189	264		215	20
C_{19}	142	193	213		183	20
C_{20}	131	133	200		155	25
C_{21}	289	318	335		314	7
C_{22}	183	161	189		178	8
C_{23}	234	178	257		223	18
C_{24}	242	302	297		280	12
C_{25}	440	513	472		475	8
C_{26}	340	371	393		368	7
C_{27}	1159	1140	840		1046	17
C_{28}	345	366	421		377	10
C_{29}	857	834	768		820	6
C_{30}	827	736	815		793	6
C_{31}	1159	1349	1017		1175	14
C_{32}	310	309	265		295	9

---

*Coefficient of variation - Standard Deviation/Mean

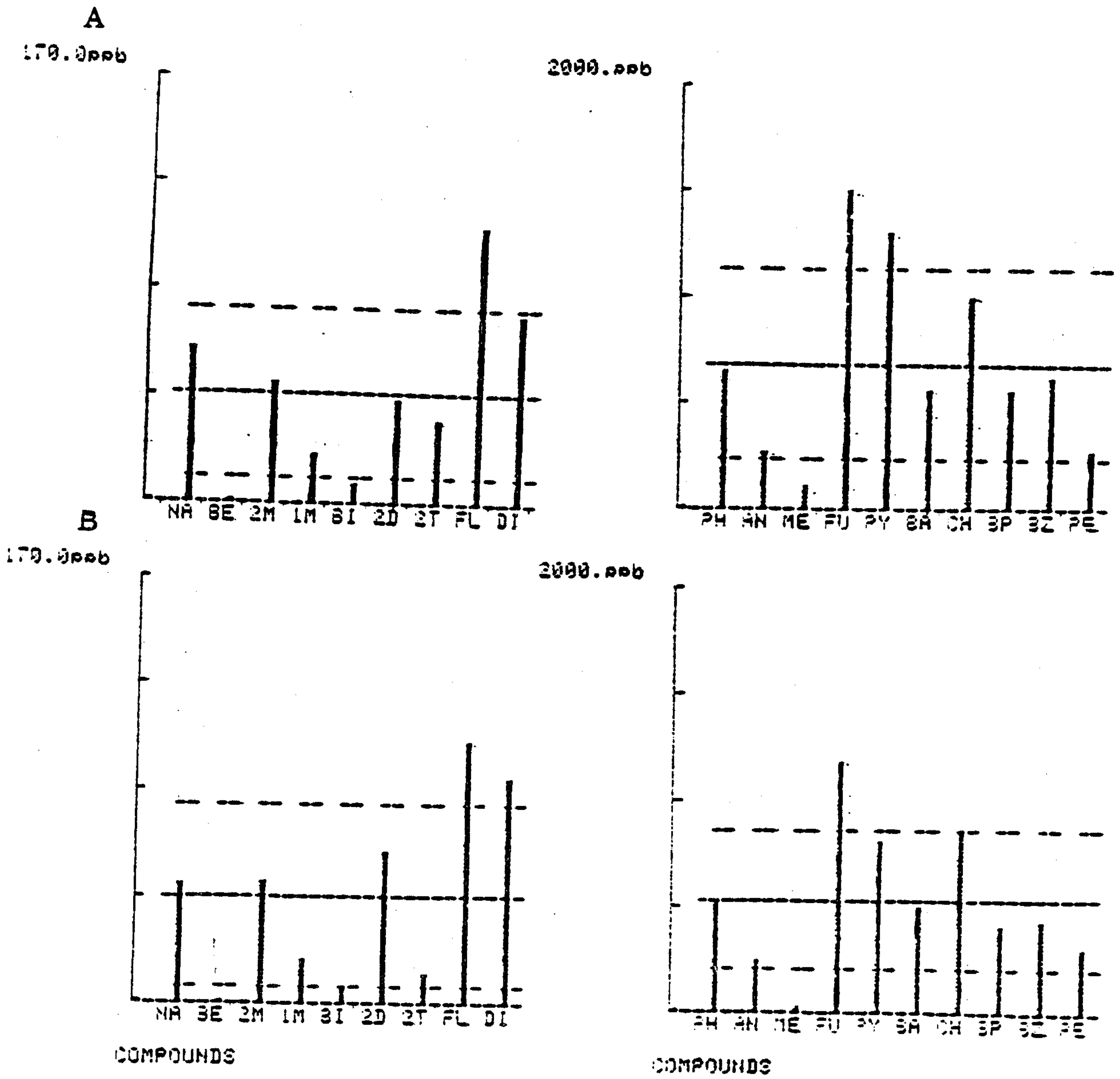

FIGURE 8-1. RELATIVE ABUNDANCE PLOTS FOR POLYNUCLEAR AROMATIC HYDROCARBONS DETECTED IN THE DUWAMISH II INTERCALIBRATION SAMPLES. (A) NOAA NATIONAL MARINE FISHERIES RESULTS AND (B) SCIENCE APPLICATIONS, INC. RESULTS. NOTE CHANGE IN CONCENTRATION SCALES BETWEEN DIBENZOTHIOPHENE (DI) AND PHENANTHRENE (PH); COMPOUND IDENTIFICATIONS FOR OTHER COMPONENTS ARE GIVEN IN TABLE 5-37.

dynamic range, and the overall concentrations of materials are well within one standard deviation. As the data suggest, very good agreement between our laboratory and the National Marine Fisheries Quality Control Laboratory was obtained. In general, when we conduct replicate analyses to evaluate laboratory precision, our results show that coefficients of variations for specific compounds at nanogram levels are near 20 percent or better.

For the Sinclair Inlet sediment intercalibration program the same shaker table extraction and sample workup procedure was used as in the Duwamish II intercalibration program (methods are presented in Appendix H). However, upon recommendation from Dr. William MacLeod of NOAA/NMFS-Seattle, an additional gel permeation step was performed on the aromatic fraction to remove interfering compounds (described by Ramos and Prohaska, 1981). The aromatic fractions were analyzed by both FID-GC and GC-MS; and the results are presented in Tables 8-2 and 8-3. The NOAA/NMFS-Seattle laboratory has not yet released the results of this inter-calibration, so no inter-laboratoy comparisons of absolute concentration can be made. The precision of measurement within our own laboratory was quite high, however, as the coefficient of variation for individual compound measurements ranged from 1-19% for the FID-GC and from 3-25% for the GC/MS. Depending on which of the three internal standards was used for recovery determinations, different portions of the chromatogram exhibited higher precision. However, the majority of compounds measured by FID-GC and GC/MS exhibited analytical coefficients of variation (C.V.) less than 10% and 15%, respectively.

In the most recent NOAA/OCSEAP intercalibration program no extraction or sample workup was required. A vial of Test Extract (TE-1) and its associated standard (vial A) were analyzed in triplicate by FID-GC and GC/MS. Because the concentrations of aromatic analytes in the standard (vial A) were not released to the participating laboratories, compound concentrations for both vials were reported as percent (%) of one of the three internal standards present. The results from the FID-GC analyses are presented in Tables 8-4 and 8-5. Coefficients of variation for the triplicate FID-GC analyses ranged from

TABLE 8-2. NOAA/NMFS INTERCALIBRATION III - SINCLAIR INLET SEDIMENT RESULTS FROM TRIPLICATE FID-GC ANALYSIS

ANALYTE	Concentrations in ng/g dry wt.					
	Calculations Based on d-naphthalene I-Std		Calculations Based on d-acenaphthene I-Std		Calculations Based on d-perylene I-Std	
	$\bar{x} \pm$ Sd	C.V.[a]	$\bar{x} \pm$ Sd	C.V.	$\bar{x} \pm$ Sd	C.V.
naphthalene	NR[b]	—	NR	—	NR	—
benzothiophene	ND[c]	—	ND	—	ND	—
2-methylnaphthalene	57.3 ± 6.4	11%	45.2 ± 4.6	10%	50.3 ± 6.4	13%
1-methylnaphthalene	24.3 ± 1.3	5%	19.3 ± 0.9	5%	21.3 ± 1.5	7%
biphenyl	16.8 ± 2.5	15%	13.4 ± 2.5	19%	14.7 ± 2.2	15%
2,6-dimethylnaphthalene	58.1 ± 4.8	8%	46.1 ± 4.3	9%	51.0 ± 5.2	10%
acenaphthene	19.1 ± 1.8	9%	15.2 ± 1.7	11%	16.8 ± 1.9	11%
trimethylnaphthalene	70.5 ± 5.2	7%	55.9 ± 2.5	5%	61.7 ± 3.8	6%
fluorene	35.0 ± 3.2	9%	27.8 ± 3.0	11%	30.7 ± 3.4	11%
dibenzothiophene	42.4 ± 3.3	8%	35.0 ± 5.1	15%	37.3 ± 3.9	10%
phenanthrene	207 ± 3	1%	164 ± 4.9	3%	181 ± 1	6%
anthracene	79.8 ± 3.3	2%	63.3 ± 3.1	5%	69.9 ± 4.6	7%
1-methylphenanthrene	65.1 ± 5.1	8%	51.7 ± 5.0	10%	57.5 ± 5.7	10%
fluoranthrene	472 ± 33	7%	374 ± 29	8%	440 ± 85	19%
pyrene	730 ± 92	13%	578 ± 64	11%	641 ± 92	14%
benz(a)anthracene	209 ± 18	9%	166 ± 15	9%	184 ± 19	10%
chrysene	327 ± 25	8%	259 ± 15	6%	290 ± 32	11%
benzo(e)pyrene	403 ± 36	9%	320 ± 32	10%	351 ± 35	10%
benzo(a)pyrene	281 ± 27	10%	223 ± 14	6%	246 ± 20	8%
perylene	109 ± 13	12%	86.2 ± 8.5	10%	96.8 ± 10.4	11%

[a] Coefficient of Variation is $(sd/\bar{x}) \cdot (100)$

[b] The peak of interest was Not Resolved from a neighboring peak

[c] Peak was Not Detected

TABLE 8-3. NOAA/NMFS INTERCALIBRATION III - SINCLAIR INLET SEDIMENT RESULTS FROM TRIPLICATE GC/MS ANALYSIS UTILIZING A SPECIFIC ION AREA (generally the base peak) FOR DATA REDUCTION

ANALYTE	Concentrations in ng/g dry wt.					
	Calculations Based on d-naphthalene I-Std		Calculations Based on d-acenaphthene I-Std		Calculations Based on d-perylene I-Std	
	$\bar{x}$ ± Sd	C.V.[a]	$\bar{x}$ ± Sd	C.V.	$\bar{x}$ ± Sd	C.V.
naphthalene	54.4 ± 6.2	11%	50.8 ± 8.3	16%	39.1 ± 5.2	13%
benzothiophene	ND[B]	—	ND	—	ND	—
2-methylnaphthalene	42.0 ± 5.7	14%	39.1 ± 6.4	16%	30.2 ± 4.6	15%
1-methylnaphthalene	20.5 ± 2.2	11%	19.1 ± 2.8	15%	14.8 ± 1.9	13%
biphenyl	9.1 ± 2.0	22%	8.5 ± 2.1	25%	6.6 ± 1.6	24%
2,6-dimethylnaphthalene	40.7 ± 3.6	9%	37.9 ± 5.1	13%	29.2 ± 3.2	11%
acenaphthene	10.8 ± 1.2	11%	10.0 ± 1.6	16%	7.7 ± 1.0	13%
trimethylnaphthalene	49.7 ± 4.5	9%	46.3 ± 6.7	14%	35.7 ± 4.0	11%
fluorene	26.6 ± 3.8	14%	24.8 ± 4.6	19%	19.1 ± 3.1	16%
dibenzothiophene	11.7 ± 0.9	8%	10.9 ± 1.3	12%	8.4 ± 0.8	10%
phenanthrene	254 ± 9	4%	237 ± 19	8%	182 ± 10	6%
anthracene	80 ± 8	10%	75 ± 11	15%	57.5 ± 6.9	12%
1-methylphenanthrene	161 ± 12	8%	149 ± 14	9%	115 ± 10	9%
fluoranthrene	585 ± 38	7%	545 ± 66	12%	420 ± 34	8%
pyrene	1009 ± 77	8%	940 ± 122	13%	725 ± 65	9%
benz(a)anthracene	316 ± 24	8%	294 ± 38	13%	227 ± 20	9%
chrysene	447 ± 34	8%	417 ± 55	13%	321 ± 29	9%
benzo(e)pyrene	429 ± 12	3%	399 ± 34	9%	308 ± 14	5%
benzo(a)pyrene	401 ± 11	3%	373 ± 30	8%	288 ± 14	5%
perylene	154 ± 6	4%	143 ± 11	8%	110 ± 7	6%

[a] Coefficient of Variation is (sd/$\bar{x}$)·(100)

[b] Peak was Not Detected

TABLE 8-4. NOAA/NMFS INTERCALIBRATION IV - VIAL A RESULTS FROM TRIPLICATE FID-GC ANALYSIS

	Concentrations as Percent(%) of I-Std					
	Calculations Based on d-naphthalene I-Std		Calculations Based on d-acenaphthene I-Std		Calculations Based on d-perylene I-Std	
ANALYTE	$\bar{x} \pm$ Sd	C.V.[a]	$\bar{x} \pm$ Sd	C.V.	$\bar{x} \pm$ Sd	C.V.
naphthalene	79.6 ± 5.7	7%	63.4 ± 3.7	6%	190 ± 39	20%
2-methylnaphthalene	123.2 ± 3.5	3%	98.3 ± 1.3	1%	294 ± 51	17%
1-methylnaphthalene	124.5 ± 3.6	3%	99.2 ± 1.3	1%	296 ± 51	17%
biphenyl	133.4 ± 3.3	2%	106.3 ± 1.1	1%	317 ± 54	17%
2,6-dimethylnaphthalene	131.5 ± 3.2	2%	104.9 ± 1.0	1%	313 ± 53	17%
acenaphthene	115.3 ± 2.2	2%	91.9 ± 0.4	<1%	274 ± 44	16%
2,3,5-trimethylnaphthalene	119.2 ± 1.9	2%	95.0 ± 0.2	<1%	283 ± 45	16%
fluorene	107.4 ± 1.1	1%	85.6 ± 0.7	<1%	255 ± 39	15%
phenanthrene	113.7 ± 3.5	3%	90.7 ± 4.0	4%	269 ± 30	11%
anthracene	105.3 ± 4.2	4%	84.0 ± 4.6	5%	249 ± 26	10%
1-methylphenanthrene	107.2 ± 5.9	6%	85.5 ± 5.8	7%	253 ± 23	9%
3,6-dimethylphenanthrene	94.1 ± 6.2	7%	75.0 ± 5.9	8%	222 ± 17	8%
fluoranthrene	90.5 ± 7.0	8%	72.2 ± 6.5	9%	213 ± 14	7%
pyrene	87.3 ± 8.1	9%	69.7 ± 7.4	11%	205 ± 10	5%
benz(a)anthracene	74.3 ± 9.4	13%	59.4 ± 8.2	14%	174.4 ± 2.6	1%
chrysene	43.6 ± 7.0	16%	34.8 ± 6.0	17%	101.8 ± 3.6	4%
benzo(e)pyrene	63.1 ± 9.7	15%	50.4 ± 8.4	17%	147.6 ± 2.0	1%
benzo(a)pyrene	63.3 ± 9.4	15%	50.6 ± 8.1	16%	148.2 ± 1.4	<1%
perylene	46.0 ± 7.0	15%	36.7 ± 6.0	16%	107.6 ± 1.1	1%
dibenz(a,h)anthracene	45.7 ± 9.3	20%	36.5 ± 7.9	22%	106.5 ± 6.8	6%
<u>Internal Standards</u>						
d_8 - naphthalene	100	—	80.9 ± 0.8	<1%	242 ± 41	17%
d_{10} - acenaphthene	125.4 ± 1.9	2%	100	—	265 ± 22	8%
d_{12} - perylene	42.7 ± 6.1	14%	34.1 ± 5.3	16%	100	—

[a]Coefficient of Variation is $(sd/\bar{x})\cdot(100)$

TABLE 8-5 . NOAA/NMFS INTERCALIBRATION IV - TEST EXTRACT 1 RESULTS FROM TRIPLICATE FID-GC ANALYSIS

	Concentrations as Percent(%) of I-Std					
	Calculations Based on d-naphthalene I-Std		Calculations Based on d-acenaphthene I-Std		Calculations Based on d-perylene I-Std	
ANALYTE	$\bar{x}$ ± Sd	C.V.[a]	$\bar{x}$ ± Sd	C.V.	$\bar{x}$ ± Sd	C.V.
naphthalene	39.9 ± 3.5	9%	34.1 ± 2.6	8%	110 ± 10	9%
2-methylnaphthalene	37.1 ± 0.6	2%	31.7 ± 0.4	1%	102 ± 2	2%
1-methylnaphthalene	22.9 ± 0.1	<1%	19.5 ± 0.4	2%	63.0 ± 1.3	2%
biphenyl	10.2 ± 0.3	3%	8.72 ± 0.42	5%	28.1 ± 0.8	3%
2,6-dimethylnaphthalene	19.8 ± 0.5	3%	16.9 ± 0.3	2%	54.6 ± 1.7	3%
acenaphthene	65.6 ± 0.9	1%	56.0 ± 0.5	<1%	181 ± 4	2%
2,3,5-trimethylnaphthalene	ND[b]	—	ND	—	ND	—
fluorene	70.7 ± 1.2	2%	60.3 ± 0.4	<1%	195 ± 5	3%
phenanthrene	394 ± 9	2%	336 ± 11	3%	1085 ± 7	<1%
anthracene	87.9 ± 3.0	3%	75.1 ± 3.1	4%	242 ± 4	2%
1-methylphenanthrene	17.2 ± 1.2	7%	14.7 ± 1.2	8%	47.4 ± 2.6	5%
3,6-dimethylphenanthrene	4.3 ± 1.5	34%	3.7 ± 1.3	35%	11.7 ± 3.8	33%
fluoranthrene	488 ± 19	4%	417 ± 20	5%	1342 ± 28	2%
pyrene	525 ± 21	5%	448 ± 22	5%	1443 ± 31	2%
benz(a)anthracene	157 ± 7	4%	134 ± 7	5%	431 ± 11	3%
chrysene	237 ± 8	3%	202 ± 9	4%	651 ± 10	2%
benzo(e)pyrene	124 ± 4	3%	106 ± 5	5%	342 ± 5	1%
benzo(a)pyrene	122 ± 5	4%	104 ± 5	5%	337 ± 6	2%
perylene	25.9 ± 1.7	7%	22.1 ± 1.6	7%	71.3 ± 3.3	5%
dibenz(a,h)anthracene	6.52 ± 0.47	7%	5.57 ± 0.48	9%	17.9 ± 1.3	7%
<u>Internal Standards</u>						
d_8 - naphthalene	100	—	85.4 ± 1.3	2%	276 ± 5	2%
d_{10} - acenaphthene	117 ± 2	2%	100	—	323 ± 9	3%
d_{12} - perylene	36.4 ± 0.7	2%	31.0 ± 0.9	3%	100	—

[a] Coefficient of Variation is $(sd/\bar{x}) \cdot (100)$

[b] Peak was Not Detected

<1% to 22% for vial A and from <1% to 35% for TE-1. The high C.V. in TE-1 belongs to dimethylphenanthrene, which was present at a concentration near the detection limit of the FID-GC. If this one high value is excluded from the list, the next highest coeficient of variation is only 9%, indicating that very high precision was obtained in the FID-GC determinations.

The GC/MS data was quantified using two different methods. The first method of GC/MS data reduction utilized a specific ion area, generally the base peak, for quantitation. This method eliminates the contributions from co-eluting peaks in the sample (and is the same method that was used in data reduction for the Sinclair Inlet GC/MS data). Tables 8-6 and 8-7 present the results obtained on vial A and TE-1 using this method. The second method utilized the total peak area of the compound on the reconstructed ion chromatogram (RIC) for data reduction. Tables 8-8 and 8-9 present the results obtained using this method. Although this type of quantitation parallels the quantitation method utilized in FID-GC data reduction (and gives best agreement with FID-GC results), this method would be inaccurate if co-eluting peaks were present. Generally, the specific ion method is accepted as a more accurate representative of what is truly present in the sample.

TABLE 8-6. NOAA/NMFS INTERCALIBRATION IV - VIAL A RESULTS FROM TRIPLICATE GC/MS ANALYSIS UTILIZING A SPECIFIC ION AREA (generally the base peak) FOR DATA REDUCTION

ANALYTE	Concentrations as Percent(%) of I-Std					
	Calculations Based on d-naphthalene I-Std		Calculations Based on d-acenaphthene I-Std		Calculations Based on d-perylene I-Std	
	$\bar{x}$ ± Sd	C.V.[a]	$\bar{x}$ ± Sd	C.V.	$\bar{x}$ ± Sd	C.V.
naphthalene	132 ± 10	8%	268 ± 40	15%	241 ± 55	23%
2-methylnaphthalene	73.6 ± 3.0	4%	149 ± 17	11%	134 ± 26	19%
1-methylnaphthalene	72.7 ± 5.7	8%	148 ± 22	15%	133 ± 29	22%
biphenyl	96.4 ± 5.1	5%	196 ± 25	13%	176 ± 38	22%
2,6-dimethylnaphthalene	66.5 ± 2.5	4%	135 ± 15	11%	121 ± 25	21%
acenaphthene	51.3 ± 2.6	5%	104 ± 3	3%	94 ± 21	22%
2,3,5-trimethylnaphthalene	57.0 ± 2.3	4%	116 ± 13	11%	104 ± 24	23%
fluorene	63.1 ± 1.6	3%	128 ± 12	9%	115 ± 25	22%
phenanthrene	97 ± 19	19%	198 ± 51	26%	175 ± 42	24%
anthracene	89 ± 18	20%	181 ± 47	26%	159 ± 36	23%
1-methylphenanthrene	67 ± 13	20%	137 ± 35	26%	120 ± 27	23%
3,6-dimethylphenanthrene	44.5 ± 7.4	17%	91 ± 20	22%	80 ± 15	19%
fluoranthrene	82 ± 19	22%	168 ± 46	27%	147 ± 30	20%
pyrene	85 ± 18	22%	173 ± 46	27%	151 ± 28	19%
benz(a)anthracene	78 ± 21	27%	159 ± 48	30%	137 ± 18	13%
chrysene	45 ± 13	29%	91 ± 29	31%	78.7 ± 9.4	12%
benzo(e)pyrene	79 ± 26	33%	161 ± 57	35%	138 ± 17	12%
benzo(a)pyrene	84 ± 28	33%	172 ± 61	35%	147 ± 18	12%
perylene	90 ± 24	27%	182 ± 53	29%	158 ± 8	5%
dibenz(a,h)anthracene	44 ± 14	33%	90 ± 30	34%	77.3 ± 7.6	10%
<u>Internal Standards</u>						
d_8 - naphthalene	100	—	203 ± 15	7%	182 ± 37	20%
d_{10} - acenaphthene	49.5 ± 3.7	7%	100	—	91 ± 20	22%
d_{12} - perylene	57 ± 13	23%	115 ± 28	24%	100	—

[a] coefficient of Variation is (sd/$\bar{x}$)·(100)

TABLE 8-7. NOAA/NMFS INTERCALIBRATION IV - TEST EXTRACT 1 RESULTS FROM TRIPLICATE GC/MS ANALYSIS UTILIZING A SPECIFIC ION AREA (generally the base peak) FOR DATA REDUCTION

	Concentrations as Percent(%) of I-Std					
	Calculations Based on d-naphthalene I-Std		Calculations Based on d-acenaphthene I-Std		Calculations Based on d-perylene I-Std	
ANALYTE	$\bar{x} \pm$ Sd	C.V.[a]	$\bar{x} \pm$ Sd	C.V.	$\bar{x} \pm$ Sd	C.V.
naphthalene	69.6 ± 1.0	1%	170 ± 15	3%	115 ± 27	23%
2-methylnaphthalene	12.9 ± 1.5	12%	31.5 ± 3.2	10%	21.0 ± 3.5	17%
1-methylnaphthalene	4.7 ± 1.8	38%	11.4 ± 4.1	36%	7.3 ± 1.4	19%
biphenyl	1.9 ± 1.5	79%	4.7 ± 3.5	74%	2.8 ± 1.6	57%
2,6-dimethylnaphthalene	2.3 ± 0.9	39%	5.6 ± 2.1	38%	3.6 ± 0.9	25%
acenaphthene	21.8 ± 1.9	9%	53.4 ± 5.5	10%	37 ± 12	32%
2,3,5-trimethylnaphthalene	ND[b]	—	ND	—	ND	—
fluorene	27.9 ± 4.4	16%	67.9 ± 8.8	13%	45.0 ± 5.0	11%
phenanthrene	414 ± 12	3%	1010 ± 21	2%	685 ± 167	24%
anthracene	76.7 ± 8.9	12%	187 ± 15	8%	125 ± 21	17%
1-methylphenanthrene	13.0 ± 4.3	33%	31.7 ± 9.8	31%	20.5 ± 3.6	18%
3,6-dimethylphenanthrene	ND	—	ND	—	ND	—
fluoranthrene	600 ± 40	7%	1466 ± 62	4%	990 ± 226	23%
pyrene	720 ± 51	7%	1758 ± 79	4%	1186 ± 267	23%
benz(a)anthracene	204 ± 33	16%	497 ± 63	13%	330 ± 41	12%
chrysene	296 ± 37	13%	722 ± 66	9%	482 ± 77	16%
benzo(e)pyrene	201 ± 37	18%	490 ± 73	15%	325 ± 39	12%
benzo(a)pyrene	231 ± 38	16%	563 ± 74	13%	374 ± 51	4%
perylene	57 ± 16	28%	138 ± 35	25%	89.4 ± 4.3	5%
dibenz(a,h)anthracene	6.6 ± 4.7	71%	16 ± 11	69%	9.7 ± 4.7	48%
<u>Internal Standards</u>						
d_8 - naphthalene	100	—	244 ± 8	3%	166 ± 41	25%
d_{10} - acenaphthene	50.0 ± 1.3	3%	100	—	68 ± 15	23%
d_{12} - perylene	63 ± 17	27%	153 ± 37	24%	100	—

[a] Coefficient of Variation is (sd/$\bar{x}$)·(100)

[b] Peak was Not Detected

TABLE 8-8. NOAA/NMFS INTERCALIBRATION IV - VIAL A RESULTS FROM TRIPLICATE GC/MS ANALYSIS UTILIZING THE TOTAL PEAK AREA FOR DATA REDUCTION

	Concentrations as Percent(%) of I-Std					
	Calculations Based on d-naphthalene I-Std		Calculations Based on d-acenaphthene I-Std		Calculations Based on d-perylene I-Std	
ANALYTE	$\bar{x}$ ± Sd	C.V.[a]	$\bar{x}$ ± Sd	C.V.	$\bar{x}$ ± Sd	C.V.
naphthalene	127 ± 13	10%	148 ± 34	23%	191 ± 77	40%
2-methylnaphthalene	109 ± 12	11%	126 ± 29	23%	164 ± 66	40%
1-methylnaphthalene	117 ± 15	13%	137 ± 34	25%	178 ± 75	42%
biphenyl	120 ± 2	2%	139 ± 19	14%	178 ± 56	31%
2,6-dimethylnaphthalene	111 ± 10	9%	129 ± 26	21%	167 ± 63	38%
acenaphthene	97 ± 7	7%	111 ± 6	5%	141 ± 34	24%
2,3,5-trimethylnaphthalene	101 ± 7	7%	117 ± 23	19%	151 ± 56	37%
fluorene	92 ± 4	4%	106 ± 13	12%	136 ± 41	30%
phenanthrene	123 ± 26	21%	139 ± 19	14%	174 ± 27	15%
anthracene	112 ± 24	21%	128 ± 15	12%	159 ± 19	12%
1-methylphenanthrene	120 ± 25	21%	136 ± 17	12%	169 ± 21	12%
3,6-dimethylphenanthrene	92 ± 23	25%	104 ± 16	16%	129 ± 12	9%
fluoranthrene	112 ± 24	21%	127 ± 15	12%	159 ± 17	10%
pyrene	119 ± 24	20%	135 ± 13	10%	168 ± 19	11%
benz(a)anthracene	105 ± 23	22%	119 ± 13	11%	148 ± 16	11%
chrysene	68 ± 16	24%	77 ± 10	13%	96 ± 11	12%
benzo(e)pyrene	231 ± 37	16%	264 ± 24	9%	331 ± 59	18%
benzo(a)pyrene	103 ± 27	26%	116 ± 18	16%	144 ± 17	12%
perylene	123 ± 41	33%	138 ± 32	23%	170 ± 14	9%
dibenz(a,h)anthracene	49 ± 18	37%	54 ± 14	26%	67 ± 9	14%
<u>Internal Standards</u>						
d_8 - naphthalene	100	——	115 ± 15	13%	148 ± 45	30%
d_{10} - acenaphthene	88 ± 10	12%	100	——	126 ± 24	19%
d_{12} - perylene	72 ± 22	31%	81 ± 17	20%	100	——

[a]Coefficient of Variation is (sd/$\bar{x}$)·(100)

TABLE 8-9. NOAA/NMFS INTERCALIBRATION IV - TEST EXTRACT 1 RESULTS FROM TRIPLICATE GC/MS ANALYSIS UTILIZING THE TOTAL PEAK AREA FOR DATA REDUCTION

	Concentrations as Percent(%) of I-Std					
	Calculations Based on d-naphthalene I-Std		Calculations Based on d-acenaphthene I-Std		Calculations Based on d-perylene I-Std	
ANALYTE	$\bar{x} \pm$ Sd	C.V.[a]	$\bar{x} \pm$ Sd	C.V.	$\bar{x} \pm$ Sd	C.V.
naphthalene	67.8 ± 4.9	7%	82.5 ± 5.6	7%	138 ± 57	41%
2-methylnaphthalene	29.8 ± 0.9	3%	36.3 ± 0.8	2%	61 ± 24	39%
1-methylnaphthalene	16.1 ± 0.8	5%	19.5 ± 1.0	5%	32 ± 10	31%
biphenyl	5.9 ± 1.6	27%	7.1 ± 1.9	27%	11.3 ± 2.6	23%
2,6-dimethylnaphthalene	10.6 ± 1.2	11%	12.9 ± 1.5	12%	21.0 ± 5.2	25%
acenaphthene	50.6 ± 1.7	3%	61.6 ± 1.7	3%	103 ± 41	40%
2,3,5-trimethylnaphthalene	ND[b]	——	ND	——	ND	——
fluorene	51.8 ± 5.5	11%	63.1 ± 6.6	10%	103 ± 32	31%
phenanthrene	388 ± 2	<5	473 ± 4	<1%	788 ± 294	37%
anthracene	79 ± 10	13%	96 ± 13	14%	155 ± 35	23%
1-methylphenanthrene	23.3 ± 4.0	17%	28.4 ± 4.9	17%	45.4 ± 9.1	20%
3,6-dimethylphenanthrene	ND	——	ND	——	ND	——
fluoranthrene	549 ± 2	<1%	668 ± 5	<1%	1112 ± 409	37%
pyrene	717 ± 68	9%	873 ± 85	10%	1420 ± 380	27%
benz(a)anthracene	200 ± 27	14%	244 ± 33	14%	393 ± 91	23%
chrysene	291 ± 26	9%	354 ± 32	9%	577 ± 162	28%
benzo(e)pyrene	370 ± 128	35%	450 ± 154	34%	812 ± 588	72%
benzo(a)pyrene	197 ± 35	18%	240 ± 43	18%	384 ± 78	20%
perylene	58 ± 17	29%	71 ± 21	30%	111 ± 25	22%
dibenz(a,h)anthracene	8.3 ± 2.8	34%	10.1 ± 3.4	34%	15.5 ± 2.3	15%
Internal Standards						
d_8 - naphthalene	100	——	121.7 ± 0.7	<1%	203 ± 75	37%
d_{10} - acenaphthene	82.2 ± 0.4	<1%	100	——	167 ± 63	38%
d_{12} - perylene	54 ± 18	33%	65 ± 21	33%	100	——

[a] Coefficient of Variation is $(sd/\bar{x}) \cdot (100)$

[b] Peak was Not Detected

9.0 BIBLIOGRAPHY

Adams, C.E., Jr and Weatherly, G.L. (1981). Some Effects of Suspended Sediment Stratification on an Oceanic Bottom Boundary Layer. J. Geophy. Res, Vol 86, No. C5, pp 4161-4172.

API (1976). Technical Data Book - Petroleum Refining. American Petroleum Institute, Washington, D.C.

Atlas, R. M. and R. Bartha (1981). Microbial Ecology Fundamentals and Applications. Addison-Wesley, Reading, MA.

Azam, F., and O. Holm-Hansen (1973). Use of Tritiated Substrates in the Study of Heterotrophy in Seawater. Marine Biology. 23:191-196.

Bailey, N. J. L., A. M. Jobson, and M. A. Rogers (1973). Bacterial Degradation of Crude Oil: Comparison and Experimental Data. Chem. Geol. 11:203-221.

Baker, E.T. (1983). Suspended Particulate Matter Distribution, Transport, and Physical Characteristics in the North Aleutian Shelf and St. George Basin Lease Areas. NOAA Project No. R7120897.

Ball, J. S., and H. T. Rall (1962). Nonhydrocarbon Components of a California Petroleum. Division of Refining, 42(3):128-145.

Bartha, R., and R. M. Atlas (1983). Transport and Transformations of Petroleum: Biological Processes (unpublished manuscript).

Bassin, J. J., and T. Ichiye (1977). Flocculation Behavior of Suspended Sediments and Oil Emulsions. Journal of Sedimentary Petrology, 47(2):671-677.

Bellar, T. A., and J. J. Lichtenberg (1974). Journal of American Water Works, 66:703.

Blumer, M., M. Ehrhardt, and J. H. Jones (1973). The Environmental Fate of Stranded Crude Oil. Deep Sea Research, 20:239-259.

Boehm, P. D., and D. L. Fiest (1980). Aspects of the Transport of Petroleum Hydrocarbons to the Offshore Benthos During the IXTOC-I Blowout in the Bay of Campeche. Proceedings of a Symposium on Preliminary Results from the Sept. 1979 Researcher/Pierce IXTOC-I Cruise. Key Biscayne, Florida, (June 9-10). NOAA Off. Mar. Poll. Assessment.

Butler, J. N. (1975). Evaporative Weathering of Petroleum Residues: The Age of Pelagic Tar. Marine Chemistry, Vol. 3, p. 9.

Cacchione, D. A. and Drake, D. E. (1982). Measurements of Storm-Generated Bottom Stresses on the Continental Shelf. J. Geophys Res. Vol 87, No. C3, pp 1952-1960.

Caparello, D. M., and P. A. La Rock (1975). A Ratioisotope Assay for the Quantification of Hydrocarbon Biodegradation Potential in Environmental Samples. Microbial Ecology. 2:28-42.

Carslaw, H. S., and J. C. Jaeger (1959). Conduction of Heat in Solids, Oxford University Press.

Chase, R. R. P. (1979). Settling Behavior of Natural Aquatic Particulates. Limnol. Oceanogr. Vol 24, No. 3, pp 417-426.

Clark, R. C., and W. D. MacLeod, Jr. (1977). Inputs, Transport Mechanisms and Observed Concentrations of Petroleum in the Marine Environment, p. 91-223. In: D. C. Malins (ed.), Effects of Petroleum on Arctic and Subarctic Marine Environments and Organisms. Academic Press, New York.

Coleman, H. J., E. M. Shelton, D. T. Nichols, and C. J. Thompson (1978). Analyses of 800 Crude Oils from United States Oil Fields. BETC/RRI-78/14, Bartlesville Energy Technology Center, Bartlesville, Oklahoma.

Davies, J. T. (1957). Spontaneous Emulsification. Proceedings of the International Congress on Surface Activity, 2nd, London, 1, 417.

Davies, J. T. (1972). Turbulence Phenomena. Academic Press, Inc., New York, New York.

de Lappe, B. W., R. W. Riseborough, J. C. Shropshire, W. R. Sisteck, E. F. Letterman, D. R. de Lappe, and J. R. Payne (1979). The Partitioning of Petroleum Related Compounds Between the Mussel Mytilus californianus and Seawater in the Southern California Bight. Draft Final Report II-15.0, Intertidal study of the Southern California Bight, submitted to Bureau of Land Management, D.C. by the Bodega Marrine Laboratory, University of California, and Science Applications, Inc.

Delaune, R. D., G. A. Hambrick, and W. H. Patrick, Jr. (1980). Degradation of Hydrocarbons in Oxidized and Reduced Sediments. Mar. Poll. Bull. 11:103-106.

Drake, D. E. (1976). Suspended Sediment Transport and Mud Deposition on Continental Shelves. In: Marine Sediment Transport and Environment Managment, edited by D. J. Stanley and D. J. Swift, pp 127-158. Wiley-Interscience, New York.

Duda, J. L. and J. S. Vrentas (1969). Perturbation Solutions for Diffusion - Controlled Moving Boundary Problems. Chemical Engineering Science 24:461-670.

Evaluations of World's Import Crudes (1973). The Oil and Gas Journal, The Petroleum Publishing Co., Tulsa, Oklahoma, U.S.A.

Fallon, J. F., and K. M. Watson (1944). Thermal Properties of Hydrocarbons. National Petroleum News, June 7, p. 372.

Feely, R. A., J. D. Cline, and G. J. Massoth (1978). Transport Mechanisms and Hydrocarbon Adsorption Properties of Suspended Matter in Lower Cook Inlet. Quarterly Report, Pacific Marine Environmental Laboratory, NOAA, Seattle, Wash.

Fuhrman, J. A., Ammerrman, J. W., and F. Azam (1980). Bacterioplankton in the Coastal Euphotic Zone: Distribution, Activity and Possible Relationships with Phytoplankton. Marine Biology, 60, 20:201-207.

Fuhrman, J. A., and F. Azam (1980). Bacterioplankton Secondary Production Estimates for Coastal Waters of British Columbia, Antarctica, and California. Applied and Environmental Microbiology. 39(6):1085-1095.

Fuhrman, J. A., and F. Azam (1981). Thymidine Incorporation as a Measure of Heterotrophic Bacterioplankton Production in Marine Surface Waters: Evaluation and Field Results. Marine Biology (in press).

Gad, J. (1878). Arch. Anat. Physiol, pg. 181.

Gamson, B. W., and K. M. Watson (1944). Vapor Pressures and Critical Properties of Organic Compounds. National Petroleum News, May 3, p. 259.

Gearing, J. N. and Gearing P. J. (1982). Effects of Suspended Load and Solubility on Sedimentation of Petroleum Hydrocarbons in Controlled Estuarine Ecosystems. Canadian Journal of Fisheries and Aquatic Science.

Gearing, J. N., P. J. Gearing, T. Wade, J. G. Quinn, H. G. McCarty, J. Farrington, and R. F. Lee (1979). The Rates of Transport and Fates of Petroleum Hydrocarbons in a Controlled Marine Ecosystem and a Note on Analytical Variability, p. 555-564, In: Proceedings, 1979 Oil Spill Conference (Prevention, Behavior, Control, Cleanup) 19-22 March, Los Angeles, Calif.

Gold, P. I. (1969). Estimating Thermophysical Properties of Liquid, Part 10; Viscosity. Chemical Engineerring, July 14.

Gordon, D. C., P. D. Keizer, W. R. Hardstaff, and D. G. Aldous (1976). Fate of Crude Oil Spilled on Seawater Contained in Outdoor Tanks. Environmental Science and Technology, 10(6):580-585.

Grant, H. L., Moilliet, H. L., Vogel, W. M. (1968). Some Observations of the Occurrence of Turbulence in and Above the Thermocline. J. Fluid Mech; Vol 34, part 3, pp 443-448.

Griffiths, R. P., and R. Y. Morita (1980). Study of Microbial Activity and Crude Oil-Microbial Interactions in the Waters and Sediments of Cook Inlet and the Beaufort Sea. Final Reporrt to the NOAA OCSEAP Office, Juneau, Alaska.

Groves, M. J. (1978). Spontaneous Emulsification. Chemistry and Industry, (12), p. 417.

Gundlach, E. R., and M. O. Hayes (1978). Investigations of Beach Processes. In: The Amoco Cadiz Oil Spill. A Preliminary Scientific Report, W. N. Hess (ed.), NOAA/EPA Special Report, pp. 85-196.

Gundlach, E. R., P. D. Boehm, M. Marchand, R. M. Atlas, D. M. Ward, and D. A. Wolfe (1983). Science 221:4606, 122-129.

Gurwitsch. Wissenschaftliche Grundlagen der Erdolbearbeitung (1913). Translation by Moore, London, 1932, pg. 430. Chapman and Hall ltd.

Harrison, W., M. A. Winnik, P. T. Y. Kwong, and D. Mackay (1975). Crude Oil Spills. Disappearance of Aromatic and Aliphatic Components from Small Sea-Surface Slicks. Environmental Science and Technology, 9:231-234.

Hawley, N. (1982). Settling Velocity Distributions of Natural Aggregates. J. Geophys. Res., Vol 87, No. C12, pp 9489-9498.

Hayes, M. O., P. J. Brown, and J. Michel (1976). Coastal Morphology and Sedimentation, Lower Cook Inlet, Alaska: With Emphasis on Potential Oil Spill Imports: Tech. Rept. No. 12-CRD, Coastal Research Division, Dept. of Geology, Univ. of South Carolina, 107 pp.

Hayes, M. O. E. R. Gundlach, and L. D'Ozouville (1979). Role of Dynamic Coastal Processes in the Impact and Dispersal of the Amoco Cadiz Oil Spill (March, 1978), Brittany, France, p 193-200. In Proceedings of the 1979 Oil Spill Conference, March 19-22, Los Angeles, CA.

Hobbie, J. E., Daley, R. J., and S. Jasper (1977). Use of Nucleopore Filters for Counting Bacteria by Fluorescence Microscopy. Applied and Environmental Microbiology. 33(5):1225-1228.

Hodson, R. E., Azam, F., and R. F. Lee (1977). Effects of Four Oils on Marine Bacterial Populations: Controlled Ecosystem Pollution Experiment. Bulletin of Marine Science. 27(1):119-126.

Hougen, O. A., K. M. Watson, and R. A. Ragatz (1965). Chemical Process Principles, Part I. John Wiley & Sons, Inc., New York.

Huang, C. P. (1976). Solid-Solution Interface: its Role in Regulating the Chemical Composition of Natural Waters. Transport Processes in Lakes and Oceans. Proceedings of a Symposium held at the 82nd National Meeting of the American Institute of Chemical Engineers.

Hunt, J.R. (1982a). Particle Dynamics Seawater: Implication for Predicting the Fate of Discharged Particles. Environ. Sci. Technol, Vol 16, No. 6. pp 303-309.

_______ (1982b). Self-Similar Particle-Size Distributions during Coagulation: Theory and Experimental Verification. J. Fluid Mech, Vol 22, pp 169-185.

Jaeger, J. C. (1945). Conduction of Heat in a Slab in Contact with a Well Stirred Fluid. Cambridge Philosophical Society, Proceedings, Vol. 41, p. 43.

John, P., and I. Souter (1976). Anal. Chem. 48:520.

Jordan, R. E., and J. R. Payne (1980). Fate and Weathering of Petroleum Spills in the Marine Environment: A Literature Review and Synopsis. Ann Arbor Science Publishers, Inc., Ann Arbor, Michigan.

Kaminski and McBain (1949). Proc. Roy. Soc. A 198, pg. 447.

Karickhoff, S. W., D. S. Brown, and T. A. Scott (1979). Sorption of Hydrophobic Pollutants on Natural Sediments. Water Research, 13, p. 241.

Kovats, E. (1958). Helv. Chim. Acta, 41:1915.

Liss, P. G., and P. G. Slater (1974). Flux of Gases Across the Air-Sea Interface. Nature, Vol. 247, January 25, p. 181.

Lloyd, J. B. F. (1971). Nature, 231(64).

Lloyd, J. B. F. (1971). J. Forensic Sci. Soc., 11(83).

Mackay, D., A. Bobra, and D. W. Chan (1982). Vapor Pressure Correlations for Low-volatility Environmental Chemicals. Environ. Sci. Tech. 16(10):645-649.

Mackay, D., J. Buist, R. Mascarenhas, and S. Paterson (1980). Oil Spill Processes and Models, report submitted to Research and Development Division, Environmental Emergency Branch, Environmental Impact Control Directorate, Environmental Protection Service, Environment Canada, Ottawa, Ontario, K1A 1C8.

Mackay, D. and K. Hossain (1982). An Exploratory Study of Naturally and Chemically Dispersed Oil. Department of Chemical Engineering and Applied Chemistry, University of Toronto.

Mackay, D. P. J. Leinonen, J. C. K. Overall, and B. R. Wood (1975). The Behavior of Crude Oil Spilled on Snow. Arctic 28:9-20.

Mackay, D., and R. S. Matsugu (1973). Evaporation Rates of Liquid Hydrocarbon Spills on Land and Water. The Canadian Journal of Chemical Engineering, Vol. 51, p. 434.

Mackay, D., and W. Y. Shiu (1977). Aqueous Solubility of Polynuclear Aromatic Hydrocarbons, Journal of Chemical Engineering Data, Vol. 22, #4, p. 399.

Malinky, G. and D. G. Shaw (1979). Modeling the Association of Petroleum Hydrocarbons and Sub-Arctic Sediments, p. 621-624, In: Proceedings, 1979

Oil Spill Conference (Prevention, Behavior, Control, Cleanup), 19-22 March, Los Angeles, Calif.

McAuliffe, C. (1966). Solubility in Water of Paraffin, Cycloparaffin, Olefin, Acetylene, Cycloolefin, and Aromatic Hydrocarbons. J. Phys. Chem. 70:1267-1275.

McAuliffe, C. (1977). Evaporation and Solution of C_2 to C_{10} Hydrocarbons from Crude Oils on the Sea Surface. In: D. A. Wolfe (ed.), Fate and Effects of Petroleum Hydrocarbons in Marine Organisms and Ecosystems, Pergamon Press.

Means, J. C., S. G. Wood, J. J. Hassett, and W. L. Banwart (1980). Sorption of Polynuclear Aromatic Hydrocarbons by Sediments and Soils. Environmental Science and Technology, 14(12), p. 1524.

Meyers, P. A., and J. G. Quinn (1973). Association of Hydrocarbons and Mineral Particles in Saline Solutions. Nature, 244:23-24.

Meyers, P. A. and J. G. Quinn (1973). Factors Affecting the Association of Fatty Acids with Mineral Particles in Sea Water. Geochimica et Cosmochimica Acta, 37,p. 1745.

Mooney, M. (1951). The Viscosity of a Concentrated Suspension of Spherical particles. Journal of Colloid Science, Vol. 6, pp. 162-170.

Owen, M. W. (1977). Problems in the Modeling of Transport, Erosion and Deposition of Cohesive Sediments. In: The Sea. Vol 6, edited by E. D. Goldberg, I. N. McCave, J. J. O'Brien, and J. H. Steele, pp 515-537, Interscience, New York.

Parker, P. L. and S. Macko (1978). An Intensive Study of the Heavy Hydrocarbons in the Suspended Particulate Matter of Seawater, Ch. 11 of South Texas Outer-Continental BLM Study.

Pavlou, S. P. and R. N. Dexter (1979). Distribution of Polychlorinated Byphenyls (PCB) in Estuarine Ecosystems. Testing the Concept of Equilibrium Partitioning in the Marine Environment. Environmental Science and Technology, 13(10), p. 65.

Payne, J. R. (1981). A Review of the Formation and Behavior of Water-in-Oil Emulsions (Mousse) from Spilled Petroleum and Tar Ball Distributions, Chemistries and Fates in the World's Oceans. Background Information for Ocean Sciences Board on "Inputs, Fates and Effects of Petroleum in the Marine Environment," National Academy of Sciences.

Payne, J. R., N. W. Flynn, P. J. Mankiewicz, and G. S. Smith (1980b). Surface Evaporation/Dissolution Partitioning of Lower-Molecular-Weight Aromatic Hydrocarbons in a Down-Plume Transect from the IXTOC-I Wellhead, p. 239-265. In: Proceedings of a Symposium, Preliminary Results from the Sept.

1979 Researcher/Pierce IXTOC-I Cruise (June 9-10, Key Biscayne, Fla.) NOAA, Off. Mar. Poll. Assess.

Payne, J. R., B. E. Kirstein, G. D. McNabb, Jr., J. C. Lambach, C. De Oliveira, R. E. Jordan, and W. Hom (1983). Multivariate Analysis of Petroleum Hydrocarbon Weathering in the Subarctic Marine Environment. pp. 423-434. In: Proceedings of the 1983 Oil Spill Conference, San Antonio, TX. February 28 - March 3, 1983.

Payne, J. R., B. E. Kirstein, R. F. Shokes, N. L. Guinasso, L. Carrer, K. R. Fite, R. E. Jordan, P. J. Mankiewicz, G. S. Smith, W. J. Paplawsky, T. G. Fanara, and J. Lambach (1980). Multivariant Analysis of Petroleum Weathering Under Marine Conditions. Interim Quarterly Report Submitted to National Oceanographic and Atmospheric Administration.

Payne, J. R., P. J. Mankiewicz, J. E. Nemmers, R. E. Jordan, S. Brenner, M. I. Venkatesan, B. W. de Lappe, R. W. Risebrough, G. F. Gould, and M. L. Moberg (1979a). Southern California Outer Continental Shelf Baseline Studies: Intercalibration of Participating Hydrocarbon Laboratories. Manuscript submitted in Oceans '79 Conference Proceedings for Oceans Conference, San Diego, California, 16-19 September, 1979.

Payne, J. R., J. E. Nemmers, R. E. Jordan, P. J. Mankiewicz, A. D. Oesterle, S. Laughon, and G. Smith (1979b). Measurement of Petroleum Hydrocarbon Burdens in Marine Sediments by Three Commonly Accepted Procedures: Results of a NOAA Inter-Laboratory Calibration Exercise, Fall, 1978. Submitted to Dr. John A. Calder, Staff Chemist, OCSEAP, U.S. Department of Commerce, National Oceanic and Atmospheric Administration, Environmental Research Laboratory, Boulder, CO, January 1979. pp. 1-34, plus appendix.

Payne, J. R., G. S. Smith, P. J. Mankiewicz, R. F. Shokes, N. W. Flynn, V. Moreno, and J. Altamirano (1980a). Horizontal and Vertical Transport of Dissolved and Particulate-Bound Higher-Molecular-Weight Hydrocarbons from the IXTOC-I Blowout, p. 119-167. In: Proceedings of a Symposium, Preliminary Results from the Sept. 1979 Researcher/Pierce IXTOC-I Cruise (June 9-10, Key Biscayne, Fla.) NOAA, Off. Mar. Poll. Assess.

Poirier, O. A., and G. A. Thiel (1941). Deposition of Free Oil by Sediments Settling in Sea Water. Bulletin of the American Association of Petroleum Geologist, 25(1), p. 2170.

Postma, H. (1967). Sediment Transport and Sedimentation in the Estuarine Environment. In: ESTUARIES, Ed. by George H. Lauff., American Association for the Advancement of Science. Pub No. 83.

Ramos, L. S. and P. G. Prohaska (1981). Sephadex LH-20 Chromatography of Extracts of Marine Sediment and Biological Samples for the Isolation of Polynuclear Aromatic Hydrocarbons. Jour. of Chromatography 211:284-289.

Raschevsky (1928). Z. Phys., 46, pg. 585.

Reid, R. C., J. M. Prausnitz, and T. K. Sherwood (1977). The Properties of Gases and Liquids, McGraw-Hill Book Company, New York.

Rohsenow, W. M., and J. P. Hartnett (1973). Handbook of Heat Transfer, McGraw-Hill Book Company, New York.

Ruby, A. and Majero, D. J., (1979). Environmental Sensitivity Index (ESI) for Lower Cook Inlet (unpublished manuscript).

Smith, C. L., and W. G. MacIntyre (1971). Initial Aging of Fuel Oil Films of Seawater. In: Proceedings of the 1971 Joint Conference on Prevention and Control of Oil Spills, p. 457-461. American Petroleum Institute, Washington, D.C.

Smith, J. (1977). Modeling of Sediments Transport on Continental Shelves. In: The Sea, Vol 6, edited by E. D. Goldberg, I. N. McCave, J. J. O'Brien, and J. H. Steele, pp 539-577, Interscience, New York.

Smith, J. D. and McLean, S. R. (1977a). Spatially Averaged Flow over a Wavy Surface. J. Geophys. Res. Vol 32, No. 12, pp 1735-1746.

Smith, J. D. and McLean, S. R. (1977b). Boundary Layer Adjustments to Bottom Topography and Suspended Sediment. In: Bottom Turbulence, edited by J. C. J. Nihoul, pp 123-152, Elsevier Scientific Publishing Co., The Netherlands.

Stackelberg, W., Klockner and Mohrhauer (1949). Kolloidzschr, 115, pg. 53.

Steen, W. C., D. F. Paris and G. L. Baughman (1978). Partitioning of Selected Polychlorinated Biphenyls to Natural Sediments. Water Research, 12, p.655.

Suess, E. (1968). Calcium Carbonate Interactions with Organic Compounds. Ph.D. Thesis. Lehigh University, Bethlehem, PA.

Sullivan, K. F., E. L. Atlans, and C. S. Giam (1982). Adsorption of Phthalic Acid Esters from Seawater. Environmental Science and Tecynology, 16(7), p. 428.

Sutton, C. and J. A. Calder (1974). Solubility of Higher-Molecular-Weight n-Paraffins in Distilled Water and Seawater. Environmental Science and Technology, 8:654-647.

Sutton, W. G. L. (1943). On the Equation of Diffusion in a Turbulent Medium, Proceedings of the Royal Society (London), A182, p. 48.

Tambo, N. and Watanabe, Y. (1979). Physical characteristics of flocs - I. The floc density function and aluminum floc. Water Research, Vol 13, pp 409-419.

Tebean, P. A (LCDR-USCG), D. Mackay, W. Y. Shin, W. Stiver, K. Hassain, D. McCurdy and S. Paterson (1982). Oil Weathering Under Arctic Conditions. Paper from Department of Chemical Engineering, University of Toronto, Toronto, Ontario, Canada, M5S 1A4.

Teige, R. W. (1980). Petroleum Distillation Using Kontes/Martin MK IV-B Fractionators and Hi-Vac Skills. Kontes/Martin Co. 68 pp.

Treybal, R. E. (1955). Mass-Transfer Operations, McGraw-Hill Book Company, New York.

Twardus, E. M. (1980). A Study to Evaluate the Combustibility and Other Physical and Chemical Properties of Aged oils and Emulsions. R and D Div., Environmental Emergency branch, Environmental Protection Serrvice, Ottawa, Ontario, Canada.

Twomey, S. (1977). Atmospheric Aerosols. Elsevier Scientific Publishing Company. New York.

Vo-Dinh, T., R. B. Gammage, A. R. Hawthrone, and J. H. Thorngate (1978). Synchronous Spectroscopy for Analysis of Polynuclear Compounds. Environmental Science and Technology, 12(12):1297-1302.

Wade, T. L. and J. G. Quinn (1979). Incorporation, Distribution, and Fate of Saturated Petroleum Hydrocarbons in Sediments from a Controlled Marine Ecosystem. Marine Environmental Research, 3, p. 15.

Wakeham, S. F. (1977). Synchronous Fluorescence Spectroscopy and Its Application to Indigenous and Petroleum-Derived Hydrocarbons in Lacustrine Sediments. Environmental Science and Technology, 11(3):272-276.

Walker, J. D., and R. R. Colwell (1976). Measuring the Potential Activity of Hydrocarbon-Degrading Bacteria. Applied and Environmental Microbiology. 31(2):189-197.

Ward, D. M. and T. D. Brock (1978). Hydrocarbon Biodegradation in Hypersaline Environments. Appl. Environ. Microbiol. 35:353-359.

Ward, D., R. M. Atlas, P. D. Boehm, and J. A. Calder (1980). Microbial Biodegradation and the Chemical Evolution of Amoco Cadiz Oil Pollutants. Ambio 9:277-283.

Watson, S. W., Novitsky, T. J., Quinby, H. L., and F. W. Valois (1977). Determination of Bacterial Number and Biomass in the Marine Environment. Applied and Environmental Microbiology. 33(4):940-946.

Winters, J. K. (1978). Fate of Petroleum Derived Aromatic Compounds in Seawater Held in Outdoor Tanks, Ch. 12, South Texas Outer-Continental Shelf BLM Study.

Yang, W. C., and H. Yang. (1977). Modeling of Oil Evaporation in Aqueous Environment. Water Research, Vol. 11, p. 879.

Zurcher, F. and M. Thuer (1978). Rapid Weathering Processes of Fuel Oil in Natural Waters. Analysis and Interpretations. Environmental Science and Technology, 12(7):838-843.

U. S. DEPARTMENT OF COMMERCE
NATIONAL OCEANIC AND ATMOSPHERIC ADMINISTRATION
N/OMS33x3 (OCSEAP)
P.O. Box 1808
Juneau, Alaska 99802

OFFICIAL BUSINESS
PENALTY FOR PRIVATE USE, $300

POSTAGE AND FEES PAID
U.S. DEPARTMENT OF COMMERCE
COM-210

PRINTED MATTER

CLASS OF POSTAL SERVICE

U.S.MAIL

[illegible]
[illegible]
[illegible]
[illegible]

NOAA FORM 61-32A (11-77)
See NDM 61-50 for Class of Postal Service